KWARA STATE UNIVERSITY, MALETE, NIGERIA

SCHOOL OF POSTGRADUATE STUDIES (SPGS)

GEOPHYSICAL AND HYDROCHEMICAL CHARACTERIZATION FOR QUANTITATIVE AND QUALITATIVE ANALYSES OF GROUNDWATER WITHIN ILORIN NW, SHEET 223 SOUTHWESTERN NIGERIA

Umar ISSA

17/27/PGE002

MAY, 2022

SCHOOL OF POSTGRADUATE STUDIES (SPGS)

GEOPHYSICAL AND HYDROCHEMICAL CHARACTERIZATION FOR QUANTITATIVE AND QUALITATIVE ANALYSES OF GROUNDWATER WITHIN ILORIN NW, SHEET 223 SOUTHWESTERN NIGERIA

A Ph.D. THESIS SUBMITTED

BY

Umar ISSA

(17/27/PGE002)

In Partial Fulfillment of the requirements of the award of Doctor of Philosophy (Ph.D.) in Geology

DEPARTMENT OF GEOLOGY AND MINERAL SCIENCES, FACULTY OF PURE AND APPLIED SCIENCES, KWARA STATE UNIVERSITY, MALETE, NIGERIA

MAY, 2022.

DECLARATION PAGE

I hereby declare that this thesis titled (Geophysical and Hydrochemical characterization for quantitative and qualitative analyses of Groundwater within Ilorin Northwest, sheet 223 southwestern Nigeria) is a record of my research. It has neither been presented nor accepted in any previous application for a higher degree.

---------- ----------

UMAR ISSA Signature /Date

APPROVAL PAGE

This is to certify that this thesis by Umar ISSA has been read and approved as meeting the requirements of the Department of Geology and Mineral Sciences, Kwara State University, Malete for the award of the degree of Doctor of Philosophy (Ph.D.) in Geology.

Dr. Jimoh Ajadi

Main Supervisor

30/6/2022

Signature and Date

Dr. Saminu Olatunji

Co- Supervisor

30/06/202

Signature and Date

Dr. Jimoh Ajadi

Head of Department

30/6/2022

Signature and Date

Dr. Suraju A. Adepoju

Internal Examiner

30/6/2022

Signature and Date

Dr. Lukman B. Abdulrauf

Internal Examiner

30/06/20

Signature and Date

Prof. L.A. Sunmonu

External Examiner

20/06/2

Signature and Date

Prof. Hamzat .I. AbdulRaheem

Dean, School of Postgraduate Studies (SPGS)

5-8-22

Signature and Date

KWARA STATE UNIVERSITY, MALETE
School of Postgraduate Studies
Office of the Dean
RECEIVED

DEDICATION

This research work is dedicated to the Almighty Allah for seeing me through this program, and to my late Parents (Alhaji Issa and Alhaja Fatimoh Issa) for their care for me and the love, they have for education. May Almighty Allah be please with them.

ACKNOWLEDGEMENTS

I thank the Almighty Allah; the sustainer of life; He who has sustained my life from the beginning of this program to the end. All adorations, glorifications, and praises are due to Him alone.

I express my unquantifiable appreciation to my main and co-supervisors: Dr. Jimoh Ajadi and Ass. Prof. Saminu Olatunji for their motivation, support, constructive criticisms, encouragement, and words of advice given to me during this research work.

My gratitude also goes to members of the academic and non-academic staff of the Department for their support, starting from my former supervisor Late Professor Peter I. Olasehinde, Professor Victor O. Olanrewaju, Dr. Y.A Jimoh, Dr. S.A Adepoju, Dr. Olubunmi Owoyemi, Dr. Olufemi Olaniyan, Dr. M.O Awojobi, Dr. Olufemi Bamigboye, and my other colleagues.

I shall never forget my Ph.D. colleagues; Mr. Bamidele Toba Emmanuel, Mrs. Aminu Shakirat, Mrs. Saad Mariam, Mr. Taofeeq Issa, Mr. Ojulari Bashiru Alaba, Mr. Akim Olawumi, Mr. Awe and others numerous to mention.

My special acknowledgment goes to my children (Muhammad Sulton, Hawwau, Abdulwadood, Abdulquddus, and Muhammad Mahi) and my wife; a virtuous and loving woman (Mrs. Umar Amudat) for their understanding and support given to me during the study.

To my brothers and sisters, friends, my spiritual fathers, and other well-wishers, I appreciate you all and value your contributions.

TABLE OF CONTENTS

TITLE PAGE		i
DECLARATION PAGE		iii
APPROVAL PAGE		iv
DEDICATION		v
ACKNOWLEDGEMENTS		vi
TABLE OF CONTENTS		vii
LIST OF FIGURES		xiii
LIST OF TABLES		xvii
ABSTRACT		xviii
CHAPTER ONE		1
1.0	INTRODUCTION	1
1.1	The study area	3
1.1.1	Description of the area	3
1.1.2	Relief and Drainage	3
1.1.3	Climate, Vegetation, and Land use	4
1.2	Statement of problems	9
1.3	Justification for the study	9
1.4	Aim and Objectives of the study	9
1.5	Scope of the study	10
CHAPTER TWO		11
2.0	LITERATURE REVIEW	11
2.1	General Geology of Nigeria	11
2.1.1	The Precambrian Basement Complex rocks	11
2.1.1.1.	The Migmatite – Gneiss- Complex (MGQC)	15

2.1.1.2	The schist belts	16
2.1.1.3	Charnockitic- Gabroic-Dioritic Rocks	22
2.1.1.4	The Older Granites	24
2.1.1.5	Un-deformed Acid and Basic Dykes	26
2.1.2	The Sedimentary rocks	26
2.1.2.1	The Iullemmeden Basin	27
2.1.2.2	The Chad Basin	27
2.1.2.3	The Dahomey Basin	28
2.1.2.4	The Niger Delta Basin	29
2.1.2.5	The Benue Trough Basin	30
2.1.2.6	The Bida Basin	30
2.1.2.7	The Anambra Basin	31
2.2	Geology of Kwara State	31
2.3	Hydrogeology of Kwara State	33
2.4	Geophysical studies	34
2.4.1	Principle of Magnetic Method	34
2.4.2	The Earth' Magnetic Field	35
2.4.3	The Geomagnetic Field	36
2.4.4	The International Geomagnetic Reference Field (IGRF)	37
2.4.5	Magnetic Susceptibility	39
2.4.6	Magnetic induction	39
2.4.7	Classification of magnetic materials	40
2.4.8	Magnetism of Rocks and Minerals	42
2.4.9	Aeromagnetic Survey	42
2.5	Principle of Electrical Resistivity	43

2.5.1	Review of Previous Geophysical Works	44
2.5.2	Dar Zarouk Parameters	52
2.6	Related Previous works on Hydrogeophysical studies	53
2.7	Review of previous Hydrochemical assessment of groundwater	55
CHAPTER THREE		58
3.0	MATERIALS AND METHODS	58
3.1	Geological Survey Materials	58
3.1.1	Geological Mapping	58
3.1.2	Hydrogeological Survey Data	59
3.1.3	Hydrogeological Survey Method	59
3.1.3.1	Pumping Test Survey	59
3.1.3.2	Water Level Measurements	63
3.2	Aeromagnetic data	64
3.3	High-Resolution Aeromagnetic Data (HRAM) Processing	65
3.3.1	The Regional – Residual Separation	65
3.3.2	Filtering of Residual Field Data	68
3.3.3	Reduction to the Equator (RTE)	68
3.3.4	Tilt Angle Derivative (TDR)	69
3.4	Electrical Resistivity Survey data	70
3.4.1	Electrical Resistivity survey method	70
3.5	Hydrochemical Test Materials	74
3.5.1	Hydrochemical Test Method	74
CHAPTER FOUR		76
4.0	RESULTS AND DISCUSSION	76
4.1	Mapping of the Study Area	76

4.1.1	Rock Types in the Area	77
4.1.1.1	Migmatite gneiss	77
4.1.1.2	Banded Gneiss	81
4.1.1.3	Augen Gneiss	84
4.1.1.4	Granite Gneiss	84
4.1.1.5	Quartz-Mica-Schist	93
4.1.1.6	Fine-Grained Granite	93
4.1.2	Geologic structures of the study area	99
4.2	Aquifer types in the study area	102
4.2.1	The overburden aquifer	102
4.2.2	The fractured crystalline aquifer	103
4.3	Hydraulic Characteristics of Aquifers in the Study Area	106
4.4	Evaluation of Groundwater level Time-Dependent Variation	114
4.4.1	Evaluation of thickness of unsaturated/Vadose zone	119
4.5	Geophysical Method	121
4.5.1	Magnetic Method	121
4.5.1.1	Total Magnetic Field Intensity (TMI) Anomaly Map	121
4.5.1.2	Regional Magnetic Intensity (RMI) map	124
4.5.1.3	Residual Magnetic Intensity (RMI) map	126
4.5.1.4	Reduction to the Magnetic Equator (RTE)	128
4.5.1.5	Tilt Derivative (TDR) Map	130
4.5.2	Electrical Resistivity Method	134
4.5.2.1	VES Results	134
4.5.2.2	Inferred Geologic Layers, equivalence of Geo-electric sections	139
4.5.2.3	Isoresistivity maps	144

4.5.2.4	Isopach map	150
4.5.2.5	Dar- Zarouk parameters	154
4.5.2.6	Groundwater potential evaluation through Reflection Coefficient and Overburden Thickness	164
4.5.2.7	Aquifer Parameters	167
4.6	Physico-chemical quality assessment of groundwater of the area	179
4.6.1	Quality of groundwater for drinking and domestic purposes	181
4.6.1.1	Physico-chemical parameters	181
4.6.1.2	Water Quality Index	197
4.6.2	Quality of Groundwater for Irrigation Purpose	202
4.6.2.1	Bicarbonate Hazard/Residual Sodium Carbonates (RSC)	202
4.6.2.2	Sodium Hazard or Sodium Adsorption Ratio (SAR)	205
4.6.2.3	Salinity Hazard	209
4.6.2.4	Toxic Elements Hazard	211
4.6.2.5	Kelly Index (KI)	211
4.6.2.6	Magnesium Adsorption Ratio (MAR)	213
4.6.2.7	Percentage Sodium (%Na)	215
4.6.3	Gibbs Diagram	219
4.6.4	Classification and Evolution of Groundwater in the Study Area	221
4.6.4.1	Piper classification	221
4.6.4.2	Stiff classification	222
4.6.5	Correlation Analysis of the Chemical Species	225
4.6.5.1	Correlation Analysis	225

CHAPTER FIVE 227

5.0 CONCLUSION, RECOMMENDATIONS AND CONTRIBUTIONS TO KNOWLEDGE 227

5.1 Conclusion 227

5.2 Recommendations 228

5.3 Contributions to Knowledge 228

REFERENCES 229

APPENDIX 1: GEOPHYSICAL CURVES AND THEIR PSEUDO SECTIONS 243

APPENDIX 2: SUMMARY OF THE REMAINING RESULTS OF VERTICAL ELECTRICAL SOUNDING 317

APPENDIX 3: TABLE 4(a-f) SHOWING CALCULATED VALUES OF DAR- ZAROUK PARAMETERS 344

APPENDIX 4: TABLE 6(a-e) SHOWING CALCULATED VALUES OF AQUIFER PARAMETERS 354

APPENDIX 5: PRINCIPLES AND PROCEDURES OF THE METHODS USED IN THE WATER SAMPLES' ANALYSIS 363

LIST OF FIGURES

Figure 1:	Topographical map of the study area	5
Figure 2:	Topographical map of the study area showing its relief	6
Figure 3:	Map of drainage pattern of the study area	7
Figure 4:	Mean Monthly Rainfall Data of the Area	8
Figure 5:	Geological map of Nigeria showing the litho-petrological components	12
Figure 6:	Geological Map of Nigeria showing Basement Complex and Sedimentary terrains	13
Figure 7:	A migmatitic gneiss rock from Basement complex rocks along NRDC – Emir's palace	17
Figure 8:	Schist belt localities within the context of the Geology of Nigeria	18
Figure 9:	Elements of Earth's Magnetic Field; Z: Vertical component H: Horizontal component.	38
Figure 10:	Geological map of the study area	78
Figure 11:	Field photograph of migmatite gneiss showing joints, simple and asymmetrical folds	79
Figure 12:	Photomicrograph of migmatite gneiss in cross polarized light	80
Figure 13:	Photomicrograph of migmatite gneiss in plane polarized light (PPL)	80
Figure 14:	Field photograph of Banded Gneiss at Odo-ode	82
Figure 15:	Photomicrograph of Banded gneiss in cross-polarized light (XPL).	83
Figure 16:	Photomicrograph of banded gneiss in plane polarized light (PPL).	83
Figure 17:	Field photograph of Augen Gneiss at Osin-Idiemi with pegmatite vein intrusion.	85
Figure 18:	Field photograph of Augen Gneiss at Osin-Olokete	86
Figure 19:	Field photograph of Augen gneiss with relics of pegmatite intrusion at Malubi	87
Figure 20:	Photomicrograph of Augen gneiss in cross polarized light.	88
Figure 21:	Photomicrograph of Augen gneiss in plane polarized light.	88

Figure 22:	Field photograph of Granite Gneiss at Asa River	89
Figure 23:	Field photograph of Granite Gneiss at Sokoto community	90
Figure 24:	Photomicrograph of granite gneiss at Sokoto and Tewure communities, in cross-polarized light.	92
Figure 25:	Photomicrograph of granite gneiss at Sokoto and Tewure communities, in plane polarized light	92
Figure 26:	Field photograph of Quartz-Mica-Schist intruded by pegmatite rich in potassic feldspar at Igborese.	94
Figure 27:	Photomicrograph of Quartz-Mica-schist in cross polarized light.	95
Figure 28:	Photomicrograph of quartz- mica- schist in plane polarized light	95
Figure 29:	Field photograph of fine grained granite with quartzo-feldsparthic	96
Figure 31:	Photomicrograph of fine-grained granite at Ansarul Islam Secondary School premises, Laduba, in cross-polarized light.	98
Figure 30:	Photomicrograph of fine-grained granite at Ansarul Islam Secondary School premises, Laduba, in plane-polarized light.	98
Figure 32:	Rose diagram showing the structural trends of joints in the study area	100
Figure 33:	Rose diagram showing the foliation planes in the study area	101
Figure 34:	Borehole log of Ago- Agbona in the study area depicting an overburden aquifer	104
Figure 35:	Borehole log of Ila-Oja in the study area depicting a fractured aquifer	105
Figure 36:	Plot of drawdown versus time for Reke water side	108
Figure 37:	Plot of drawdown versus time for Ganmo water side	109
Figure 38:	Plot of drawdown versus time for Amayo water side	110
Figure 39:	Plot of drawdown versus time for Osin- Aremu water side	111
Figure 40:	Plot of drawdown versus time for Ita - Elepa water side	112
Figure 41:	Plot of drawdown versus time for Budo-Ojoku water side	113
Figure 42:	Groundwater contour map at the end of raining season	115
Figure 43:	Groundwater flow net, end of rainy season	116

Figure 44:	Groundwater contour map at the peak of the Dry season	117
Figure 45:	Groundwater flow net, the peak of the dry season	118
Figure 46:	Peizometric surface variation at the end of raining season	120
Figure 47:	Peizometric surface variation at the peak of dry season	120
Figure 48:	Total Magnetic Intensity anomaly map of the study area	123
Figure 49:	Regional Magnetic field Intensity map of the study area	125
Figure 50:	Residual Magnetic Intensity map of the study area	127
Figure 51:	Reduction to equator (RTE) map of the study area	129
Figure 52:	Tilt Angle Derivative Map of the study area	131
Figure 53:	Inferred structures from Tilt Derivative Map of the study area	133
Figure 54:	Location map of the study area showing VES points	135
Figure 55:	Pie chart showing frequency distribution of observed curve types	137
Figure 56:	Bar chart showing frequency distribution of observed curve types	138
Figure 57:	Typical Field Curve and its Equivalent 2D Section for Ganmo location	141
Figure 58:	Typical field Curve and its Equivalent 2D Section for Eleru location	141
Figure 59:	Typical Field Curve and its Equivalent 2D Section for Akanbi Ade location	141
Figure 60:	Top soil Isoresistivity map for the study area	145
Figure 61:	Laterite isoresistivity map for the study area	146
Figure 62:	Isoresitivity map of Weathered Basement for the study area	148
Figure 63:	Isoresistivity of Fresh basement rock within the study area	149
Figure 64:	Isopach map of top soil for the study area	151
Figure 65:	Isopach of Laterite within the study area	152
Figure 66:	Isopach map of weatherd Basement within the study area	153
Figure 67:	Longitudinal conductance distribution map within the study area	159
Figure 68:	Transverse Resistance distribution map within the study area	160

Figure 69:	Longitudinal Resistivity distribution mapwithin the study area	161
Figure 70:	Transverse Resistivity distribution mapwithin the study area	162
Figure 71:	Coefficient of anisotropy distribution mapwithin the study area	163
Figure 72:	Reflection coefficient variation mapwithin the study area	165
Figure 73:	Overburden thickness variation mapwithin the study area	166
Figure 74:	Aquifer resistivity variation map within the study area	168
Figure 75:	Aquifer Depth variation map within the study area	170
Figure 76:	3-D Impression of aquifer depth variation within the study area.	171
Figure 77:	Aquifer thickness distribution map within the study area	173
Figure 78:	Aquifer Potential map within the study area	174
Figure 79:	Hydraulic Conductivity distribution map within the study area	176
Figure 80:	Aquifer Transmissivity distribution map within the study area	178
Figure 81:	Map of the study area showing groundwater sampling locations.	180
Figure 82:	Graph comparing the obtained average concentrations of physical parameters	195
Figure 83:	Graph comparing the obtained average concentrations of chemical parameters	196
Figure 84:	Graphical representation of water quality index rating for groundwater locations	200
Figure 85:	Graphical representation of water quality index rating for groundwater locations	200
Figure 86:	Water Quality map for groundwater sampling locations in the study area	201
Figure 87:	Wilcox quality classification of irrigation waters	207
Figure 88:	Wilcox (1948) and Mohammad *et al*., (2019)'s quality classification of irrigation waters .	217
Figure 89:	Gibbs diagram showing the distribution of the water samples in the area.	220
Figure 90:	Piper trilinear diagram showing the distribution of water samples.	223
Figure 91:	Stiff diagram showing the chemical parameters of groundwater	224

LIST OF TABLES

Table 1:	Calculated Values of Hydraulic Conductivity, Transmissivity and Storage coefficient	107
Table 2:	Various curve types, their frequencies and percentages	136
Table 3:	Summary of Results of Vertical Electrical Sounding	143
Table 4:	Modified longitudinal conductance/protective capacity rating	158
Table 5:	Physico-chemical Analysis of Groundwater samples in the area	183
Table 6:	Average values obtained for Physico-chemical parameters.	194
Table 7:	Calculated values of water quality index for groundwater samples of the area	198
Table 8:	Classification of the quality of water for drinking purposes.	199
Table 9:	Calculated values of Residual Sodium Carbonate of groundwater samples in the area	204
Table 10:	Calculated values of Sodium Adsorption ratio for groundwater in the area	206
Table 11:	United State Science Laboratory (USSL) classification for Sodium Adsorption Ratio	208
Table 12:	Suitability of water for irrigation in respect of Salinity Hazard	210
Table 13:	Calculated values of salinity Hazard for groundwater of the study area	210
Table 14:	Kelley Index for suitability of groundwater for irrigation purpose in the study area	212
Table 15:	Calculated values of Magnesium Adsorption Ratio (MAR) for groundwater in the area	214
Table 16:	Calculated values of Percentage sodium for groundwater samples in the area	216
Table 17:	Wilcox water classification in respect of percentage sodium	218
Table 18:	Correlation Analysis of Physico-chemical parameters Results	226

ABSTRACT

The study area covers parts of Ilorin Northwest Sheet 223 which is underlain by the Basement Complex rocks of southwestern Nigeria. The need for groundwater system evaluation within the study area arises to provide a standard database for consumption and Agrarian purposes. The study aims at determining the quantity and quality of the groundwater in the area. The objectives of the study are to determine the groundwater time-dependent variations to obtain the perennial groundwater level fluctuation, analyze the magnetic anomalies to derive lineaments' distribution, investigate the geophysical study of vertical electrical sounding to establish the potentiality of the groundwater, and, conduct the hydrochemical analysis of groundwater samples of 35 sampling points within the area to determine their quality for human and agrarian usability. The methodology adopted for this research includes; (i) Peizometric measurement of water level in the area for perennial groundwater level fluctuation determination, (ii) analyzing aeromagnetic dataset to obtain magnetic anomalies of the underlain rocks within the area (iii) vertical electrical sounding of Schlumberger array techniques to investigate resistivity changes of the underlying lithologies and, (iv) assessment of groundwater quality through in-situ and laboratory methods. The findings from this study revealed that the area is underlain by lithologies comprising; migmatite gneiss, banded gneiss, augen gneiss, granite gneiss, quartz-mica-schist, and fine-grained granite. The time-dependent variation studies show higher groundwater levels in the southern part of the study area than in the rest parts. The magnetic anomalies are also higher in the southern part, while they are moderate and low in the western and the eastern parts respectively. The vertical electrical sounding (VES) identified three to five geo-electric layers; the topsoil, the lateritic horizon, the weathered basement, the sandy clay/clayey sand, and the underlying fractured basement rock with the depth varying from 1.05 to 41.8 m. The range of concentrations of the measured physical parameters; including turbidity (50-470 NTU), pH (3.7-7.9), temperature (29-35 °C) and electrical conductivity (50-940 µS/cm) and average of chemical parameters (mg/l) Ca (0.85), Na (1.23), K (0.35), Mg (0.56), Cu (0.03), Fe (0.03), Mn (0.1), Zn (0.02). Pb (0.03), Cd (0.05), SO_4^{3-} (0.02), PO_4^{2-} (0.11), Cl^- (1.43), HCO_3^- (65), CO_3^- (157), and NO_3^- (0.47), fall below the World Health Organization (WHO) standards. The study concludes that the crystalline rocks within the Ilorin Northwest Sheet 223 have a moderate to low permeability, therefore, are aquiferous with modest groundwater potential, especially in the southern part. The high lineament density mapped also confirms the above deductions. The physio-chemical assessment of groundwater samples revealed values that fall below the maximum desirable and permissible limits of the WHO standard, which suggest that the groundwater in the study area is good for human consumption and suitable for Agricultural purposes.

CHAPTER ONE

1.0 INTRODUCTION

Water is one of the most significant natural resources which support both human needs and economic development. Water is available in many forms such as ice caps, glaciers, ocean water, groundwater, etc. For more than 50% of the world's population, groundwater is a more dependable source of water (Alabi *et al.*, 2010). The size of a region's groundwater resources is determined by the limit of a group of rocks there. According to Lawrence and Ojo (2012), groundwater with the lowest dissolved solid content is typically free of color and odor. It is also not usually affected by natural factors such as drought.

Due to the government's inability to meet the nation's ever-increasing water needs, residents in Nigeria are forced to find alternate sources, among which groundwater resources like shallow wells and boreholes are a component (LAWMA, 2000). The majority of Nigeria's rural areas rely on hand-dug wells, rivers, and streams for their water supply, while urban areas rely on treated piped water and boreholes. Studies show that Nigeria has sufficient water resources that could meet the needs of its people. However, the actual potable water supply is very poor in various areas of the country. Olatunji *et al.* (2021) informed that population explosion and technological development result in sporadic development of dumpsites where rubbish is kept; this causes pollution. In addition, the natural contaminants below surface rocks add up to the artificial/manmade contaminant earlier mentioned. These pose a danger to the consumption of exploited underground water. Thus, a thorough chemical analysis is imperative to ascertain the quality of the exploited subsurface water at an instance.

In exploring underground water, different methods have been employed by various researchers in which geophysical methods have been extensively utilized due to their capacity to deliver precise results. Because of its advantages, such as simplicity in field methodology

and data handling procedures, the electrical resistivity method has been the most frequently utilized for groundwater study among geophysical techniques (Anomohanran, 2013). Investigators such as Olasehinde *et al.* (1998), Raji and Bale (2008), Olawuyi, A.K. (2012), Oseji *et al*.(2009), Nejad (2009), Egbai (2013), Anudu *et al*.(2011), Sirhan *et al*.(2011), Ibrahim *et al*. (2012), Utom *et al*. (2012), and Anomohanran (2013), among others, have all utilized the electrical resistivity method (ERM) to explore for groundwater in varying locations. Electrical resistivity methods are effectively used for groundwater exploration in areas where good electrical resistivity contrast exists between the water-bearing formation and the underlying rocks (Nejad, 2009). By injecting an electric current into the earth and observing the electrical potential it creates, the resistivity method can determine the subsurface resistance. Also, researchers such as Adetona *et al.* (2007), Labbo and Ugodulunwa (2007), Nwankwo (2015), and Kamba *et al. (*2016) have all used magnetic method to delineate groundwater potential zones in different locations. The magnetic method gives information about the sub-surface's deeper source by indicating the high and low magnetic intensity areas. It also shows the presence of lineament equivalence of fractures. Hydrogeophysical studies were carried out at some selected areas in the North-Eastern and South-Eastern parts of Ilorin Metropolis, Kwara State by Olasehinde *et al.* (1998), Raji and Bale (2008) and Olawuyi A.K (2012). However, the present study area which covers parts of Ilorin North-west, Sheet 223 has not received much attention.

Ilorin Sheet 223 North- West which is the study area has important features for water supply. The area has the north-flowing major River Asa (Figure 1). The first major Dam- Asa Dam is sited northwest of the area. The tributaries take off from the southwestern upland area. Apart from the numerous surface water sources, the area is poorly attended to in terms of water supply. The population of the Asa Local government Area is about 50,000 people (Personal communication from the secretary, Asa Local government). The people of Afon

which is the headquarters of the local government do not fully benefit from the Asa Dam project talking less of the small towns and villages in the local government.

The present study is aimed at proffering solutions to the water supply problem facing the dwellers in the area by determining the potentiality and quality of groundwater in the area. This would be done through detailed geo-hydrological investigations using Geological mapping, lithological log data, direct measurement of depth to water-table, pump-testing data, aeromagnetic data, and vertical electrical sounding (VES) survey and physico-chemical assessment. This is to fill the gap in the need for good domestic and agricultural water sources which are lacking in the study area.

1.1 The study area

1.1.1 Description of the area

The study area covers a part of sheet 223, (Ilorin NW), on a scale of 1:25,000. The area is bounded by latitudes 8°15' N and 8°25'N and lines of longitude 4°30'E and4°37.5'E, covering an approximate area of 72km^2 (Figure1). The study area includes some notable settlements like Egbejila, Laduba, Afon, Okeso, Ganmo Market, Ogbondoroko, and Gbaija. The area was accessible through motorable roads and footpaths.

1.1.2 Relief and Drainage

The relief of Ilorin is that of a dissected topography with the main Rivers Asa and Oyun truncating the rather peneplanar surface in a dendritic pattern. The highest point is 357 m and the lowest is188 m above mean sea level (Figure 2). Other notable rivers in the area are rivers Sagbeluka, Iwo-nto, and Elelela which also flow in the North-South direction as the main rivers. Figure 3 shows the drainage pattern of the area.

1.1.3 Climate, Vegetation, and Land use

The study area lies within the humid tropical climate with a total annual rainfall of about 1200 mm. The area is characterized by two seasons; the rainy season and the dry season. The rainy season begins in early March and lasts till October while the dry season is from November to early March. Figure 4 shows the mean monthly average rainfall from 2005 to 2016 with a mean annual of 1,309 mm, September has the highest rainfall and December has the least. Appendix 1 contains the average rainfall information for each year. March has the highest average temperature of 31º C and August has the lowest monthly average temperature of 25.5º C (Figure 4).

The vegetation of Ilorin is that of derived wooded guinea savanna type. The vegetation is characterized by woody trees, tall grasses, and herbs. The grasses and herbs sprout up during the wet season with the assumption of various shades of green and turn brown, pale, or yellow in the dry season. This is a result of seasonal changes in rainfall.

The main occupation in the area is agriculture. Almost all the farmers in the area are peasant farmers. The land is mainly used for rain-fed agricultural purposes where farm crops such as yams, cassava, maize, guinea-corn, and vegetables are produced. Animal husbandry such as cattle rearing is also practiced.

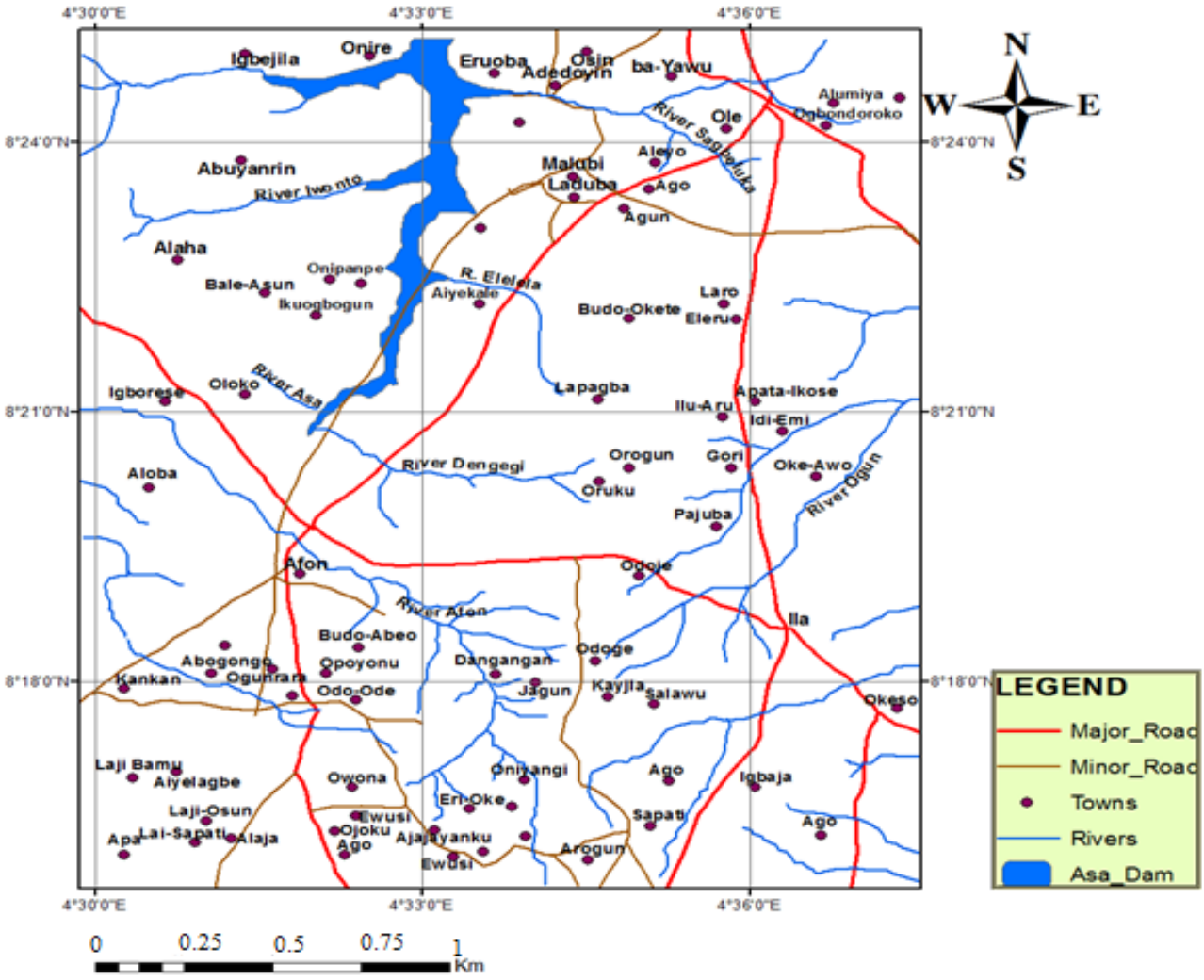


Figure 1: Topographical map of the study area

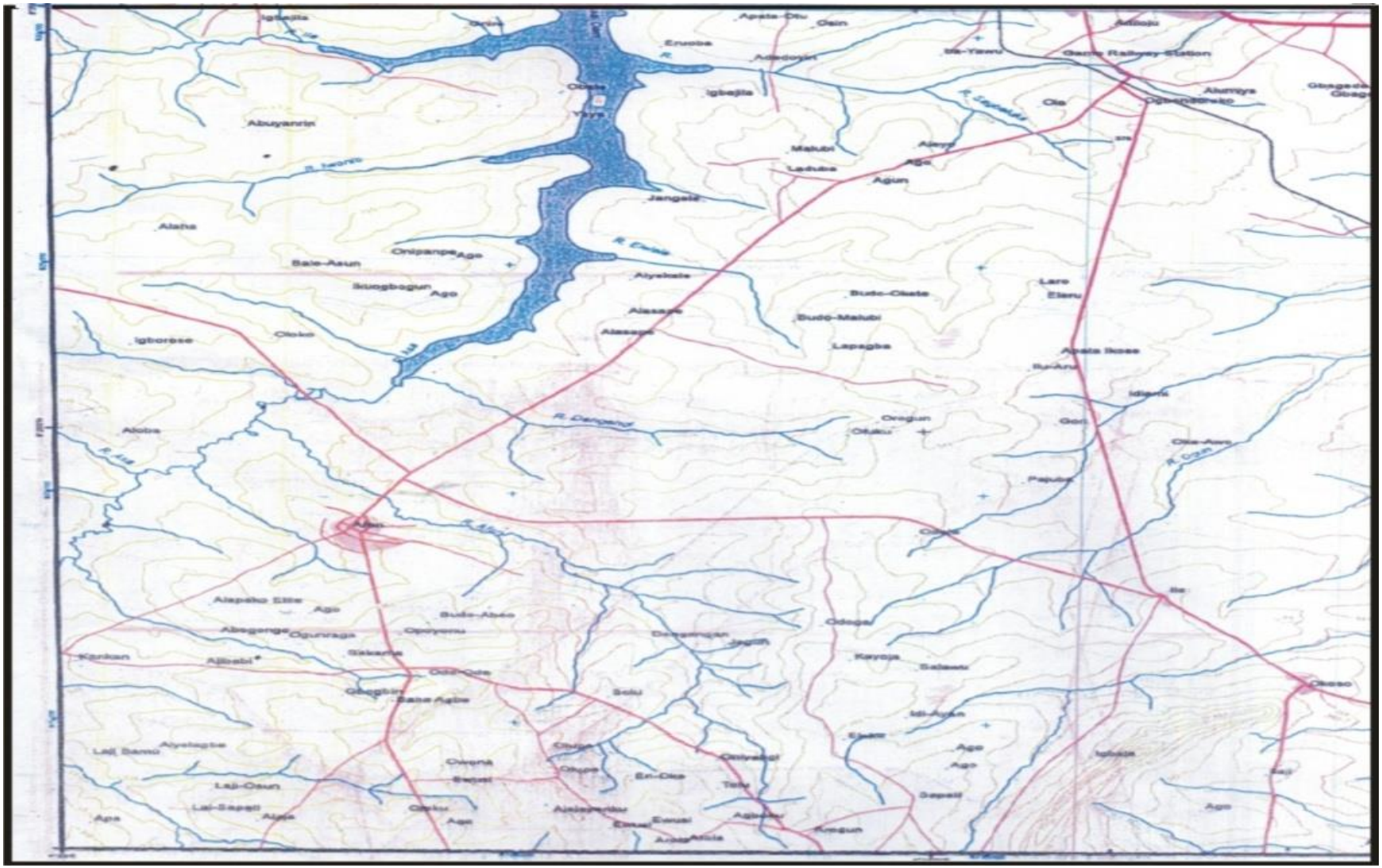


Figure 2: Topographical map of the study area showing its relief

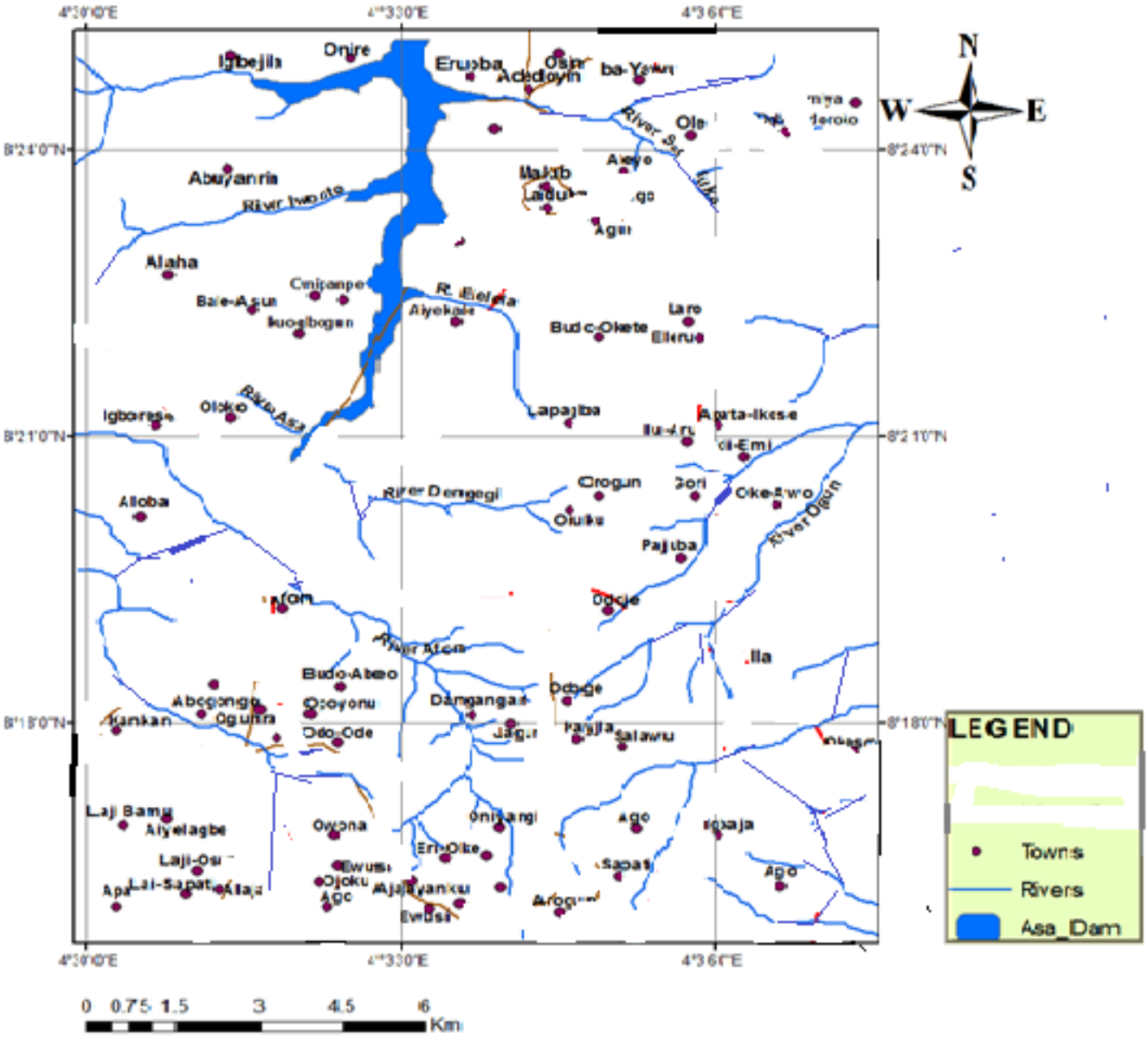


Figure 3: Map of drainage pattern of the study area

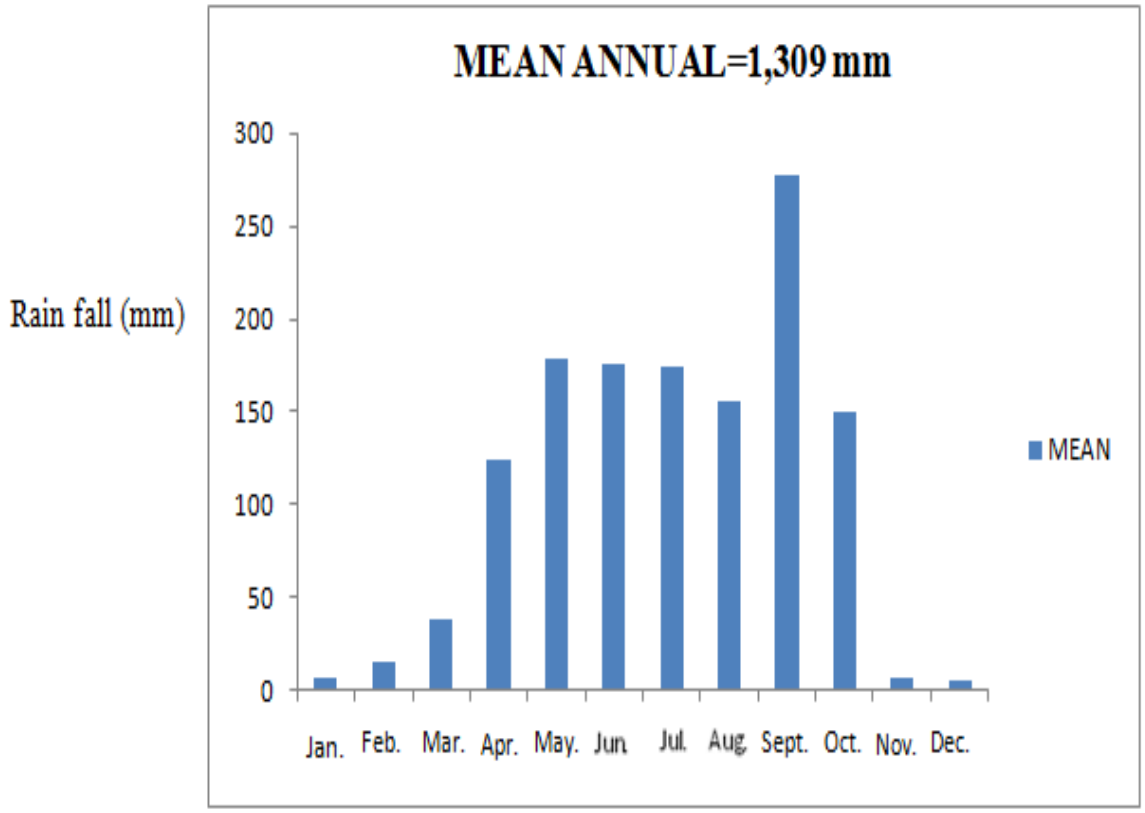


Figure 4: **Mean Monthly Rainfall Data of the Area**

(Source: Lower Niger River Basin Development Authority, Ilorin, 2005-2016)

1.2 Statement of problems

Nigeria has sufficient water resources that could meet the needs of its people, but the government has not been able to meet the ever-increasing water demand of its people. This might be due to the problem of lacking a proper hydrological information database that can be referred to in the event of selection of suitable sites for drilling of boreholes and pollution problems. Further, the lack of adequate geophysical works for exploration and poor analysis and modeling of the VES and magnetic data to determine the groundwater potentiality pose immeasurable problems in the water demand of Nigerians. However, the existing problems in the study area in which this work is set out to solve are the problems of inadequate groundwater potentials and quality due to lack of proper hydrological information database usable in drilling boreholes and controlling pollution.

1.3 Justification for the study

Different researchers such as Olasehinde *et al.* (1998) and Adekeye (2001) have worked on the quantity and quality of groundwater in some selected areas in the North-Eastern and South-Eastern parts of Ilorin Metropolis, Kwara State. However, the present study area which covers parts of Ilorin North-West, Sheet 223 has not received much attention. Hence, there is a need to evaluate groundwater systems within the study area to provide a standard hydrological database for consumption and agrarian purposes.

1.4 Aim and Objectives of the study

This study is aimed at assessing geo-hydrological settings, using geological, direct measurement, geophysical and physico-chemical methods within Sheet 223, Ilorin Northwest Kwara State, Nigeria. The following are the objectives set for achieving the aim:

1. Geological mapping of the area
2. Determination of perennial groundwater level fluctuation Analysing the magnetic anomalies

3. Execution of vertical electrical sounding in the area
4. Use of Dar-Zarouk Approach
5. Physico-chemical analysis of water samples.

1.5 Scope of the study

The Study covers the following areas:

(i) Geological mapping, to produce a geological map of the area, (ii) Direct measurement of depth to water level in wells and boreholes and its head above the mean sea level to produce groundwater contour maps and flow net for both wet and dry seasons, (iii) production of maps of thickness of dry zones for both wet and dry seasons from measured water levels, (iv) calculation of aquifer characteristics such as hydraulic conductivity, permeability and Storativity, (v) modeling and analyzing VES data to produce geo-electric sections in the area, (vi) Calculation of longitudinal conductance to know the protective capacity of aquifers in the area, (vii) Determination of low, medium and high groundwater potential of the area through reflection coefficients and resistivity values, (viii) Magnetic data interpretation to reveal areas with low and high magnetic intensities, and (ix) Physico-chemical analysis of water samples for groundwater quality valuation.

CHAPTER TWO

2.0 LITERATURE REVIEW

2.1 General Geology of Nigeria

The Geology of Nigeria is basically made up of four (4) litho-petrological components, viz: (i) Basement complex (ii) the Younger granite (iii) Tertiary to recent volcanics and (iv) Sedimentary rocks (Figure 5).

2.1.1 The Precambrian Basement Complex rocks

The Basement Complex is one of the four litho-petrological components that make up the geology of Nigeria (Figure 5). The Basement is the component that comprises of hard rocks which cover about 90% of Nigeria (Oyawoye, 1964). The Nigerian Basement Complex, which is a component of the Pan-African Mobile Belt, is located south of the Tuareg Shield, between the West African and Congo Cratons (Black, 1980).

The Mesozoic calc-alkaline ring complexes (Newer Granites) of the Jos Plateau intrude into Nigeria's Basement Complex, which is unconformably overlain by Cretaceous and younger sediments. The Nigerian Basement (Figure 6) is a reactivated zone that originated from plate collision between the passive West African craton margin and the active Pharusian continental margin. It was impacted by the 600 Ma Pan-African orogeny (Burke and Dewey, 1972; Dada, 2006).

At least four major orogenic cycles of deformation, metamorphism, and remobilization—the Liberian (2,700 Ma), Eburnean (2,000 Ma), Kibaran (1,100 Ma), and Pan-African cycles—are thought to have contributed to the development of the Basement rocks (600 Ma).

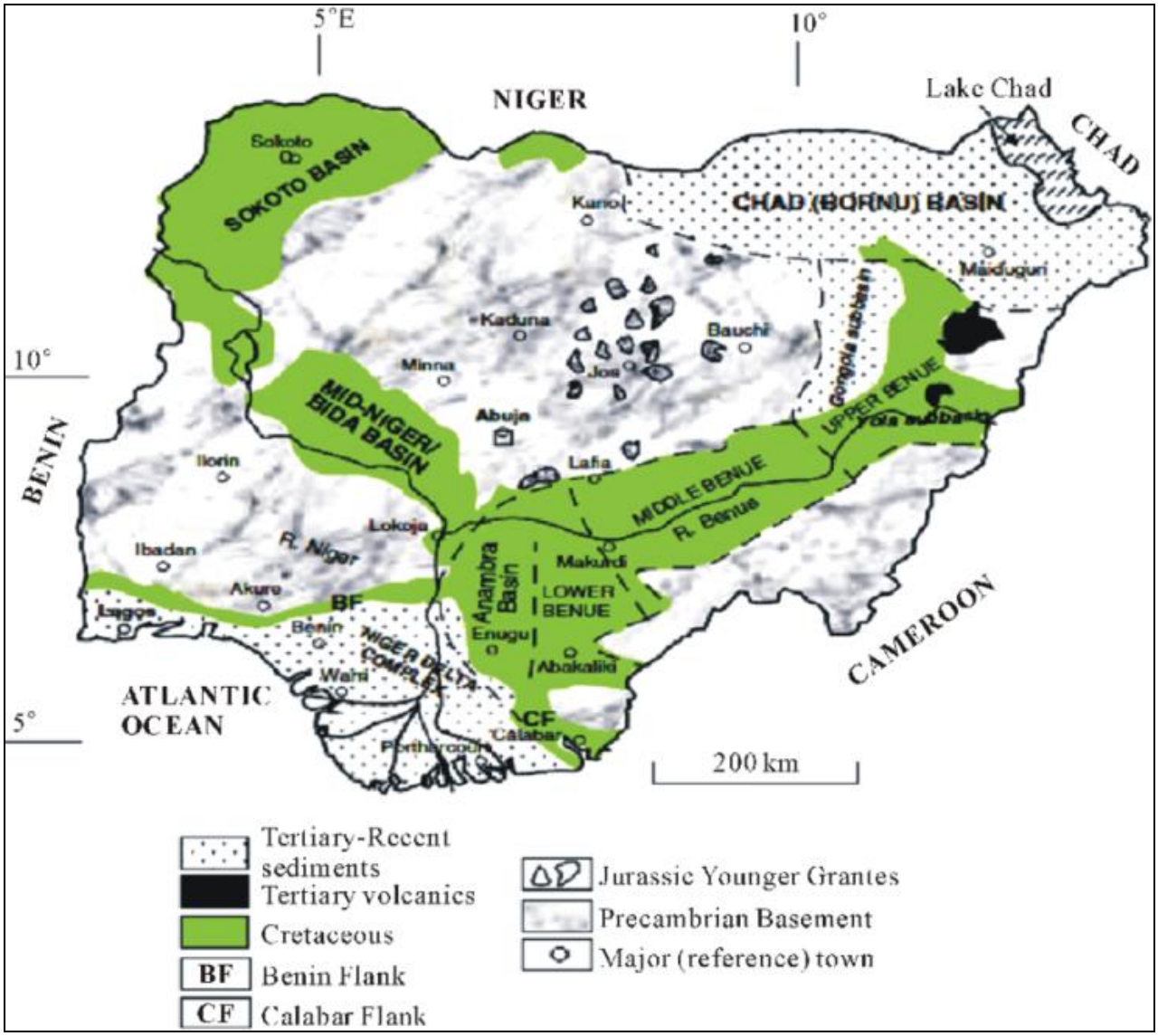


Figure 5: Geological map of Nigeria showing the litho-petrological components (Obaje *et al.*, 2009)

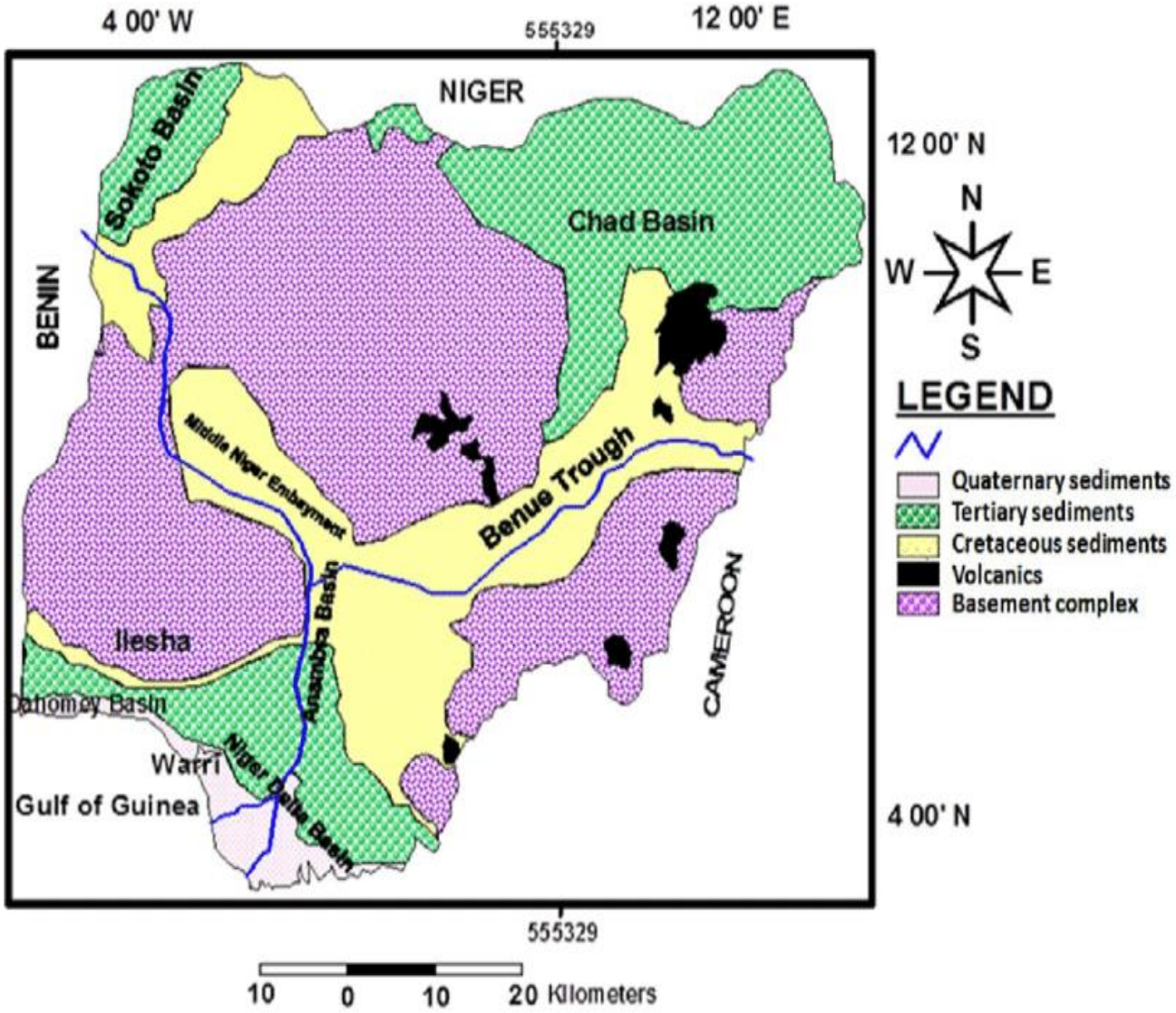


Figure 6: Geological Map of Nigeria showing Basement Complex and Sedimentary terrains (After Obaje, 2009)

The first three cycles were characterized by significant isoclinal folding and deformation, as well as localized metamorphism and substantial migmatization. Regional metamorphism, migmatization, substantial granitization, and gneissification occurred alongside the Pan-African deformation, producing syntectonic granites and homogeneous gneisses (Abaa, 1983).

The early workers on Basement Complex of Nigeria are the colonial geologists in old record of geological survey. Oyawoye (1964) worked on Basement complex of Nigeria in the North-eastern part, while Rahman (1976) worked in the western part of Nigeria.

Oyawoye (1964) based his classification of basement rocks on rock types or lithologies while Rahman (1988), based his own classification on age relationship or field relationship which gives better understanding. The Six major groups of the Basement Complex by Rahman (1988), from the oldest to the youngest, are:

1. Migmatite-Gneiss-Quartzite Complex
2. The Schist Belt is a group of meta-sedimentary and meta-igneous rocks that range from slightly migmatized to non-migmatized.
3. Charnockitic, Gabbroic and Dioritic rocks
4. Members of the Older Granite suite
5. Metamorphosed to non-metamorphosed calc alkaline volcanic and hyper-basic rocks
6. Un-metamorphosed dolerite dykes, basic dykes and syanite dykes

Obaje (2009) identified the Basement Complex's four primary petro-lithological units as follows:

1. The Migmatite – Gneiss Complex (MGC)
2. The Schist Belt (Metasedimentary and Metavolcanic rocks)

3. The Older Granites (Pan African granitoids)
4. Un-deformed Acid and Basic Dykes

2.1.1.1. The Migmatite – Gneiss- Complex (MGQC)

The most common of the component units in the Nigerian basement, the Migmatite-Gneiss Complex is typically regarded as the basement complex sensu stricto (Rahman, 1988; Dada, 2006). Migmatites, orthogneises, paragneisses, and a number of basic and ultrabasic metamorphosed rocks make up its heterogeneous assemblage. About 60% of the surface area of the Nigerian basement is made up of the Migmatitie-Gneiss Complex, also known as the "migmatite-gneiss-quartzite complex" by certain researchers (Rahman and Ocan, 1978). Many areas in northern, western and eastern Nigeria are covered by rocks of the Migmatite – Gneiss Complex. These areas include, but not limited to: Abuja, Keffi, Akwanga, Bauchi, Kaduna, Kanareo, Funtua, Okenne, Egbe, Ajaokuta (in northern Nigeria); Ibadan, Ile-Ife, Akure, Ikerre, (in western Nigeria) and Obudu and the Oban Massif areas in eastern Nigeria. Example of one of the areas is Migmatite-Gneiss rock found in Keffi, Nasarawa State (Figure 7)

Petrographic evidence suggests that many of the constituent minerals of the Migmatite-Gneiss Complex were recrystallized as a result of the Pan-African reworking by partial melting, with the bulk of the rock types exhibiting medium to upper amphibolite facies metamorphism. The migmatite structure is one of twelve (12) different structural kinds found in migmatites.

Geo-chronologically, The Migmatite–Gneiss Complex has ages ranging from Pan-African to Eburnean. Various ages dating in migmatites are:

(i) Early Archean age 3,510 ± 380 million years (Dada, 1989)

(ii) Liberian age (2800 million years) Dada, 1989.

(iii) Eburnean age 200 million years ago by Grant, 1970

(iv) Kibaran 1100 million years ago ± 200 by Ogoezi,1977

(v) Pan- African age 600 ± 150 million years ago or 650 ± 150 (Grant, 1970; Ajibade,1980)

Basement Complex rocks are generally low lying and concordant in contrast to the cross-cutting, discordant, and steeply occurring hilly outcrops in the form of ring dykes and cone sheets in the Younger Granites.

2.1.1.2 The schist belts

The migmatite-gneiss-quartzite complex has infolded these belts, which are thought to be Upper Proterozoic supracrustal rocks. In the western half of Nigeria, where they are most developed, they consist of low grade, meta-sediment-dominated belts flowing north to south (Figure 8). The schist belt does not extend beyond 80 longitudes to the north or south, according to Oyawoye (1964), although there are currently just a few gold discoveries in the region's southeast.

The carbonate rocks (marbles/dolomitic marbles), pelitic schists, phyllites, banded iron formation, and coarse to fine-grained clastics are among the lithological variations of the schist belts (amphibolites). Some of them might contain pieces of ocean floor debris from tiny back-arc basins. While Oyawoye (1972) and McCurry (1976) view the schist belts as remnants of a single supracrustal cover, Rahaman (1976) and Grant (1978) imply that there were many deposition basins. Based on structural and lithological correlations, Grant (1978), Holt (1982), and Turner (1983) hypothesize that the ages of the strata vary. Ajibade *et al.* (1979) refutes this assertion and demonstrate that the deformational histories of the two series were identical.



Figure 7: A migmatitic gneiss rock from Basement complex rocks along NRDC – Emir's palace, Keffi (NW Nigeria)

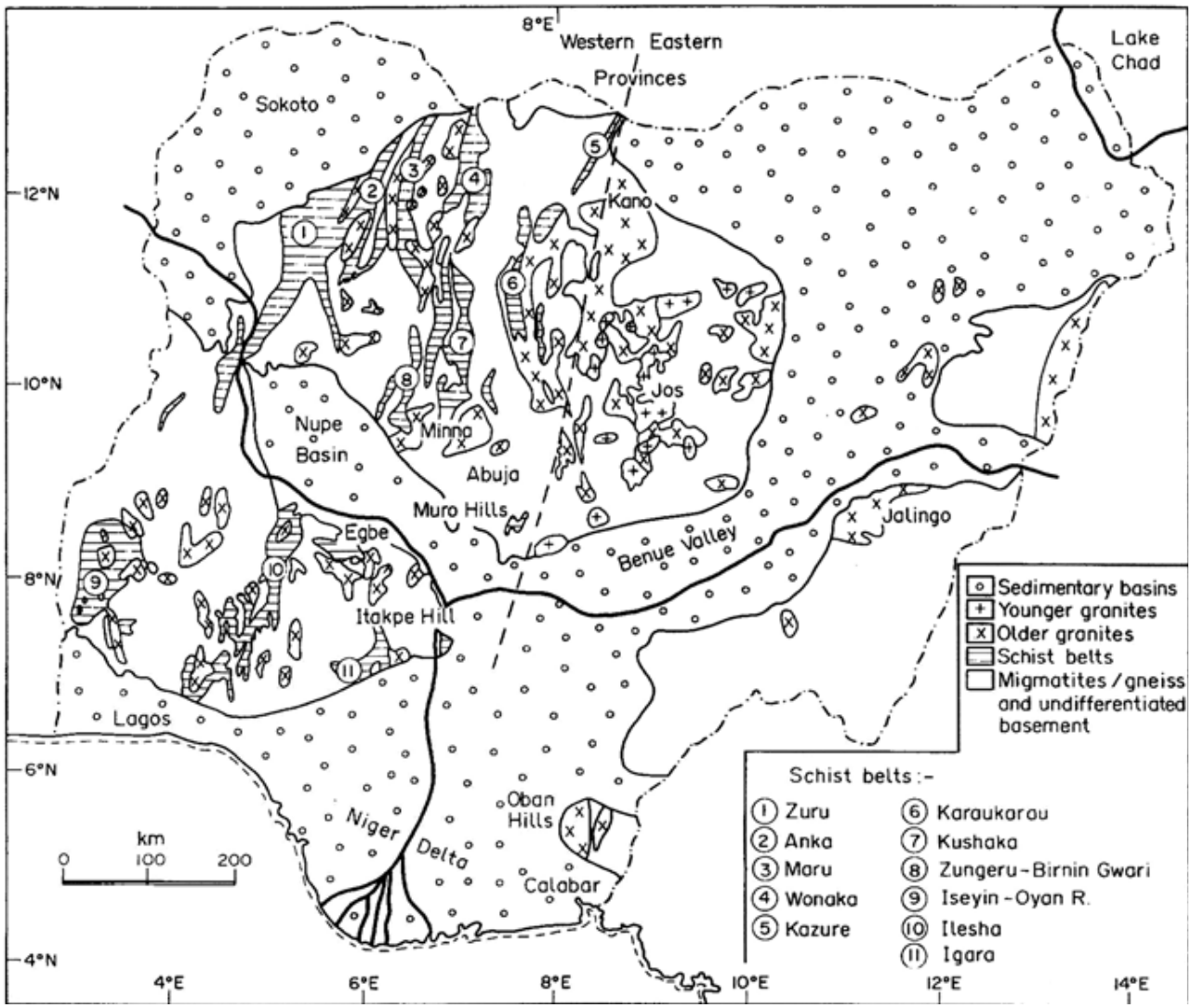


Figure 8: Schist belt localities within the context of the Geology of Nigeria (After Woakes *et al*., 1987)

The talc-schist-actinolite-tremolite schist, which was created from ultramafic rocks, is another lithology found in the schist belt.

The schist belts have been mapped and studied in detail in the following localities: Maru, Anka, Zuru, Kazaure, Kusheriki, Zungeru, Kushaka, Isheyin Oyan, Iwo, and Ilesha where they are known to be generally associated with gold mineralization.

Some of the schist belts and their brief discussion include:

(i) The Kusheriki Schist Group

The region near Kusheriki in northern Nigeria serves as a key to understanding the schist belts there. Truswell and Cope (1963) completed detailed mapping, and Ajibade expanded it south to the Zungeru region (1980). For the Kusheriki Schist Group, four formations were identified, namely:

1. The Kusheriki Psammite Formation at the base of the succession,
2. The Kushaka Schist Formation,
3. The Zungeru Granulite Formation and
4. The Birnin Gwari Schist Formation at the top.

(ii) Zungeru-Birnin Gwari Schist Belt

The Zungeru-Birnin Gwari Schist Belt is a single structural unit made up of the Zungeru Granulite Formation's overlying quartzo-feldspathic rocks and the Birnin Gwari Schist Formation. Simple N-S syncline of 150 km in length, with extra displacement in the north caused by NE-SW transcurrent fault. Both of the schist belt's flanks have outcrops of the Zungeru Granulite Formation. It is mostly composed of amphibolites and some quartzites interbedded with fine-medium grained quartzo-feldspathic rocks.

(iii) The Birnin Gwari Schist

The synclinal axis of the schist belt is occupied by this formation. The bottom portion is made up of better grade biotite-muscovite schists in the east and finely banded phyllites in the west. The Durimi pebbly schist, a metamorphosed mudstone conglomerate with some strata of impure quartzite or metagreywacke, lies on top of them.

(iv) The Kushaka Schist Formation

This results in several curved schist belts that are divided by gneiss domes and anticlines. In terms of lithology, structure, and igneous connections, they diverge from the Zungeru-Birnin Gwari belt. The predominant rock type is semi-pelitic biotite-muscovite schist, with garnet and staurolite in some locations. Phyllites, metasiltstones, and graphitic schists are examples of other rocks. The schists are embedded inside many substantial units of banded garnetgrunerite iron deposit. Numerous amphibolites and amphibole, epidote, chlorite, and talc-bearing schists are related to tholeiitic basalt at least in part (Elueze, 1981). Amphibolites are extremely thick in some places, indicating significant volcanic accumulations. The Zungeru-Birnin Gwari Belt is straight, in contrast to the curved Kushaka Schist Belt. The Kushaka Schist Formation's smaller scale formations, which show its longer and more complicated history, were reported by Grant (1978). The link between the Zungeru-Birnin Gwari and Kushaka Schist Formations and Pan-African granite plutons is another significant distinction between the two. Despite being present in both the Zungeru and Birnin Gwari Formations, granite intrusions only occur at the outermost portions of the Birnin Gwari schist belt. In contrast, granite, granodiorite, and syenite plutons extensively invade the Kushaka schist belts, frequently penetrating the axial zone of the belts.

(v) The Ilesha Schist Belt

East of the Ibadan Archaean to Lower Proterozoic massif is where this is located. It is more than 200 km long from north to south and becomes as wide as 60 km in the south. Here, it

comprises of two structural units with different lithologies that are divided by the Ife fault zone, which has a NNE trend (Hubbard, 1975). The amphibolite, amphibole schists, and pelitic schists of the western unit are closely related to the trondhjemitic granite, gneiss, and pegmatite. It displays a slightly open folding technique using N-S axis. Locally, the greenschist facies undergoes metamorphism, but primarily the amphibolite facies does. Along with quartz schist, quartzo-feldspathic gneiss, and small iron-rich schists and quartzites, quartzite predominates east of the fault. The Effon Psammite Forrnation assemblage exhibits amphibolite facies metamorphism and close isoclinal folds. It appears to overlie amphibole schists of the western type around 30 km NE of Ilesha, however it is unclear if this is a stratigraphic superposition or an over-thrust relationship.

(vi) Igarra Schist Belt

The Okene migmatitic nucleus is surrounded by the south-westernmost schist belts in Nigeria. With barely 50 km in length, it has an NNW tendency and is connected to the NW-trending Owo belt in the west as well as the Itobe belt in the east, which may have reached the Muro Hills in the north. It differs from the other schist belts described because it contains both calcareous rocks and conglomerates. These rock types can be found in bands inside the predominant biotite schists, along with quartzites. The non-migmatitic gneisses near the belt's edges are analogous to the non-migmatitic gneisses described by Furon (1960) from the margins of other schist belts in this eastern region. They may constitute a highly metamorphosed basal section of the sequence.

(vii) The Zuru Schist Belt

With a length of 280 km and a maximum width of 40 km, this is the greatest of the northern schist belts. Except for work in the NE sector, little is known about its geology (McCurry, 1976). The predominant kind of rock is quartzite, which is also occasionally feldspathic and is interspersed with quartz-muscovite schists. Truswell and Cope (1963) regarded the

structural connections between the schist belts and the basement as conformable metamorphic fronts, but it wasn't until Ajibade *et al.* (1979) that a structural break was first delineated. According to Grant (1978), Holt (1982), and Turner (1983), there are various ages of sediments based on structural and lithological relationships. Ajibade *et al.* (1979) disproves this assertion and demonstrate that the deformational histories of the two series were identical.

Although the ages of the intrusive cross-cutting Older Granites indicate a bottom limit of around 750 Ma, the geochronology of the schist belts continues to be controversial. Ogezi accepted a Rb/Sr age of 1,040 25 Ma for the Maru Belt phyllites as a metamorphic age (1977). The distribution of primary gold occurrences in certain belts but their notable absence in others may suggest that they do not represent a single supracrustal sequence, while the apparent absence of Subduction-related mineral deposits may be indicative of a limited role for the en-simatic processes. The schist belts are best developed in the western part of Nigeria, west of 8°E longitude, though smaller occurrences are found to the east but only sporadically. The belts are confined to a 300 km wide, NNE-trending zone. The Burke and Dewey Dahomeyan is made up of gneisses and migmatites in the region to the west of this zone (1972). In Cameroun, a number of schist belts that are thought to be Upper Proterozoic are found in the Pan-African granite-migmatite terrain north of the Congo Craton. Similar to the east, no schist bands are known for a distance of 700 km.

2.1.1.3 Charnockitic- Gabroic-Dioritic Rocks

The word charnockitic came from a man called Job Charnock. Charnockite is an autopyroxene quartz feldspar rock. It is a dark-greenish looking rock which distinguishes from other rocks in the field. In the Nigerian basement, charnockite was initially characterized by Falconer (1911) at Toro and was then referred to as a "quartz diorite

porphyrite," according to Dada (1989). It was believed to share some similarities with the fundamental Ivory Coast charnockitic series members. Wright (1970) defined it as three round, concentric granites surrounding an Undeformed Acid and Basic Dykes annular complex of hypersthene diorite. According to contact relations, he believed the hypersthene diorite to be older than the granites. Cooray (1975) used the occurrence of granitic veins in the diorite, dioritic xenoliths in granites, and microcline porphyroblasts in the diorite as evidence to reach the same conclusion in his review of charnockitic rocks of Nigeria.

A field study of the same hybrid rocks led by Rahaman (1981) to consider both the granites and the charnockites as either contemporaneous or the latter emplaced shortly after the former. The Basement in Toro area consists of gneisses and migmatites into which the Toro Charnockitic Complex intruded (Dada, 1989); Older Granites and charnockites which constitute the complex proper; and undeformed basic (doleritic) dykes considered to be later than the Pan-African Granites. The Toro charnockite was described by Dada (1989) to be typically greenish black, fine to medium-grained, equigranular and massive, sometimes porphyritic. The granites consist from the periphery of the complex (in contact with the migmatitic gneiss) towards the centre (in contact with the hypersthene diorite) of: a fine to medium grained biotite-muscovite granite, an equi-granular biotite hornblende granite and a porphyritic biotite-hornblende granite. In general, these granites as well as the diorites are not affected by a penetrative deformation, but undulatory extinction of the quartz and fractures in feldspar crystals indicate local brittle deformation. They usally contain quartz + plagioclase + alkali feldspar + orthopyroxene + clinopyroxene + hornblende ± biotite ± fayalite. Accessory minerals are usually zircon, apatite, and iron ores (Olarewaju, 2006). Apart from Toro, other localities of charnockite occurrence include Bauchi, Ado-Ekiti, Ikere (Ekiti), Akure, Idanre, and in the Obudu Plateau.

Structurally, Charnockitic rocks range in composition from granitic to granodioritic to dioritic and enderbitic. In general, these granites as well as the diorites are not affected by a penetrative deformation, but undulatory extinction of the quartz and fractures in feldspar crystals indicate local brittle deformation.

All charnockitic rocks produce pan-African ages using geochronology. Older Granites are related to them. On the bauchites in the vicinity of Bauchi, Van Breemen et al. (1977) determined the inaccurate ages of 663 164 Ma and 668 128 Ma. Using the U-Pb technique on zircons, Tubosun (1983) assigned the charnockites of Ikerre and Akure, respectively, exact Pan-African dates of 620 20 Ma and 634 21 Ma. In order to corroborate specific Pan-African ages for the charnockitic complexes of SW Nigeria, they got late Pan-African ages of 580 Ma and 593 Ma for the Idanre Comple.

2.1.1.4 The Older Granites

The term “Older Granite” was introduced by Falconer (1911) to distinguish the deep- seated, often concordant or semi-concordant granites of the Basement Complex from the high-level, highly discordant tin-bearing granites of Northern Nigeria. The Older Granites are believed to be pre-, syn- and post-tectonic rocks which cut both the migmatite-gneiss-quartzite complex and the schist belts. The rocks of this suite range in composition from tonalites and diorites through granodiorites to true granites and syenites. Charnockites form an important rock group emplaced during this period. They are generally high level intrusions and anataxis has played an important role (Rahaman, 1981). The Older Granites suite is notable for its general lack of associated mineralization although the thermal effects may play a role in the remobilization of mineralizing fluids.

The granitoids which outcrop with the schist belts in northwestern and southwestern Nigeria include biotite granites, biotite muscovite granites, syenites, chanockites, serpentinites and

anorthosites. Rahaman (1988) discarded the earlier classification of members of the Older Granites suite on the basis of their texture, mineraological composition and the relative timing of their emplacement. In its place, members of the Older Granite suite were classified as follows, based mainly on the textural characteristics:

1. Migmatitic granite;
2. Granite gneiss;
3. Early pegmatites and fine-grained granite;
4. Homogeneous to coarse porphyritic granite;
5. Slightly deformed pegmatite aplites and vein quarz; and
6. Un-deformed pegmatites, two-mica granites and vein quartz.

Texturally, there are three varieties of Older Granite within the Basement Complex of Nigeria; these are:

(a) The coarse-grained porphritic variety. This variety can also be sparsely porphyritic. The colour varies from very pink to whitish
(b) Medium- coarse grained non porphyritic Older granite
(c) The fine to medium grained Older Granite. E.g alphite, micro-granite. Aplite is sugary in texture.

Structurally**,** many of Older Granite bodies show features which indicate that the rocks have undergone deformation. The features include: crude foliation on observed outcrops, strain effects shown by quartz and augen structure when feldspar shows or drawn into eye like feature

Geochronologically, The Older Granites are recognized as of Pan-African age. The ages vary from 500-600 million years ago.

2.1.1.5 Un-deformed Acid and Basic Dykes

The post-tectonic Pan African acid and basic dykes are not yet present. They cut across the Schist Belts, the Older Granites, and the Migmatite-Gneiss Complex. The acid and basic dykes that haven't distorted include:

a. Felsic dykes on the ground that are connected to Pan African granitoids, such as pegmatites, microgranites, aplites, and syenite dykes that include muscovite, tourmaline, and beryl (Dada, 2006)

b. Basic dykes, which include dolerite and the less frequent basaltic, felsite, and lamprophyric dykes, are typically recognized as the youngest units in the Nigerian basement.

The older granites, the schist belts, and the migmatite-gneiss complex are structurally cut by the undamaged acid and basic dykes. In addition to the invaluable guidance, they offer in sampling for isotope geochemistry, analysis, and interpretation, when they cross-cut basement, they could be used to determine the age of metamorphic structures and rock suites. They could also suggest the existence of older basement windows in the Nigerian schist belts (Dada,2006).

According to geochronology, the felsic dykes are thought to be between 580 and 535 million years old (Matheis and Caen-Vachette, 1983; Dada, 2006), whilst the fundamental dykes are thought to be around 500 million years old (Grant, 1970).

2.1.2 The Sedimentary rocks

These are rocks that have developed at or very close to the surface of the earth as a result of the buildup and lithification of sediment (detrital rock) or as a result of precipitation from solution at typical surface temperatures (chemical rock). 73 percent of the planet's current land area is covered by sedimentary rocks, according to Wilkinson et al. (2008), although

just 8 percent of the crust is thought to be made up of these rocks (Buchner, K., and Grapes, R.) (2011). These sedimentary basins in Nigeria contain these rocks:

2.1.2.1 The Iullemmeden Basin

Locals refer to the Iullemmeden Basin in northwest Nigeria as the "Sokoto Basin." Mostly a gently sloping plain with an average elevation of 250 to 400 meters above sea level makes up this region. Low mesas sporadically break up this plain. The most noticeable feature in the basin is a low escarpment known as the "Dange Scarp," which is directly tied to the geology (Obaje, 2009).

The Iullemmeden Basin's sediments accumulated throughout the course of four major episodes of deposition. The Pre-Maastrichtian "Continental Intercalaire" of West Africa is made up of the grit- and clay-rich Illo and Gundumi Formations, which unconformably overlie the Pre-Cambrian Basement. They are separated by the fossiliferous, shelly Dukamaje Formation and are overlain irregularly by the Maastrichtian Rima Group, which is made up of mudstones and friable sandstones (Taloka and Wurno Formations). The Paleocene Sokoto Group is made up of the (mostly shale-containing) Dange and Gamba Formations and the calcareous Kalambaina Formation. The Post-Paleocene Continental Terminal is made up of the continental Gwandu Formation beneath it. These strata gently dip northwestward and gradually thicken, reaching a maximum thickness of about 1,200 m close to the border with the Niger Republic. (Obaje, 2009)

2.1.2.2 The Chad Basin

The dynamic process of plate divergence is connected to the origin of the Chad Basin, one of the African Phanerozoic sedimentary basins. The Paleozoic fold belts of Moroco and Mauritania, which were distorted as a result of the collision between Africa and North America during the Hercynian convergent motion, and the Tindouf and Ougarta basins,

which are Paleozoic successor basins, are notable exceptions (Burke, 1976; Petters, 1982). It is an intracratonic inland basin with a total area of roughly 2,335,000 km2, more than half of which is shared by the Republics of Niger and Chad. The basin is a member of a group of Cretaceous and post-Cretaceous rift basins in Central and West Africa that were formed in response to the opening of the South Atlantic (Obaje et al., 2004). The Anambra Basin, the Benue Trough, the Mid-Niger (or Bida) Basin, and the Sokoto Basin are other inland basins in Nigeria that belong to the same series. About one-tenth of the entire Chad Basin is made up of the Nigerian portion, sometimes referred to as the Bornu Basin locally. The Chad Basin's southeast corner is made up of it.

2.1.2.3 The Dahomey Basin

The Dahomey Basin, which extends from southeast Ghana through Togo and the Republic of Benin to southwest Nigeria, combines inland, coastal, and offshore basins. It is separated from the Niger Delta by the Okitipupa Ridge, a subsurface basement high. It's unclear how far offshore it extends. An east-west trend governs the deposition of sediment. The geology of the Republic of Benin is largely understood (Billman, 1976; De Klasz, 1977). Onshore, the Cretaceous strata are roughly 200 meters thick (Okosun, 1990).

Okosun (1990) conducted a thorough assessment of the Dahomey Basin's stratigraphy. The Dahomey Embayment's Cretaceous strata has received relatively little attention in the literature. This is partly because deep drill cores are not easily accessible and oil company reports are proprietary. The Cretaceous sands, grits, clays, and shale in the Nigerian area are represented by the Abeokuta Formation, which Jones and Hockey identified in 1964. The Ajali Sandstone and the Nsukka Formation are found close to the basin boundary in Ijebu-Ode and Okitipupa, according to Reyment (1965). He also mentioned the presence of Nkporo Shale in the basin's subsoil. Two unofficial lithostratigraphic units—the unnamed Older

Folded Sediments and the unnamed Albian Sands—were proposed by Billman (1976) based on a study of some offshore sequences in the Republic of Benin. The Abeokuta Formation and the Awgu and Nkporo Shales make up the remainder of the Cretaceous series.

2.1.2.4 The Niger Delta Basin

At the point where the South Atlantic Ocean, Benue Trough, and Cenozoic Niger Delta converge, a triple junction formed during the split of South America from Africa in the late Jurassic (Whiteman, 1982). This split in the early Cretaceous was followed by the subsidence of the African continental edge and cooling of the newly formed oceanic lithosphere.

The Benin Formation, a continental shallow massive sand sequence, the Agbada Formation, a coastal marine sequence of alternating sands and shales, and the Akata Formation, a basal marine shale unit, make up the geologic sequence of the Niger Delta. Clays, shales, and some trace amounts of intercalated sand make up the Akata Formation. The habitats where the sediments were deposited were pro-delta. Here, the sand content is often less than 30%. Sand and shale sediments from the lower delta plain (mangrove swamps, floodplain, marsh), as well as sediments from the coastal barrier and fluviomarine worlds, make up the Agbada Formation. The Agbada Formation contains between 30 and 70 percent sand, as a result of the several depositional off lap cycles. A complete cycle often consists of thin fossiliferous transgressive sea sand, followed by an offlap sequence that starts with marine shale and continues with laminated fluviomarine sediments before being terminated by another transgression and/or barrier (Weber, 1972; Ejedawe, 1989). The Benin Formation, which makes up the top layer of the Niger Delta depositional series, is distinguished by a high sand content (70–100%). The fluvial domains (braided and meandering channels) of the upper

delta plain comprised the continental environment where the enormous sands were deposited.

2.1.2.5 The Benue Trough Basin

The middle West African rift basin known as the Benue Trough of Nigeria spans approximately 800 km in length and 150 km in width. The Chad Basin's southern boundary serves as the southern limit, and the northern limit is the Niger Delta's northern barrier. Up to 6,000 meters of Cretaceous-Tertiary sediments can be found in the trough, and those that predate the mid-Santonian have been compressionally folded, faulted, and uplifted in various locations. Over 100 anticlines and synclines were produced by the mid-Santonian tectonic episode's severe compressional folding, which affected the entire Benue Trough (Benkhelil, 1989). The Abakaliki anticlinorium and the Afikpo syncline in the Lower Benue, the Giza anticline and the Obi syncline in the Middle Benue, and the Lamurde anticline and the Dadiya syncline in the Upper Benue Trough are among the major such deformational features. The Anambra Basin subsided as a result of the westward displacement of the depositional axis in the Benue Trough caused by mid-Santonian tectonism and magmatism. As a result, the Anambra Basin is a portion of the Lower Benue Trough and contains sediments that were formed after deformation and range in age from Campanian-Maastrichtian to Eocene. Given that the Anambra Basin is a comparable structure that emerged during the compressional stage, it makes sense to include it in the Benue Trough (Akande and Erdtmann, 1998). A lower, middle, and upper sections are arbitrarily distinguished within the Benue Trough.

2.1.2.6 The Bida Basin

The Bida Basin is an intracratonic structure with a NW-SE trend that stretches from Kontagora in Niger State in the north to a region just south of Lokoja in the south. It is

separated from the Anambra and Sokoto Basins to the SE and NW, respectively, by the Basement Complex in the NE and SW. Post-orogenic molasse and thin unfolded sea layers make up its sedimentary fill (Ladipo, 1988). The basin is a gently down-warped trough, and the Benue valley and SE Nigeria's Santonian orogenic movements are where it first formed. The basin is thought to be the northwest extension of the Anambra Basin, which was a significant depocentre during the third major transgression cycle in the Late Cretaceous. The basin trends perpendicular to the main axis of the Benue Trough and the Niger Delta Basin. According to interpretations of drill logs and Landsat pictures, as well as geophysical data, the basin is bordered by a network of linear faults flowing NW-SE (Udensi and Osazuwa, 2004). According to gravity studies, there are a number of central positive anomalies flanked by negative anomalies, which are typical of rift structures and similar to the nearby Benue Trough (Ojo, 1984; Ojo and Ajakaiye, 1989).

2.1.2.7 The Anambra Basin

The mid-santonian tectonism and magmatism to the western half of the Anambra Basin resulted in its development, which implies the post-deformational sediments of Campano-Maastrichtian to Eocene ages. The Campano-Maastrichtian marine and paralic shales of the Enugu and Nkporo formations, overlain by the coal measures of the mamu formation, were the first sediments to form. In most locations, the fluviodeltaic sandstones of the Ajali and owelli formations are the lateral equivalents of the mamu formation.

2.2 Geology of Kwara State

Tijani (1994) stated that Moro area of Kwara State lies within the Basement Complex of South Western Nigeria, which is of Precambrian to Lower Palaeozoic in age (Jones and Hockey, 1964; Odeyemi, 1976; Rahaman, 1976). Tijani further said that the oldest rock in the area comprises of the Gneissic Complex whose principal member is biotite-hornblende gneiss

and amphibolite, which underly about half of the area. According to Tijani, other rock types observed in the area are the Older Granites, mainly porphyritic granite and granite-gneiss. Tijani revealed that the superficial deposit which varies in thickness from 4 to 8 m is made up of mostly dark sandy and clayey-loamy top soils, usually less than two metres thick, followed by laterites and red soils in most cases. The author said these soils form the bulk of the superficial deposits and obscure most of the underlying geology.

Raji and Alagbe (1997) observed that the geology of Asa drainage basin in Kwara State, south western Nigeria is concordant with the general geology of the Nigerian Basement Complex as discussed by Grant (1969). The authors pointed out that rocks of the remobilized Older Granites predominate the area with few occurrences of undifferentiated schists and quartzites, which are dominated by silicate minerals such as quartz, biotite, muscovite, orthoclase feldspar, and oligoclase and trace occurrence of zircon, hornblende and apatite.

Adekeye (2001) examined and reported that over eighty percent of Kwara State (study area inclusive) is underlain by crystalline rocks of the Precambrian Basement Complex of Nigeria, while the remaining part is underlain by cretaceous and younger sediments (Jones and Hockey, 1964; Rahaman, 1976). Adekeye further said that the rocks of the Basement Complex terrain include granites, granite-gneiss, biotite-gneiss, and migmatite while the younger sediments in the remaining part of Kwara State are composed mainly of alternating beds of sandstones, shales and clays. According to the author, the superficial deposit in the Basement Complex terrain varies in thickness from 4 metres to 8 metres and is made up mainly of dark sandy and clayey-loamy top soils, usually less than two metres thick followed by laterites, in most cases. The author pointed out conclusively that these superficial deposits usually obscure the subsurface geology.

2.3 Hydrogeology of Kwara State

Ayodele *et al.*(1989) assessed the groundwater prospects in the Crystalline weathered regolith in southwestern Nigeria using geophysical, hydrochemical and hydrogeological techniques to evaluate the depth of weathering, the recharge potential and the flow characteristics. By their finding, the resistivity measurement gave an average depth of weathering of 34m. Ilesha was selected for their case study because of its central location within the Basement Complex of southwestern Nigeria and the fact that the rocks found there are fairly typical of the region.

Olasehinde *et al.* (1998) carried out a preliminary test on hydrogeological investigation in Ilorin Area, South-Western Nigeria. The authors found out that most of the hand-dug wells in the area with depth ranging between 7 and 11 metres penetrate only into the overburden aquifers. They concluded that such aquifers have been polluted by the migration of pollutants into the shallow aquifers.

For the purpose of sustainable ground water development and management in Ilorin city, Ashaolu, *et al.* (2015) evaluated the static water level and overburden pattern. The depth of the boreholes, the depth to the water, and the vertical electrical sounding VES) data with electrode spacing of (AB/2) varied from 10m to 200m were all recorded by the authors. They demonstrated that each VES curve's overburden thickness was determined manually.

Some influencing factors known as aquifer characteristics determine the ability of an aquifer to transmit water in economic quantities in to or away from that aquifer. These characteristics include hydraulic conductivity, transmissivity and storativity.

The hydraulic conductivity of an aquifer is the ability of an aquifer to transmit water. It is sometimes referred to as coefficient of permeability and is denoted by K. Hydraulic conductivity determines the rate of water flow in an aquifer. An aquifer is said to be highly

permeable and easily release water if it has a large hydraulic conductivity. The greater the permeability of an aquifer is, the lesser its resistance to flow.

The Transmissivity is the rate of flow through a cross-section of a certain width over the entire saturated thickness of an aquifer under a given hydraulic gradient (Bear, 1979; kruseman and de Ridder, 1990). According to Hantush, 1964; Bouwer, 1978; Freeze and Cherry, 1979, Transmissivity is the product of the thickness of the aquifer and the average value of the hydraulic conductivity. Fetter, 1980; Todd,1980 defined the Transmissivity as the ratio at which water of prevailing density and viscosity is transmitted through a unit width of an aquifer or confining bed under a unit hydraulic gradient. It is a function of the properties of the liquid, the porous media and the thickness of the porous media.

Storage coefficient or Storativity is the volume of water given up per unit area of an aquifer and per unit drop of the water table or potentiometric surface. It is a dimensionless ratio and always less than unity. In unconfined aquifers, it is equal to the specific yield but in confined aquifers it depends on elastic compression of the aquifer and is usually less than 10^{-3}.

2.4 Geophysical studies

2.4.1 Principle of Magnetic Method

Milsom (2011) stated that the principle underlying the operation of the Magnetic Method is based on the fact that when a magnetic material such as iron is placed within the Earth's magnetic field, an induced magnetic field is developed. The induced magnetic field is superimposed on the Earth's field at that location creating a magnetic anomaly (i.e. it is being created by a series of magnetic dipoles located within the magnetic material and oriented parallel to the direction of the inducing field, H).

The magnetic field whose amplitude is measured is the vector sum of the Earth's Main field and Induced field caused by magnetic induction in magnetically susceptible earth materials polarized by the main field. A field caused by remnant magnetism of earth materials and other less significant fields is caused by solar, atmospheric and cultural influences (Telford *et al.,* 1990).

Ninety percent of the Earth's magnetic field looks like a magnetic field that would be generated from a dipolar magnetic source located at the center of the Earth and aligned at 11.5^0, with the Earth's rotational axis. The remaining 10 % of the magnetic field cannot be explained in terms of simple dipolar sources (Telford *et al.,* 1990)

2.4.2 The Earth' Magnetic Field

From the point of view of geomagnetism, the earth may be considered as made up of three parts: core, mantle and crust. Convection processes in the liquid part of the iron core give rise to a dipolar geomagnetic field. The mantle plays little part in the earth's magnetism, while interaction of the (past and present) geomagnetic field with the rocks of the Earth's crust produces the magnetic anomalies (Telford *et al.,* 1990).

The magnetic field of the earth is a vector, that is, it has both magnitude and direction. According to Blakely 1995, ninety percent of the earth's magnetic field looks like a magnetic field that would be generated from a dipolar magnetic source located at the center of the earth and aligned with the earth's rotational axis. The strength of the magnitude is about 70,000 nT.

Doell and Cox (1967) stated that the geomagnetic field (electromagnetic interaction) of the earth consists of three (3) parts.

1. **Main field:** this is said to have an internal origin from the core of the earth and is in range of 30,000-70,000 nT with relatively long wavelength. It is the largest

component of the magnetic field and is believed to be caused by electrical currents in the earth's fluid outer core. It acts as the inducing magnetic field for exploration work.

2. **External magnetic field:** This is also known as smaller field with the range of 0-2000 nT that is generated from magnetic sources external to the earth. It is mainly caused by solar activities (i.e. interactions of the earth's ionosphere with the solar wind).
3. **Crustal field:** This is the portion of the magnetic field associated with the magnetism of crustal rocks. It is caused by local changes in magnetization of near- surface rocks. It contains magnetism caused by induction from the earth's main magnetic field and from remanent magnetization.

2.4.3 The Geomagnetic Field

This is the magnetic field that extends from the earth's interior out into space, where it meets the solar wind, a stream of charged particles emanating from the sun.

Gauss Larmor, 1919 stated that the magnitude of geomagnetic field at the Earth's surface ranges from 25 to 65 micro-teslas or 0.25 to 0.65 .The cause of the geomagnetic field is attributed to a dynamo action produced by the circulation of charged particles in coupled convective cells within the outer fluid part of the Earth's core. The exchange of dominance between such cells is believed to produce the periodic changes in polarity of the geomagnetic field revealed by palaeomagnetic studies. From spherical harmonics analysis of the observed magnetic field, over 99% of the geomagnetic field is due to the sources inside the earth (Telford *et al.,* 1990).

The main geomagnetic field at any point on the earth's surface is defined as a vector quantity requires three scalar values (Figure 9), normally expressed either as three orthogonal components (vertical, horizontal-north and horizontal-east components) or the scalar magnitude of the total field vector and its orientation in dip and azimuth. With the exception

of a few specialized surveys, aeromagnetic surveys have always measured only the scalar magnitude, making the latter system more convenient for present purposes (Blakely, 1995).

The angle the total field vector makes above or below the horizontal plane is known as the magnetic inclination, I, which is conventionally positive north of the magnetic equator and negative to the south of it ($-90° \leq I \leq +90°$). The angle between the vertical plane containing F and true (geographic) north is known as the magnetic declination, D, which is reckoned positive to the east and negative to the west. The value of D is commonly displayed on topographic maps to alert the user to the difference between magnetic north, as registered by a compass, and true north (Reeves *et al.*, 1997).

The Equation relating the three (3) vectors and two (2) angles include

$$H = FCos\,(I) \quad (1)$$

$$Z = FSin(I) = H\tan\,(I) \quad (2)$$

$$X = HCos\,(D) \quad (3)$$

$$Y = HSin\,(D) \quad (4)$$

$$X^2 + Y^2 = H^2 \quad (5)$$

$$X^2 + Y^2 + Z^2 = F^2 = H^2 + \Delta Z \quad (6)$$

2.4.4 The International Geomagnetic Reference Field (IGRF)

The International Geomagnetic Reference Field (IGRF) defines the theoretical undisturbed magnetic field at any point on the Earth's surface. Magnetic anomalies caused by rocks are localized effects superimposed on the normal magnetic field of the Earth (geomagnetic field). Nabighian (1972) said that, in magnetic surveying, the IGRF is used to remove from the magnetic data those magnetic variations attributable to this theoretical field

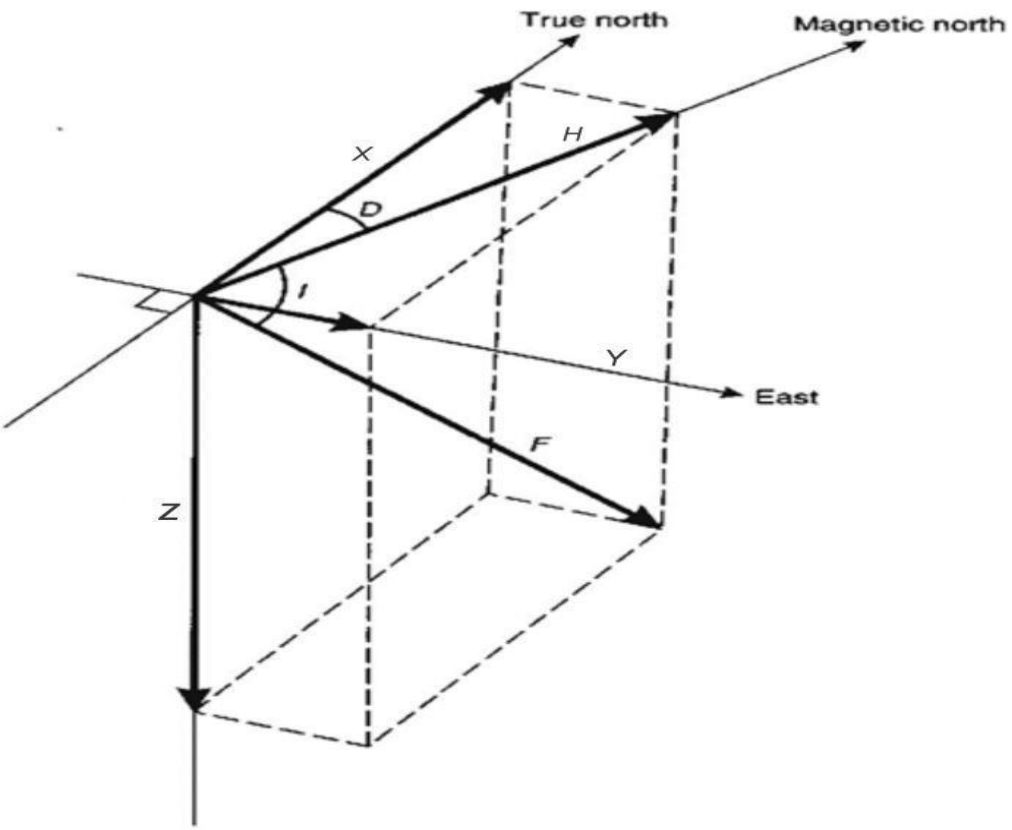


Figure 9: Elements of Earth‘s Magnetic Field; Z: Vertical component H: Horizontal component.

The magnitude of magnetic force will fall between 20, 000 and 70, 000 nT everywhere on earth and it can be expected to have local variations of several hundred nT (sometimes, but less often, than several thousand (nT) imposed upon it by the effects of the magnetization of the crustal geology.

Reeves *et al.*,1997 observed that from the point of view of exploration geophysics, undoubtedly the greatest advantage of the IGRF is the uniformity it offers in magnetic survey practice since the IGRF is freely available and universally accepted

2.4.5 Magnetic Susceptibility

It is a unitless constant that is determined by the physical properties of the magnetic material. It relates the intensity of magnetization, *I* to the strength of the inducing magnetic field *H* through the expression:

$$I = kH \qquad 7$$

Where *k* is magnetic susceptibility, 'k' may either be positive or negative. When it is positive, then it implies that the induced magnetic field is in the same direction as the inducing field *H*, while negative value implies that the induced magnetic field is in opposite direction to the inducing field. In magnetic prospecting, susceptibility is the fundamental material property whose spatial distributions are attempting to determine (Telford *et al.,* 1990).

2.4.6 Magnetic induction

The magnetic poles induced in a material by an external field *H* will produce a field of their own, *H*. It is related to the intensity of magnetization *I* by the formula:

$$\mathrm{H}' = 4\pi I' \qquad 8$$

The magnetic induction A' is defined as the total field within the body. It is given as:

$$A' = H + H' \quad 9$$

By substituting (2.18) into (2.19), we have

$$A' = H + 4\pi I' = H + 4\pi kH \quad 10$$

$A' = H(1 + 4\pi k)$, $where(1 + 4\pi k)\, is\mu$, so that;

$$A' = \mu H \quad 11$$

We can define magnetic permeability in section. 2.2.1 as the ratio of magnetic induction *A* to magnetic field strength *H*

$$\mu = {}^{A'}/_{H} \quad 12$$

In summary, magnetic induction is a measure of the force exerted on a moving charge by a magnetic field, whereas magnetic intensity is a measure of the force exerted on a magnetic pole by a magnetic field, whether the pole is moving or not (Doell and Cox, 1967).

2.4.7 Classification of magnetic materials

Magnetic materials are classified into three types based on their magnetic properties. They are:

1. **Diamagnetic material**: This type of magnetization was discovered in 1846 by Michael Faraday. It is the fundamental property of all materials and is caused by alignment of magnetic moments observed with orbital electrons in the presence of an external magnetic field.

   There is no net moment in diamagnetic material since all the electron shells are full and in the presence of an external field, the net moment opposes the external field, thus the susceptibilities of diamagnetic materials are usually negative and relatively

small. There is no interaction of atomic currents (dipoles) in diamagnetic materials. Examples of diamagnetic materials include graphite, gypsum, marble, quartz, salt and some other alkali halides.

2. **Paramagnetic materials**: Here materials contain unpaired electrons in incomplete electron shells and the magnetic moment of each atom is uncoupled from others so they all behave independently. In order words, the magnetic material has odd numbers of electrons orbiting in their outer shells. Paramagnetic materials can only be observed at relatively low temperatures. Above this temperature, paramagnetism will no longer be observed. Such temperature is referred to as Curie temperature. It is important to state that paramagnetism results in weakly magnetic materials and hence small and positive susceptibilities. Hence materials that are not diamagnetic can said to be paramagnetic.

3. **Ferromagnetism**

Unpaired electrons are magnetically connected in metals like cobalt, nickel, and iron because of strong interactions between nearby atoms and orbital overlap. Magnetic domains, which are around 1 micron in size, are collections of atoms that magnetically pair together. In the absence of an external field, magnetic domains can be directed to create a spontaneous magnetic field. Although magnetic susceptibility is high, it is temperature and applied field strength dependent. All domains are oriented in same direction. It has the following characteristics:

1. They are caused by overlapping electron orbits
2. They give rise to spontaneous magnetization even in absence of an external field.

Examples of ferromagnetic materials are cobalt, iron and nickel.

2.4.8 Magnetism of Rocks and Minerals

Many rocks that contain iron-bearing minerals act as tiny magnets. As magma or lava cool, these minerals begin to form. Magnetic anomalies are caused by magnetic minerals (mainly magnetite and pyrrhotite) contained in the rocks. Substances can be divided on the basis of their behaviour when placed in an external field (Telford *et al.*, 1990).

Magnetic susceptibility is an extremely important property of rocks. The susceptibility of a rock usually depends on its magnetite content (Milsom, 2011). Rocks that have a significant concentration of fero-and/or ferri magnetic materials (for example magnetite, illmenite, pyrrhotite and hematite) tend to have the highest susceptibilities. Consequently, basic and ultrabasic igneous rocks have the highest susceptibilities, acid igneous and metamorphic rocks have intermediate to low values, and sedimentary rocks have very small susceptibility in general (Milsom, 2011).

2.4.9 Aeromagnetic Survey

Airborne geophysics, particularly aeromagnetic and gamma-ray spectrometer (radiometric) surveys form a critical component of geological mapping and mineral resource inventory programs in many African countries (Reford *et al*., 2009). In the 60’s and 70’s, regional aeromagnetic surveys were fairly widespread over much of the continent, in both sedimentary and hard rock terrains (Barritt, 1993).

An aeromagnetic survey is a common type of geophysical survey carried out using a magnetometer aboard or towed behind an aircraft. The principle is similar to a magnetic survey carried out with a hand-held magnetometer, but allows much larger areas of the Earth's surface to be covered quickly for regional reconnaissance. The aircraft typically flies in a grid-like pattern with height and line spacing determining the resolution of the data (and cost of the survey per unit area).

As the aircraft flies, the magnetometer records tiny variations in the intensity of the ambient magnetic field due to the temporal effects of the constantly varying solar wind and spatial variations in the Earth's magnetic field, the latter being due both to the regional magnetic field, and the local effect of magnetic minerals in the Earth's crust. By subtracting the solar and regional effects, the resulting aeromagnetic map shows the spatial distribution and relative abundance of magnetic minerals (most commonly the iron oxide mineral magnetite) in the upper levels of the crust. Because different rock types differ in their content of magnetic minerals, the magnetic map allows a visualization of the geological features of the upper crust in the subsurface, particularly the spatial geometry of bodies of rock and the presence of structures (faults and folds). This is particularly useful where bedrock is obscured by surface sand, soil or water. Aeromagnetic surveys are widely used to aid in the production of geological maps and are also commonly used during mineral exploration.

2.5 Principle of Electrical Resistivity

Dobrin (1960), and Parasnis (1966), 1972 and 1986 pointed out that in this method, current is introduced artificially into the earth through a pair of electrode pinned to the ground(current electrode) and the resulting potential difference due to the current is measured through another pair of electrode (potential electrode) that is also pinned to the ground. Any subsurface variation in resistivity alters the current flow, which in turn affects the distribution of electric potential at the surface.

Emenike (2000) concluded that in the sedimentary environment, high resistivity may broadly be associated with the presence of fresh groundwater in porous medium aquifer while low resistivity maybe due to the presence of clay and/or brackish water. In hard rock environment, which is considered very resistant to the flow of electric current, a low resistivity anomaly will be the target for groundwater. In a clayey or salty environment that is

normally considered conductive, a comparatively high resistivity anomaly will most probably correspond to fresh water and thus will be the target in the case and thus will be the target in the case of groundwater exploration. In resistivity measurements, highest resistivity is associated with igneous rocks. Sedimentary rocks tend to be most conductive due to their high fluid content. Metamorphic rocks have intermediate resistivity.

Benard (2003) stated that resistivity of rocks generally depend on the water content, clay content and the content of metallic minerals.

Generally, materials that lack pore spaces will show high resistivity. Materials whose pore spaces lack water will show high resistivity such as dry sand or gravel. Materials whose water content is clean will show high resistivity such as clean gravel or sand even if water is saturated.

Weathered rocks and clay will show medium to low resistivity. Frozen ground will show much higher resistivity than unfrozen ground.

2.5.1 Review of Previous Geophysical Works

Perfect similar works of this kind are lacking in the target study area; except for some, in the suburb neighboring areas; Nigeria in particular and any other area in the world in general. The previous workers used one or combination of two geophysical methods different from the methods adopted by the present study. Some of these previous workers and their works are mentioned below:

Umego (1990) revealed major structures in the Precambrian basement beneath the sediments, and delineated areas for more detailed investigations using both gravity and magnetic data. He described a system of large scale NE-SW and NW-SE trending magnetic lineation revealed in the Basin as part of the continent-wide conjugate strike-slip fault system of

probable tectonic origin. He later concluded that the absence of major faulting even at the sediment-basement boundary tend to suggest that the southeastern sector of the Iullemmeden Basin probably originated from gentle epeirogenic warpings in contrast to the western and northeastern parts.

Adetona *et al.* (2007) determined the depth of the buried magnetic rocks under the lower Sokoto Basin Nigeria using aeromagnetic data. They employed statistical spectral analysis of the residual magnetic field to determine the depth to the magnetic basement rocks. They reported that two prominent magnetic layers originated from the depth. The first layer depth varies from 0.22 km to 0.96 km with an average value of 0.457 km; while the second layer depth varies from 0.46 km to 1.96 km with an average value of 1.45 km.

Labbo and Ugodulunwa (2007) interpreted the total intensity aeromagnetic maps of part of southeastern Sokoto basin. The two-dimensional spectral analysis indicated a two-depth source model. The deeper sources occurred at the depth of 1.25 km - 1.80 km while the shallower sources occurred at the depth of 0.31 km – 0.56 km. They reported that faults and fractures were potential channels for mineralization fluids.

Raji and Bale (2008) carried out geological and geophysical studies of gravel deposits at the Eastern part of University of Ilorin, main campus using vertical electrical drilling and horizontal profiling method of electrical resistivity. Their result revealed three to four geo-electric layers: laterite, gravel layer, weathered rock and the fresh basement rock. The authors observed that gravel deposit occurs as a laterally continuous geo-electric layer with an average thickness of 3.1m.

Olasunkanmi *et al*. (2012) carried out a geo-electrical assessment of University of Ilorin dam axis. The assessment was aimed at evaluating the geo-structural setting of the concealed

bedrock, the fracture pattern and possible dam seepage along the dam axis and its banks. The authors used Vertical Electrical Sounding (VES) technique of Schlumberger electrode configuration for the field study. Twenty seven VES stations on eight profiles were established along the West-East flank of the dam. According to the authors, three major lithologic units were delineated which are the topsoil, weak/gravelly zone and the fracture/fresh basement. The geo-electric sections reveal fractured basement beneath 4 stations of which two (i.e. VES 1 and 10) are along the dam reservoir and the two starts at the depth of 10 m, extending downward. The authors reported that the geo-electric maps show high resistivity range of about 29-2613 Ωm and thickness range of 0.8-3.1 m and is underlain by relatively low resistivity layer whose values loiters around 100 Ωm with thickness range of 1.8-11.3 m, indicating near surface bedrock straddled with basement depression or fracture. The authors concluded that the fractured basement and low resistivity zone is considered inimical to the continued water retention or zone of anomalous seepage as there is no surface manifestation and significant water reduction can be experienced. This is considered as responsible for low water retention in the reservoir during the dry season.

Olawuyi A.K. (2012) carried out the geo-electric exploration for ground water within the premises of the university of Ilorin teaching hospital, Ilorin Kwara State. The study, according to the authors, was carried out with a view to establishing the different sub-surface geo-electric layers, the aquifer units and their hydro-geologic properties. Olawuyi found out that the 2-D resistivity structures used has elicited 2 lobes of low resistivity which constitutes the prospective zone for water in the area. The author concluded that the study area contains two lobes of low resistivity which could be explored for water supply.

Ibrahim *et al.* (2012) worked on geo-electrical Soundings to investigate Groundwater Potential of Orisunmibare Village in Ilorin South Area of Kwara State, Nigeria. In their

report, A Vertical Electrical Sounding (VES) Method was employed to determine the groundwater potential of Orisunmibare Village in the neighborhood of Federal government college, Ilorin. The purpose of the study was to determine the feasibility of a potable water borehole in the study area. A total of nine VES were carried out in different parts of the study area by means of Schlumberger electrode array configuration. The results of the study indicate the occurrence of good aquifers in the first, second, third, fourth, and fifth VES stations in the form of the weathered and fractured basement. Results also indicate that borehole drilling in the study area is achievable but to a depth of 45 meters to allow large reservoir within the aquifers.

Obaje *et al.* (2013) carried out survey to shed more light on the hydrocarbon prospectivity of the Sokoto Basin. The research was assessed with the use of geological mapping, geochemical analysis and aeromagnetic geophysical investigation. The geological mapping indicates that the basin deepens towards the border with Niger Republic. The geochemical analysis shows that 90% of the samples examined have equal or more than the minimum limit of TOC value (0.5 wt %) required to initiate hydrocarbon generation from source rocks. The geophysical data processing and interpretation allows for the delineation of the prospective areas. From the limitation of the study only eight (8) areas were covered where depths to basement were derived from the processed aeromagnetic raw data map but the structures are neither delineated nor characterized.

Olatunji and Osazuwa (2012) carried out geo-electrical delineations within Kubanni basin, north-central Nigeria. According to the authors, the research site is the whole landmass of the Federal College of Education, Zaria, seated on Basement Complex of north-central Nigeria. Direct current resistivity geophysical method was employed to characterise parameters such as the basement depth and topography, aquifer depth and thickness, weathered basement

distribution as well as mapping of orientations of fractures and faults present in the premises using radial sounding technique. The conventional vertical electrical sounding (VES) Schlumberger array was carried out at 40 stations, and eight of which were radial stations. Radial sounding was used to establish resistivity anisotropy which gives clue for the choice of consistent VES profile direction used throughout the fieldwork.It was reported by the authors that the results from the resistivity interpretation suggest three layers in most parts of the premises with some minor occurrence of two and four layers. The first layer (topsoil) has its thickness ranging between 3.5 and 14.0 m; second layer (weathered basement) thickness ranges between 9.0 and 36.5 m, while the third layer (fresh basement) is deepest (40.1 m) towards the eastern corner of the area. The aquifer depth ranges from 1.5 to 4.0 m with a thickness range of 5.0 to 14.0 m. They concluded that the thickest aquifer occurs around the centre to the west in the area. Results from radial sounding show presence of resistivity anisotropy, an insight to fracturing and faulting; this is more pronounced around the west-central part of the premises.

Olatunji and Musa (2013) estimated Aquifer Hydraulic Characteristics from Surface Geo-electrical methods: Case Study of the Rima Basin, North Western Nigeria. According to the authors, forty vertical electrical resistivity soundings (VES) were acquired, using a Schlumberger array. Three soundings were additionally made at existing boreholes in the vicinity of the study area for comparison. Since the area is a basement complex terrain, a maximum current electrode spacing of 200 m which is believed to probe down to the fresh basement in the area was used. This is believed to enable fresh basement in the area to be observed. The concept of Dar Zarouk parameters (transverse unit resistance and longitudinal conductance in porous media) was used to determine aquifer hydraulic characteristics in the sedimentary formation underlying the area. The authors reported that the results of the interpreted VES data using a combination of curve matching technique and computer

iterative modeling suggest that the area is underlain by between 3–5 geo-electric layers. The geologic sections derived from the equivalent geo-electrical sections revealed lithologic sequence of mostly five layers. However, there are minor isolated cases of three layers. The geo-electrical sections showed that the resistivity of the aquifer varies between 14.1 and 128.8 m. The thickness of the aquifer ranges from 1.0 to 48 m while its depth from the surface lies between 1.0 and 50 m. The authors concluded that relationships between aquifer characteristics and the geo-electrical parameters revealed the hydraulic conductivity K and transmissivity T variations to be 3.10–28.34 m/day and 10.0–796.6 m2/day, respectively. The maximum K and T occur around VES 4 and 14; thus the maximum yield could be expected around VES 4 and 14.

Olawepo *et al.* (2013), evaluated the groundwater potential and subsurface lithologies in unilorin staff quarters using resistivity method. The results he obtained from the sounding were analyzed to determine the aquifers in the zone. The authors from their result of interpretation deduced that the test site has at least four major lithologic layers with the top most layer (top soil) predominantly laterite, the second layer is clay/sand, the third layer is weathered basement and the fourth is fractured basement rocks. Olawepo *et.al* also revealed that the aquifer in the area is located mostly within the fractured basement found at a depth ranging from 16.8 m to 88.6 m.

Nwankwo (2015) also estimated the depths to the bottom of magnetic sources and ensuing geothermal parameters from aeromagnetic data of Upper Sokoto Basin Nigeria. The result showed that the depths to the bottom of magnetic sources (DBMS) vary between 11.37 km and 28.18 km while the ensuing heat flows vary between 51.45 mW/m^2 and 127.55 mW/m^2.

Delineation of magnetic zones of Sokoto Basin in Northwestern Nigeria using aeromagnetic data revealed areas of thick sedimentations around Isah, Rabah, Talata/Mafara and Gandi in

the northeastern part of the Basin. The study suggested that these areas are of relatively thick sediments probable sites for prospecting hydrocarbon deposits

Olatunji and Ojulari (2015) investigated electrical assessment of aquifers in the basement complex of unilorin: implications for existing boreholes. According to the authors, schlumberger 4-electrode array was employed to sound 21 stations. IPI2WIN and surfer12 software were used to infer lithological series, aquifer thickness and depth. The aquifer hydraulic conductivity K and transmissivity T were calculated from the VES data using the Dar Zarouk principles. The authors reported that the field curves show that the area has 3 and 4 geo-electric layers. The layers were interpreted as the topsoil (130- 1469), clayey (wet to dry) (52.6- 8552), weathered/fractured basement (46.2-249) and fresh basement (454-5022) respectively. The aquiferious zones lie within the second and third layers. The aquifer depth is between 6.17 m and 24.9 m while the thickness ranges from 1.89 to 22.7 m. The longitudinal conductance S ranges from 0.02 to 0.468 Ω-1 and transmissivity T varies from 246 to 2419.8 2 .The authors concluded that the results conformed to the functional boreholes, such as at VES 3, sited in areas with maximum aquifers and highest transmissivity T. The NE and NW parts were found most suitable for fresh water exploitations. Low longitudinal conductance which implies low protective cover, in the vicinity of the borehole near VES 6 suggests the contamination claim of its water

Kamba *et al.* (2016) observed that the spectral depth analysis of aeromagnetic data of Lower Sokoto Basin indicated an increase in sedimentation southwards, with several depressions on the basement rock the result observed two prominent magnetization layers of depths varying from 0.589 km to 1.249 km and 2.506 km to 3.2 km

Ofoha and Ekine (2016) carried out determination of Magnetic Basement Depth over parts of Sokoto Basin, within Northern Nigeria, using Improved Source Parameter Imaging (ISPI)

Technique to determine the thickness to sediment and to delineate lithological contacts within the study area. The result estimated the sedimentary thickness ranging from 54.1 m to 3384.4 m with an average thickness of about 739 m

Babatunde *et al*. (2021) carried out study ondetermination of Aquifer Parameters from Resistivity Data: A Case of University of Ilorin Campus, Northcentral Nigeria. The authors said a total of twenty-one (21) vertical electrical sounding (VES) data were acquired using Pz-02 resistivity meter within the Precambrian basement area of part of Ilorin Metropolis north central Nigeria to evaluate the hydraulic characteristics of aquifers. The Schlumberger configuration with half-current electrode separation (AB/2) varying from 1 m to 60 m was used. According to the authors, the aquifer hydraulic characteristics such as hydraulic conductivity K and transmissivity T (Ωm^2) were calculated from the interpreted VES data using the concept of Dar-Zarrouk parameters. The data, processed with computer software IPI2WIN, indicated three to four geo-electric layers, namely; topsoil, clayey (wet to dry), weathered or fractured basement and fresh basement with resistivity values ranging from 130 to 1469 , 52.6 to 8552 , 46.2 to 249 and 454 to 5022 , respectively. The depth to aquifer ranges between 6.17 m and 24.9 m and the overburden thickness ranges between 4.1 m and 22.7 m. The assessment of the materials above the aquifers showed that longitudinal conductance lies between 0.02 and 0.468 Ω–1 , transmissivity values vary from 246 to 2419.8 2 . The authors concluded that the results obtained have offered worthwhile hydrologic information that will aid both exploration and exploitation of the groundwater system of the study area.

2.5.2 Dar Zarouk Parameters

Dar Zarouk parameters are parameters used to define or delineate areas of target of groundwater potential. The parameters are; longitudinal conductance (S), transverse resistance (T) and longitudinal resistivity (Rs).

The longitudinal conductance is used to define the aquifer's protective capacity. The higher the value of longitudinal conductance of an aquifer, the higher its protective capacity and vice versa. The transverse resistance is used in direct relations with Transmissivity (T). The higher the Transmissivity value of an aquifer, the higher its transverse resistance (T).

Ekwe, *et al*. (2010) used the concept of Dar zarouk parameter to estimate aquifer hydraulic characteristics of low permeability formation from Geo-sounding Data: A case study of Oduma Town, Enugu State. According to the authors, eight VES results using schlumberger configuration were acquired for the study area. The Eight sounding were processed using RESIST software. They said that geo-electric sections of the area were generated from which the aquiferous layers were delineated and hydraulic parameters (hydraulic conductivity and transmissivity) were computed.

Okonkwo and Ezeh (2013) used the concept to infer the subsurface lithological extent of Agbani sandstone, Enugu State, Nigeria. A total of 13 vertical electrical sounding was carried out by the authors in the area. Longitudinal resistivity, transverse resistance and apparent resistivity data was computed from the interpreted VES data. The authors concluded from their interpretation that areas with high longitudinal resistivity, transverse resistance and apparent resistivity are indicative of a thick succession of a substratum and are areas recommended for citing of productive boreholes.

Okonkwo and Ugwu (2015)used the concept to predict the protectivecapacity of Agbani sandstone aquifer within the Enugu State university of science andTechnology, Agbani campus. Thirteen (13) vertical electrical sounding (VES) was carried out within the study area. Longitudinal conductance, transverse resistance, longitudinal resistivity and apparent resistivity data was computed from the interpreted VES data. According to the author, the longitudinal conductance was used to predict the protective capacity of Agbani sandstone aquifer and three protective capacity zones were delineated; the good, moderate and poor/weak protective zones.

All the existing studies on geophysical and hydrogeophysical studies have used one geophysical method or the other. Some of the studies have combined gravity and Magnetic methods, some have used VLF-EM and electrical methods and some used Magnetic method only while many of the studies used electrical method only. It is observed that none of the studies has used the combination of Magnetic and electrical methods in the study area and its neighboring areas to solve problem of groundwater potential as this present study does.

2.6 Related Previous works on Hydrogeophysical studies

Muhammed *et al.* (2008) carried out a hydrogeophysical investigation of groundwater potential in central Minna, Nigeria. According to the authors, the investigation was aimed at delineating the aquiferous units in the central part of Minna by determining theirdepths, thicknesses, resistivities and the potential borehole depth at various locations within the area. They employed the technique of Vertical Electric Sounding (VES) using the Schlumberger array. A grid of 7 profiles with a total of 49 sounding stations was occupied. The authors said that the area was found to be underlain by 4 geological formations and the second and third formations underlying parent bedrock form the aquiferous unit. This unit was found to have an average resistivity value range of 120 – 900 Ωm and an averagethickness of 25 m. It is deeply seated in some areas with an average depth of 25 – 30 m.

Oseji and Ujuanbi (2009) carried out a hydrogeophysical investigation of groundwaterPotential in Emu kingdom, Ndokwa land of Delta State, Nigeria. The authors undertook 10 vertical electrical soundings from different quarters of Emu kingdom using Schlumberger array. According to the authors, this was an attempt to obtain useful information on the aquifer distribution withinthe area and hence delineate possible site boreholes that could be drilled for potable and sustainable water supply. The authors concluded that based on the geo-electric section which is in agreement with the driller's log; the best environments for sustainable water supply were identified. This coincides with the third layer of the aquifer in Emu kingdom and consists of medium-grained sand formation. They said the average depth to thisaquifer is 45 m whose thickness is not defined at Obiogo since it is the last layer, but in other parts ofEmu-Kingdom, the thickness ranges from 45.00 m in Ikosa quarter to 95.00 m in Etevie quarter.

Opeyemi, J.A. and Rasheed, B.A. (2016) carried out a hydrogeophysical investigation of groundwater potential and aquifer vulnerability prediction in Basement Complex terrain – A

case study from Akure, Southwestern Nigeria. According to the authors, the study provides a model for the prediction of groundwater potential and vulnerability of basement aquifers in parts of Akure, Southwestern Nigeria. Hydrogeophysical surveys involving very-low-frequency electromagnetic (VLF-EM) profiling and electrical resistivity (ER) sounding, as well as evaluation of hydraulic gradient using three-point method, were carried out. The authors said two-dimensional map of the filtered real component reveals areas of high conductivity, indicative of linear features that can serve as a reservoir or conduit for fluid flow. They further said interpretation of the VES results delineates three to four geoe-lectric units and two aquifer zones were identified, with resistivity values in the ranges of 20 to 310 and 100 to 3,000 , respectively. Transverse resistance, longitudinal conductance, coefficient of anisotropy and hydraulic gradient have values ranging from $318.2^2$to $1{,}041.8^2$, 0.11 mhos to 0.39 mhos, 1.04 to 1.74 and 0.017 to 0.05, respectively. The authors concluded that results of this study identified two prospective borehole locations and the optimum position to site the proposed septic system, based on the aquifer's protective capacity and groundwater flow properties.

2.7 Review of previous Hydrochemical assessment of groundwater

Adekeye (2001) related borehole depth to water quality so as to access its suitability for drinking, agricultural and industrial purposes. He took thirty water samples from boreholes in different parts of the Basement Complex terrain of Kwara State and analyzed. The result of the chemical analyses of the samples shows that the levels of potability of water in terms of the physical and chemical characteristics are reasonably acceptable when compared withWHO acceptable standard. Adekeye (2001) found out that the levels of iron in many of the boreholes are objectionable and require remedial action using appropriate treatment procedures.

Tijani and Ayodeji (2001) carried out hydrogeochemical assessment of surface and groundwater resources in part of Dahomey Basin south western Nigeria. The study is aimed at assessing the quality and usability of groundwater resources as well as determining the geologic influence and factors controlling the distribution of aqueous ions. The major cation concentrations are in the order K ≥Na≥ Ca ≥ Mg with mean values of 22.5 mg/l, 21.0 mg/l, 17.97 mg/l and 4.74 mg/l respectively with average value of 6.8 for pH. Conductivity and TDS values recorded indicate a fresh water grade that is suitable for domestic (drinking) and agricultural purposes. The result revealed a strong positive correlation coefficient between sodium and potassium. Hence, the overall hydrochemical characteristics of sample waters are partly affected by mixing of diverse water types, chemical weathering and dissolution of parent rocks.

Abimbola *et al.* (2002) worked on the environmental impacts assessments of waste dumpsites on the geo-chemical quality of water and soils in Warri metropolis, southwestern Nigeria. The research discovered that the pH value of the water ranges between 6.4 and 6.5, indicating that the water is slightly acidic. The TDS value ranges from 125.8 (mg/l) to 166.9 (mg/l) which are rather low but conform to the prescribed standard of World Health Organization (WHO). From the discovery, it is said that the area with low anthropogenic activities account for the elevated Total Organic Compound (TOC) values. The authors therefore concluded that there are elevated concentrations of phosphate, cadmium, iron, nickel, lead and manganese in the groundwater samples in the area

Adeyemi*et al.* (2003) worked on the chemical characteristics of some well waters in Ikire south western Nigeria aimed at determining the potability or otherwise of the well waters as well as the probable source(s) of the pollution of groundwater if any. The concentration of ions in majority of the samples is below maximum permissible levels indicated in the World

Health Organization (WHO) standards. This indicates that most of the waters in the area are potable.

Adekunle*et al.* (2007) assessed the groundwater quality in a typical rural settlement (Igbo-Ora), Oyo State, south western Nigeria. Their assessment was aimed at studying the levels of some physical, chemical, biochemical and microbial water quality parameters in twelve hand-dug wells in the area. All the parameters were determined up to 200m from pollution source and most of them increased in concentration during the rainy season over the dry periods, pointing to infiltrations from storm water. Coliform population, Pb, NO_3 and Cd in most cases exceeded the World Health Organization recommended thresholds for potable water. The mean values for the parameters measured are as follows: pH (6.91), turbidity (42.12), electrical conductivity (421 µS/cm), temperature (30.33^{o}C), TDS (273.43mg/l), PO_4^{3-} (0.02mg/l), NO_3 (19.28 mg/l), Cu (0.12 mg/l), Pb (0.16 mg/l), Cd (0.30 g/l), BOD (2.55 mg/l) and COD (43.59mg/l). From this result, it was concluded that the quality of the well water samples were not suitable for human consumption without adequate treatment.

CHAPTER THREE

3.0 MATERIALS AND METHODS

3.1 Geological Survey Materials

The materials used for the geological survey of the area include the topographical maps of the area (Figures 1 and 2) which were used to study the relief and drainage characteristics of the area. The relief map was used to study possible surface water flow directions. A dendritic drainage pattern is a characteristic of surface water sources while a trellis pattern is characteristic of fractured terrain. A global positioning system was used to take coordinates of the area, a geological hammer and chisel were used to collect fresh samples of rocks in the area and compass clinometers were used to measure strikes and dips as well as trends of fractures in rocks of the area.

3.1.1 Geological Mapping

Geological mapping of the study area was done in the dry season on an approximate scale of 1:25,000 using appropriate and suitable field instruments. An extensive traversing using the many footpaths and roads available was done in the study area. A topographical map on the scale of 1:25,000 was used as the base map for the exercise and field data on outcrops of

basement rocks such as strikes and dips, as well as geological boundaries were plotted and indicated on the geological map respectively. Fresh rock samples were collected for petrographic study and coordinates were measured using a Global Positioning System (GPS).

Here, the laboratory works involve the petrographic study of the freshly collected rock samples in the field. The samples were prepared in thin sections at KWASU geological laboratory. The thin sections were observed through a petrographic microscope using plane polarized light and cross-polarized light to reveal the mineral constituents of the rock samples

3.1.2 Hydrogeological Survey Data

The hydrogeological survey data include water level measurements from 80 hand-dug wells in the study area. The data were taken both at the end of raining season and the peak of the dry season (2019-2020) using weighted survey tape for in situ measurements. The water level measurement data were used to prepare hydrogeological maps for both ends of raining season and the peak of the dry season. Meteorological and pumping test data were obtained as secondary data from the Ministry of Water Resources and Lower Niger River Basin Development Authority, Ilorin, Kwara State. The meteorological data were used to prepare to mean monthly averages for rainfall, temperature, and relative humidity while the pumping test data were used to calculate aquifer characteristics; Hydraulic conductivity, Transmissivity, and Storativity of the area.

3.1.3 Hydrogeological Survey Method

3.1.3.1 Pumping Test Survey

Geology, climate, and structures of an area control its hydrogeology. According to Davis and De Wiest (1966), Todd (1980), and Tijani (1994), geological formations underlying an area

and the associated structures do determine the type and nature of aquifers to be encountered while climate determines the amount and rate of recharge of the aquifers.

Groundwater is held in porous formations which are rocks containing a relatively large portion of void spaces (Deming, 2002). Crystalline Basement rocks (study area inclusive) generally have porosities of less than 3% (Bouwer, 1978). As such rocks of the Basement Complex, when not weathered are practically impermeable and have no storage capacity. However, appreciable porosity and permeability might have been developed in the rocks through fracturing and weathering processes (Davis and De Wiest, 1966), depending on the lithology and texture of the original rock.

The Basement rock units are described to be more productive at the base of the weathered zone where the rocks have been broken down to sand size and larger fragments that are not subjected to extensive weathering process i.e. sap rock zone (Offodile (1983), Jones (1985) and Egboka (1988). Therefore, groundwater occurs in the Basement Complex in the weathered overburden or the joints and fractures' system within un-weathered rock units of the study area.

The aquifer characteristics determined were:

i. **Hydraulic conductivity**

Hydraulic conductivity was calculated using Darcy's law which states that the rate of water that flows through a porous medium is directly proportional to the difference in hydraulic head and inversely proportional to the length of the flow path (Darcy,1856). Darcy mathematically stated the law as:

$q \propto dh$ 13

$q \propto \frac{1}{dl}$ 14

$q = k\frac{dh}{dl}$ 15

i.e. $q = \frac{Q}{A}$ 16

$Q = KA\frac{dh}{dl}$ 17

$Q = KA_i$ 18

Where q = discharge rate (m^3/day), K= hydraulic conductivity (m/day), i= hydraulic gradient= dh/dl, i.e. loss of head (h) over the distance (l), A= cross-sectional area perpendicular to the flow (m^2), Q= quantity discharged (m^3). Therefore, hydraulic conductivity

$K = \frac{Q}{iA}$ 19

Hydraulic conductivity can alternatively be calculated using a formula relating it with Transmissivity after the value of Transmissivity has been calculated. The formula is:

T= Kb 20

K= T/b 21

Where T= transmissivity coefficient, b= aquifer saturated thickness, and K= hydraulic conductivity. Hence, the hydraulic conductivity of the study area was calculated using a formula relating it to Transmissivity and aquifer thickness.

ii. Coefficient of Transmissivity

Transmissivity or transmissibility (T) is the rate at which water will flow through a unit cross-section of the aquifer of unit width and extend through the full saturated thickness under a unit hydraulic gradient. It is the product of hydraulic conductivity (K) and aquifer thickness (b), that is, T= Kb 22

Where:

T= transmissivity (m^2/day), K= hydraulic conductivity (m/day), b= aquifer thickness (m)

Alternatively, Transmissivity can be calculated using Jacob's modified method (1987). The formula is given as;

$$S_2\text{-}s_1 = 2.30Q/4\pi T \times \log_{10}(t_2/t_1) \quad (23)$$

$$\Delta s = 2.30Q/4\pi T \times \log_{10}(t_2/t_1)$$

$$\text{Hence, } T = 2.30Q/4\pi\, \Delta s \times \log_{10}(t_2/t_1) \quad (24)$$

Where: T = transmissivity (m^2/day), Q= discharge rate, Δs = change in drawdown, t_2 and t_1 = time (days) since pumping started.

Transmissivity (T) was estimated by plotting the drawdown values (m) of water level in wells against time in minutes since pumping started on a semi-logarithmic co-ordinate paper.

From the pumping test data available in the study area, T was calculated using equation 24 above.

iii. Coefficient of Storativity (storage coefficient)

Storage coefficient is defined as the volume of water that an aquifer releases from or takes into storage per unit surface area of the aquifer per unit change in the component of head normal to that surface. For a vertical column of a unit area extending through a confined aquifer, the storage coefficient 'S' equals the volume of water released from the aquifer when the piezometric surface declines a unit distance. In most confined aquifers, 'S' falls in the range $5\times10^{-5} < S < 5.0\times10^{-3}$.

Storage coefficient can also be calculated using the pumping test method by extrapolating the straight line of the semi-log curve to a point at which it intersects with the zero draw-down axes which permit the computation of 'S' as:

$$S = 2.25Tt_0/r^2 \quad 25$$

Where:

S= storage coefficient, T = transmissivity (m^2/day), t_o = time intercept on zero draw-down axis, r = distance of the borehole.

The storage co-efficient of the aquifers in the study area was calculated using equation 25 above.

3.1.3.2 Water Level Measurements

Water level measurements are measurements of the levels at which water remains static in hand-dug wells from the ground surface without being pumped naturally or artificially. The measurements were done by taking a reference point at the rim of the well and then lowering a weighted surveyor's tape into the well until its zero mark just touched the surface of the water in the well. The reference point helps in knowing the point at which the exact depth of the well begins. The depth to water level from the surface was read thereafter on the tape concerning the reference point. The depth to water level measurements was carried out in eighty (80) hand-dug wells in the study area. The number of the measurements was according to the available wells in the area. This exercise was carried out at the end of the rainy season (October 2018) and at the peak of the dry season (March 2018).

The water levels of groundwater available in the study area were used to prepare the following hydrogeological maps;

i. Water level contour maps
ii. Maps of the depth to water level (i.e. map of unsaturated/vadose zone)

I. Water Level Contour Maps

These are hydrogeological maps that show the configuration of the phreatic surface and the regional direction of groundwater flow in the study area. The maps were prepared by plotting the altitudes of water levels measured in dug-wells on a topographical map. The altitude of the water level in each of the wells was calculated by deducting the measured water levels below the ground surface (depth to water level) from the altitude of the well locations. Lines were then drawn to join points of equal water level elevation. The maps were prepared for the end of raining season and at the peak of the dry season.

II. Map of unsaturated/Vadose zone

These are maps that show the depth to water level from the ground surface. It was prepared by plotting values of measured water levels from the ground surface on a topographical map using a suffer software. Lines were then drawn to join points of equal values of the unsaturated zone of thicknesses. These maps were prepared for both end of raining season and the peak of the dry season.

3.2 Aeromagnetic data

The total-field high resolution digital aeromagnetic airborne data used in this study were acquired from the Nigerian Geological Survey Agency (NGSA), Abuja. The digital data covered sheet 223 Ilorin North- West and it is bounded between latitudes 8°15' N and 8°25' N and lines of longitude 4°30' E and4°37.5' E. The aeromagnetic data were acquired as part of a

nationwide aeromagnetic survey conducted in two phases by Fugro Airborne Surveys. Phase I data sets was acquired in 2007 while Phase II data were acquired from 2007-2009. The data set were acquired along a series of NW– SE flight lines with a line spacing of 500m and an average of 80m terrain clearance. This new data offers a lot of advantages in terms of resolution over the old data (acquired in 1974) in which most of the earlier interpretations were made (Zahran *et al*., 2017)

3.3 High-Resolution Aeromagnetic Data (HRAM) Processing

3.3.1 The Regional – Residual Separation

For accurate interpretation of aeromagnetic data, the residual anomalies must be separated from the regional field. Since a composite magnetic map comprises disturbances of different order sizes and patterns, the residual field which is usually of interest must be generated by subtracting the estimated regional field from the measured total field. There are various methods of removing the unwanted regional, from the total field map. This includes graphical and analytical methods. The graphical method is an old method where total field data are manually plotted and the regional is to represent a smooth regional field.

The earliest non-graphical approach also known as the analytical method employs various mathematical tools to obtain the regional field considered the regional field at a point to be the average of observed values around a circle centered on the point, where the residual field is simply the difference between this average value and the value observed at the central point (Griffin, 1949). It was shown by Henderson (1949) and Roy (1958) that this method was equivalent to calculating the second vertical derivative except for a constant factor.

Regional residual separation is equivalent to filtering in other geophysical techniques like seismic, but the difference is that the noise that is removed as a result of filtering is the object of importance in magnetic studies. This noise or residue is of little or no interest in seismic

data and other geophysical techniques. Residual anomalies, which are the smaller local disturbances are of primary interest in many magnetic interpretations and also reveal the subsurface features which frequently distort the larger features mainly caused by the deeper heterogeneity on the Earth's crust and appear as trends over a considerable distance. These trends are known as regional and are considered as the value of the field which would exist if there were no local disturbance due to the source we are trying to interpret.

Another analytical method based on frequency-domain Wiener filtering for gravity data and is equally applicable to magnetic data was proposed by Pawlowski and Hansen (1990). Matched filters and Wiener filters have much in common with other linear bandpass filters but have the distinct advantage of being optimal for a class of geologic models. Spector and Grant (1970) analyzed the shape of power spectra calculated from observed data. Clear breaks between low- and high-frequency components of the spectrum were used to design either band-pass or matched filters. However, the signal overlap of the discontinuities often affects the accuracy of this technique. In hydrocarbon exploration, this is the most common approach to separating different depth ranges of interest based on their frequency content.

Polynomial fitting is considered one of the analytical methods for determining a regional magnetic field. This approach was proposed by Agocs (1951) and is considered a widely used approach. In this method, the fitting is based on the statistical theory since the observed data are computed by the least square method to obtain a surface that has the closest fit to the magnetic field. This surface is considered to be the regional field while the residual is the difference between the magnetic field value obtained in the field and the regional field value computed.

In this research, the least squares method was employed because the geology of the area is not complex. This method has a lot of advantage**s** over the other method**s** because;

1. Bodies of arbitrary shapes are considered
2. The solution may take known geological structures into consideration
3. Many points of the maps or profile are used to obtain the solution
4. It is free from the interpreter's bias.

The procedures are as follows:

1. The linear surface trend equation has the form

$$Y = d_0 + d_1X_1 + d_2X_2 + \cdots, \quad 26$$

Where Y is the regional field, X's geographic coordinates of the map, and d's are the polynomial regression coefficients. The values obtained for the coefficients are

$d_0 = 33188.44151, d_1 = -9.86082$ *and* $d_2 = -0.49269$ respectively.

Substituting the above coefficients into equation (3.11) we have:

$$Y = 33188.44151 - 9.86082X_1 - 0.49269X_2 \quad 27$$

2. The linear surface trend must minimize the sum of squares of the vertical distance from the points.

The observations are represented as a point

$$P_i = (xi; yi) \quad 28$$

Where I range from 1 to N. If the vertical projection of Pi on the line is indicated as U_i, then the distance P_iU_i represents the residual or deviation from the line.

However, all the regional were calculated as a two-dimensional first-degree polynomial surface since the regional field is a polynomial fitting of the first order surface. Hence, Surfer

V.12.0 software was used to subtract values of the regional field from the total magnetic field value at grid points.

3.3.2 Filtering of Residual Field Data

The preliminary beginning stages of magnetic data interpretation generally involve the application of mathematical filters to the observed data. The choice of the filter to apply often depends on the aim of the study. The general purpose is to simplify the appearance of the anomalies and enhance features of particular interest subtle at the expense of others that are of less interest. Horizontal and vertical derivatives are routinely used to enhance details in magnetic data. The total horizontal derivative and analytical signal are two effective tools that are used to detect the edges of magnetized structures (Pilkington and Keating, 2004; Cooper and Cowan, 2008; Cooper, 2009). Furthermore, specific functions of these filters are employed to map subsurface structures.

However, the upward continuation in this research was enhanced by both vertical derivatives (i.e. FVD and SVD). Hence, the shape, dimensions, and amplitude of an induced magnetic anomaly are a function of the orientation, geometry, size depth, and magnetic susceptibility of the body as well as the intensity and inclination of the earth's magnetic field (Sharrma, 2002).

3.3.3 Reduction to the Equator (RTE)

Generally, the shape of the magnetic anomaly depends on the inclination and declination of the magnetic field of the Earth in order words, the same magnetic body will produce a different anomaly depending on the location of the study area on the globe. RTE was applied to transform the anomaly of non-zero inclination into an anomaly that would be observed on the same body with zero inclination. The RTE is mathematically expressed as:

$$RTE = \sin I + i \cos I \sin (D - \theta)^2 \quad 29$$

Where I is geomagnetic inclination also called Dip, D is geomagnetic declination, $\sin I$ is the amplitude component, and $i \cos I \sin (D - \theta)^2$ is the phase component. The software Geosoft of Oasis Montaj v.6.4.2 using the convolution of *Fourier transformation* made it possible to obtain the map of Total magnetic Intensity (TMI) reduced to the equator and other relevant maps. To realize this map, Inclination (*I*) and Declination (*D*) values were computed; these values are: $I = 2.7850$ and $D = -2.0050$ respectively. Further, due to the dipolar nature of the magnetic field, the peaks of the anomalies are skewed from the centre of the source bodies. For accurate interpretations, a place shift correction known as a reduction to the equator is applied in low latitude regions to minimize the problem by aligning the peak of the magnetic anomalies over the center of their sources.

3.3.4 Tilt Angle Derivative (TDR)

Since the amplitude of magnetic signature depends on magnetic field strength and to some extent the depth of magnetic sources, lower amplitude signature may be suppressed at the expense of higher amplitudes. For this reason, the edge-detection filters area is normally applied for delineating linear features without necessarily diminishing the long-wavelength anomalies (Salem *et al.*, 2008). The tilt angle derivative filter is one of the filters employed for this purpose. According to Verduzco *et al.* (2004) the tilt derivative tends to equalize the response from both weak and strong anomalies. Miller and Singh (1994) showed that structural boundaries can be relatively mapped by the method.

Tilt angle is defined as the arctan value of the ratio of the vertical derivative of the potential field to its horizontal derivative (Miller and Singh, 1994; Verduzco *et al.*, 2004). The

advantage of the tilt angle method compared to some other methods is that parametersuch as magnetic susceptibility it is largely independent of magnetic inclination.

According to Miller and Singh (1994), the tilt angle is expressed as:

$$TDR = arctan\left[\frac{\left(\frac{\partial T}{\partial z}\right)}{\left(\frac{\partial T}{\partial h}\right)}\right] \quad 30$$

Where $$\frac{\partial T}{\partial h} = \left[\left(\frac{\partial T}{\partial x}\right)^2 + \left(\frac{\partial T}{\partial y}\right)^2\right]^{\frac{1}{2}} \quad 31$$

Equation (30) is the first-order derivative of the potential field in the *x*, *y*, and *z* directions. The data is transformed from space to frequency domain using fast Fourier transform (FTT) then the Fourier transformed data is multiplied with the tilt angle derivative filter (Equation 31) and the product is inversely Fourier transformed with the space domain to obtain the TDR values. In this study, the tilt derivative was computed with the aid of Oasis Montaj v6.4.2 software.

3.4 Electrical Resistivity Survey data

Resistivity data were acquired with a *Herojat* resistivity meter, manufactured in Nigeria. This was used to acquire data from two hundred and ten (210) points following Schlumberger vertical electrical sounding (VES) array mode. The data were interpreted from curve matching using computer iteration modeling to reveal the geo-electric layers of the study area.

3.4.1 Electrical Resistivity survey method

Two hundred and ten (210) vertical electrical resistivity surveys were carried out in the study area along 63 profiles using schlumberger sounding electrode arrangement with electrode separation of 200m (i.e. AB). Figure 54 shows the location map of the VES stations. Partial

curve matching techniques using two-layer model curves and corresponding auxiliary curves were used to arrive at the different curve types and their appropriate resistivity values. The parameters obtained from curve matching were used by the computer software IPI2win as input data for the computer iterative modeling.

The data were obtained through a geophysical survey. The Geophysical method used for the study was the electrical resistivity method. The method involved investigating the electrical resistivity of points in the area through vertical sounding. This was done by choosing a reference point at the center of the electrodes while both current and potential electrodes were laid out with non-conducting measuring tapes. The field procedure involves expanding the current electrodes while keeping the potential electrodes fixed. Readings for both current and potential electrodes were taken and recorded in the data sheet from which the resistivity values were calculated. The resistivity values were plotted against current electrodes to give different curve patterns (Appendix 1). Partial curve matching and computer iteration techniques were used to reveal the geo-electric layers occurring in the area. Isopach (thickness of weathered basement) and Isoresistivity (layers of the same resistivity) maps were also prepared from the geophysical data. Longitudinal conductance, transverse unit resistance, longitudinal resistivity, transverse resistivity, coefficient of anisotropy, and reflection coefficients were calculated from the resistivity values of the geo-electrical layers to characterize the properties of the delineated aquifers.

A, H, Q, and K curve types are three geo-electric layer curves with resistivity variation of each as $\rho1 < \rho2 < \rho3$, $\rho1 > \rho2 < \rho3$, $\rho1 > \rho2 > \rho3$, and $\rho1 < \rho2 > \rho3$ respectively. HA, KH, QH, AA and QA are four geo-electric layer curve with resistivity variation of each as$\rho1 > \rho2 < \rho3 < \rho4$, $\rho1 < \rho2 > \rho3 < \rho4$, $\rho1 > \rho2 > \rho3 < \rho4$, $\rho1 < \rho2 < \rho3 < \rho4$ and $\rho1 > \rho2 > \rho3 < \rho4$ respectively. The five geo-electric layer curve types in the area are HKH, QHA, HAA and KQA with resistivity

variation of each, as ρ1>ρ2<ρ3>ρ4>ρ5, ρ1>ρ2>ρ3>ρ4<ρ5, ρ1>ρ2>ρ3<ρ4<ρ5 and ρ1<ρ2>ρ3>ρ4<ρ5.

A-curve type (ρ1< ρ2< ρ3) is a curve type characterized by a consistent increase in apparent resistivity of the layers. This layer is not desirous for groundwater exploration. **H-curve type** (ρ1>ρ2<ρ3) is characterized by low apparent resistivity in layer two indicating that the layer is of high conductivity and high groundwater potential .**Q-curve type** (ρ1>ρ2>ρ3) is a curve type with low apparent resistivity in layers two and three, thus indicating high groundwater potential in the layers. **K-curve type** (ρ1<ρ2>ρ3) is characterized by low apparent resistivity in layers one and three which indicate an overburdened aquifer with high groundwater potential.

HA-curve type (ρ1>ρ2<ρ3<ρ4) is a combination of the minimum and ascending segment. The first elevated apparent resistivity value (ρ1) may be associated with the effect of dehydration from sun radiation (especially in the dry season). The relatively low resistivity values in the second and third geo-electric layers, commonly due to the presence of pore fluid (water), may have been facilitated by the weathered nature of basement rock. Thus, these layers are the major hydrogeologic interest of the curve type. The fourth geo-electric layer has continuously elevated apparent resistivity values with limited water-bearing potential. **KH-curve type** (ρ1<ρ2>ρ3<ρ4), is another four-geo-electric layer curve. This curve type has two regimes of low apparent resistivity values (i.e. the first and third layers). The Hydrogeologic significance of a KH curve will be determined by low apparent value, degree of weathering, and mineral types. **QH-curve type** is the a-curve type that is characterized by the consistent reduction in apparent resistivity (ρ1>ρ2>ρ3>ρ4). This shows that the subsequent geo-electric layer is less resistive. This type of curve is typical of thick overburdened material and is desirous in groundwater exploration. However, it requires a

high level of technicality during drilling to prevent the collapse of less resistive lithologies. The **AA-curve type** is not desired in groundwater exploration because of its consistent elevation in apparent resistivity ($\rho1<\rho2<\rho3<\rho4$). This situation will consequently lead to limited groundwater accumulation or flow. **QA- curve type** ($\rho1>\rho2>\rho3<\rho4$) is the last four geo-electric layer curves in the study area. It is characterized by low apparent resistivity in layers 2 and 3. The third layer indicates a weathered aquifer unit with high groundwater potential.

The **HKH curve type** ($\rho1>\rho2<\rho3>\rho4>\rho5$), is characterized by low apparent resistivity values in layers two, four, and five. This indicates one of the aquiferous units in the area which is a fractured crystalline aquifer at layer five. **QHA curve type** ($\rho1>\rho2>\rho3>\rho4<\rho5$) is characterized by a consistent reduction in apparent resistivity from layer one to layer four and high apparent resistivity at layer five. The low apparent resistivity at layer three is a weathered aquifer unit that enhances groundwater potential. **HAA-curve type** ($\rho1>\rho2<\rho3<\rho4<\rho5$) is characterized by two regimes; low apparent resistivity at layers two and three and high apparent resistivity at layers four and five. The two regimes indicate the two aquifers in the area; three and five layers. **KQA-curve type**($\rho1<\rho2>\rho3>\rho4<\rho5$) is characterized by an increase in apparent resistivity at layers two and five and low apparent resistivity at layers three and four.

Lenkey *et al*. (2005), Omosuyi (2000), and Meju*et al*. (1999) stated that in assessing the groundwater potential of any area in the crystalline Basement Complex, the cardinal focus for well aquiferous units is where the overburden and fractured crystalline aquifers are complementary or connected.

Olayinka (1996) observed that in evaluating the groundwater potential of any area in the basement terrain, the resistivity cannot be solely relied on, to identify areas of the promising aquifer.

Hence its reflection coefficient has to be considered in the evaluation.

3.5 Hydrochemical Test Materials

The Hydrochemical parameters tested include both the physical and chemical parameters. The physical parameters are PH, temperature, electrical conductivity, and turbidity. These parameters were measured using a PH meter, thermometer, conductivity meter, and turbidity metre respectively in a 4-in-1 instrument known as HANNA instrument. The chemical parameters on the other hand include the major cations and anions. The major cations including heavy metals are Na, K, Ca, Mg, Fe, Mn, Pb, Cu, Zn, and Cd. All these cations were analyzed using Atomic Absorption Spectrophotometer (AAS). The major anions analyzed were Cl using silver nitrate reagent, CO_3 and HCO_3using phenolphthalein and methyl orange indicators, PO_4 and SO_4 using UV spectrophotometer, and NO_3 using $CuSO_4$, $NaSO_4$, selenium powder, Kjeldahal digestion flask, concentrated H_2SO_4, HCl acid and boric acid for digestion, distillation, and titration.

3.5.1 Hydrochemical Test Method

The water samples were collected in 0.5 liter sample bottles which had been previously thoroughly washed and later rinsed more than three times with the water being sampled before filling the bottles. Two separate samples were collected for each water point; one was for the determination of anion while the second was for the determination of cation. The samples collected for cation determination were acidified with concentrated nitric acid (HNO_3) to a pH of approximately 2. This is done to reduce the adsorption of ions from the

solution and the formation of bonds between the container and the ions. Samples were preserved in a deep freezer before being taken to the laboratory for analysis.

The physical parameters were measured *in situ* by dipping the instruments in the water samples at the points of collection and their readings from the instruments were taken and recorded. The in-situ measurements are necessary because the values of the parameters might change significantly soon after collection. The chemical parameters were analyzed at UNILORIN central research laboratory, University of Ilorin. The cations analyzed were done by Atomic Absorption Spectrophotometer (AAS). The samples for cation determination were firstly digested before running through the AAS machine. The NO_3^- was analyzed by digestion, distillation, and titration methods, PO_4^- and SO_4^{2-} by UV Spectrophotometer, Cl^- by silver nitrate titration in the presence of potassium chromate as an indicator; this is also known as the argentimetric method, and CO_3^-/ HCO_3 were analyzed by the alkalinity test method. The procedure for each analysis is in Appendix 5.

The suitability of groundwater of the area for Agricultural purposes was assessed on the toxic elements level in the water. Toxic elements hazard is caused by excessively high concentrations of cadmium, lead, manganese, zinc, copper, chromium, arsenic, and boron.

CHAPTER FOUR

4.0 RESULTS AND DISCUSSION

The various field and laboratory-acquired data are hereby discussed. This was done in terms of geology, hydrogeology, geophysical studies and physico-chemical assessment of groundwater of the study area.

4.1 Mapping of the Study Area

The Geological mapping confirmed that the study area is within Sheet 223, Ilorin North-West and it is underlain by the rocks of the Basement Complex of Nigeria, comprising migmatite gneiss, banded gneiss, augen gneiss, granite gneiss, quartz-mica-schist and fine-grained granite (Figure 10). The study area lies within the Basement Complex of South Western Nigeria, which is of Precambrian to Lower Palaeozoic in age as evidenced by Jones and Hockey (1964); Odeyemi, (1976) and Rahaman (1976). The lithologies of the area, observed in this study, are dominantly gneissic which include migmatite gneiss, banded gneiss, augen gneiss, and granite gneiss which concurs with the submission of Adekeye's (2001). Also observed in the study area are quartz-mica schist and fine-grained granite which are among the Older Granite in Kwara State, according to Rahman (1988). Thus, the geology of the study area is concordant with the general geology of the Nigerian Basement Complex as discussed by Grant (1969). The identified rock types in the area are presented as well as structural features such as foliations, folds and fractures were observed and measured on the rocks. These are discussed in the steps below.

4.1.1 Rock Types in the Area

4.1.1.1 Migmatite gneiss

Migmatite gneiss is one of the high-grade metamorphic rocks found in the study area. The rock occurs in the northern part of the study area occupying 10% of the study area (Figure 10). It is a low-lying body, light to pinkish and fine-grained in texture at Ago-Oja and Ansarul Islam Secondary School, Laduba. The outcrop has simple and asymmetrical folds (Figure 11). Joints with strike values of $N60^0E$, $N34^0E$ and $N36^0E$ were measured on the outcrop.

The petrographic study of the rock has shown through the visual estimate method that the estimated modal compositions of the rock are Microcline (45%), Quartz (35%), biotite (10%), Plagioclase feldspar (5%) and accessories (5%) (Figure 12). Microcline is the dominant mineral in the rock, colourless but cloudy with low relief in plain polarized light (PPL) (Figure 13) but greyish in cross-polarized light (XPL) with cross-hatch twinning (Figure 12). Quartz is anhedral, in-equigranular and has no cleavage. Biotite is light brown but pleichroic from light to dark brown, sub-heudral in shape and has perfect cleavage. Plagioclase feldspar is sub-heudral in its habit and shows a multiple albite twinning (Figure 12)

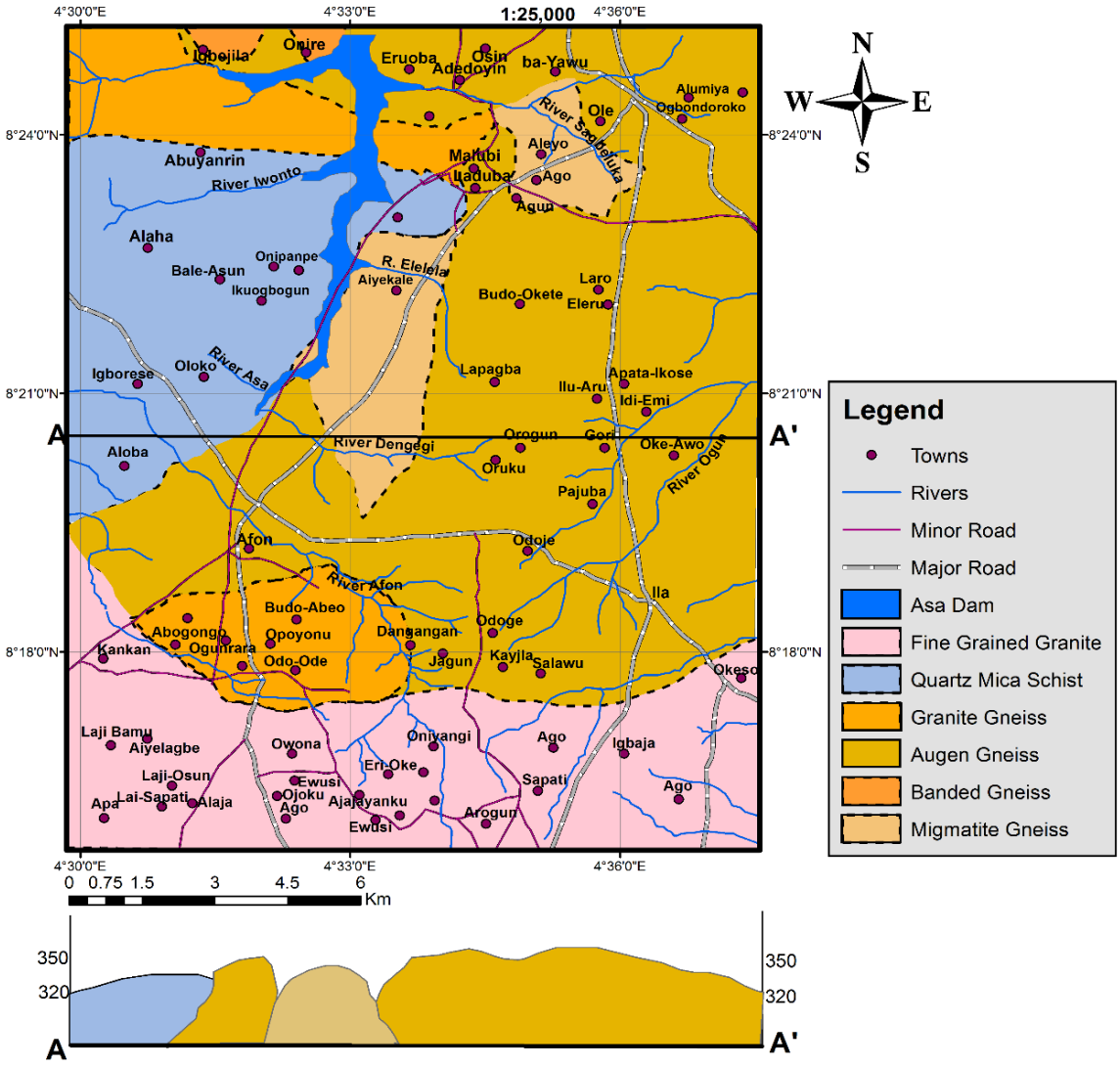


Figure 10: Geological map of the study area



Figure 11: Field photograph of migmatite gneiss showing joints, simple and asymmetrical folds at Ansarul Islam Secondary School premises, Laduba.

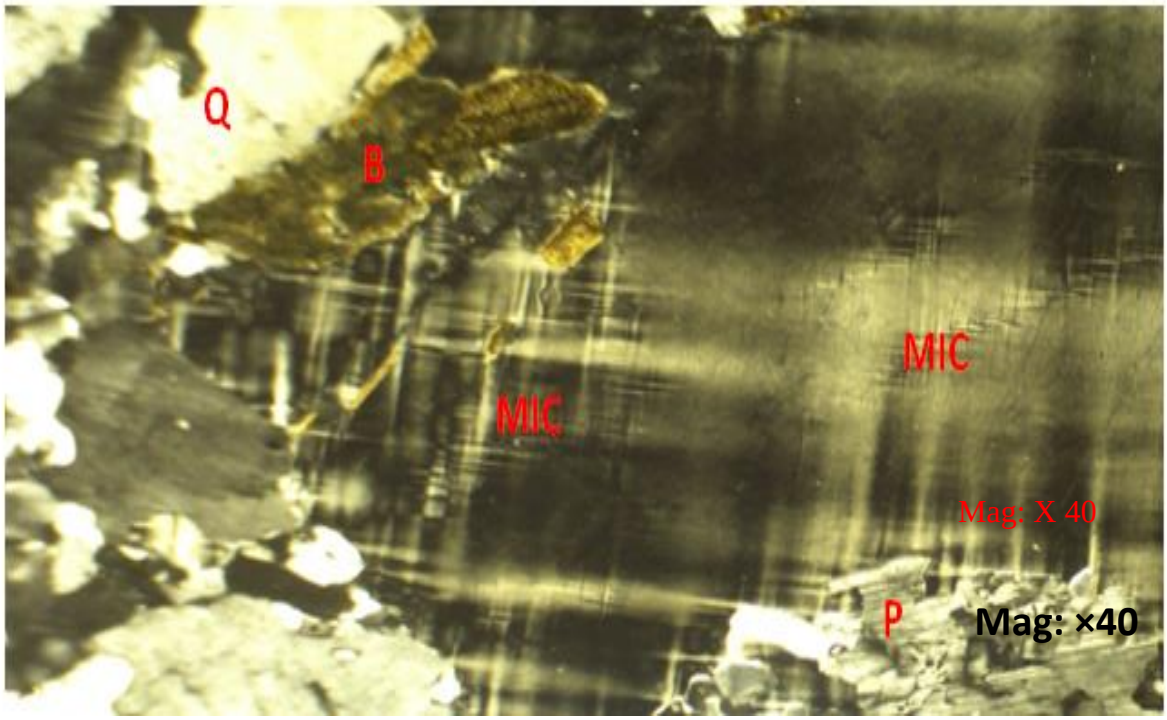


Figure 12: Photomicrograph of migmatite gneiss in cross polarized light (XPL).B = Biotite, MIC= microcline, Q= Quartz, and P= Plagioclase

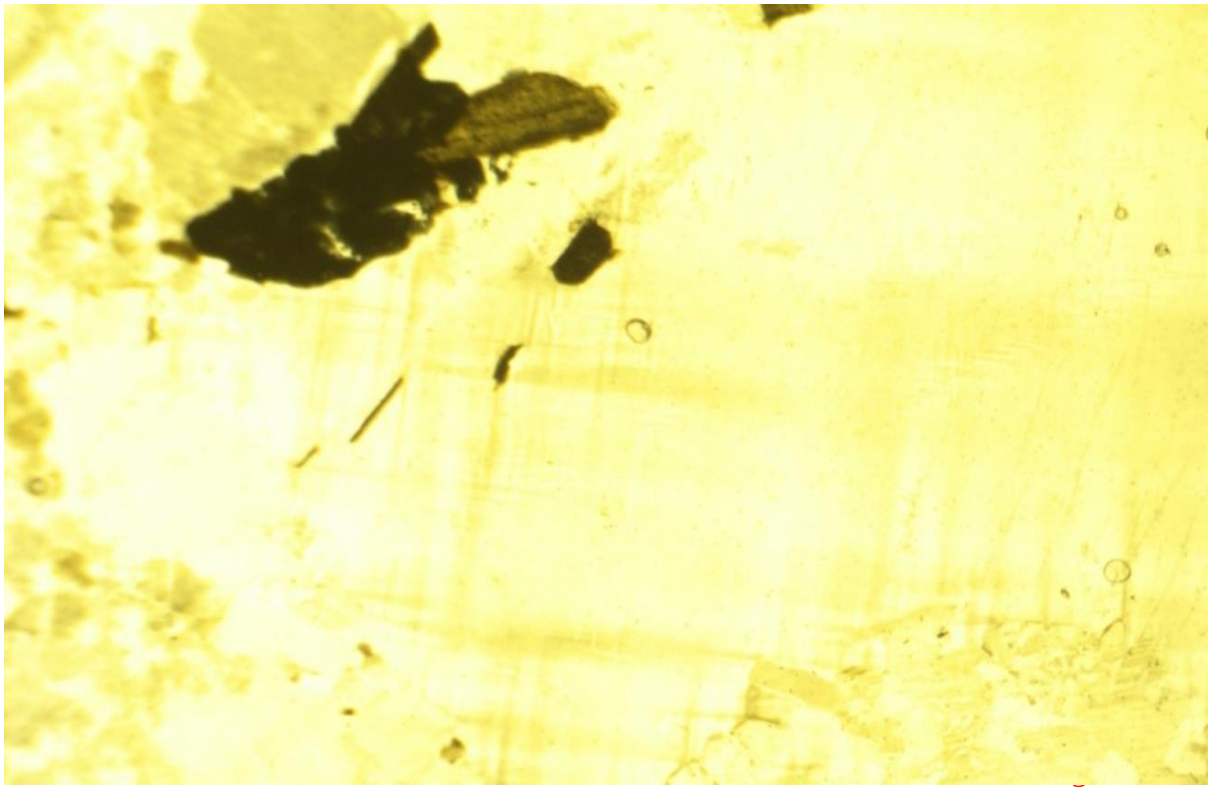


Figure 13: Photomicrograph of migmatite gneiss in plane polarized light (PPL)

4.1.1.2 Banded Gneiss

Banded Gneiss is one of the metamorphic rocks in the area, which shows banding characteristics with alternating layers of dark and light-coloured minerals (Figure 14).

The occurrence of this rock was found in the south-western part of the mapped area occupying about 5 % of the area (Figure 10). It is a high rising body of about 20 metres in height, dark greyish in colour and medium to coarse in texture. The outcrop at Odo-Ode has a foliation plane striking $S186^0W$ and dipping 68^0W as well as a prominent joint direction of $N50^0E$ (Figure 14).

The petrography, using the visual estimate method, revealed that the estimated modal compositions of the rock are Microcline (40%), quartz (30%), Biotite (25%), and opaque (5%) (Figure 15). Microcline is the dominant mineral in the rock; it is colourless but cloudy with low relief in PPL (Figure 16) but greyish in XPL with cross-hatch twinning (Figure 15). Quartz is anhedral, in equigranular and has no cleavage. Biotite is light brown but pleichroic from light to dark brown, sub-heudral in shape and has perfect cleavage.



Figure 14: Field photograph of Banded Gneiss at Odo-ode

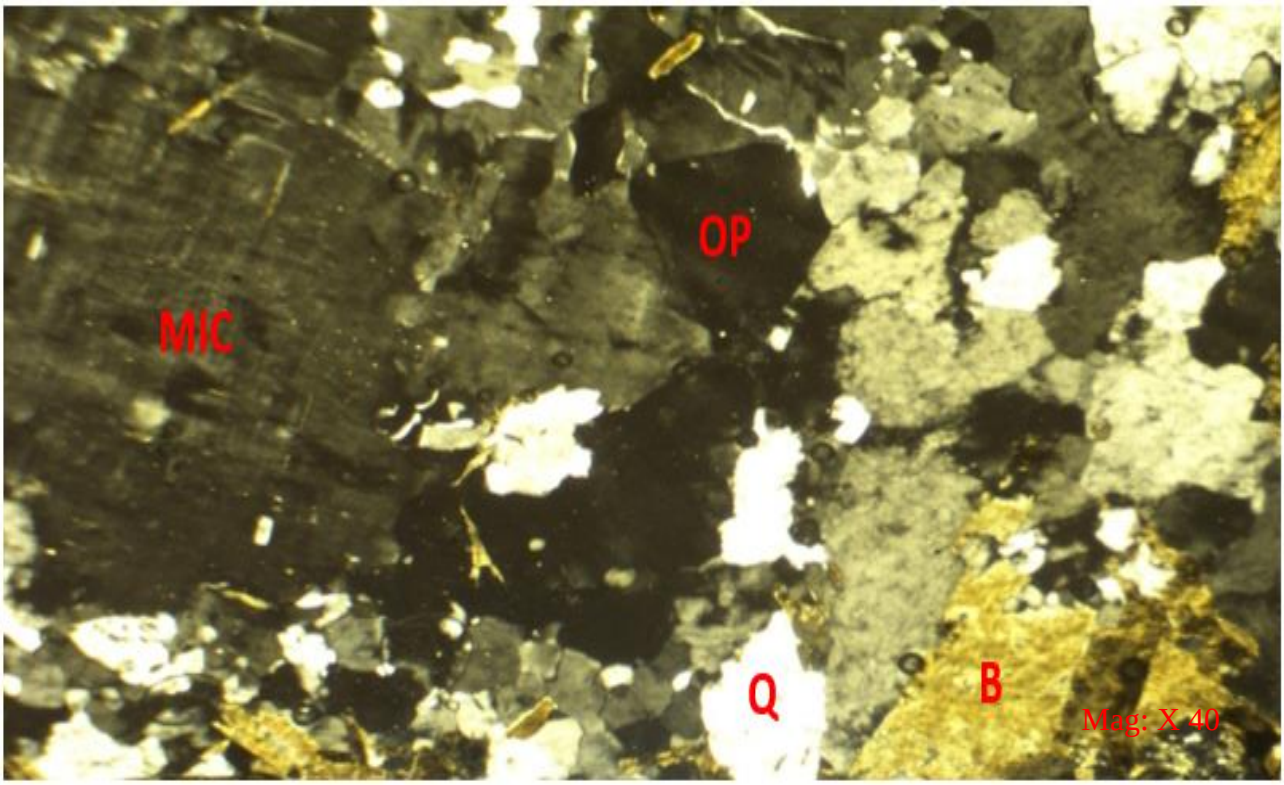


Figure 15: Photomicrograph of Banded gneiss in cross-polarized light (XPL).
B= biotite, MIC= microcline, Q= quartz, and OP= opaque

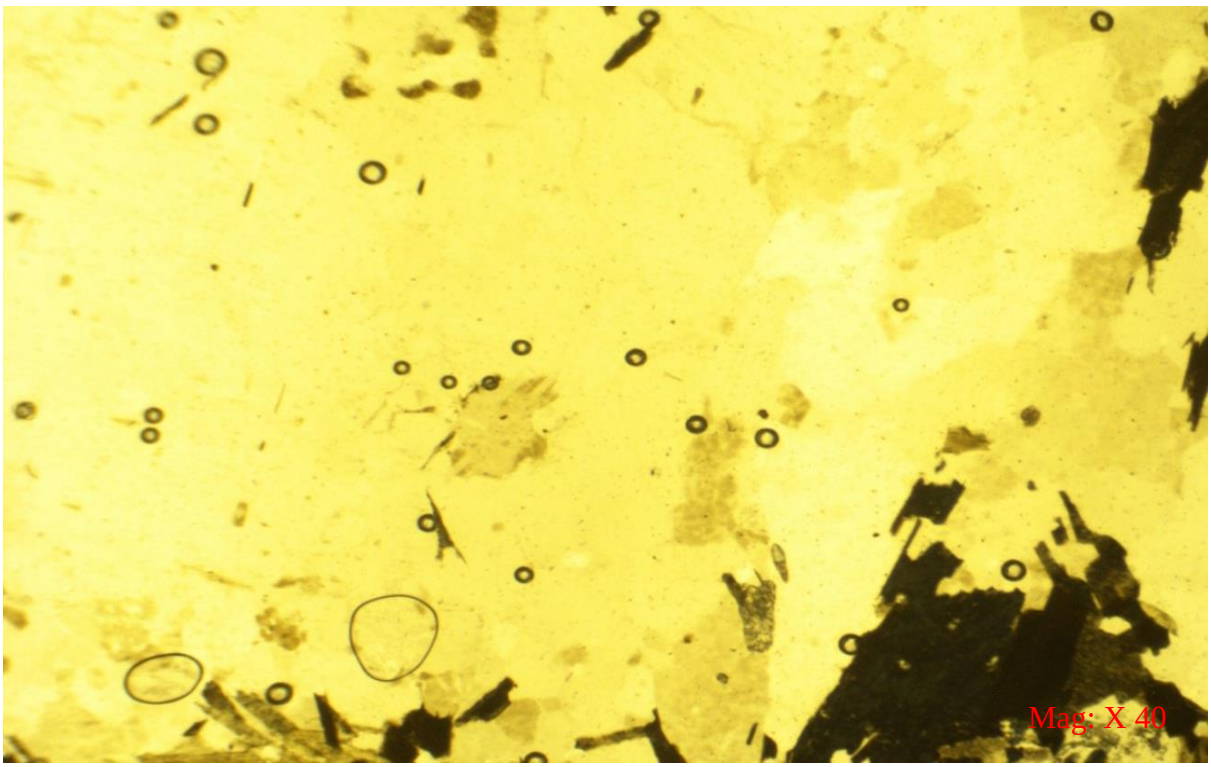


Figure 16: Photomicrograph of banded gneiss in plane polarized light (PPL).

4.1.1.3 Augen Gneiss

This is a high-grade metamorphic rock with eye structure. This eye structured gneiss, occupies the south-western part of the mapped area making up about 15% (Figure 10). The rock outcrops a low-lying body, it is light to pinkish in colour and coarse in texture. Settlements in the area where the rock is found include Osin Okete, Osin Idiemi, Osin Olokoto, Osin Aremu, Malubi and Ita-Elepa (Figure 10). At Osin Idiemi, the outcrop has a quartz-feldspar pegmatite intrusion with the width of 0.12cm (Figure 17). The Joint observed on the outcrop strikes S208^{0}W. The rock was also found in Osin Okete area (Figure 18) and Malubi with relics of pegmatite intrusion (Figure 19).

The petrographic study of the rock revealed that the mineral constituents of the rock are Quartz, microcline, myrmekite and biotite. From the visual estimate, the modal compositions of these minerals are Biotite (45%), Microcline (25%), Quartz (20%), and Myrmekite (10%). Biotite is the dominant mineral while myrmekite is the least (Figure 20) Myrmekite is an intergrowth between quartz and microcline feldspar. Quartz is the dominant mineral which is colourless in plane polarized light and anhedral in shape (Figure 21).

4.1.1.4 Granite Gneiss

This is a high-grade metamorphic rock found in the study area. Granite gneiss occurs essentially in the extreme north-western part of the study area which includes areas like Asa River, Sokoto and Tewure communities (Figure 10). At Asa River, the rock strikes in the North-South direction while the river flows in the East-West direction. At Asa River, on longitude 004^0 32' 46.4" E and latitude 08^0 25' 15.4" N the rock contains a prominent quartz-feldspar rich pegmatite vein of 0.1m width. There is a sinistral fault also observed on the outcrop (Figure 22).

At Sokoto and Tewure communities, the rock outcrops as low-lying bodies, light greyish in colour and medium to coarse in texture (Figure 23). Mineralogically, the rock contains quartz, K and Ca-rich feldspar and biotite.



Figure 17: Field photograph of Augen Gneiss at Osin-Idiemi with pegmatite vein intrusion.



Figure 18: Field photograph of Augen Gneiss at Osin-Olokete



Figure 19: Field photograph of Augen gneiss with relics of pegmatite intrusion at Malubi

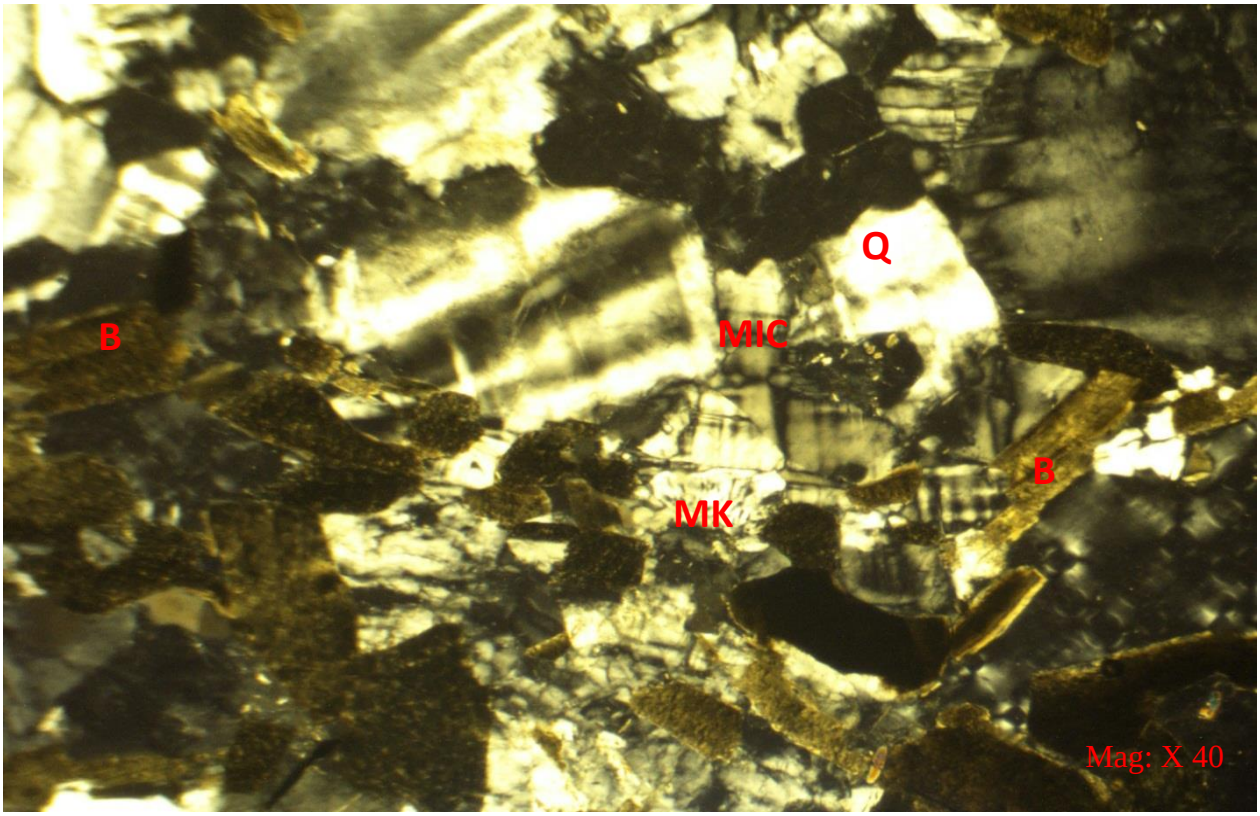


Figure 20: **Photomicrograph of Augen gneiss in cross polarized light. Q= quartz, IC= Microcline, B= biotite and MK= myrmekite.**

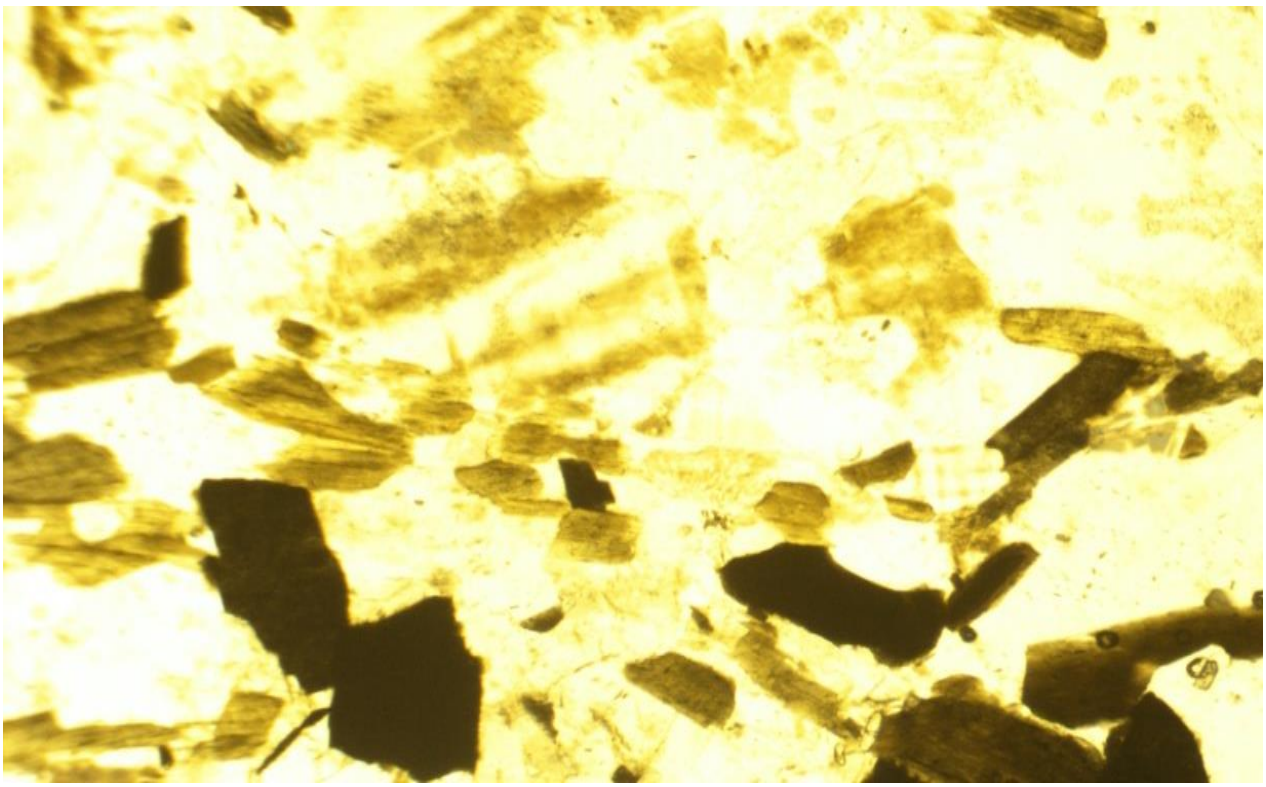


Figure 21: **Photomicrograph of Augen gneiss in plane polarized light.**



Figure 22: Field photograph of Granite Gneiss at Asa River on longitude 004^0 32' 46.4'' E and latitude 08^0 25' 15.4'' N showing sinistral fault and pegmatite vein.



Figure 23: Field photograph of Granite Gneiss at Sokoto community

The petrographic study shows that the rock contains quartz, microcline, plagioclase feldspar and biotite as its mineral constituents. The estimated modal compositions of the rock are quartz (40%), microcline (25%), plagioclase feldspar (20%) and biotite (15%) using the visual estimate method (Figure 24). Quartz is the dominant mineral which is colourless in plane polarized light and anhedral in shape (Figure 25). The microcline is the next abundant to quartz with across-hatch twinning, plagioclase feldspar that is sub-heudral in its habit shows a multiple albite twinning and biotite is sub-heudral and pleichroic from light brown to dark brown.

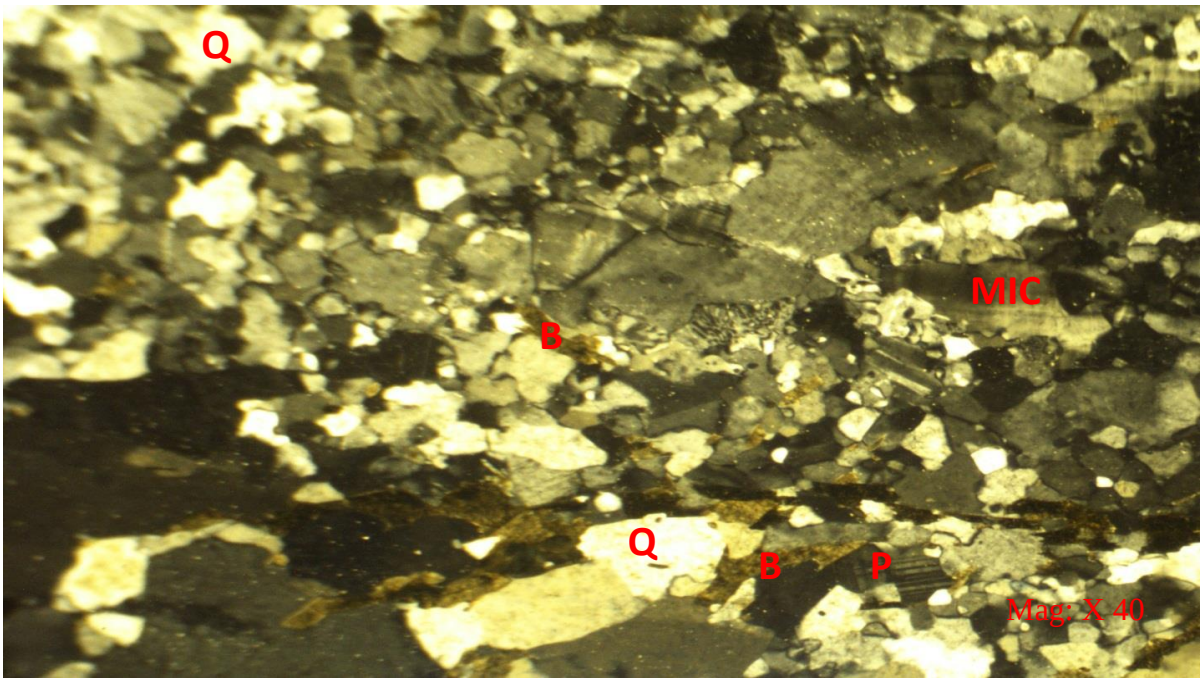


Figure 24: **Photomicrograph of granite gneiss at Sokoto and Tewure communities, in cross-polarized light. MIC = microcline, Q = quartz, B = biotite, P=plagioclase feldspar.**

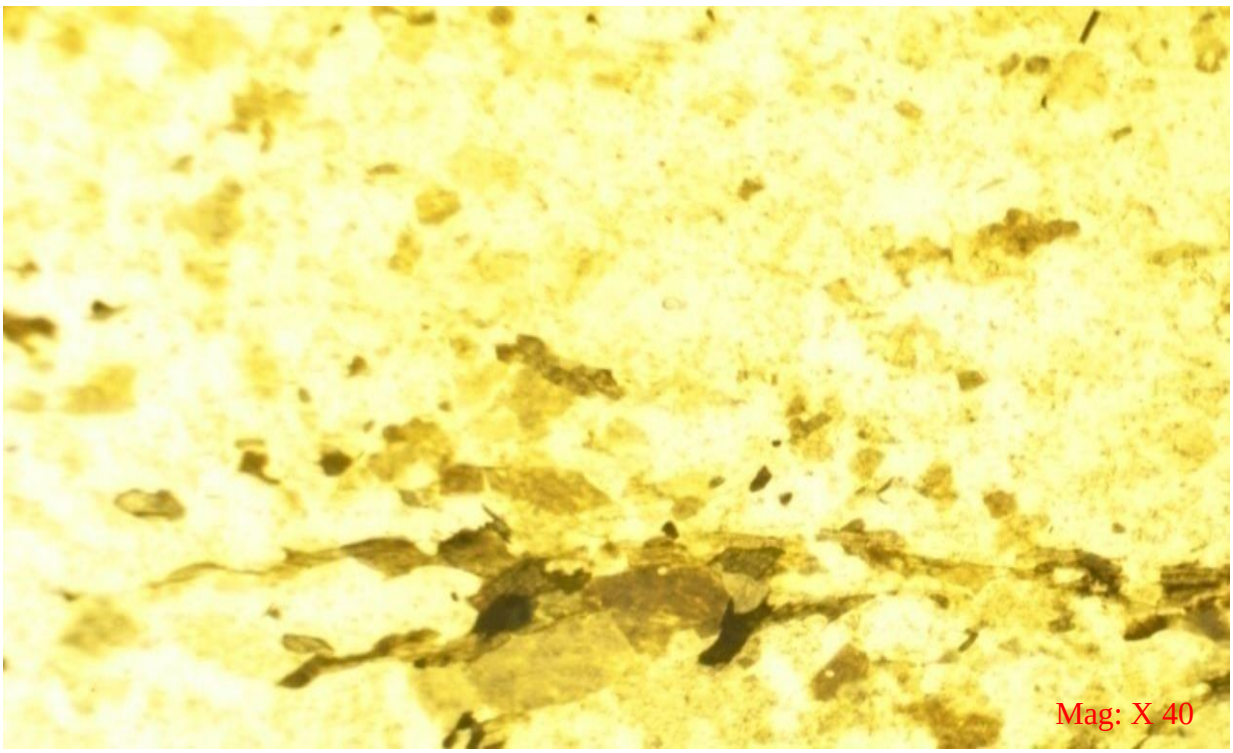


Figure 25: **Photomicrograph of granite gneiss at Sokoto and Tewure communities, in plane polarized light**

4.1.1.5 Quartz-Mica-Schist

This Schist is characterised with having quartz and mica as the dominant minerals in it. The outcrop occurs as a low-lying body which is exposed at the north-western part of the mapped area (Figure 10). It is light greyish in colour and medium to coarse grain in texture. The notable settlements in the area where the rock is found include Igbo-rese, Alaha, Abuyanrin and Arowosaye, covering about 10% of the study area. Using the hand lens specimen, the schist is composed of quartz, plagioclase feldspar, microcline and biotite. At Igborese, the schist is intruded by pegmatite of 0.3m wide that is rich in potassium feldspar (Figure 26).

The petrographic study of the rock in plane polarized light and cross-polarized light shows that the rock contains quartz, biotite, plagioclase feldspar, microcline and muscovite. Using the visual estimate method, the modal compositions of the rock are quartz (30%), biotite (35%), plagioclase feldspar (10%), microcline (10%), muscovite (10%) and myrmekite (5%) (Figure 27). Quartz dominates the rock while myrmekite occurs as the least. Quartz is colourless, anhedral and has un-equal grain. Biotite shows a moderate relief and has perfect cleavage in plane-polarized light (Figure 28). Plagioclase feldspar is sub-heudral in its habit and shows a multiple albite twinning. Microcline is greyish in cross-polarized light with cross hatch twinning, muscovite is greenish in cross-polarized light and brownish in plane polarized light and myrmekite is an intergrowth between quartz and feldspar.

4.1.1.6 Fine-Grained Granite

This fine-grained rock, dark greyish was exposed in the southern part of the mapped area (Figure 10). The outcrop is exposed as a low-lying body at Alapako Etile, Ewusi, Kankan and along Sapati Oko road. At Alapako Etile and Ewusi, the granite was found intruded by quartz-feldspar pegmatite of about 1.5 m long and 0.5m wide (Figure 29).



Figure 26: Field photograph of Quartz-Mica-Schist intruded by pegmatite rich in potassic feldspar at Igborese.

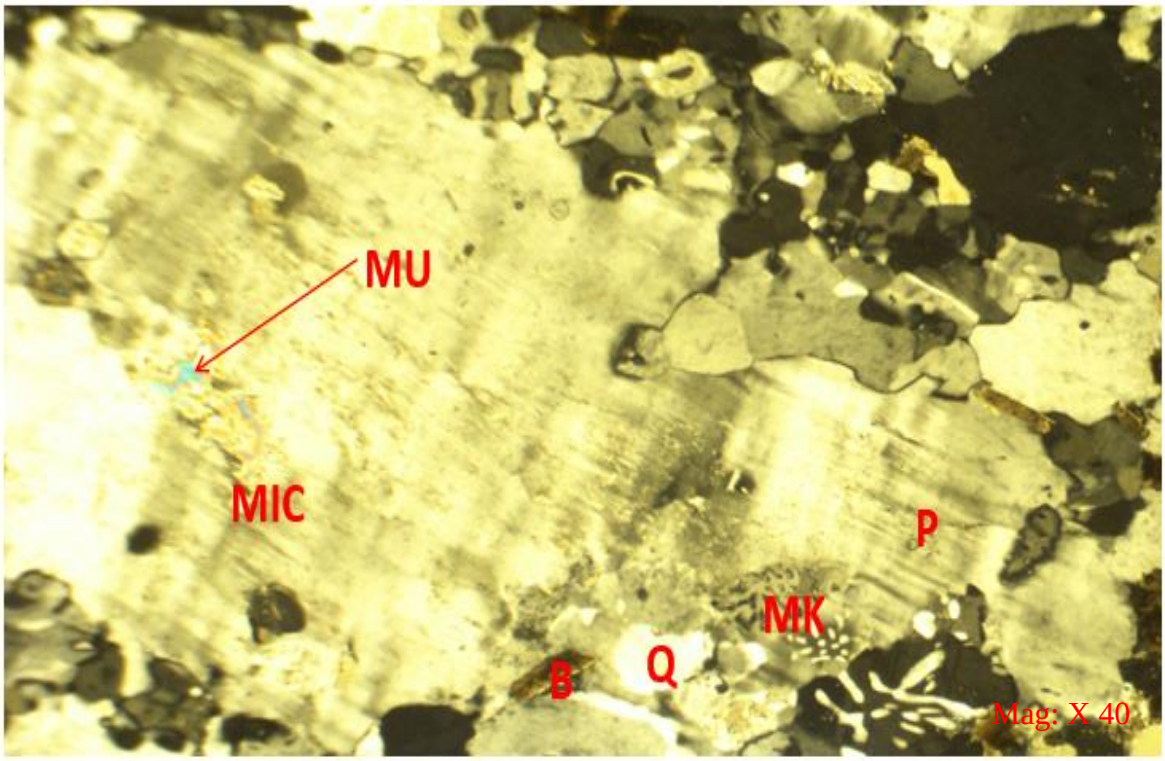


Figure 27: **Photomicrograph of Quartz-Mica-schist in cross polarized light. Q=quartz, B= biotite, P= plagioclase feldspar, MIC= microcline, MU= muscovite, MK=myrmekite**

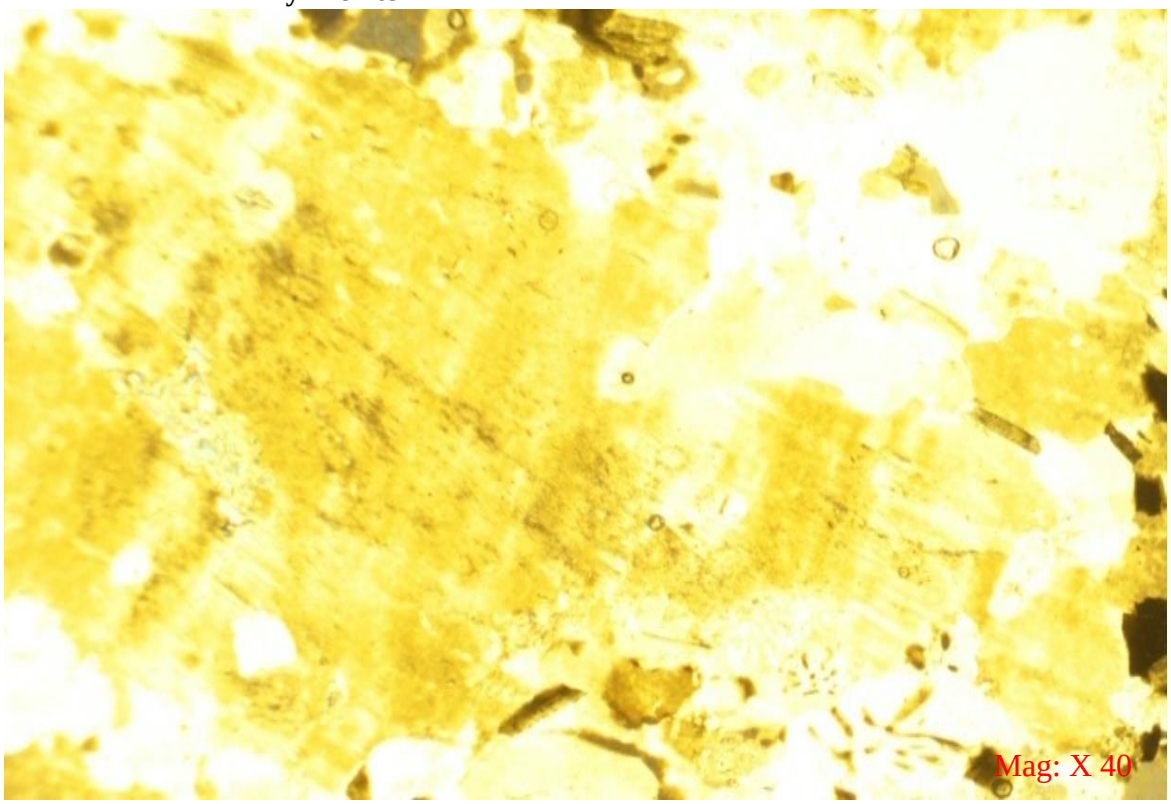


Figure 28: **Photomicrograph of quartz- mica- schist in plane polarized light**



Figure 29: Field photograph of fine grained granite with quartzo-feldsparthic Pegmatite vein and an anticlinal fold at Alapako Etile

The petrographic study of the rock in plane-polarized light and cross-polarized light has shown that the rock contains quartz, biotite, microcline, and sericite as its mineral constituents. The modal analysis was visually estimated from the microscope is quartz (35%), biotite (30%), microcline (20%), plagioclase feldspar (10%) and sericite (5%). Quartz is the dominant mineral with the highest percentage while sericite is the least (Figure 30). Quartz is anhedral and in-equigranular, biotite has perfect cleavage in plane polarized light and pleichroic, and microcline is greyish in plane-polarized light (Figure 31) with cross-hatch twinning in cross-polarized light. Sericite is an accessory mineral of the composition.

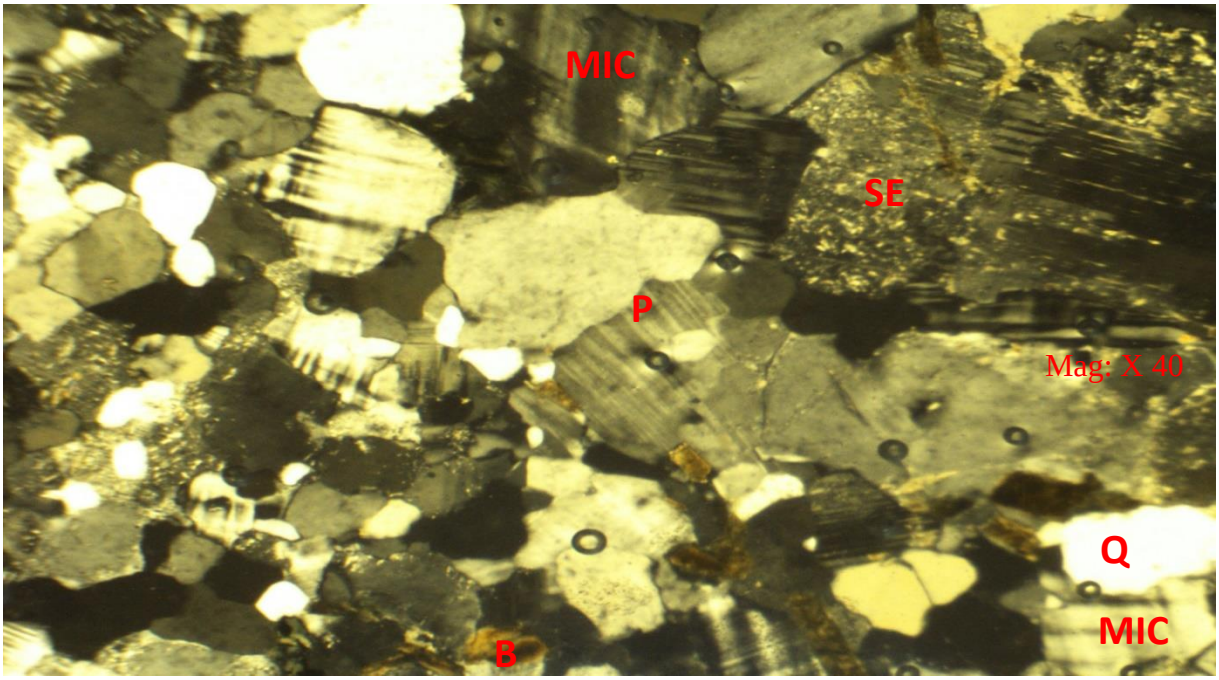


Figure 31: **Photomicrograph of fine-grained granite at Ansarul Islam Secondary School premises, Laduba, in cross-polarized light. Q= quartz, B= biotite, MIC= microcline, P= plagioclase and SE= sericite**

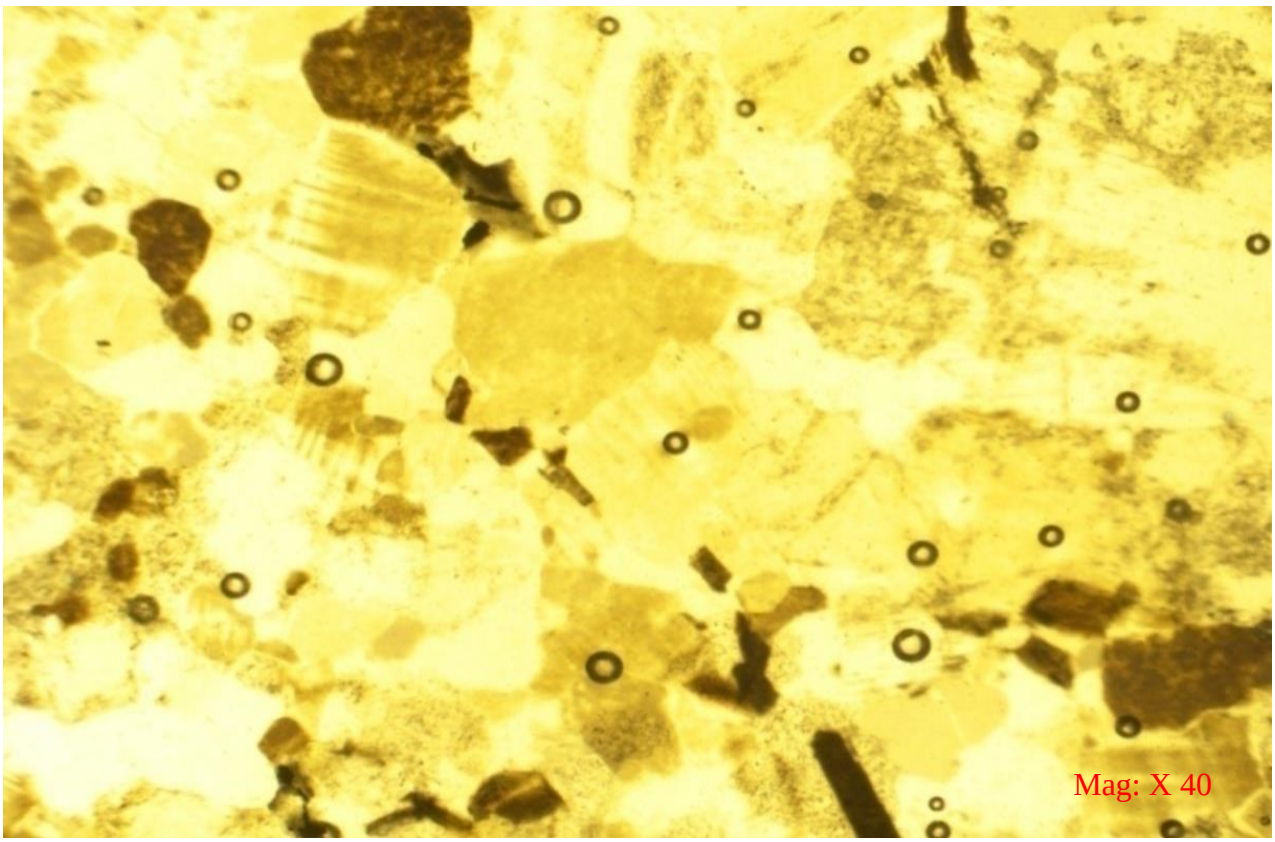


Figure 30: **Photomicrograph of fine-grained granite at Ansarul Islam Secondary School premises, Laduba, in plane-polarized light.**

4.1.2 Geologic structures of the study area

The study area has undergone some tectonic events resulting in the deformation of the rocks in the area. The structural elements resulting from the deformation are ductile and brittle features. The ductile structures include foliations and folds while the brittle structures include joints and faults.

1. Foliations

Foliations were in the porphyroblastic gneiss, augen gneiss, granite gneiss and quartz mica-schist. The foliations in the gneisses are marked by alternating bands of dark and coloured minerals. The dark minerals include biotite, and hornblende while the light minerals include quartz and feldspar. The foliations in the area trend majorly in NWN-SES (Figure 33).

2. Folds

Folds were observed in the migmatite gneiss and fine-grained granite of the area. The folds include simple, asymmetrical and anticlinal folds. The simple and asymmetrical folds were found at Ansarul Islam Secondary school, Laduba (Figure 11). The anticlinal fold was found at Alapako etile (Figure 29).

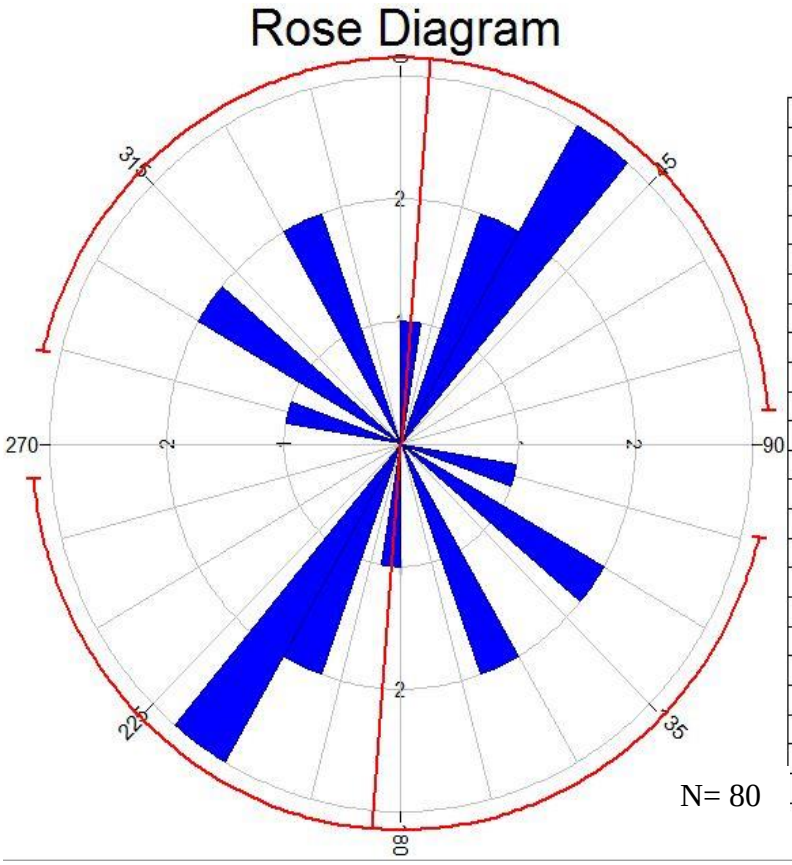
3. Micro faults

The micro fault occurred in the granite gneiss and the sense of its displacement is sinistral as observed at the Asa river extreme edge (Figure 22)

4. Joints

An open joint was observed in Banded gneiss at Odo-ode and Sokoto community (Figure 14) The joints trend majorly in NNE- SSW direction.

a. Rose Diagram Depicting Orientations of Joints



Statistical Summary	
Calculation Method:	Frequency
Class Interval:	10.0 Degrees
Azimuth Filtering:	Deactivated
Data Type:	Bidirectional
Population:	11
Total Length of All Lineations:	22.0
Maximum Bin Population:	3.0
Mean Bin Population:	1.83
Standard Deviation of Bin Population:	0.72
Maximum Bin Population (%):	13.64
Mean Bin Population (%):	8.33
Standard Deviation of Bin Population (%):	3.26
Maximum Bin Length:	3.0
Mean Bin Length:	1.83
Standard Deviation of Bin Lengths:	0.72
Maximum Bin Length (%):	13.64
Mean Bin Length (%):	8.33
Standard Deviation of Bin Lengths (%):	3.26
Vector Mean:	4.5 Degrees
	184.48 Degrees
Confidence Interval:	80.5 Degrees
	(95 Percent)
R-mag:	0.29

Figure 32: Rose diagram showing the structural trends of joints in the study area

The joints occurring in the rocks of the area were a result of compressional forces acting on the rocks, thereby creating a strain in form of joints in the rock. These joints are usually perpendicular or in opposite direction to the forces. From the diagram, the major joints in the area trend in the NNE-SSW direction with other ones trending in the NNW-SSE direction.

b. Rose Diagram Depicting Orientations of Foliations

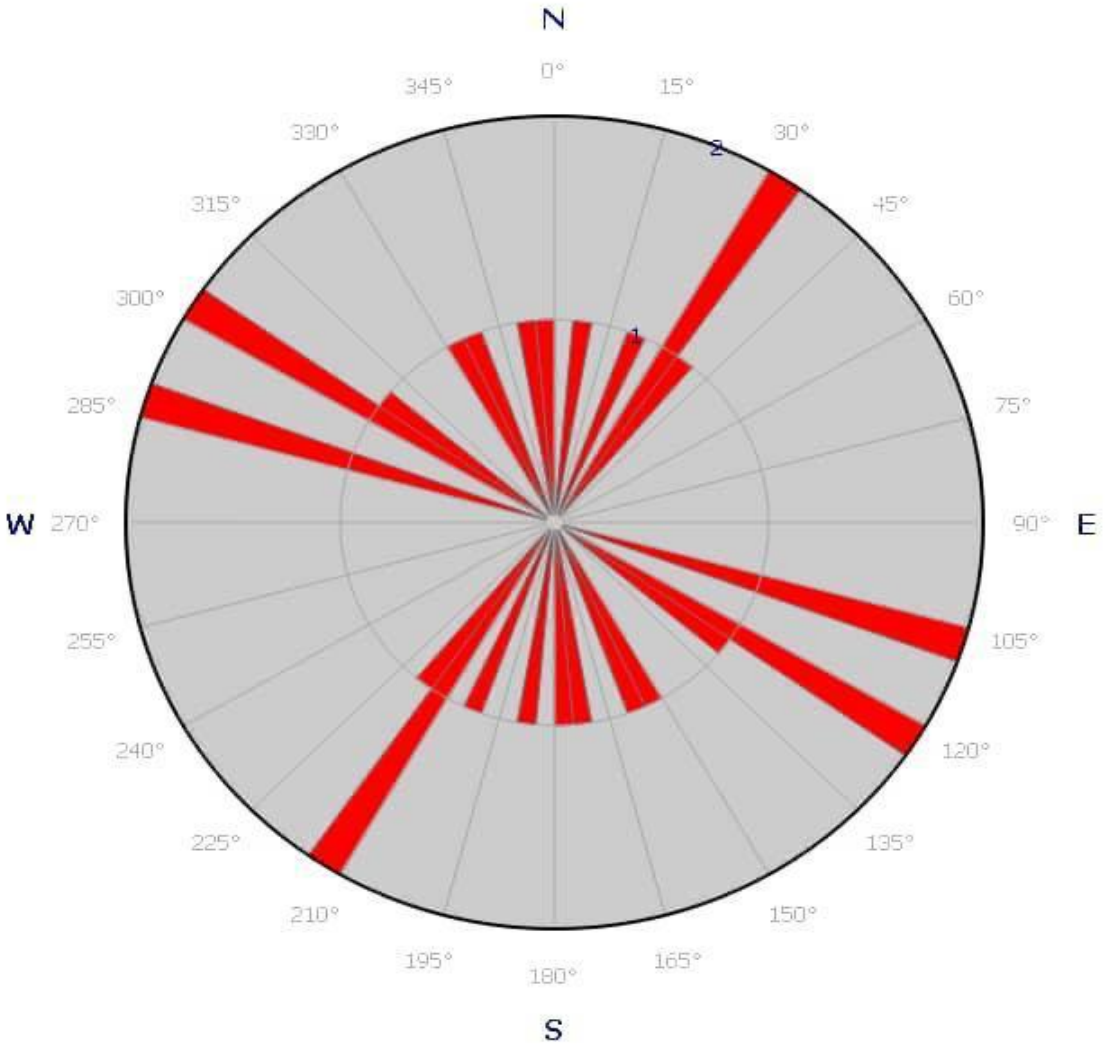


Figure 33: Rose diagram showing the foliation planes in the study area

The major trend of the foliations is in the NWN-SES direction with minors in the NNE-SSW direction.

The structural trends of the rocks in the area from the rose diagram are basically in NNE-SSW and NWN-SES directions. The NNE-SSW conforms with the observation of Umego (1990) while the NWN-SES conforms to the global structural trend existing in the Basement Complex of Nigeria, as reported by McCurry (1976), Oluyide (1988) and Oyawoye (1964).

4.2 Aquifer types in the study area

There are two major aquiferous units in the area and these are (i) overburden and (ii) Fractured crystalline aquifers. These two aquifers are of different groundwater potentials and characteristics. The depth to the weathered zone varies and depends largely on the composition and texture of the parent rock together with the density of the regional fracture field.

4.2.1 The overburden aquifer

The overburden aquifer in the study area is found within the weathered profiles of the Basement rocks that overly the fresh bedrock units and includes the in-situ decomposed rock. Figure 34shows the weathered profiles of weathered pegmatite overlying the dark grayish and fractured granite at Ago Agbona village in the study area.

The overburden materials which include laterites, clay/sandy material and broken rocks of the weathered Basement show that the aquifer is highly heterogeneous and the groundwater potentials of the Basement Complex have been greatly enhanced due to the breakdown of these basement rocks. This is so because appreciable porosity and permeability which are the key factors for groundwater potentials might have been developed through the breaking down or weathering process of the basement rocks.

The most important factor governing groundwater resources in this aquifer is the thickness of the aquifer which ranges from 1.58 m to 27.5m in the different rock settings occurring in the boreholes available in the area. Relating this aquifer thickness range with the depth of the aquifer which ranges from 2.34 m to 36.8 m in the boreholes of the area, it is justified that groundwater occurrence in this aquifer provides high yields. This is so because the aquifer thickness is high and optimally, boreholes should be sited in zones of maximal aquifer thickness, which will provide the highest yield.

4.2.2 The fractured crystalline aquifer

The fractured crystalline aquifer underlies the overburden aquifer in the study area. The availability of groundwater in this aquifer depends on the volume and the extent of joints and fractures in the aquifer (Clark, 1985, Tijani, 1994). The occurrence of groundwater in the crystalline basement rocks is in facture systems within the fresh bed rocks.

In the study area, figure 35 depicts a fractured crystalline aquifer at Ila-Oja. The figure shows the weathered profiles of quartz intrusions and feldspar grains overlying the slightly fractured pegmatite vein in quartz granite which also overlies the fractured basement plus pegmatite, quartz intrusions and water.

In borehole drilling, the fractured crystalline aquifer is commonly regarded as a source of groundwater because of its extensive depth, but yields are typically low in some boreholes and the low storage capacity makes some boreholes prone to drying up during the dry season. High yields in boreholes are encountered where overburden aquifer and fractured crystalline aquifer are complementary or connected.

Wright and Burgess (1992) stated that the optimum drilling depth in the crystalline Basement Complex can be the minimum depths at which adequate yield can be obtained and with a specific capacity which keeps pumps and costs to a minimum. However, the maximum depth determined from the borehole logs available in the study area is 40 m which taps a fractured crystalline aquifer.

Location: Ago-Agbona.

measurements are in meters. Hole and casing diameters are in inches scale: 1cm=2units

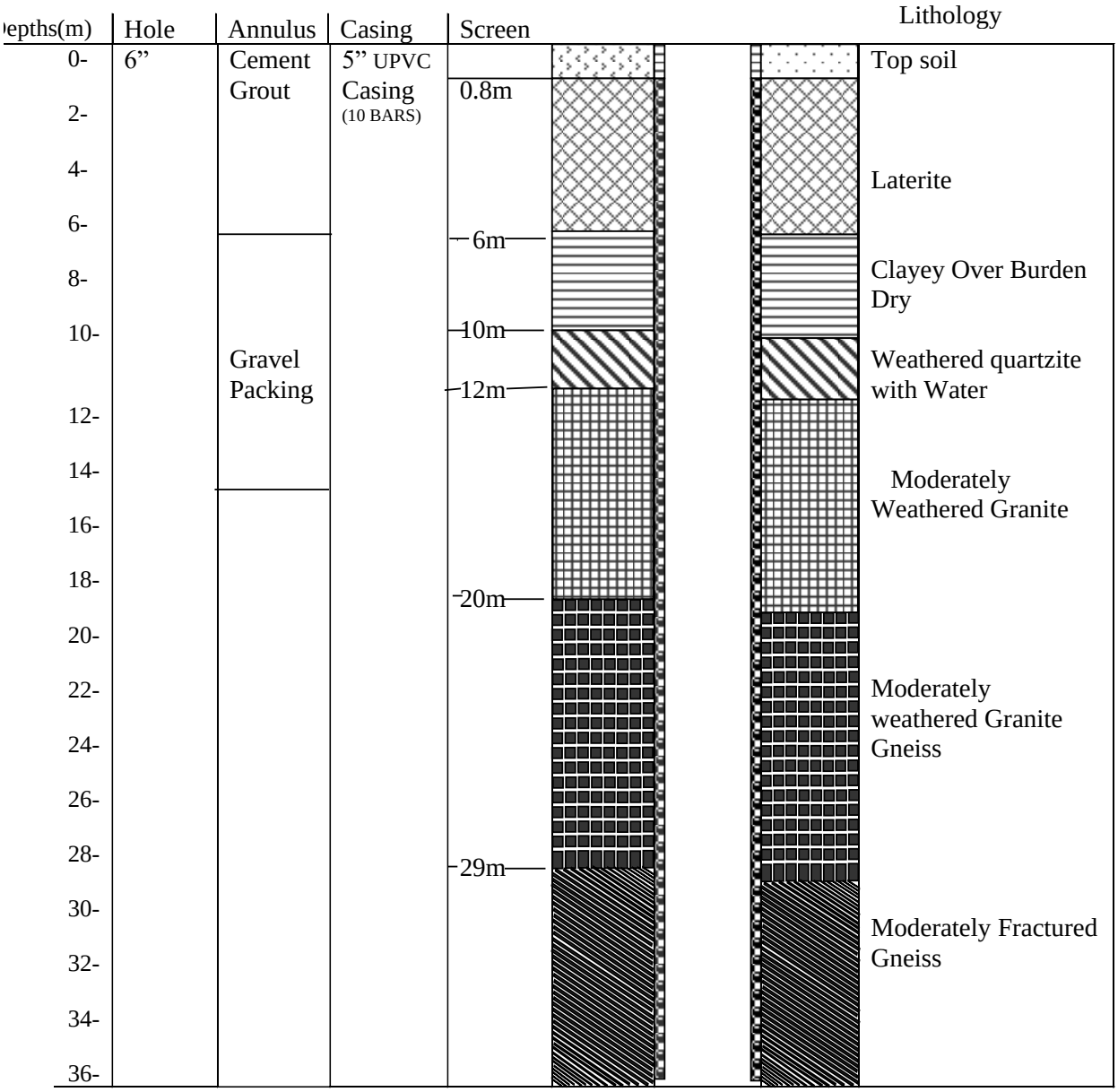


Figure 34: Borehole log of Ago- Agbona in the study area depicting an overburden aquifer

Source: Kwara State Ministry of Water Resources, Ilorin. Drill-Date: 14-06-1996

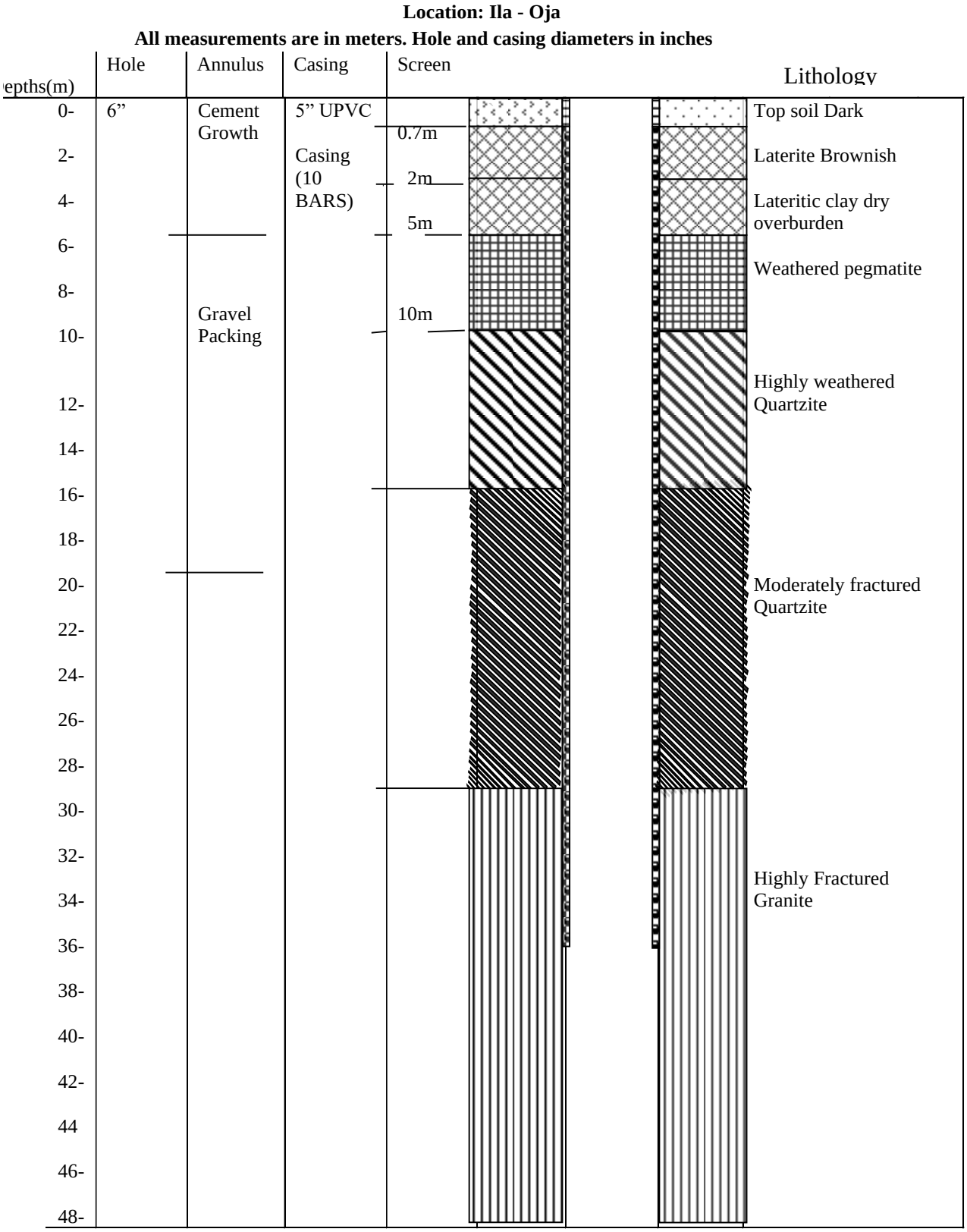


Figure 35: Borehole log of Ila-Oja in the study area depicting a fractured aquifer

Source: Kwara State Ministry of Water Resources, Ilorin. Drill-Date: 14-06-1996

Results show that groundwater in the study area occurs in the weathered overburden of the Basement Complex rocks and the joints and fracture system of unweathered rock units. This is in line with Deming (2002) who equally confirmed that Groundwater is held in porous formations which are rocks containing a relatively large portion of void spaces.

4.3 Hydraulic Characteristics of Aquifers in the Study Area

The assessment of aquifer hydraulic characteristics from well performance data is complicated by some factors which include; interdependence of well design, the aim of each drilling testing program, the sitting techniques used and the hydrogeological setting of the aquifers.

The hydraulic aquifer characteristics calculated in the study area are hydraulic conductivity denoted by (K) which sometimes is referred to as the coefficient of permeability, coefficient of transmissivity denoted by (T) and coefficient of Storativity or storage coefficient denoted by (S). These parameters were calculated for the available six boreholes in the study area as shown below and the summary of the results obtained is presented in Table 1.

The hydraulic conductivity values of the aquifers range from 3.23×10^{-2} m /day to 2.99×10^{-1}m/day with a mean of 2.83×10^{-1}m/day, Transmissivity values of the aquifers range between 3.49 m^2/day and 8.50 m^2/day with an average value of 5.61 m^2/day and Storage coefficient values vary from 3.45 to 9.15 with a mean of 5.03.

From Table 1, it was observed that the storage coefficients of Reke,Ita-Elepa, Ganmo, Osin-Aremu and Amayo boreholes (3.45, 3.57, 4.28, 5.72 and 9.15 respectively) are of metamorphic origin with thicker overburden than that of Budo-Ojoku (4.06) which is of granitic origin

Table 1: Calculated Values of Hydraulic Conductivity, Transmissivity and Storage coefficient obtained from available boreholes in the area

Names of the boreholes	Hydraulic Conductivity(m/day)	Transmissivity (m^2/day)	Storage coefficient	Bedrock types
Reke Village	2.99×10^{-1}	6.19	3.45	Porphyroblasic gneiss
Ita –Elepa	3.23×10^{-2}	3.68	3.57	Augen gneiss
Ganmo	2.84×10^{-1}	8.50	4.28	Porphyroblasic gneiss
Osin Aremu	8.10×10^{-2}	5.91	5.72	Augen gneiss
Budo- Ojoku	7.64×10^{-2}	3.49	4.06	Fine grained granite
Amoyo	2.18×10^{-1}	5.90	9.15	Porphyroclasic gneiss

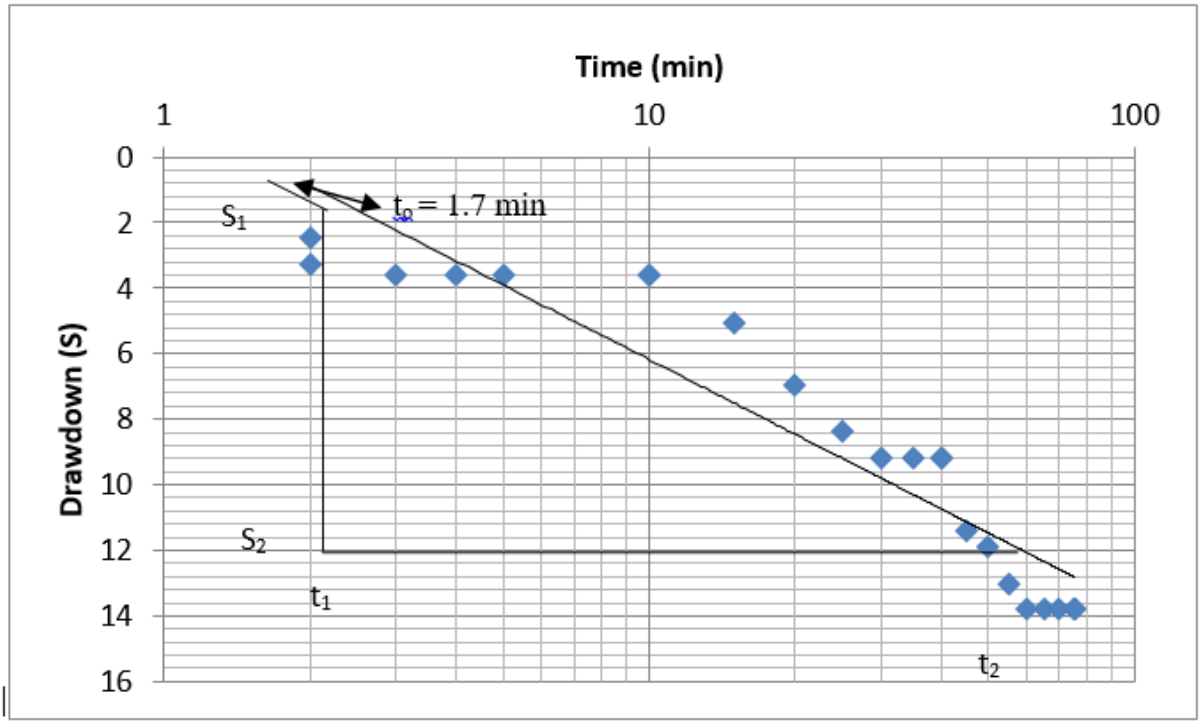


Figure 36: Plot of drawdown versus time for Reke water side

$$\textbf{\textit{Transmissivity}}\ (T) = \frac{2.30Q\log\frac{t_2}{t_1}}{4\pi\Delta S} = \frac{2.3X0.25X10^3 log30}{4X3.142X10.9} = 6.19\ m^2/day$$

$$\textbf{\textit{Hydraulic conductivity}}\ (K) = \frac{T}{b} = \frac{6.19}{20.7} = 2.99X10^{-1}\frac{m}{day}$$

Where T= transmissivity, b= Aquifer saturated thickness = Total depth of borehole – Static water level

T = 6.19m^2/day b= 25m- 4.3m = 20.7m

$$\textbf{\textit{Storativity}}\ (S) = \frac{2.25Tt_0}{r^2} = \frac{2.25X6.19X0.001}{(0.635)^2} = 3.45\ units$$

Where T= transmissivity, $t_{0=}$ time intercept at zero drawdown = 1.7min, r = radius of the borehole = 0.0635

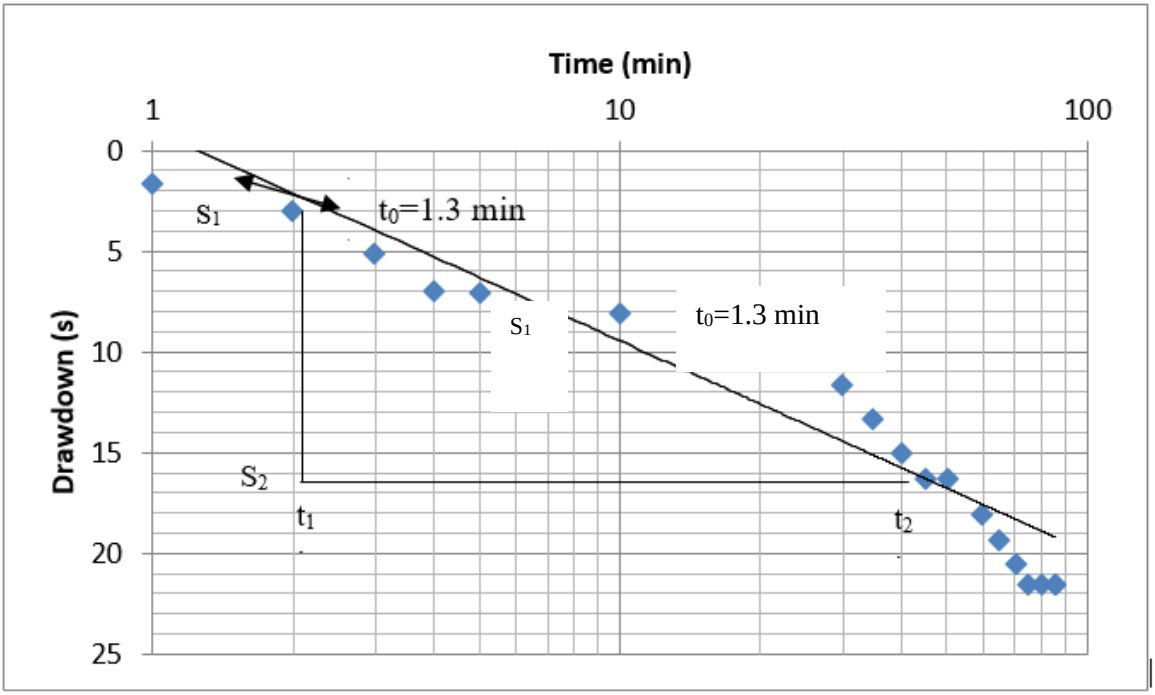


Figure 37: Plot of drawdown versus time for Ganmo water side

$$\textbf{\textit{Transmissivity}}(T) = \frac{2.30Q\log\frac{t_2}{t_1}}{4\pi\Delta S} = \frac{2.3X0.5X10^{3}log20}{4X3.142X14.0} = 8.57\ m^2/day$$

Where Q = quantity discharged (l/s) = 0.5×10^{-3}, t_2= 40 min, t_1= 2 min, ΔS = 16m- 2.0m= 14.0m

$$\textbf{\textit{Hydraulic conductivity}}\ (K) = \frac{T}{b} = \frac{8.50}{29.9} = 2.84X10^{-1}\ m/day$$

Where T= transmissivity, b= Aquifer saturated thickness = Total depth of borehole – Static water level

$$\textbf{\textit{Storativity}}\ (S) = \frac{2.25Tt_0}{r^2} = \frac{2.25X8.50X9.0277X10^{-4}}{(0.635)^2} = 4.28\ units$$

Where T= transmissivity, t_0 = time intercept at zero drawdown = 1.3min, r = radius of the borehole = 0.0635

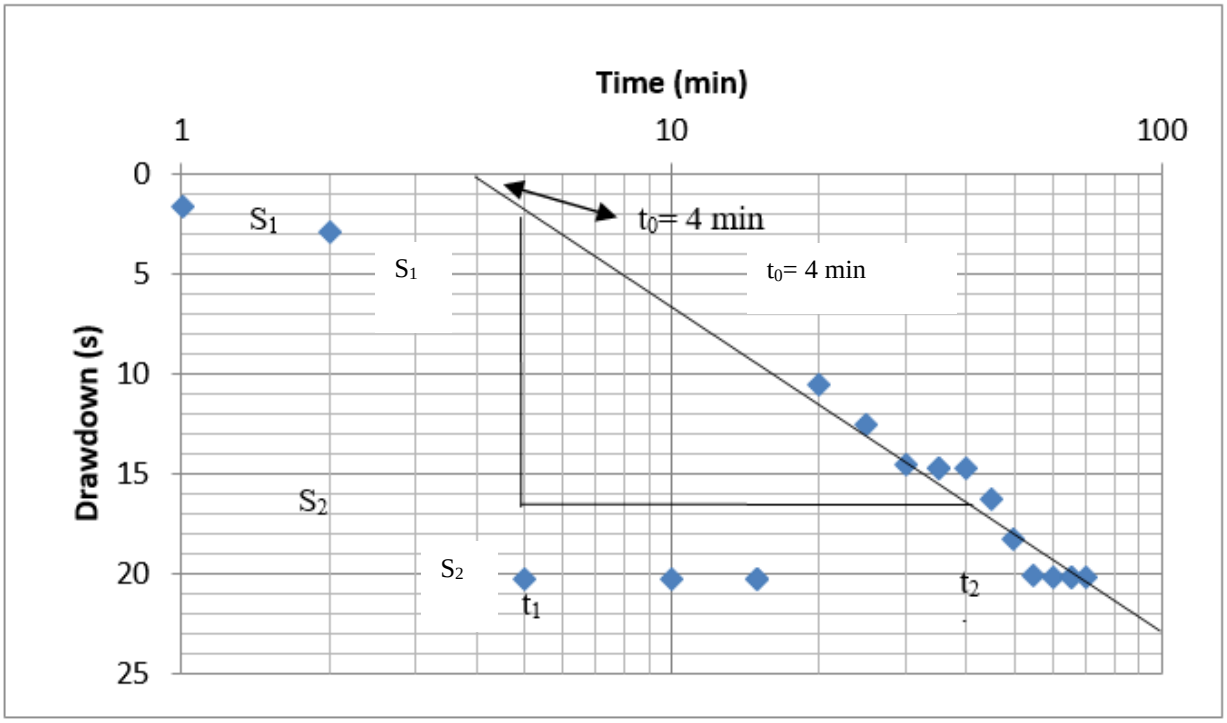


Figure 38: Plot of drawdown versus time for Amayo water side

$$\textbf{\textit{Transmissivity}}\ (T) = \frac{2.30Q\log\frac{t_2}{t_1}}{4\pi\Delta S} = \frac{2.3X0.5X10^{-3}log8}{4X3.142X14.0} = 5.90\ m^2/day$$

Where Q = quantity discharged (l/s) = 0.5×10^{-3}, t_2= 40 min, t_1= 5 min, ΔS = 16m- 2.0m= 14.0m

$$\textbf{\textit{Hydraulic conductivity}}\ (K) = \frac{T}{b} = \frac{5.90}{27.1} = 2.18X10^{-1}\ m/day$$

Where T= transmissivity, b= Aquifer saturated thickness = Total depth of borehole – Static water level

T = 5.90 m^2/day, b= 31m- 3.90 m = 27.1 m

$$\textbf{\textit{Storativity}}\ (S) = \frac{2.25Tt_0}{r^2} = \frac{2.25X5.90X2.778X10^{-3}}{(0.635)^2} = 9.15\ units$$

Where T= transmissivity, t_0 = time intercept at zero drawdown = 4 min, r = radius of the borehole = 0.0635

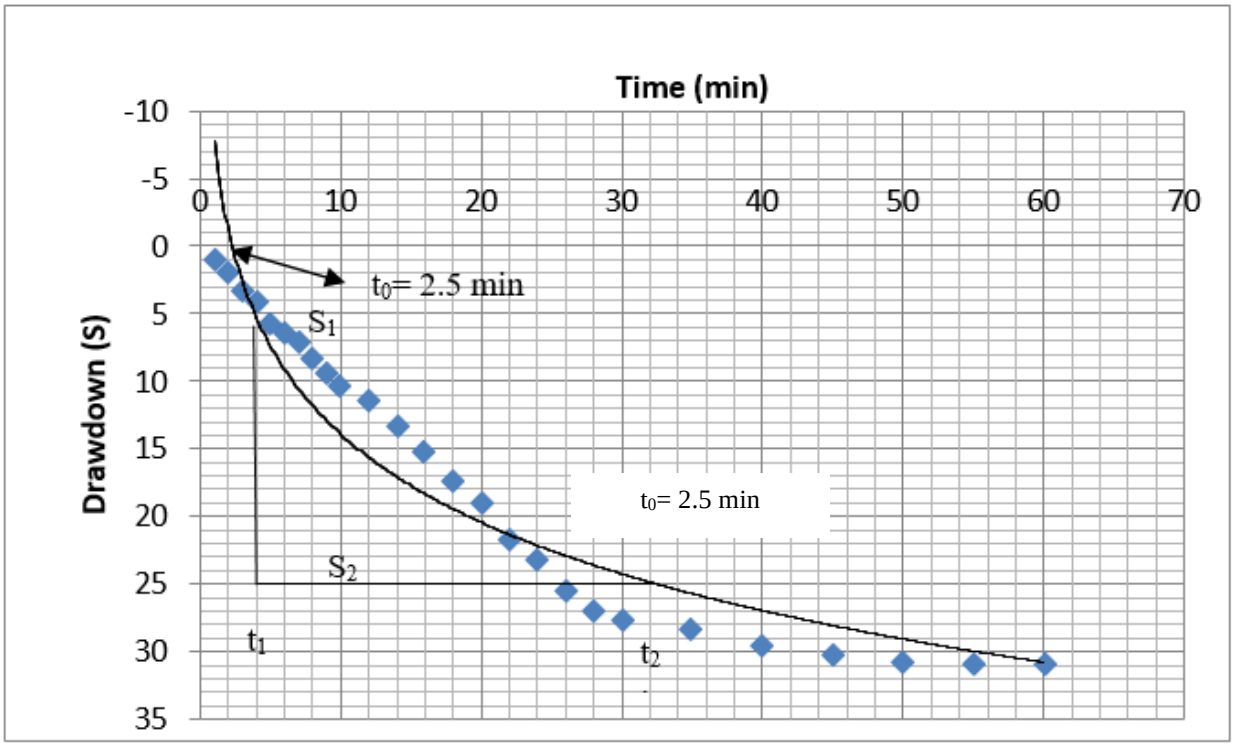


Figure 39: Plot of drawdown versus time for Osin- Aremu water side

$$\textbf{\textit{Transmissivity}}\ (T) = \frac{2.30Q\log\frac{t_2}{t_1}}{4\pi\Delta S} = \frac{2.3X0.68X10^{-3}log8}{4X3.142X19.0} = 5.91\ m^2/day$$

Where Q = quantity discharged (l/s) = 0.68× 10^{-3}, t_2= 32 min, t_1= 4 min, ΔS = 25m- 6.0m= 19.0m

$$\textbf{\textit{Hydraulic conductivity}}\ (K) = \frac{T}{b} = \frac{5.91}{72.93} = 8.10X10^{-2}\ m/day$$

Where T= transmissivity, b= Aquifer saturated thickness = Total depth of borehole – Static water level

T = 5.91 m^2/day, b= 82.12m- 9.19 m = 72.93 m

$$\textbf{\textit{Storativity}}\ (S) = \frac{2.25Tt_0}{r^2} = \frac{2.25X5.91X1.736X10^{-3}}{(0.635)^2} = 5.72\ units$$

Where T= transmissivity, t_0 = time intercept at zero drawdown = 2.5 min, r = radius of the borehole = 0.0635

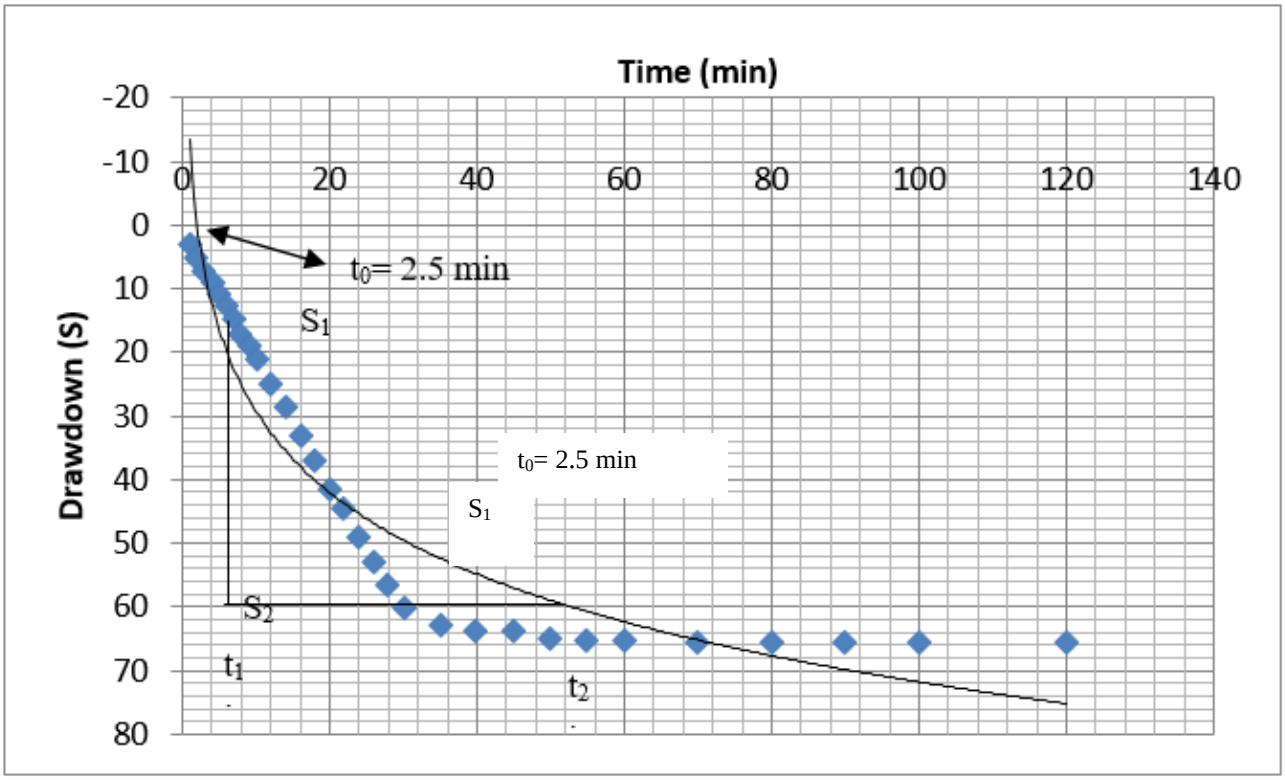


Figure 40: Plot of drawdown versus time for Ita - Elepa water side

$$\textbf{\textit{Transmissivity}}\ (T) = \frac{2.30Q\log\frac{t_2}{t_1}}{4\pi\Delta S} = \frac{2.3X0.83X10^{-3}log13}{4X3.142X19.0} = 3.68\,m^2/day$$

Where Q = quantity discharged (l/s) = 0.83× $10^{-3,}$ t_2= 52 min, t_1= 4 min, ΔS = 60m- 14m= 46m

$$\textbf{\textit{Hydraulic conductivity}}\ (K) = \frac{T}{b} = \frac{3.68}{114.01} = 3.23X10^{-2}\frac{m}{day}$$

Where T= transmissivity, b= Aquifer saturated thickness = Total depth of borehole – Static water level

T = 3.68 m^2/day, b= 128.57m- 14.56 m = 114.01 m

$$\textbf{\textit{Storativity}}\ (S) = \frac{2.25Tt_0}{r^2} = \frac{2.25X3.68X1.736X10^{-3}}{(0.635)^2} = 3.57\ units$$

Where T= transmissivity, t_0 = time intercept at zero drawdown = 2.5 min, r = radius of the borehole = 0.0635

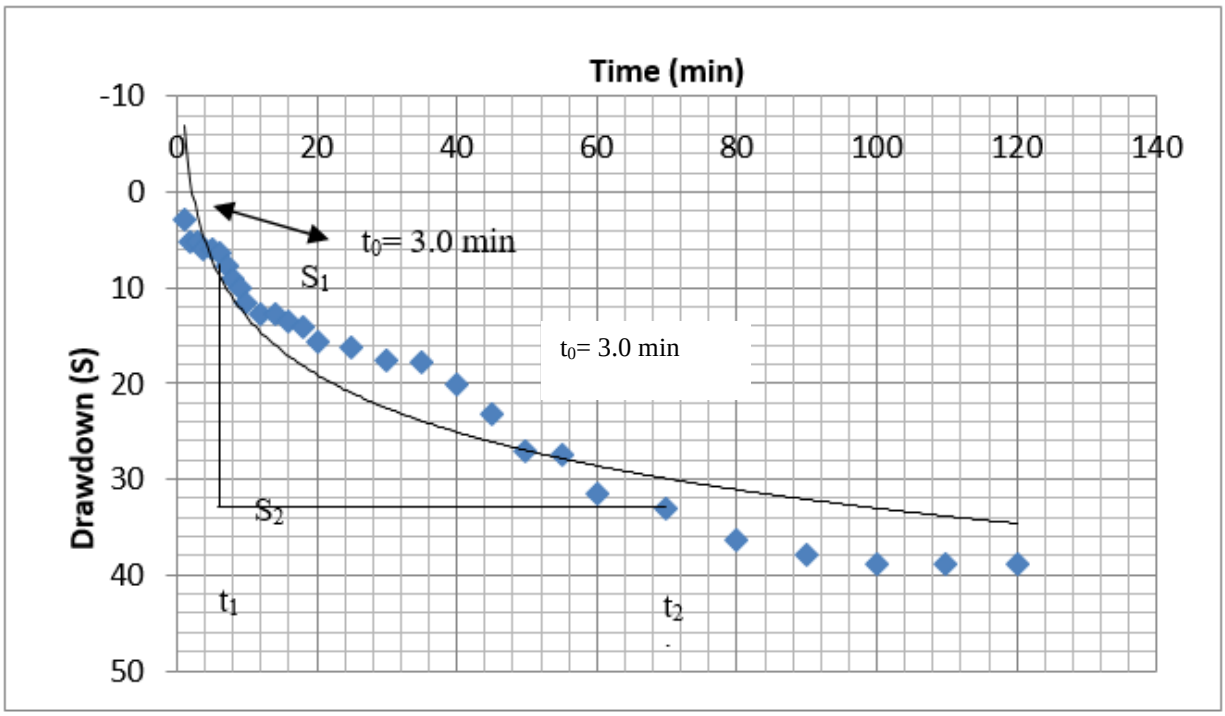


Figure 41: Plot of drawdown versus time for Budo-Ojoku water side

$$\textbf{\textit{Transmissivity}}\ (T) = \frac{2.30Q\log\frac{t_2}{t_1}}{4\pi\Delta S} = \frac{2.3X0.38X10^{-3}log16}{4X3.142X24} = 3.49\ m^2/day$$

Where Q = quantity discharged (l/s) = 0.38× $10^{-3,}$ t_2= 64 min, t_1= 4 min, ΔS = 30m- 6m= 24m

$$\textbf{\textit{Hydraulic conductivity}}\ (K) = \frac{T}{b} = \frac{3.49}{45.69} = 7.64X10^{-2}\ m/day$$

Where T= transmissivity, b= Aquifer saturated thickness = Total depth of borehole – Static water level

T = 3.49 m^2/day, b= 58m - 12.31 m = 45.69 m

$$\textbf{\textit{Storativity}}\ (S) = \frac{2.25Tt_0}{r^2} = \frac{2.25X3.49X2.083X10^{-3}}{(0.635)^2} = 4.06\ units$$

Where T= transmissivity, t_0 = time intercept at zero drawdown = 3.0 min, r = radius of the borehole = 0.0635

4.4 Evaluation of Groundwater level Time-Dependent Variation

Groundwater level configuration maps were prepared for both the end of raining season (October) and the peak of dry season (March). Figures 42 and 44 show the groundwater configurations while figures 43 and 45 show the corresponding groundwater flow directions.

The water level contours in the study area have been drawn at 5m intervals for both seasons and the contours are observed to be very similar to the ground surface except where they are interrupted by the crystalline outcrops. The shape of the water level contours is identical in both seasons.

The direction of groundwater flow is also known as the direction of groundwater movement which is indicated in the map by the arrows drawn perpendicular to the groundwater level contours (equipotential lines). Groundwater in the study area flows from the higher groundwater elevation contour (445 m above sea level [a.s.l])to the lower groundwater elevation contour (295 m a.s.l) and the flow is largely in the north-western direction.

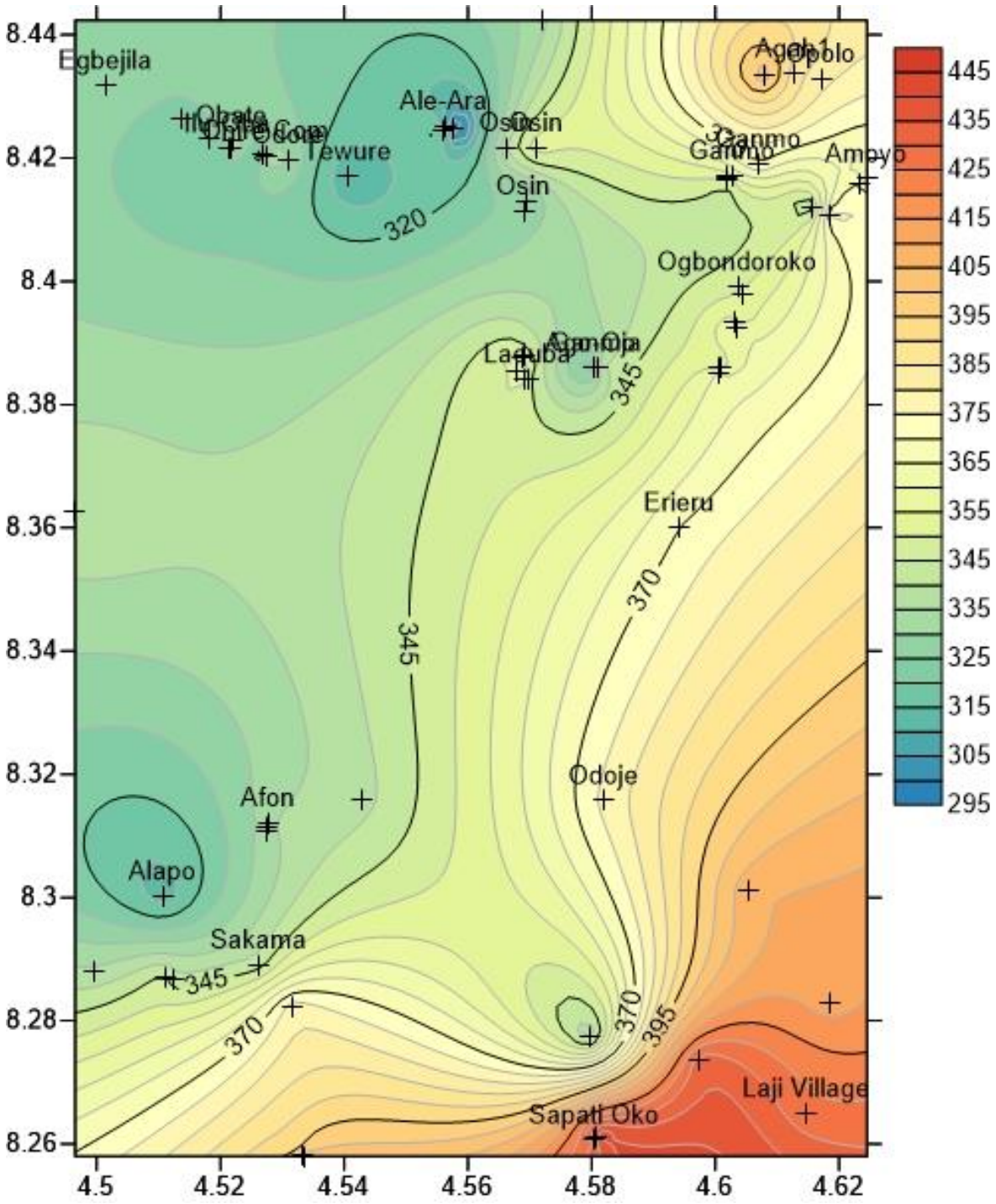


Figure 42: Groundwater contour map at the end of raining season (Cont. Int. 5 m) (2019)

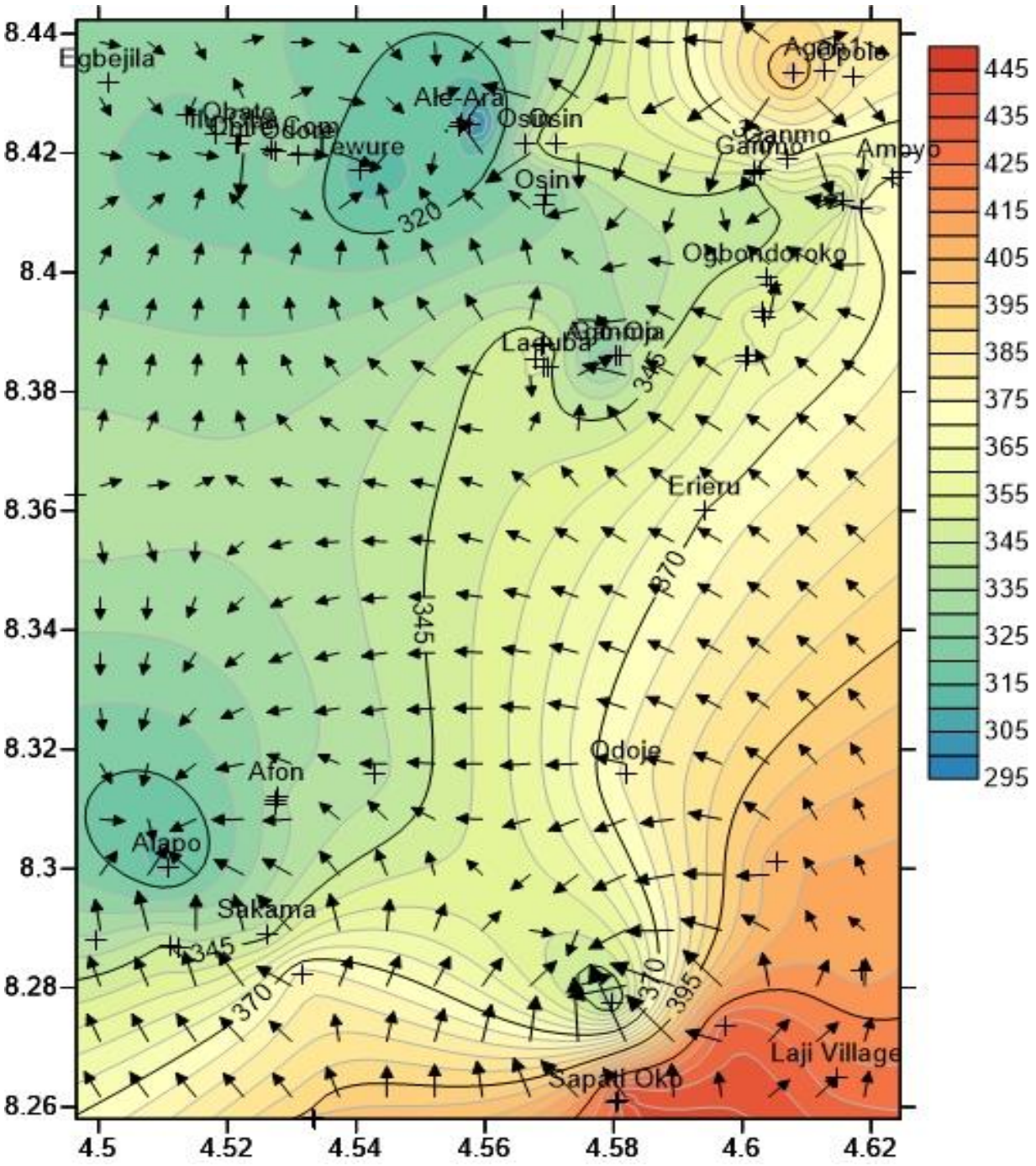


Figure 43: Groundwater flow net, end of rainy season (2019)

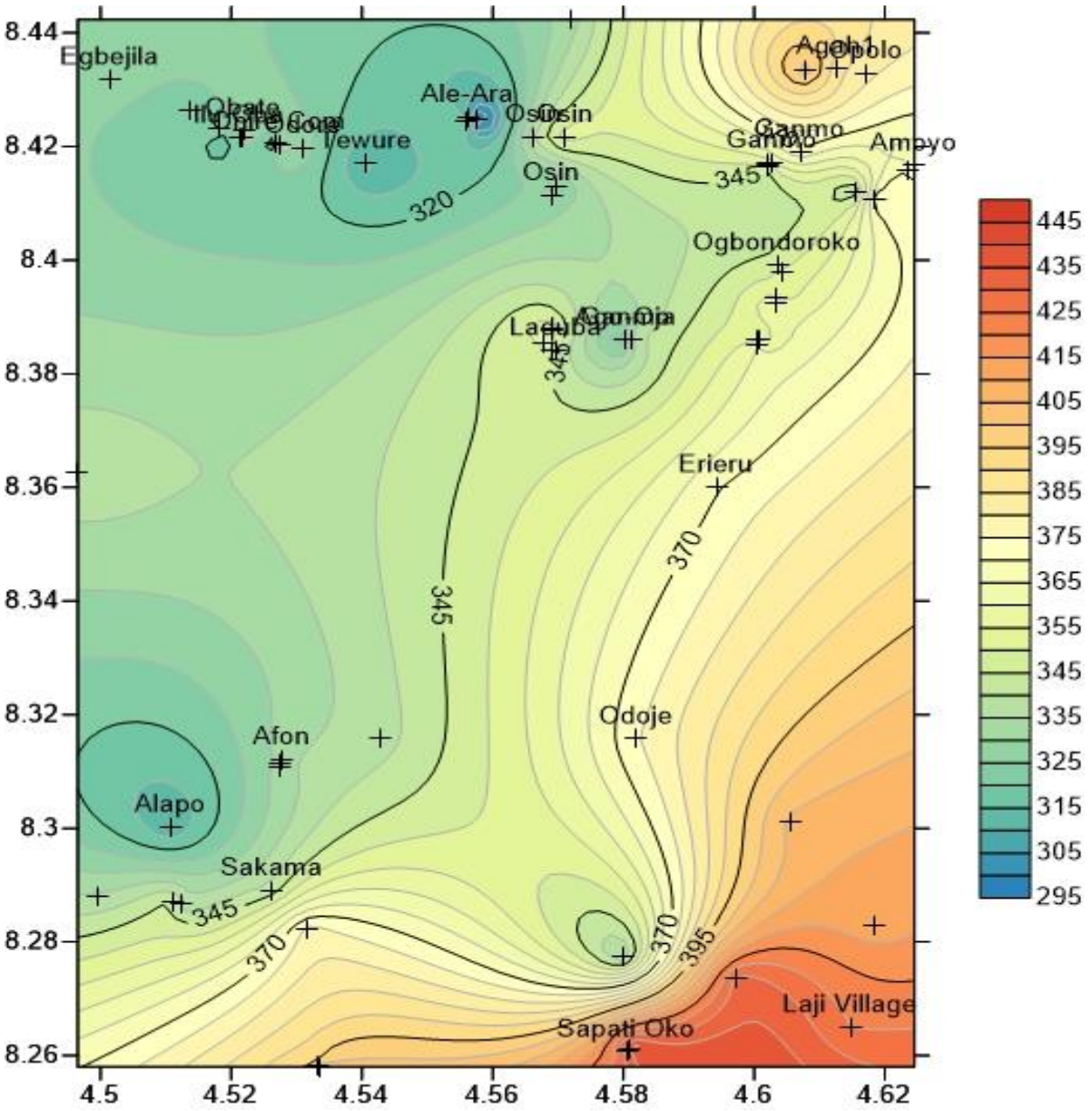


Figure 44: Groundwater contour map at the peak of the Dry season (Cont. Int. 5 m) (2019)

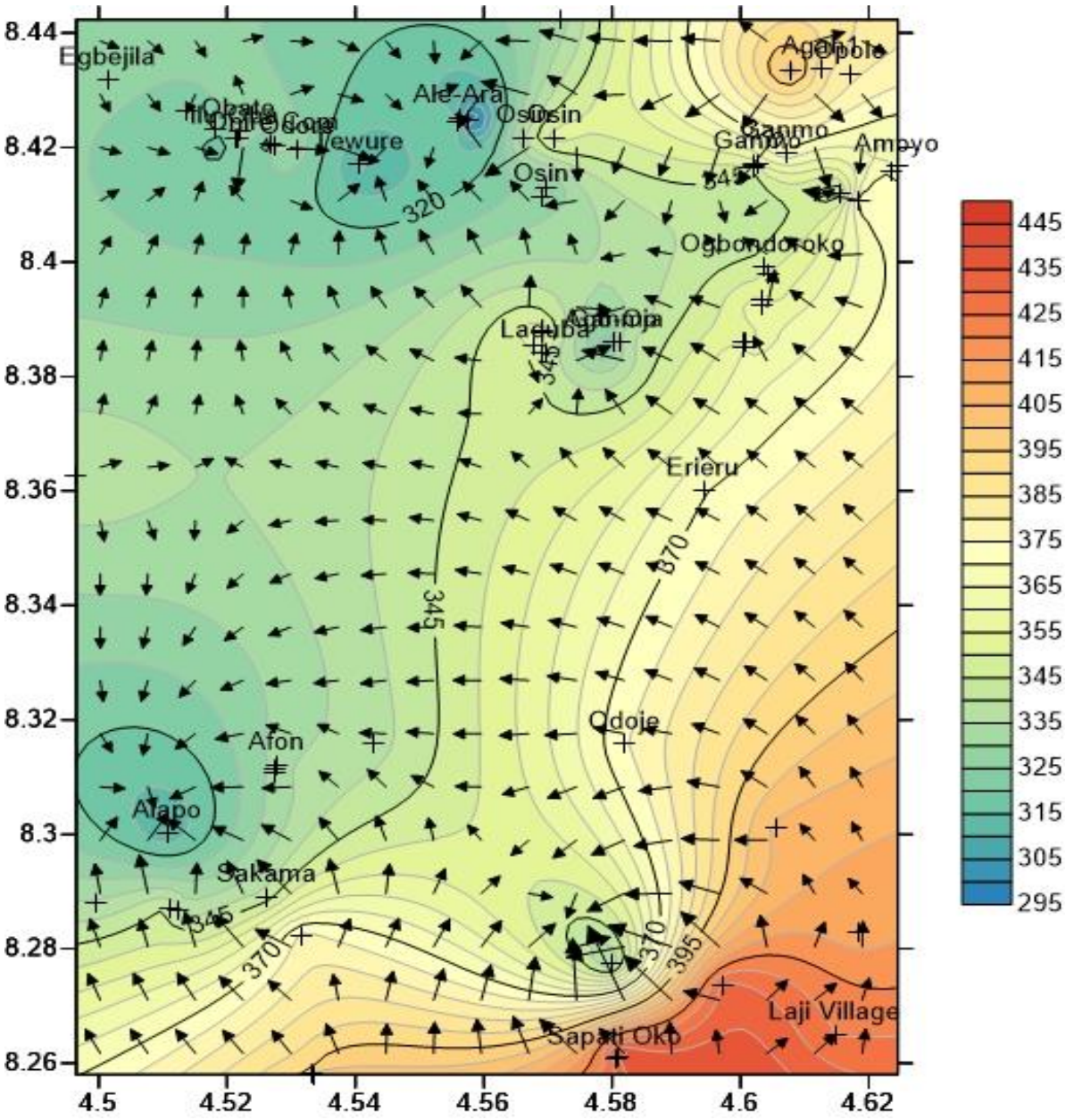


Figure 45: Groundwater flow net, the peak of the dry season (2019)

4.4.1 Evaluation of thickness of unsaturated/Vadose zone

The maps of the unsaturated zone in the study area (Figures 46 and 47) have been drawn at 0.5m intervals for the end of the rainy season and the peak of the dry season. The highest contour of thickness is 11.5 m while the lowest is 1m. For the end of the raining season, areas with a depth to water level range between 1 m and 2 m are areas with low water levels which include Okeso and gbaija villages while areas with a depth to water level range between 9.5 m and 11m are areas with high water level which include Eri-eru, Alomilaya and Ba-yawu. At the peak of the dry season, areas with depth to water level range between 2.5 m and 3.5 m are areas with low water levels which include Okeso and gbaija villages while areas with depth to water level range between 10 m and 11.5 m are areas with high water level which include Eri-eru, Alomilaya and laji villages. The water level during this season has receded to about 1.5 m below the ground surface.

These maps are of use in the water mining industry, by helping the miners to know the depth to which the hole will be dug to get to where water is. It is also of importance to agriculturists to know the water depth of the crops, whether the crops need more water or need removal of water from them.

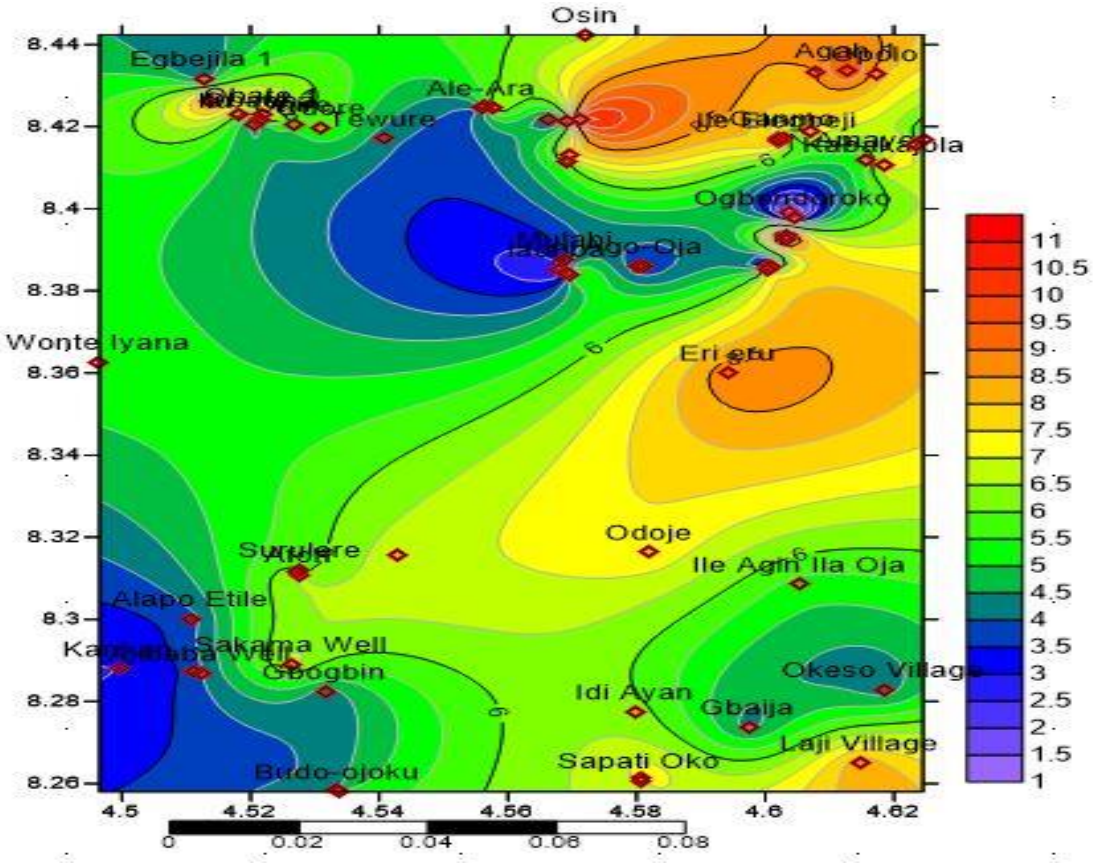


Figure 46: Peizometric surface variation at the end of raining season (2019)

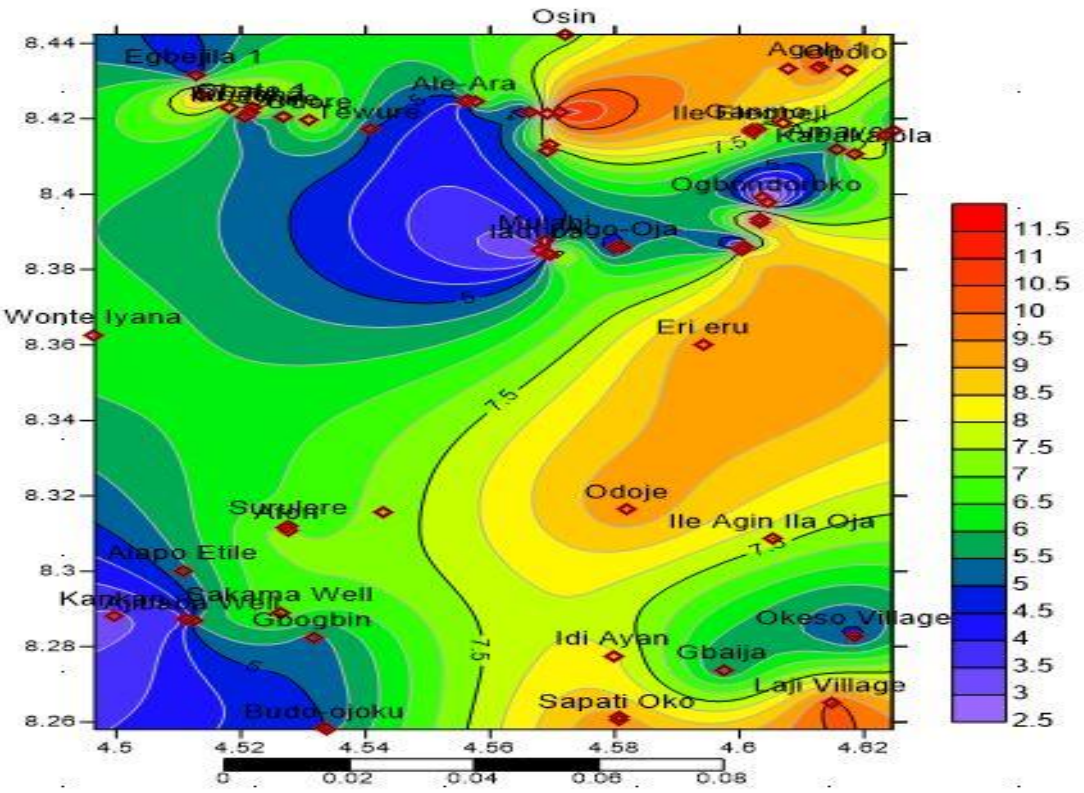


Figure 47: Peizometric surface variation at the peak of dry season (2019)

4.5 Geophysical Method

4.5.1 Magnetic Method

The magnetic survey interpretation of the study area is discussed under the following headings:

4.5.1.1 Total Magnetic Field Intensity (TMI) Anomaly Map

This is a magnetic field intensity that shows acute variation in magnetic intensity. TMI anomaly map (Figure 48) reveals three main types of magnetic anomalies ranging in intensity from -102.68 to 101.40 nT that are depicted in pink, red, yellow, green and blue colours. The anomalies were classified into high, moderate and low amplitude anomalies. The high amplitude total-field magnetic anomalies associated with intensity between 54.36 and 101.40 nT, which are shown in pink and red colours, occupied predominant portions of the northern, north-eastern, southern, south western and south eastern of the study area. The portions include settlements like Eru-Oba, Alaha, Alomilaya, Ewusi, Kankan and Okeso respectively. These settlements are dominated by fine-grained granite with high magnetic susceptibilities across the total and residual magnetic intensities dominated by banded gneiss. The moderate amplitude magnetic anomalies range in values from 24.61 to 54.36 nT and are shown in yellow and green colours. These are predominant in the western part of Aloba and Igborese areas. Also, Parts of the south-western and south-eastern portions of the area were occupied by yellow and green colours. These areas include Odo-Ode and Ila-Oja respectively. The prominent low amplitude anomalies ranging in intensity from -102.68 to 24.61nT are shown in blue colour. The blue colour is found extending from the eastern part around Oke-Awo, pajuba and Apata- Ikose to some western part which includes the Oloko and Dangagi areas of the study area. These portions are dominated by quartz-mica schist.

Generally, the anomalous closures were depicted as short and long wavelength anomalies which are linear and circular trending along ENE-WSW, W-E and NE-SW directions respectively. The rate of magnetization of a material depends on the length of its wavelength; the longer the wavelength of the anomalies, the higher the rate of magnetization because the longer wavelength shows greater amplitude.

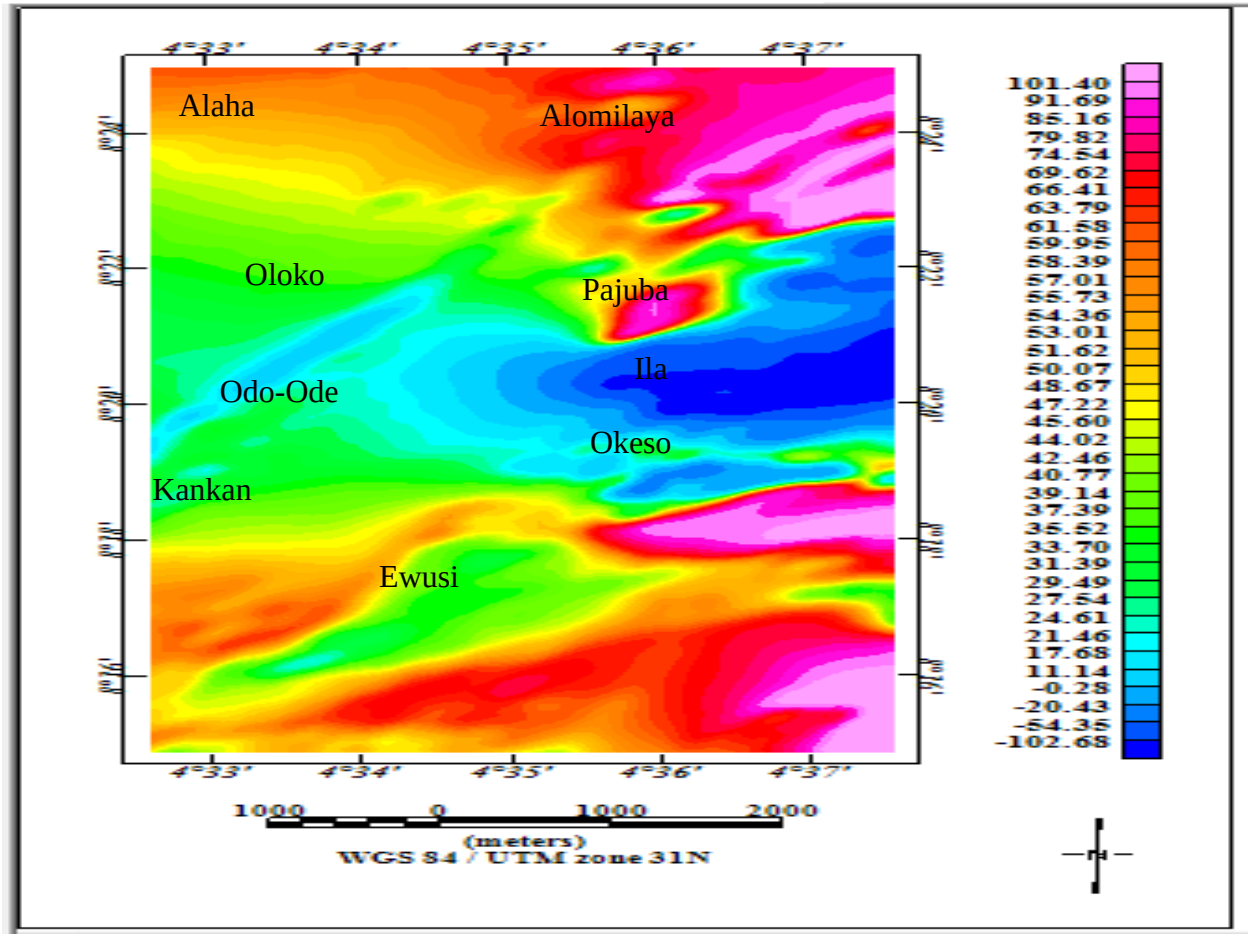


Figure 48: Total Magnetic Intensity anomaly map of the study area

4.5.1.2 Regional Magnetic Intensity (RMI) map

The regional magnetic intensity field reflects the major global tectonic elements of deeper and regional extent which affect and control the structural framework of the study area (Telford *et al.*, 1990). Figure 49 shows the contour map representing the estimated regional magnetic field intensities over the study area. The map shows a uniform trend along the NW-SE direction, which conforms to the global structural trend existing in the Basement Complex of Nigeria, as reported by McCurry (1976), Oluyide (1988) and Oyawoye (1964). The magnitude ranges from -18.55 to 82.35 nT. In general, the regional field increases in magnitude from the northern to the southern portion of the study area.

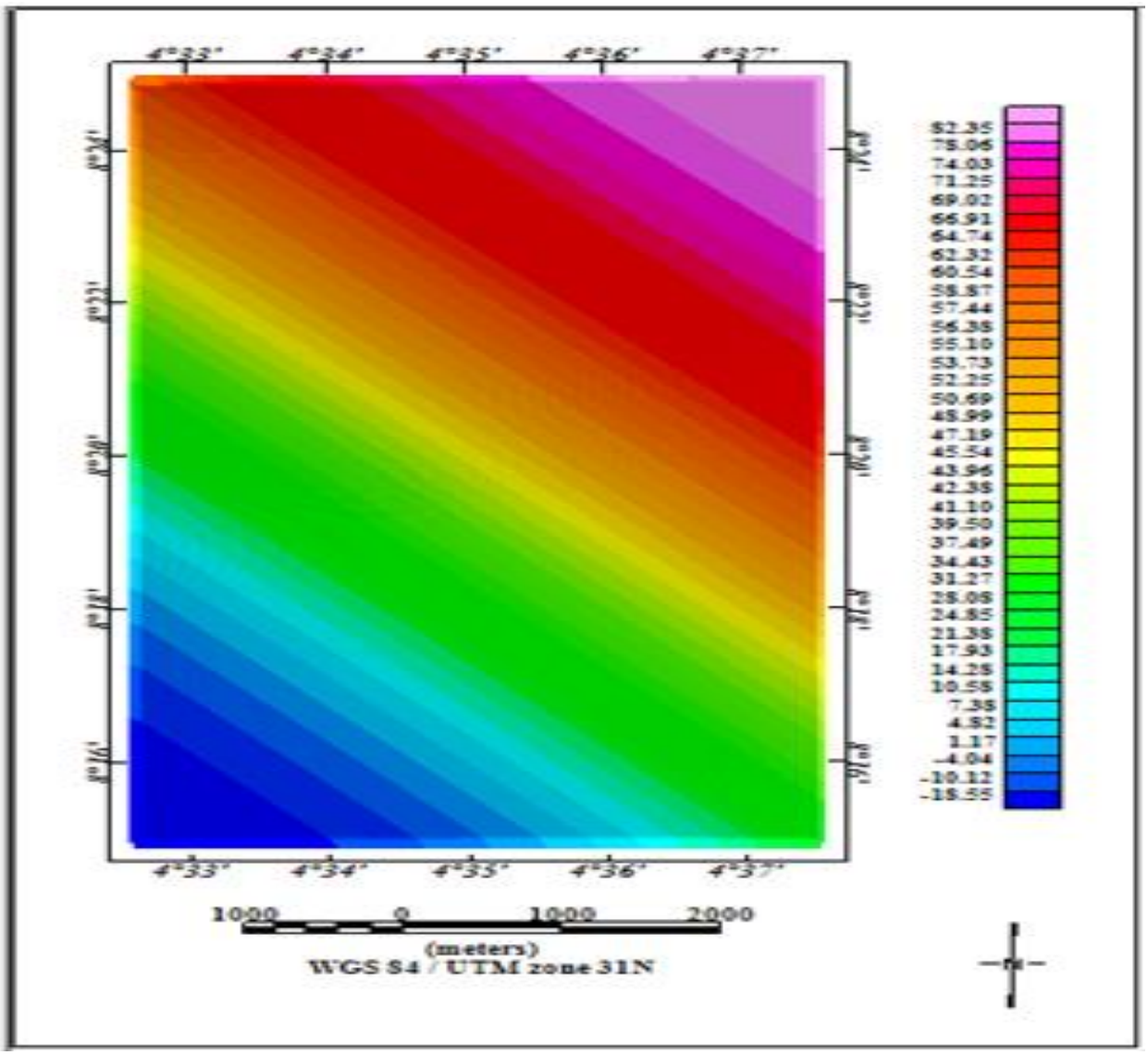


Figure 49: Regional Magnetic field Intensity map of the study area

4.5.1.3 Residual Magnetic Intensity (RMI) map

RMI represents the responses due to the bodies of interest in the study area. Residual magnetic Intensity map shows the colour shaded of the residual magnetic field intensity over the study area ranging from -35.87 to 35.74 nT and depicted in red, pink, yellow, green and blue colours (Figure 50). The positive residual intensities range from 0.63 to 35.74 nT with the high amplitudes ranging between 4.16 and 35.74 nT and depicted in pink and red colours while the low positive amplitude ranges from 0.63 to 4.16 nT and is depicted in yellow colour. The negative residual intensities are ranging between –35.87 and -0.07 nT. The high positive amplitude anomalies are found in the north-eastern (around Alomilaya, Gbagede and Ogbondoroko) and south western(around Kankan, Abogongo and Laji Bamu) parts while the low positive amplitude is widespread throughout the study area. Similarly, the negative amplitude anomalies are widespread throughout the study area with dominance in the half northern, eastern and western regions.

However, areas of deep Basement surface or areas containing minerals of low magnetic contents such as shale, silica, limestone and sandstone are areas associated with low magnetization and negative residual intensities. The residual field anomalies were depicted in form of long and short wavelength anomalies that are linear and circular. The short wavelength anomalies suggest near-surface magnetized intrusions while the long wavelength suggests deep-seated bodies typical of areas associated with thick sediments. The long wavelength anomalies are dominant in the northern and southern parts of the study area while the low wavelength anomalies are dominant in the eastern part of the study area. The general trends of these anomalies were observed to be in the NE-SW direction.

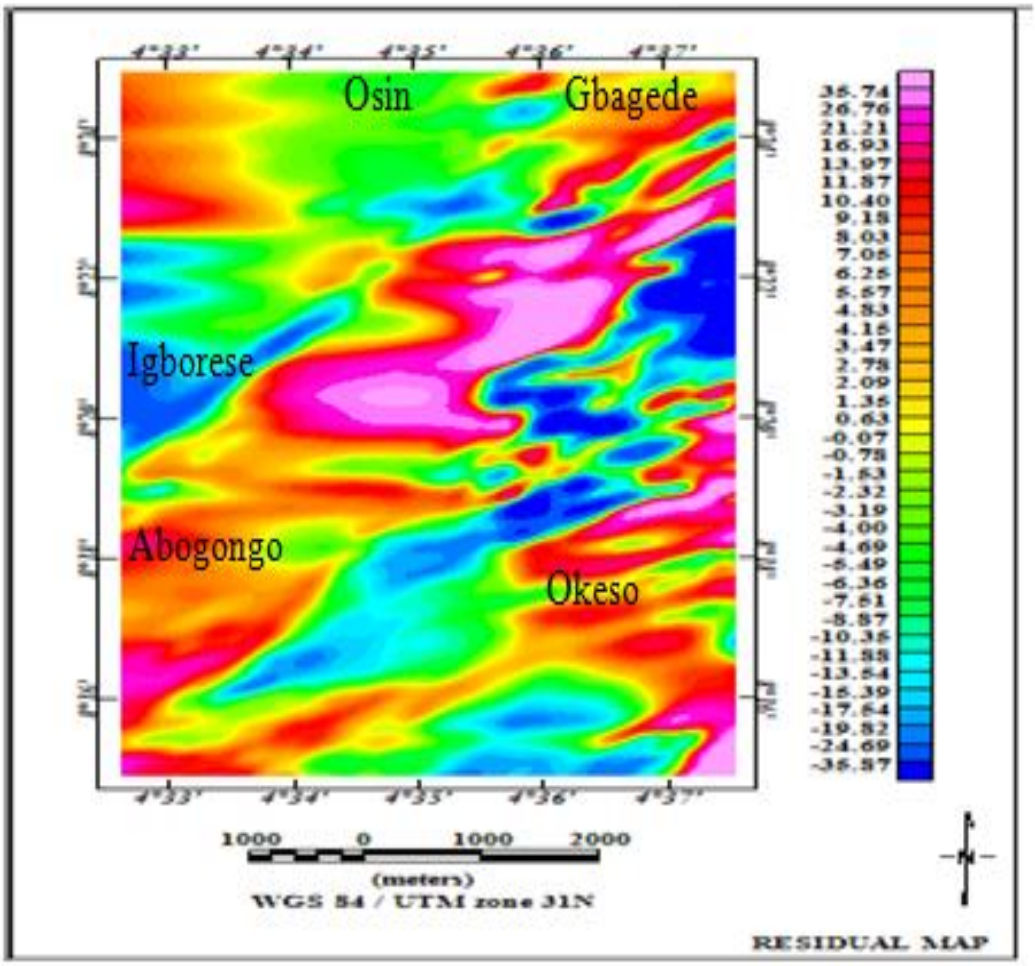


Figure 50: Residual Magnetic Intensity map of the study area

4.5.1.4 Reduction to the Magnetic Equator (RTE)

This is a process of reducing and simplifying non-zero magnetic anomalies from any part other than the equator to the centre of the equator where the magnetic inclination is zero. The angle of inclination is the angle between the surface horizontal and total magnetic intensity. The angle of declination on the other hand is the angle between the geographic and magnetic poles.

The colour shaded map of the RTE residual magnetic field intensity (Figure 51) exhibits negative and positive values ranging from -99.3395 to 74.7526 nT shown in red, pink, yellow, green and blue colours. The positive RTE is broadly characterized by intensities ranging from 0.9524 to 74.7526 nT with a high amplitude ranging from 14.2069 to 74.7526 nT and depicted in red and pink colours. The intermediate positive value is shown in yellow colour with the range between 0.9524 and 14.2069 nT and the negative RTE intensities range between -99.3395 and -1.0155 nT with the high amplitude ranging from -20.5305 to -1.0155 nT and depicted in green colour while the negative amplitudes are ranging between -99.3395 to -20.5305 nT and depicted in blue colour. The shape of the anomalies on the RTE map are of short and long wavelength form and also circular and elongated in shape.

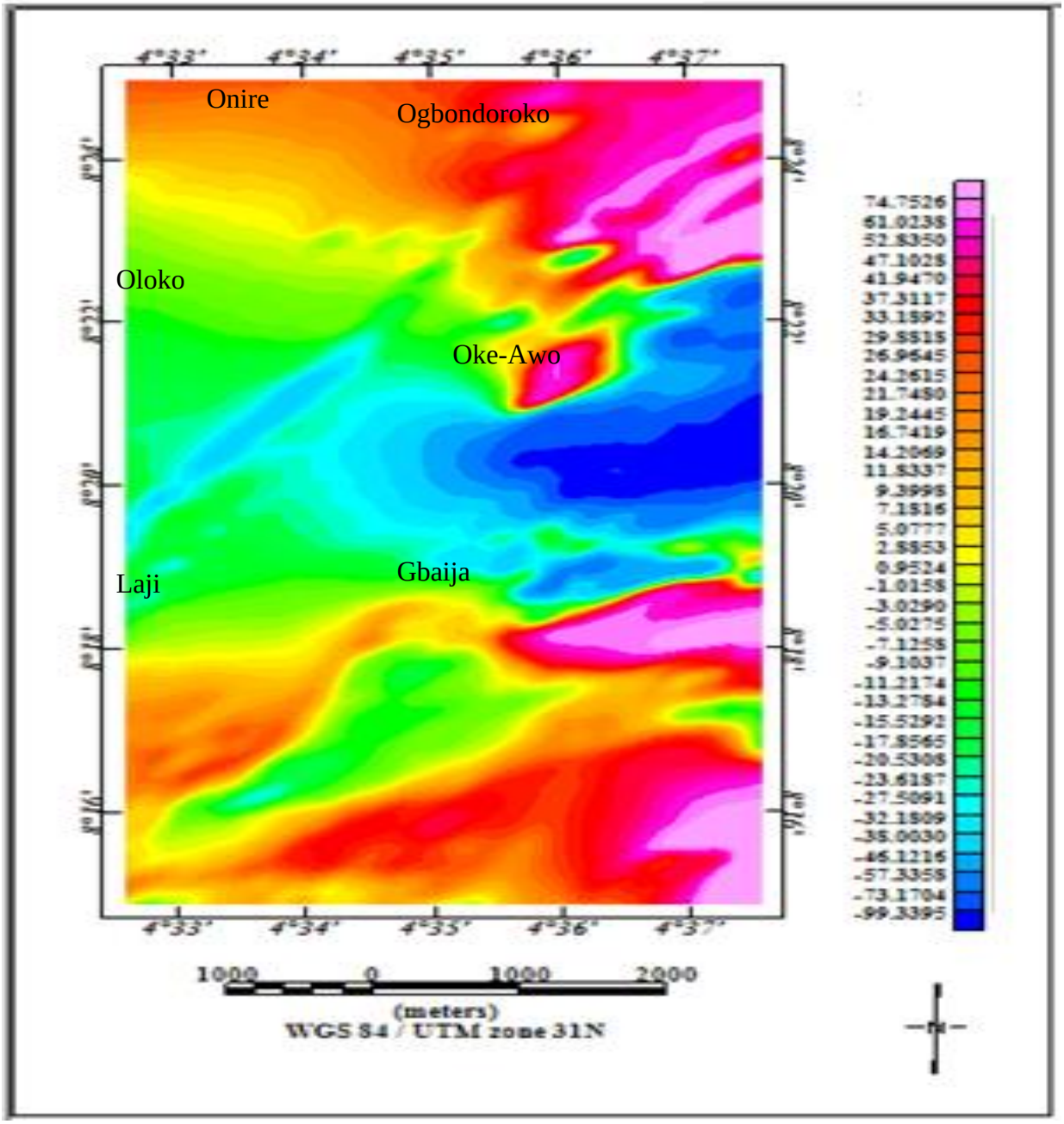


Figure 51: Reduction to equator (RTE) map of the study area

The high prominent negative amplitude anomalies, shown in green colour, are widespread throughout the study area with dominance in the half western region while the very low amplitude negative anomalies displayed in blue colour with circular and elongated shapes are dominant in the half eastern region. Generally, the negative amplitude anomalies are circular and linear in shape trending along the NE-SW, direction, which is consistent with the trends of the TMI and RMI anomalies. A comparison between the RMI and RTE-RMI anomalies suggests a slight eastward shift of the RTE-RMI anomalies compared with the positions of the RMI anomalies.

4.5.1.5 Tilt Derivative (TDR) Map

The wavelength anomalies of tilt derivative are circular and elliptical ranging from -1.3624 to 1.3634 nT and depicted in pink, red, yellow, green and blue colours (Figure 52). The high positive gradient TDR anomalies which are prevalent throughout the study area are depicted in pink and red colours. The intensities of these anomalies vary between 0.4478 and 1.3634nT and are predominantly linear in shape.

The low positive TDR values shown in yellow colour range between 0.0292 and 0.4478 nT and are depicted as the boundary separating the high positive and negative TDR gradient values. As the high positive gradient TDR values reflect magnetic sources, the low positive TDR intensities which are close to zero were interpreted to reflect geologic boundaries. The prevalence of high gradient positive TDR intensities suggests the presence of mafic to ultramafic rocks that are covered by the overlying sediments. Also, the negative gradient TDR anomalies (Figure 52) shown in green and blue colours with intensities between -1.3624 to -0.2332 nT occupy the study area and are linear and elliptical.

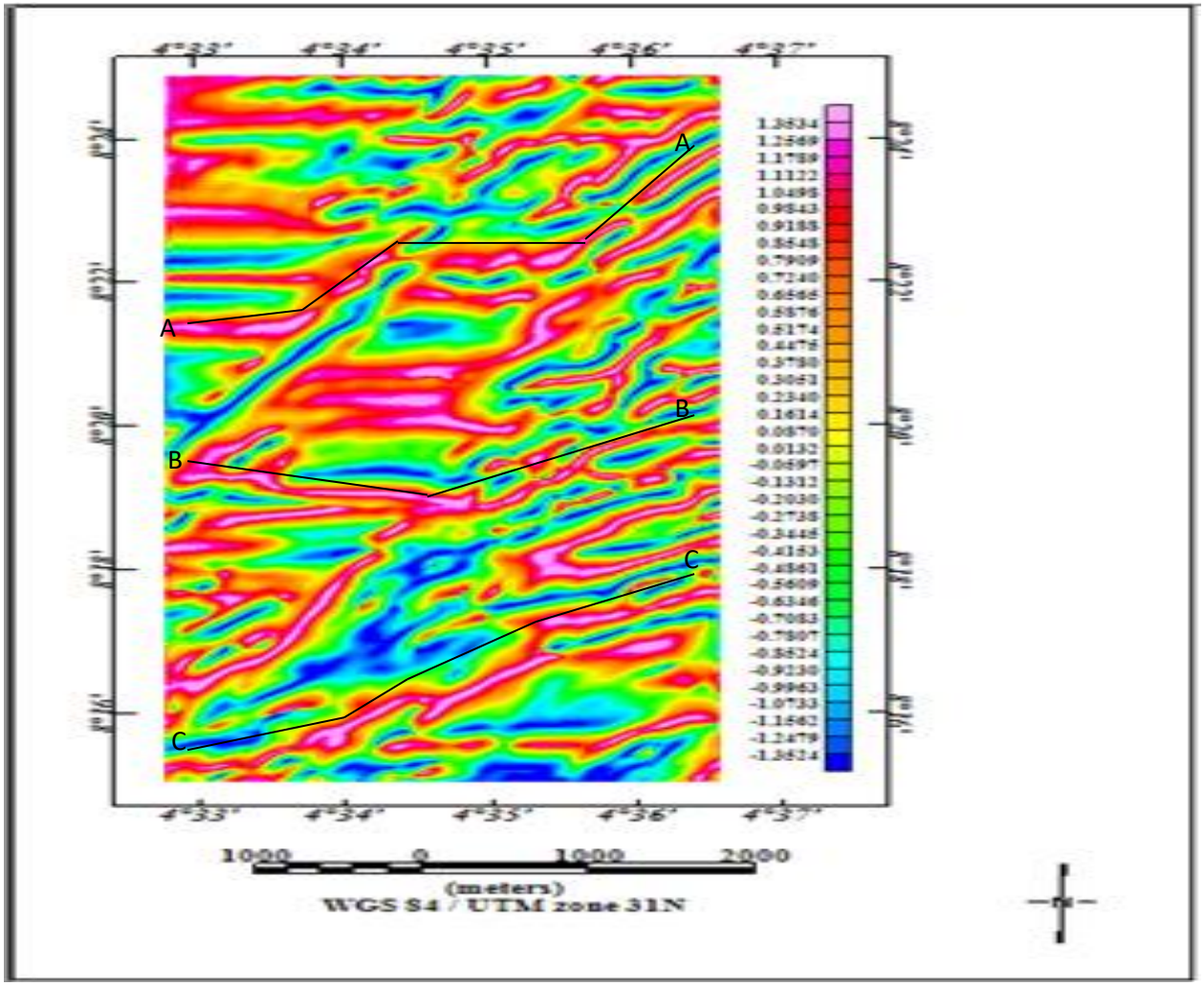


Figure 52: **Tilt Angle Derivative Map of the study area**

The low gradient negative TDR intensities are interpreted to reflect the presence of low magnetic content sediments such as limestone and sandstone in the area. The TDR anomalies identified in this area are trending along NE-SW, NW-SE, E-W and ENE-WSW directions.

The inferred lineament map (Figure 53) shows three major (regional) and minor lineaments trending in different directions beneath the study area. The major lineaments are tagged AA', BB',' and CC'

The fault "AA" is curve-linear in shape and spans from ENE around Alaha to the WSW around Alomilaya. There is a change in the trend of this fault from ENE-WSW to NE-SW direction and finally along E-W direction. This reflects the change in the stress regime around this region. Similarly, fault "BB" is also curve-linear in shape spanning from the western part of Aloba area to the eastern part of the area around Idiemi and Oke-awo (W-E). The region between faults AA and BB contain minor lineaments. Fault "CC" is observed extending from SW around Laji Bamu to NE around Ila. The region between faults BB and CC contains minor lineaments. These major lineament areas indicate major locations of high promising groundwater potential.

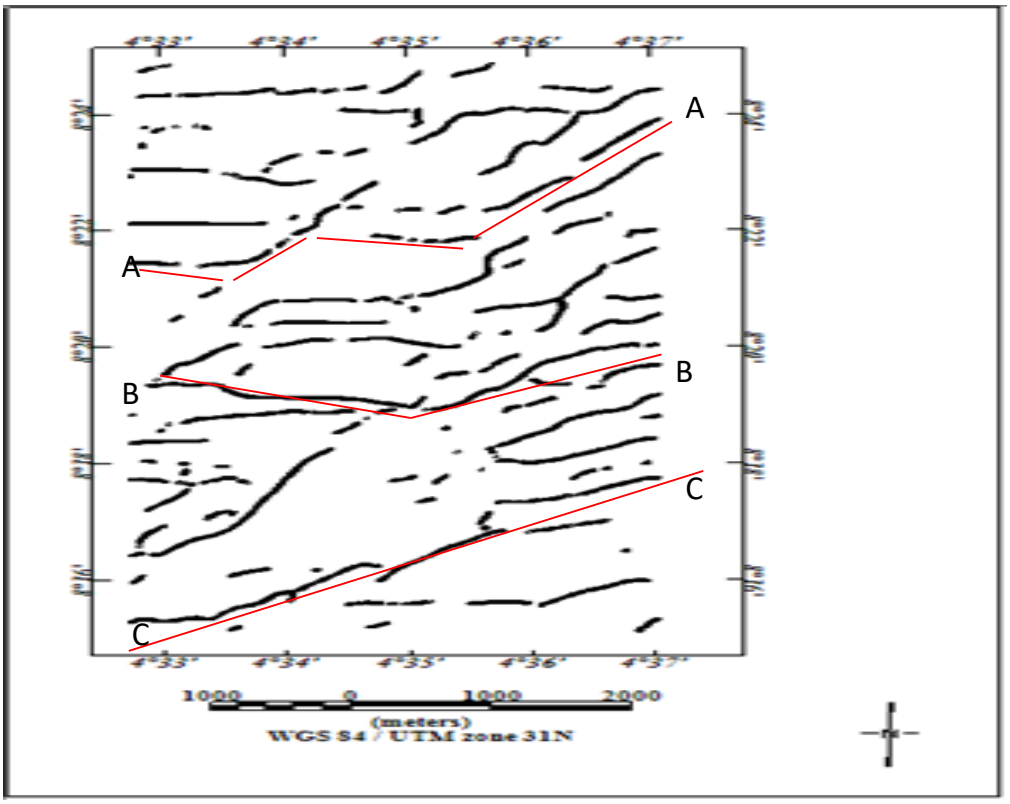


Figure 53: Inferred structures from Tilt Derivative Map of the study area

4.5.2 Electrical Resistivity Method

4.5.2.1 VES Results

From curve matching analysis, the subsurface layering is depicted by thirteen (13) types of the sounding curves (Table 2); comprising three-layer curves (A, H, Q, and K,) at 105 VES stations (i.e. 50%), four-layer curves(QH, KH, HA, QA and AA) at 79 VES stations (i.e. 37.6%) and five-layer curves (HKH, QHA, HAA, and KQA) at 26 VES stations(i.e. 12.4%) characterizing the vertical changes and the typology of sounding curves in the study area; this is illustrated in Figure 55. The lithology of the subsurface is dominated by geo-electrical and lithological 2D models derived from the H, KH, and HA curve types. These models are characterized by the presence of conductive layers and fractured/weathered layers derived from the tectonic activities of the region. Also, the resistivity method (VES) applied in this study brings information about the variation of the resistivity with depth, geological structures and thicknesses of layers underground.

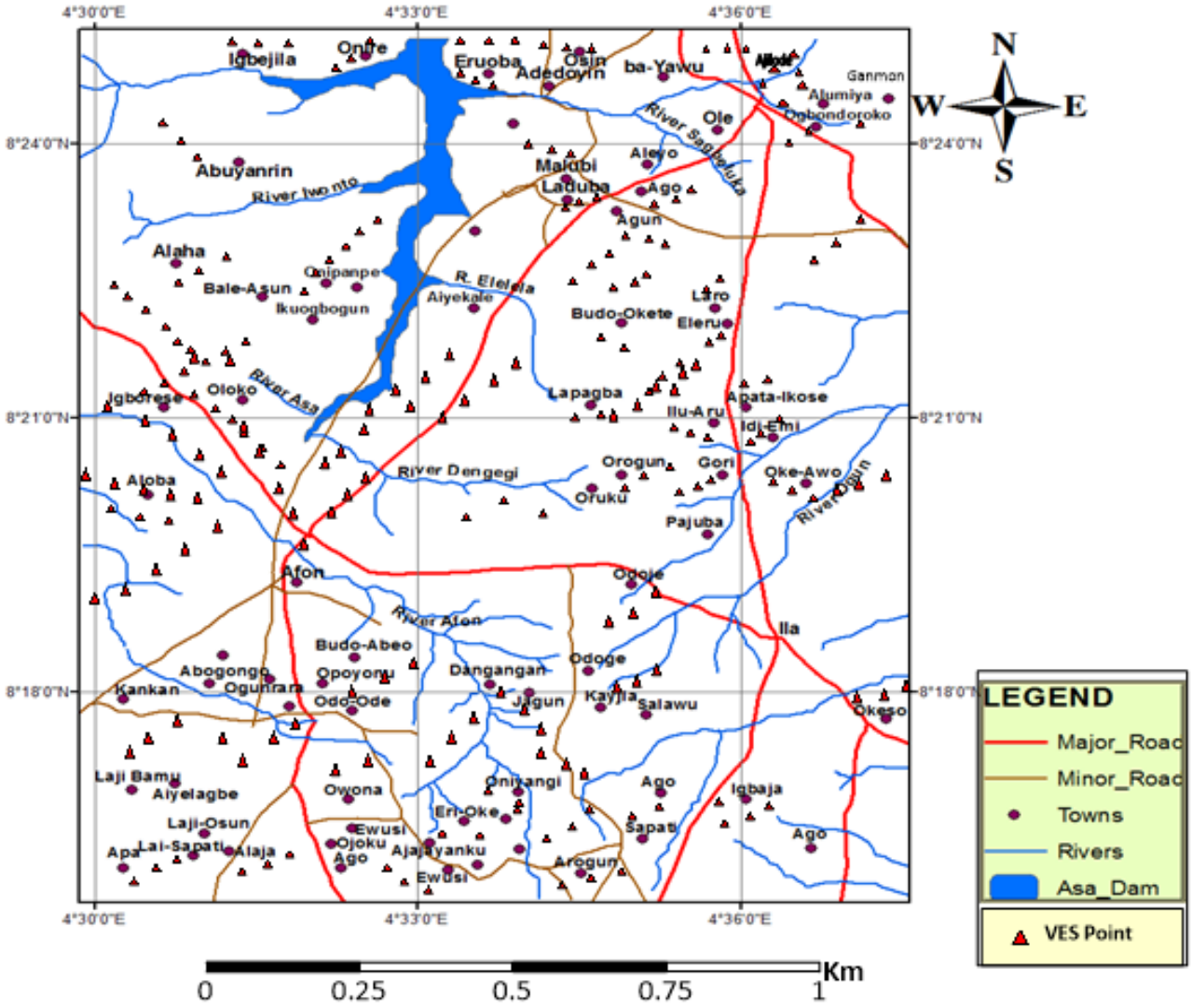


Figure 54: Location map of the study area showing VES points

Table 2: Various curve types, their frequencies and percentages from the study area

S.N.	Curve types	Frequency	Percentage
1	A	13	6.19
2	H	82	39.05
3	Q	2	0.95
4	K	8	3.81
5	KH	44	20.95
6	HA	19	9.04
7	QH	5	2.38
8	AA	10	4.76
9	QA	1	0.48
10	HKH	23	10.95
11	QHA	1	0.48
12	HAA	1	0.48
13	KQA	1	0.48

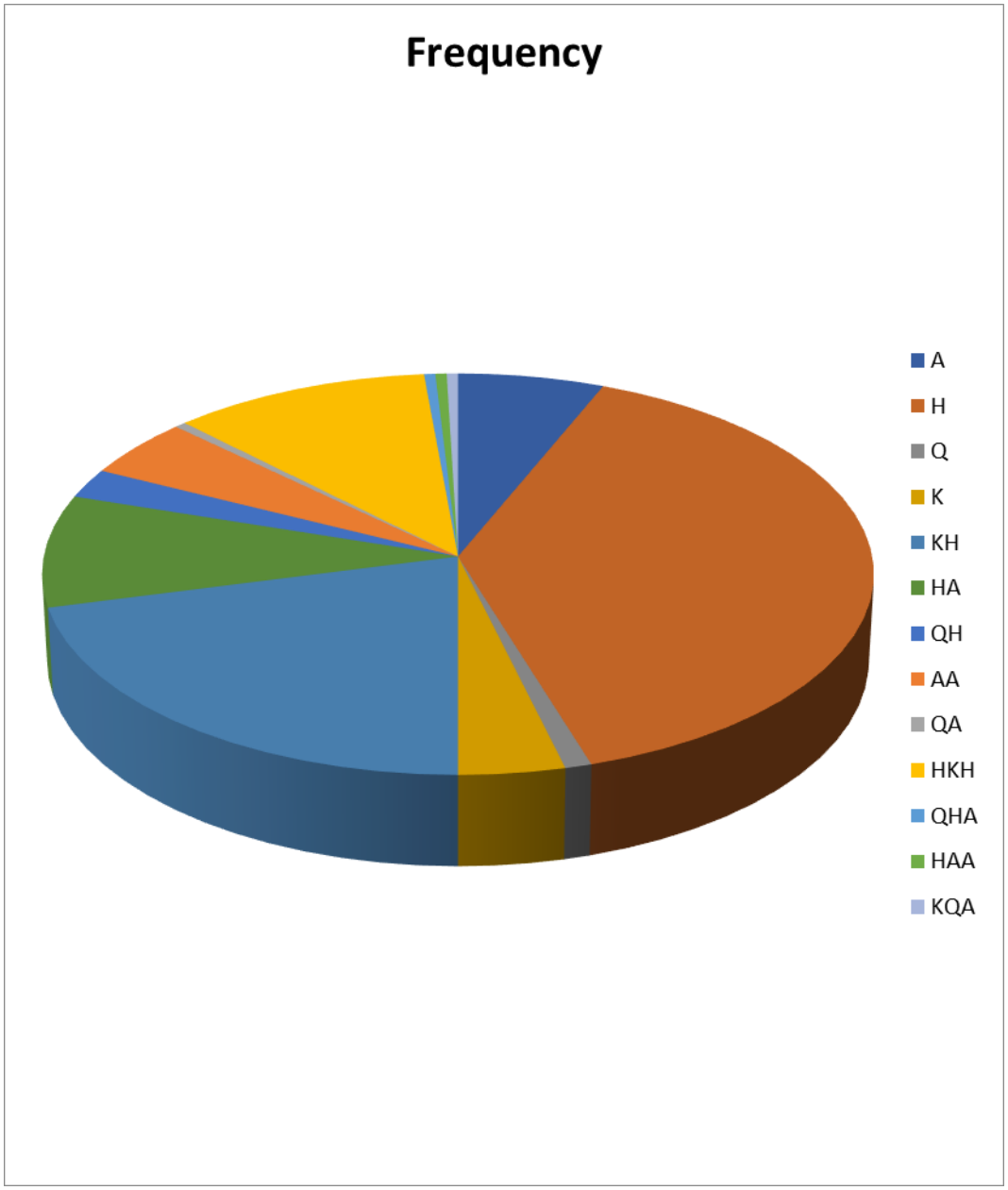


Figure 55: **Pie chart showing frequency distribution of observed curve types in the study** area

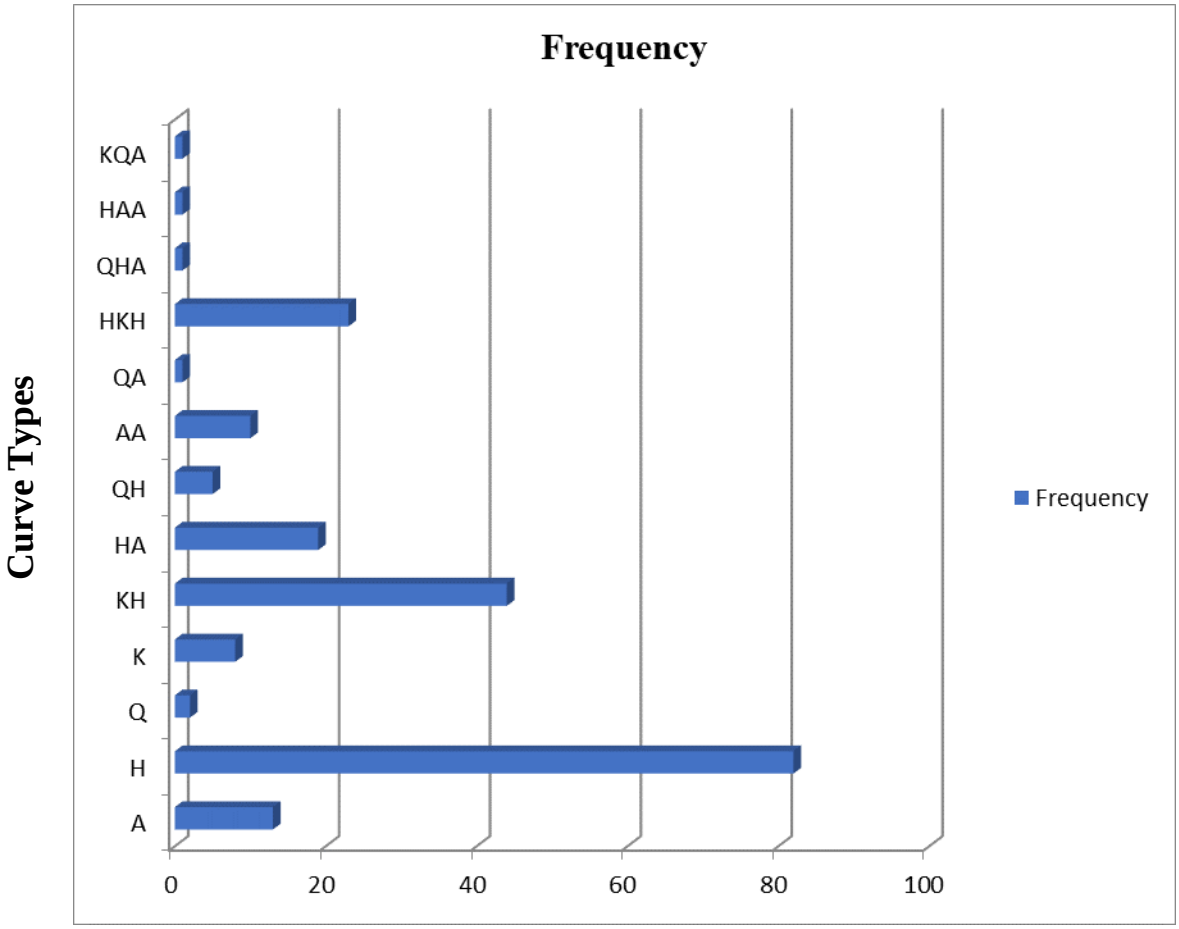


Figure 56: Bar chart showing frequency distribution of observed curve types in the studyarea

4.5.2.2 Inferred Geologic Layers, equivalence of Geo-electric sections

The geo-electric sections are sections that show the variations of resistivity and thickness values of layers within the depth penetrated in the study area at the indicated VES stations along certain profile. The profiles were taken along E-W directions. The typical 2-D profile generated from inversion of the resistivity data of3 layer, 4 layer and 5 layer cases together with their geo-electric pseudo-sections are shown in Figures 57, 58 and 59. The 2-D profiles were therefore generated from inversion of the 210 VES point data and their respective geo-electric sections are obtained and the summarized outcome are partly shown in Table 3; the rest are shown in Appendix 1.

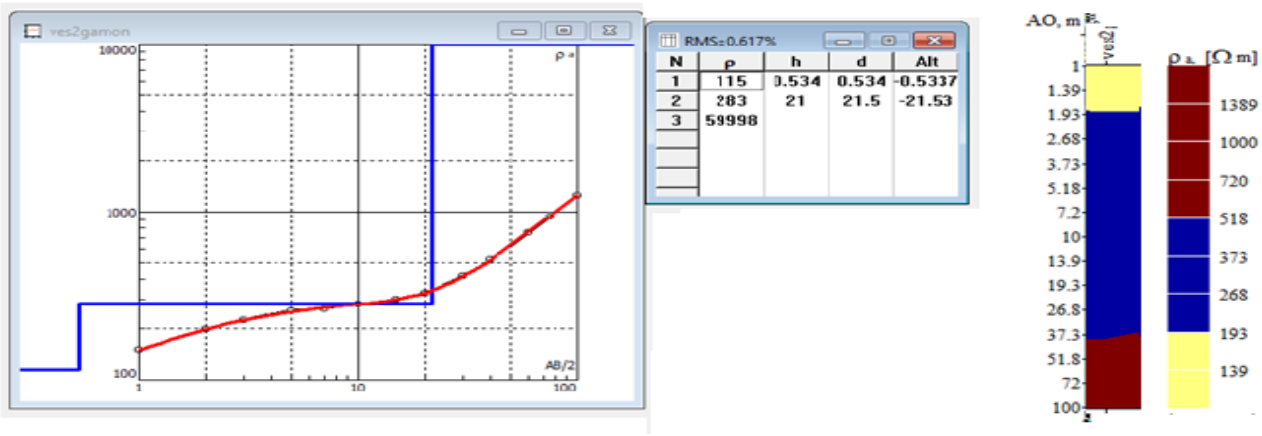
Analysis of the 2-D resistivity profile produced a system of three to five geo-electric layers (Table 3) which are the top soil, lateritic layer, weathered basement, Sandy clay/clayey sand and fractured rock/ underlying fresh basement.

The first layer was top soil characterised with apparent resistivity values varying from 12.9 at VES 75 to 2203 at VES 41while the thickness of the layer varies from 0.5 m to a maximum of 5.07 m at VES170 which is relatively thick (Table 3). This thickness is an indication of high potential for water holding capacity in the area.

The second layer is the lateritic layer which marks the contact with the weathered layer and has good water retention capacity but limited flow potential due to non-interconnectivity of the pores. It has apparent resistivity ranges from 95 to 2884 at VES 210 and VES 181 respectively. The thicknesses of the lateritic layer varied from 0.46 m at VES 161 to 9.7 m at VES 87 (Table 3).

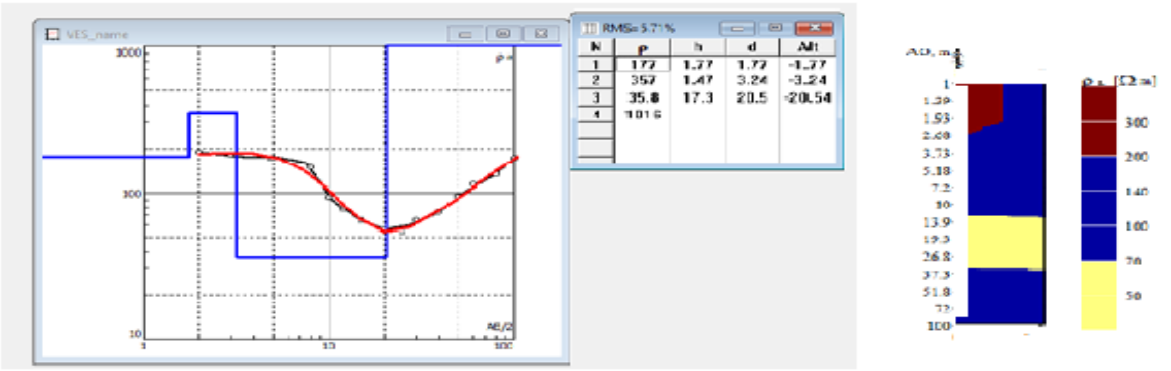
The third layer is the weathered Basement layer whose apparent resistivity ranges from 9.57 at VES 64 to 399 at VES 111. Also, the thickness of this layer varies from 0.2 m to 39.2 m at

VES 64 and VES 75 respectively. This layer is common in Basement Complex areas and characterized by moderate to highly weathered lithology. The layer serves as pathway or conduit for percolating water. The wide variation in the thickness of the layer may have influenced the variability in the availability of water in the borehole since most boreholes actually depend on recharge from this unit.



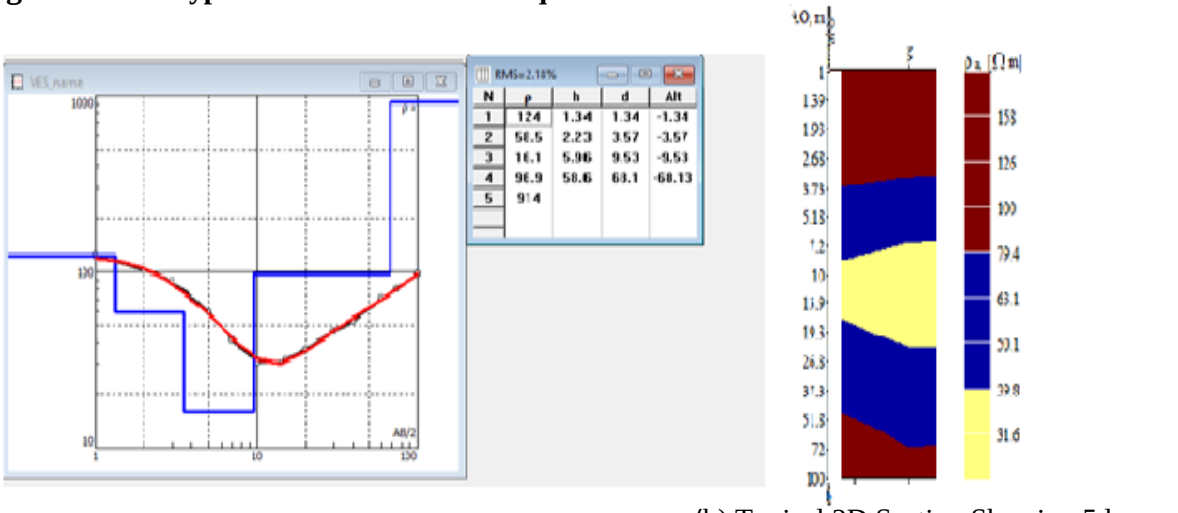
(a) A-Type Curve for VES 2 (b) Typical 2D Section Showing 3 layers

Figure 57: Typical Field Curve and its Equivalent 2D Section for Ganmo location



(a) KH-Type Curve for VES 50 (b) Typical 2D Section Showing 4 layers

Figure 58: Typical field Curve and its Equivalent 2D Section for Eleru location



(a) QHA-Type Curve for VES 47 (b) Typical 2D Section Showing 5 layers

Figure 59: Typical Field Curve and its Equivalent 2D Section for Akanbi Ade location

The fourth layer is the Sandy clay/ clayey sand layer which ranges in its apparent resistivity from 32.8 to 683 at VES 76 and VES 59 respectively (Table 3).

The fifth and the last layer is the fractured/fresh basement layer whose apparent resistivity range from 12.3 (VES 96) to 941 (VES 157) and 41.2 (VES 94) to 453276m (VES 110) respectively with an un-determined thickness (Table 3).

The weathered and fractured Basement layers constituted the major aquifers in the area based on their thick overburden and relatively low resistivity values which enhance groundwater exploration in the area. The fresh basement layer is a lithologic unit known to be generally impervious, hence, non-water bearing. Therefore, aquifer setting is generally heterogeneous and anisotropic in the study area. Groundwater flow and its accumulation can be controlled by topography, weathered mineral types, degree of tectonic deformation and thickness of overburden. All these are in line with findings by Musa and Olatunji (2013) and Olawuyi (2012).

Table 3: Summary of Results of Vertical Electrical Sounding

TOWN	VES STATION	No. of Layers	Layer Resistivity ()	Thickness (m)	Depth to Bedrock (m)	Curve Type	Inferred lithology
GANMO	VES1	4	82.5	0.5		KH	Topsoil
			594	2			Laterite
			273	18.8			Weathered Basement
			170989	--	20.8		Fresh Basement.
	VES2	3	115	0.5	21.5	A	Topsoil
			283	21.5			Weathered Basement
			59998				Fresh Basement.
	VES3	3	125	0.6		A	Topsoil
			285	7.82			Laterites,
			207812	--	8.46		Weathered Basement
AJILODE	VES4	3	867	1.78		H	Topsoil
			17.5	7.04			Weathered Basement
			10206	--	8.82		Fresh Basement.
	VES5	3	82.8	1.72		H	Topsoil
			18.4	6.07			Weathered Basement
			451	--	7.79		Fractured Basement.
	VES6	3	116	2.01		H	Topsoil
			21.9	4.45			Weathered Basement
			148	--	6.46		Fractured Basement.
ALOMILAYA	VES7	3	610	0.701		H	Topsoil
			44.3	2.98			Weathered Basement
			353	--	3.68		Fractured Basement.
	VES8	4	231	0.5		KH	Topsoil
			830	0.79			Laterite
			38.4	13.7			Weathered Basement
			25646	--	15		Fresh Basement.
	VES9	3	201	2.26		H	Topsoil
			54.6	7.11			Weathered Basement
			2790	--	9.37		Fresh Basement.
OGBODOROKO	VES10	3	117	1.02		H	Topsoil
			41.7	12			Weathered Basement
			36812	--	13.1		Fresh Basement.
	VES11	4	660	1.09		HKH	Topsoil
			104	1.68			Weathered Basement
			316	14.4			Fractured Basement.
			92904	--	6.17		Fresh Basement
	VES12	3	113	2.01		H	Topsoil
			24.9	10.6			Weathered Basement
			209	--	12.6		Fractured Basement.

4.5.2.3 Isoresistivity maps

Isoresistivity map is a map whose contours link points of equal electrical apparent resistivity. According to Ishola *et al*. (2013), Isoresistivity contour map representing a low resistivity region could be potential groundwater zones due to high thickness of the aquifer. The Isoresistivity map showing the resistivity distribution of the aquifer layers had been proven useful in mapping promising areas for groundwater abstraction. The Isoresistivity is discussed under the following headings:

a. Isoresistivity of the top soil

The Isoresistivity map shows that the high resistivity region is found in isolated spots in the south-eastern portion of the study area which include areas like Budo Omo Abeo, Alaja and Laji sapati indicating low potential groundwater zones (Figure 60). Also, low resistivity region is found in the western and southern parts of the study area which include Onipampo, Igborese, Gbaija and Okeso indicating high potential ground water zones (Figure 60).

b. Isoresistivity map of the lateritic soil layer

Generally, the resistivity of this layer ranges between 200 and 4800 Ωm (Figure 61). The iso-resistivity map of lateritic soil reveals that the high resistivity region is found at isolated spots in the central portion of the area with resistivity values ranging from 2800 to 4600 Ωm. The settlements in this region include Budo malubi and Ogbondoroko indicating areas of low groundwater potential (Figure 61). On the other hand, the north western and south-eastern parts of the area are areas of low resistivity (200 – 800 Ωm), indicating high groundwater potential zones. These areas include Onipampo, Igborese, Ila and Gbaja and Okeso (Figure 61).

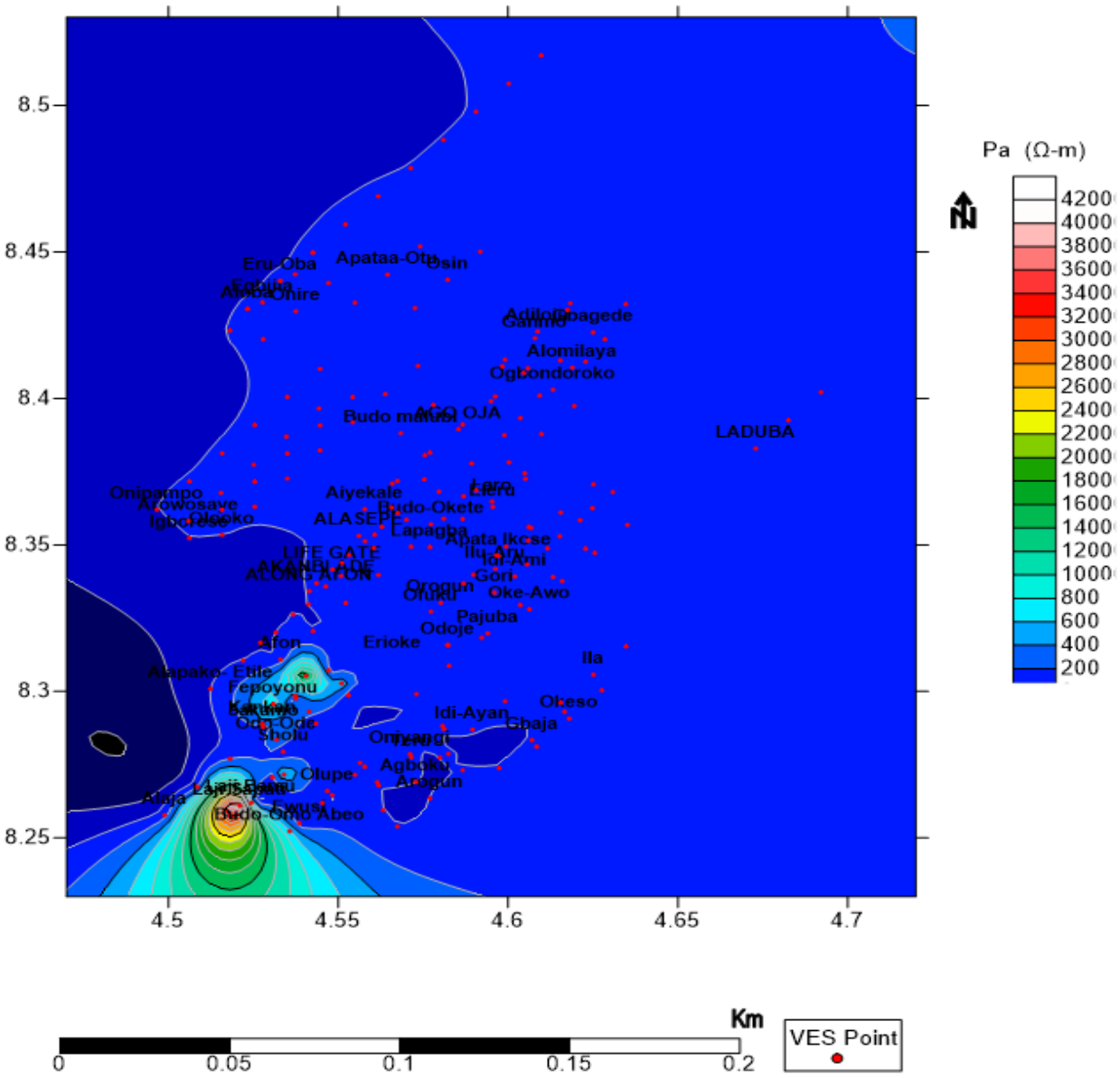


Figure 60: Top soil Isoresistivity map for the study area

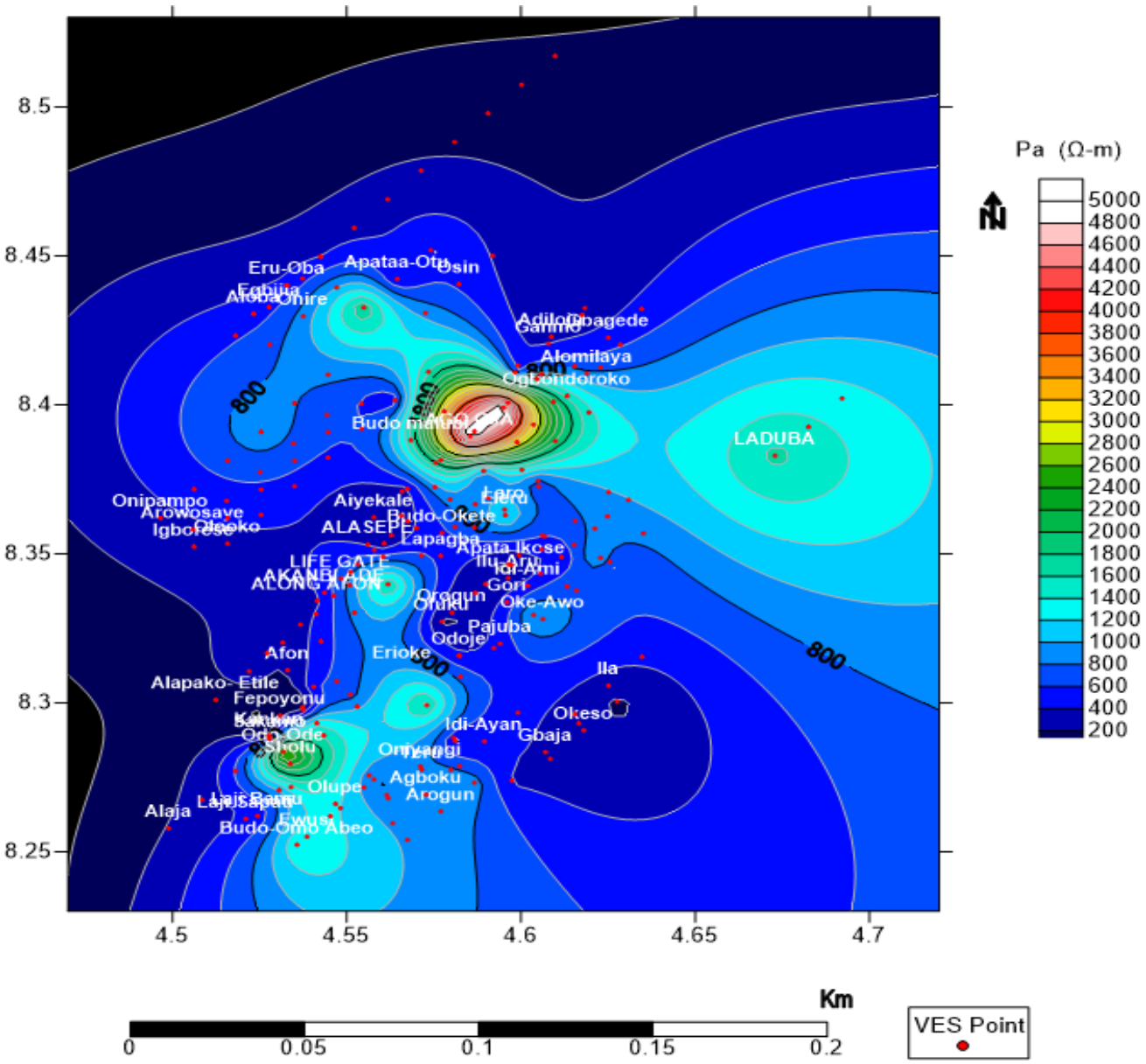


Figure 61: Laterite isoresistivity map for the study area

c. Isoresistivity map of the weathered Basement

The resistivity values of this layer ranges from 50 Ωm to 750 Ωm. The Iso-resistivity map shows that isolated spots in the north central and southern portions of the study area are areas of high resistivity with resistivity values ranging from 500 to 700 Ωm and a low groundwater potential (Figure 62). These areas include Osin, Budo-omo Abeo and Arogun. Areas comprising North-eastern, western and south eastern parts of the study area are low resistivity region (50- 300 Ωm), indicating high groundwater potential zones. The areas include pajuba,Oke awo, Aloba and Odoge (Figure 62).

d. Isoresistivity map of the Fresh Basement

The resistivity value of this layer lies between 200 and 4400 Ωm (Figure 63). The map reveals that at isolated spots in the north-western, western and southern portions of the study area are high resistivity region with resistivity values ranging between 3000 and 4000 Ωm where low groundwater potential is found (Figure63). The areas include Alaha, Abogongo and Ewusi while areas in the south-eastern of the study area are areas of low resistivity (200-800 Ωm) having high groundwater potential. These areas include Ila, Gbaija, Ago, Idi Ayan and Okeso.

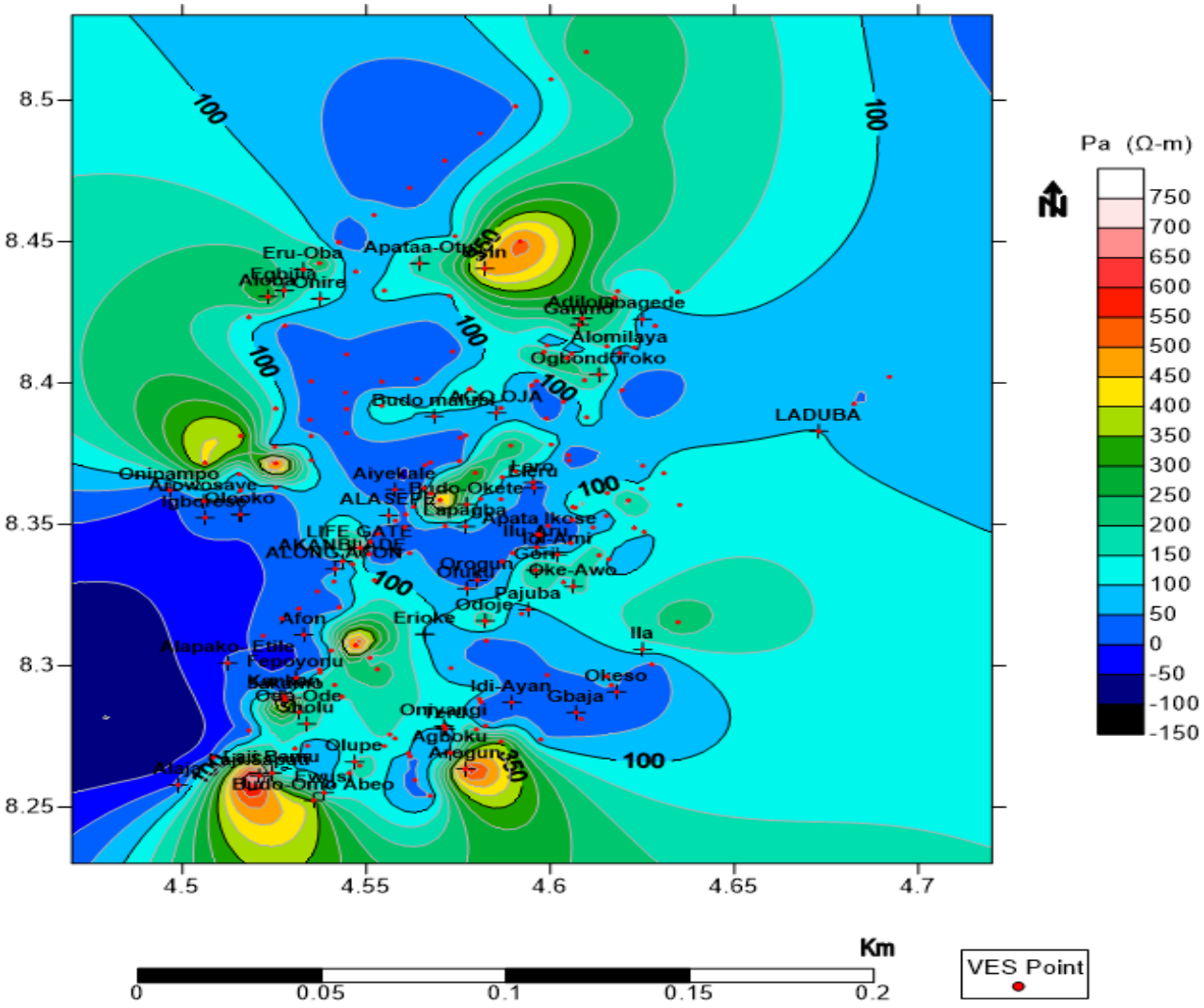


Figure 62: Isoresitivity map of Weathered Basement for the study area

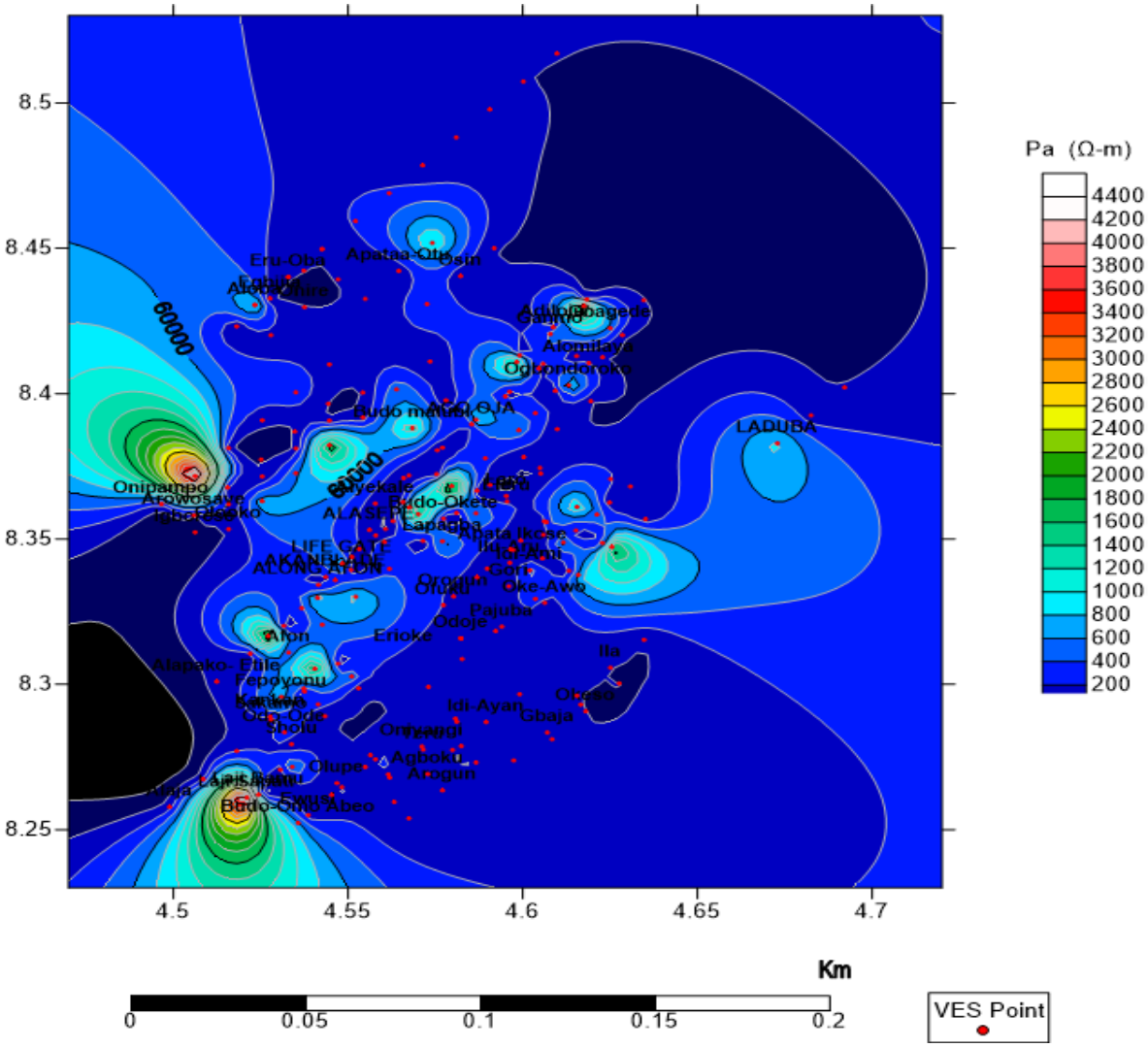


Figure 63: Isoresistivity of Fresh basement rock within the study area

4.5.2.4 Isopach map

This is a map of different lithological layers showing area of equal thicknesses within each layer. This map is discussed under the following headings:

(a) Isopach of Topsoil

The thickness of the topsoil varied from 0.5m to 11 m with the thickest values ranging from 7.5 m to 10.5 m at the North-eastern and south-western portions of the study area which include areas like Alapako Etile, Laduba and Gbagede. (Figure 64).

(b) Isopach of Lateritic soil

The thickness of this map varied from 0 m to 12.5 m with the thickest values ranging from 7m to 8.5 m towards the Northern and southern portions of the study area which include areas like Oke-Awo, Odoje, Arogun and Adigbongbo (Figure 65)

(c) Isopch of Weathered Basement

The thickness of this map varied from 0 m to 42 m with the thickest values ranging from 30 m to 42 m towards the North-eastern, North-western and southern portions of the study area which include areas like Onire, Osin, and Budo-Abeo (Figure 66).

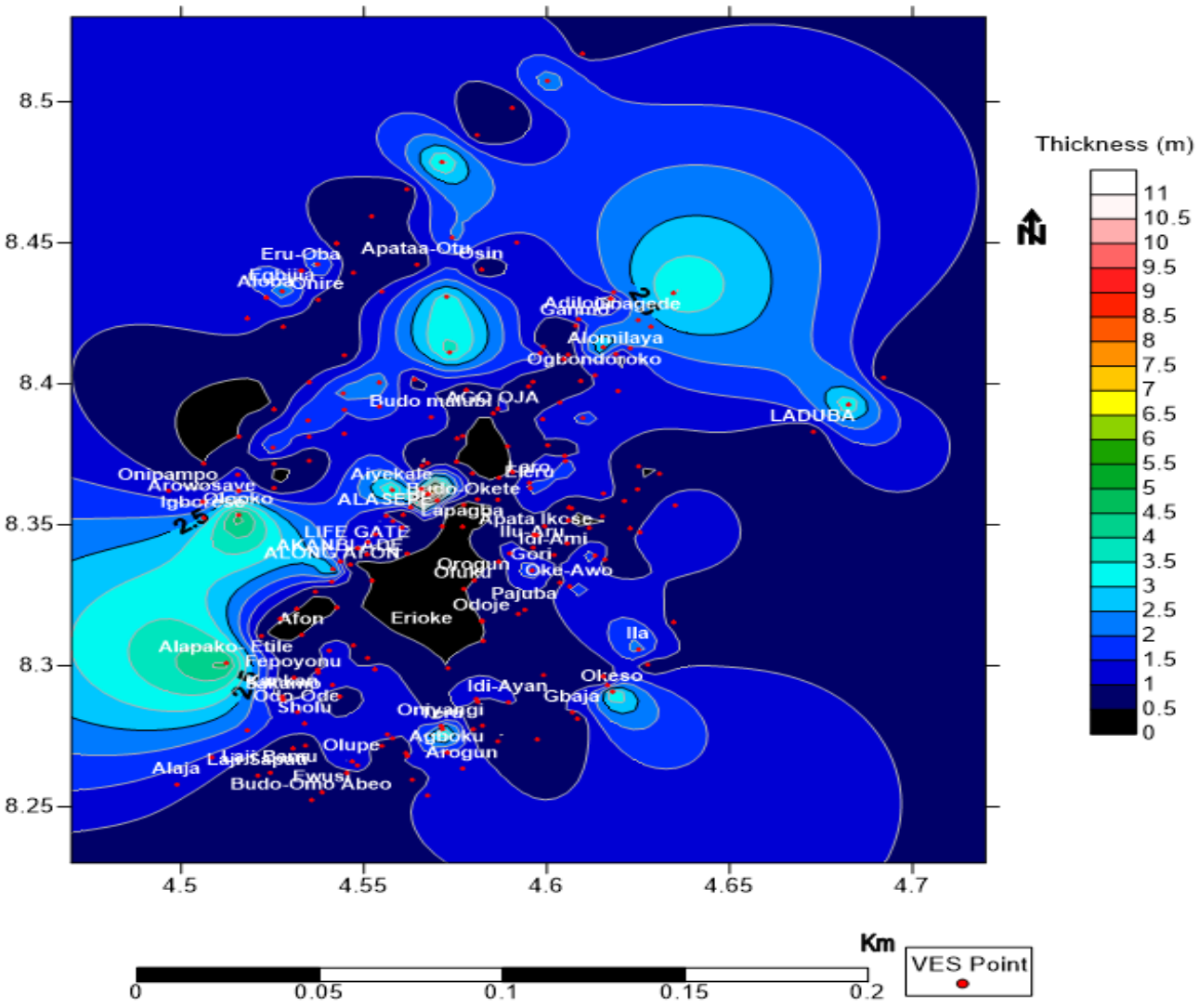


Figure 64: Isopach map of top soil for the study area

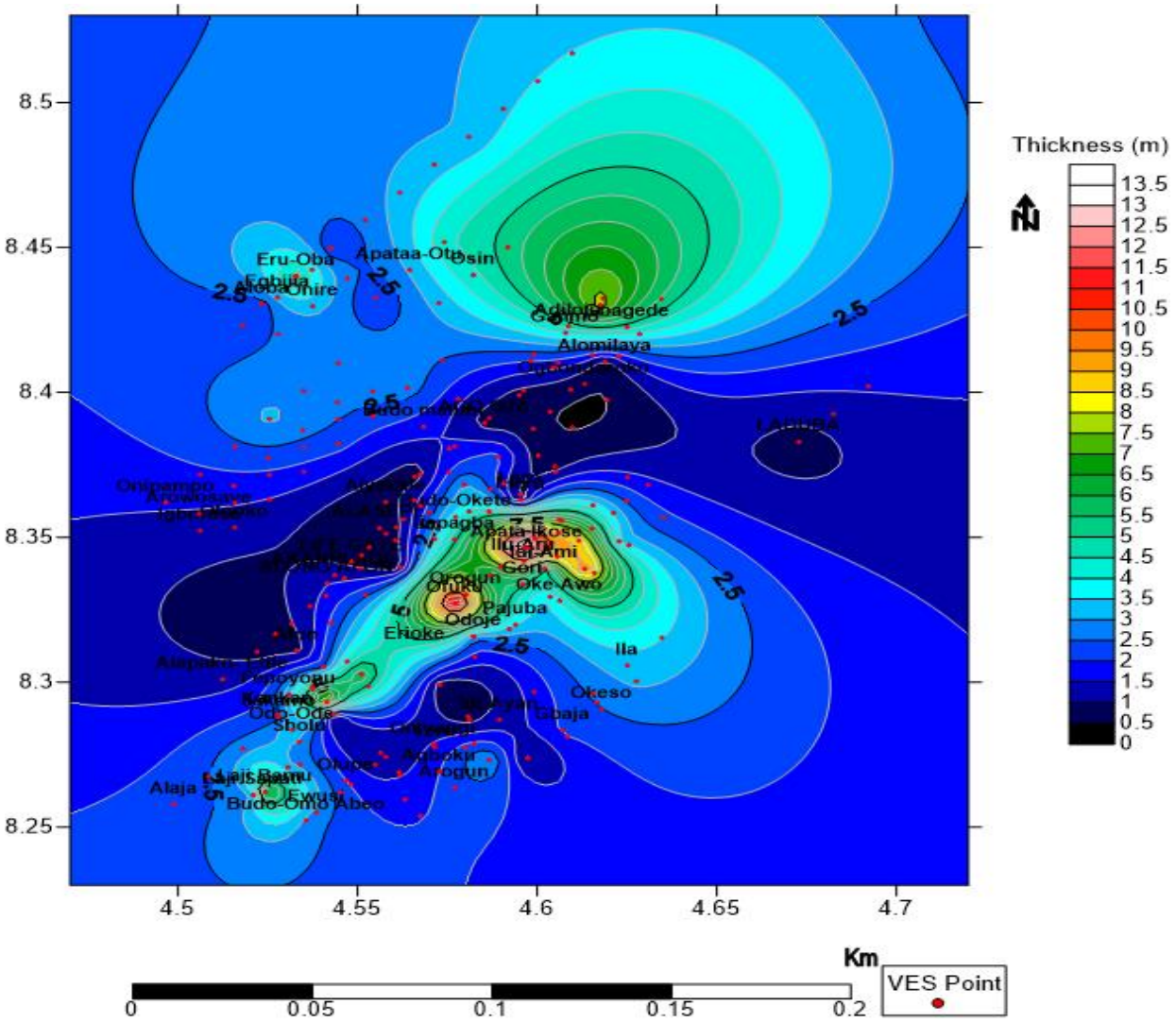


Figure 65: Isopach of Laterite within the study area

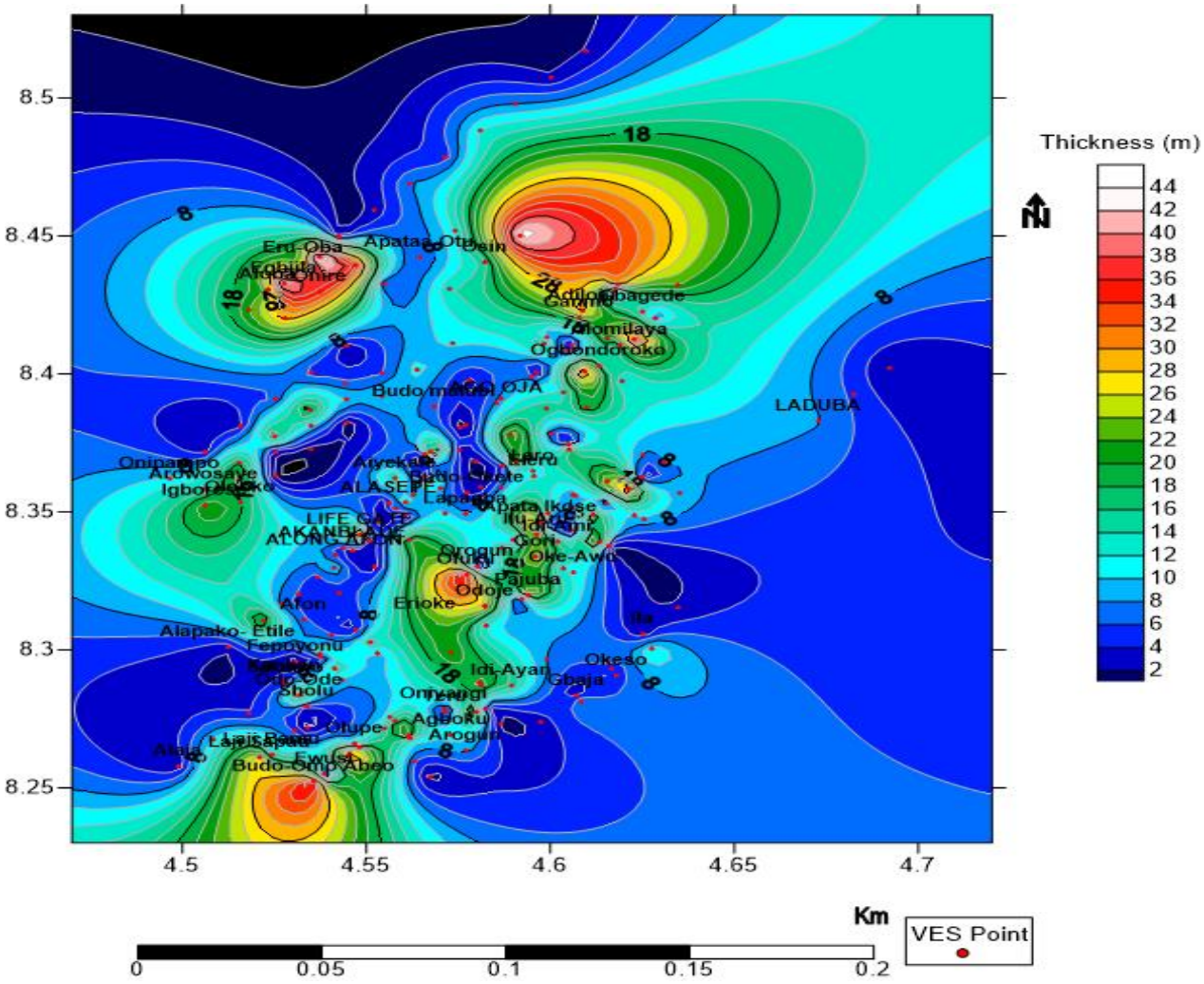


Figure 66: Isopach map of weatherd Basement within the study area

4.5.2.5 Dar- Zarouk parameters

As employed by Ekwe *et al*. (2010), Okonkwo *et al*. (2013) and Okonkwo and Ugwu, (2015), Dar- Zarouk parameters such as longitudinal conductance (S), total transverse resistance (T), transverse resistivity(ρ_t), longitudinal resistivity(ρ_L) and coefficient of anisotropy (λ) were also used to delineate and define areas of target of groundwater potential in the study. The parameters are discussed as follows:

a. Longitudinal conductance (S) to evaluate aquifer protective capacity

Aquifer protective capacity is the ability of aquifers to be less vulnerable to surface contaminants. Aquifer protective capacity is a function of its longitudinal conductance. The longitudinal conductance (S) is a measure of the impermeability of a rock layer (Billing, 1972). According to Golam *et al*., 2014; Oborie and Udom, 2014, longitudinal conductance is computed using combination of resistivity and thickness of layers of the aquifer. High longitudinal conductance indicates relatively high protective capacity while low longitudinal conductance indicates low protective capacity. The protective capacity of aquifers provide visual information for more vulnerable zones which help to protect groundwater resources and also employ to evaluate the potential for water quality improvement.

The calculated longitudinal conductance of the overburden at each station was obtained from mathematical model of Henriet, (1976) (Equation 32)

$$S = \frac{h_1}{\rho_1} + \frac{h_2}{\rho_2} + \frac{h_3}{\rho_3} + \cdots + \frac{h_{n-1}}{\rho_{n-1}} \qquad 32$$

Whereh_1, h_2, etc. are the thicknesses and ρ_1, ρ_2, are the resistivities of successive layers. Hence, the calculated values in the study area are presented in Table 4(a-e). Table 5 shows the longitudinal conductance/ protective capacity rating used for comparison of the result obtained in Table 4(a-f) which is in Appendix 3.

Comparing the calculated values of longitudinal conductance in the area with the standard rating by Oladapo and Akintorinwa, 2007 (Table 5), it is observed that the protective capacity rating of the study area shows very poor, weak, moderate, good and excellent protective capacity rating. Ten VES stations show very poor protective capacity and the areas include Amayo, Ogbondoroko, Laduba/Malubi, Afon road, Kankan and Ajibaba which are found in the northern, North-eastern, southern and south western parts, twelve (12) VES stations show weak protective capacity which are areas like Egbejila, Sakamo, Gbogbin, Alapako Etile, Odo-ode and Fepoyonu in the south western part of the area because of their longitudinal conductance values ranging from 0.1 to 0.19, nine VES stations show moderate protective capacity which include Reke, Ogbondoroko, Ago-Oja, Alaha, Onipampo, Oloko and Aloba in the northern and western parts of the area due to their longitudinal conductance values ranging between 0.2 and 0.69, two VES stations show good protective capacity and the stations are Amayo and Orisunbare Egbejila in the north-eastern part due to their longitudinal conductance values which fall between 0.7 and 4.9, and the remaining one and hundred and seventy eight (178) VES stations have their longitudinal conductance values greater than 10; making them to be of excellent protective capacity. Further, the overall distribution of longitudinal conductance over the area is depicted in Figure 67. From this analysis, it is observed that most parts of the study area have excellent protective capacities which indicate that they are zones of low vulnerability to contaminants; hence the groundwater quality of the parts is good.

b. Transverse unit Resistance (T)

The transverse unit resistance is the product of a layer's true resistivity and its thickness. It is used in direct relations with transmissivity and the highest T values reflect most likely the highest transmissivity values of the aquifers or aquiferous zones and vice-versa (Kumar *et al*., 2001). The transverse resistance parameter for the saturated zone of the aquifer makes it

possible to delineate the most favourable zones, with the objective of hydrogeological exploration (Gilli*et al*., 2004).

The highest T valuewas determined at VES station 47 (32,733.87 Ωm^2) and the lowest was at VES station 206 (8.6 Ωm^2) and therefore, depict that the aquifers or aquiferous zones delineated at these two mentioned VES stations might have the highest and lowest transmissivity values respectively in the study area, thus indicating high and low groundwater potential respectively. The total transverse unit resistance can be obtained from

$$T = \sum_i^n = h_1\rho_1 + h_2\rho_2 + h_3\rho_3 + \ldots\ldots h_n\rho_n \quad 33$$

Where T is the total transverse resistance, Σ is summation sign, h_1 is the thickness of the ith layer and ρi is the resistivity of the ith layer

Using equation 33, the calculated values of the total transverse resistance for the two hundred and ten VES stations in the area is summarized in the Table 4(a-f).Figure 68 shows that areas in the northern part of the study area such as Apata-Otu and Osin are marked with the higher total transverse resistance, indicating low groundwater potential while places like Ila, Okeso and Gbaija in the southern part are areas of lower total transverse resistance, indicating high groundwater potential.

c. Longitudinal resistivity(ρ_L)

The Longitudinal resistivity is calculated using

$$\rho_L = \frac{H}{S} = \frac{\sum_{i=1}^{n} h_i}{\frac{\sum_{i=1}^{n} h_i}{\rho_i}} \quad 34$$

Where h = thickness of layers, ρ = resistivity of layer

The calculated values for longitudinal resistivity of the VES stations in the area are presented in Table 4(a-f). From table 4(a-f), it is revealed that the longitudinal resistivity in the area ranges from 0.1951Ωm (VES 20) to 8095.63 Ωm (VES 120). Figure 69 shows the variation of longitudinal resistivity over the study area. An isolated very high longitudinal resistivity is shown at the south-eastern part of the area such as at Pajuba, Odoje and Ila areas, thus indicating low groundwater potential but generally the southern parts show low resistivity, indicating high groundwater potential.

d. Transverse resistivity

The transverse resistivity in the area was obtained using

$$\rho_t = \frac{T}{H} = \frac{\sum_{i=1}^{n} h_i \rho_i}{\sum_{i=1}^{n} h_1} \qquad 35$$

Where h = thickness of layers, ρ = resistivity of layer,

The highest transverse resistivity value (63697.66 Ωm) was obtained at VES 67 in the eastern part indicating low groundwater potential while the lowest transverse resistivity was at VES 3 in the southern part, indicating high groundwater potential. The calculated values for transverse resistivity in the area are shown in Table 4 (a-f) which is shown in Appendix 3.

e. Coefficient of anisotropy (λ)

The coefficient of an isotropy of a particular area could be calculated by using

$$\lambda = \sqrt{\frac{\rho_t}{\rho_L}} = \sqrt{\frac{ST}{H}} \qquad 36$$

Where ρ_t= transverse resistivity, ρ_L = longitudinal resistivity, S= longitudinal conductance. T= transverse resistance and H= summation of thicknesses of layers.

According to Olorunfemi and Olorunnnwo, 1985, a range of 1.39-1.66 anisotropy coefficient has been judged necessary for boreholes to be considered productive in some parts of south-western Nigeria's Basement complex. Based on Olorunfemi and Olorunnnwo's observation, the first 30 VES stations in the study area fall within the range, hence the boreholes in the areas are considered productive. Generally, the values of coefficient anisotropy in the area range between 0.029 and 5349.78**(λ).** Groundwater yield increases with anisotropy coefficient (Olorunfemi *et al*., 1991). The calculated values for coefficient of anisotropy in the area are presented in Table 4(a-f) shown in Appendix 3.

Table 4: Modified longitudinal conductance/protective capacity rating (After Oladapo and Akintorinwa, 2007)

Longitudinal Conductance (Ω^{-1})	Protective Capacity Rating
>10	Excellence
5–10	Very good
0.7–4.9	Good
0.2–0.69	Moderate
0.1–0.19	Weak
0.1	Poor

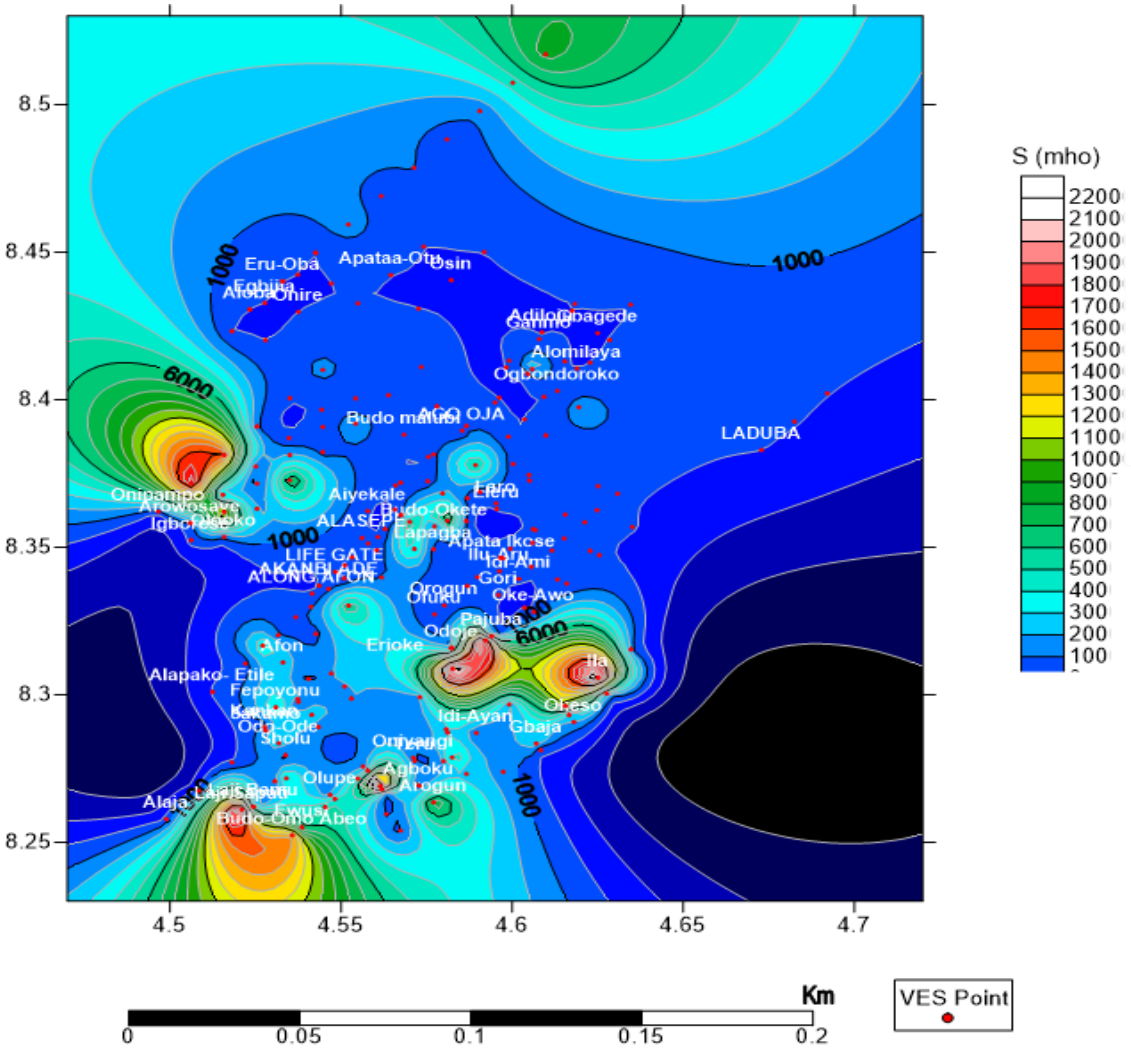


Figure 67: Longitudinal conductance distribution map within the study area

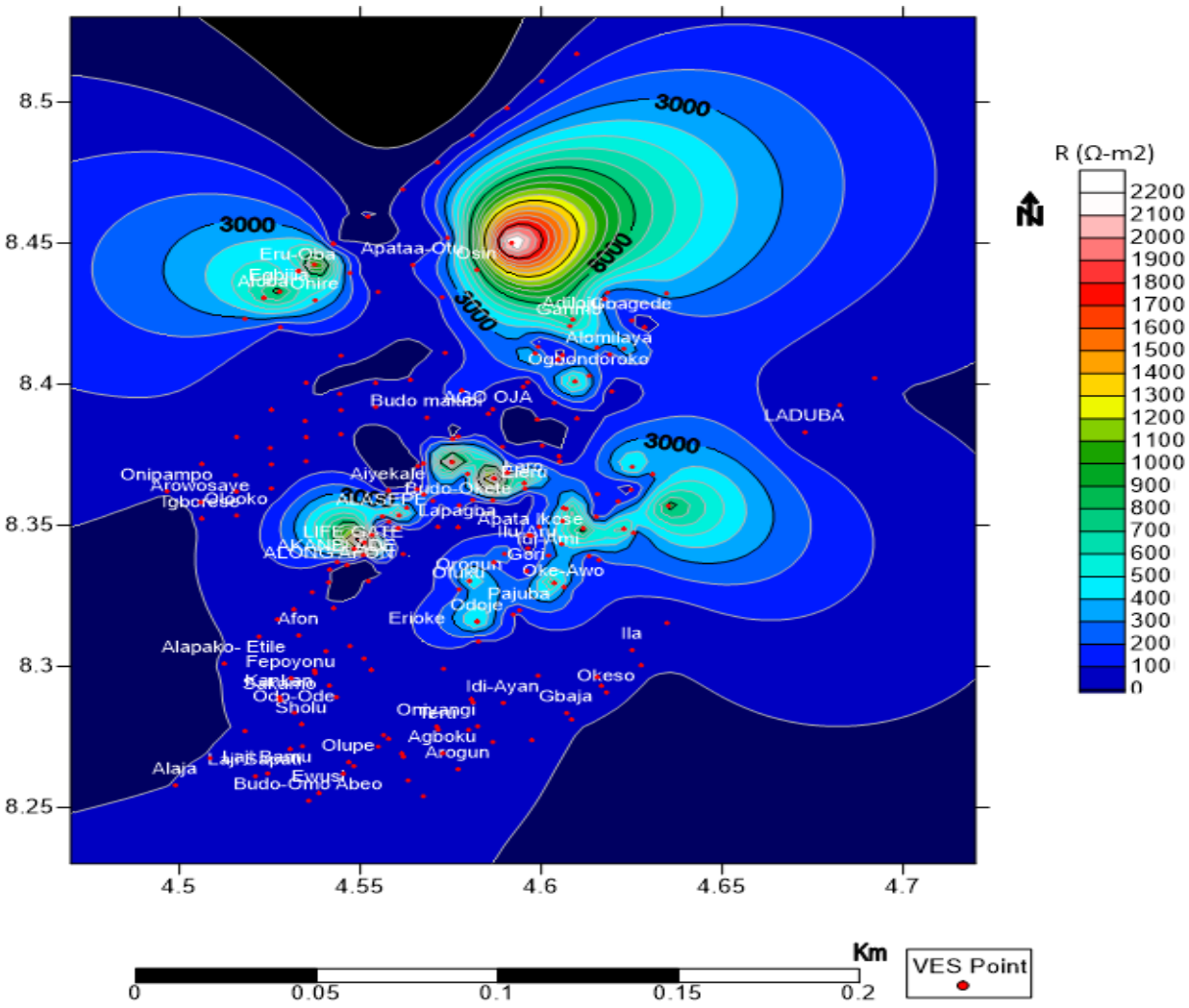


Figure 68: Transverse Resistance distribution map within the study area

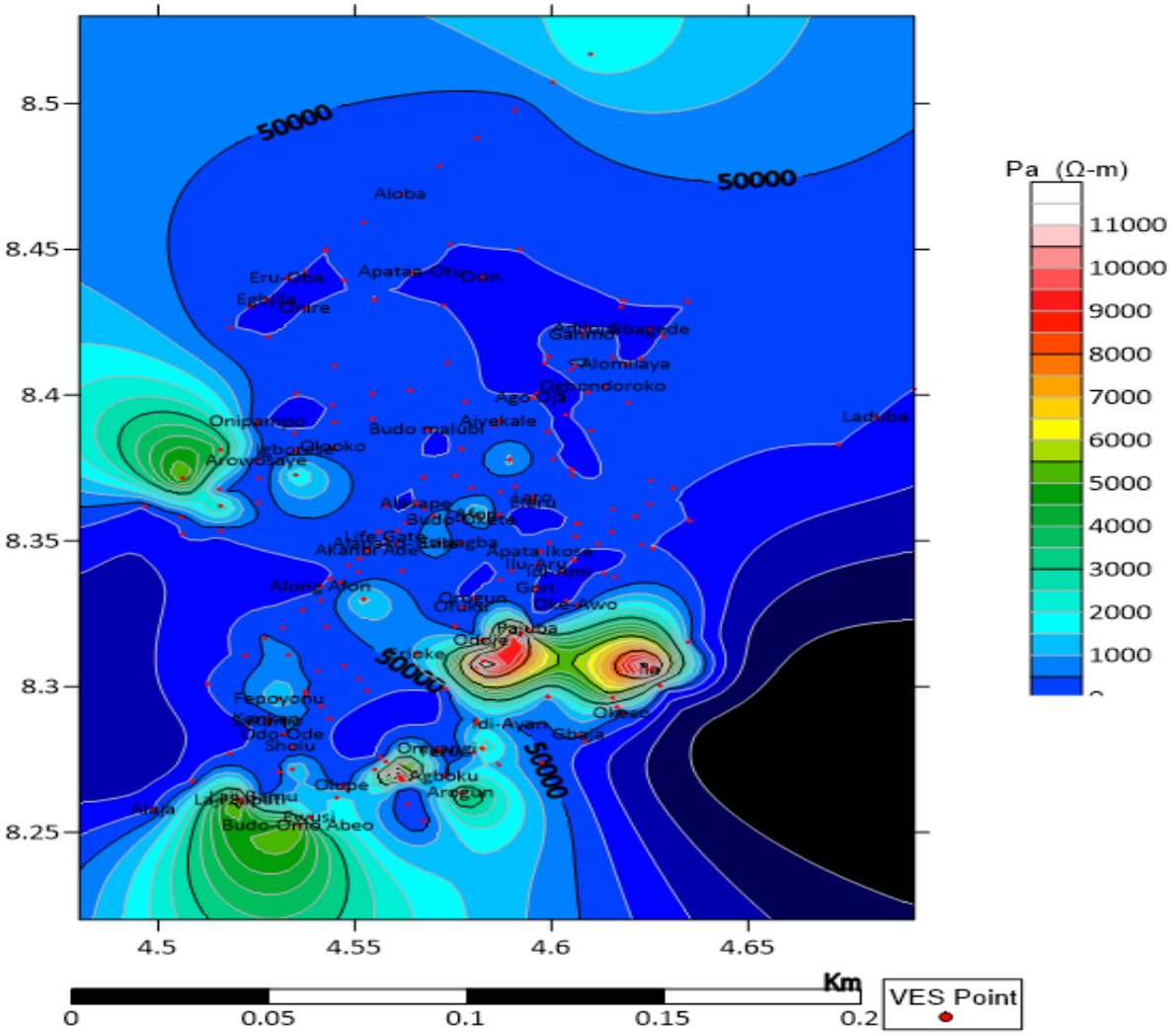


Figure 69: Longitudinal Resistivity distribution mapwithin the study area

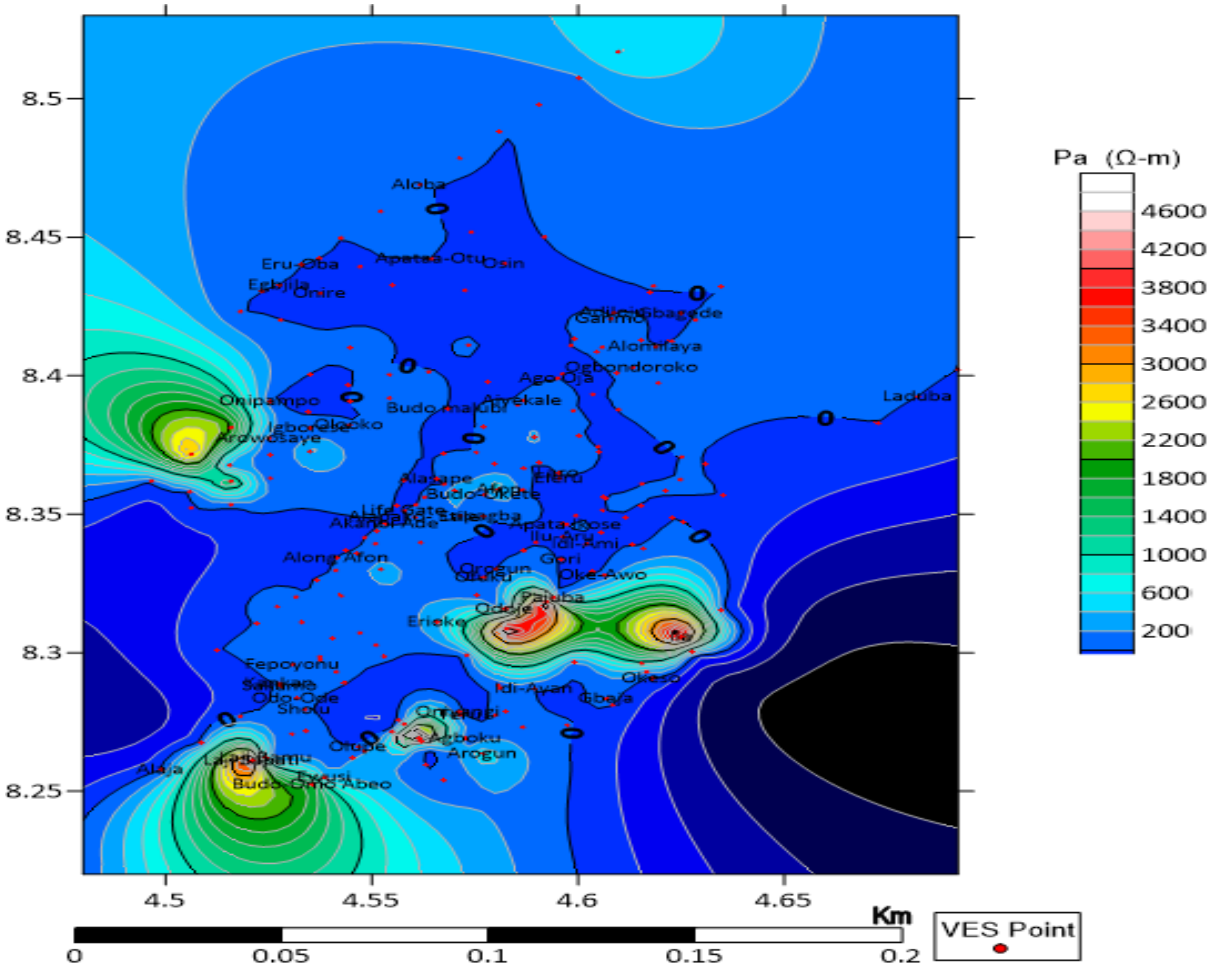


Figure 70: Transverse Resistivity distribution mapwithin the study area

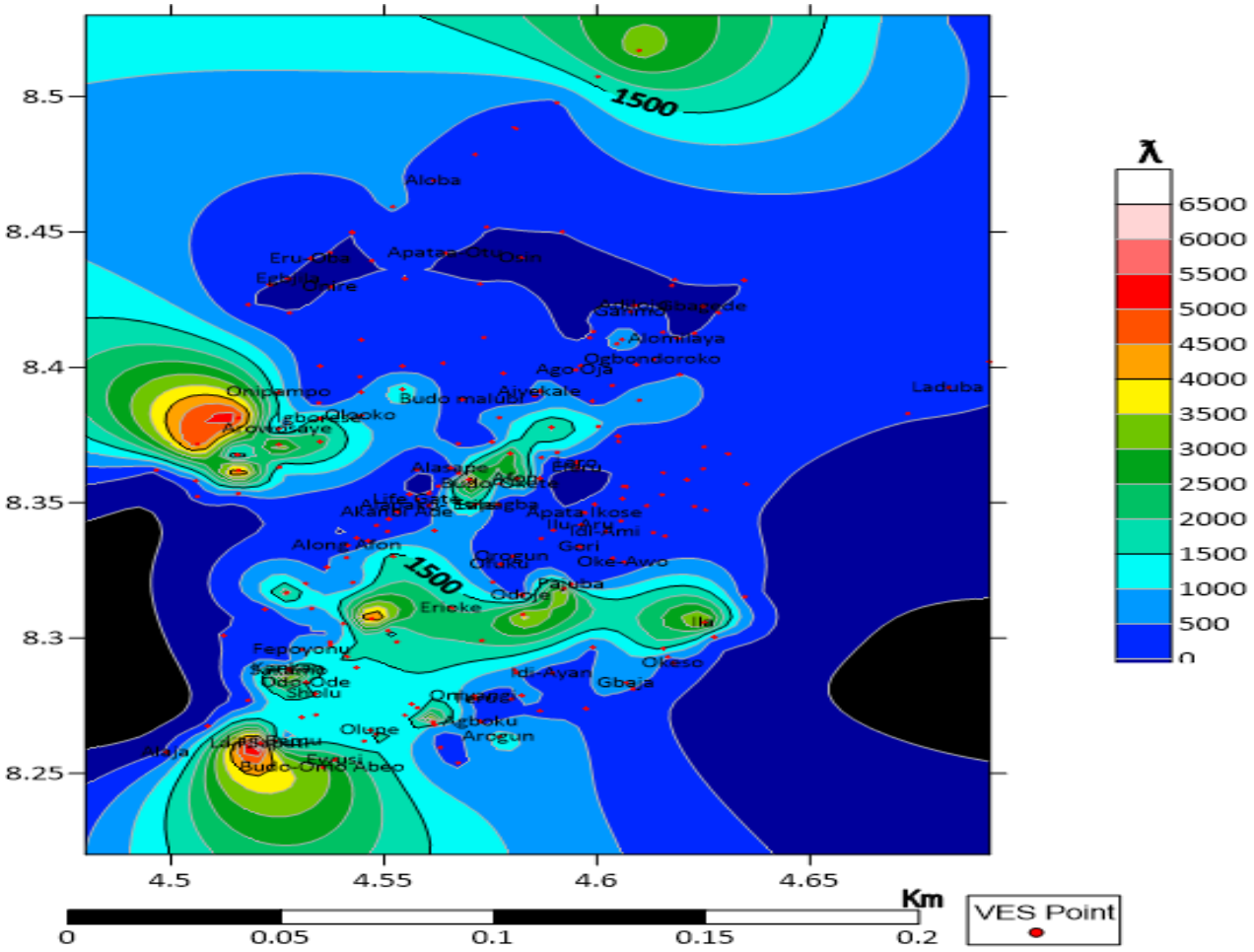


Figure 71: Coefficient of anisotropy distribution mapwithin the study area

4.5.2.6 Groundwater potential evaluation through Reflection Coefficient and Overburden Thickness

Reflection coefficients show the degree of fracturing of the underlying basement better than depending solely on the resistivity values. The reflection coefficients (r) of the study area were calculated using the method of Olayinka (1996), Bhattacharya and Patra (1968) and Loke (1999) as seen in equation 4.15.

$$r = \frac{\rho_n - \rho(n-1)}{\rho_n + \rho(n-1)} \qquad 37$$

Where ρ_n is the layer resistivity of the nth layer, $\rho(n-1)$ is the layer resistivity overlying the nth layer.

In the Basement terrain, good aquiferous zones are usually found either where the overburden is relatively thick and/or where the reflection coefficient is low (< 0.8).

In evaluating promising points for groundwater potential evaluation, three criteria have to be considered, they are:

I. Areas with high groundwater yield: These are the areas with overburdenthickness greater than>13m and with reflection coefficientless than 0.8.
II. Areas with medium groundwater yield: These are areas with overburden thickness greater than 13m and with reflection coefficient greater than or equal to 0.8
III. Areas with low groundwater yield: Areas with overburden thickness less than 13m and with reflection coefficient greater than or equal to 0.8.

Based on thesecriteria, the maps of reflection coefficient (Figure 72) and overburden thickness (Figure 73) show the low, medium and high groundwater potential locations, indicated on Figure 72 as red, green and blue respectively. The promising areas, based on the thickness of overburden, lie in the navy-blue, green, yellow and red colours on Figure 73. Thus, the most promising areas fall in the southern part of the area as shown in Figures 72 and 73.

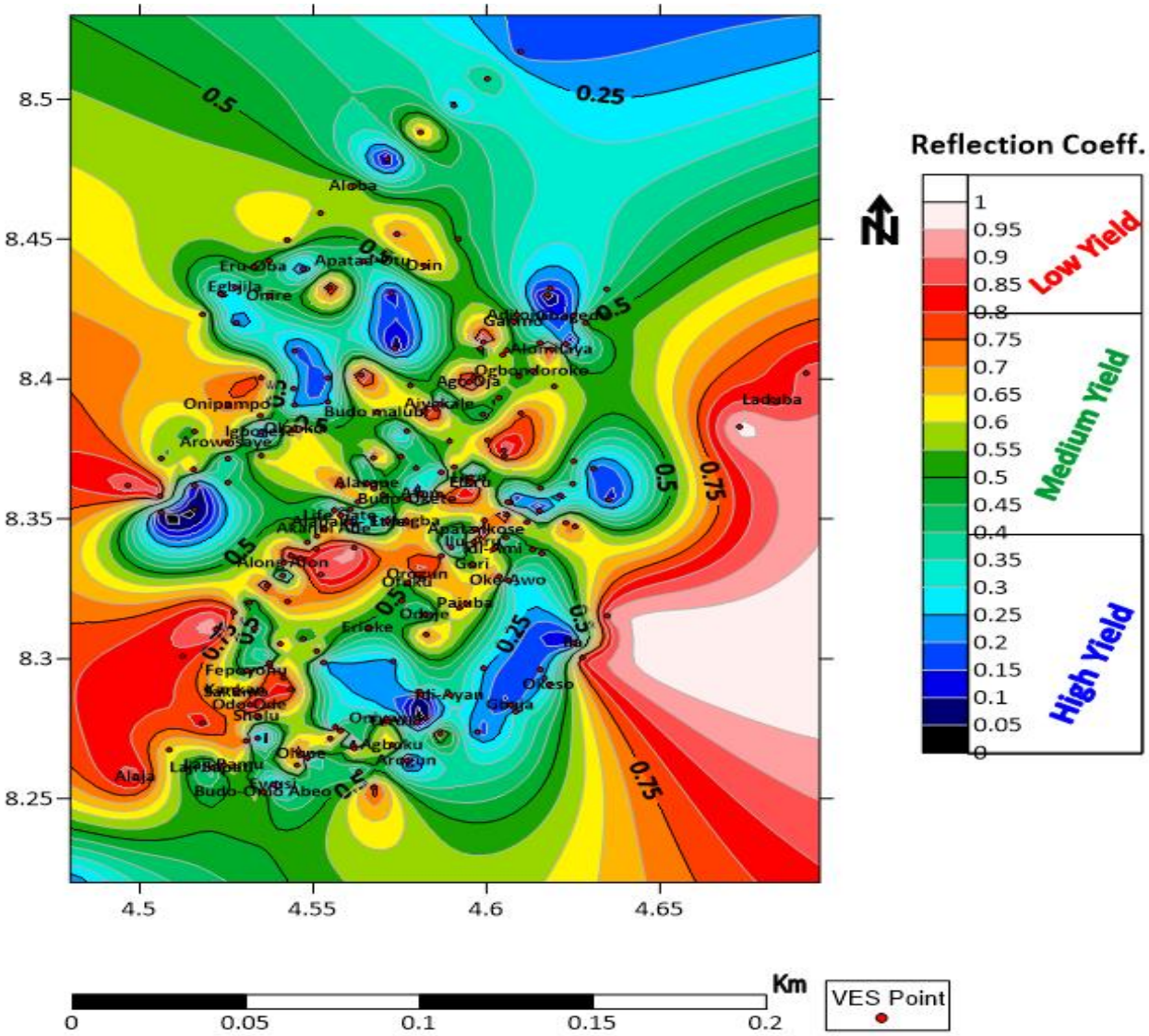


Figure 72: Reflection coefficient variation mapwithin the study area

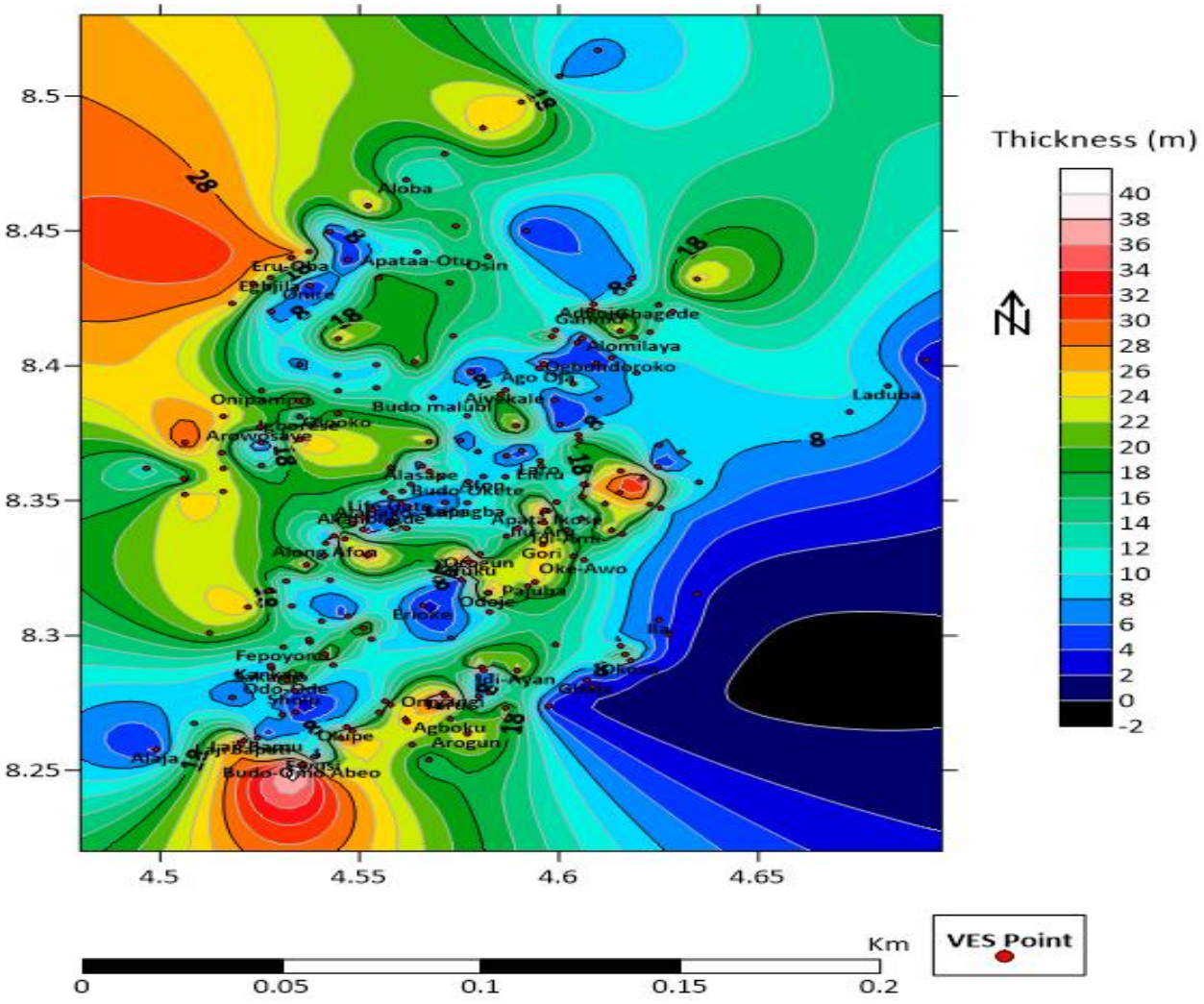


Figure 73: Overburden thickness variation mapwithin the study area

4.5.2.7 Aquifer Parameters

Aquifer parameters are parameters measured from both weathered and fractured crystalline aquifers present in the study area. These parameters include: a. resistivity b. depth (i.e. depth to aquifer) c. Thickness d. hydraulic conductivity, e.Transmissivity. These parameters were obtained for the study area and are shown in Table 6(a-e).These parameters play immesurable roles in the decission making regarding the exploration and exploitation endeavours in the study area. Thus, the parameters shown in Table 6(a-e)were utilised to obtain figures 74 – 81, needed for further meaningful decision makings, discussed in subsections vii(a-e). The table 6 (a-e) is shown in Appendix 4.

a. Aquifer resistivity

This is the resistivity of both weathered and fractured crystalline aquifers in the area. The resistivity ranges from 9.57 Ωm to 784 Ωm. The resistivity values obtained are plotted in the map shown in figure 74. Areas of high resistivity indicate areas of low conductivity which are areas of low groundwater potential. The areas are found in northern, eastern and southern parts of the study (Apata Otu, Onipampo and Budo-Omo Abeo).

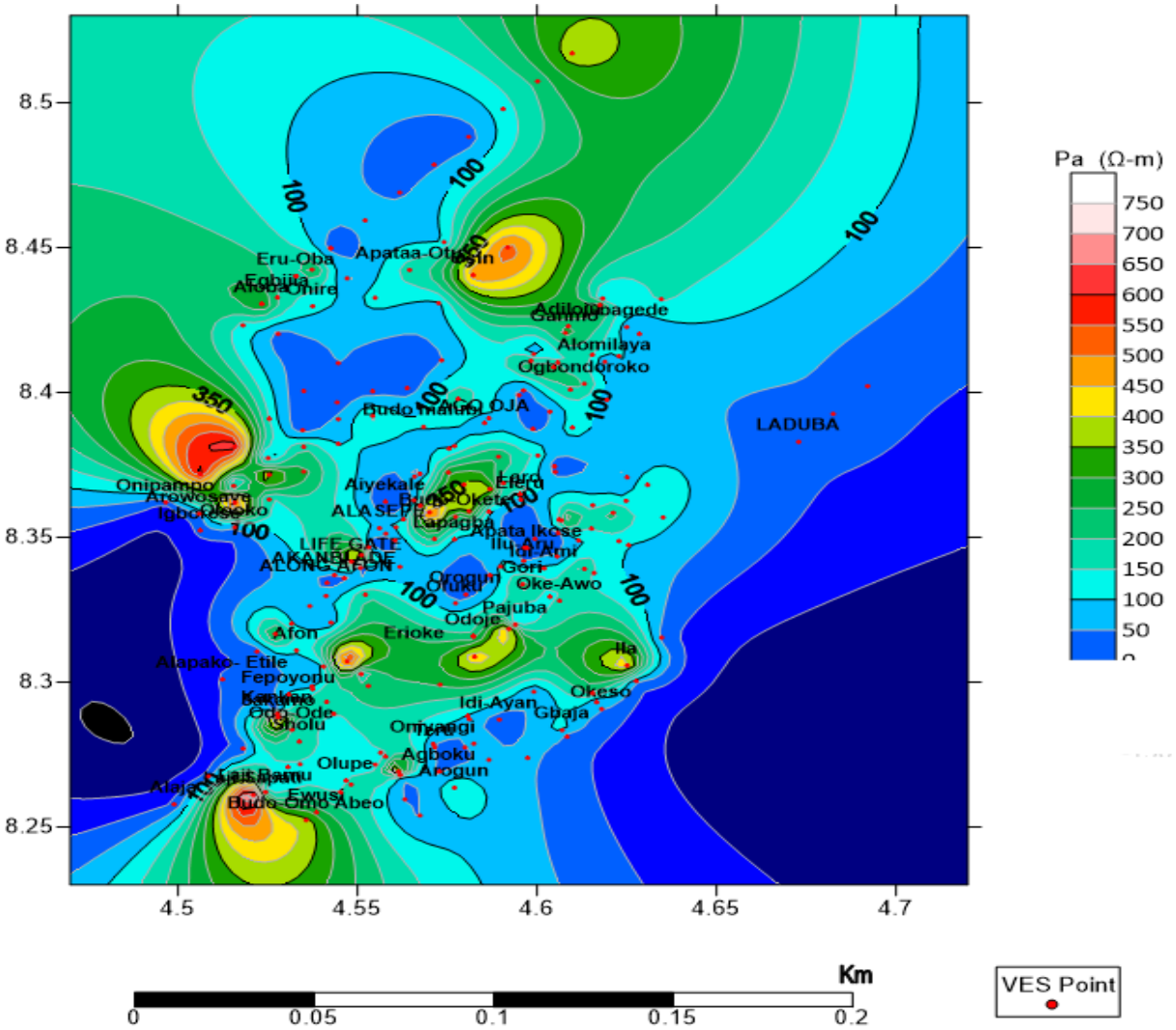


Figure 74: Aquifer resistivity variation map within the study area

b. Aquifer depth

This is the depth to the aquifer in the area. Areas with higher depth (20 to 30 m) such as Abogongo and Aloba areas in the western part of the area (Figure 75) will have their water table farther from the ground surface; hence people in the areas will tap groundwater at a farther depth than those people in the eastern and south eastern parts with lower depth to the aquifer (2 to 8 m). Such areas include Laduba, Ila , Okeso and Gbaija.

The 3-dimensional map of aquifer depth in the study area is shown in figure 76.The map shows variations in the depth of aquifer in the study area. Areas with highest depth where water table is farther to the ground surface allow tapping of groundwater at a farther depth to the surface; indicating that the water is of good quality because of its devoid of surface contaminations. These areas include Kankan, Igborese, Alaha and Onipampo in the western portion of the study area. Also, areas with lower depth are areas with water table nearer to the surface for easier tapping but having lower quality.The areas include Gbaija, Idi-Ayan, Ila and Oniyangi in the south-eastern part of the study area.

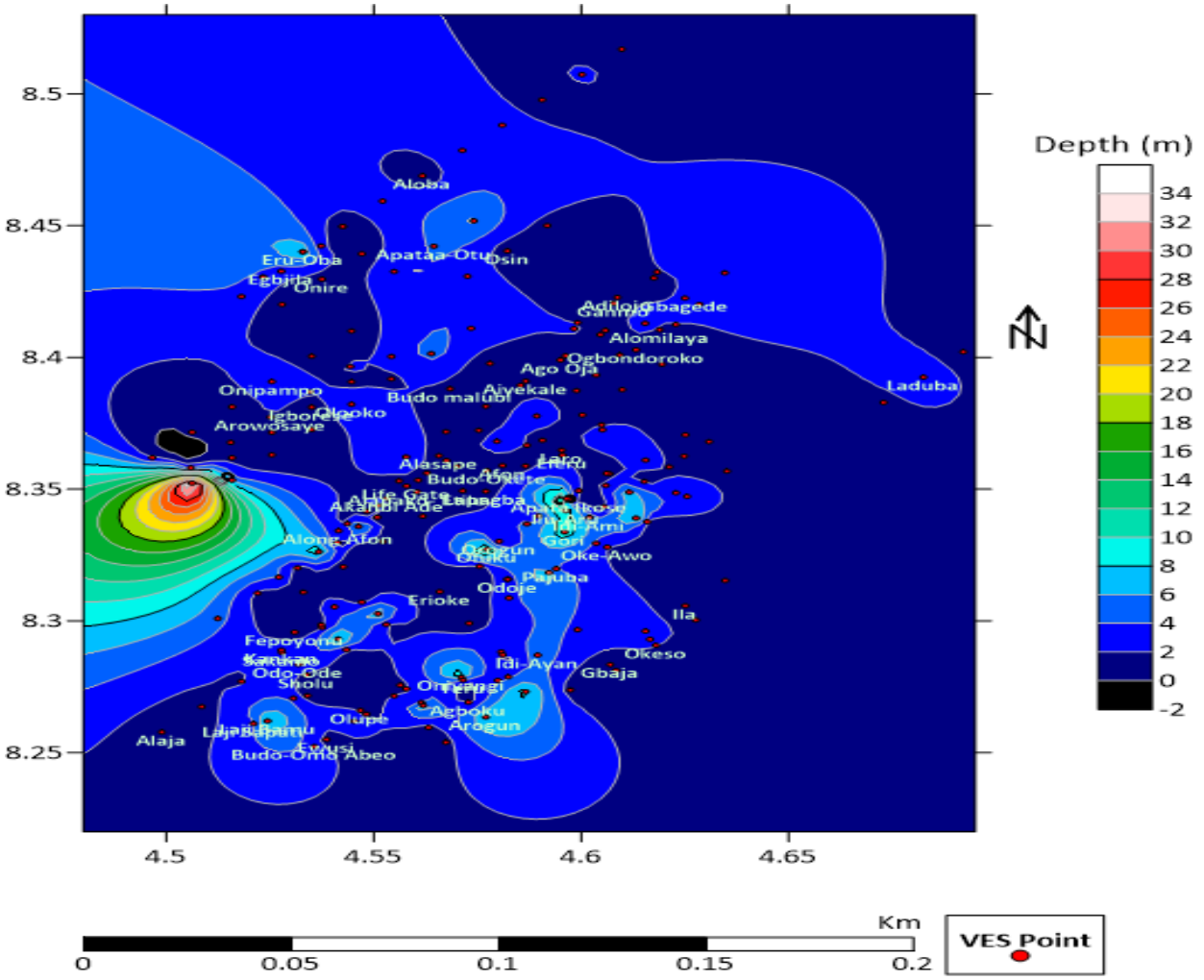


Figure 75: Aquifer Depth variation map within the study area

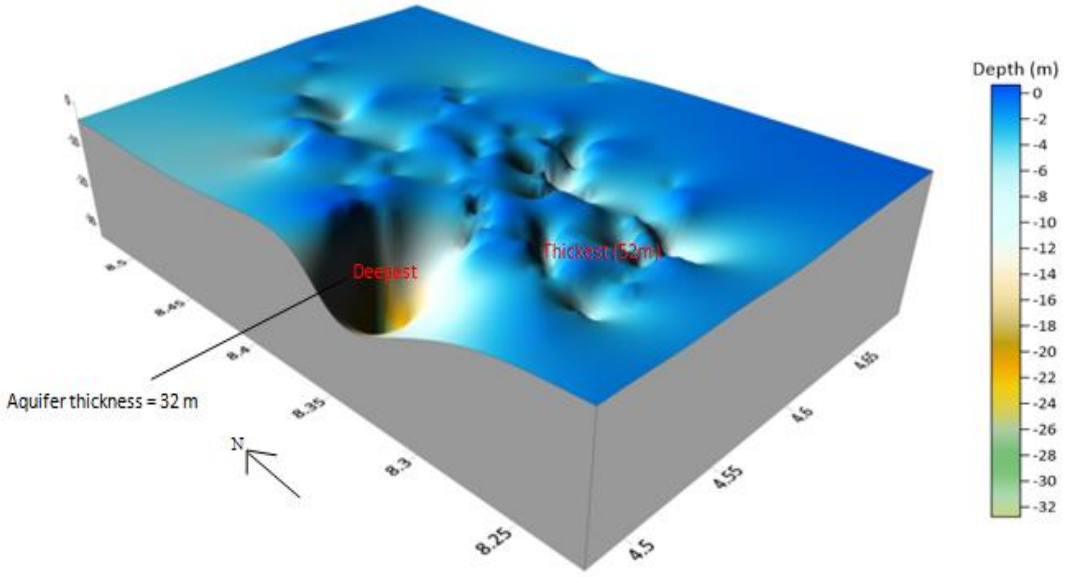


Figure 76: 3-D Impression of aquifer depth variation within the study area.

c. Thickness

The thickness of aquifers in the study area varies from 0.8 m at VES 119 to 63.8 m at VES 47{Table 6 (a-e)}. From thickness distribution map (Figure 77), areas with thickness values ranging from 24 m to 52 m are areas of high groundwater potential. This is due to the fact that the thicker an aquifer is the more groundwater potential would be produced by the aquifer. Those areas are indicated by green, yellow and red colours found around Gbaija, Ila, Okeso and Arogun dominantly in the southern part of the study area. Other areas such as Laduba, Ago-Oja, Budo Malubi and Alaja are areas of low groundwater potential indicated by sky and deep blues dominated in the eastern to western parts of the study area. Aquifer potential map (Figure 78) shows low, medium and high yields areas.

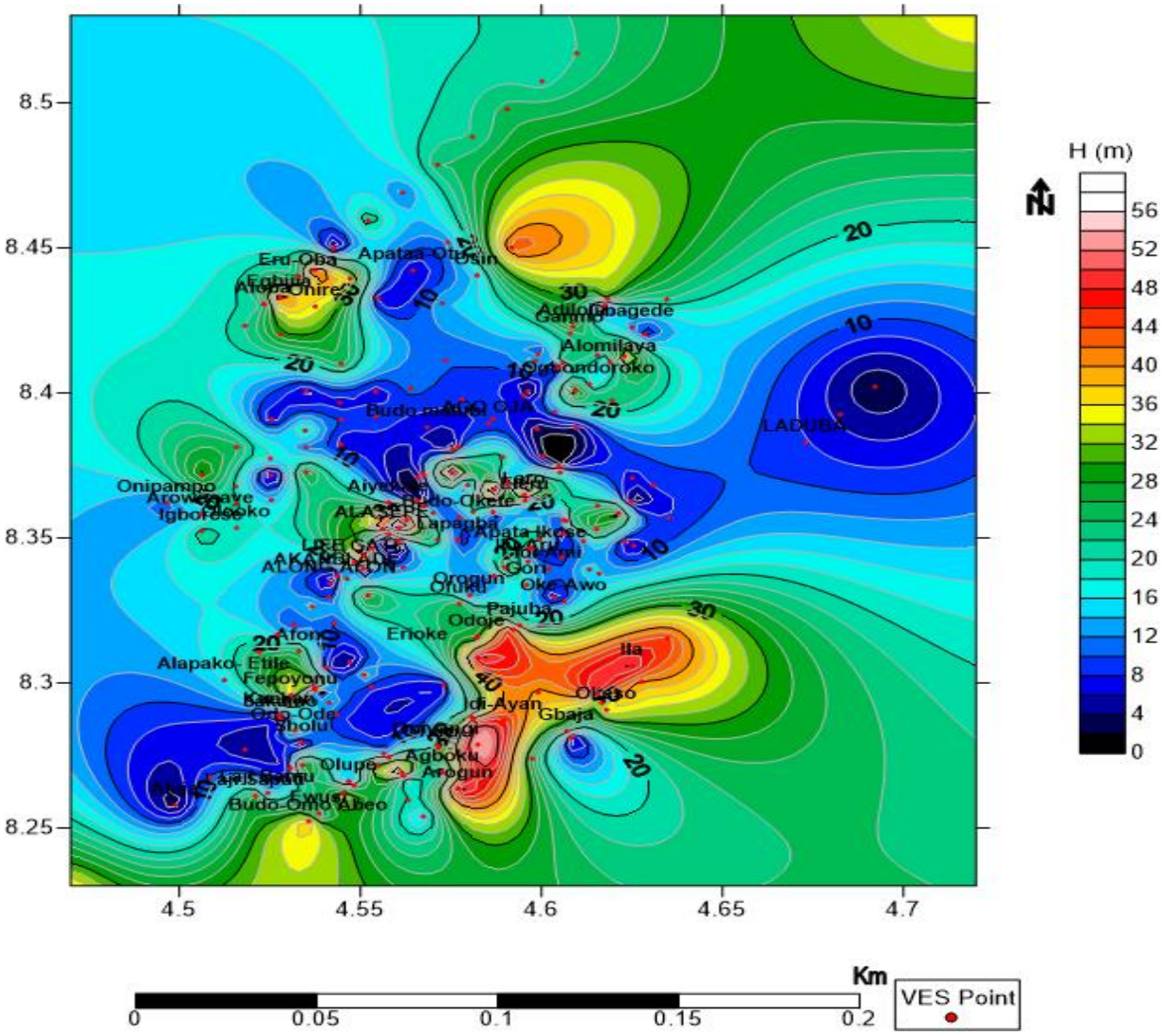


Figure 77: Aquifer thickness distribution map within the study area

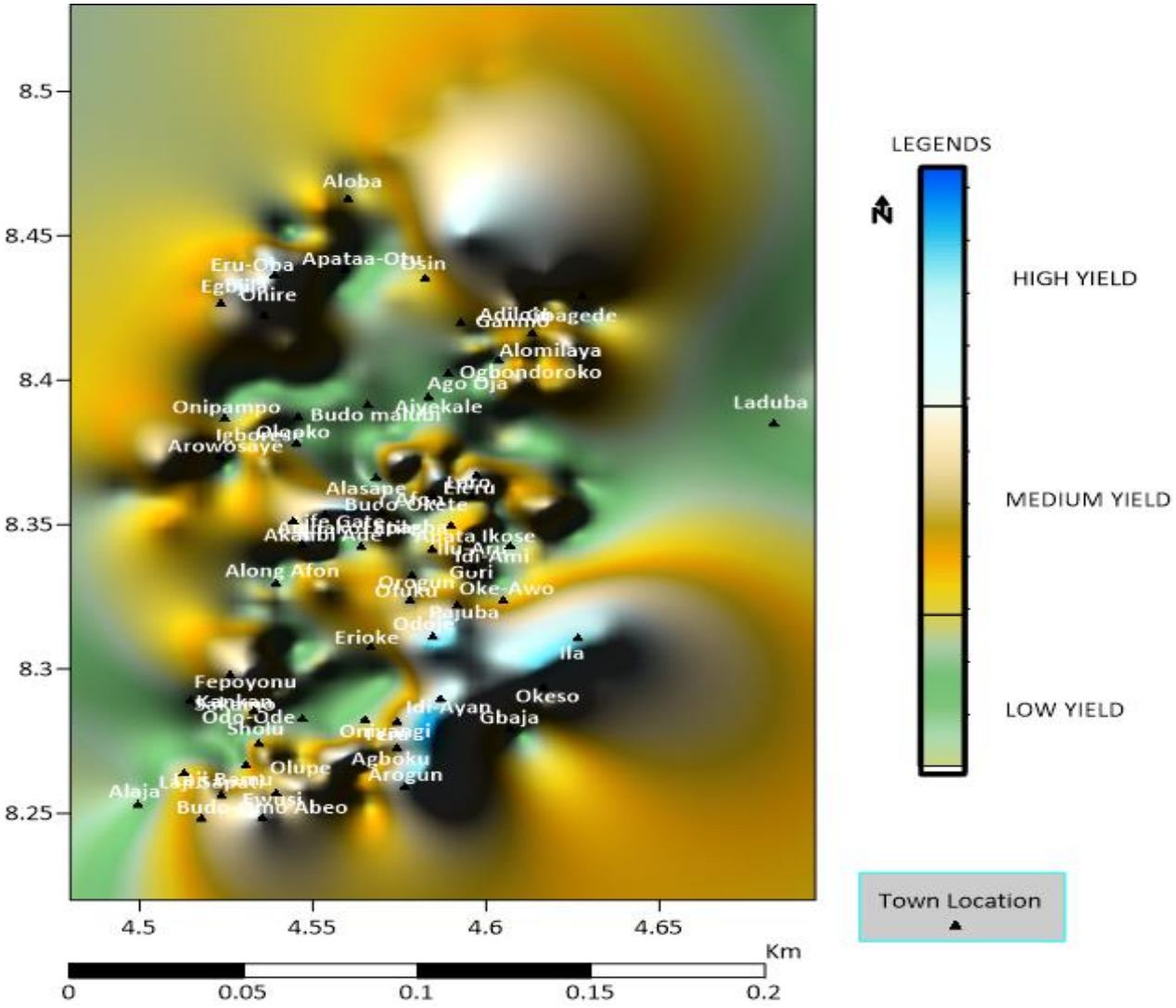


Figure 78: Aquifer Potential map within the study area

The above aquifer potential map was generated from aquifer thickness map

d. Hydraulic conductivity

This is the flow of groundwater in an aquifer through a medium. The hydraulic conductivity of aquifer in the area was calculated using the formular relating it with transmissivity.

$$T = Kb \quad (38)$$

Where T= transmissivity, K= hydraulic conductivity and b= aquifer thickness. Areas with high hydraulic conductivity are concentrated in the western portion of the study area. The areas include Onipampo, igborese and Alapako Etile (Figure 79). This implies that the areas are of high permeability, thus having high porosity. Areas in the northern and eastern parts of the study area which include Apata Otu, Osin, Eru-Oba and Laduba are having low hydraulic conductivity (Figure 79).

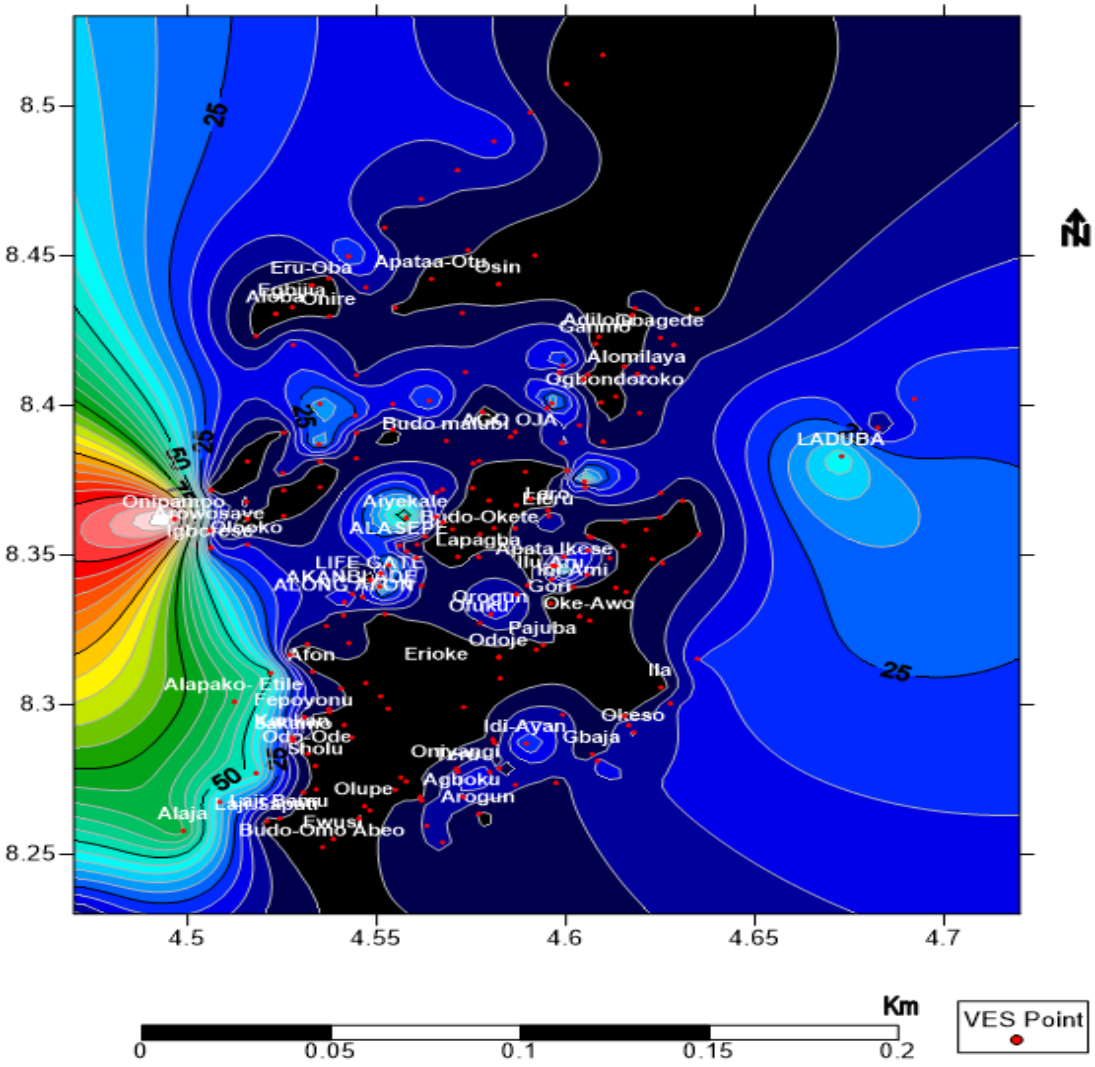


Figure 79: Hydraulic Conductivity distribution map within the study area

e. Transmissivity: Aquifer transmissivity was calculated by a formular showing relationship between hydraulic conductivity (K), electrical conductivity (σ), Transverse resistance (R) and aquifer thickness (h). The formular is given as:

$T_r = K \sigma R = Kh.$ 39

Where T_r = Aquifer Transmissivity, K= hydraulic conductivity, σ = electrical conductivity, R = Transverse resistance and h= aquifer thickness.

The aquifer transmissivity in the area ranges from 0.77 m^2/day to 3,777 m^2/day {Table 6(a-e)} The widely spread areas of transmissivity are areas with transmissivity ranging from 1 m^2/day to 200 m^2/day found in the northern, southern and parts of eastern and western portions of the study area (Figure 80).

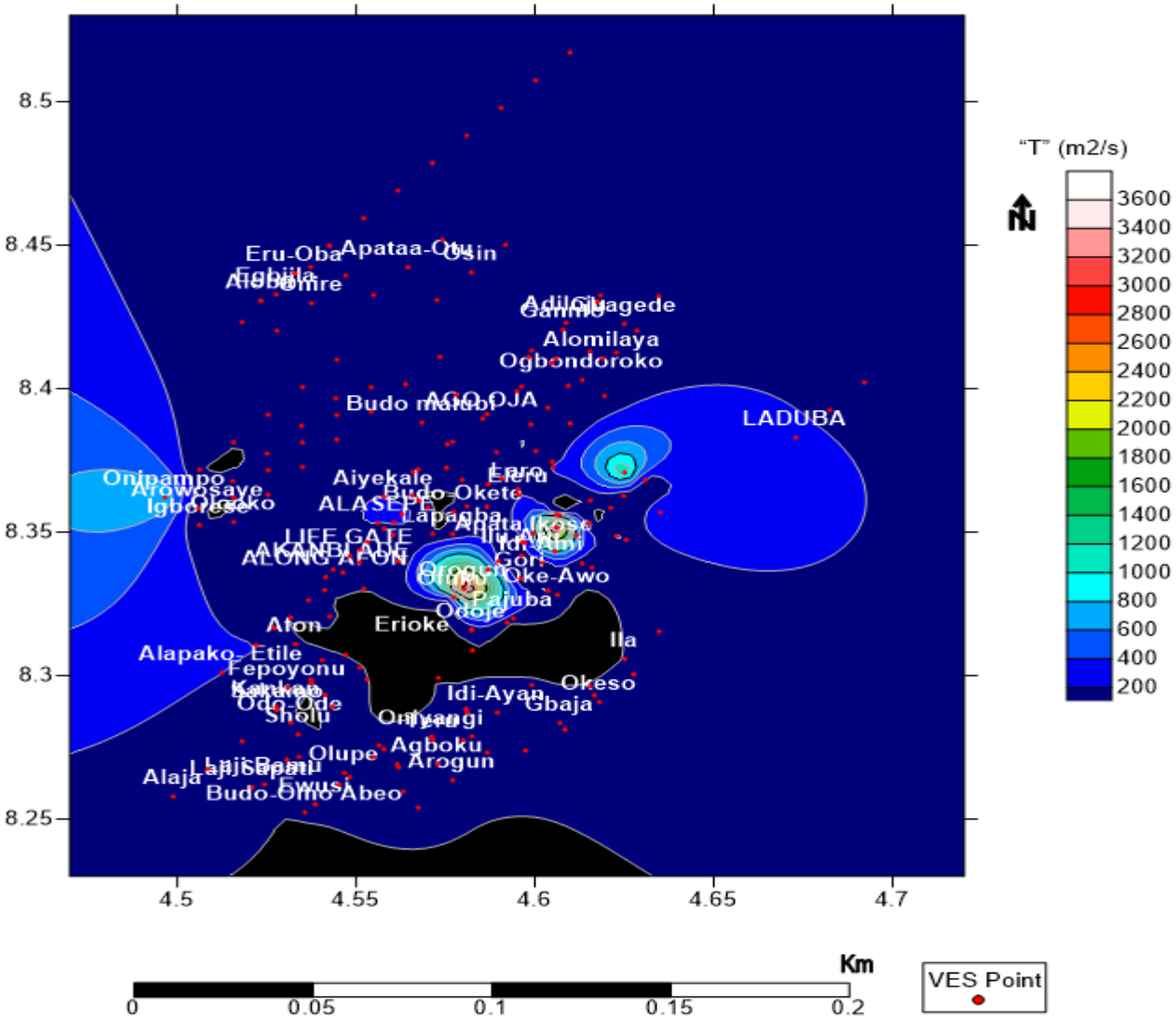


Figure 80: Aquifer Transmissivity distribution map within the study area

4.6 Physico-chemical quality assessment of groundwater of the area

Locations of 35 groundwater samples from both boreholes and wells collected from the study area are shown in Figure 81. 20 groundwater samples were taken from boreholes while the remaining 15 groundwater samples were taken from hand-dug wells. The size was based on the available tapeable groundwater in the area.

The groundwater quality of the area was assessed using physical and chemical parameters. The physical parameters assessed include colour, turbidity, temperature, pH and electrical conductivity. The chemical parameters on the other hand include Calcium (Ca), Sodium (Na), Potassium (K), Magnesium (Mg), Cupper (Cu), Iron (Fe), Manganese (Mn), Zinc (Zn), Lead(Pb), cadmium (Cd), Sulphate (SO_4^-), Phosphate (PO_4^{-}),Chloride (Cl^-) ,Bicarbonate (HCO_3-) , Carbonate (CO_3-) and Nitrate (NO_3^-). Also, the total dissolved solids (TDS) and total hardness of the water samples were analysed. Table 7 displays the comprehensive results of the physico-chemical analysis of the groundwater samples collected in the area. The analysis was done at University of Ilorin central research laboratory, University of Ilorin, Ilorin and the result is discussed sequentially next. The comparison of the obtained result with WHO standard is shown in table 4.8 and represented in Figures 82 and 83.

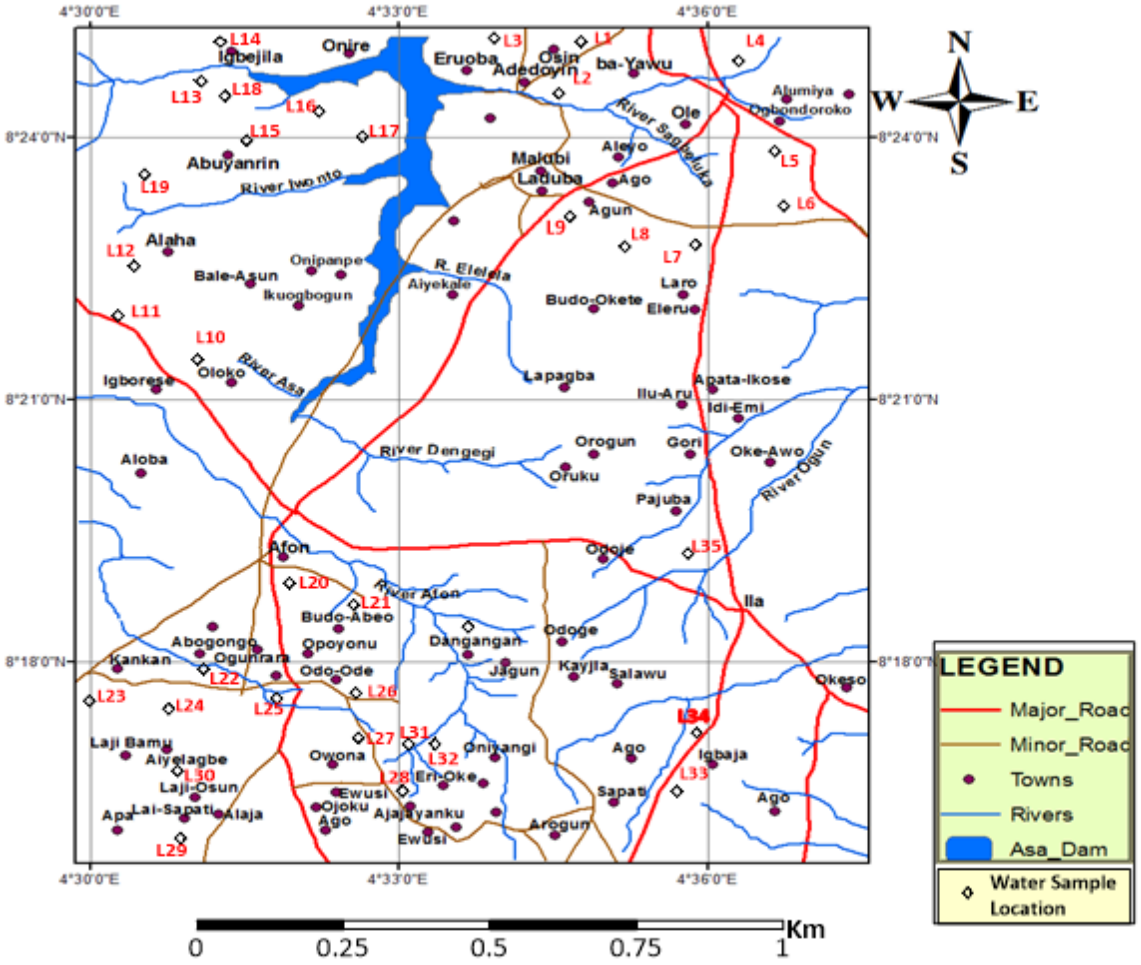


Figure 81: Map of the study area showing groundwater sampling locations.

4.6.1 Quality of groundwater for drinking and domestic purposes

The quality of groundwater in the area for drinking and domestic purposes was discussed under two headings; (a) the physico-chemical parameters and (b) water quality Index.

4.6.1.1 Physico-chemical parameters

i. Colour

According to World Health Organization guide line(2017) for drinking water, it is said that drinking-water should ideally have no visible colour. Sources of colour in drinking-water are due to the presence of coloured organic matter (primarily humic and fulvic acids) associated with the humus fraction of soil, presence of iron and other metals, either as natural impurities or as corrosion products, contamination of the water source with industrial effluents and may be the first indication of a hazardous situation. The source of colour in a drinking-water supply should be investigated, particularly if a substantial change has taken place. Most people can detect colours above 15 true colour units (TCU) in a glass of water. Levels of colour below 15 TCU according to WHO are usually acceptable to consumers, but acceptability may vary. High colour could also indicate a high propensity to produce by-products from disinfection processes. No health-based guideline value is proposed for colour in drinking-water (WHO).

ii. Turbidity

This is the presence of suspended materials such as clay, silt, finely divided organic material, plankton and other organic and inorganic materials in groundwater. It is a measure of water's ability to scatter and absorb light, and is expressed in NTU (nephelometric turbidity units). The World Health Organization, 2017 said that the desirable limit for turbidity is 5 NTU while its maximum permissible limit is 1000 NTU.

Hence, the average value of turbidity for groundwater samples in the area is 182.3 NTU which is within the permissible limit of WHO

iii. pH Value

The PH of water is the negative common logarithm of the hydrogen ion activity: pH= -log ($H^{+)}$. It is a measure of acidity or basicity on a scale from 0-14. pH is sensitive to small changes in water chemistry. Like conductance, pH can be considered a good preliminary indicator that your water quality is changing for some reason, but it alone cannot be used to identify the culprit (Colorado Water Energy Research Centre, 2014). It usually depends on free carbon dioxide picked up from atmosphere as rain falls, presence of acids of peaty origin, decaying vegetation and presence of sulphates. Depending on pH, water is described as neutral (pH from 6.8 to 7.2), weakly alkaline (pH 7.2 to 7.8), alkaline (pH 7.8 to 8.2) or strongly alkaline (pH > 8.2). Also, water can be described as weakly acid (pH 6.0 to 6.8), acid (4.5 to 6.0), and strongly acid (pH< 4.5) (Schoeneich, 2001).

Table 5: Physico-chemical Analysis of Groundwater samples in the area

Lat.(deg.)	Long.(deg.)	Locations	Villages	pH	Temp.(oC)	Elect.Cond.	Turbidity	TH (mgl)	TDS (mgl)	Ca^{2+} (mg/l)	Na^{+} (mg/l)	K^{+} (mg/l)	Mg^{2+} (mg/l)	Cu^{2+} (mg/l)	Fe^{2+} (mg/l)	Mn^{+} (mg/l)	Zn^{+} (mg/l)	Pb^{2+} (mg/l)	Cd^{+} (mg/l)	SO_4^{2-} (mg/l)	PO_4^{-} (mg/l)	Cl^{-} (mg/l)	HCO_3^{-} (mg/l)	CO_3^{-} (mg/l)	NO_3^{-} (mg/l)
8.43	4.57	L1	Osin Aremu	4.6	29	160	80	2.2815	112	0.765	0.66	0.17	0.09	0.015	0.06	0.045	ND	ND	0.015	0.1064	1.4299	40	125	0	0.6977
8.42	4.57	L2	Osin Idiem	5.2	32	330	160	4.447	231	0.475	1.405	0.72	0.795	0.015	0.2	0.01	ND	ND	ND	0.1065	1.4269	75	90	0	0.7365
8.43	4.55	L3	Apata out	4.8	34	400	200	4.3755	280	0.635	1.75	0.52	0.68	0.045	0.305	0.02	ND	ND	ND	0.1065	1.4289	35	130	230	0.6202
8.42	4.6	L4	Ganmo	5.6	30	530	260	3.525	371	0.795	1.36	0.4	0.375	0.02	0.05	0.01	ND	ND	ND	0.1064	1.43	230	100	0	0.6202
8.39	4.6	L5	Ogbondokc	5.3	31	460	230	3.4325	322	0.635	0.95	0.95	0.45	0.01	0.06	0.01	ND	ND	ND	0.1065	1.4302	115	155	220	0.6978
8.39	4.6	L6	Ogbondokc	4.1	30	270	130	2.95	189	0.77	0.73	0.2	0.25	0.055	0.085	0.025	ND	ND	0.02	0.1065	1.4272	40	135	125	0.3101
8.39	4.58	L7	Ago-Oja	3.7	31	390	190	5.96	273	0.58	2.01	0.475	1.1	0.03	0.425	0.055	0.015	ND	ND	0.1065	1.4268	40	160	220	0.8528
8.38	4.57	L8	Laduba	4.9	32	470	230	6.6725	329	0.865	1.06	0.3	1.1	0.025	0.035	0.01	ND	ND	ND	0.1065	1.4277	80	160	0	0.7365
8.38	4.56	L9	Malubi	4.6	30	420	210	8.889	294	1.44	1.465	0.515	1.29	0.035	0.08	0.01	0.01	ND	0.02	0.1065	1.4288	60	140	215	0.5815
8.35	4.52	L10	Olooko	4.7	35	610	300	6.648	427	0.97	1.515	0.21	1.03	0.045	0.065	0.01	ND	ND	ND	0.1065	1.4284	60	245	0	0.3876
8.36	4.5	L11	Arowosaye	4.3	30	120	250	3.88	84	0.855	0.935	0.235	0.425	0.03	0.03	0.01	0.025	ND	0.02	0.1065	1.4305	50	90	200	0.4652
8.37	4.51	L12	Alaha	4.1	29	280	140	2.7225	196	0.72	2.725	0.145	0.225	0.015	0.445	0.05	ND	ND	0.015	0.1065	1.4309	55	125	140	0.4264
8.42	4.52	L13	Ilu-Oba	4.5	29	460	230	6.365	322	1.07	1.705	0.25	0.9	0.01	0.08	0.025	ND	ND	0.03	0.1065	1.4304	40	175	455	0.3489
8.43	4.52	L14	Aloba	5.5	31	250	120	4.8185	175	0.845	1.27	0.135	0.66	0.03	0.045	0.01	ND	ND	0.02	0.1065	1.4317	70	195	130	0.1551
8.42	4.53	L15	Onire	4.8	32	430	210	4.2985	301	1.17	1.095	0.355	0.335	0.04	0.065	0.025	0.04	ND	ND	0.1064	1.4289	70	50	225	0.6202
8.42	4.52	L16	Obate	6.2	32	110	50	3.814	77	1.05	1.36	0.21	0.29	0.02	0.045	0.015	ND	ND	ND	0.1065	1.4288	70	100	205	0.6202
8.42	4.53	L17	Abeokuta	6.8	32	410	200	5.5135	287	1.41	1.18	0.33	0.485	0.01	0.03	0.015	ND	ND	ND	0.1064	1.4278	40	30	100	0.6589
8.42	4.52	L18	Ilu-Oba2	6.2	31	100	50	2.965	70	1.145	0.895	0.155	0.025	0.03	0.04	0.015	ND	ND	0.035	0.1076	1.4318	45	245	0	0.6202
8.41	4.52	L19	Egbejila	7.1	29	240	120	6.2585	168	1.995	0.7	0.115	0.31	0.045	0.05	0.01	0.01	ND	ND	0.1065	1.4281	35	200	135	0.3101
8.32	4.53	L20	Afon Elera	5.7	29	940	470	9.538	658	1.675	1.06	0.265	1.305	0.01	0.265	0.12	ND	ND	ND	0.1065	1.4296	160	165	0	0.3489
8.31	4.53	L21	Afon2	6.5	30	150	70	1.5615	105	0.395	0.84	0.14	0.14	0.01	0.015	0.015	0.01	ND	0.01	0.1064	1.4299	50	115	600	0.3877
8.3	4.51	L22	Alapako	6.8	30	410	200	5.573	287	0.54	1.475	0.345	1.03	0.02	0.075	0.03	ND	ND	ND	0.1064	1.4277	65	115	205	0.3101
8.28	4.49	L23	Kankan	6.5	30	240	120	4.198	168	0.81	2.075	0.435	0.53	0.03	0.18	0.025	ND	ND	ND	0.1065	1.425	40	90	155	0.3101
8.29	4.51	L24	Ajibaba	7.3	30	770	380	9.65	539	1.81	1.62	1.62	1.25	0.02	0.065	0.085	ND	ND	0.025	0.1065	1.4279	60	370	210	0.3877
8.28	4.53	L25	Sakamo	7.9	31	390	190	1.657	273	0.425	0.18	0.18	0.145	0.03	0.03	0.015	ND	ND	ND	0.1065	1.4292	35	125	210	0.3489
8.28	4.53	L26	Odo-Ode	6.2	31	180	90	1.591	126	0.415	0.885	0.205	0.135	0.015	0.065	0.015	0.11	ND	ND	0.1065	1.4299	75	115	0	0.3489
8.28	4.54	L27	Gbogbin	6.4	32	680	340	4.268	476	0.92	0.815	0.515	0.48	0.01	0.065	0.055	ND	ND	ND	0.1065	1.4262	45	300	0	0.6977
8.25	4.53	L28	Budo-Ojoku	6.9	31	280	140	3.9495	196	0.645	1.17	0.235	0.57	0.03	0.035	0.015	ND	0.165	0.02	0.1064	1.4297	35	210	0	0.2714
8.23	4.51	L29	Ajila	6.3	33	380	190	4.931	266	0.685	1.11	0.17	0.785	0.02	0.035	0.015	ND	ND	0.015	0.1064	1.43	60	285	310	0.7365
8.26	4.51	L30	Lajisapati	6.5	33	210	100	2.814	147	0.65	1.295	0.25	0.29	0.035	0.045	0.01	ND	0.025	ND	0.1065	1.4293	55	70	0	0.1939
8.26	4.53	L31	Ewusi	6.3	35	150	70	1.768	105	0.535	0.955	0.21	0.105	0.02	0.095	0.02	ND	0.015	ND	0.1064	1.4272	65	140	0	0.3101
8.28	4.55	L32	Sholu	6.8	36	830	410	6.783	581	0.245	1.91	0.52	1.505	0.05	0.03	0.01	ND	0.01	ND	0.1065	1.4308	80	245	0	0.6978
8.26	4.58	L33	SapatiOko	5.7	31	50	20	2.0665	35	0.72	0.92	0.32	0.065	0.02	0.16	0.01	ND	0.015	ND	0.1065	1.4276	80	165	0	0.1551
8.28	4.58	L34	Idi-Ayan	6.3	31	120	60	1.5445	84	0.585	0.81	0.185	0.02	0.06	0.065	0.01	ND	ND	ND	0.1064	1.4291	70	170	0	0.1551
8.32	4.58	L35	Odoje	6.7	33	350	170	2.8215	245	0.53	1.145	0.29	0.365	0.01	0.09	0.02	ND	ND	ND	0.1064	1.4299	40	155	0	0.1551
		SUM		**201.8**	**1095**	**12570**	**6380**	**154.531**	**8799**	**29.78**	**43.04**	**12.28**	**19.54**	**0.92**	**3.51**	**0.85**	**0.22**	**0.23**	**0.25**	**3.73**	**50.01**	**2265**	**5485**	**4290**	**16.28**
		AVERAGES		**5.77**	**31.29**	**359.14**	**182.29**	**4.415**	**251.4**	**0.85**	**1.23**	**0.35**	**0.56**	**0.03**	**0.1**	**0.02**	**0.03**	**0.05**	**0.02**	**0.11**	**1.43**	**64.71**	**156.71**	**122.57**	**0.47**

According to World Health Organization standard (2006), the desirable range for pH in drinking water is from 6.5 to 8.5 which is also supported by Colorado Water Energy Research Centre (CWERC, 2014).Schoeneich, 2001, also stated that pH value in groundwater in the crystalline hydrogeological province (the study area inclusive) is slightly lower than the WHO desirable range while that of surface water is within the range. This is due to excessive precipitation of iron in groundwater than in surface water. Hence, the pH values of groundwater samples in the area average 5.8, indicating that the groundwater of the area is acidic and slightly lower than the WHO desirable range as evidenced by Schoeneich, 2001.

iv. Temperature

This is a measure of hotness or coldness of the groundwater samples. Groundwater temperature at depths from one to five metres both in hand dug wells and boreholes, fluctuates seasonally and is close although lagging behind to the mean seasonal earth thermometers temperature. Groundwater temperature from the depth of about 10 metres down, increases with increase in geothermal gradient. From the measurement of temperature taken in the study area, the average temperature value for groundwater samples of the area is 31.29^0 C.

v. Electrical Conductivity (EC)

The Electrical conductivity (EC) measures the ability of a material to conduct an electric current such that the higher EC indicates enrichment of salts in the groundwater. Thus, the EC can be classified as type I, if the enrichments of salts are low (EC <1,500 µS/cm); type II, if the enrichment of salts are medium (EC between 1,500 and 3,000 µS/cm); and type III, if the enrichments of salts are high (EC >3,000 µS/cm)(Sarath Prasanth *et al*., 2012). The average value of the total electrical conductivity measured by HANNA instrument in groundwater samples of the area is 359.14µS/cm falling under type1 classification

Electrical conductivity is the conductivity of water at temperature 20^0C, contained between two metallic electrodes, 1 cm^2 each located at a distance of 1 cm from each other. It is a proxy for the amount of inorganic dissolved solids in water; as dissolved substances increase, so does conductance. Conductance is also used to describe the salinity hazards in assessment of water quality for irrigation. In an oil and gas context, changes in conductance could indicate contamination by produced water, which is usually high in salts, or hydrologic communication between geologic zones, seepage, or spills (Colorado Water Energy Research Centre (CWERC, 2014).

vi. Total hardness:

Hardness of water is the amount of dissolved calcium and magnesium in the water. Hard water is high in dissolved minerals largely calcium and magnesium. Hardness is a traditional measure of water to form lather when react with soap. Many industrial and domestic water users are concerned about the hardness of their water. When hard water is heated such as in a home water heater, solid deposits of calcium carbonate can form. This scale can reduce the life of equipment, raise the costs of heating the water, lower the efficiency of electric water heaters, and clog pipes (USGS, science for a changing world). According to WHO (2004), hard water can benefit humans because Humans need minerals to stay healthy. The World Health Organization (WHO) states that drinking-water may be a contributor of calcium and magnesium in the diet and could be important for those which states that depending on the interaction of other factors, such as pH and alkalinity, water with hardness above approximately 200 mg/l may cause scale deposition in the treatment works, distribution system and pipe work and tanks within buildings.

Based on USGS science for a changing world, the general guidelines for classification of waters are: 0 to 60 mg/l (milligrams per liter) as calcium carbonate is classified as soft; 61 to 120 mg/l as moderately hard; 121 to 180 mg/l as hard; and more than 180 mg/l as very hard.

In the study area, the average value for total hardness calculated is 4.4 mg/l which shows that the groundwater of the area is soft and the value is a very good value far below its maximum desirable level in drinking water which is 100mg/l $CaCO_3$ and permissible level of 500mg/l $CaCO_3$.

vii. **Total Dissolved Solids (TDS)**

This is also known as mineralization of water. It is the term used to describe the inorganic salts and small amounts of organic matter present in solution in water. Total Dissolved Solids (TDS) can be measured directly in laboratory as residue left after the water is vaporized in temperature of 105^0C (Schoeneich, 2001). This method is usually used for hard waters with mineralization not less than 500mg/l. It can also be measured indirectly by multiplying the electrical conductivity value with a factor of 0.7. This indirect method is applicable to soft and very soft waters to achieve more accurate result. In the study area, the TDS was calculated by indirect method since the water is soft (Schoeneich, 2001). The average value of TDS for the groundwater in the area is 251mg/l which is a good value far below the WHO desirable value of 500mg/l.Degree of groundwater quality can be classified as fresh, if the TDS is less than 1,000 mg/l; brackish, if the TDS is between 1,000 and 10,000 mg/l; saline, if the TDS is varied from 10,000 to 1,000,000 mg/l; and brine, if the TDS is more than 1,000,000 mg/l (Todd, 1980). Accordingly, the quality of groundwater in the present study area is classified as fresh.

viii. Calcium (Ca)

This is a common ion in groundwater. It is released to water in process of weathering of feldspar, amphibole and pyroxene. According to Schoeneich and Aku, 1998, calcium in groundwater of the Soft overburden and in fractured crystalline aquifers is the same as in surface water and it ranges from0.67mg/l to 7.57mg/l on average of 3.0mg/l. The average value of calcium ion in groundwater samples of the area is 0.85mg/l. This average value corresponds to Alagbe (1988) value of 0.8mg/l. The average value is far below upper desirable limit of 75mg/l of World Health Organization (WHO, 2006) standard for drinking water.

ix. Sodium (Na)

Sodium is a major ion in groundwater and is released by weathering of plagioclases. There is no sodium in the atmosphere unless in particulate matter. According to World Health Organisation standard (2004), the desirable limit for Sodium in groundwater is 200 mg/l. Schoeneich and Aku (1998) stated that groundwater from the soft overburden and fractured crystalline aquifers contain the same low concentration of sodium as surface water which is on average of 1.7 mg/l. Hence, the average concentration of sodium in the study area is 1.23mg/l far below the WHO desirable limit which is 75 mg/l. There is evidence that high dietary intakes of sodium play a significant role in the development of hypertension among genetically susceptible persons (WHO, 1993). Persons suffering from hypertension or congestive heart failure may require a sodium-restricted diet, and in such cases the intake of Sodium is 1.23 mg/l.

x. Potassium (K)

This refers to an ion in groundwater that is released by weathering of orthoclase and microcline. Schoeneich and Aku, 1998, stated that concentration of potassium in groundwater

of the soft overburden and fractured crystalline aquifers is higher than that of surface water and it ranges from 0.4mg/l to 5.9mg/l on average of 3.0 mg/l. The desirable limit of potassium according to WHO (2006) is 20 mg/l. From the study area, the average value of potassium in groundwater of the area is 0.35 mg/l which is far below the desirable limit of World Health Organization.

xi. Magnesium (Mg)

Magnesium is released in to groundwater by weathering of feldspar, biotite and pyroxene. It is a major contributor to water hardness. Magnesium concentrations in both soft overburden and fractured crystalline aquifers of the Basement crystalline hydrogeological province varies from 0.10mg/l to 5.74mg/l on average of 1.08 mg/l (Schoeneich and Aku, 1998). According to World Health Organization standard (2006), the maximum desirable and permissible limits of Magnesium are 30 mg/l and 150 mg/l respectively. Concentration of magnesium greater than 125 mg/l negatively affects taste of beverages (Schoeneich and Aku, 1998). The average value of magnesium in groundwater of the study area is 0.56 mg/l which is deeply below the maximum desirable limit of the World Health Organization standard.

xii. Cupper (Cu)

Copper is generally low in groundwater. It may be introduced by mining, farming, manufacturing, or industrial wastewater and can also occur in water due to corrosion of household plumbing systems by acidic water. According to world Health Organization (2006) drinking water standard, the highest desirable level of copper is 0.05 mg/l while maximum permissible limit is 1.5 mg/l. The average value of copper in groundwater of the area is 0.03 mg/l which is also below the desirable limit of the World Health organization standard.

xiii. Iron (Fe)

Iron is commonly found in groundwater from weathering of iron bearing minerals, rocks, and soils such as hematite and magnetite. It may also be introduced by industrial wastewater, acid-mine drainage, sewage, landfill leachate and the leaching of cast-iron pipes in plumbing systems, or iron bacteria. According to the National Secondary Drinking Water Standard (2014), the iron's desirable limit is 0.3 mg/l. The World Health Organization standard (2006) for drinking water stated that the maximum desirable level of iron in groundwater is 0.1 mg/l while its maximum permissible limit is 1.0 mg/l. In the study area, the average concentration of iron in groundwater is 0.1 mg/l which corresponds to the desirable limit of World Health Organization standard.

xiv. Manganese (Mn)

There is no evidence of seasonal variation in concentration of manganese. Manganese in groundwater varies from 0.010 mg/l to 0.200 mg/l on average of 0.063 mg/l (Schoeniech and Aku, 1998).Manganese produces a black stain in the presence of oxygen. The National Secondary Drinking Water Standard for manganese is 0.05 mg/l. According to World Health Organization standard for drinking water, the health-based guideline value for manganese is 4 times higher than this acceptability threshold of 0.1 mg/l, hence the maximum desirable level of manganese in groundwater is 0.05 mg/l and its maximum permissible level is 0.5 mg/l. The average concentration of manganese in groundwater of the study area is 0.02 mg/l which is below the desirable limit of World Health Organization (2006) standard.

xv. Zinc (Zn)

According to Schoeniech and Aku (1998), Zinc in crystalline hydrogeological province of Nigeria, ranges from 0.002 mg/l to 0.007 mg/l on average of 0.007 mg/l. The World Health Organization (WHO) 1996 stated that concentration of zinc in groundwater ranges from

0.010 mg/l to 0.040 mg/l. According to World Health Organization (2004), the desirable limit of Zinc is given as 3 mg/l. The average concentration of zinc in groundwater of the study area is 0.03 mg/l which is below the desirable level of World Health Organization guide line value indicating that the water is good for drinking and other domestic purposes.

xvi. Lead (Pb)

Lead is a known neurotoxin. It occurs naturally in certain drilling geologic deposits. Lead was also a component of plumbing solder used in homes with copper plumbing installed before 1985. It may be leached from lead soldered joints, as well as from faucets and lead pipe. The World Health guideline value for Lead in drinking water is 0.01 mg/l. The average concentration of lead in groundwater of the area is 0.05 mg/l which is higher than the World Health Organization standard.

xvii. Cadmium (Cd)

According to World Health Organization, the World Health standard value for cadmium in groundwater is 0.003 mg/l. Aku and Schoeneich (1998), also gave an average value of cadmium in crystalline hydrogeological province of Nigeria to be 0.0004 mg/l. In the study area, the average concentration of cadmium is 0.02 mg/l which is higher than the World Health Organization standard.

xviii. Sulphate (SO_4^{2-})

Sulphate is an indicator of organic pollution of water especially in shallow water aquifers and in hand dug wells. . Sulfate often leaches into groundwater from shale deposits. Byproducts of coal mining, industrial wastes and sewage are also high in sulfate. Bacterial process often changes sulfate concentrations as well. Sulphate enters water by oxidation of sulphides. Since sulphides are not very common in the crystalline rocks, water in the crystalline hydrogeological province tends to contain fewer sulphates than water in the sedimentary

hydrogeological province. According to World Health Organization standard for drinking water, the highest desirable limit for sulphate in groundwater is 200 mg/l while its maximum permissible level is 400 mg/l. Concentrations of sulphate above 250 mg/l in groundwater may cause gastrointestinal irritation, especially when combined with high concentration of magnesium or sodium. The average concentration of sulphate in groundwater samples of the study area is 0.11mg/l which is far below the desirable level of WHO standard (2017).

xix. Phosphate (PO_4^-)

This ion occurs both in surface and groundwater of crystalline hydrogeological province. According to World Health Organization standard for drinking water, the maximum desirable level for sulphate is 0.3 mg/l. Schoeneich and Aku (1998) stated that phosphate varies in groundwater from 0.02 mg/l to 6.20 mg/l on average of 1.43 mg/l. In the study area, the average value of phosphate in groundwater is 1.43 mg/l which corresponds to Schoeneich and Aku (1998).

xx. Chloride (Cl^-)

The chloride ion is the most predominant natural form of the element chlorine and is extremely stable in water. The chloride in groundwater may be from diverse sources such as weathering, leaching of sedimentary rocks and soil, domestic and municipal effluents (Sarath Prasanth *et al*. 2012). A significant increase in chloride could indicate hydrologic communication between geologic zones, seepage or spills. Changes in chloride may also be tied to the presence or absence of other major ions, which can shift for many reasons. According to World health organization 2017, the desirable level for chloride in groundwater, is 250 mg/l while its maximum permissible level is 600 mg/l. The average concentration of

chloride in groundwater of the study area is 65 mg/l which is far below the desirable level of WHO standard.

xxi. Bicarbonate (HCO_3)

Bicarbonate has its source from atmospheric carbon dioxide dissolved by rain water and carbon dioxide present in the humus soil which is absorbed by water during percolation. Schoeneich (2001) said if concentration of bicarbonate in water is higher than concentration of calcium, then all carbon dioxide which formed bicarbonate was of atmospheric origin. The available data for bicarbonate in the study area shows this situation. According to World Health Organization standard for drinking water, the desirable level for bicarbonate is 125 mg/l while its maximum permissible level is 350 mg/l. In the study area, the average concentration of bicarbonate in groundwater is 157 mg/l which is within the maximum permissible level of WHO.

xxii. Carbonate (CO_3)

Carbonate occurs in groundwater occasionally, only in every 10^{th} sample in concentrations ranging from 0.02 mg/l to 0.04 mg/l. In the study area, the average concentration of carbonate in groundwater of the area is 123mg/l

xxiii. Nitrate (NO_3)

Most chemicals arising in drinking-water are of health concern only after extended exposure of years, rather than months. The principal exception is nitrate (WHO, 2017). Typically, changes in water quality occur progressively, except for those substances that are discharged or leached intermittently to flowing surface waters or groundwater supplies from, for example, contaminated landfill sites (WHO, 2017). Nitrogen compounds are the most widespread contaminants in subsurface environments, mainly originating from non-point and multi-point agricultural sources (Pang *et al*., 2013).Nitrate originates from organic matter.

When organic matter decays in the soil, ammonia is produced. The ammonia is oxidized by nitrosifying bacteria to nitrites (NO_2) and nitrite is oxidized to nitrate by nitrifying bacteria. According to World health Organization standard, the maximum desirable limit of nitrate is 45 mg/l and the maximum permissible level is 500 mg/l. The average concentration of nitrate in groundwater of the study area is 0.47 mg/l which is far below the desirable limit of WHO. For drinking and domestic uses, highest safe level of nitrate is 45 mg/l when water is drunk by adults, but infants should not consume more than 10 mg/l of NO_3. A higher concentration intake of NO_3 by infants may cause infant cyanosis (methaemolobinaemia) or blue baby disease.

The obtained average concentrations of physico-chemical parameters of groundwater in the study area are compared with World Health Organization (WHO) standard and the comparison is shown in Table 8

Table 6: Average values obtained for Physico-chemical parameters from study area compared with WHO standard (2006) for drinking water.

S/N	Parameters	Average concentrations Obtained	WHO acceptable limits	WHO permissible limits
1	Colour (TCU)	5	5	15
2	Turbidity (NTU)	182.3	5	1000
3	PH	5.8	6.5-8.5	9.2
4	Temperature (^{0}C)	31.29		
5	Conductivity (µS/cm)	359.14		1400
6	Total Hardness (mg/l $CaCO_3$)	4.4	100	500
7	TDS	251	500	1000
8	Calcium (mg/l)	0.85	75.0	200
9	Sodium (mg/l)	1.23	20	200
10	Potassium (mg/l)	0.35	20	200
11	Magnesium (mg/l)	0.56	30	150
12	Copper (mg/l)	0.03	0.05	1.5
13	Iron (mg/l)	0.1	0.1	1.0
14	Manganese (mg/l)	0.02	0.05	0.5
15	Zinc (mg/l)	0.03	3.0	1.5
16	Lead (mg/l)	0.05	0.01	
17	Cadmium (mg/l)	0.02	0.003	
18	Sulphate (mg/l)	0.11	200	400
19	Phosphate (mg/l)	1.43	0.3	
20	Chloride (mg/l)	65	250	600
21	Bicarbonate (mg/l)	157	125	350
22	Carbonate (mg/l)	123		
23	Nitrate (mg/l)	0.47	45	500

The compared values of average concentrations of physico-chemical parameters obtained in the study area with World Health Organization acceptable and permissible limits are graphically presented in Figures 82 and 83.

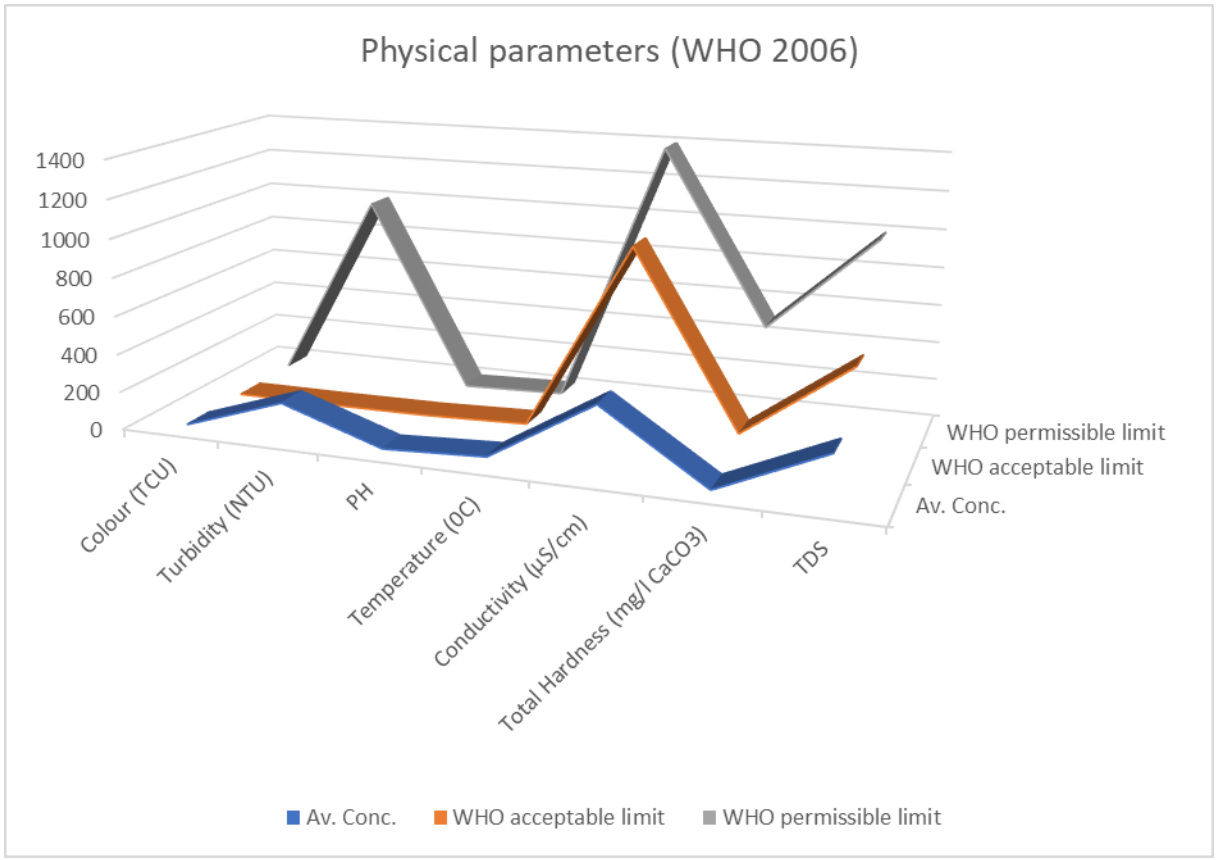


Figure 82: Graph comparing the obtained average concentrations of physical parameters with World Health Organization (WHO) standard

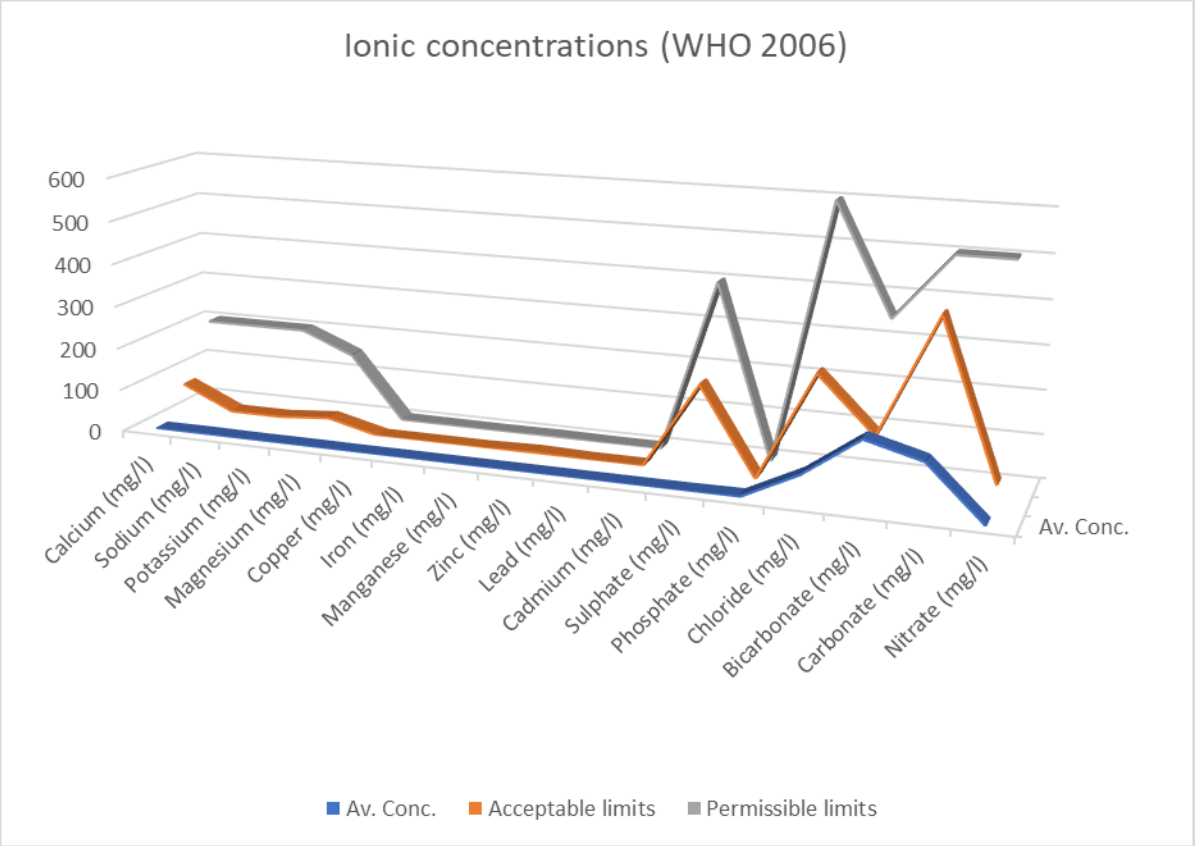


Figure 83: Graph comparing the obtained average concentrations of chemical parameters with World Health Organization (WHO) standard

4.6.1.2 Water Quality Index

WQI is defined as a rating that reflects the composite influence of different physico-chemical parameters of water (Sahu and Sikdar, 2008).It is an important tool for demarcating groundwater quality for drinking purposes (Tiwari and Mishra, 1985; Singh, 1992; Naik and Purohit, 2001; Singh *et al*., 2005). To calculate the WQI, the weight has been assigned for the physico-chemical parameters according to the parameters' relative importance in the overall quality of water for drinking water purposes. The assigned weight ranges from 1 to 5. The weight 1 is assigned for magnesium, 2 for Ca, Na, K, 3 for HCO_3, Cl, 4 for pH, EC, SO_4 and maximum weight of 5 has been assigned for nitrate and TDS (Vasanthavigar *et al*., 2010). The relative weight is computed from this equation;

$$w_i = \frac{w_i}{\sum_{i=1}^{n} w_i} \quad (40)$$

Where W_i is the relative weight, w_i is the weight of each parameter, n is the number of parameters. The quality rating scale for each parameter is calculated by dividing its concentration in each water sample by its respective standards (World Health Organization, 2011) and multiplied the results by 100. The equation is given as:

$$q_i = \frac{C_i}{S_i} \times 100 \quad (41)$$

Where q_i is the quality rating scale, C_i is the concentration of each chemical parameter in each sample in milligrams per litre; S_i is the World Health Organization standard for each chemical parameter in milligrams per liter according to the guidelines of the (WHO 2011).Therefore, water quality index is calculated by multiplying index rating with the relative weight. i.e

$$WQI = w_i \times q_i \quad (42)$$

Where WQI = water quality index, w_i = relative weight, q_i = index rating,

The calculated WQI for the 35 groundwater samples of the area is shown in Table 9 and the graphical representation of its rating is shown in Figures 84 and 85. The water quality map based on water quality index is shown in Figure 86.

Table 7: Calculated values of water quality index for groundwater samples of the area

Location ID	Location Names	WQI
L1	OsinAremu	15.38
L2	OsinIdiemi	18.12
L3	Apata out	24.80
L4	Ganmo	29.12
L5	Ogbondoko	30.88
L6	Ogbondoko	33.78
L7	Ago-Oja	33.47
L8	Laduba	39.99
L9	Malubi	35.04
L10	Olooko	28.63
L11	Arowosaye	34.99
L12	Alaha	29.02
L13	Ilu-Oba	31.02
L14	Aloba	21.80
L15	Onire	22.19
L16	Obate	16.24
L17	Abeokuta	18.32
L18	Ilu-Oba2	28.81
L19	Egbejila	34.21
L20	AfonEleran	32.07
L21	Afon2	35.04
L22	Alapako	28.63
L23	Kankan	34.99
L24	Ajibaba	35.04
L25	Sakamo	28.63
L26	Odo-Ode	14.63
L27	Gbogbin	17.202
L28	Budo-Ojoku	19.43
L29	Ajila	14.63
L30	Lajisapati	17.20
L31	Ewusi	19.43
L32	Sholu	21.28
L33	SapatiOko	21.77
L34	Idi-Ayan	24.66
L35	Odoje	24.02

According to Saba and Umer, 2016 the values of WQI of potable waters are classified into 5 groups and the classification is shown in Table 10

Table 8: Classification of the quality of water for drinking purposes based on the values of Water Quality Index (WQI) (After Sabar and Umer, 2016).

WQI range	Type of water
<50	Excellent
50-100	Good
100-200	Poor
200-300	Very poor
>300	Unsuitable

Based on Horton, 1965, as well as Saba and Umer (2016), the graphical representations of water quality index rating for groundwater in the area are thus presented in Figures 84 and 85.

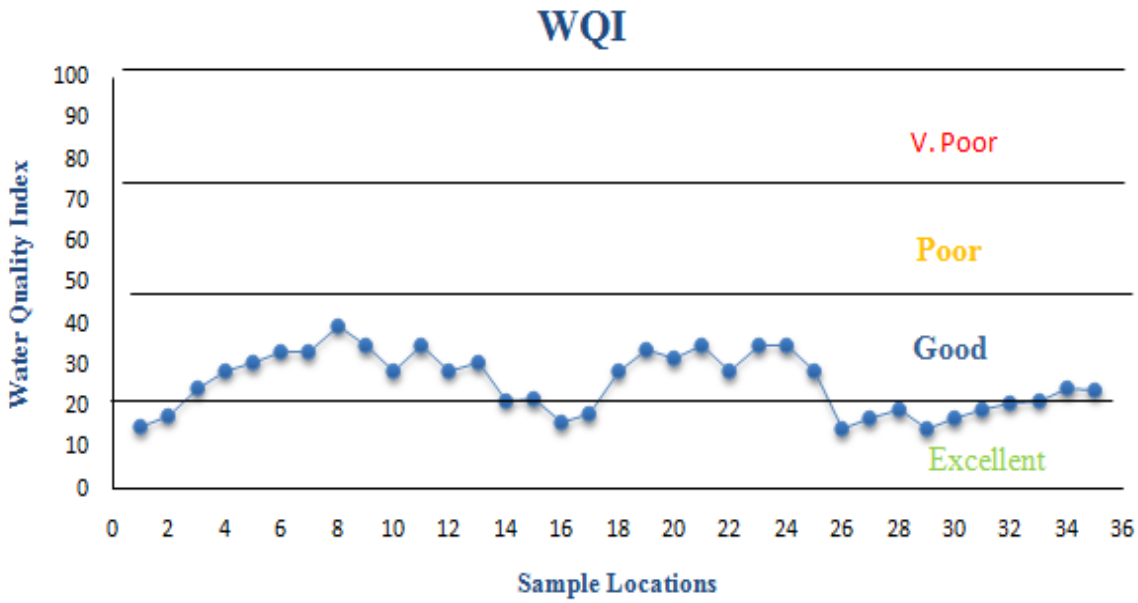


Figure 84: **Graphical representation of water quality index rating for groundwater locations (After Horton, 1965)**

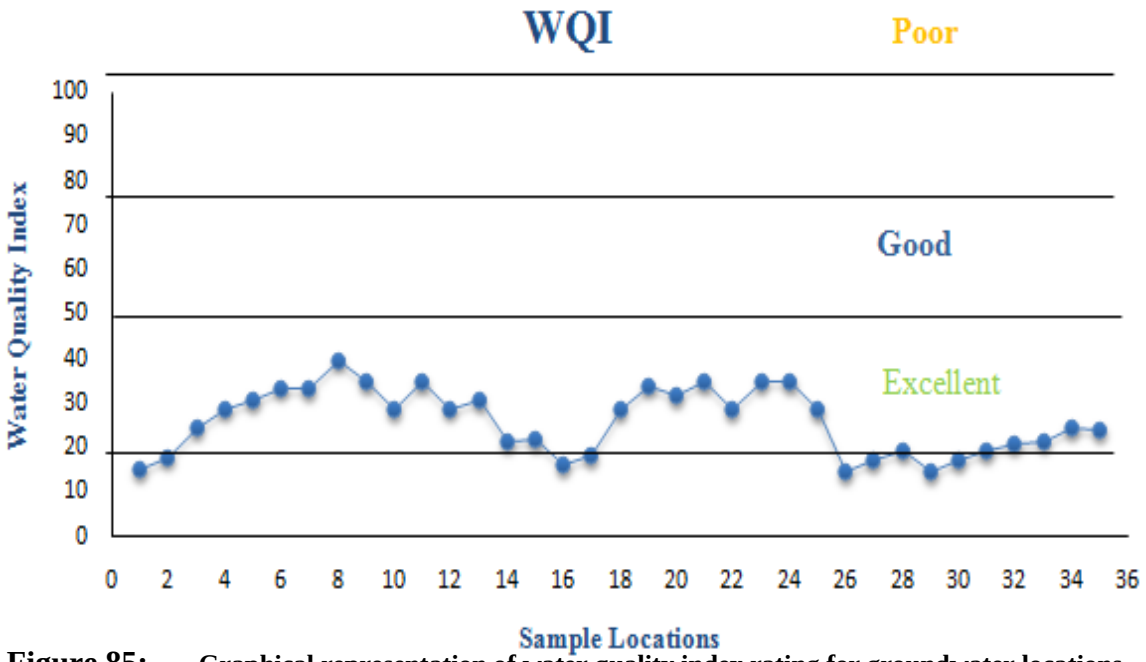


Figure 85: **Graphical representation of water quality index rating for groundwater locations (After Saba and Umer, 2016)**

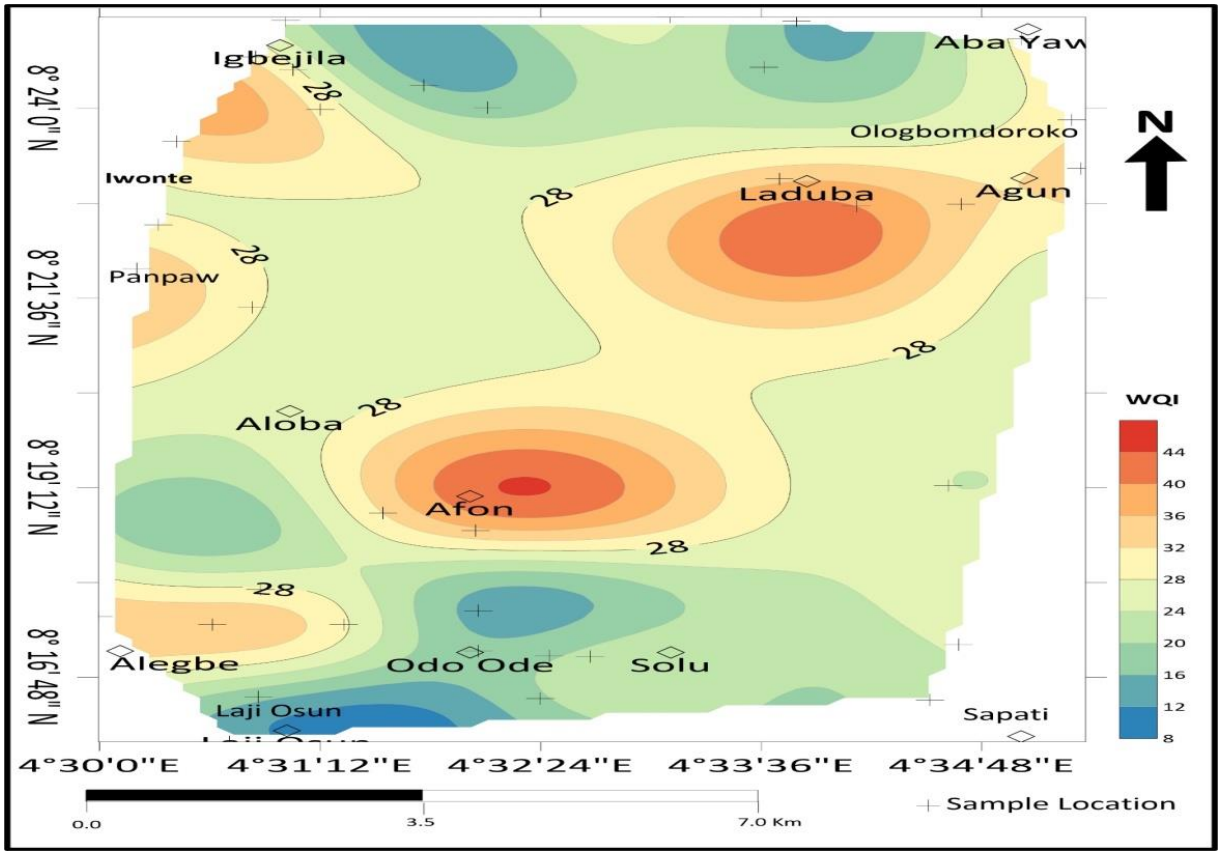


Figure 86: Water Quality map for groundwater sampling locations in the study area

4.6.2 Quality of Groundwater for Irrigation Purpose

In assessing the quality of water for irrigation the following parameters are to be considered:

i. Bicarbonate hazard or Residual Sodium carbonates (RSC)

ii. Sodium hazard or Sodium adsorption Ratio (SAR)

i. Salinity hazard

ii. Toxic elements hazard

iii. Kelley's Index (K.I)

iv. Magnesium adsorption ratio (MAR) and

v. Percentage sodium.

4.6.2.1 Bicarbonate Hazard/Residual Sodium Carbonates (RSC)

RSC means residual sodium carbonates which represent the amount of sodium carbonate ($NaCO_3$) and sodium bicarbonate ($NaHCO_3$) present in the irrigation water. If the concentration of carbonate (CO_3^{2-}) and bicarbonate (HCO_3^-) ions exceeds the concentrations of Ca^{2+} and Mg^{2+}ions, precipitation of Ca^{2+} and Mg^{2+} occurs (Raghunath 1987), but if the carbonates are less than alkaline earths ($Ca^{2+} + Mg^{2+}$), it outlined the residual $NaCO_3$ which is absent in this study. Generally, RSC is expressed as milli-equivalents per liter (meq/l) of $NaCO_3$. An excess of CO_3^{2-} and HCO_3^- causes precipitation of soil Ca^{2+} and Mg^{2+}thereby impairing the soil structure as well as potentially activating soil sodium. The RSC was defined by Richards (1954) and calculated by using the formula given below:

$$RSC= (HCO_3^- + CO_3^{2-}) - (Ca^{2+} + Mg^{2+}) \quad 43$$

On the basis of RSC range, bicarbonate hazard has been classified into three classes as follows:

a. RSC < 1.25 is Low and the water having this value is referred to as safe or suitable water for irrigation.
b. RSC between 1.25 and 2.5 is medium and the water having this value is referred to as marginally safe water for irrigation.
c. RSC > 2.5 is high and the water having this value is referred to as un-suitable water for irrigation.

In the study area, the Residual Sodium Carbonate (RSC) of groundwater has been calculated to reveal the safe, marginal and un-suitable water for irrigation (Table 11). From table 11, It shows that 25 groundwater locations are unsuitable for irrigation due to their Residual Sodium Carbonate (RSC) values which are higher than 2.5. 9 groundwater locations are marginally suitable due to their RSC values falling between 1.25 and 2.5 while only groundwater of location 30 which is at Laji Sapati town is suitable and safe for irrigation purpose due to its RSC value which is lesser than 1.25. This result reveals that most of groundwater in the study area is not suitable and safe for irrigation purpose based on bicarbonate hazard or Residual Sodium Carbonate analysis.

Table 9: Calculated values of Residual Sodium Carbonate of groundwater samples in the area

LOCATION I.D	$HCO_3 + CO_3$	Ca + Mg	RSC	Remarks
L1	2.049	0.045	2.0033	M. Suitable
L2	1.475	0.090	1.3850	M. Suitable
L3	5.964	0.088	5.8756	Unsuitable
L4	1.639	0.071	1.568	M. Suitable
L5	5.552	0.069	5.4828	Unsuitable
L6	4.296	0.059	4.2367	Unsuitable
L7	6.290	0.121	6.1693	Unsuitable
L8	2.623	0.135	2.4881	M. Suitable
L9	5.878	0.179	5.6985	Unsuitable
L10	4.016	0.134	3.8817	Unsuitable
L11	4.808	0.078	4.7298	Unsuitable
L12	4.382	0.055	4.3273	Unsuitable
L13	10.452	0.129	10.3235	Unsuitable
L14	5.364	0.0973	5.2668	Unsuitable
L15	4.569	0.086	4.4826	Unsuitable
L16	5.056	0.077	4.9793	Unsuitable
L17	2.159	0.110	2.0481	M. Suitable
L18	4.016	0.059	3.9567	Unsuitable
L19	5.529	0.126	5.4034	Unsuitable
L20	2.705	0.192	2.5125	M. Suitable
L21	11.885	0.031	11.8536	Unsuitable
L22	5.302	0.113	5.1892	Unsuitable
L23	4.058	0.0845	3.9733	Unsuitable
L24	9.566	0.195	9.3713	Unsuitable
L25	5.549	0.033	5.5157	Unsuitable
L26	1.885	0.032	1.853	M. Suitable
L27	4.918	0.086	4.832	Unsuitable
L28	3.442	0.079	3.3623	Unsuitable
L29	9.839	0.099	9.7393	Unsuitable
L30	1.148	0.057	1.0913	Suitable
L31	2.295	0.035	2.2595	M. Suitable
L32	4.016	0.137	4.0022	Unsuitable
L33	2.705	0.041	2.6636	Un Suitable
L34	2.787	0.030	2.7561	Un Suitable
L35	2.541	0.056	2.4841	M. Suitable

4.6.2.2 Sodium Hazard or Sodium Adsorption Ratio (SAR)

Sodium hazard or Sodium Adsorption Ratio is calculated using this formular:

$$SAR = \frac{Na}{\sqrt{(Ca+Mg)/2}} \quad 44$$

Where: Na= Sodium concentration, Ca= calcium concentration, Mg= magnesium concentration all the concentrations are expressed in milli-equivalents per litre. Evaluation of sodium hazard calculated for groundwater samples in the area according to equation 4.21 is shown in Table 12. Figure 87 shows the Wilcox quality classification of water for irrigation based on sodium adsorption ratio and electrical conductivity of groundwater in the area.From the figure, all the groundwater samples in the area fall within conductivity C2 and Sodium adsorption ratio S1 range which according to Table 13 (USSL classification) the ground waters are considered to have medium salinity and low sodium.

This reveals that groundwater of the study area is excellent for irrigation purpose based on Sodium Adsorption Ratio.

Table 10: Calculated values of Sodium Adsorption ratio for groundwater in the area

LOCATION I.D	Na	(Ca+Mg)	√(Ca+Mg)	√(Ca+Mg)/2	SAR = (Na/√(Ca+Mg)/2	Remark
L1	0.02900	0.04575	0.213892	0.106946	0.27116	Excellent
L2	0.06100	0.09	0.3	0.15	0.40666	Excellent
L3	0.07600	0.088417	0.297349	0.148675	0.51118	Excellent
L4	0.05900	0.071	0.266458	0.133229	0.44284	Excellent
L5	0.04100	0.06925	0.263154	0.131577	0.31160	Excellent
L6	0.03200	0.059333	0.243584	0.121792	0.26274	Excellent
L7	0.08700	0.120667	0.347371	0.173686	0.50090	Excellent
L8	0.04600	0.134917	0.36731	0.183655	0.25047	Excellent
L9	0.06400	0.1795	0.423674	0.211837	0.302119	Excellent
L10	0.06600	0.134333	0.366515	0.183258	0.36015	Excellent
L11	0.04100	0.078167	0.279583	0.139792	0.29329	Excellent
L12	0.11800	0.05475	0.233987	0.116994	1.00859	Excellent
L13	0.07400	0.1285	0.358469	0.179234	0.41287	Excellent
L14	0.05500	0.09725	0.311849	0.155925	0.35273	Excellent
L15	0.04800	0.086417	0.293967	0.146984	0.32657	Excellent
L16	0.05901	0.076667	0.276887	0.138444	0.42617	Excellent
L17	0.05100	0.110917	0.333042	0.166521	0.30627	Excellent
L18	0.03911	0.059333	0.243584	0.121792	0.32021	Excellent
L19	0.03000	0.125583	0.354377	0.177189	0.16931	Excellent
L20	0.04611	0.1925	0.438748	0.219374	0.20969	Excellent
L21	0.03712	0.031417	0.177247	0.088624	0.41749	Excellent
L22	0.06411	0.112833	0.335907	0.167953	0.38106	Excellent
L23	0.09000	0.084667	0.290975	0.145488	0.61861`	Excellent
L24	0.07000	0.194667	0.44121	0.220605	0.31731	Excellent
L25	0.00811	0.033333	0.182574	0.091287	0.08764	Excellent
L26	0.03811	0.032	0.178885	0.089443	0.42485	Excellent
L27	0.03512	0.086	0.293258	0.146629	0.23869	Excellent
L28	0.05111	0.07975	0.2824	0.1412	0.36119	Excellent
L29	0.04810	0.099667	0.3157	0.15785	0.30409	Excellent
L30	0.05611	0.056667	0.238048	0.119024	0.47049	Excellent
L31	0.04211	0.0355	0.188414	0.094207	0.44583	Excellent
L32	0.08301	0.137667	0.371035	0.185517	0.44739	Excellent
L33	0.04000	0.041417	0.203511	0.101755	0.39310	Excellent
L34	0.03512	0.030917	0.175831	0.087916	0.39811	Excellent
L35	0.04911	0.056917	0.238572	0.119286	0.41078	Excellent

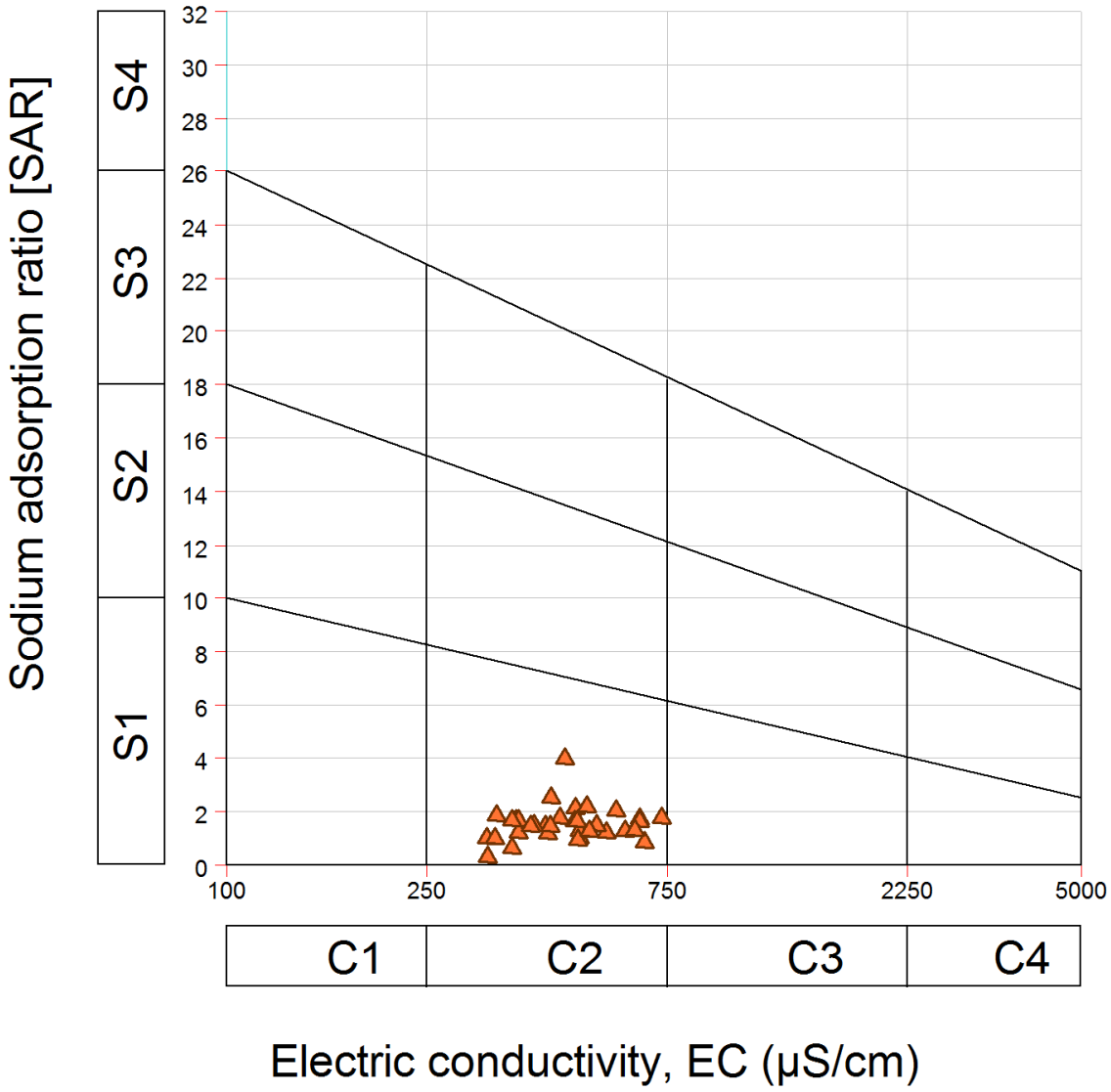


Figure 87: **Wilcox quality classification of irrigation waters (1948) showing position of the collected groundwater samples between electric conductivity and Sodium Adsorption ratio** = Collected groundwater samples

Table 11: United State Science Laboratory (USSL) classification for Sodium Adsorption Ratio

Classification type	Obtained		Remarks
	Sample numbers	% Numbers	
C1 – S1	-	-	Low salinity, low sodium
C1 – S2	-	-	Low salinity, medium sodium
C1 – S3	-	-	Low salinity, high sodium
C2 – S1	All samples	100	Medium salinity, low sodium
C2 – S2	-	-	Medium salinity, medium sodium
C2 – S3	-	-	Medium salinity, High sodium
C3 – S1	-	-	High salinity, low sodium
C3 – S2	-	-	High salinity, medium sodium
C3 – S3	-	-	High salinity, high sodium

4.6.2.3 Salinity Hazard

Salinity hazard of water for irrigation is according to the electro-conductivity of water. The salinity can be low, medium, high or very high and the dividing points between the classes are 0-250, 250-750 and 750-2250 and above 2250 µs/cm respectively (Table 14). Water of medium, high or very high salinity hazard should be used for irrigation only on permeable soils with good drainage, provided that other hazards are low (Schoeneich, 2001).

Table 15 shows the electro-conductivity values for the groundwater locations and their respective salinity hazards. From the table, 13 groundwater locations are of low salinity hazard, 19 groundwater locations are of medium salinity hazard while only 3 groundwater locations are of high salinity hazard. This analysis reveals that most of groundwater in the area is of medium salinity hazard due to their electro-conductivity values falling between 250 and 750 µS/cm which should be used for irrigation purpose only on permeable soils with good drainage, provided that other hazards are low (Schoeneich, 2001).

Table 12: Suitability of water for irrigation in respect of Salinity Hazard (After Wilcox, 1948 and Mohammad *et al*., 2019)

Salinity Hazard	Range of Electrical conductivity (µS/cm)
Low	Less than 250
Medium	250 to 750
High	750 to 2250
Very high	Greater than 2250

Table 13: Calculated values of salinity Hazard for groundwater of the study area

LOCATION I.D	ELECTROCONDUCTIVITY (µs/cm)	SALINITY HAZARD
L1	160	LOW
L2	330	MEDIUM
L3	400	MEDIUM
L4	530	MEDIUM
L5	460	MEDIUM
L6	270	MEDIUM
L7	390	MEDIUM
L8	470	MEDIUM
L9	420	MEDIUM
L10	610	MEDIUM
L11	120	LOW
L12	280	MEDIUM
L13	460	MEDIUM
L14	250	LOW
L15	430	MEDIUM
L16	110	LOW
L17	410	MEDIUM
L18	100	LOW
L19	240	LOW
L20	940	HIGH
L21	150	LOW
L22	410	MEDIUM
L23	240	LOW
L24	770	HIGH
L25	390	MEDIUM
L26	180	LOW
L27	680	MEDIUM
L28	280	MEDIUM
L29	380	MEDIUM
L30	210	LOW
L31	150	LOW
L32	830	HIGH
L33	50	LOW
L34	120	LOW
L35	350	MEDIUM

4.6.2.4 Toxic Elements Hazard

In the study area, the average values for Zn, Mn, Pb, Cd, and Cu are 0.03 mg/l, 0.02 mg/l, 0.05mg/l, 0.02 mg/l and 0.03 mg/l respectively. Comparing these values with the limits of FAO (1985) and Ewulu (1983), almost all the toxic elements are below the limits. This reveals that toxic elements hazard is absent in groundwater of the study area, hence the groundwater is good for irrigation based on toxic elements hazard evaluation.

4.6.2.5 Kelly Index (KI)

Kelly (1951) considered parameters for assessing water quality for irrigation. Kelly's ratio is the measure of concentration of sodium in milli-equivalent per litre against the addition of calcium and magnesium in milli-equivalent per litre i.e. Na^{+} against Ca^{2+}+ Mg^{2+}. Kelly's ratio is used to find whether a water sample is suitable for irrigation purpose or not. Water having Kelly's ratio greater than one (1) is generally considered unfit for irrigation. The formula is as follows:

$$KI = \frac{Na}{Ca+Mg} \qquad 45$$

Table 16 shows the calculated values for Kelley index of groundwater samples in the study area. From the table, 29 groundwater samples are suitable for irrigation while only 6 groundwater samples are unsuitable for irrigation purpose. This analysis shows that most of groundwater of the area is suitable for irrigation purpose based on Kelley Index ratio.

Table 14: Kelley Index for suitability of groundwater for irrigation purpose in the study area

LOCATION I.D	Na	Mg + Ca	K.I = Na/(Mg+Ca)	Remarks
L1	0.02869	0.0458	0.6272	**Suitable**
L2	0.06108	0.09	0.6787	**Suitable**
L3	0.07608	0.0884	0.8605	**Suitable**
L4	0.0591	0.071	0.8328	**Suitable**
L5	0.0413	0.0693	0.5965	**Suitable**
L6	0.0317	0.0593	0.5349	**Suitable**
L7	0.0874	0.1207	0.7242	**Suitable**
L8	0.0460	0.1349	0.3416	**Suitable**
L9	0.06369	0.1795	0.3549	**Suitable**
L10	0.0658	0.1343	0.4903	**Suitable**
L11	0.04065	0.0782	0.5200	**Suitable**
L12	0.11847	0.0548	2.1639	**Unsuitable**
L13	0.0741	0.1285	0.5769	**Suitable**
L14	0.05521	0.0973	0.5678	**Suitable**
L15	0.04760	0.0864	0.5509	**Suitable**
L16	0.0591	0.0767	0.7713	**Suitable**
L17	0.0513	0.1109	0.4625	**Suitable**
L18	0.0389	0.0593	0.6558	**Suitable**
L19	0.0304	0.1256	0.2423	**Suitable**
L20	0.0460	0.1925	0.2394	**Suitable**
L21	0.0365	0.0314	1.1625	**Unsuitable**
L22	0.06413	0.1128	0.5684	**Suitable**
L23	0.0902	0.0847	1.0656	**Unsuitable**
L24	0.0704	0.1947	0.3618	**Suitable**
L25	0.0078	0.0333	0.2348	**Suitable**
L26	0.0384	0.032	1.2024	**Unsuitable**
L27	0.0354	0.086	0.4120	**Suitable**
L28	0.0508	0.0797	0.6379	**Suitable**
L29	0.0482	0.0997	0.4842	**Suitable**
L30	0.0563	0.0567	0.994	**Suitable**
L31	0.0415	0.0355	1.1696	**Unsuitable**
L32	0.0830	0.1377	0.6032	**Suitable**
L33	0.0400	0.0414	0.9658	**Suitable**
L34	0.0352	0.0309	1.1391	**Unsuitable**
L35	0.0497	0.0569	0.8747	**Suitable**

4.6.2.6 Magnesium Adsorption Ratio (MAR)

Thisis a means of assessing groundwater quality for irrigation by finding theratio of concentration of magnesium in milli-equivalent per litre against the addition of calcium and magnesium in milli-equivalent per litre. The formular for calculating it is given as:

$$MAR = \frac{Mg}{Mg+Ca} \times 100 \qquad 46$$

Where MAR= Magnesium Adsorption Ratio, Mg = Magnesium, Ca = calcium

According to Raghunath, 1987, groundwater with MAR less than 50% is considered suitable for irrigation while groundwater with MAR greater than 50% is considered unsuitable for irrigation purpose. The calculated MAR is given in Table 17. From the table, 18 groundwater samples were suitable for irrigation while 17 were unsuitable. This reveals that most of groundwater in the area is suitable for irrigation purpose based on magnesium adsorption ratio.

Table 15: Calculated values of Magnesium Adsorption Ratio (MAR) for groundwater in the area

LOCATION I.D	Mg	Mg + Ca	MAR (%)	Remarks
L1	0.0075	0.04575	16.39344	Suitable
L2	0.06625	0.09	73.61111	Un suitable
L3	0.056667	0.088417	64.09048	Un Suitable
L4	0.03125	0.071	44.01408	Suitable
L5	0.0375	0.06925	54.15162	Un suitable
L6	0.020833	0.059333	35.11236	Suitable
L7	0.091667	0.120667	75.96685	Un Suitable
L8	0.091667	0.134917	67.94317	Un Suitable
L9	0.1075	0.1795	59.88858	Un Suitable
L10	0.085833	0.134333	63.89578	Un Suitable
L11	0.035417	0.078167	45.30917	Suitable
L12	0.01875	0.05475	34.24658	Suitable
L13	0.075	0.1285	58.36576	Un Suitable
L14	0.055	0.09725	56.55527	Un Suitable
L15	0.027917	0.086417	32.30473	Suitable
L16	0.024167	0.076667	31.52174	Suitable
L17	0.040417	0.110917	36.43877	Suitable
L18	0.002083	0.059333	3.511236	Suitable
L19	0.025833	0.125583	20.57067	Suitable
L20	0.10875	0.1925	56.49351	Un Suitable
L21	0.011667	0.031417	37.13528	Suitable
L22	0.085833	0.112833	76.0709	Un suitable
L23	0.044167	0.084667	52.16535	Un Suitable
L24	0.104167	0.194667	53.51027	Un Suitable
L25	0.012083	0.033333	36.25	Suitable
L26	0.01125	0.032	35.15625	Suitable
L27	0.04	0.086	46.51163	Suitable
L28	0.0475	0.07975	59.56113	Un Suitable
L29	0.065417	0.099667	65.63545	Un suitable
L30	0.024167	0.056667	42.64706	Suitable
L31	0.00875	0.0355	24.64789	Suitable
L32	0.125417	0.137667	91.10169	Un Suitable
L33	0.005417	0.041417	13.07847	Suitable
L34	0.001667	0.030917	5.390836	Suitable
L35	0.030417	0.056917	53.4407	Un Suitable

4.6.2.7 Percentage Sodium (%Na)

This is the ratio of concentration of sodium in milli-equivalent per litre against the addition of calcium, magnesium, sodium and potassium in milli-equivalent per litre. The formular for calculating it is given as:

$$\%Na = \frac{Na}{(Ca+Mg+Na+K)} \text{x } 100 \qquad 47$$

According to Wilcox (1948), Mohammad *et al*., 2019 and Todd (1980), groundwater with percentage sodium lessthan50% is considered suitable for irrigation while the groundwater with greater than 50% percentage sodium is considered unsuitable for irrigation based on percentage sodium analysis. Table18 shows the calculated percentage sodium for groundwater samples collected in the area. From the table, four groundwater locations (12, 21, 26 and 31) are rated unsuitable for irrigation purpose while the remaining thirty one (31) groundwater locations are rated suitable for irrigation purpose based on percentage sodium formular (equation 47) used.

Figure 88 is a Wilcox quality classification of water for irrigation based on sodium percentage. The figure shows that all the groundwater samples in the area fall within excellent range. This is also confirmed by Table 19 (Wilcox classification system)

Table 16: Calculated values of Percentage sodium for groundwater samples in the area

LOCATION I.D	Na	Ca+Mg+Na+ K	%Na	Ratings
1	0.028696	0.078805	36.41366	Suitable
2	0.061087	0.169548	36.02919	Suitable
3	0.076087	0.177837	42.78467	Suitable
4	0.05913	0.140387	42.11964	Suitable
5	0.041304	0.134913	30.61547	Suitable
6	0.031739	0.096201	32.99263	Suitable
7	0.087391	0.220237	39.68049	Suitable
8	0.046087	0.188696	24.42393	Suitable
9	0.063696	0.256401	24.84222	Suitable
10	0.06587	0.205588	32.03967	Suitable
11	0.040652	0.124844	32.56225	Suitable
12	0.118478	0.176946	66.95722	Unsuitable
13	0.07413	0.209041	35.4622	Suitable
14	0.055217	0.155929	35.4119	Suitable
15	0.047609	0.143128	33.26304	Suitable
16	0.05913	0.141182	41.8825	Suitable
17	0.051304	0.170683	30.05834	Suitable
18	0.038913	0.102221	38.06766	Suitable
19	0.030435	0.158967	19.14537	Suitable
20	0.046087	0.245382	18.78173	Suitable
21	0.036522	0.071528	51.05925	Un suitable
22	0.06413	0.18581	34.514	Suitable
23	0.090217	0.186038	48.49409	Suitable
24	0.070435	0.30664	22.96987	Suitable
25	0.007826	0.045775	17.09693	Suitable
26	0.038478	0.075735	50.80667	Unsuitable
27	0.035435	0.13464	26.31819	Suitable
28	0.05087	0.136645	37.22748	Suitable l
29	0.048261	0.152287	31.69084	Suitable
30	0.056304	0.119381	47.16347	Suitable
31	0.041522	0.082406	50.38657	Unsuitable
32	0.083043	0.234043	35.48207	Suitable
33	0.04	0.089622	44.632	Suitable
34	0.035217	0.070878	49.68758	Suitable
35	0.049783	0.114135	43.61724	Suitable

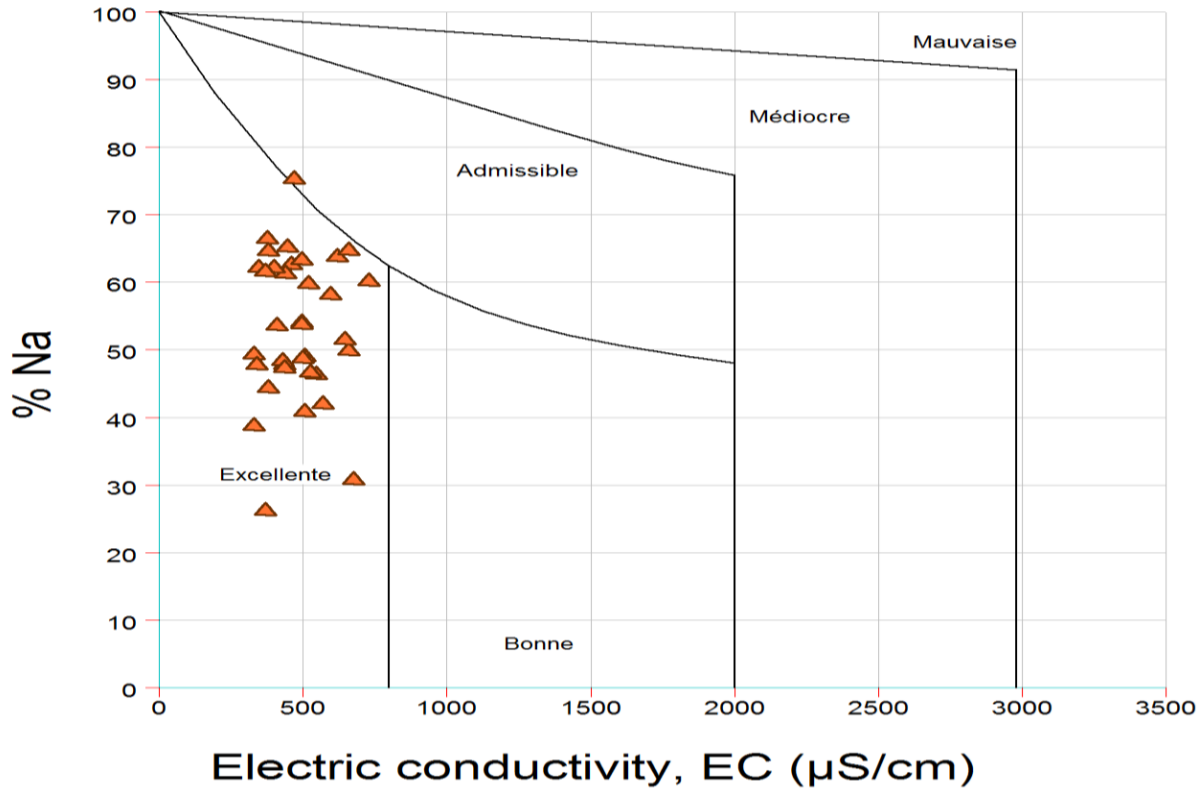


Figure 88: **Wilcox (1948) and Mohammad *et al*., (2019)'s quality classification of irrigation waters showing location of the collected water samples between electric conductivity and percentage sodium in the study area.**

Table 17: Wilcox water classification in respect of percentage sodium

Classification type	Category	Sample numbers	% Numbers
A	Excellent to Good	All samples	100
B	Good to Permissible	-	-
C	Permissible to Doubtful	-	-
D	Doubtful to Unsuitable	-	-

4.6.3 Gibbs Diagram

This is a diagram that shows relationship between groundwater of an area and its associated geology. Gibbs 1970 proposed a gibb's plot (Figure 89) which was employed to illustrate the natural mechanism controlling groundwater chemistry of an area.Three distinct fields such as precipitation dominance, evaporation dominance and rock–water interaction dominance areas are shown in the Gibbs diagram (Gibbs, 1970). The predominant groundwater samples of the study area fall in the rock–water interaction dominance field indicating the interaction between rock chemistry and the chemistry of the percolated waters under the subsurface. As stated above, the interaction between rocks and water results in leaching of ions into the surface water and penetrates in to groundwater as well, thereby influences the water chemistry.

Gibbs ratio I (for anion) = $Cl^- / Cl^- + HCO3$ 48

Gibbs ratio II (for cations) = $\frac{Na + K}{Na + K + + Ca}$ 49

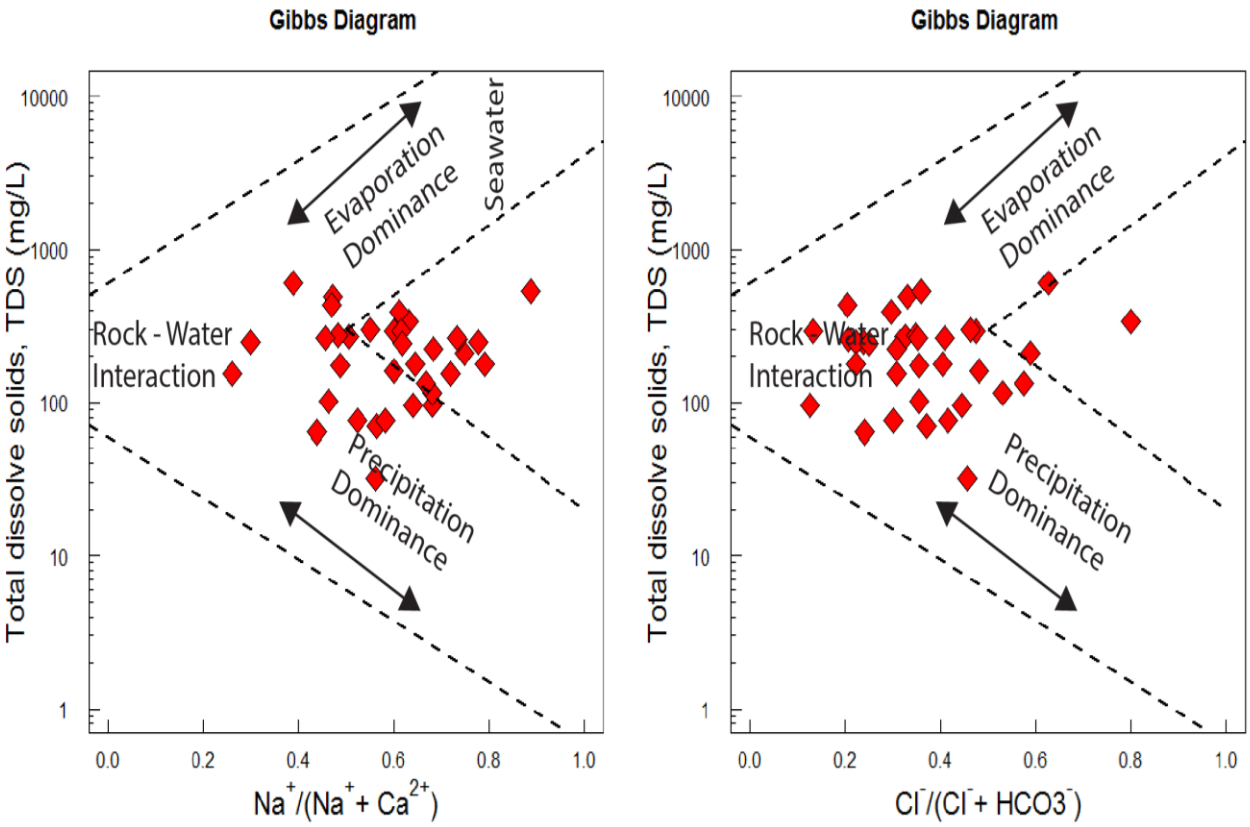


Figure 89: Gibbs diagram showing the distribution of the water samples in the area (After Gibbs (1970) and Mohammad *et al*. (2019).

4.6.4 Classification and Evolution of Groundwater in the Study Area

4.6.4.1 Piper classification

The major types of water in the study area are classified by plotting the concentrations against coordinate of water samples using Piper's trilinear diagram (Piper, 1944). The Piper trilinear diagram is a graphical representation of the chemistry of a water sample or samples. It illustrates the various percentages of anions and cations in the two triangular fields and a combined position of all major ions in the diamond-shaped field (Figure 90). The cations and anions are shown by separate ternary plots. The apexes of the cation plot are calcium, magnesium and sodium as the most abundant or major cations. The minor cations constituents are Barium, Strontium, Potassium, Caesium, Rubidium, Lithium and Ammonium. The apexes of the anion plot are bicarbonate, sulfate, and chloride as the most common or major anions. The minor constituents are Carbonate, Tetraborate, Iodide, Bromide, Fluoride, Nitrate and Nitrite. The two ternary plots are then projected onto a diamond. Percentages of anions and cations are based on total equivalents per litre of the major ions whose unit is in milligram/litre (mg/lt), obtained in the table 4.7. The mg/lt is converted to miliequivalent per litre (meq/lt) using

$$miliequivalent\ per\ litre = \frac{\left(\frac{mg}{lt}\right) valency\ of\ the\ ion}{mass\ number\ of\ the\ ion} \qquad 50$$

Piper diagram shows the effects of mixing between waters, because mixtures of two different waters will plot on a straight line. Thus, based on the major ions on the Piper plot (Figure 90) method of groundwater classification therefore, two major water types were observed in the study area*viz*:

i. Sodium potassium bicarbonate (Na-K (HCO_3) water
ii. Calcium bicarbonate water (Ca (HCO_3)

(Na-K (HCO_3) water type is the most abundant water type in the area amounting to about62.9 % of water samples from groundwater in the study area. The Ca would have been from weathering of alkali feldspar, amphibole and pyroxene of rock constituents in the area

The (Ca (HCO_3) class is the next abundant water type of water samples collected from groundwater in the study area which amounts to about 37.1%. The Ca would have been leached from weathering of feldspar present in rocks of the area.

4.6.4.2 Stiff classification

This is a graphical representation of chemical analyses, first developed by H.A. Stiff in 1951. It is widely used by hydrogeologists such as Mohammad *et al*., 2019 and geochemists to display the major ion composition of a water sample. A polygonal shape is created from four parallel horizontal axes extending on either side of a vertical zero axis. Cations are plotted in milli-equivalents per liter on the left side of the zero axis, one to each horizontal axis, and anions are plotted on the right side. Stiff patterns are useful in making a rapid visual comparison between water from different sources. The interpretation is based on the edges pointing out from each polygon. The longer the polygon the more polluted the water sample is. From the diagram (Figure 91) the samples 4, 13 and 21 are the samples with more than concentration of 5 meq/ lt.

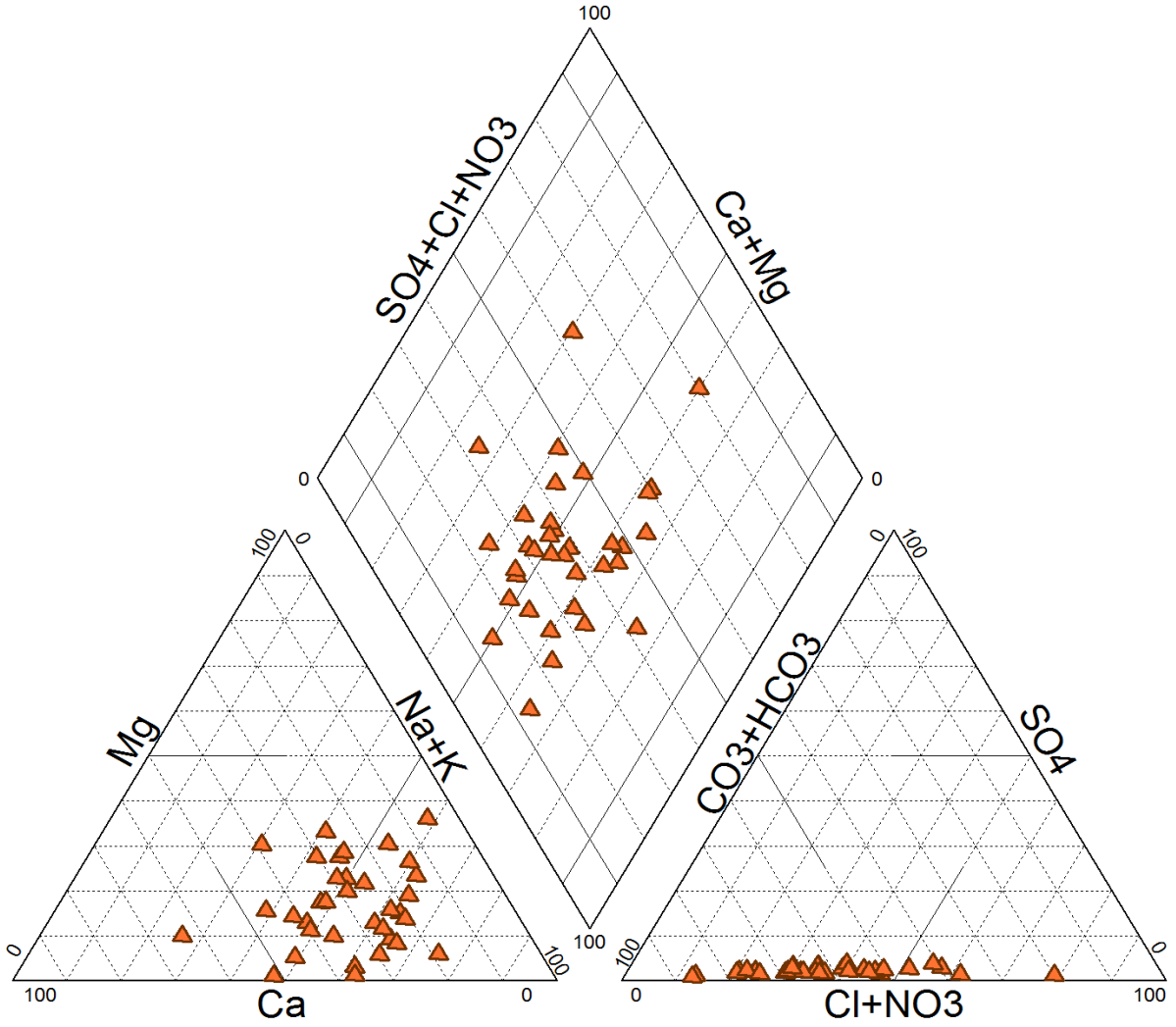


Figure 90: **Piper trilinear diagram showing the distribution of water samples in the area (After Piper, 1944 and Mohammad *et al.* 2019Piper trilinear diagram plotted for the**

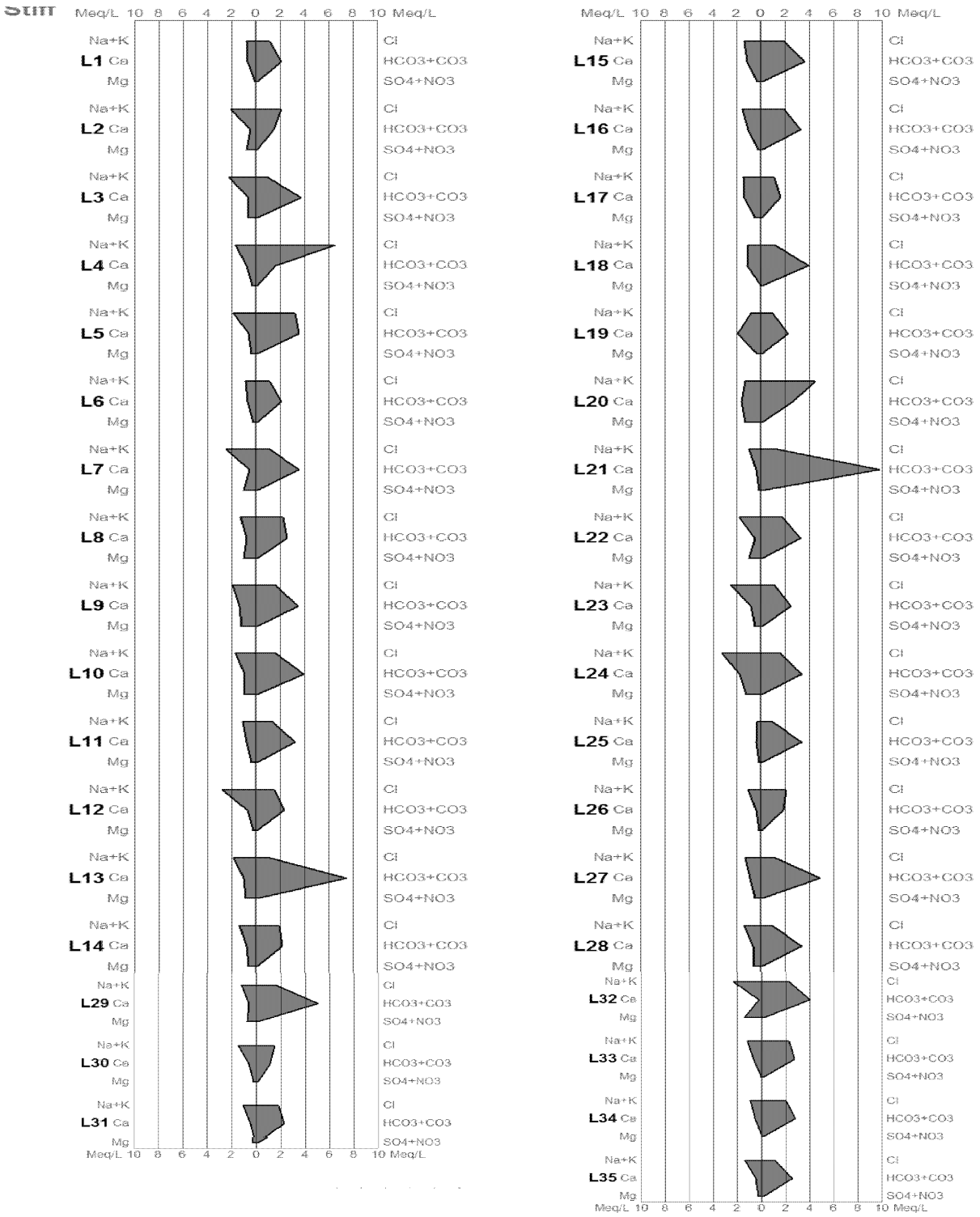


Figure 91: Stiff diagram showing the chemical parameters of groundwater in the study area (After Stiff, 1951 and Mohammad *et al*., 2019)

4.6.5 Correlation Analysis of the Chemical Species

4.6.5.1 Correlation Analysis

Correlation analysis is an analysis that shows the relationship between two variables. It is a simple measure to exhibit how well one variable predicts the other (Bahar and Reza, 2010).Correlation coefficient was the measure used to assess the relationship, using North-western University's version of the statistical package for the social scientists (SPSS). The Validity and reliability of data is the backbone of any research work for easy analysis and to achieve objectives set for the study. The relationship among the physico-chemical parameters was tested, so as to establish their validity and reliability or otherwise and the result is presented in Table 20.

Correlation coefficient is a commonly used measure to assess the relationship between two variables.

Table 20 shows the correlation between the parameters, it was shown that, there is a very strong positive correlation (0.953) ** between Turbidity and Electric conductivity and the relationship between them is significant. This means that the two parameters are directly proportional to each other; indicating that the higher the turbidity, the higher the conductivity and vice-versa. More so, a strong positive correlation (0.732)** exists between TH and Electric conductivity and a strong positive correlation (0.730*) between TH and Turbidity and the relationship between them is significant respectively. This also shows a direct relationship between them.

Table 18: Correlation Analysis of Physico-chemical parameters Results

Variables	pH	Temp	Elect_Cond	Turbidity	TH (mg/l)	TDS (mg/l)	Ca (mg/l)	Na (mg/l)	K (mg/l)	Mg (mg/l)	Cu (mg/l)	Fe (mg/l)	Mn (mg/l)	Zn (mg/l)	Pb (mg/l)	Cd (mg/l)	SO4 (mg/l)	PO4 (mg/l)	Cl (mg/l)	HCO3 (mg/l)	CO3 (mg/l)	NO3 (mg/l)
pH	1																					
Temp	.160	1																				
Elect_Cond	.057	.156	1																			
Turbidity	-.019	.112	.953**	1																		
TH (mg/l)	-.090	-.058	.732**	.730**	1																	
TDS (mg/l)	.057	.156	1.000**	.953**	.732**	1																
Ca (mg/l)	.029	-.387*	.287	.296	.646**	.287	1															
Na (mg/l)	-.324	.074	.248	.220	.359*	.248	-.026	1														
K (mg/l)	.092	.023	.491**	.473**	.453**	.491**	.222	.254	1													
Mg (mg/l)	-.132	.153	.764**	.755**	.894**	.764**	.234	.473**	.446**	1												
Cu (mg/l)	-.094	.262	-.078	-.066	.029	-.078	-.007	-.006	-.143	.041	1											
Fe (mg/l)	-.480**	-.139	.089	.059	.098	.089	-.057	.622**	.077	.159	-.065	1										
Mn (mg/l)	-.060	-.347*	.547**	.527**	.455**	.547**	.405*	.185	.327	.341*	-.313	.464**	1									
Zn (mg/l)	-.069	-.072	-.173	-.122	-.181	-.173	-.095	-.139	-.102	-.175	-.042	-.052	-.079	1								
Pb (mg/l)	.220	.055	-.097	-.108	-.080	-.097	-.133	-.022	-.083	-.023	.068	-.119	-.102	-.076	1							
Cd (mg/l)	-.210	-.395*	-.141	-.070	.137	-.141	.249	.051	.025	.027	-.021	-.141	.076	-.103	.167	1						
SO4 (mg/l)	.008	-.042	-.158	-.156	-.035	-.158	.166	-.060	-.059	-.142	.080	-.025	-.034	-.038	-.096	.458**	1					
PO4 (mg/l)	-.051	-.067	-.065	-.007	-.131	-.065	-.095	-.048	-.265	-.111	-.052	-.197	-.142	.106	.073	.450**	.285	1				
Cl (mg/l)	-.059	-.089	.367*	.348*	.139	.367*	.052	.012	.142	.146	-.194	-.005	.155	.004	-.131	-.267	-.106	.182	1			
HCO3 (mg/l)	.225	.137	.417*	.378*	.386*	.417*	.226	.013	.358*	.358*	.071	-.120	.292	-.217	.107	.356*	.248	.081	-.087	1		
CO3 (mg/l)	-.100	-.292	-.064	-.036	.081	-.064	.041	.119	.063	.078	-.153	.003	-.018	-.002	-.205	.291	-.150	.104	-.246	-.071	1	
NO3 (mg/l)	-.324	.166	.284	.290	.236	.284	.004	.151	.260	.298	-.154	.129	.042	-.014	-.220	-.063	.137	-.069	.119	.023	.085	1

CHAPTER FIVE

5.0 CONCLUSION, RECOMMENDATIONS AND CONTRIBUTIONS TO KNOWLEDGE

5.1 Conclusion

The study area is a Precambrian Basement Complex terrain consisting of crystalline rocks which are mainly metamorphic and igneous. The rocks are of modest characteristics in terms of groundwater potentiality and potability. There are generally two aquiferous units in the study area which are overburden and fractured crystalline aquifers and these aquifers are of different groundwater potentials and characteristics. The transmissivity and Storativity values indicate that the drawdown is high; signifying that short pumping can be sustained in the area. The southern part of the study area has low depth to water level; indicating high groundwater potential but low quality while the western part has high depth to water level; indicating low groundwater potential but high quality.

The magnetic survey of geophysical methods adopted revealed that the general trend of rocks in the area is NNW-SSE which conforms to the global structural trend existing in the Basement Complex of Nigeria. The main magnetic lineaments show that the promising areas for groundwater potential are the northern and southern parts of the area but the most promising is the southern parts. Also, the electrical resistivity survey indicated that analysis of the 2-D resistivity profile produced a system of three to five geo-electric layers with depth to bedrock of 1.05 to 41.8 m and curve matching analysis depicting thirteen types of sounding curves with dominant H, KH, and HKH curve types. The southern part of the area has the most reliable protective capacity based on the Dar Zarouk's method of assessment.

The result of a physico-chemical assessment of groundwater samples in the study area shows that the concentrations of ions in the groundwater fall within the desirable and permissible

limits of the World Health Organization (WHO) standards. This confirms that the groundwater in the area is potable for domestic purposes.

Based on major parameters analyzed to reveal the suitability of groundwater in the area for irrigation purposes, the groundwater is of excellent to good for irrigation purposes

5.2 Recommendations

A study on microbial assessment of groundwater in the area should be carried out to know its potability biologically. This enriches the knowledge of water quality in the area. Further study should also be carried out on 3 identified water samples (locations 4, 13, and 21) by the stiff diagram to know the cause of their poor quality.

5.3 Contributions to Knowledge

1) Enriching the comprehensive database, usable for the hydrological activities in the area
2) Production of the local geological map of the study area, as a modification for that of NGSA (2005).
3) Characterization of groundwater level of the area for both seasons.
4) Identification of promising groundwater potential zones in the area.
5) Production of groundwater potential distribution, quality, and protective capacity maps for the area.

REFERENCES

Abaa, S.I. (1983). The structure and petrography of alkaline rocks of the Mada Younger Granite Complex, Nigeria. J. Afr. Earth Sci. 3:107–113.

Abimbola, A.F. and Ehinola, O.A. (2002). Preliminary assessment of major and trace elements content in the Middle Cretaceous black shales of the Abakaliki fold belt, southeastern Nigeria. 23rd IAS Meeting of Sedimentology, p. 108.

Adekeye, J.I.D. (2001). Borehole depths and chemical impurities in Groundwater in the Basement Complex terrain of Kwara State, North central Nigeria,12: 9-12

Adetona, A. A., Udensi, E. E. and Agelaga A. G. (2007). Determination of Depth to Buried Magnetic Rocks under the Lower Sokoto Basin. N*igerian Journal of Physics*, 19*(2):* 281 282.

Adekunle, I.M.; Adetunji, M.T; Gbadebo, A.M; and Banjoko, O.B. (2007). Assessment of groundwater in a typical rural settlement in Southwest, Nigeria. International Journal of Environmental Research and Public Health 2007, Vol.4 (4), 307-318.

Adeyemi, G.O; Adesile,A.O; Obayomi, O.B. (2003). Chemical characteristics of source well type in Ikire southwestern Nigeria.14: pp. 12-18.

Agocs, W. B. (1951). Least-Squares Residual Anomaly Determination: *Geophysics*, 16:686 696.

Ajibade, A.C, Fitches, W.R, and Wright, J.B. (1979). The Zungeru mylonites, Nigeria: recognition of a major unit. Rev. de Geol. Geog. Phys. 21:359–363.

Ajibade, A.C. (1980). Geotectonic evolution of the Zungeru Region, Nigeria. Unpublished Ph.D. thesis, University of Wales, Aberystwyth.

Akande, S.O. and Erdtmann, B.D. (1998). Burial metamorphism (thermal maturation) in cretaceous sediments of the Southern Benue Trough and Anambra Basin, Nigeria. AAPG Bull 82: 1191–1206.

Alabi, A.A., Bello, R., Bello, A.S., Ogungbe, H.O and Oyerinde, H.O. (2010). Determination of groundwater potential in Lagos State University,Ojo: using geo-electric methods (Vertical electrical sounding and horizontal profiling), Rep. Opin. 2 p 68-75.

Alagbe, S.A. (1988). Hydrogeology of the River Kan-Gini Catchment Area, Kaduna State. Unpublished M.Sc thesis; Department of Geology, Ahmadu Bello University, Zaria

Anomohanran, O. (2013). Geophysical investigation of groundwater potential in Ukelegbe, Nigeria. Journal of Applied Sciences, 13, pp. 119-125.

Anomohanran, O. (2014). Hydrogeophysical and Hydrogeological Investigations of Groundwater Resources in Delta Central District of Nigeria, Journal of Taibbah University for Science, 9: 57-68.

Anudu, G.K, Onuba, L.S, and Ufondu, L.S. (2011). Geo- electric sounding for groundwater exploration in the crystalline basement terrain around Onipe and adjoining areas, south western Nigeriaa. Journal of Applied Technology Environmental Sanitation 1: 343-354.

Ashaolu, E.D. and Omotosho,O. (2015). Assesment of static water level and overburden pattern for sustainable groundwater development and management in Ilorin city,Nigeria. Geografia-Malaysian Journal of Society and Space 11 (9), 2017.

Ayodele,O., Hutton, L.G., Moffat, W.S. and Bako, M.D. (1989). Hydrogeology and Water chemistry in the weathered crystalline rocks of southwestern Nigeria. Groundwater Management: Quantity and Quality (Proceedings of the Benidorn Symposium (October, 1989) LAHS Publ. No, 188-198.

Babatunde, R. O., Saminu, O., Oluwatoyin, O. and Razak O. J (2021): Determination of Aquifer Parameters from Resistivity Data: A Case of University of Ilorin Campus, North-central Nigeria *Tanzania Journal of Science-AJOL series.*47(1); 91-103, Published by College of Natural and Applied Sciences, University of Dar es Salaam.

Bahar, M.M., and Reza M.S (2010). Hydrochemical characteristics and quality assessment of shallow groundwater in a coastal area of southwest Bangladesh. Environmental Earth Sci., 61: 1065-1073.

Barritt, S.D., (1993). The African Magnetic Mapping Project: *ITC Journal, **2**:*122-131.

Bhattacharya, P. K. and Patra, H. P. (1968). Direct Current Electric Sounding (Methods in Geochemistry and Geophysics, 9.) ix + 135 p., 47 figs., 16 tables. Elsevier Publishing Co., Amsterdam, London, New York. Price £3 15*s*

Bear, J. (1979). Hydraulics of Groundwater. New York: McGraw-Hill International Book.

Benkhelil, J. (1989). The origin and evolution of the Cretaceous Benue Trough, Nigeria. J. Afr. Earth Sci. 8:251–282.

Billing, M.P. (1972). Structural Geology, Eaglewood Cliffr. N. (third ed.), Prentice-Hall .

Billman, H.G. (1976). Offshore stratigraphy and paleontology of the Dahomey embayment. Proceedings, 7th African micropaleontology colloquium, lle-Ife.

Black, R. (1980). Precambrian of West Africa. Episodes 4:3–8.

Blakely, R.J. (1995). Potential Theory in Gravity and Magnetic Applications. *Cambridge UniversityPress, Australia,*pp.43-46.

Bouwer, H. (1978). Groundwater Hydrology, McGraw-Hill, New York. p.210.

Buchner, K. and Grapes, R. (2011). "Metamorphic rocks". Petrogenesis of Metamorphic rocks. Springer. pp. 21–56.

Burke, K.C. and Dewey, J.F. (1972). Orogeny in Africa. In: Dessauvagie T.F.J, Whiteman A.J (eds.), Africa geology. University of Ibadan Press, Ibadan, pp. 583–608.

Burke, K. (1976). The Chad Basin: an active intra-continental basin. Tectonophysics 36:197 206.

Clark, L. (1985). Groundwater abstraction from Basement Complex areas of Africa. Quarterly Journal of Engineering Geology, 18, 25-34.

Cooray, P.G (1975). The charnockitic rocks of Nigeria. Pitchamutu Volume, Banglore University, India, pp. 50–73.\

Cooper, G.R.J., (2009). Balancing Images of Potential-Field Data. *Geophysics, 74(3):* 17-20.

Cooper, G.R.J. and Cowan, D. R.(2008). Edge Enhancement of Potential-Field Data Using Normalized Statistics. *Geophysics, 73(3):* 1-4.

Dada, S.S. (1989). Evolution de la croute continental au Nord Nigeria: apport de la geochimie, de la geochronologie U-Pb et des traceurs isotopiques Sr, Nd et Pb. Ph.D. Thesis University of Science and Technology Languedoc, Montpellier, France.

Dada, S.S. (2006). Proterozoic evolution of Nigeria. In: Oshi O (ed.). The Basement Complex of Nigeria and its mineral resources (A Tribute to Prof. M. A. O. Rahaman). Akin Jinad and Co. Ibadan, pp. 29–44.

Darcy, H. (1856). Les fontaines publiques de la ville de Dijon: Exposition et application des principes à suivre et des formules à employer dans les questions de distribution d'eau: Ouvrage terminé par un appendice relatif aux fournitures d'eau de plusieurs villes, au filtrage des eaux et à la fabrication des tuyaux de fonte, de plomb, de tôle et de bitume (Vol. 2). V. Dalmont.

Davis, S.N. and De Wiest, R.M.J. (1966). Hydrogeology, New York: John Wiley and Sons, New York463p.

Deming, D. (2002). Introduction to hydrogeology. McGraw-Hill Higher Education, N.J. p.466.

De Klasz, I. (1977). The West African Sedimentary Basins. In: Moullade M, Nairn AEM (eds.) The phanerozoic geology of the world. The Mesozoic 1. Elsevier, Amsterdam, pp. 371–399.

Dobrin, M.B. (1960). Introduction to geophysical prospecting, German Edition

Doell, R. and Cox, A. (1967). Magnetization of Rocks. Mining Geophysics, Theory. Society of Exploration Geophysics, 2: 446-456.

Egbai, J.C. (2013). Aquifer comparability and formation strata in Orogun and Osubi (Ugolo) area of delta State using electrical resistivity method. Int. J. Rev. Appl. Sci. 14: 682-691.

Egboka, B.C.E. (1988). The Hydrogeological Provinces of Nigeria. In water quality Bulletin (13) No 4, 117-125pp.

Ejedawe, J.E. (1989). The Eastern Niger Delta: geological evolution and hydrocarbon occurrences. SPDC Internal Report, Exploration Note 89. 002

Ekwe, A. C. Nnodu, I. N., Ugwumbah, K. I. and. Onwuka, O. S (2010).Online Journal of Earth Sciences. Vol.4, 19-26pp.

Elueze, A.A. (1981). Petrographic studies of metabasic rocks and meta-ultramafics in relation to mineralization in Nigerian schist belts. J. Mining Geol. 18:31–36.

Ezeh, C. C. (2011). International Journal of Physical Sciences. Vol. 6, pp.3319-3329. Ewulu, P.Ch. (1983). Effects of poluutional discharges on Kaduna River Quality. M.sc thesis, Department of chemistry, Ahmadu Bello University, Zaria.

Falconer, J.D. (1911). The Geology and Geography of Northern Nigeria. Macmillan, London, pp.135

Food Agricultural Organization (F.A.O) (1985). Water Quality for Agriculture. Irrigation and Drainage paper, No 29 (Rev. 1), FAO, Rome.

Freeze, R.A. and Cherry, J.A. (1979). Groundwater. Prentice-Hall Inc., Englewood Cliffs, Vol. 7632, p.604.

Furon, R. (1960). G´eologie de l'Afrique Payot, Paris, pp. 40.

Fetter, C. W. (1980). "Applied Hydrogeology," Charles E. Merrill Publishing Company, Amherst.

Gilliet, N. P., Weaver, A. J., Zwiers, F. W. and Flannigan, M. D. (2004). Detecting the effect of climate change on Canadian forest fires. Journal of Geophysical Research, Vol. 3, (18).

Golam, S.S., Keramat, M. and Shalid, M. (2014). Deciphering transmissivity and hydraulic conductivity of the aquifer by vertical electrical sounding (VES) experiments in northwest Bangladesh, Appl. Water Sci. 2014

Grant, H.K. (1969). The late Precambrian to early Palaeozoic Pan- African orogeny in Ghana, Togo, Dahomey and Nigeria. Geol. Soc. Am Bull 80: 45-56.

Grant, N.K. (1970). Geochronology of Precambrian Basement rocks from Ibadan, South-Western Nigeria. Earth Planet Sci. Lett., 10:19–38

Grant, N.K. (1978). Structural distinction between a metasedimentary cover and an underlying Basement in the 600 my old Pan-African domain of Northwestern Nigeria, Geol. Soc. Am. Bull. 89:50–58.

Gibbs, R. J. (1970) Mechanism controlling world water chemistry Sciences 170: 795–840.

Griffin, W. R. (1949). Residual Gravity in Theory and Practice: *Geophysics, 14:*39–56.

Hantush, M.S. (1964). Drawdown around wells of variable discharge. Journal of geophysical research, Vol. 69 (20), pp.4221-4235.

Henderson, R. and Zietz, H. (1949). A Comprehensive System of Automatic Computation in Magnetic and Gravity Interpretation: *Geophysics, **25**: 569– 585*.

Henriet, J.P. (1975). Direct application of the Dar-Zarouk parameters in groundwater survey Geo-physics prospect 24: 344-353.

Holt, R.W. (1982). The Geotectonic Evolution of the Anka Belt in the Precambrian Basement Complex of N.W. Nigeria. Unpublished Ph.D. Thesis, the Open University.

Horton, R.K. (1965). An Index Number System for Rating Water Quality. Journal of the Water Pollution Control Federation, 37, pp. 300-306.

Hubbard, F.H. (1975). Precambrian crustal development in Western Nigeria: indications from Iwo Region, Geol. Soc. Am. Bull. 86:548–554.

Ishola1, K., Ogunsanya , S., Adiat, K., and Abdulrahman,A. (2013). Assessing Groundwater Potential Zones in Basement Complex Terrain Using Resistivity Depth Soundings: A Case of Challenge and Oluyole in Ibadan, Southwestern Nigeria. Journal of Science, Vol. 1 No. 1: pp. 11-32.

Jacob, C.E. (1987). Drawdown test to determine effective Radius of Artesian Well. Trans. A.S.C.E., Vol.112, pp. 1047-1070.

Jones, H.A. and Hockey, R.D. (1964). The geology of part of South Western Nigeria. Geological Survey Bulletin, Pp.31-101.

Jones, M.J. (1985). The weathered zone aquifers of the Basement Complex Area of Africa. Quaternary Journal of Engineering Geology. Vol.18. P 35-46

Kamba, A. H., Bonde,D.S.and Udensi, E. E.(2016). Spectral Depth Analysis of Some Part in Lower Sokoto Basin, North - West Nigeria, Using Aeromagnetic Data. *Standard Global Journal of Geology and Explorational Research,**3**(5):* 226- 232.

Kelly, W.P. (1951). Alkali soils; their formations, properties and reclamation. Reinhold publication, New York.

Kruseman, G.P. and de Ridder, J.M. (1990). Analysis and Evaluation of Pumping Test Data. ILRI Publication 47, p. 377

Kumar, M. S., Gnanasundar, D. and Elango, L. (2001). Geophysical studies to determine Hydraulicccharacteristics of an alluvial aquifer. Journal of Environmental Hydrology, 9 (15): 1-7.

Labbo, Z. and Ugodulunwa, F.X.O. (2007). An Interpretation of Total Intensity Aeromagnetic Maps of Part of Southeastern Sokoto Basin. *Journal of Engineering and Applied Sciences*3: 15-20

Ladipo, K.O (1988). Paleogeography, sedimentation and tectonics of the Upper Cretaceous Anambra Basin, south-eastern Nigeria. J. Afr. Earth Sci. 7:865–871. (Lagos State Waste Management Authority) LAWMA, (2000). Management of Landfills waste: The journey so far. L.E.P.A.

Lawrence, A.O. and Ojo, T.A. (2012). The use of combined geophysical survey methods for groundwater prospecting in a typical Basement Complex terrain: case study of Ado-Ekiti south western Nigeria. Res. J. Eng. Appl. Sci. 1, pp. 362-376.

Lenkey, L., Hamori, Z. and Mihalffy, P. (2005). Investigating the hydrogeology of a water supply area using direct-current vertical electrical soundings. Geophysics 70 (4), H1–H19.

Loke, M. H. (1999). A Practical Guide to 2D and 3D Surveys. Electrical Imaging Surveys for Environmental and Engineering Studies, 8-10

Matheis, G. and Caen-Vachette, M. (1983). Rb-Sr isotopic study of rare-metal-bearing and barren pegmatites in the Pan-African reactivation zone of Nigeria, J. Afr. Earth Sci. 1:35–40.

McCurry, P. (1976). The Geology of the Precambrian to Lower Palaeozoic Rocks of Northern Nigeria – A Review. In: Kogbe CA (ed) Geology of Nigeria. Elizabethan Publishers, Lagos, *Pp.*15–39.

Meju, M.A., Fontes, S.L., Oliveira, M.F.B., Lima, J.P.R., Ulugerger, E.U. and Carrasquilla, A.A. (1999). Regional aquifer mapping using combined VES-TEM-AMT-EMAP methods in the semi-arid eastern margin of Parnaiba Basin, Brazil. Geophysics 64 (2), pp. 337–356.

Mele, M., Bersezio, R., Giudici, M., Rusnighi, Y., and Lupis, D. (2010). The architecture of alluvial aquifers: An integrated geological –geophysical methodology for multiscale characterization. Mem Descr Carta Geol. D'lt xc, 209-224.

Miller, H.G. and Singh, V. (1994). Potential Field Tilt-A New Concept for Location of Potential Field Sources. *Journal of Applied Geophysics, 32:*213-217.

Milsom, J. (2011). *Field Geophysics*, The Geological Field Guide Series, Wileyand Sons Ltd., Publication, ***4****:* 123-125.

Mohammad, S., Mohammad, T. A, Janardhana, M.R. , Mohamed, M. A. (2019). Hydrochemical processes and groundwater quality assessment in North eastern region of Jordan valley, Jordan. Hydro-Research regional studies, Global impact, Vol. 4

Mohammed, I. N, Aboh, H. O. and Emenike, E. A. (2008). Hydrogeophysical investigation for groundwater Potential in central Minna, Nigeria. Science world journal vol. 3 (4) 2008.

Nabighian, M.N., (1972). The Analytic Signal of Two Dimensional Magnetic Bodies with PolygonalCross section: Its Properties and Uses for Automated Anomaly Interpretation. *Geophysics* 37: 507-517.

National Secondary Drinking Water Standard (2014). Groundwater Quality Interpretation Guide, Colorado Water and Energy Research Centre, p.6

Nejad, H.T. (2009). Geo-electric investigation of the aquifer characteristics and groundwater potential in Behbahan Azad University farm, Khuzestan Province, Iran. J. Appl. Sci. 9: 3691-3698.

Naik, S., Purohit, K.M. (2001). Studies on water quality of river Brahmani in Sundargarh district, Orissa. Indian Journal of Environment and Eco-planning 5 (2), 397–402

Nwankwo, L. I. (2015). Estimation of Depths to the Bottom of Magnetic Sources and Ensuing Geothermal Parameters from Aeromagnetic Data of Upper Sokoto Basin, Nigeria. *Geothermics*, 54*:*76-81.

Obaje, N.G., Wehner, H., Scheeder, G., Abubakar, M.B, and Jauro, A. (2004). Hydrocarbon prospectivity of Nigeria's inland basins: from the viewpoint of organic geochemistry and organic petrology. AAPG Bull 87:325–353.

Obaje, N.G. (2009). Geology and mineral resources of Nigeria, Berlin: Springer, p.221

Obaje, N. G., Abdullahi, I. N., Issa, G. and Dantata,S. H. (2013).New assessment for Central Nigeria's Bida basin highlights geological prospects. Oil and Gas Journal, 113(4):52-59.

Oborie, E.L. and Udom, G.J. (2014). Determination of aquifer transmissivity using geo-electrical sounding and pumping test in parts of Bayelsa State, Nigeria. Peak J. Phys. Environ. Sci. Res. 2 (2), 32–40.

Odeyemi, I.B. (1976). Preliminary Report on the Field Relationship of the Basement Complex around Igarra, Midwest Nigeria. In: Kogbe, C.A., Ed., Geology of Nigeria, Elizabethan Press, Lagos, 365-369.

Offodile, M.E. (1983). The occurrence and exploitation of groundwater in Nigeria Basement rocks, Nig. Journ. Geol. 20 (1&2), pp.131-146.

Ofoha, C. and Ekine, A. (2016). Interpretation of Aeromagnetic Anomalies of Degema and Oloibiri area of Niger Delta, Nigeria, Using Qualitative Approach, Journal of Scientific research and Reports, 18 (4):1-12.

Ogezi, A.E.O. (1977). Geochemistry and Geochronology of Basement Rocks from Northwestern Nigeria. Unpublished Ph.D. Thesis, University of Leeds.

Ojo, S.B. (1984). Middle Niger Basin revisited: magnetic constraints on gravity interpretations. Abstract, 20th Conference of the Nigeria Mining and Geosciences Society, Nsukka, pp. 52–53.

Ojo, S.B, Ajakaiye, D.E. (1989). Preliminary interpretation of gravity measurements in the Mid-Niger Basin area, Nigeria. In: Kogbe, C.A. (Ed.), Geology of Nigeria. 2nd edition, Elizabethan Publishers, Lagos, pp. 347–358.

Okonkwo, A. C. and Ezeh, C. C. (2013). International Resource Journal of Geology and Minerals 3, 31-39

Okonkwo, A. C. and. Ugwu,G. Z. (2015). International Resource Journal of Geology and Minerals, **5**, 12-19.

Okosun, E.A. (1990). A review of the Cretaceous stratigraphy of the Dahomey Embayment, West Africa. Cretaceous Res 11:17–27

Oladapo, M.I. and Akintorinwa O.J. (2007). Hydrogeophysical study of Ogbese, southwestern, Nigeria. Global journal of pure and applied sciences 13, pp.55-61.

Olarewaju, V.O. (2006). The Charnockitic Intrusives of Nigeria. In: Oshi (ed.). The Basement Complex of Nigeria and its mineral resources (A Tribute to Prof. M. A. O. Rahaman), Akin Jinad & Co. Ibadan, pp. 45–70.

Olasehinde, P.I., Virbka, E.A. and Esan, E. A. (1998). Preliminary result of hydrogeological investigation in Ilorin area, south western Nigeria. Global Journal of Pure and Applied Sciences, 15 (2): 195-204.

Olasunkanmi, N. K., Sunmonu, L. A., Adabanija, M. A. and Oladejo, O. P. (2012). Interpretation of high resolution aeromagnetic data for mineral prospect in Igbeti-Moro area, Southwestern Nigeria, IOP conference series: Earth and Environmental Science

Olatunji S & Musa, A. (2013): Estimation of Aquifer Hydraulic Characteristics from Surface geoelectrical Methods: Case Study of Rima Basin, North Western Nigeria. *Arabian Journal fo Science and Engineering.* 39(7); 5475-5487, Published by Springer.

OlatunjiS. & Ojulari B.A. (2015): Electrical Assessment of the Aquifers in the Basement Complex of Unilorin: Implication for Existing Boreholes. *Journal of Science, Technology, Mathematics and Education.* 11(2); 1-16, Published by School of Science and Technology Education, Federal University of Technology, Minna.

Olatunji, S.& Osazuwa I. B. (2012): Geo-Electrical Delineations within Kubanni Basin, North Central Nigeria.*Arabian Journal of Geosciences.*6(10); 4079-4089, Published by Springer.Available online at https://doi.org/10.1007/s12517-012-0702-7

Olatunji1, S., Emiola, A. M. and Adebisi, A. W. (2021): Aquifer Vulnerability Evaluation in Southwestern Nigeria from AHP-GODT model using Geo-electrical Derived Parameters. Journal of meteorology and Geophysics (Journal of Meteorological and

Geophysical).22(1); 9-18, Published by Research and Development Center of the meteorology, Climatology and Geophysics Agency, Indonesia.

Olawuyi, A.K. (2012). Geo- electric exploration for groundwater within the premises of University of Ilorin Teaching Hospital, Ilorin, Kwara State. Nigerian Journal of Technological Development. 9 (2), p.8.

Olayinka, A.I. (1996). Non uniqueness in the interpretation of bedrock resistivity from sounding curves and its hydrological implications. Water Resource, NAH 7 (1&2), Pp.55–60.

Olorunfemi, M.O; Ojo, J.S and Akintunde, O.M. (1999). Hydro-geophysical evaluation of the groundwater potential of the Akure metropolis, south western Nigeria. Journal of mineral geology 35;207-228.

Olorunfemi, M.O. and Olorunnwo, M.A. (1985). Geo-electric parameters andaquifers characteristics of some parts of south-western Nigeria. Geological Application Indiogeologic, Vol. 20, pp. 99-109.

Olorunfemi, M.O., Olanrewaju, V.O. and Alade, O. (1991). Electrical nisotropy and groundwater yield in Basement Complex area of south-western Nigeria. Journal of Africa Earth Sciences, Vol. 12, No. 93, pp. 247-327.

Onuoha, K. M. and. Mbazi, F. C. C (1988). *Groundwater and Mineral Resources of Nigeria*, edited by C. O.Ofoegbu (Springer, Berlin, 1988), pp. 17-29.

Oluyide, P.O. (1988). Structural Trends in the Nigerian Basement Complex. Precambrian Geology of Nigeria, Geological Survey of Nigeria, pp. 93-98.

Omosuyi, G.O. (2010). Geoelectric assessment of groundwater prospect, a vulnerability of overburden aquifers at Idanre, Southwestern Nigeria. Ozean J. Appl. Sci. 3 (1), 19–28.

Opeyemi, J. A. and Rasheed B. A. (2016). Hydrogeophysical investigation of groundwater potential and aquifer vulnerability prediction in basement complex terrain A case study from Akure, Southwestern Nigeria RMZ – M&G | 2016 | Vol. 63 pp. 55–066

Oseji,I., Julius, O. and Ujuanbi, O. (2009). Hydrogeophysical investigation of groundwater potential in Emu kingdom, Ndokwa land of Delta State, Nigeria. International Journal of Physical Sciences Vol. 4 (5), pp. 275-284.

Oyawoye, M. O. (1964). The Geology of the Nigeria Basement Complex, *Journal of Nigeria Mining, Geology and Metallurgy Soc*., Vol. 1, pp.56-65.

Oyawoye, M.O. (1972). The Basement Complex of Nigeria. In: Dessauvagie TFJ, Whiteman AJ African geology. Ibadan University Press, pp. 66–102.

Pang, Z., Yuan, L., Huang, T., Kong, Y., Liu, J., Li Y (2013). Impacts of human activities on the occurrence of groundwater nitrate in an alluvial plain: a multiple isotopic tracers approach. J Earth Sci 24(1):111–124.

Parasins, D.S. (1966). “Principles of Applied Geophysics” Third Edition.

Parasnis, D.S. (1972). “Principles of Applied Geophysics” (2nd Ed.), Chapman and Hall, London.

Parasnis, D.S. (1986). “Principles of Applied Geophysics”. Chapman and Hall, London.

Pawlowski, R. S. and Hansen,R. O. (1990). Gravity Anomaly Separation by Wiener Filtering *Geophysics, 55:*539–548.

Petters, S.W. (1982). Central West African Cretaceous-Tertiary benthic foraminifera and stratigraphy. Palaeontographica Abt A 179:1–104

Pilkington, M..and Keating, P.(2004). Contact Mapping from Gridded Magnetic Data Comparison of Techniques, *Exploration Geophysics*, 35*:*206-311.

Piper, A.M (1944). A graphical interpretation of water—analysis. Trans Am Geophys Union 25:914–928.

Raghunath, H.M. (1987). Groundwater. Wiley Eastern Ltd., Delhi, 563.

Rahaman, M.A. (1976). Review of the Basement geology of South-Western Nigeria. In: Kogbe C.A. (ed.) Geology of Nigeria, 2nd Edition, Elizabethan Publishers, Lagos, pp. 41–58.

Rahaman, M.A, and Ocan, O. (1978). Relationships in the Precambrian Migmatite-gneisses of Nigeria. Nigeria Journal of Mineral Geology, 15:23–32.

Rahaman, M.A. (1981). Recent advances in the study of the Basement Complex of Nigeria. Abstract, 1st Symposium on the Precambrian Geology of Nigeria.

Rahaman, M.A. (1988). Recent advances in the study of the Basement Complex of Nigeria. In: Geological Survey of Nigeria (ed.) Precambrian Geology of Nigeria, pp. 11– 43.

Rajasekhar, P., Vimal, K.P., and Mansoor, M. D. (2014). Determination of confined aquifer parameters by Sushil, K. Singh method. Am. Int. J. Res. Sci. Technol. Eng. Math. 5. Pp. 158-163

Raji, B.A. and Alagbe S.A. (1997). A topo-geochemical sequence in Asa drainage basin Kwara State, Nigeria.

Raji, W.O. and Bale, R.B. (2008). The Geology and Geophysical studies of a gravel deposits in University of Ilorin, South western Nigeria. Journal of Earth Science 13(1):40-46.

Roy, A. (1958). Letter on Residual and Second Derivative of Gravity and Magnetic Maps: *Geophysics*, 23:860–861.

Reeves, C., Reford, S. and Millingan, P. (1997). Airborne Geophysics: Old Methods, New Images in a Gubins (Ed.), Proceedings of the Fourth Decennial International Conference on Mineral Exploration,Australia, pp. 13-30.

Reford, S. W., Kwan, K., Nyakaana, J., Katumwehe, A. and Wane, O.(2009). Airborne Geophysics as a tool to Promote mineral investment in Africa: *20th Geophysical Conference, ASEG*, pp. 23-24.

Reyment, R.A. (1965). Aspects of the geology of Nigeria, Ibadan University Press, pp.133.

Richards, L., 1954. Diagnosis and improvement of saline and alkali soils. US Department of Agriculture Handbook-60 (Washington DC, 160 p.)

Salem, A.S., William, S., Richard, S.M. and Dhananjay R. (2008). Interpretation of magnetic data using tilt angle derivatives. Article in Geophysics, Vol. 73, No 1,

Sarath Prasanth ,S.V, Magesh, N.S, Jitheshlal ,K.V, Chandrasekar, N (2012) . Evaluation of groundwater quality and its suitability for drinking and agricultural use in the coastal stretch of Alappuzha District, Kerala, India. Appl Water Sci 2(3):165–175

Saba, N.V., Umer, R., 2016. Hydrogeochemical assessment of Moradabad city, an important industrial town of Uttar Pradesh, India. Sustainable Water Resource Management 2, 217–236.

Sahu, P. and Sikdar, P.K., (2008). Hydrochemical framework of the aquifer in and around East Kolkata Wetlands, West Bengal, India. Environ. Geol. 55, 823–835.

Salameh, E.N., Bannayan, H., (1993). Water resources of Jordan: present status and future potentials. Fridrich Ebert Stiftung 1, 151–260

Amman, Jordan. Saleh, A., Al-Ruwaiah, F., Shehata, M., 1999. Hydrogeochemical process.

Salem, A., Williams, S., Fairhead, J. D., Smith, R. and Ravat, D. J.(2008). Interpretation of Magnetic Data Using Tilt-Angle Derivatives, *Geophysics*, 73*:* 1-10.

Schoeneich, K. and Aku, M. I. (1998). The study of Degraded Mine lands of Jos Bukuru, Riyom, B/Ladi and Bokkos Areas of Jos Plateau for Development Possibilities. Un published report for Government of plateau State, Plateau State Environmental Protection Agency.

Schoeneich, K. (2001). Water quality lecture note for Postgraduate students of hydrogeology, Geology Department, Ahmadu Bello University, Zaria.

Sharma, C. B.(2002). Airborne and Ground Magnetics, Geophysical and Remote Sensing Methodsfor Regolith Exploration, pp. 33–45.

Singh, D.F., (1992). Studies on the water quality index of some major rivers of Pune, Maharashtra. Procedings of Academy of Environmental Biology 1 (1), 61–66

Singh, A.K., Mondal, G.C., Singh, P.K., Singh, S., Singh, T.B., Tewary, B.K., (2005). Hydrochemistry of reservoirs of Damodar River basin, India: weathering processes and water quality assessment. Environ. Geol. 8, 1014–1028

Sirhan, A., Hamidi,M. and Andrieux, P. (2011). Electrical resistivity tomography, an assessment tool for water resource; a case study of Al- Aroub basin, West bank Palestine, Asian. Journal of Earth Sciences, 4:45-48.

Spector, A. and Grant, F. S. (1970). Statistical Models for Interpreting Aeromagnetic Data Geophysics 35: 293-302.

Stiff, H. A. (1951). The Interpretation of Chemical Water Analysis by Means of Patterns Environmental Science, Journal of Petroleum Technology

Telford, W.M., Geldart, L.P. and Sheriff, R.E. (1990). Applied Geophysics, Second Edition.

Tijani, M.N. (1994). Hydrogeochemical assessment of groundwater in Moro area, Kwara State, Nigeria. Environmental Geology, Vol. 24, pp.194-202.

Tijani, M.N. and Ayodeji O.A. (2001): Hydrogeochemical Assessment of surface and Groundwater Resources in parts of Dahomey Basin, SW Nigeria: *Water Resources*, (Jour. of Nigerian Assoc. of Hydrogeologists, NAH); Vol. 12: 88 - 93.

Tiwari, T.N., Mishra, M.A., (1985). A preliminary assignment of water quality index of major Indian rivers. Indian Journal of Environmental Protection 5, 276–279

Todd, D.K. (1980). Groundwater Hydrology. Wiley, New York

Truswell, J.F. and Cope, R.N. (1963). The geology of parts of Niger and Zaria Provinces, Northern Nigeria. Geol. Survey Nigeria Bull. 29:1–104.

Tubosun, I.A. (1983). Geochronologie U/Pb du Socle Precambrian du Nigeria. Unpublished 3 thesis, Univ. des Sciences et Techniques du Languedoc Montpellier.

Turner, D.C. (1983). Upper Proterozoic schist belts in the Nigerian sector of the Pan-African Province of West Africa. Precambrian Res. 21:55–79.

Udensi E.E, Osazuwa I.B. (2004). Spectral determination of depths to magnetic rocks under the Nupe Basin, Nigeria. Nigerian Association of Petroleum Explorationists (NAPE) Bull., 17:22–27.

Umego, M. N. (1990). Structural Interpretation of Gravity and Aeromagnetics Anomalies over Sokoto Basin, Northwestern Nigeria. Ph.D Thesis Dept of Physics ABU, Zaria, Nigeria pp. 34-38.

Utom, A.U., Odoh, B.I., and Okoro, A.U. (2012). Estimation of aquifer transmissivity using Dar Zarrouk parameters derived from surface resistivity measurements: a case history from parts of Enugu town, Nigeria. Journal of Water Resource Protect 4 : 993-1000.

Vasanthavigar, M., Srinivasamoorthy, k., Vijayaragaven, K., and Rajiv, R. G. (2010). Application of water quality index for groundwater quality assessment: Thirumanimuttar sub-basin, Tamilnadu, India. Environ Monit. Assess 171:595–609

Van Breemen, O., Pidgeon, R.T. and Bowden, P. (1977). Age and isotopic studies of some Pan-African granites from north central Nigeria. Precambrian Res. 4:317–319.

Verduzco, B., Fairhead, J.D., Green, C.M. and MacKenzie, C.(2004). New Insights into Magnetic Derivatives for Structural Mapping, *The Leading Edge,* 23*:*116-119.

Weber, K.J. (1972). Sedimentological aspects of oil fields in the Niger Delta. Geologe en Mijnbouw 50:559–576.

Whiteman, A. (1982). Nigeria: its petroleum geology, resources and potential. Graham and Trotman, London, pp. 381.

Wilcox, L.V., (1948). The Quality of water for irrigation use. US Department of Agriculture l Bulletin 1962, 40.

Wilkinson, Bruce, H.; McElroy, Brandon, J.; Kesler, Stephen E.; Peters, Shanan E.; Rothman,

Edward, D. (2008). "Global geologic maps are tectonic speedometers – Rates of rock cycling from area-age frequencies". Geological Society of America Bulletin. 121 (5–6): 760–779.

Woakes, M., Rahaman, M.A. and Ajibade, A.C. (1987). Some metallogenetic features of the Nigerian Basement. J. Afr. Earth Sci. 6:54–64.

World Health Organization, (1993).Guidelines for drinking water quality (2nd edition). Volume 1 Published by World Health Organization, Geneva.

World Health Organization, (1996).Guidelines for drinking water quality (2nd edition). Volume 2- Health criteria and other supporting; volume 3 – Surveillance and control of community supplies. Published by World Health Organization, Geneva.

World Health Organization, (2004). The World health report : changing history, Published by World Health Organization, Geneva.

World Health Organization, (2006).Guidelines for drinking water quality (3rd edition). Published by World Health Organization, Geneva.

World Health Organization-defined eosinophilic disorders: 2011 update on diagnosis, risk stratification, and management.

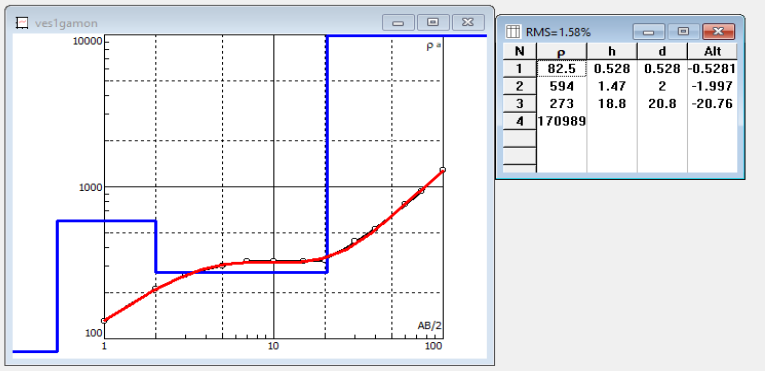
World health statistics (2017). Monitoring health for the SDGs, Sustainable Development Goals. Geneva: World Health Organization; Licence: CC BY-NC-SA 3.0 IGO.

Wright, E.P. and Burgess, W.G. (1992). Hydrogeology of crystalline Basement Aquifers in Africa.

Wright, J.B. (1970). Controls of mineralization in the Older and Younger tin fields of Nigeria, Econ. Geol. 65:945–951.

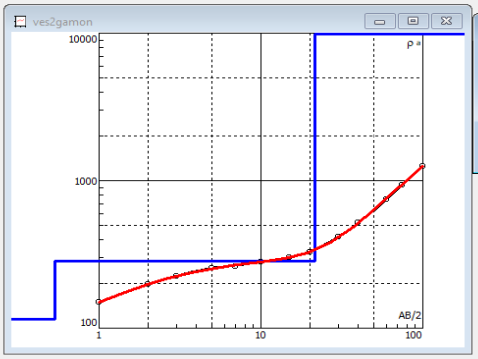
Zahran,H.M., Sherif, M.E. and Helmy, S.O. (2017). Aeromagnetic data over Harrat Lunayyir and surrounding areas, western Saudi Arabia. Arabian Journal of Geosciences, 10(3)

APPENDIX 1: GEOPHYSICAL CURVES AND THEIR PSEUDO SECTIONS GANMO



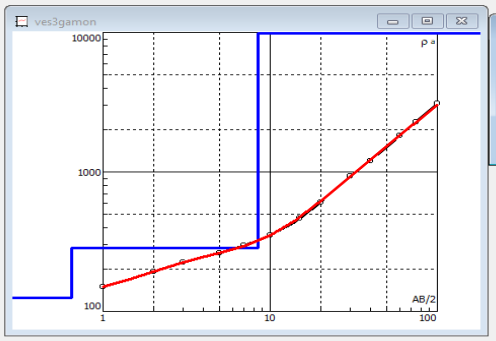
RMS=1.58%

N	ρ	h	d	Alt
1	82.5	0.528	0.528	-0.5281
2	594	1.47	2	-1.997
3	273	18.8	20.8	-20.76
4	170989			



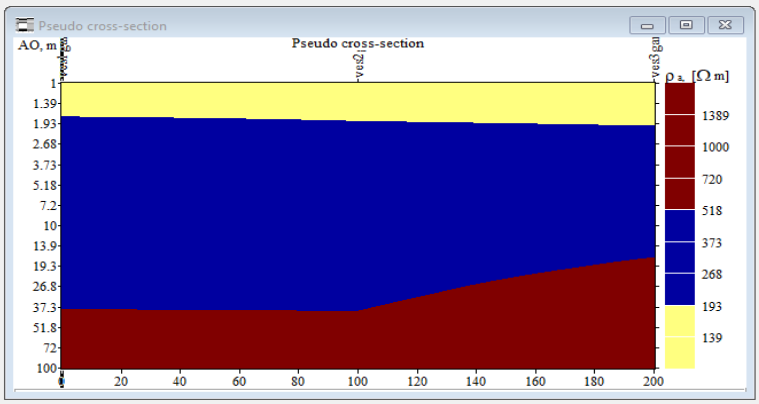
RMS=0.617%

N	ρ	h	d	Alt
1	115	0.534	0.534	-0.5337
2	283	21	21.5	-21.53
3	59998			

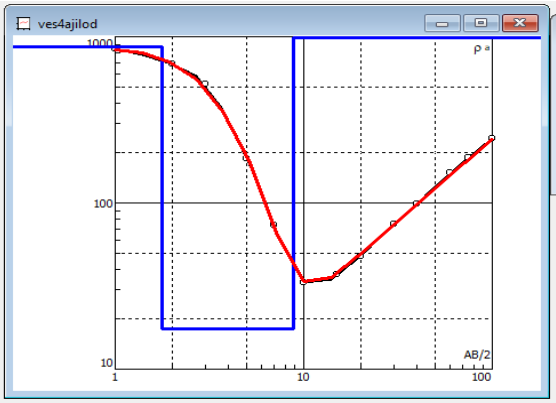


RMS=1.12%

N	ρ	h	d	Alt
1	125	0.648	0.648	-0.6481
2	285	7.82	8.46	-8.463
3	207812			

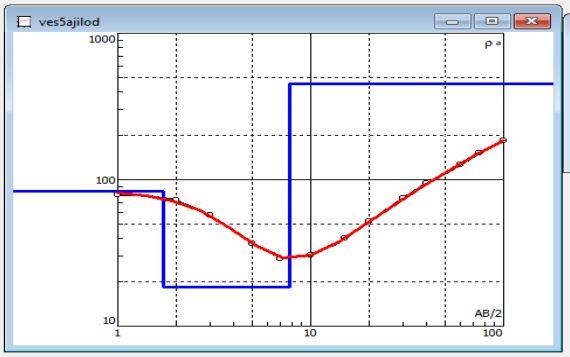


AJILODE



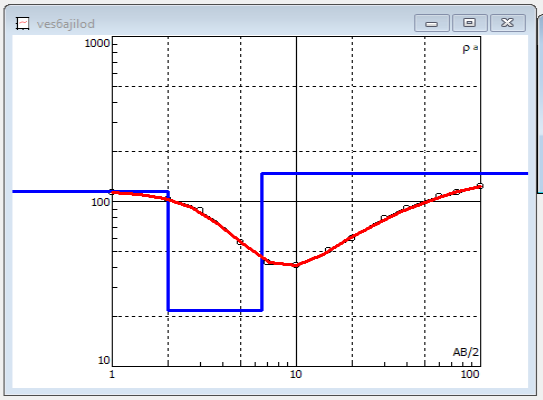
RMS=2.3%

N	ρ	h	d	Alt
1	867	1.78	1.78	-1.78
2	17.5	7.04	8.82	-8.82
3	10206			



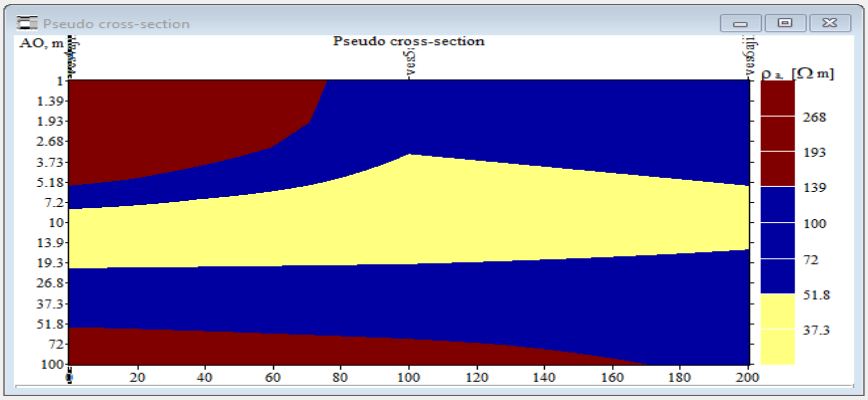
RMS=1.03%

N	ρ	h	d	Alt
1	82.8	1.72	1.72	-1.72
2	18.4	6.07	7.79	-7.787
3	451			

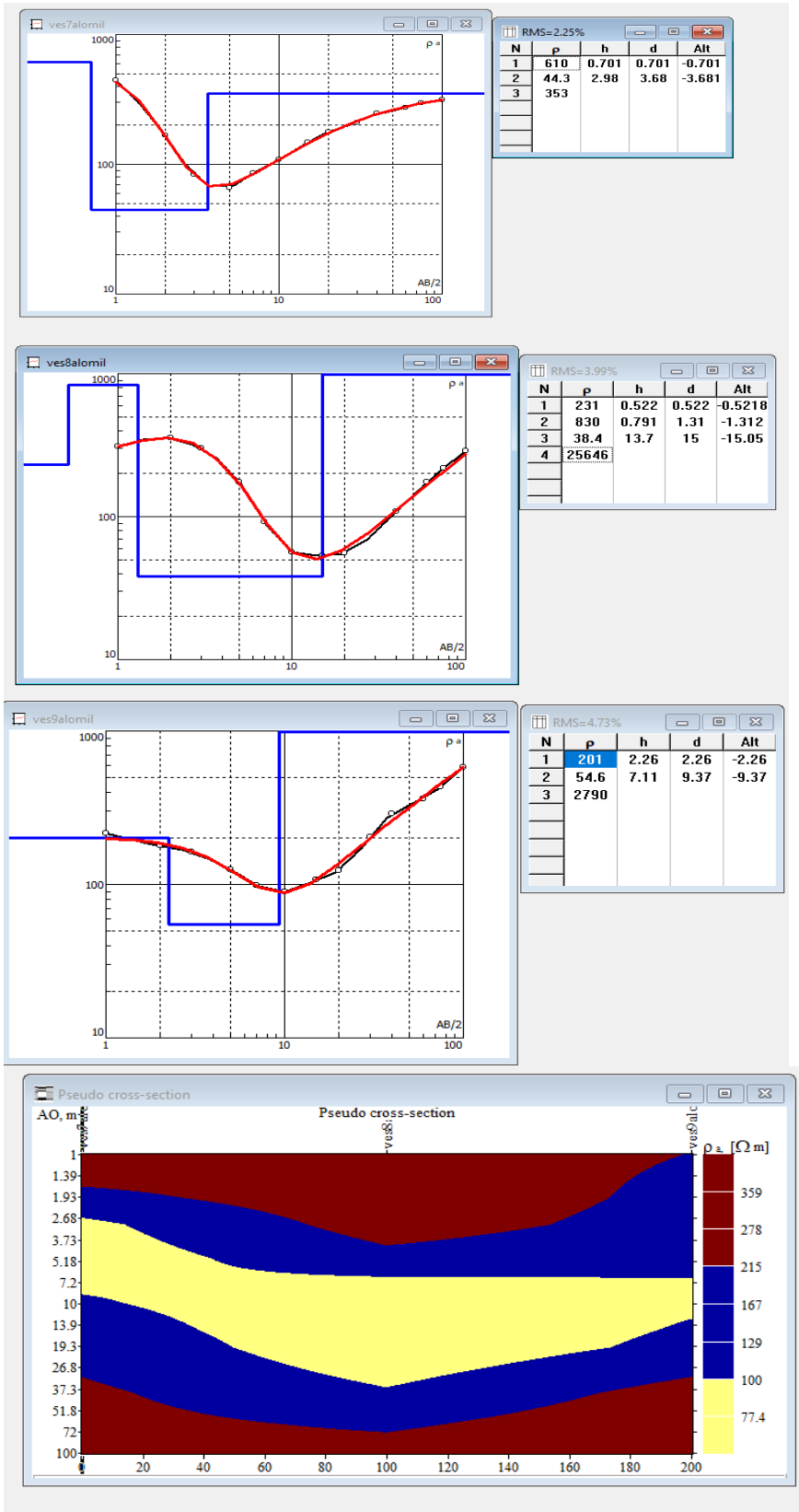


RMS=0.969%

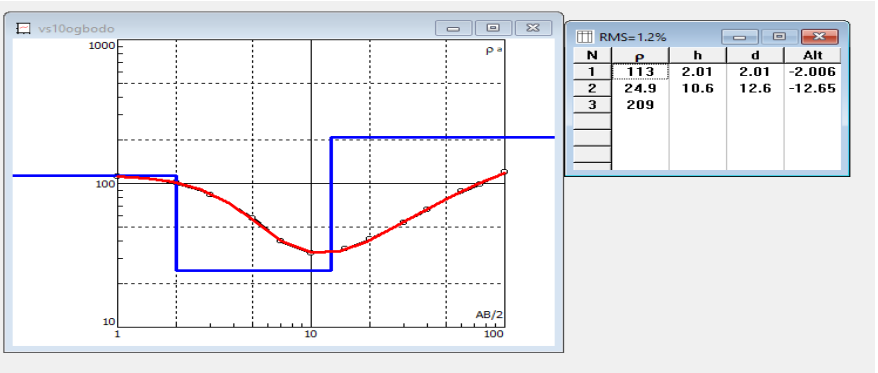
N	ρ	h	d	Alt
1	116	2.01	2.01	-2.01
2	21.9	4.45	6.46	-6.461
3	148			



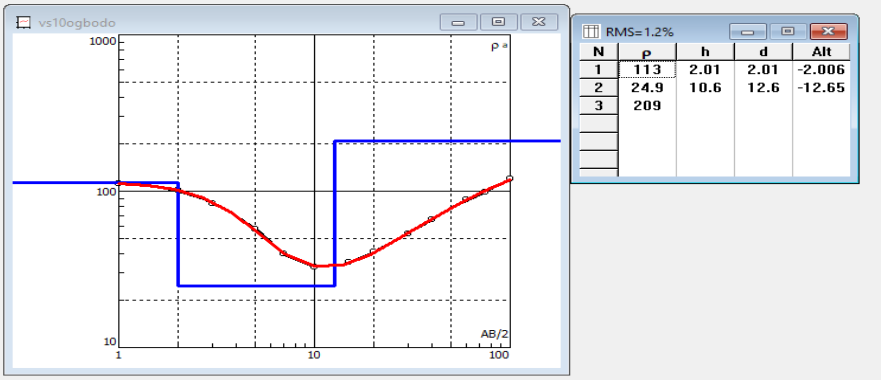
ALOMILAYA


ves7alomil
ρ a
1000
100
10
1
10
100
AB/2
RMS=2.25%
N ρ h d Alt
1 610 0.701 0.701 -0.701
2 44.3 2.98 3.68 -3.681
3 353
ves8alomil
ρ a
1000
100
10
1
10
100
AB/2
RMS=3.99%
N ρ h d Alt
1 231 0.522 0.522 -0.5218
2 830 0.791 1.31 -1.312
3 38.4 13.7 15 -15.05
4 25646
ves9alomil
ρ a
1000
100
10
1
10
100
AB/2
RMS=4.73%
N ρ h d Alt
1 201 2.26 2.26 -2.26
2 54.6 7.11 9.37 -9.37
3 2790
Pseudo cross-section
AO, m
Pseudo cross-section
ρ a [Ω m]
359
278
215
167
129
100
77.4
1
1.39
1.93
2.68
3.73
5.18
7.2
10
13.9
19.3
26.8
37.3
51.8
72
100
20
40
60
80
100
120
140
160
180
200

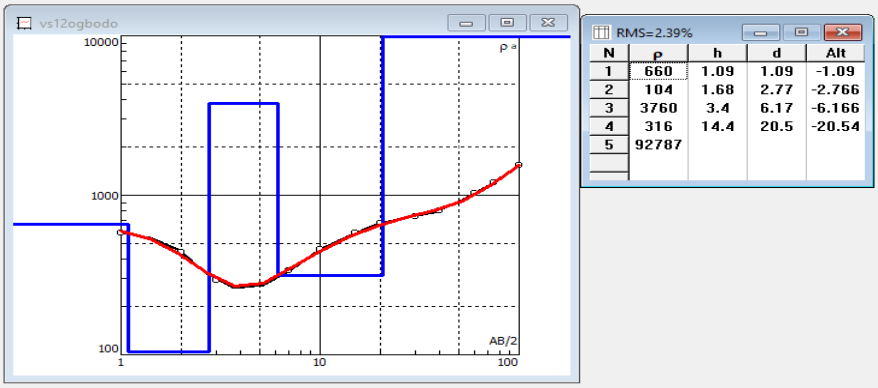
OGBONDOROKO



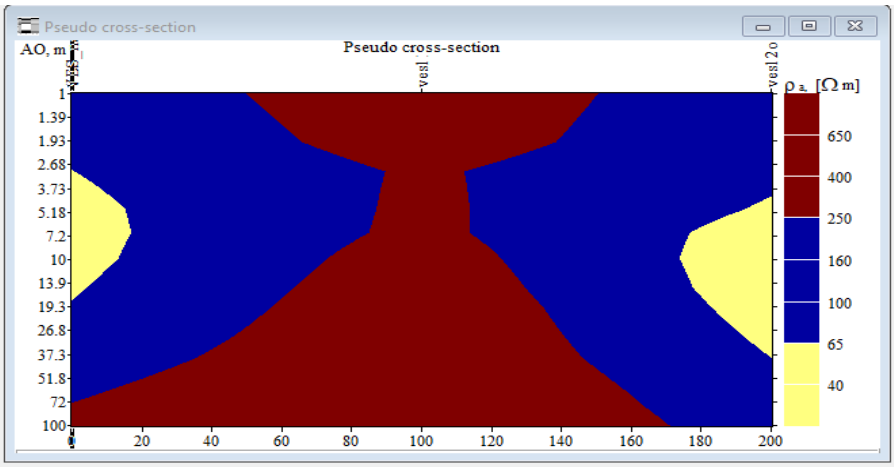
N	ρ	h	d	Alt
1	113	2.01	2.01	-2.006
2	24.9	10.6	12.6	-12.65
3	209			



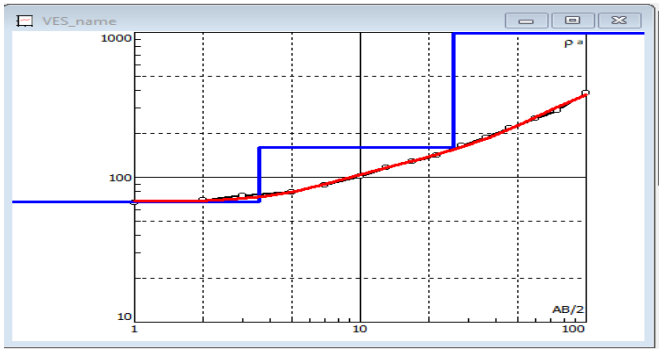
N	ρ	h	d	Alt
1	113	2.01	2.01	-2.006
2	24.9	10.6	12.6	-12.65
3	209			



N	ρ	h	d	Alt
1	660	1.09	1.09	-1.09
2	104	1.68	2.77	-2.766
3	3760	3.4	6.17	-6.166
4	316	14.4	20.5	-20.54
5	92787			

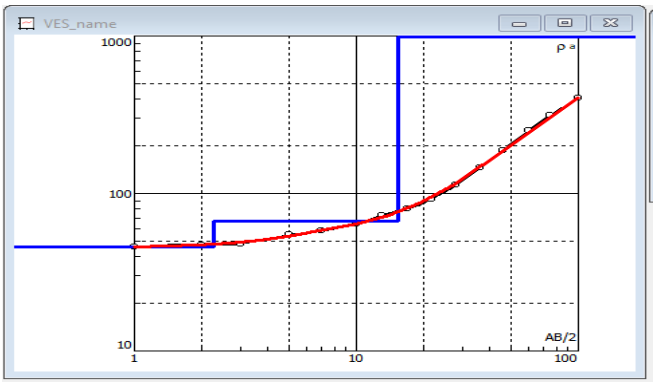


GBAGEDE



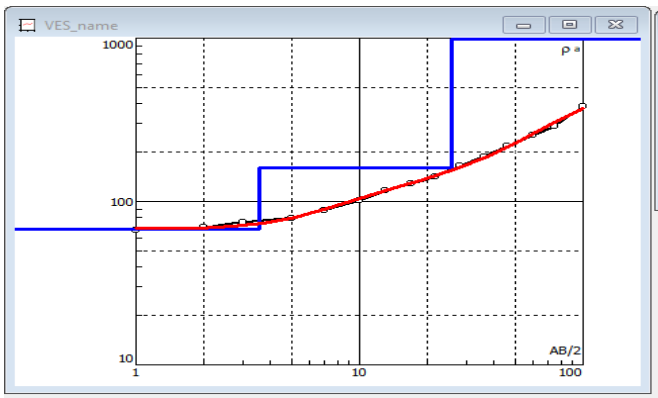
RMS=2.5%

N	ρ	h	d	Alt
1	68	3.57	3.57	-3.57
2	160	22.1	25.7	-25.67
3	1059			



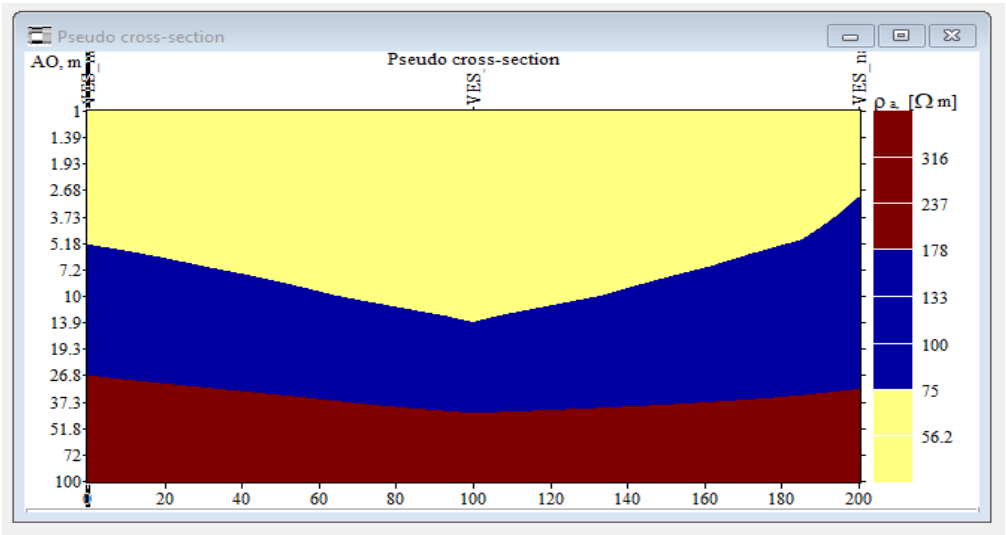
RMS=1.86%

N	ρ	h	d	Alt
1	45.8	2.27	2.27	-2.273
2	67	13.1	15.4	-15.36
3	57187			

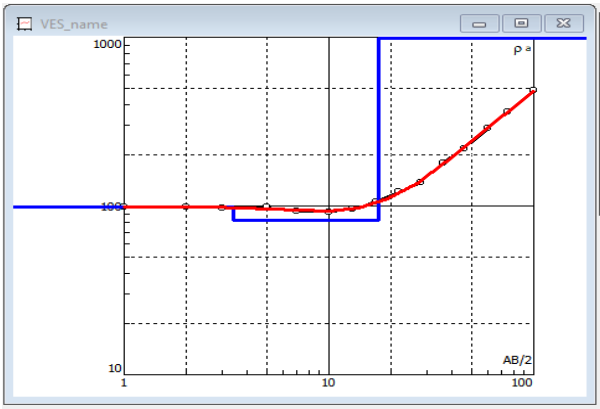


RMS=2.5%

N	ρ	h	d	Alt
1	68	3.57	3.57	-3.57
2	160	22.1	25.7	-25.67
3	1059			

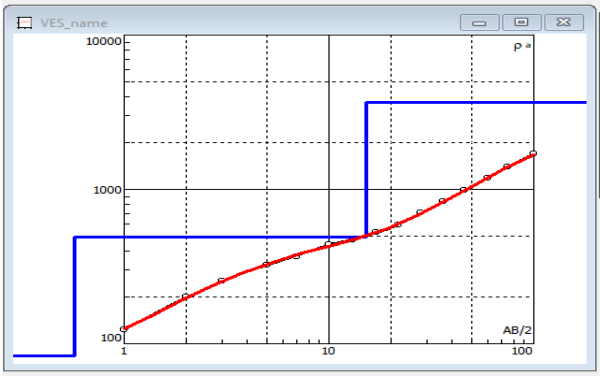


OSIN



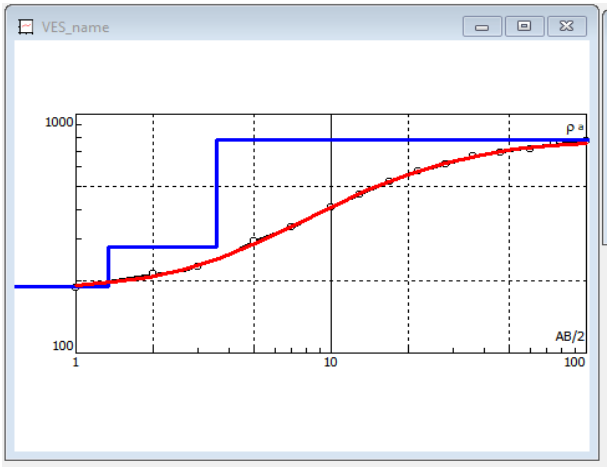
RMS=1.38%

N	ρ	h	d	Alt
1	99.1	3.41	3.41	-3.406
2	82.3	14.1	17.5	-17.5
3	39086			



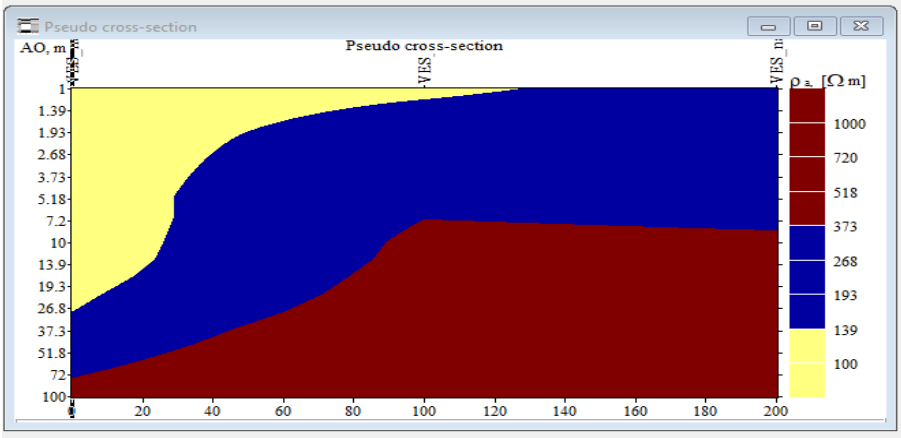
RMS=1.09%

N	ρ	h	d	Alt
1	83.3	0.571	0.571	-0.5706
2	494	14.7	15.3	-15.3
3	3666			

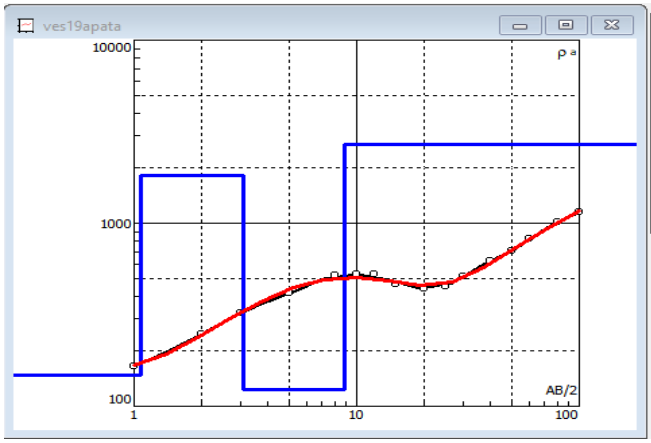


RMS=1.44%

N	ρ	h	d	Alt
1	189	1.34	1.34	-1.339
2	277	2.23	3.57	-3.571
3	784			

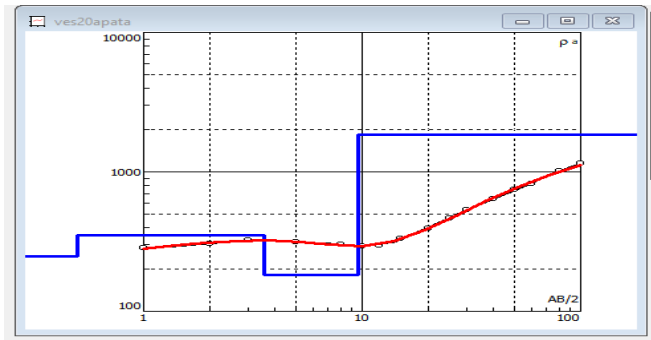


APATA



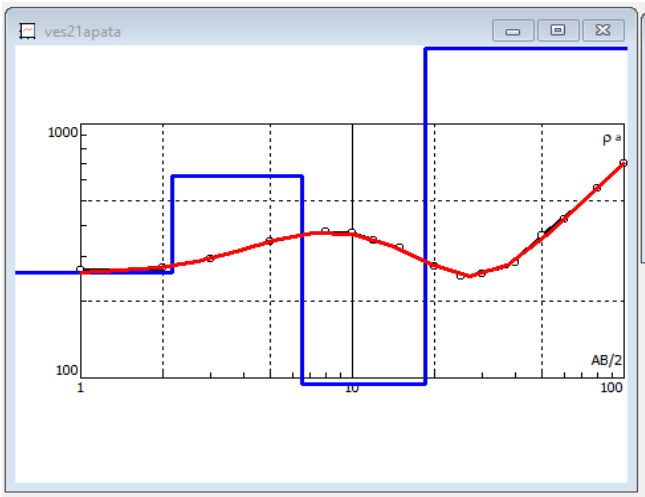
RMS=2.78%

N	ρ	h	d	Alt
1	147	1.07	1.07	-1.07
2	1810	2.03	3.1	-3.1
3	123	5.67	8.77	-8.77
4	2696			



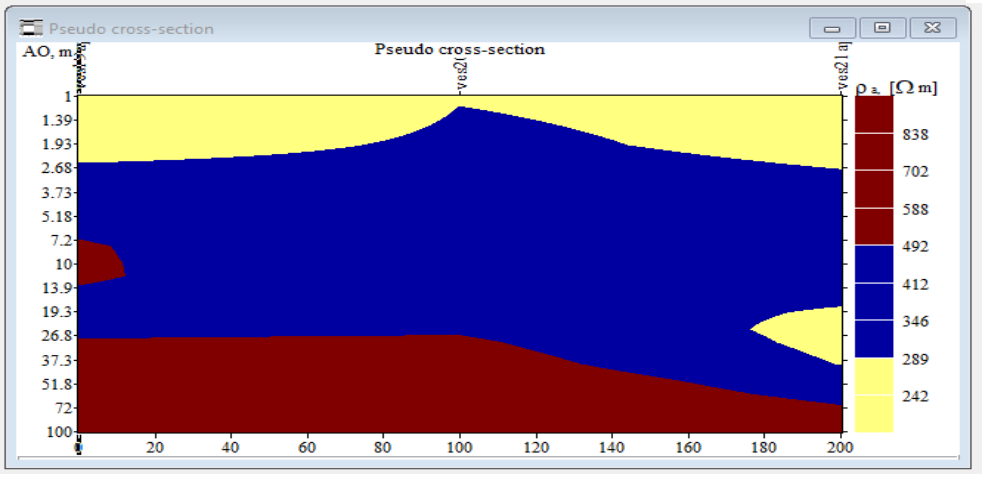
RMS=1.33%

N	ρ	h	d	Alt
1	248	0.5	0.5	-0.5
2	352	3.08	3.58	-3.579
3	182	5.96	9.54	-9.541
4	1860			

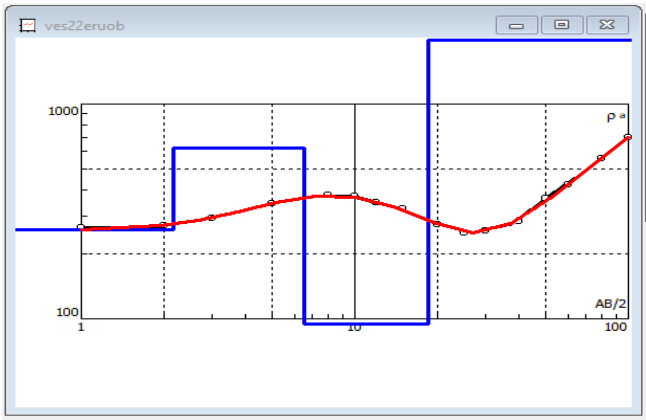


RMS=1.08%

N	ρ	h	d	Alt
1	259	2.18	2.18	-2.175
2	625	4.38	6.56	-6.557
3	94.1	11.9	18.5	-18.49
4	107151			

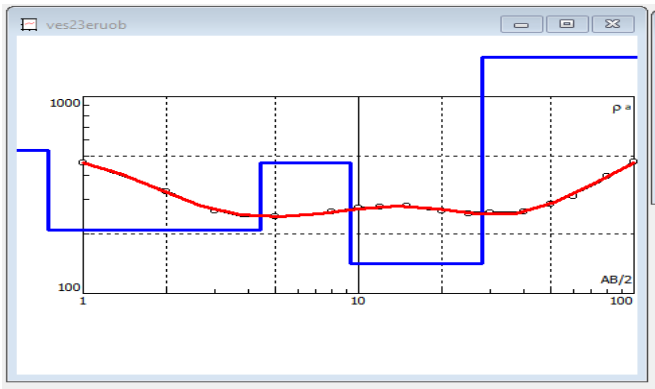


ERUOBA



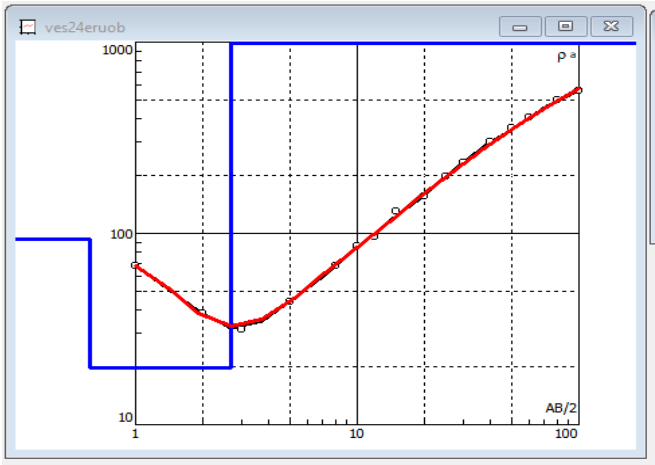
RMS=1.08%

N	ρ	h	d	Alt
1	259	2.17	2.17	-2.175
2	625	4.38	6.56	-6.557
3	94.1	11.9	18.5	-18.49
4	107151			



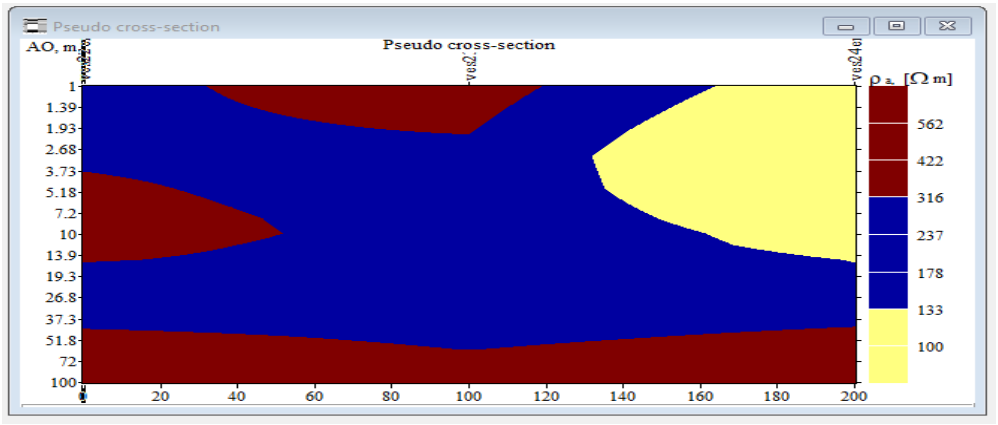
RMS=0.569%

N	ρ	h	d	Alt
1	531	0.751	0.751	-0.7505
2	210	3.68	4.43	-4.429
3	463	4.91	9.34	-9.339
4	141	18.9	28.2	-28.21
5	1592			

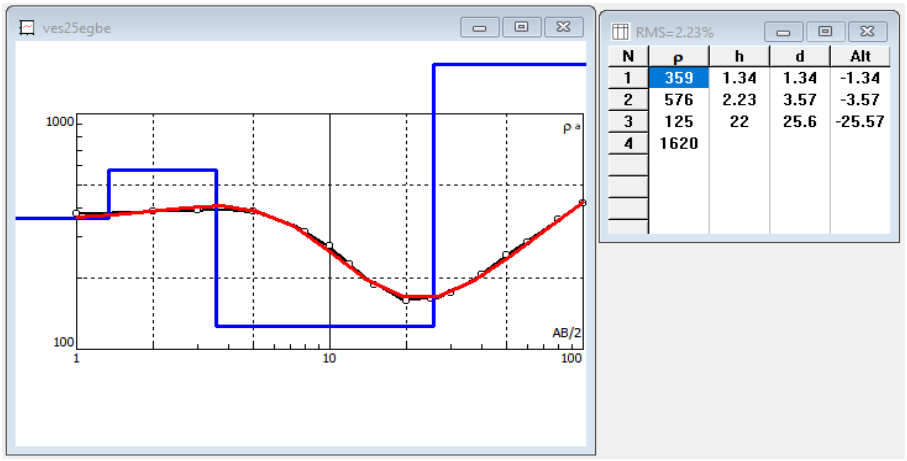


RMS=2.04%

N	ρ	h	d	Alt
1	93.4	0.621	0.621	-0.621
2	19.8	2.07	2.69	-2.691
3	1383			

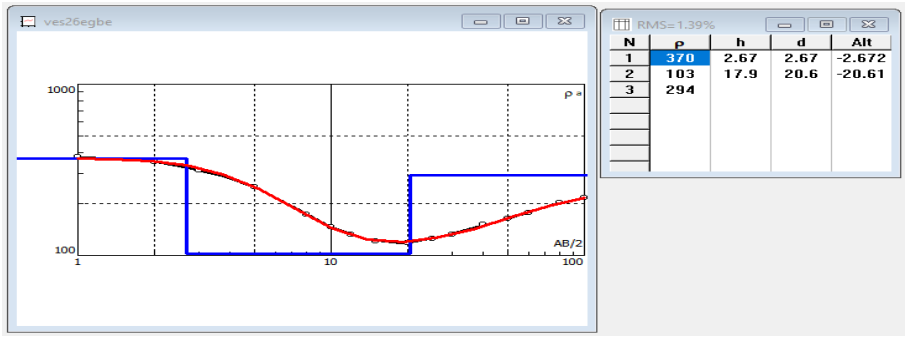


EGBEJILA



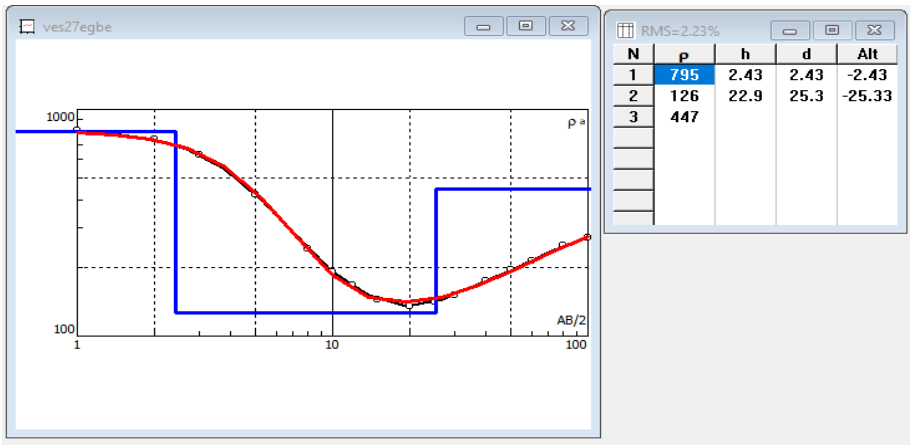
RMS=2.23%

N	ρ	h	d	Alt
1	359	1.34	1.34	-1.34
2	576	2.23	3.57	-3.57
3	125	22	25.6	-25.57
4	1620			



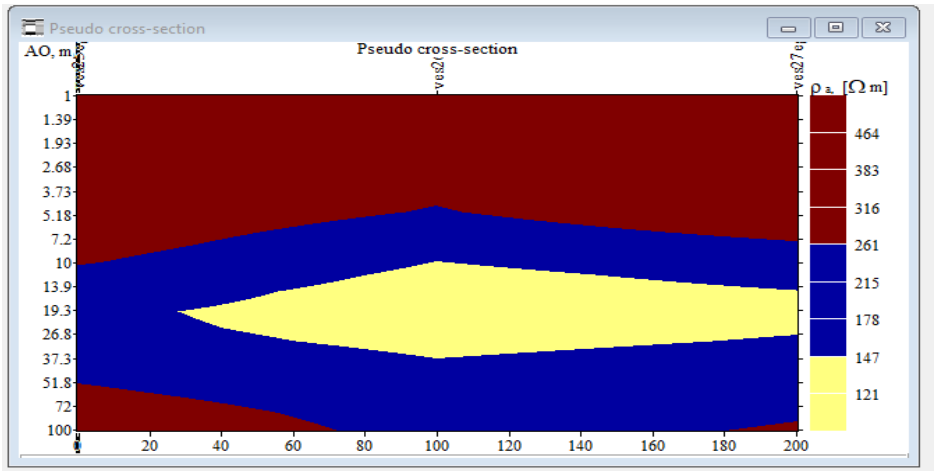
RMS=1.39%

N	ρ	h	d	Alt
1	370	2.67	2.67	-2.672
2	103	17.9	20.6	-20.61
3	294			

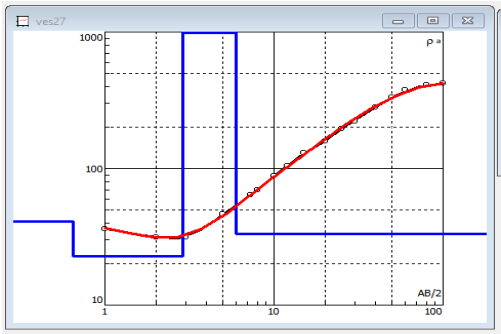


RMS=2.23%

N	ρ	h	d	Alt
1	795	2.43	2.43	-2.43
2	126	22.9	25.3	-25.33
3	447			

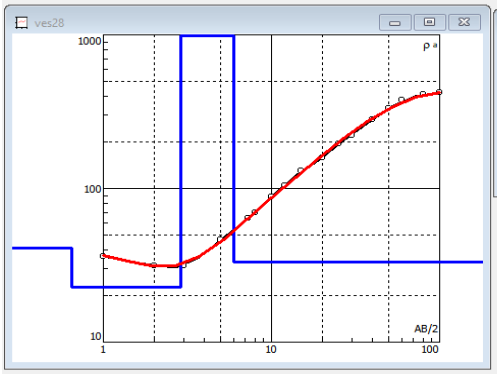


ONIRIN



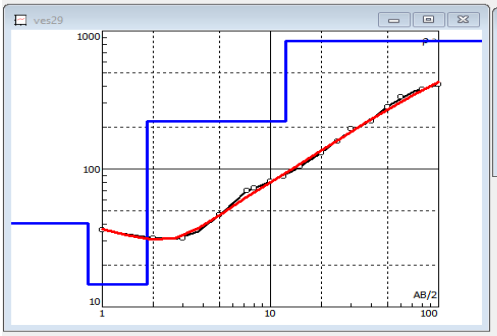
RMS=1.93%

N	ρ	h	d	Alt
1	41.1	0.648	0.648	-0.6481
2	22.9	2.23	2.88	-2.877
3	15327	3.11	5.99	-5.992
4	33.3			



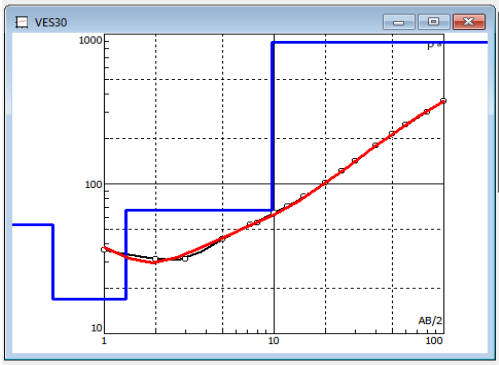
RMS=1.93%

N	ρ	h	d	Alt
1	41.1	0.648	0.648	-0.6481
2	22.9	2.23	2.88	-2.877
3	15327	3.12	5.99	-5.992
4	33.3			



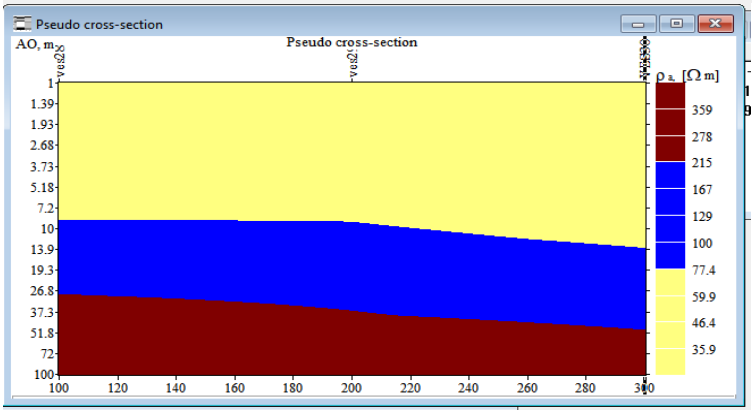
RMS=4.08%

N	ρ	h	d	Alt
1	40.5	0.822	0.822	-0.822
2	14.5	1.02	1.84	-1.842
3	223	10.5	12.3	-12.34
4	850			

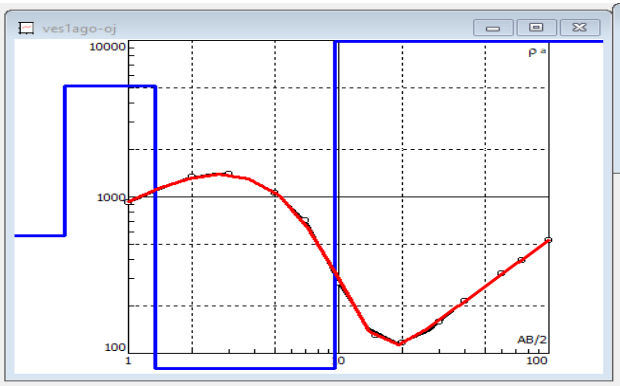


RMS=3.3%

N	ρ	h	d	Alt
1	53.4	0.5	0.5	-0.5
2	17	0.836	1.34	-1.336
3	66.9	8.39	9.73	-9.728
4	881			

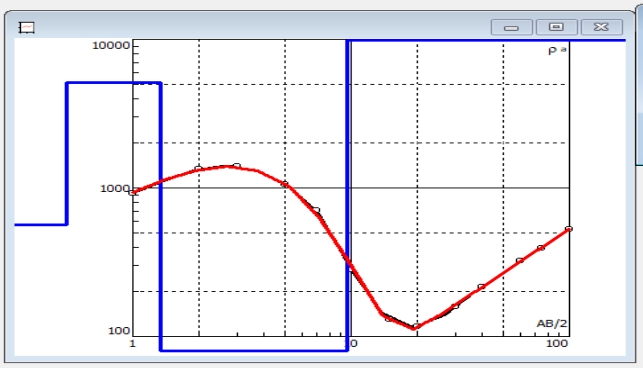


AGO OJA



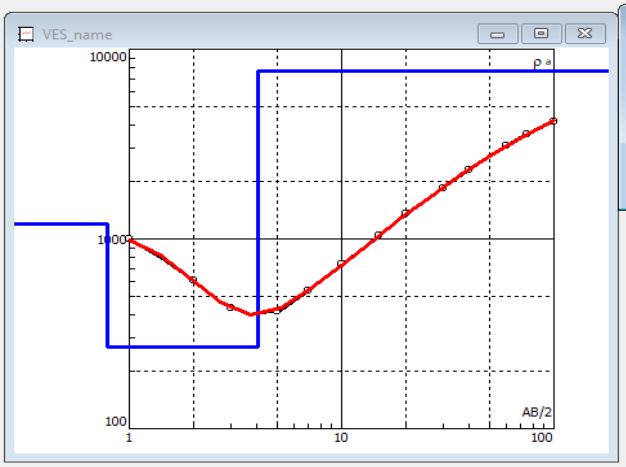
RMS=2.69%

N	ρ	h	d	Alt
1	565	0.5	0.5	-0.5
2	5108	0.836	1.34	-1.336
3	45	8.22	9.56	-9.556
4	18559			



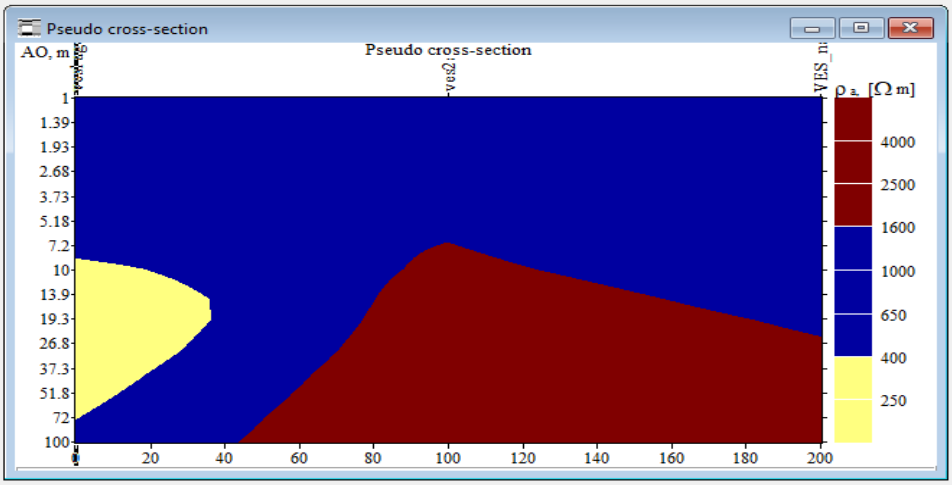
RMS=2.69%

N	ρ	h	d	Alt
1	565	0.5	0.5	-0.5
2	5109	0.836	1.34	-1.336
3	45	8.22	9.56	-9.556
4	18559			

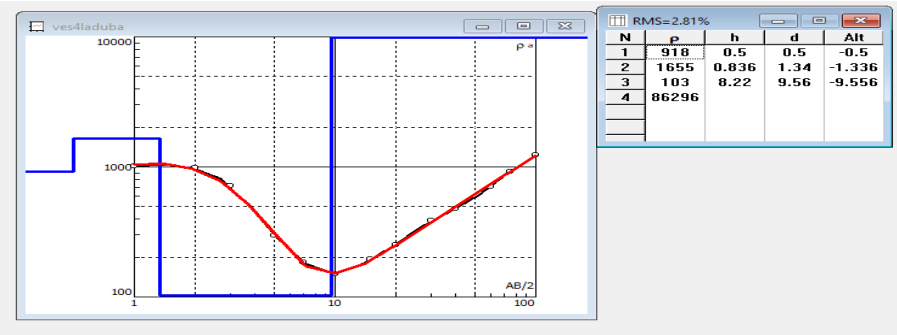


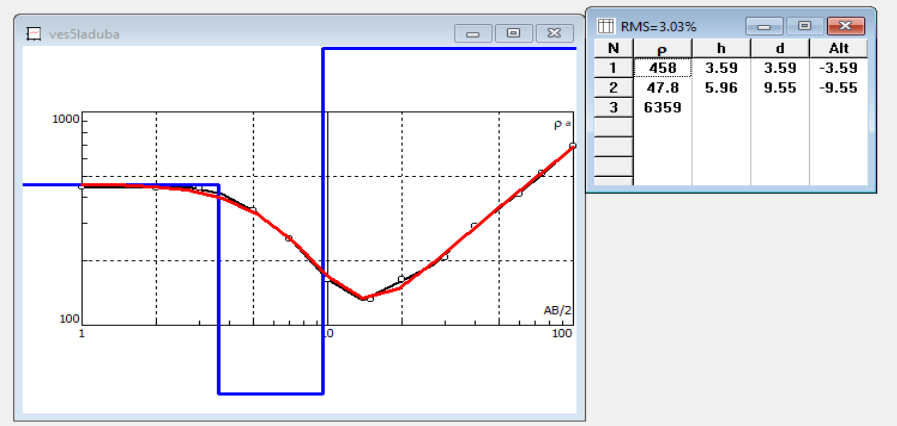
RMS=1.14%

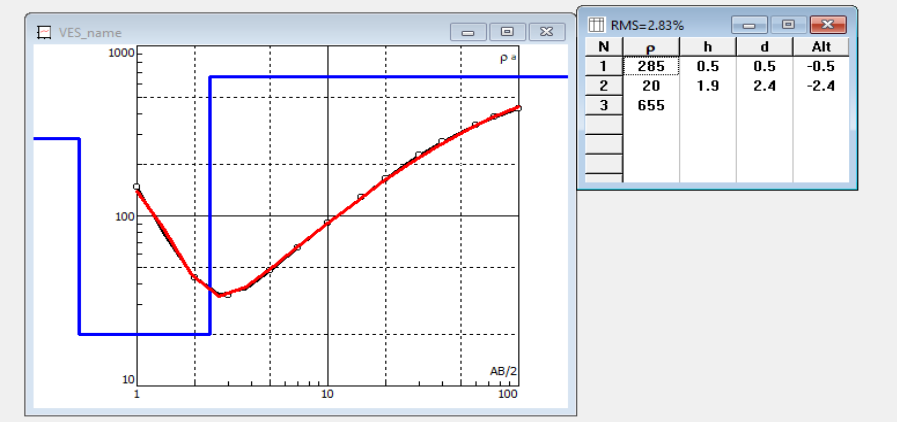
N	ρ	h	d	Alt
1	1195	0.793	0.793	-0.7926
2	271	3.24	4.04	-4.037
3	7646			

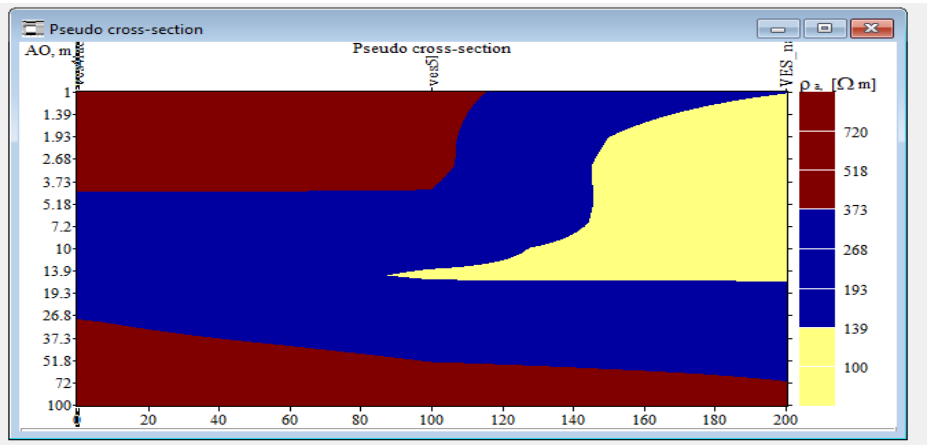


LADUBA

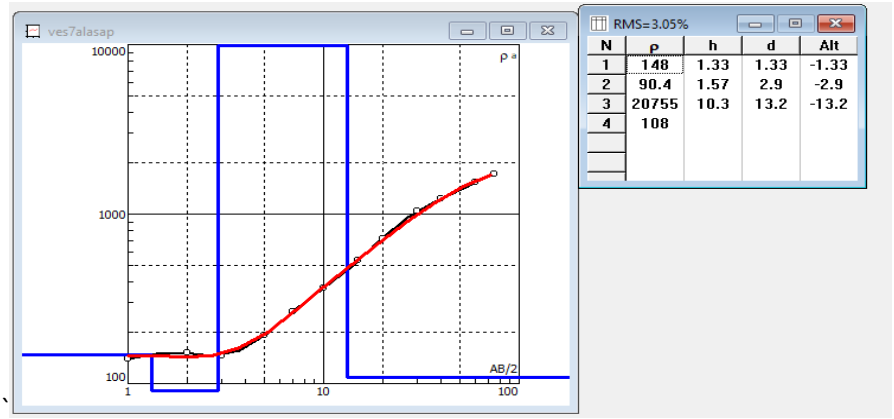

ves4laduba
10000
1000
100
1
10
100
ρ a
AB/2
RMS=2.81%
N ρ h d Alt
1 918 0.5 0.5 -0.5
2 1655 0.836 1.34 -1.336
3 103 8.22 9.56 -9.556
4 86296


ves5laduba
1000
100
1
10
100
ρ a
AB/2
RMS=3.03%
N ρ h d Alt
1 458 3.59 3.59 -3.59
2 47.8 5.96 9.55 -9.55
3 6359

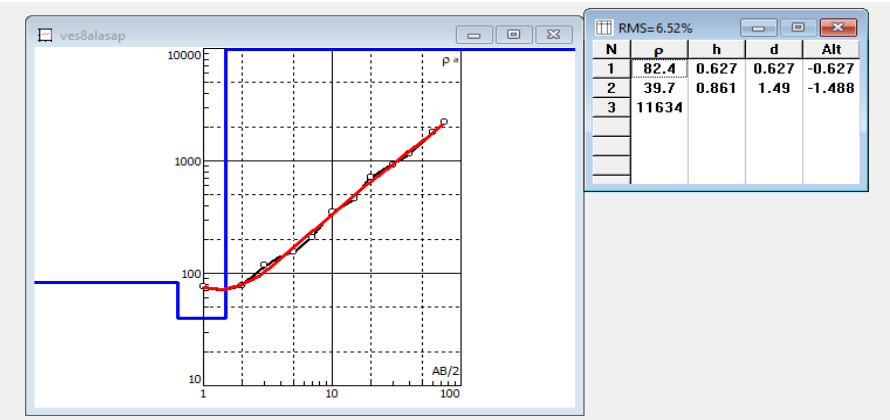

VES_name
1000
100
10
1
10
100
ρ a
AB/2
RMS=2.83%
N ρ h d Alt
1 285 0.5 0.5 -0.5
2 20 1.9 2.4 -2.4
3 655


Pseudo cross-section
Pseudo cross-section
AO, m
1
1.39
1.93
2.68
3.73
5.18
7.2
10
13.9
19.3
26.8
37.3
51.8
72
100
0
20
40
60
80
100
120
140
160
180
200
ρ a, [Ω m]
720
518
373
268
193
139
100

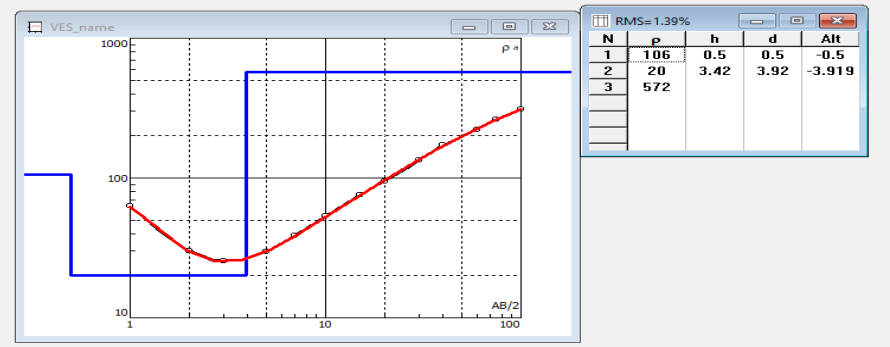
ALASEPE



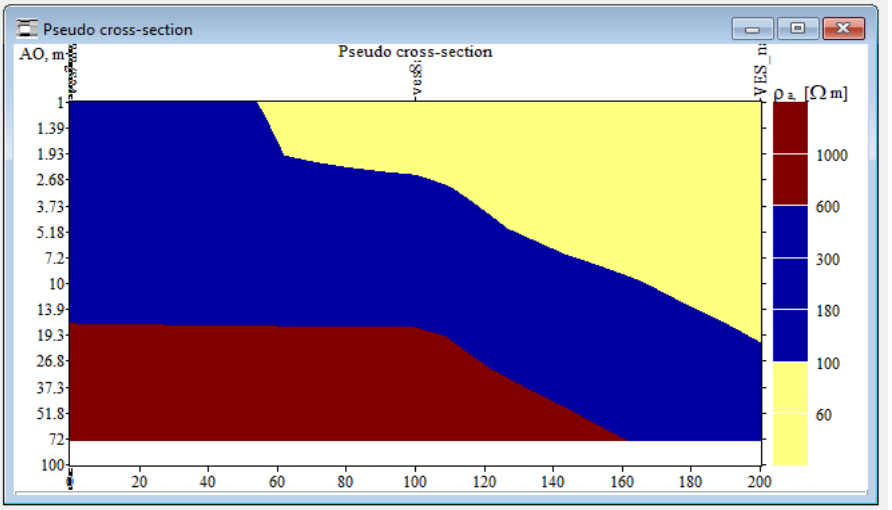
N	ρ	h	d	Alt
1	148	1.33	1.33	-1.33
2	90.4	1.57	2.9	-2.9
3	20755	10.3	13.2	-13.2
4	108			



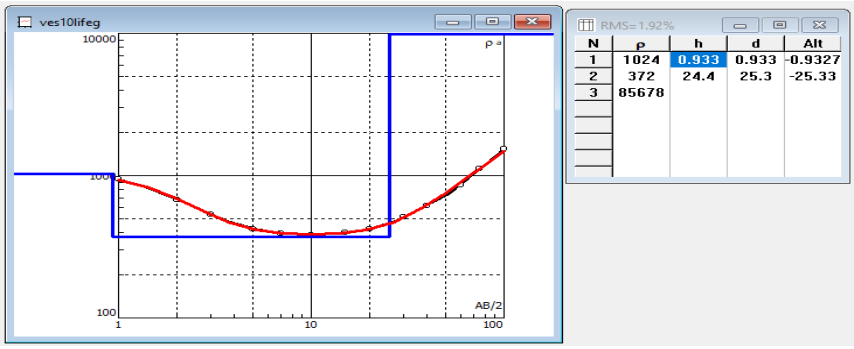
N	ρ	h	d	Alt
1	82.4	0.627	0.627	-0.627
2	39.7	0.861	1.49	-1.488
3	11634			



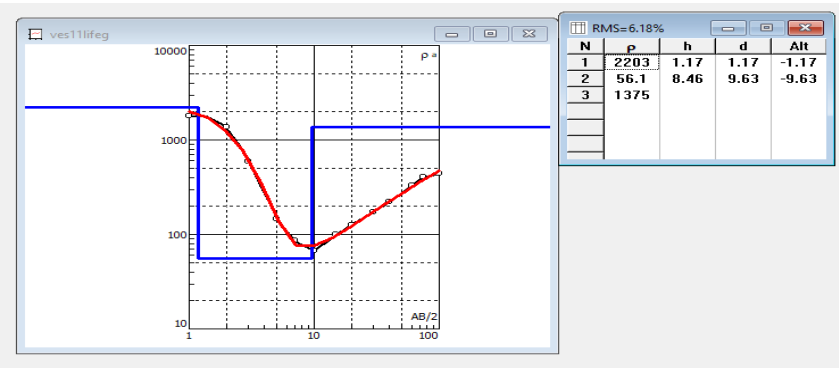
N	ρ	h	d	Alt
1	106	0.5	0.5	-0.5
2	20	3.42	3.92	-3.919
3	572			



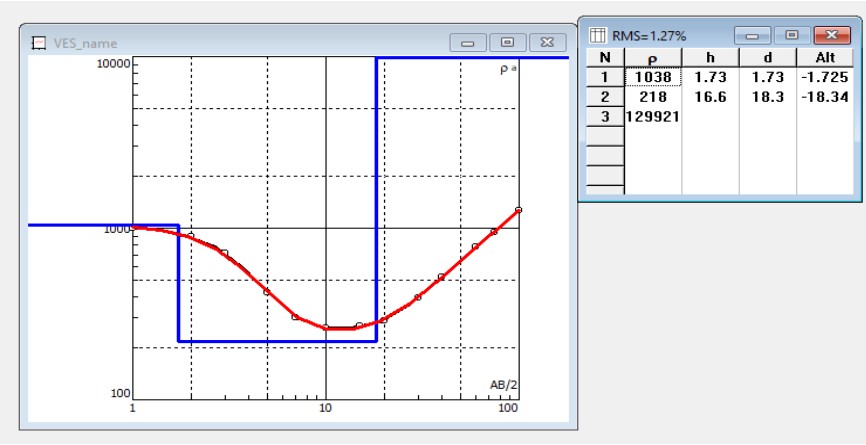
LIFE GATE



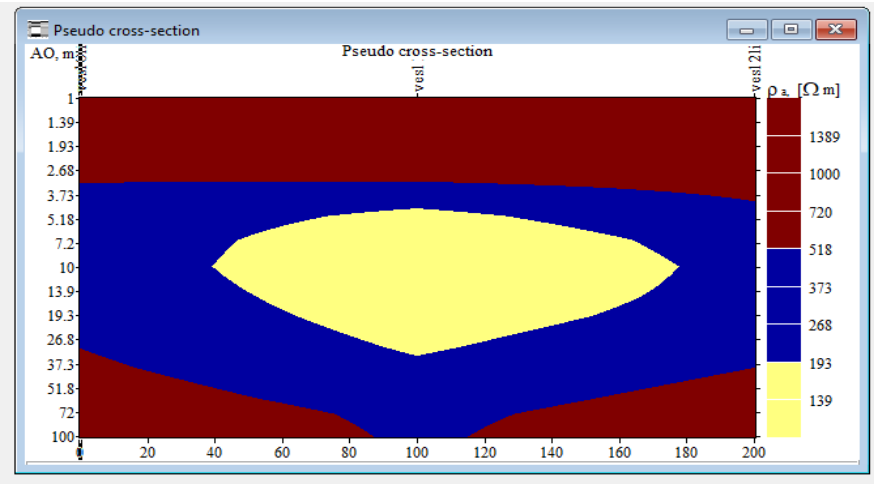
N	ρ	h	d	Alt
1	1024	0.933	0.933	-0.9327
2	372	24.4	25.3	-25.33
3	85678			



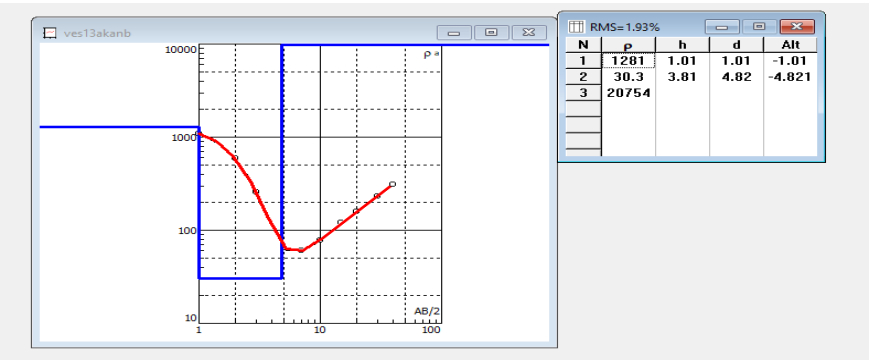
N	ρ	h	d	Alt
1	2203	1.17	1.17	-1.17
2	56.1	8.46	9.63	-9.63
3	1375			



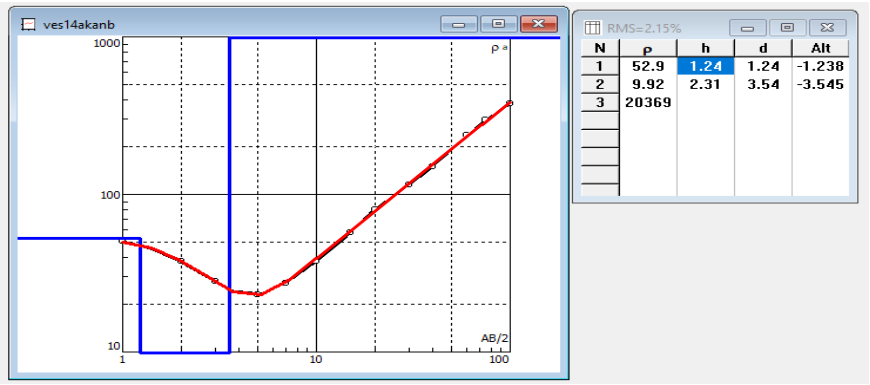
N	ρ	h	d	Alt
1	1038	1.73	1.73	-1.725
2	218	16.6	18.3	-18.34
3	129921			



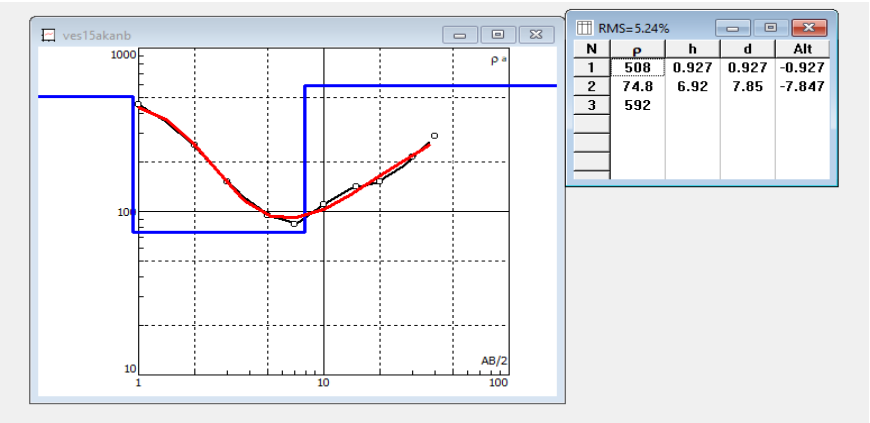
AKANBI ADE



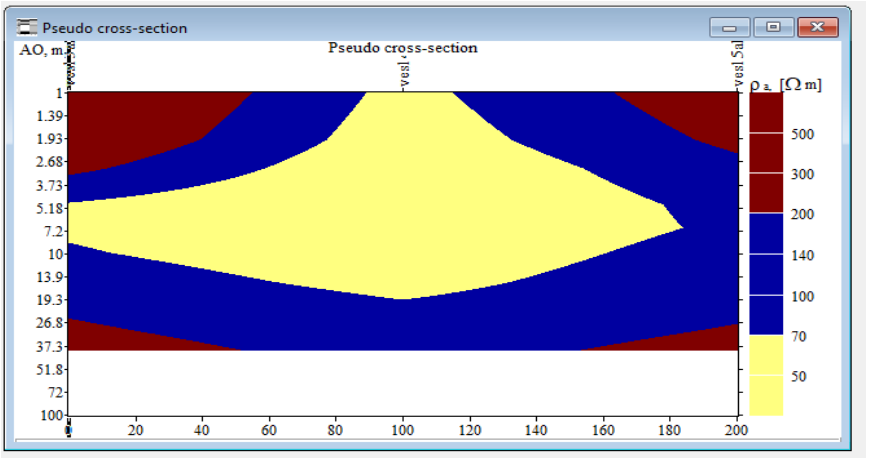
N	ρ	h	d	Alt
1	1281	1.01	1.01	-1.01
2	30.3	3.81	4.82	-4.821
3	20754			



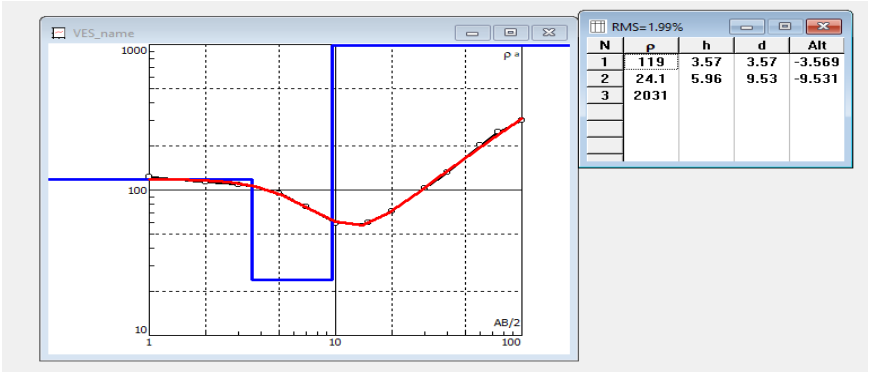
N	ρ	h	d	Alt
1	52.9	1.24	1.24	-1.238
2	9.92	2.31	3.54	-3.545
3	20369			



N	ρ	h	d	Alt
1	508	0.927	0.927	-0.927
2	74.8	6.92	7.85	-7.847
3	592			

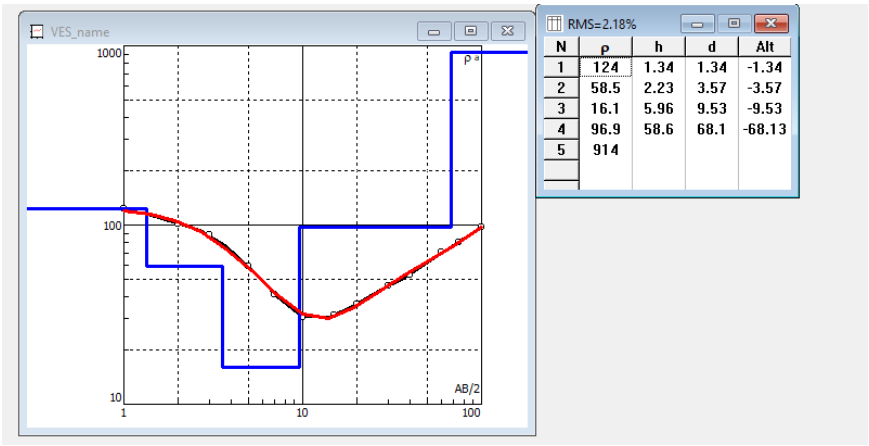


ALONG AFON



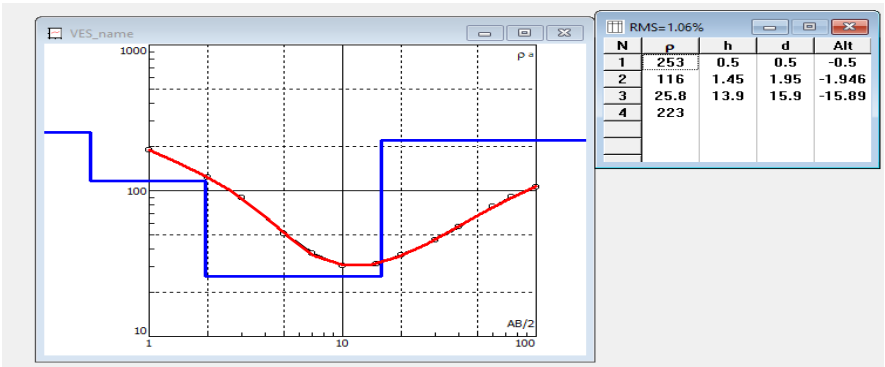
RMS=1.99%

N	ρ	h	d	Alt
1	119	3.57	3.57	-3.569
2	24.1	5.96	9.53	-9.531
3	2031			



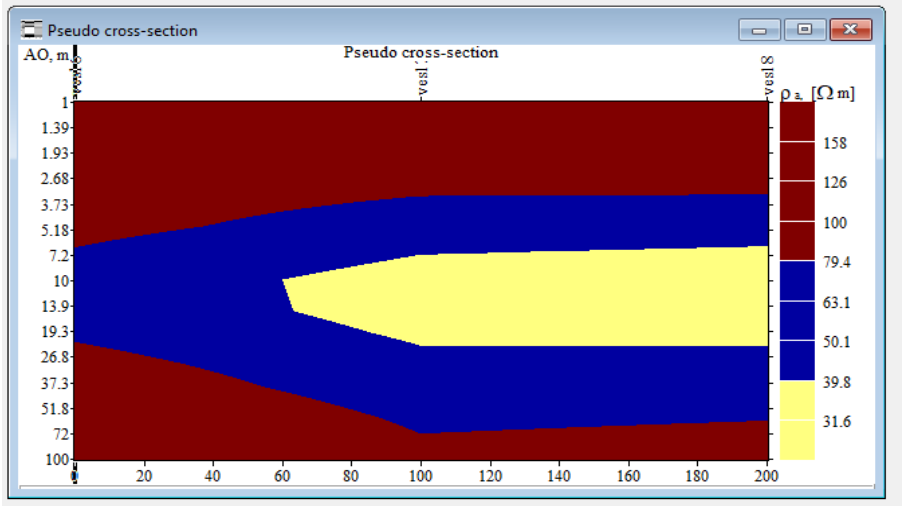
RMS=2.18%

N	ρ	h	d	Alt
1	124	1.34	1.34	-1.34
2	58.5	2.23	3.57	-3.57
3	16.1	5.96	9.53	-9.53
4	96.9	58.6	68.1	-68.13
5	914			

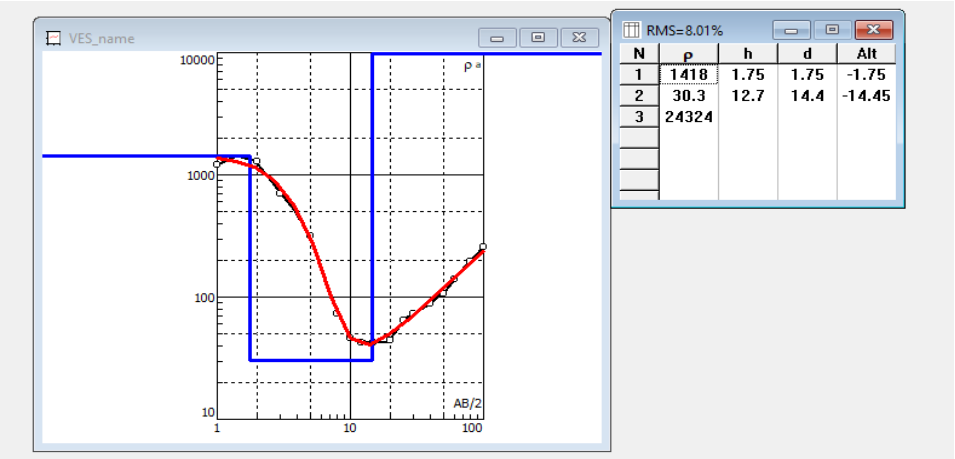


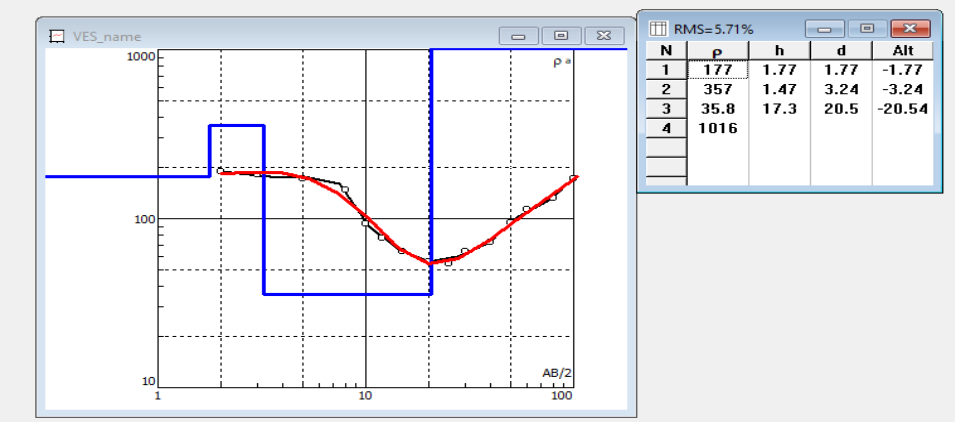
RMS=1.06%

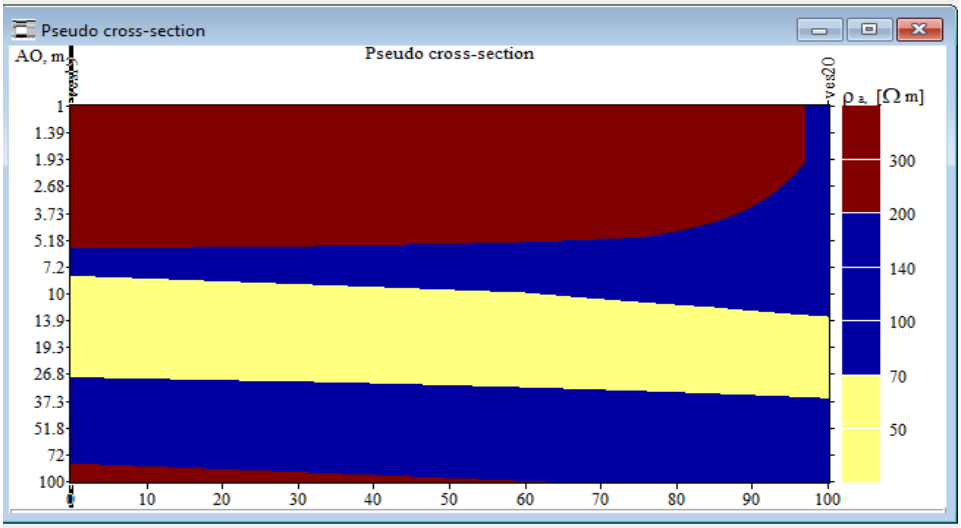
N	ρ	h	d	Alt
1	253	0.5	0.5	-0.5
2	116	1.45	1.95	-1.946
3	25.8	13.9	15.9	-15.89
4	223			



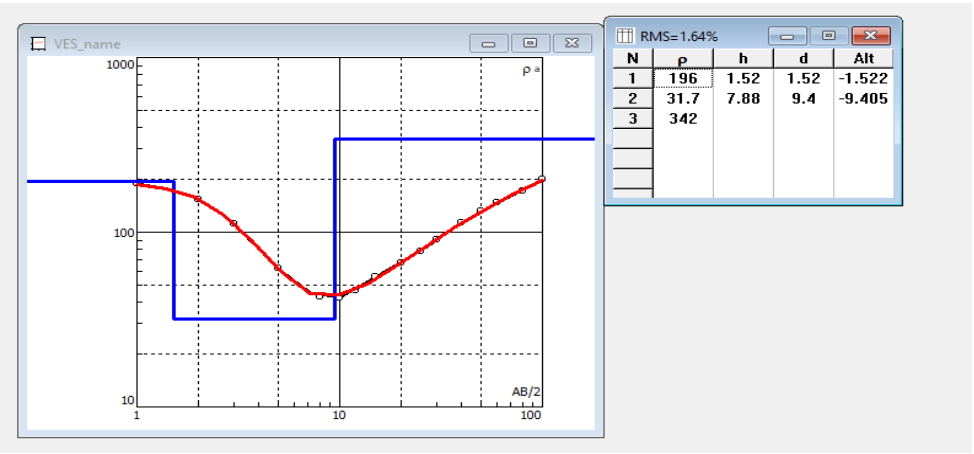
ELERU


VES_name
ρ a
10000
1000
100
10
1
10
100
AB/2
RMS=8.01%
N ρ h d Alt
1 1418 1.75 1.75 -1.75
2 30.3 12.7 14.4 -14.45
3 24324

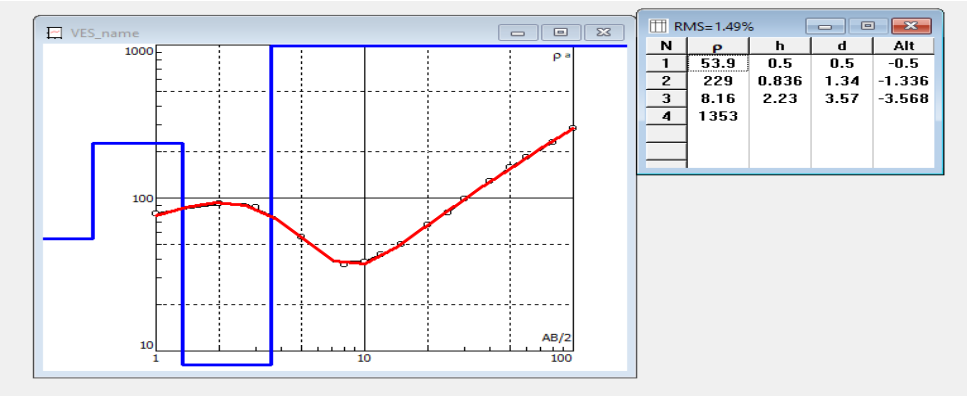

VES_name
ρ a
1000
100
10
1
10
100
AB/2
RMS=5.71%
N ρ h d Alt
1 177 1.77 1.77 -1.77
2 357 1.47 3.24 -3.24
3 35.8 17.3 20.5 -20.54
4 1016


Pseudo cross-section
Pseudo cross-section
AO, m
ρ a, [Ω m]
300
200
140
100
70
50
1
1.39
1.93
2.68
3.73
5.18
7.2
10
13.9
19.3
26.8
37.3
51.8
72
100
10
20
30
40
50
60
70
80
90
100

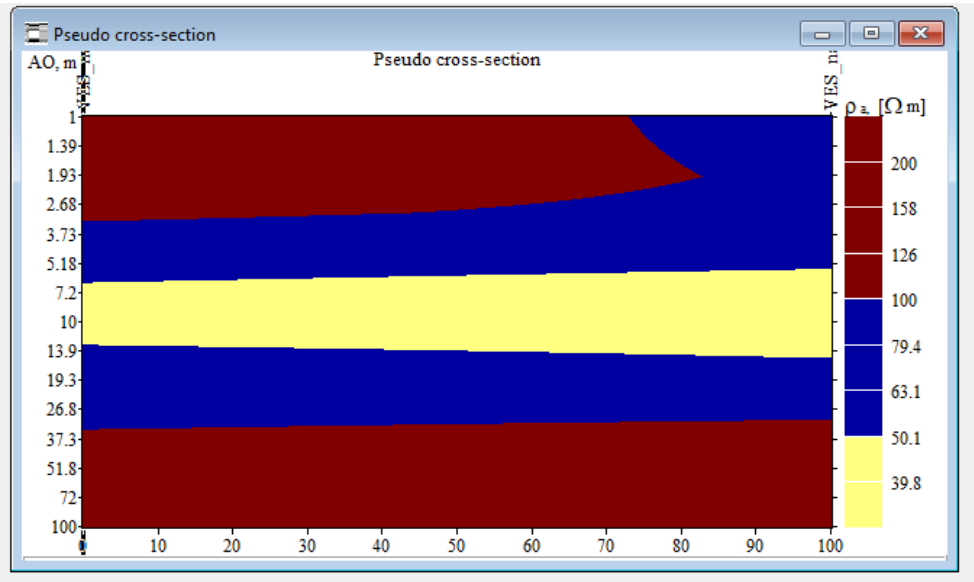
LARO



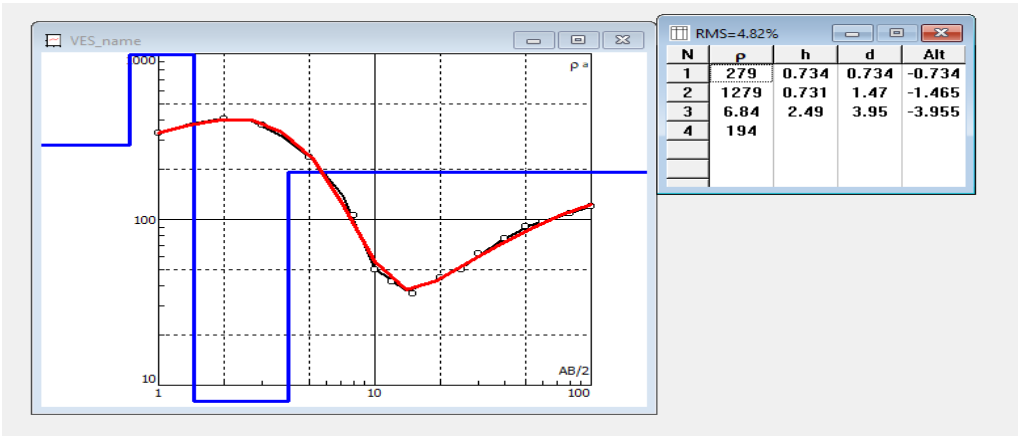
N	ρ	h	d	Alt
1	196	1.52	1.52	-1.522
2	31.7	7.88	9.4	-9.405
3	342			



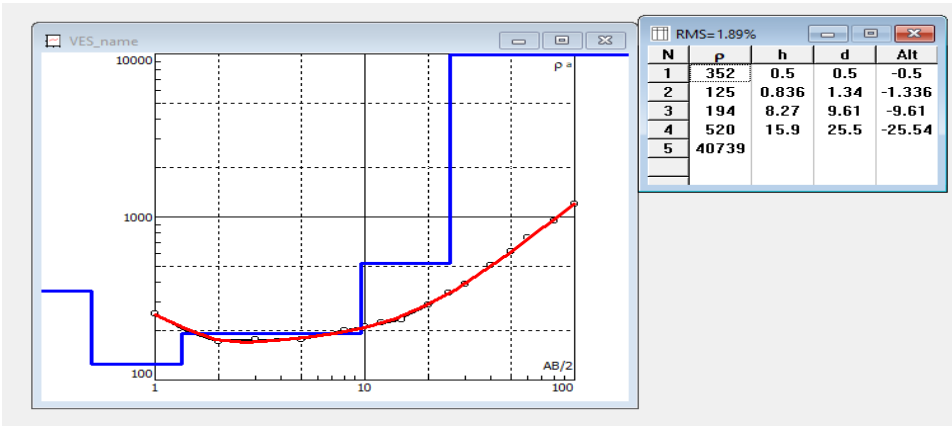
N	ρ	h	d	Alt
1	53.9	0.5	0.5	-0.5
2	229	0.836	1.34	-1.336
3	8.16	2.23	3.57	-3.568
4	1353			



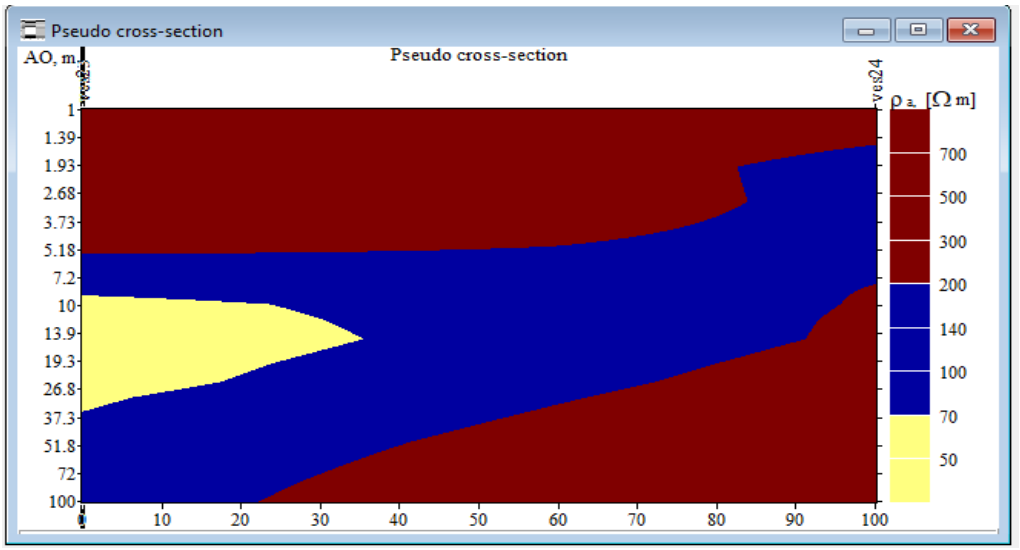
APATA



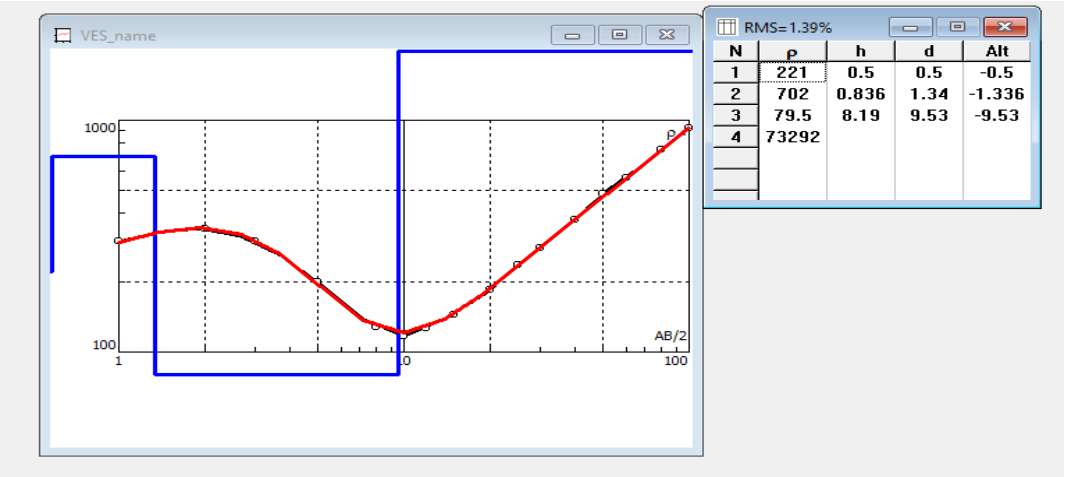
N	ρ	h	d	Alt
1	279	0.734	0.734	-0.734
2	1279	0.731	1.47	-1.465
3	6.84	2.49	3.95	-3.955
4	194			



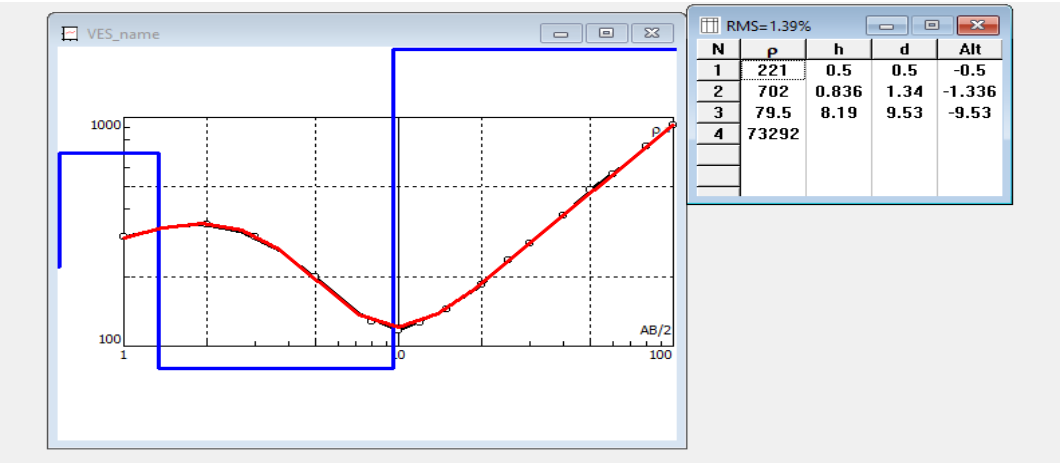
N	ρ	h	d	Alt
1	352	0.5	0.5	-0.5
2	125	0.836	1.34	-1.336
3	194	8.27	9.61	-9.61
4	520	15.9	25.5	-25.54
5	40739			



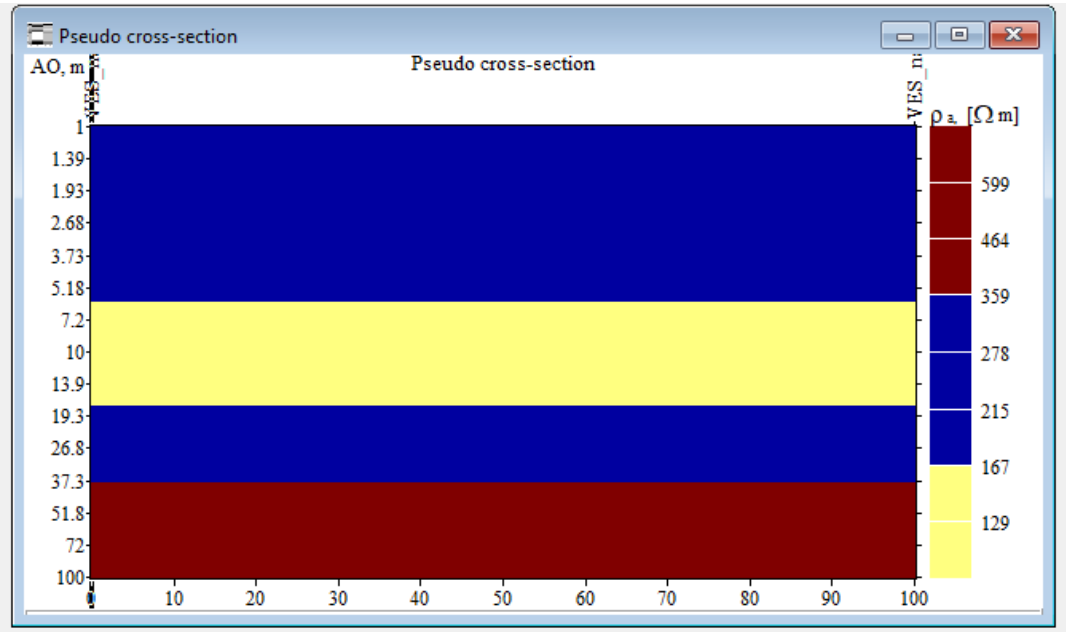
LAGBAPA



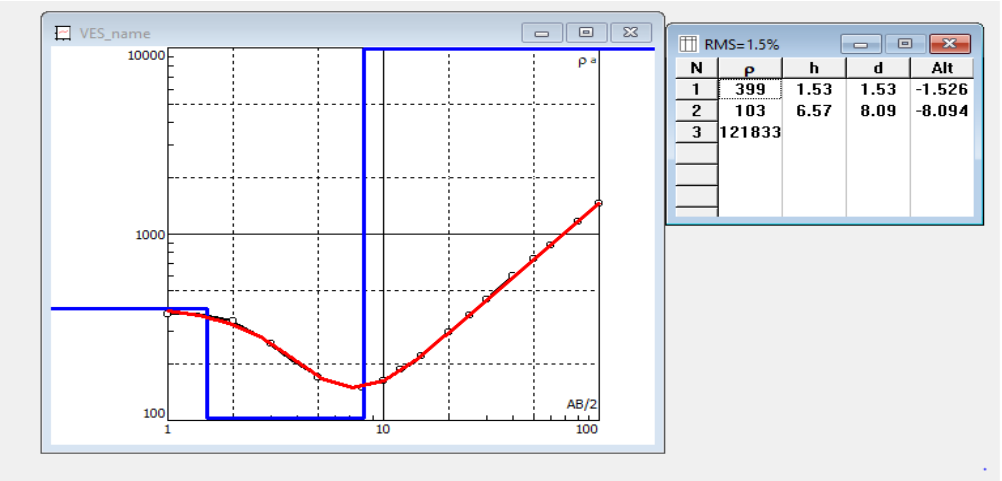
N	ρ	h	d	Alt
1	221	0.5	0.5	-0.5
2	702	0.836	1.34	-1.336
3	79.5	8.19	9.53	-9.53
4	73292			



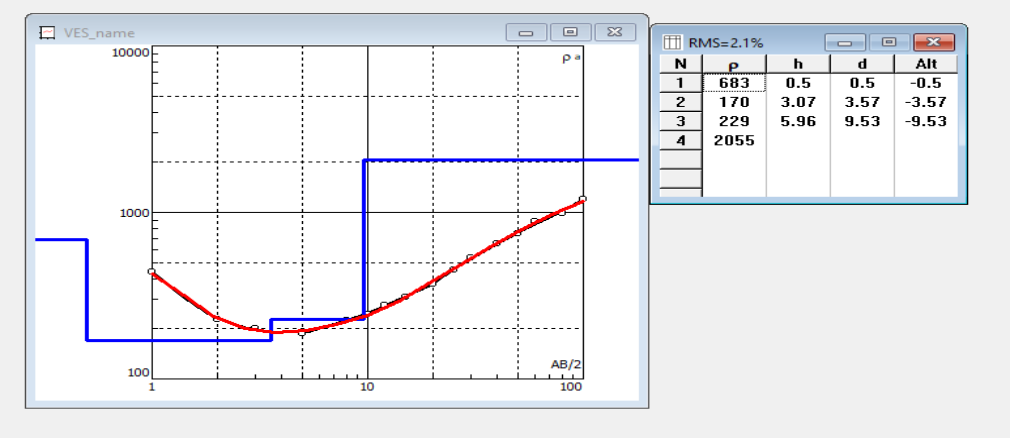
N	ρ	h	d	Alt
1	221	0.5	0.5	-0.5
2	702	0.836	1.34	-1.336
3	79.5	8.19	9.53	-9.53
4	73292			



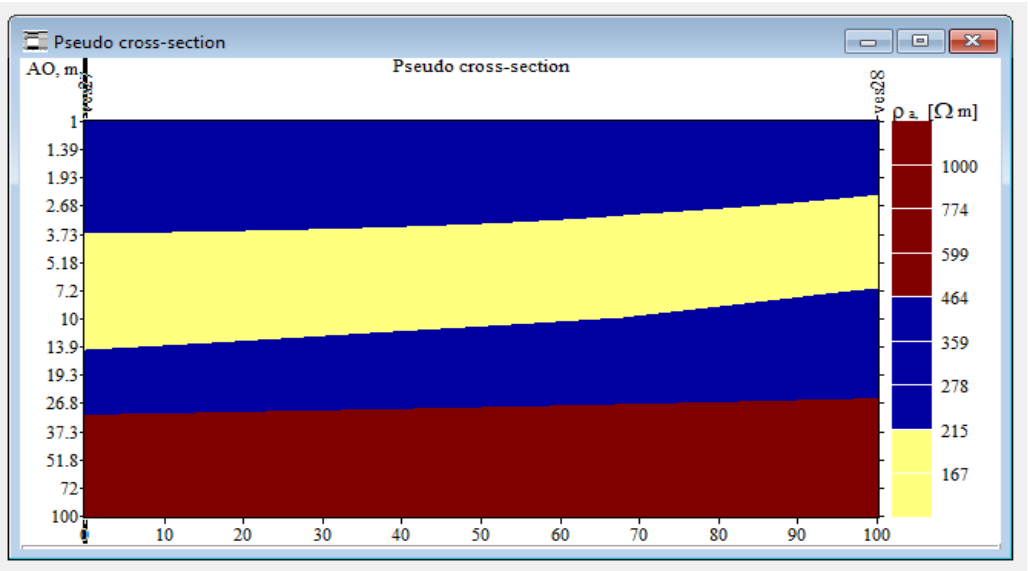
BUDO MOLUABI



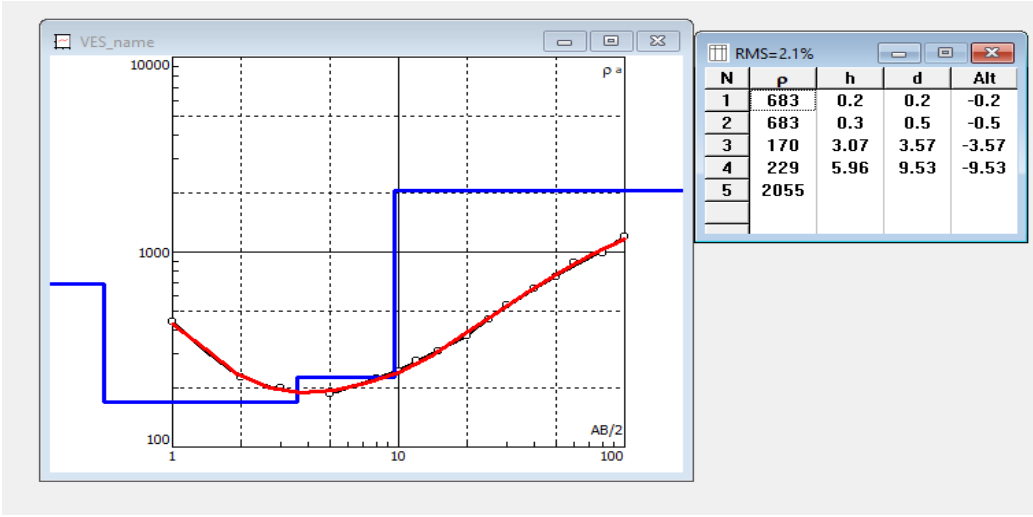
N	ρ	h	d	Alt
1	399	1.53	1.53	-1.526
2	103	6.57	8.09	-8.094
3	121833			



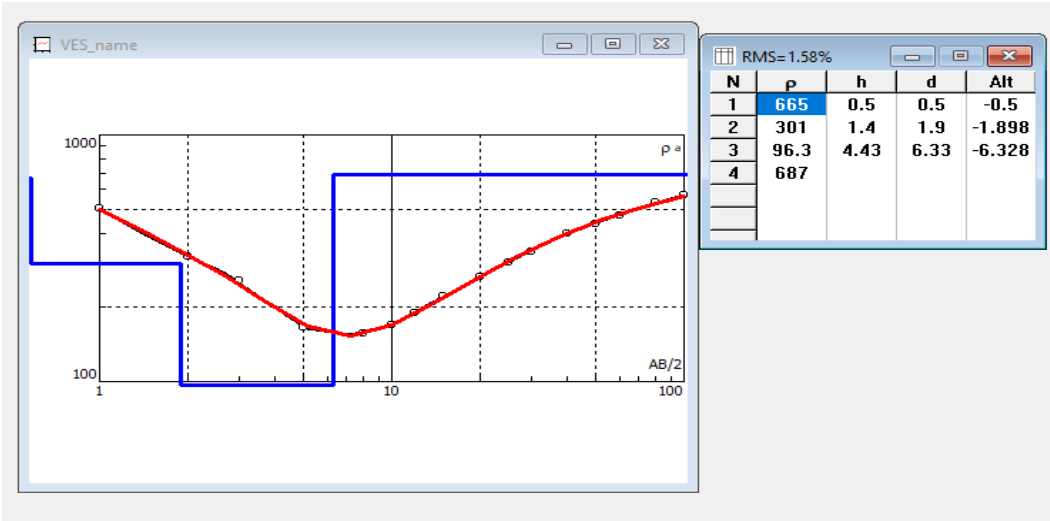
N	ρ	h	d	Alt
1	683	0.5	0.5	-0.5
2	170	3.07	3.57	-3.57
3	229	5.96	9.53	-9.53
4	2055			



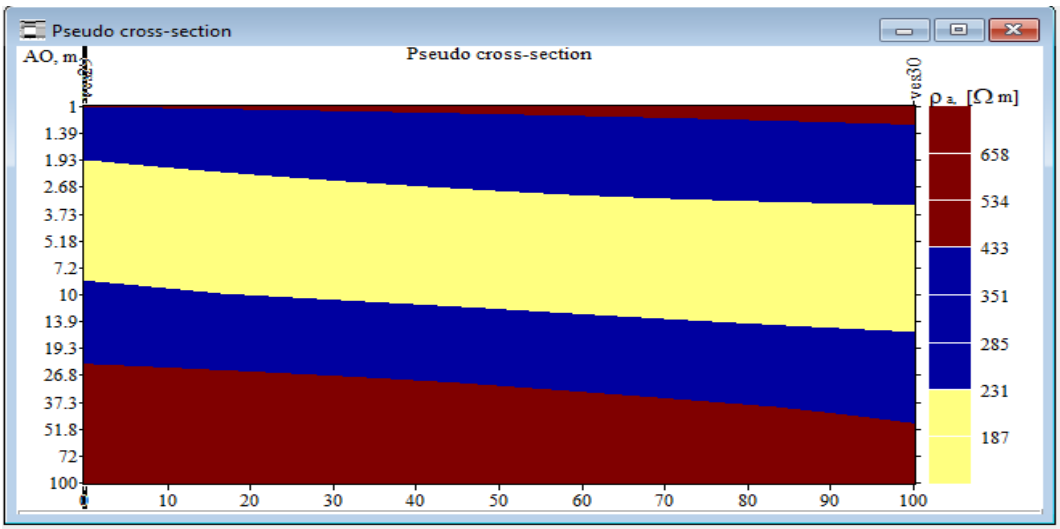
BUDO KETE



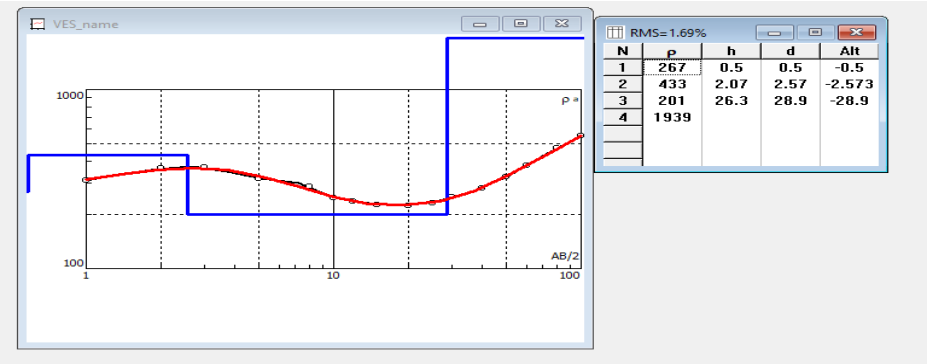
N	ρ	h	d	Alt
1	683	0.2	0.2	-0.2
2	683	0.3	0.5	-0.5
3	170	3.07	3.57	-3.57
4	229	5.96	9.53	-9.53
5	2055			



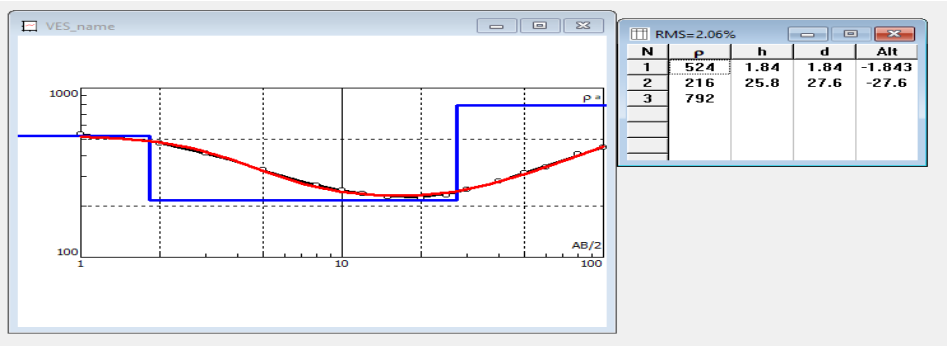
N	ρ	h	d	Alt
1	665	0.5	0.5	-0.5
2	301	1.4	1.9	-1.898
3	96.3	4.43	6.33	-6.328
4	687			



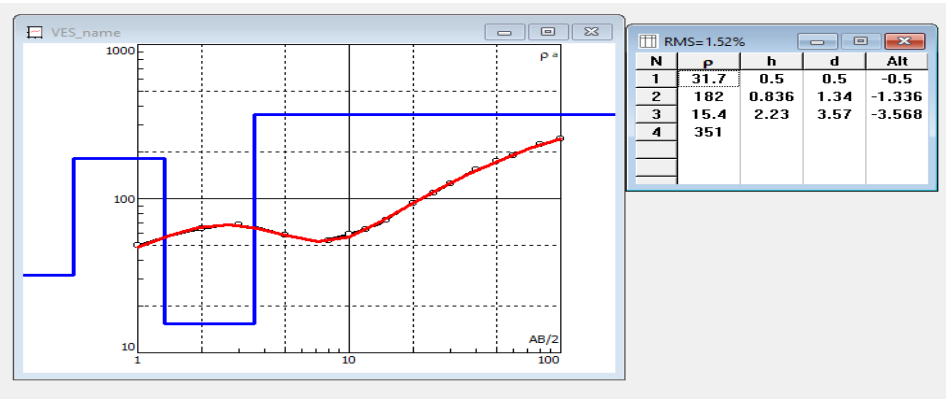
ODOJE



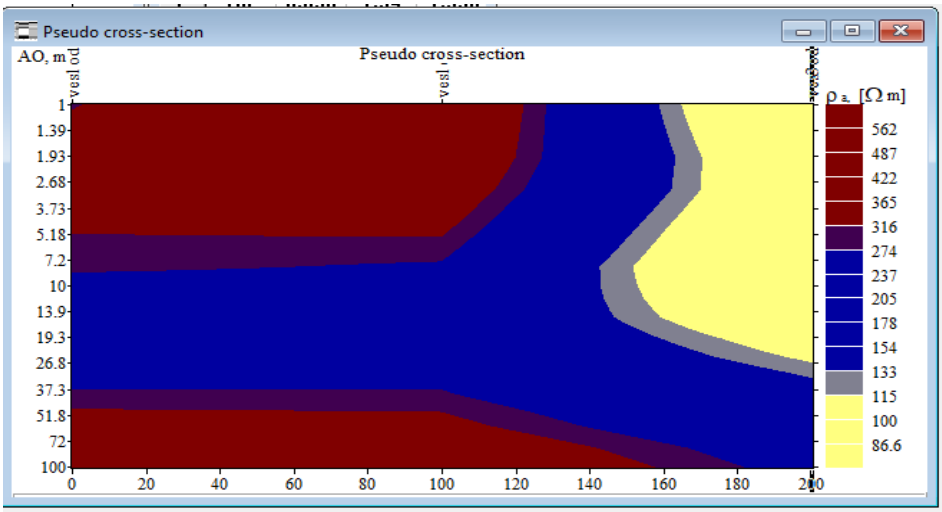
N	ρ	h	d	Alt
1	267	0.5	0.5	-0.5
2	433	2.07	2.57	-2.573
3	201	26.3	28.9	-28.9
4	1939			



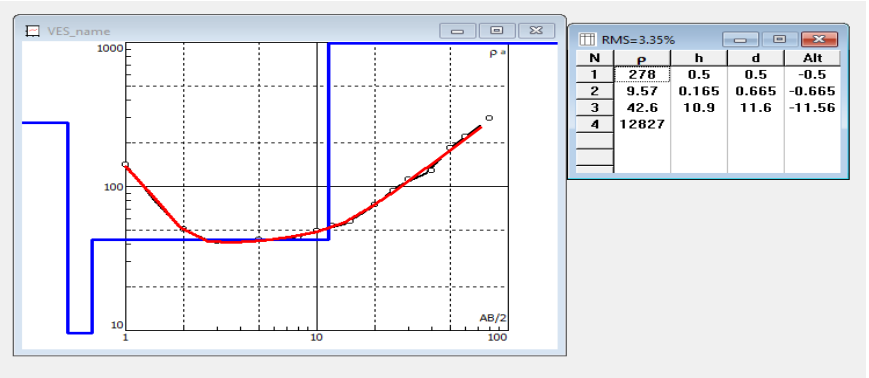
N	ρ	h	d	Alt
1	524	1.84	1.84	-1.843
2	216	25.8	27.6	-27.6
3	792			



N	ρ	h	d	Alt
1	31.7	0.5	0.5	-0.5
2	182	0.836	1.34	-1.336
3	15.4	2.23	3.57	-3.568
4	351			

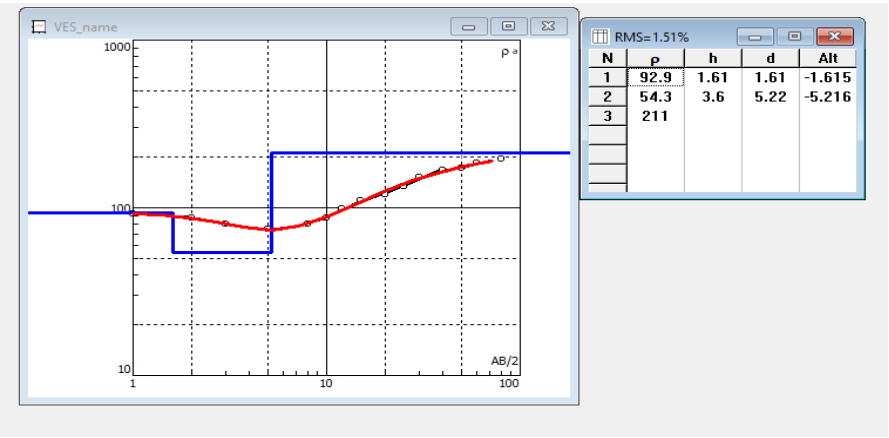


OROGUN



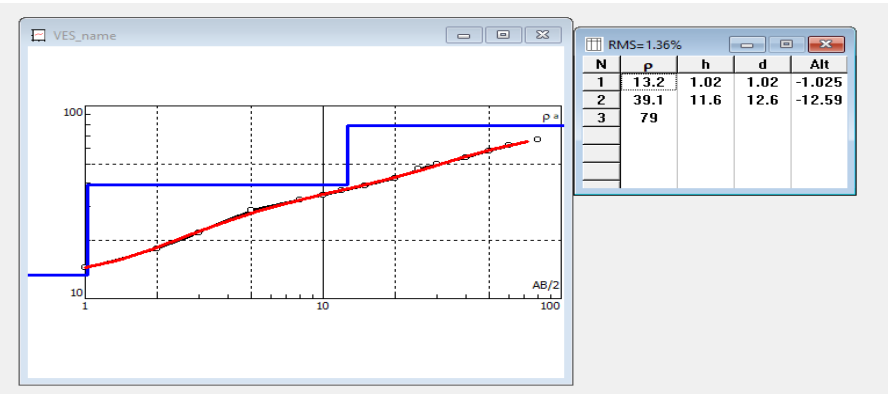
RMS=3.35%

N	ρ	h	d	Alt
1	278	0.5	0.5	-0.5
2	9.57	0.165	0.665	-0.665
3	42.6	10.9	11.6	-11.56
4	12827			



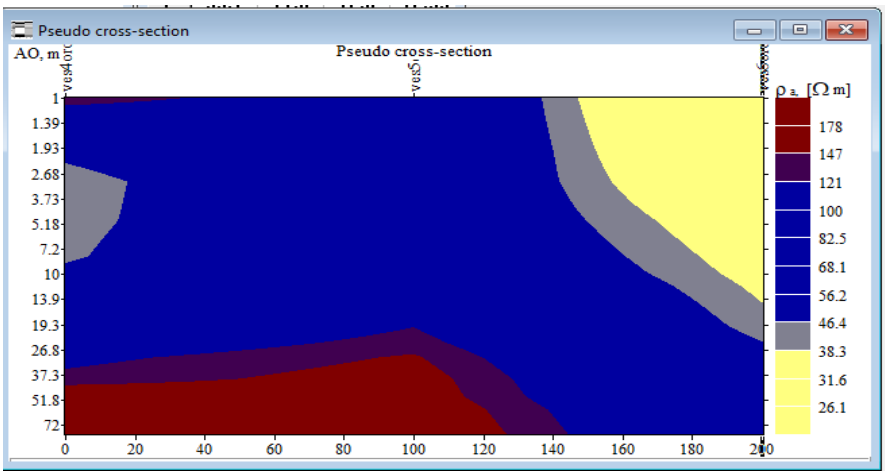
RMS=1.51%

N	ρ	h	d	Alt
1	92.9	1.61	1.61	-1.615
2	54.3	3.6	5.22	-5.216
3	211			

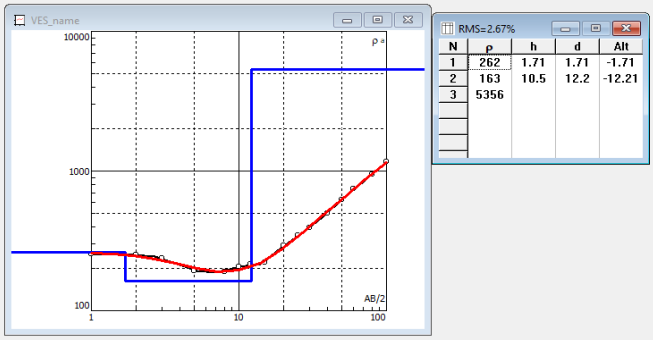


RMS=1.36%

N	ρ	h	d	Alt
1	13.2	1.02	1.02	-1.025
2	39.1	11.6	12.6	-12.59
3	79			

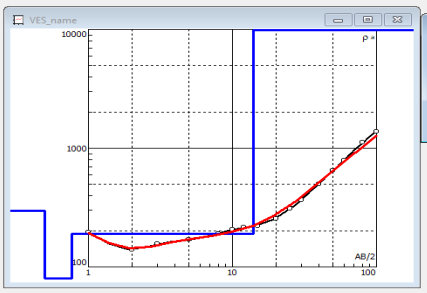


OKE AWO



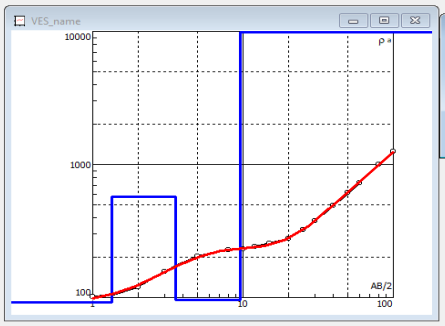
RMS=2.67%

N	ρ	h	d	Alt
1	262	1.71	1.71	-1.71
2	163	10.5	12.2	-12.21
3	5356			



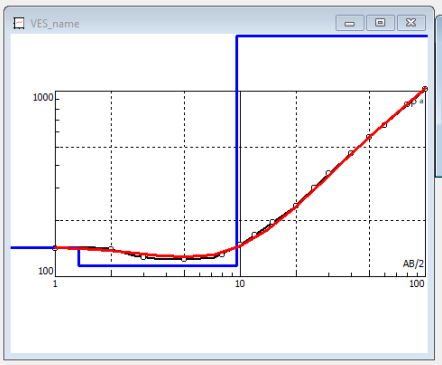
RMS=4.34%

N	ρ	h	d	Alt
1	299	0.5	0.5	-0.5
2	47.3	0.272	0.772	-0.772
3	189	13.2	14	-13.97
4	78790			



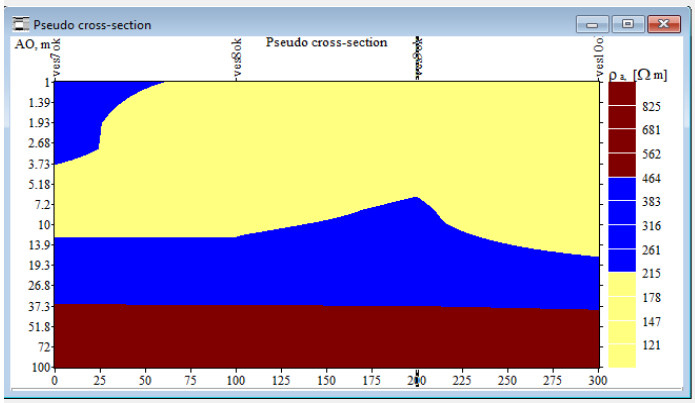
RMS=1.33%

N	ρ	h	d	Alt
1	92.4	1.34	1.34	-1.337
2	569	2.23	3.57	-3.569
3	95.6	5.96	9.53	-9.531
4	182612			

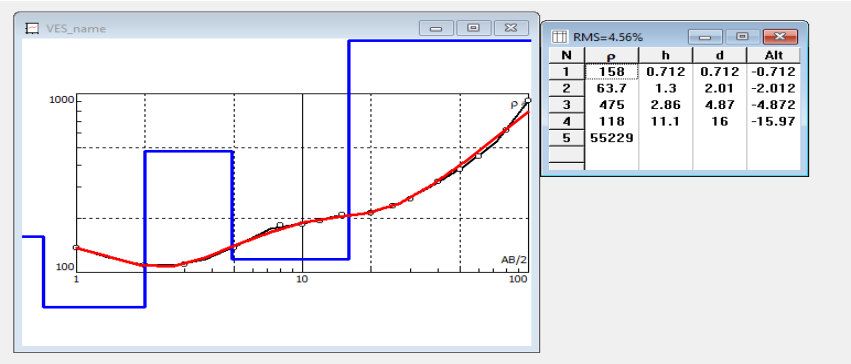


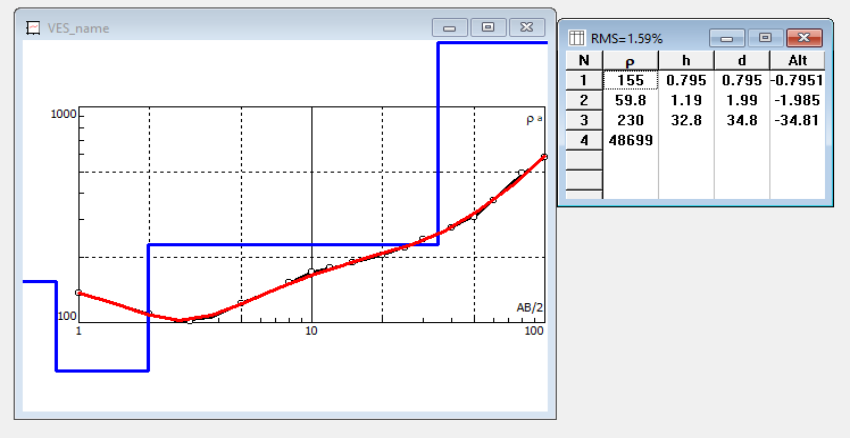
RMS=2.36%

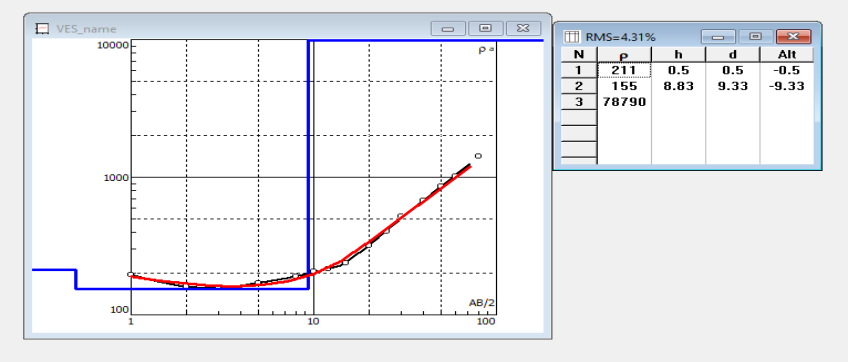
N	ρ	h	d	Alt
1	144	1.34	1.34	-1.34
2	115	8.24	9.58	-9.58
3	5717			

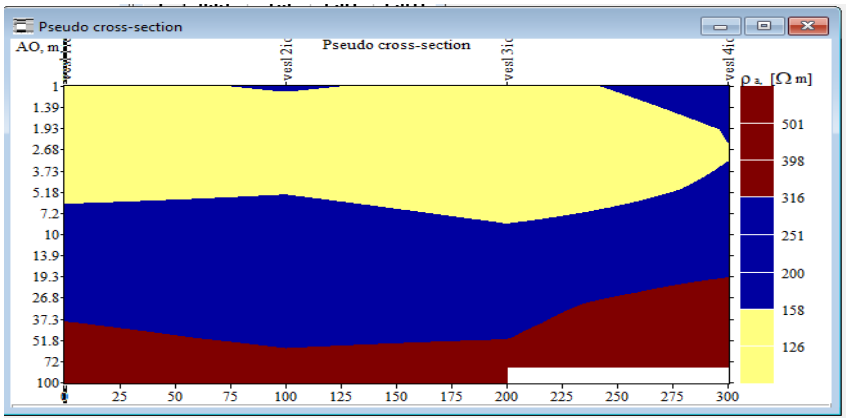


IDIAMI

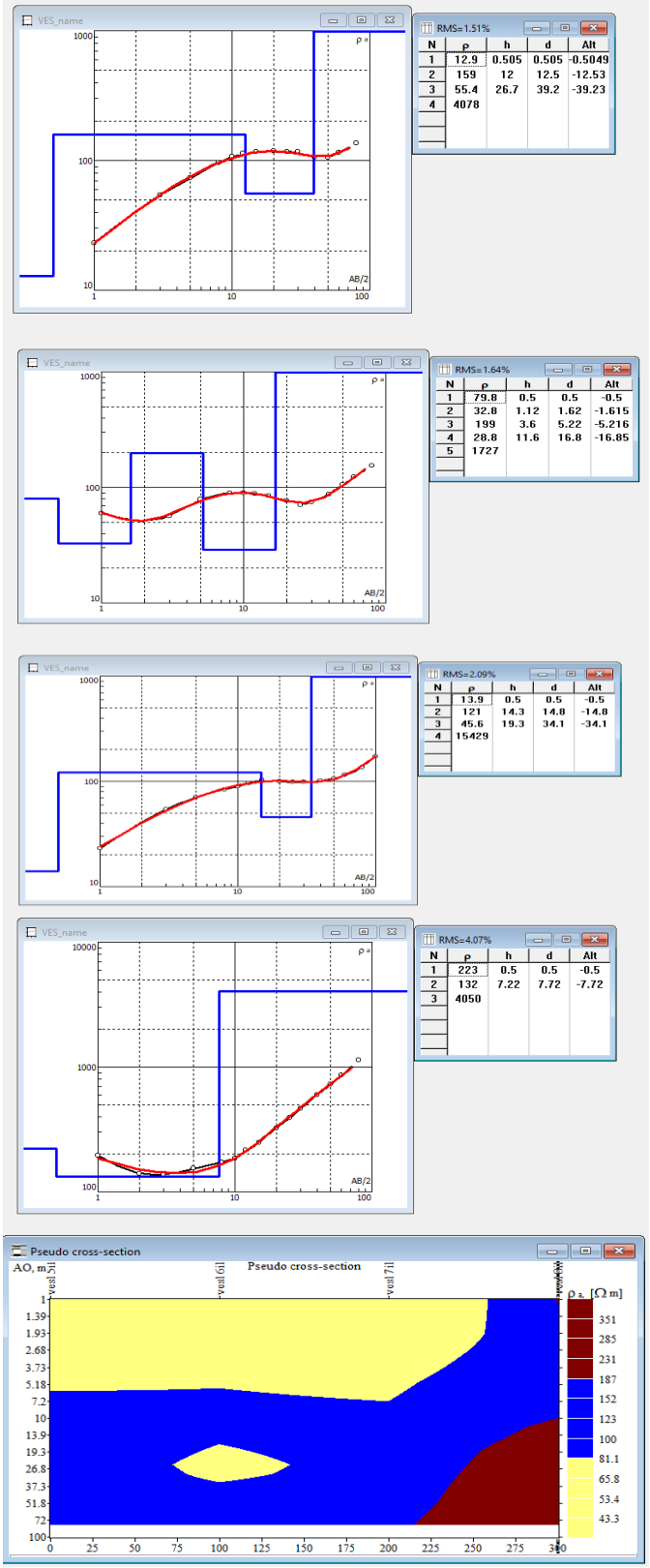

VES_name
RMS=4.56%
N ρ h d Alt
1 158 0.712 0.712 -0.712
2 63.7 1.3 2.01 -2.012
3 475 2.86 4.87 -4.872
4 118 11.1 16 -15.97
5 55229
1000
100
1
10
100
ρ
AB/2


VES_name
RMS=1.59%
N ρ h d Alt
1 155 0.795 0.795 -0.7951
2 59.8 1.19 1.99 -1.985
3 230 32.8 34.8 -34.81
4 48699
1000
100
1
10
100
ρ a
AB/2

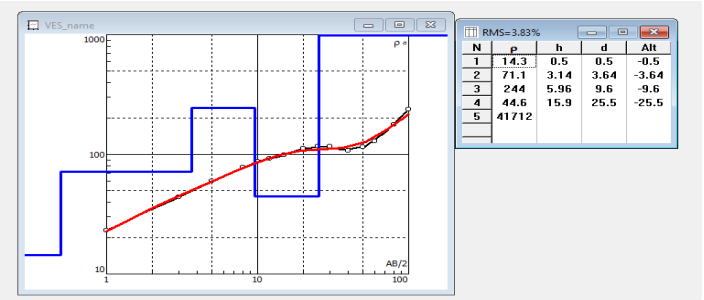

VES_name
RMS=4.31%
N ρ h d Alt
1 211 0.5 0.5 -0.5
2 155 8.83 9.33 -9.33
3 78790
10000
1000
100
1
10
100
ρ a
ρ
AB/2


Pseudo cross-section
Pseudo cross-section
AO, m
vesl2(
vesl3(
vesl4(
ρ a [Ω m]
1
1.39
1.93
2.68
3.73
5.18
7.2
10
13.9
19.3
26.8
37.3
51.8
72
100
501
398
316
251
200
158
126
25
50
75
100
125
150
175
200
225
250
275
300

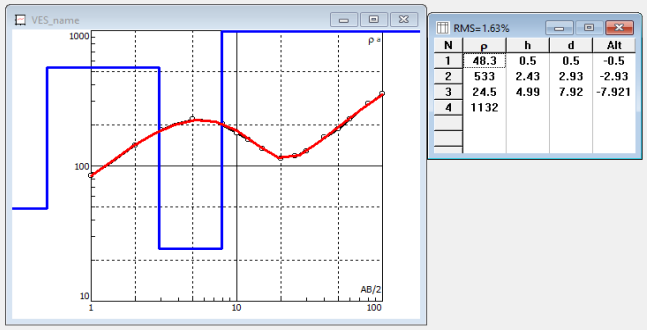
ILUIRU


VES_name
RMS=1.51%
N ρ h d Alt
1 12.9 0.505 0.505 -0.5049
2 159 12 12.5 -12.53
3 55.4 26.7 39.2 -39.23
4 4078
RMS=1.64%
N ρ h d Alt
1 79.8 0.5 0.5 -0.5
2 32.8 1.12 1.62 -1.615
3 199 3.6 5.22 -5.216
4 28.8 11.6 16.8 -16.85
5 1727
RMS=2.09%
N ρ h d Alt
1 13.9 0.5 0.5 -0.5
2 121 14.3 14.8 -14.8
3 45.6 19.3 34.1 -34.1
4 15429
RMS=4.07%
N ρ h d Alt
1 223 0.5 0.5 -0.5
2 132 7.22 7.72 -7.72
3 4050
AB/2
Pseudo cross-section
AO, m
Pseudo cross-section
ρ a, [Ω m]
351
285
231
187
152
123
100
81.1
65.8
53.4
43.3

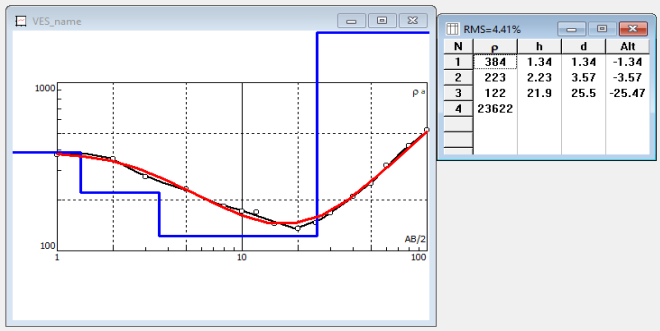
AFUKU



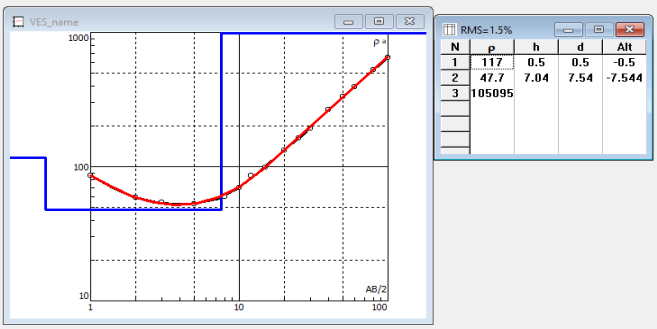
N	ρ	h	d	Alt
1	14.3	0.5	0.5	-0.5
2	71.1	3.14	3.64	-3.64
3	244	5.96	9.6	-9.6
4	44.6	15.9	25.5	-25.5
5	41712			



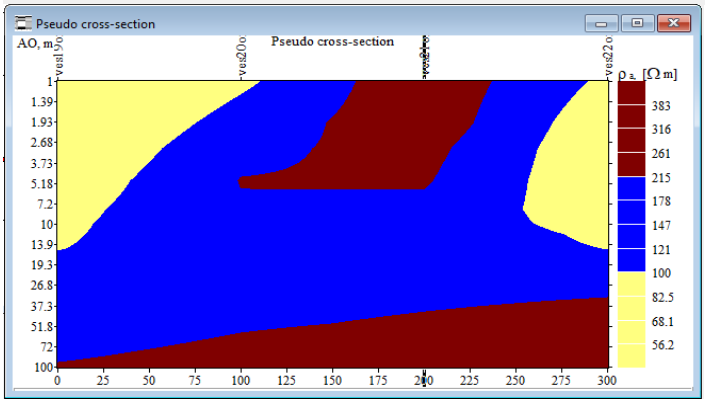
N	ρ	h	d	Alt
1	48.3	0.5	0.5	-0.5
2	533	2.43	2.93	-2.93
3	24.5	4.99	7.92	-7.921
4	1132			



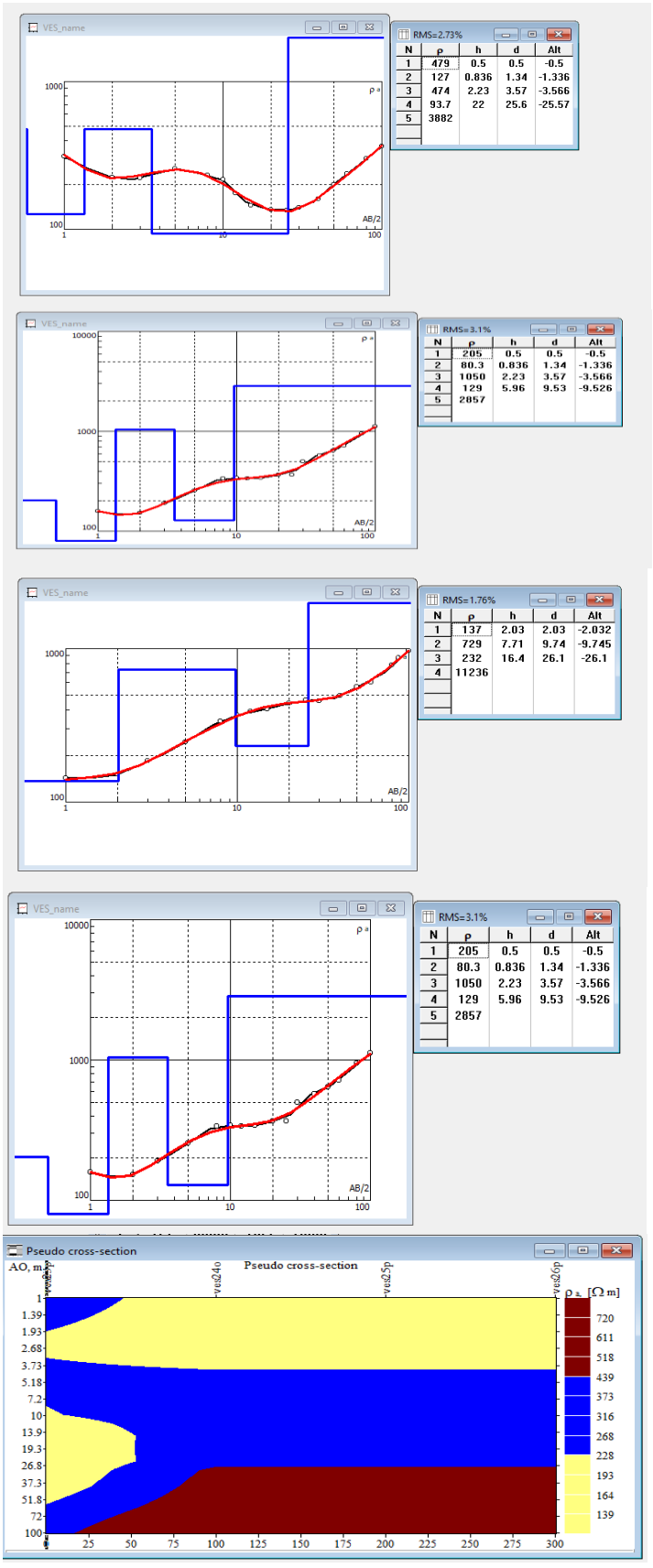
N	ρ	h	d	Alt
1	384	1.34	1.34	-1.34
2	223	2.23	3.57	-3.57
3	122	21.9	25.5	-25.47
4	23622			



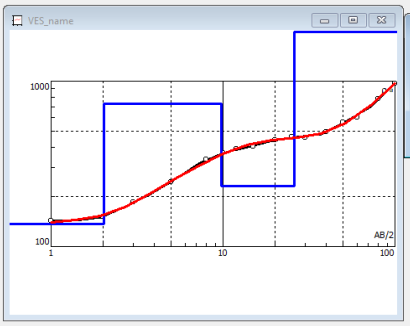
N	ρ	h	d	Alt
1	117	0.5	0.5	-0.5
2	47.7	7.04	7.54	-7.544
3	105095			



PAJUBA

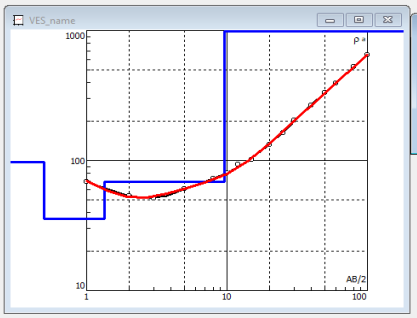

VES_name
ρ a
AB/2
RMS=2.73%
N ρ h d Alt
1 479 0.5 0.5 -0.5
2 127 0.836 1.34 -1.336
3 474 2.23 3.57 -3.566
4 93.7 22 25.6 -25.57
5 3882
RMS=3.1%
N ρ h d Alt
1 205 0.5 0.5 -0.5
2 80.3 0.836 1.34 -1.336
3 1050 2.23 3.57 -3.566
4 129 5.96 9.53 -9.526
5 2857
RMS=1.76%
N ρ h d Alt
1 137 2.03 2.03 -2.032
2 729 7.71 9.74 -9.745
3 232 16.4 26.1 -26.1
4 11236
RMS=3.1%
N ρ h d Alt
1 205 0.5 0.5 -0.5
2 80.3 0.836 1.34 -1.336
3 1050 2.23 3.57 -3.566
4 129 5.96 9.53 -9.526
5 2857
Pseudo cross-section
AO, m
Pseudo cross-section
ρ a [Ω m]
720
611
518
439
373
316
268
228
193
164
139

GORI



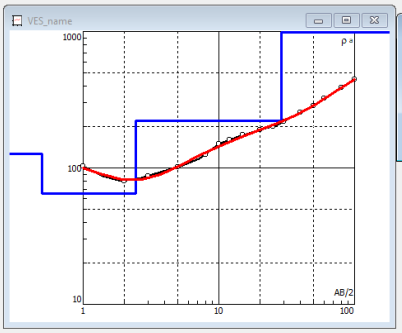
RMS=1.76%

N	ρ	h	d	Alt
1	137	2.03	2.03	-2.032
2	729	7.71	9.74	-9.745
3	232	16.4	26.1	-26.1
4	11236			



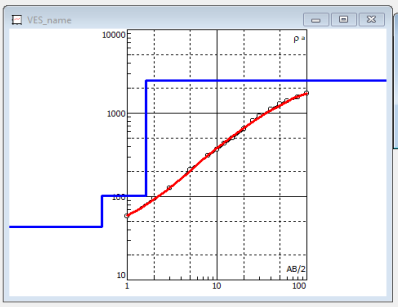
RMS=1.93%

N	ρ	h	d	Alt
1	97.3	0.5	0.5	-0.5
2	35.4	0.836	1.34	-1.336
3	68.2	8.2	9.54	-9.537
4	19952			



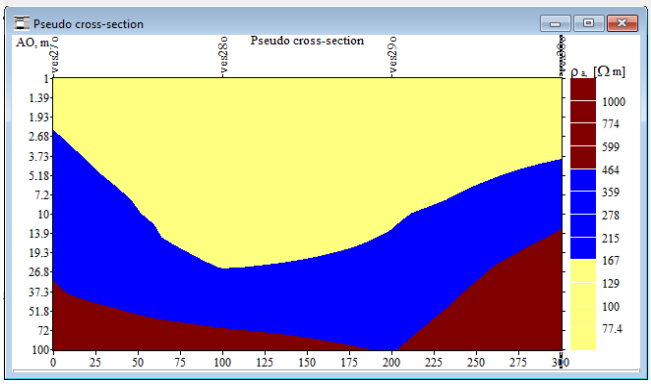
RMS=2.58%

N	ρ	h	d	Alt
1	126	0.5	0.5	-0.5
2	65.1	1.94	2.44	-2.44
3	222	26.5	28.9	-28.94
4	1110			

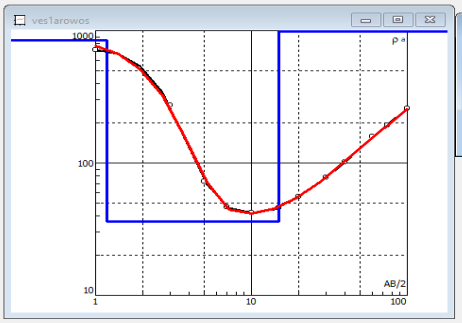


RMS=2.4%

N	ρ	h	d	Alt
1	43	0.518	0.518	-0.518
2	102	1.1	1.62	-1.618
3	2460			

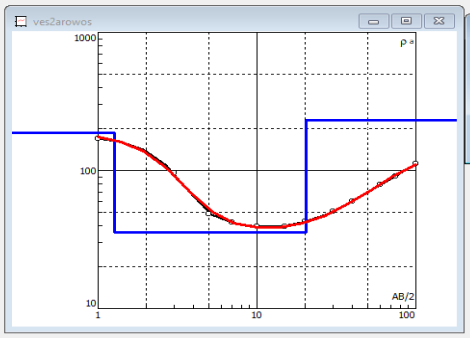


AROWOSAYE



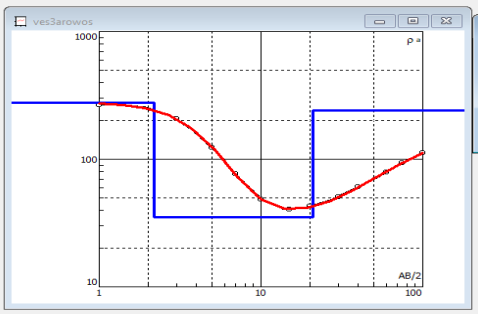
RMS=3.23%

N	ρ	h	d	Alt
1	842	1.19	1.19	-1.19
2	36.2	13.9	15.1	-15.09
3	21541			



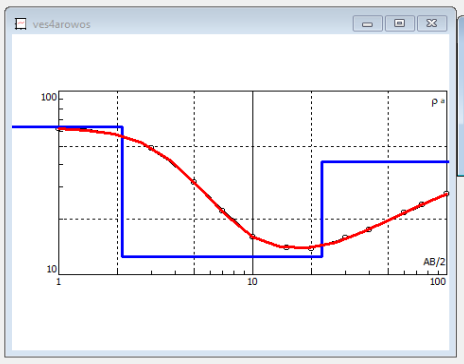
RMS=2.7%

N	ρ	h	d	Alt
1	187	1.27	1.27	-1.27
2	35.7	19.2	20.5	-20.47
3	231			



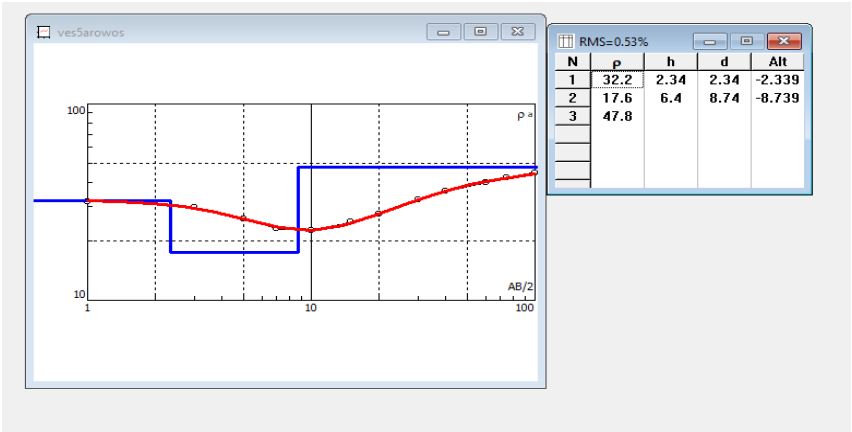
RMS=1.14%

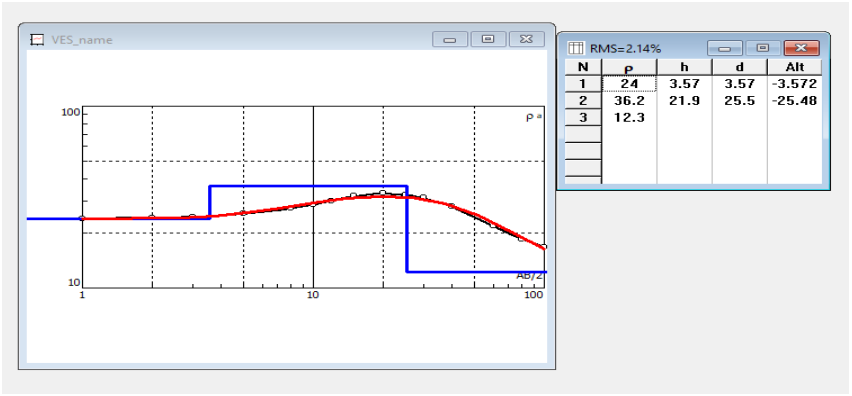
N	ρ	h	d	Alt
1	276	2.17	2.17	-2.175
2	34.9	18.9	21.1	-21.09
3	241			

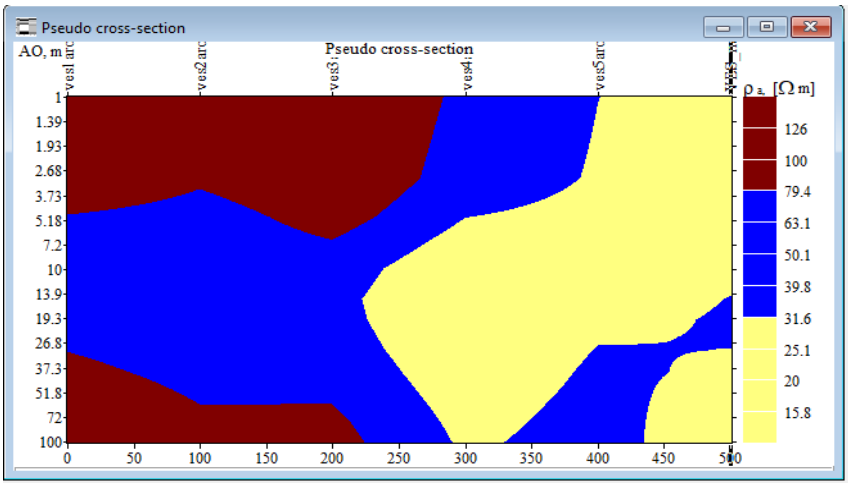


RMS=0.787%

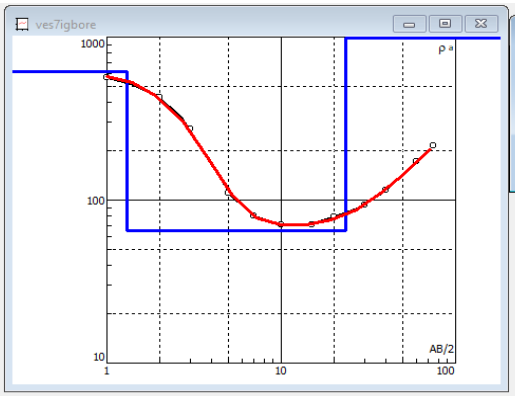
N	ρ	h	d	Alt
1	63.6	2.13	2.13	-2.134
2	12.5	20.7	22.8	-22.8
3	41.2			


ves5arowos
ρ a
100
10
1
10
100
AB/2
RMS=0.53%
N ρ h d Alt
1 32.2 2.34 2.34 -2.339
2 17.6 6.4 8.74 -8.739
3 47.8


VES_name
ρ a
100
10
1
10
100
AB/2
RMS=2.14%
N ρ h d Alt
1 24 3.57 3.57 -3.572
2 36.2 21.9 25.5 -25.48
3 12.3

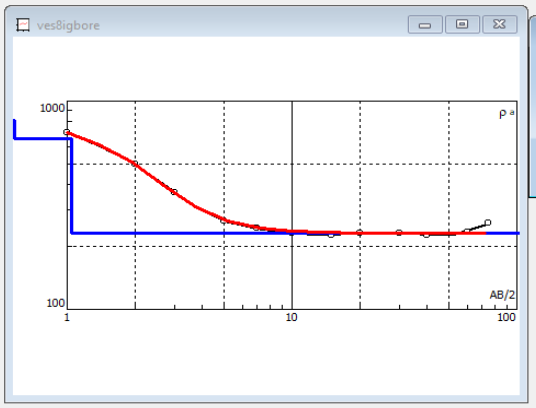

Pseudo cross-section
Pseudo cross-section
AO, m
ves1 arc
ves2 arc
ves3 arc
ves4 arc
ves5 arc
ρ a [Ω m]
126
100
79.4
63.1
50.1
39.8
31.6
25.1
20
15.8
1
1.39
1.93
2.68
3.73
5.18
7.2
10
13.9
19.3
26.8
37.3
51.8
72
100
0
50
100
150
200
250
300
350
400
450
500

IGBORESE



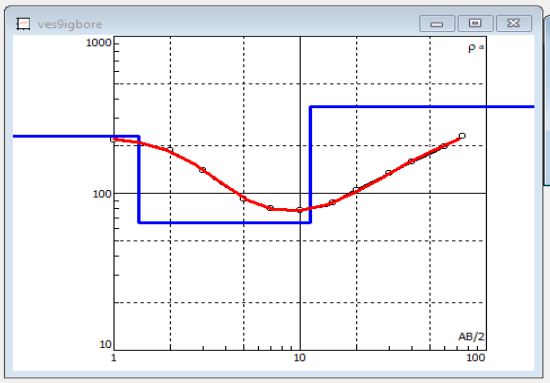
RMS=1.95%

N	ρ	h	d	Alt
1	616	1.3	1.3	-1.301
2	64.5	22.3	23.6	-23.55
3	17307			



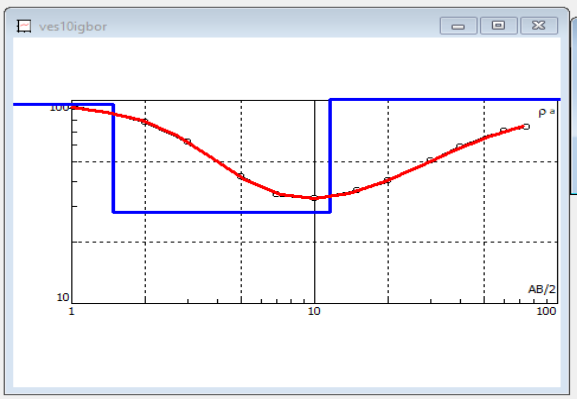
RMS=2.76%

N	ρ	h	d	Alt
1	812	0.5	0.5	-0.5
2	663	0.55	1.05	-1.05
3	231			



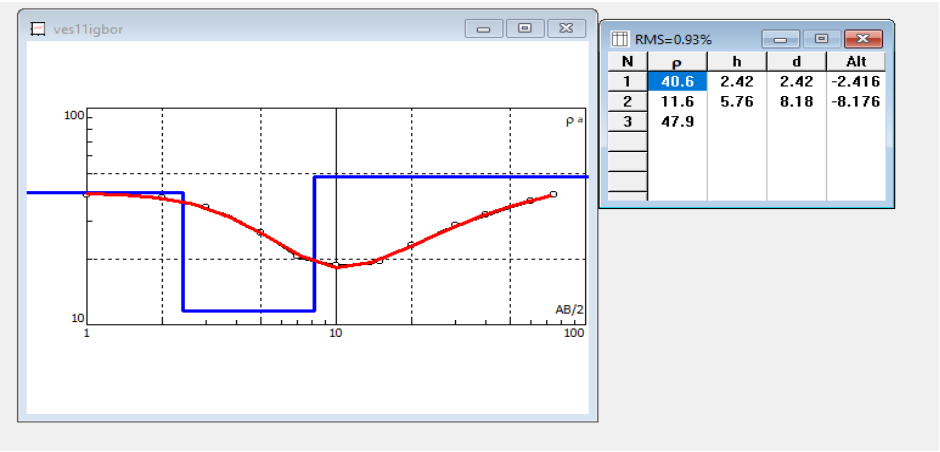
RMS=1.23%

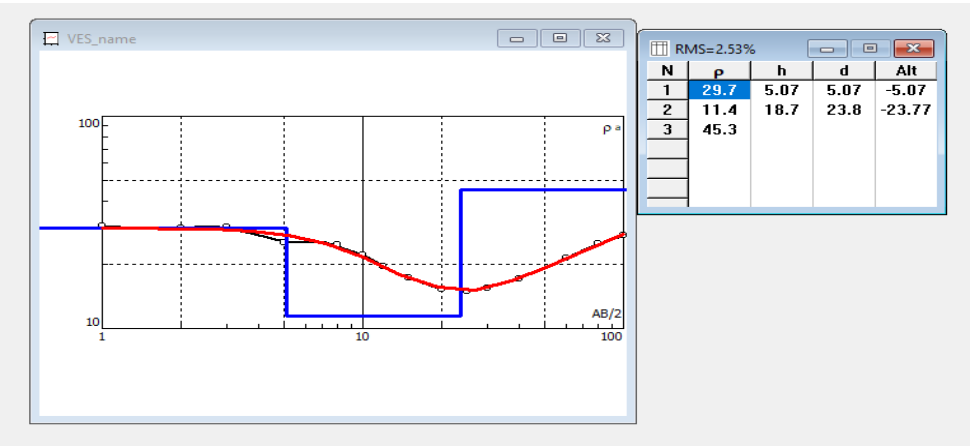
N	ρ	h	d	Alt
1	232	1.37	1.37	-1.368
2	65	9.97	11.3	-11.34
3	357			

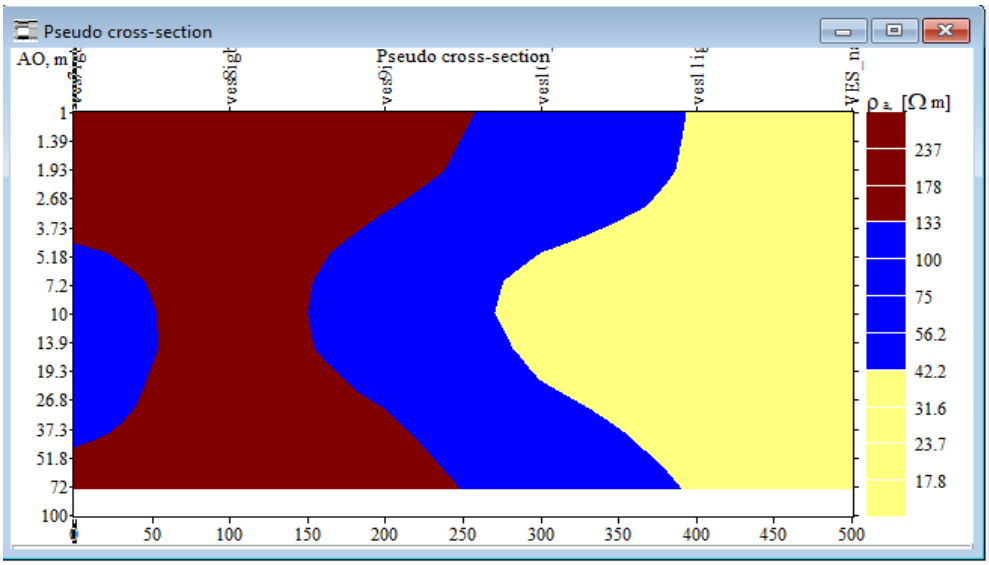


RMS=1.04%

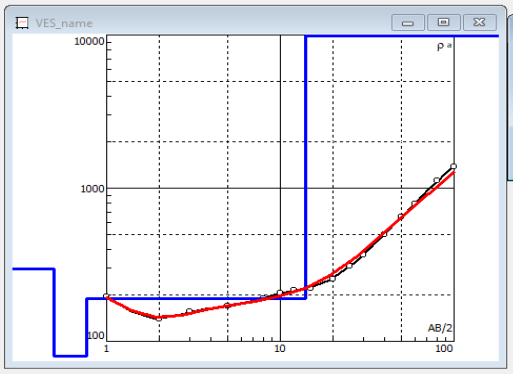
N	ρ	h	d	Alt
1	95.2	1.48	1.48	-1.478
2	28	10.1	11.5	-11.54
3	101			


ves11igbor
100
10
1
10
100
ρ a
AB/2
RMS=0.93%
N ρ h d Alt
1 40.6 2.42 2.42 -2.416
2 11.6 5.76 8.18 -8.176
3 47.9


VES_name
100
10
1
10
100
ρ a
AB/2
RMS=2.53%
N ρ h d Alt
1 29.7 5.07 5.07 -5.07
2 11.4 18.7 23.8 -23.77
3 45.3

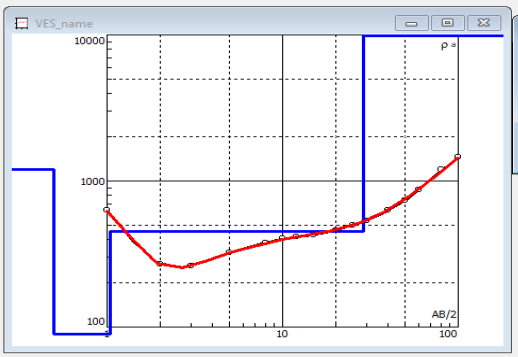

Pseudo cross-section
AO, m
Pseudo cross-section
ρ a [Ω m]
237
178
133
100
75
56.2
42.2
31.6
23.7
17.8
1
1.39
1.93
2.68
3.73
5.18
7.2
10
13.9
19.3
26.8
37.3
51.8
72
100
50
100
150
200
250
300
350
400
450
500

OLOKO



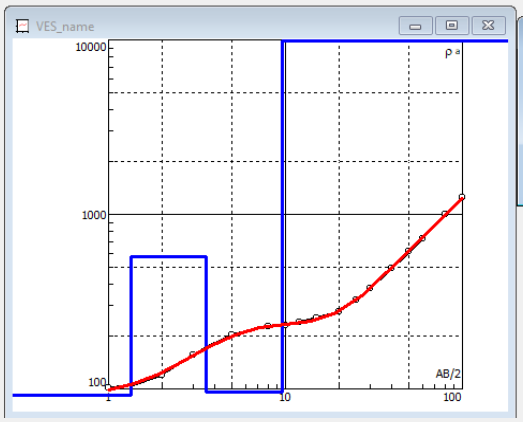
RMS=4.34%

N	ρ	h	d	Alt
1	299	0.5	0.5	-0.5
2	47.3	0.272	0.772	-0.772
3	189	13.2	14	-13.97
4	78790			



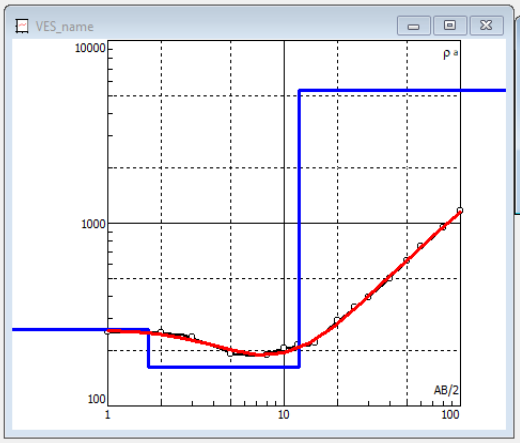
RMS=1.49%

N	ρ	h	d	Alt
1	1207	0.5	0.5	-0.5
2	89.2	0.539	1.04	-1.039
3	452	27.8	28.8	-28.82
4	57017			



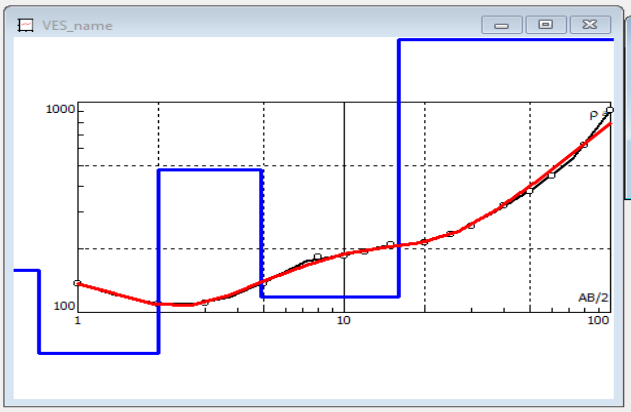
RMS=1.33%

N	ρ	h	d	Alt
1	92.4	1.34	1.34	-1.337
2	569	2.23	3.57	-3.569
3	95.6	5.96	9.53	-9.531
4	182612			



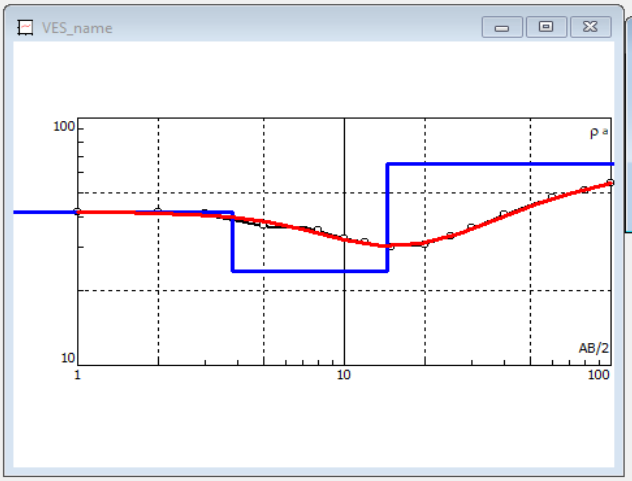
RMS=2.66%

N	ρ	h	d	Alt
1	262	1.71	1.71	-1.709
2	163	10.5	12.2	-12.17
3	5356			



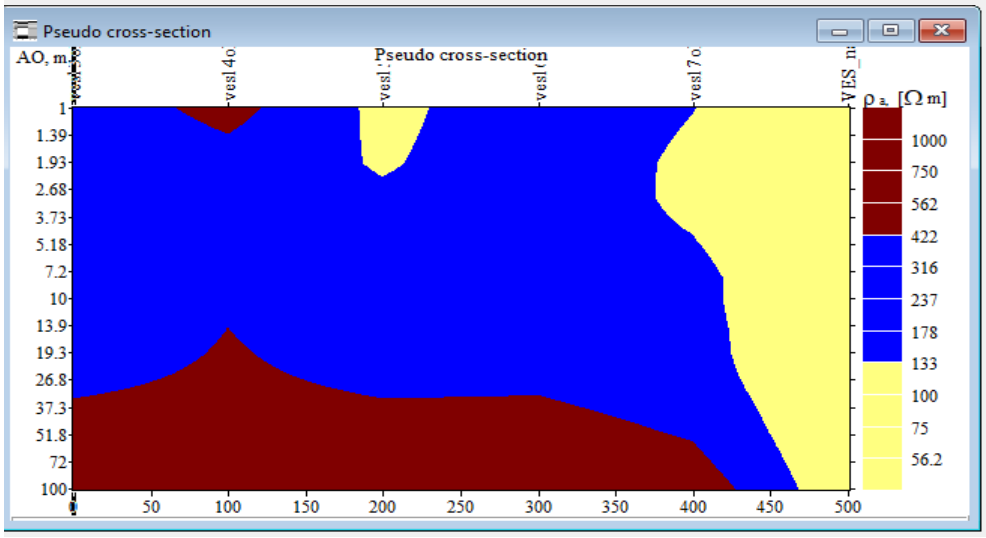
RMS=4.56%

N	ρ	h	d	Alt
1	158	0.712	0.712	-0.712
2	63.7	1.3	2.01	-2.012
3	475	2.86	4.87	-4.872
4	118	11.1	16	-15.97
5	55229			

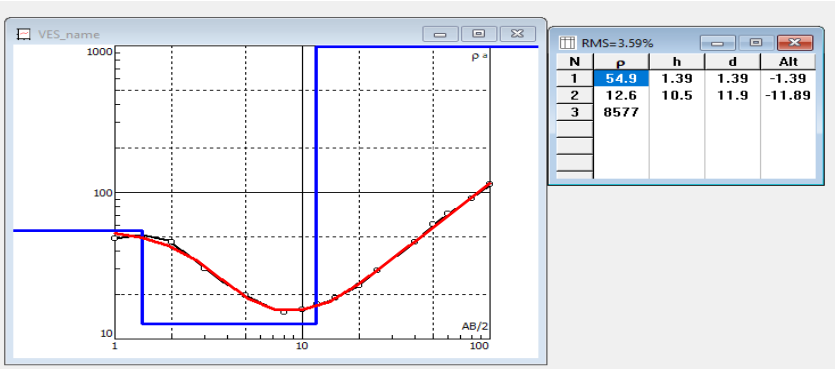


RMS=1.46%

N	ρ	h	d	Alt
1	41.6	3.81	3.81	-3.805
2	23.9	10.7	14.5	-14.53
3	65.2			

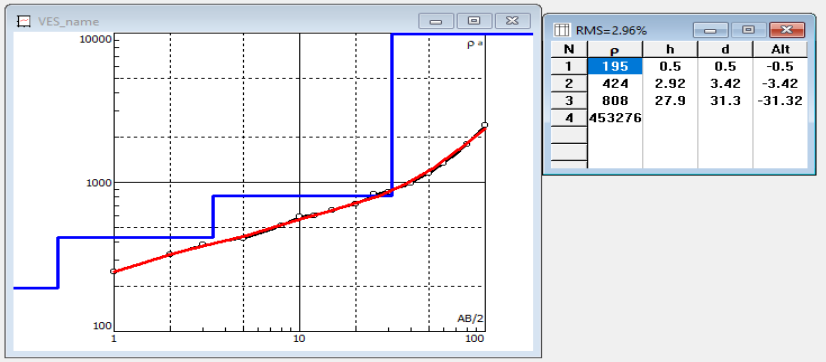


ONIPANPO



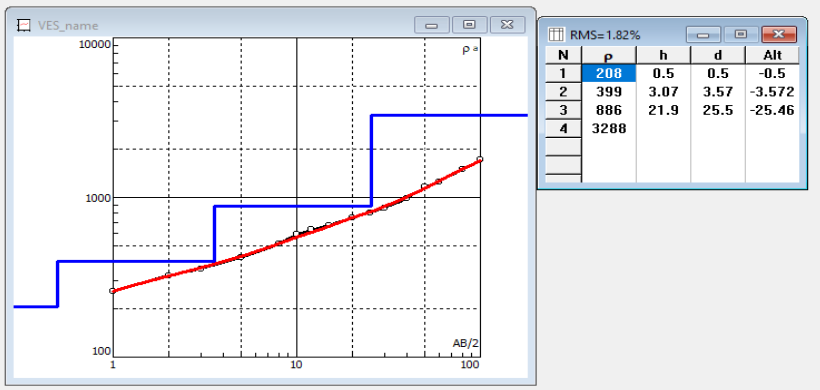
RMS=3.59%

N	ρ	h	d	Alt
1	54.9	1.39	1.39	-1.39
2	12.6	10.5	11.9	-11.89
3	8577			



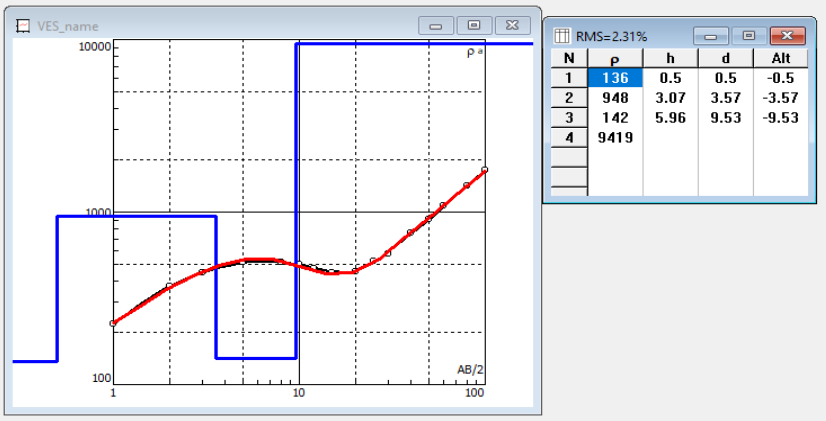
RMS=2.96%

N	ρ	h	d	Alt
1	195	0.5	0.5	-0.5
2	424	2.92	3.42	-3.42
3	808	27.9	31.3	-31.32
4	453276			



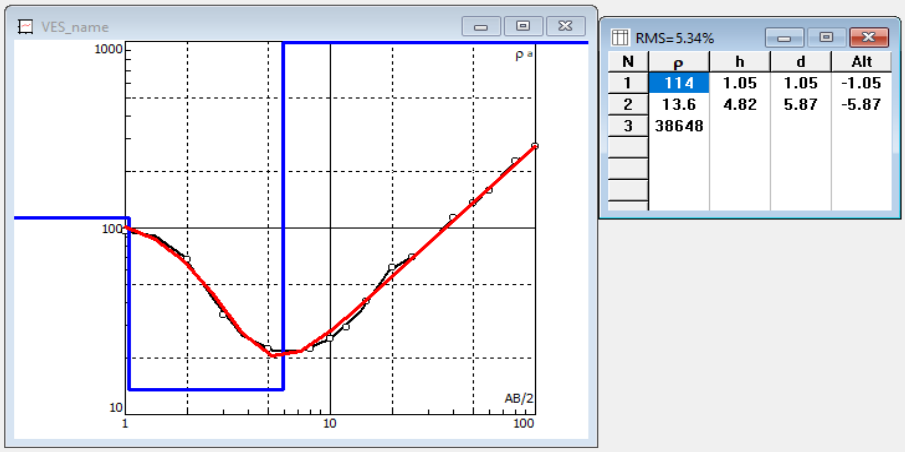
RMS=1.82%

N	ρ	h	d	Alt
1	208	0.5	0.5	-0.5
2	399	3.07	3.57	-3.572
3	886	21.9	25.5	-25.46
4	3288			



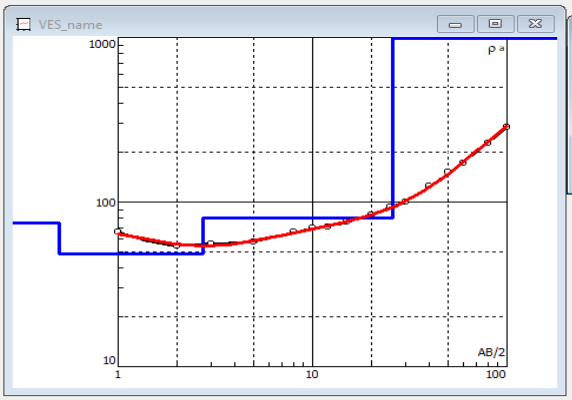
RMS=2.31%

N	ρ	h	d	Alt
1	136	0.5	0.5	-0.5
2	948	3.07	3.57	-3.57
3	142	5.96	9.53	-9.53
4	9419			



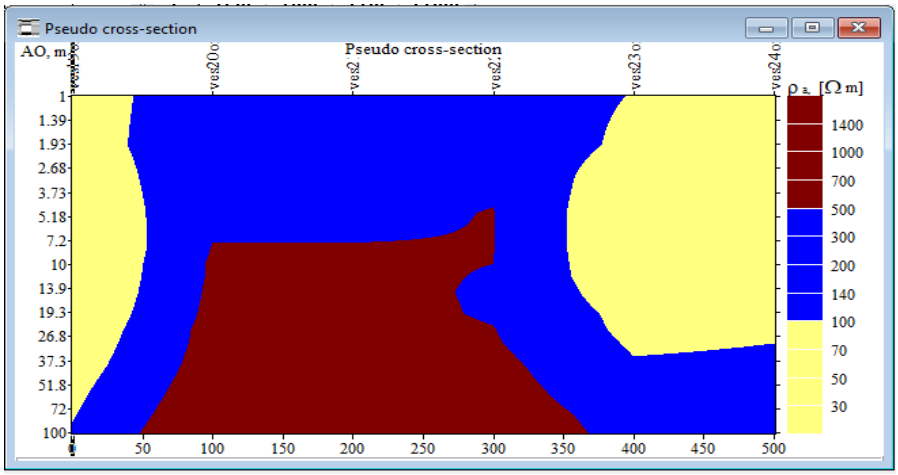
RMS=5.34%

N	ρ	h	d	Alt
1	114	1.05	1.05	-1.05
2	13.6	4.82	5.87	-5.87
3	38648			

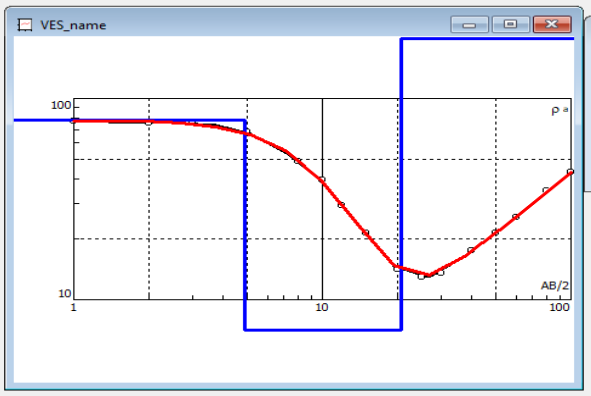


RMS=1.51%

N	ρ	h	d	Alt
1	75	0.5	0.5	-0.5
2	48.5	2.24	2.74	-2.739
3	80.2	23	25.8	-25.78
4	11662			

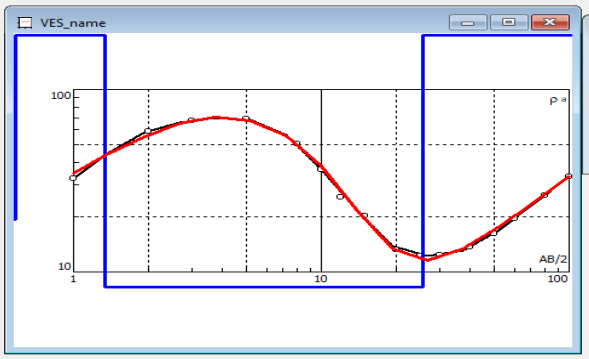


AIYEKALE



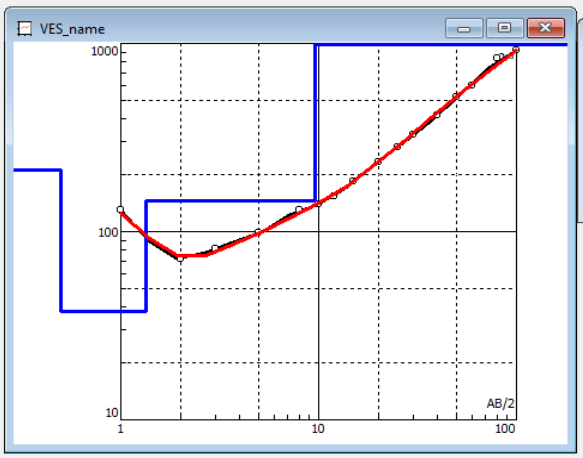
RMS=1.26%

N	ρ	h	d	Alt
1	77.7	4.89	4.89	-4.889
2	7.08	16	20.9	-20.85
3	6973			



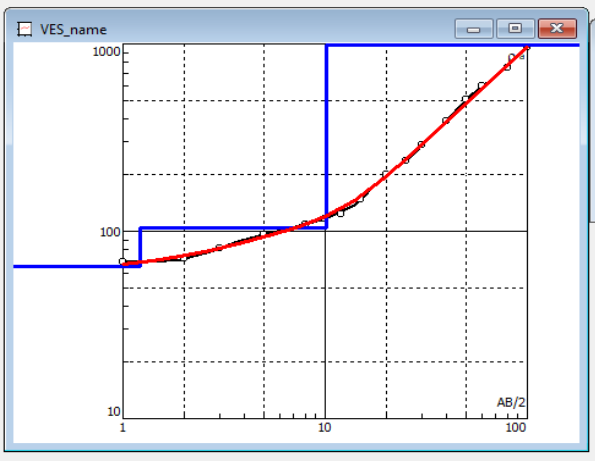
RMS=3.3%

N	ρ	h	d	Alt
1	19.4	0.5	0.5	-0.5
2	359	0.836	1.34	-1.336
3	8.27	24.4	25.7	-25.74
4	2311			



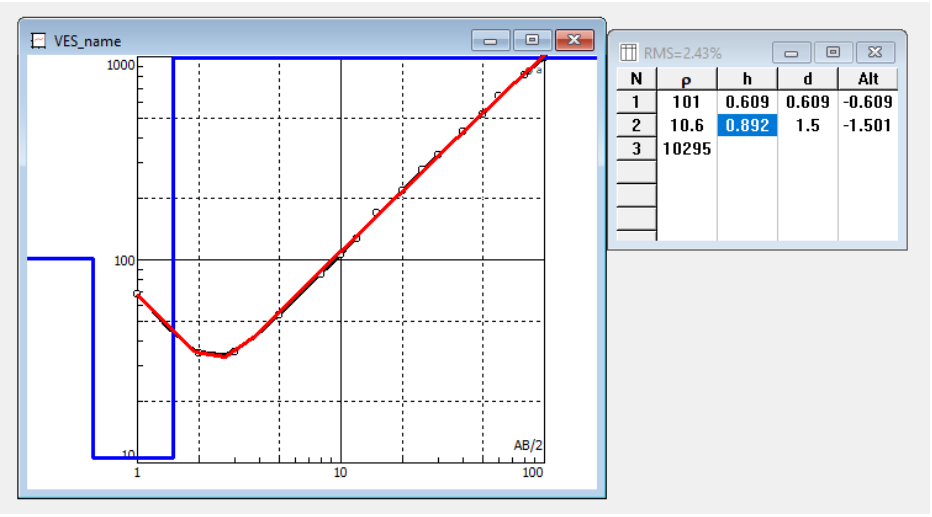
RMS=2.87%

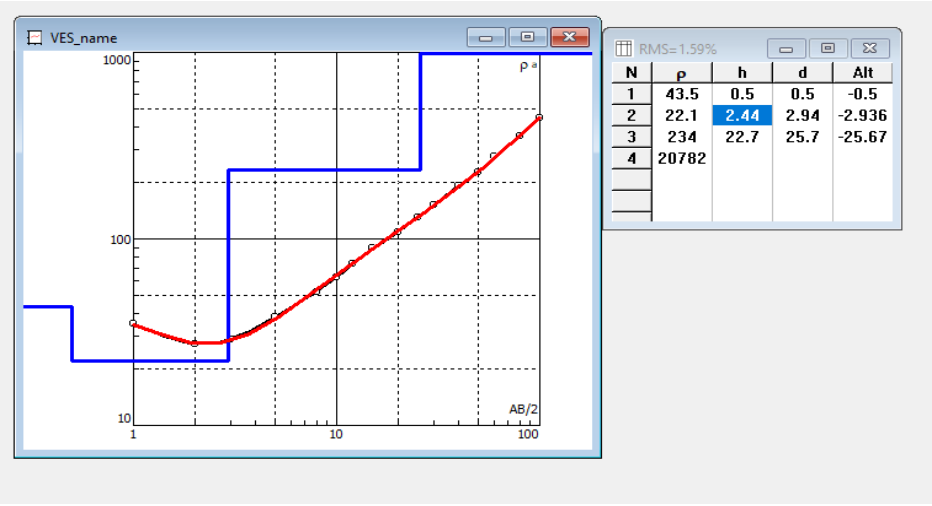
N	ρ	h	d	Alt
1	211	0.5	0.5	-0.5
2	37.6	0.836	1.34	-1.336
3	145	8.31	9.65	-9.646
4	3210			

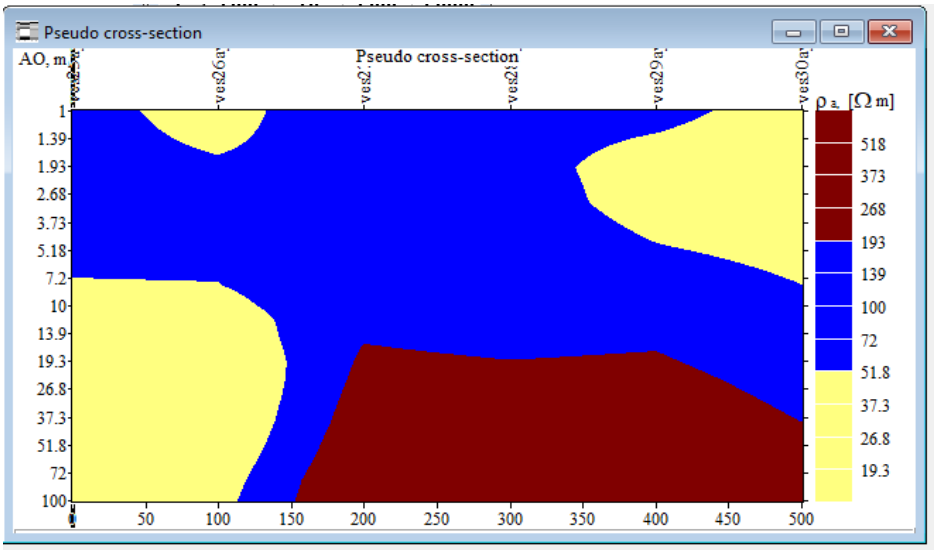


RMS=2.52%

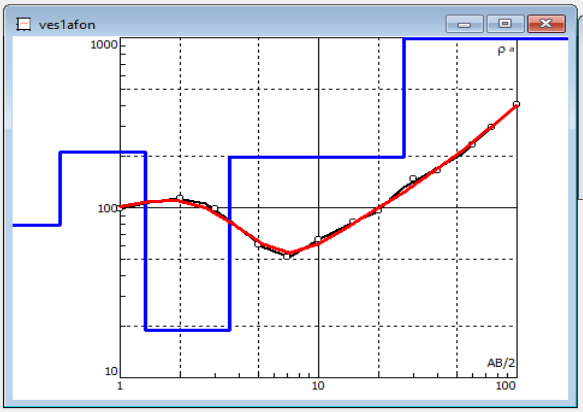
N	ρ	h	d	Alt
1	65.2	1.21	1.21	-1.21
2	105	8.88	10.1	-10.09
3	94326			


VES_name
1000
100
10
1
10
100
AB/2
RMS=2.43%
N ρ h d Alt
1 101 0.609 0.609 -0.609
2 10.6 0.892 1.5 -1.501
3 10295


VES_name
ρ a
1000
100
10
1
10
100
AB/2
RMS=1.59%
N ρ h d Alt
1 43.5 0.5 0.5 -0.5
2 22.1 2.44 2.94 -2.936
3 234 22.7 25.7 -25.67
4 20782

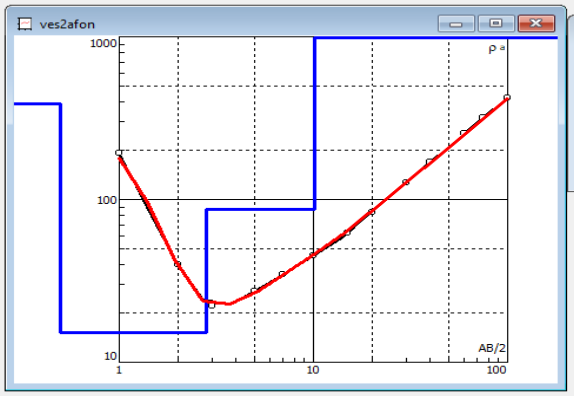

Pseudo cross-section
AO, m
Pseudo cross-section
ρ a, [Ω m]
518
373
268
193
139
100
72
51.8
37.3
26.8
19.3
1
1.39
1.93
2.68
3.73
5.18
7.2
10
13.9
19.3
26.8
37.3
51.8
72
100
50
100
150
200
250
300
350
400
450
500

AFON



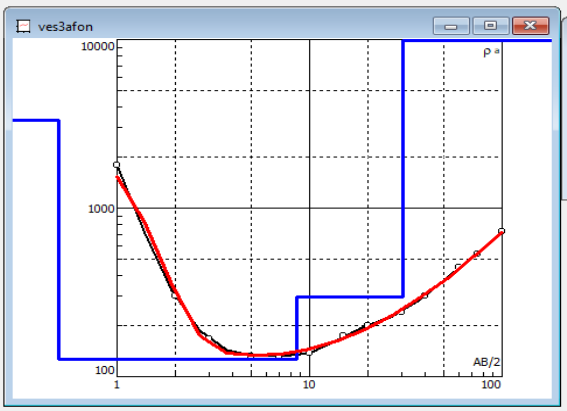
RMS=4%

N	ρ	h	d	Alt
1	79.1	0.5	0.5	-0.5
2	211	0.836	1.34	-1.336
3	18.9	2.23	3.57	-3.566
4	197	23.4	27	-26.97
5	39541			



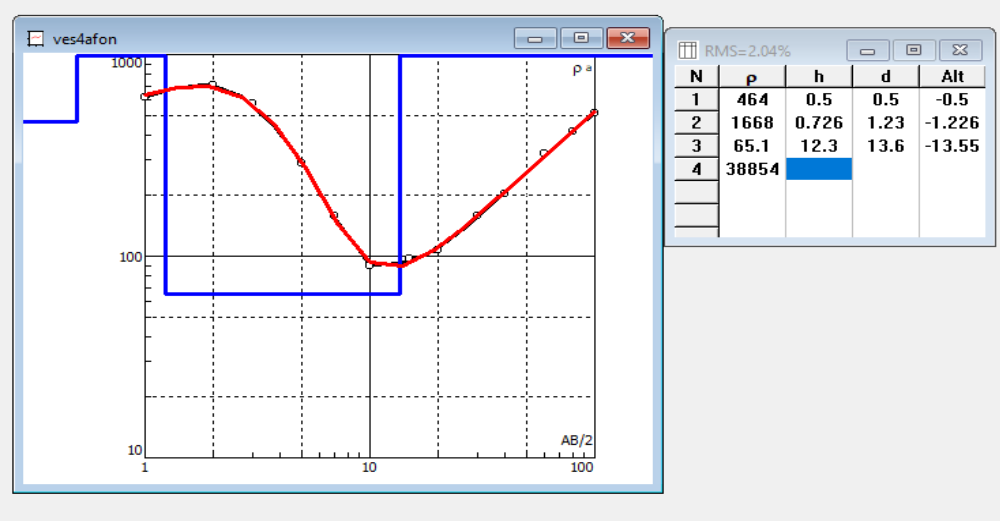
RMS=3.33%

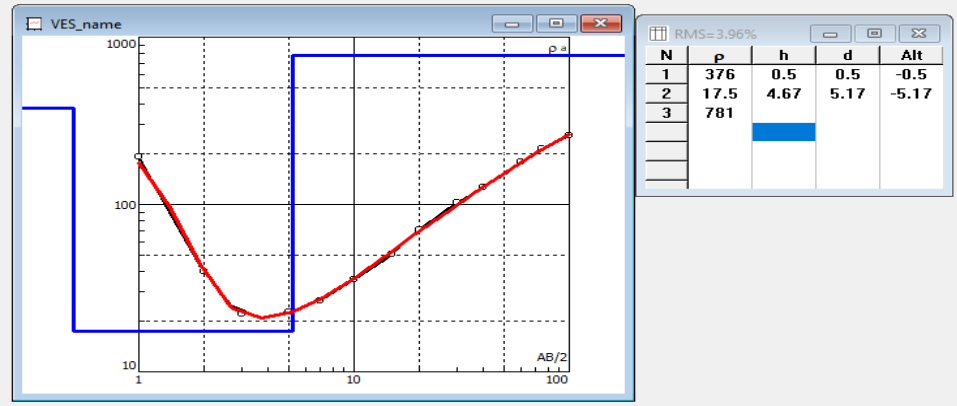
N	ρ	h	d	Alt
1	389	0.5	0.5	-0.5
2	15.1	2.29	2.79	-2.79
3	87.1	7.39	10.2	-10.18
4	51652			

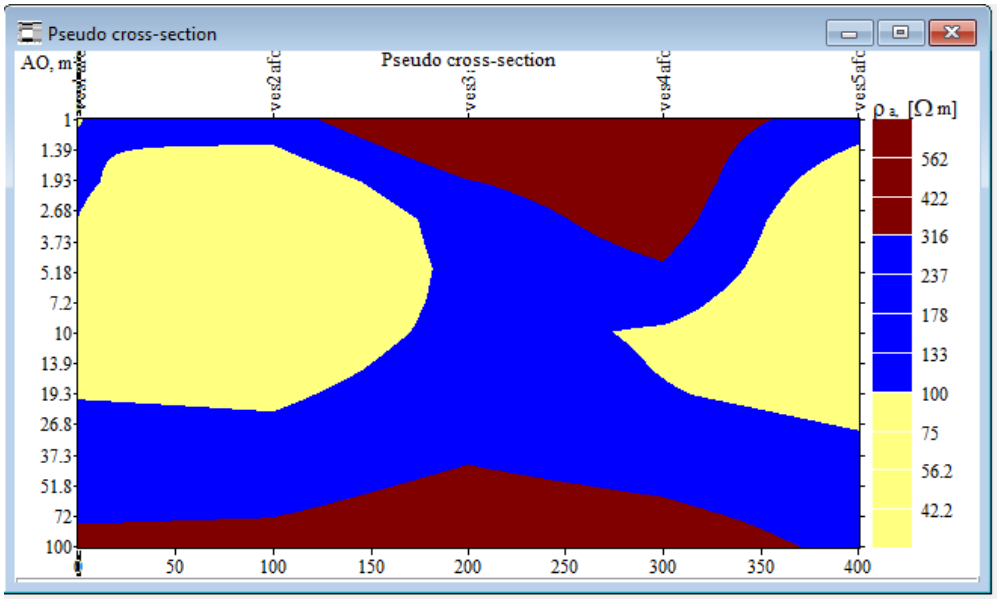


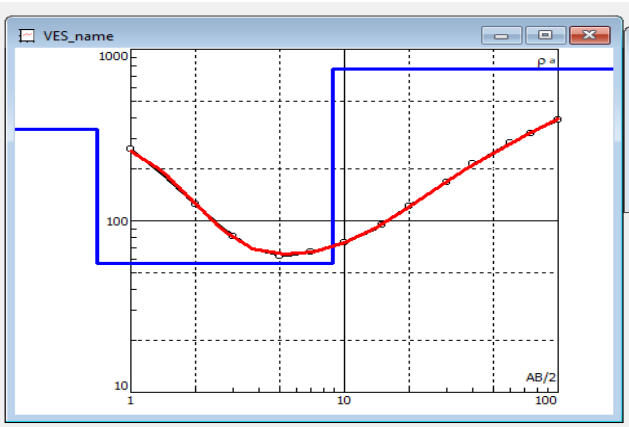
RMS=6.44%

N	ρ	h	d	Alt
1	3309	0.5	0.5	-0.5
2	127	8.08	8.58	-8.58
3	296	21.9	30.5	-30.48
4	86766			


ves4afon
ρ a
1000
100
10
1
10
100
AB/2
RMS=2.04%
N ρ h d Alt
1 464 0.5 0.5 -0.5
2 1668 0.726 1.23 -1.226
3 65.1 12.3 13.6 -13.55
4 38854

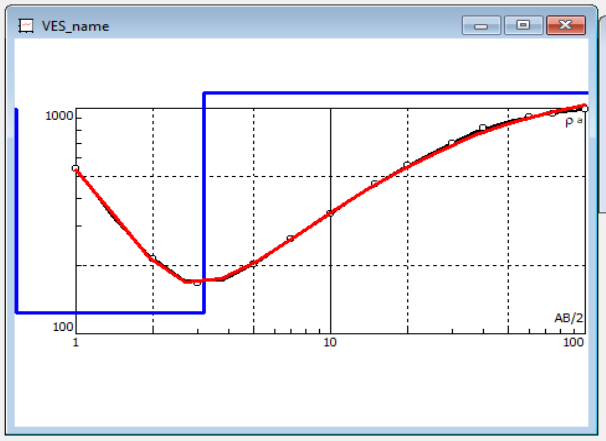

VES_name
ρ a
1000
100
10
1
10
100
AB/2
RMS=3.96%
N ρ h d Alt
1 376 0.5 0.5 -0.5
2 17.5 4.67 5.17 -5.17
3 781


Pseudo cross-section
Pseudo cross-section
AO, m
ves2afc
ves3afc
ves4afc
ves5afc
ρ a, [Ω m]
562
422
316
237
178
133
100
75
56.2
42.2
1
1.39
1.93
2.68
3.73
5.18
7.2
10
13.9
19.3
26.8
37.3
51.8
72
100
0
50
100
150
200
250
300
350
400



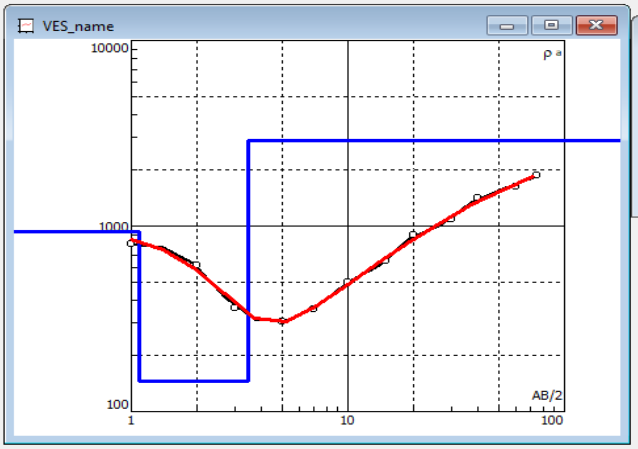
RMS=1.84%

N	ρ	h	d	Alt
1	341	0.696	0.696	-0.6964
2	56.6	8.08	8.78	-8.775
3	763			



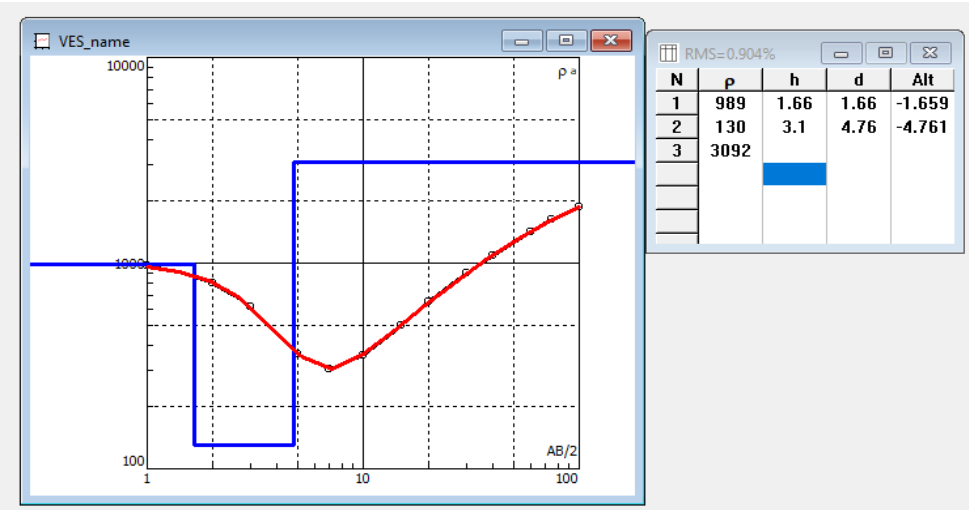
RMS=2.07%

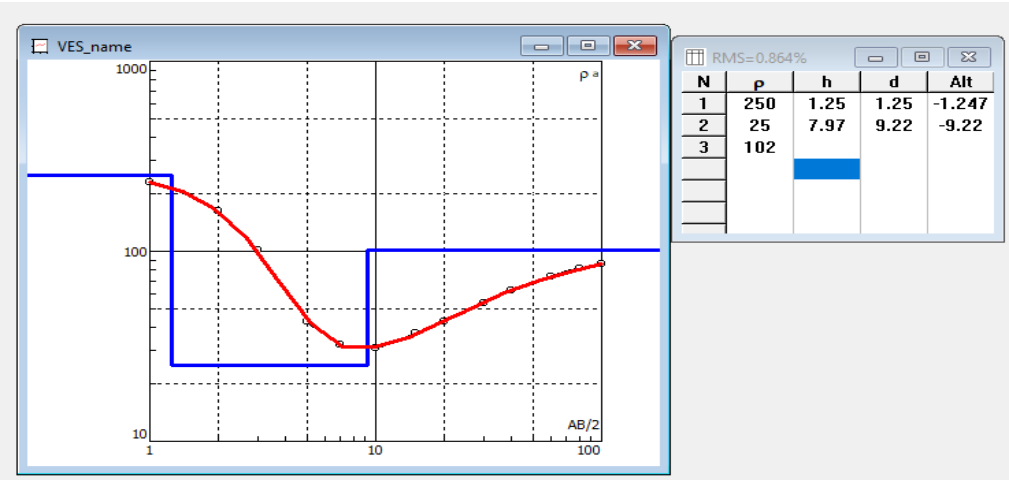
N	ρ	h	d	Alt
1	984	0.503	0.503	-0.503
2	124	2.66	3.16	-3.163
3	1168			

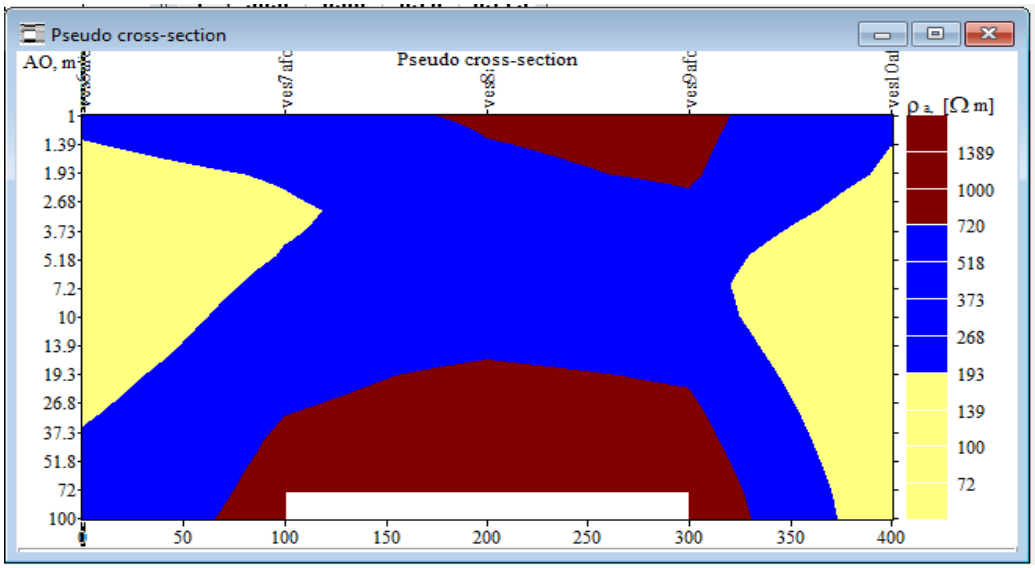


RMS=3.32%

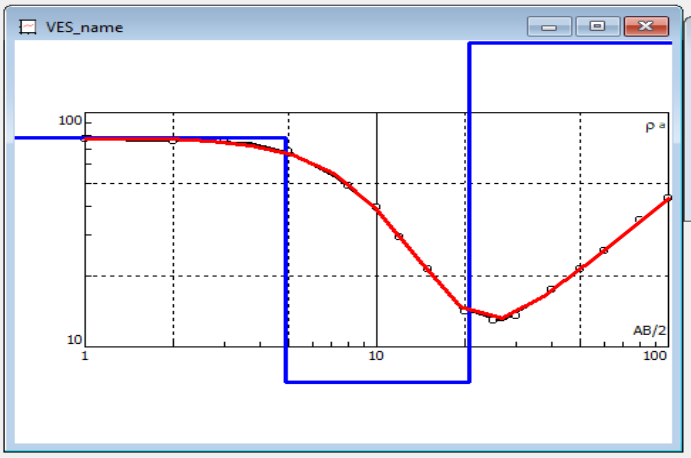
N	ρ	h	d	Alt
1	933	1.08	1.08	-1.08
2	145	2.39	3.47	-3.47
3	2873			


VES_name
10000
1000
100
ρ a
AB/2
1
10
100
RMS=0.904%
N ρ h d Alt
1 989 1.66 1.66 -1.659
2 130 3.1 4.76 -4.761
3 3092


VES_name
1000
100
10
ρ a
AB/2
1
10
100
RMS=0.864%
N ρ h d Alt
1 250 1.25 1.25 -1.247
2 25 7.97 9.22 -9.22
3 102

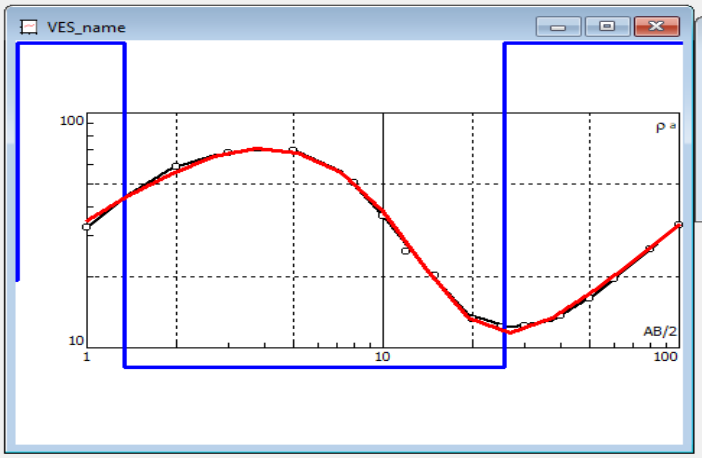

Pseudo cross-section
Pseudo cross-section
AO, m
ρ a, [Ω m]
1389
1000
720
518
373
268
193
139
100
72
1
1.39
1.93
2.68
3.73
5.18
7.2
10
13.9
19.3
26.8
37.3
51.8
72
100
50
100
150
200
250
300
350
400

ALAPAKOETILE



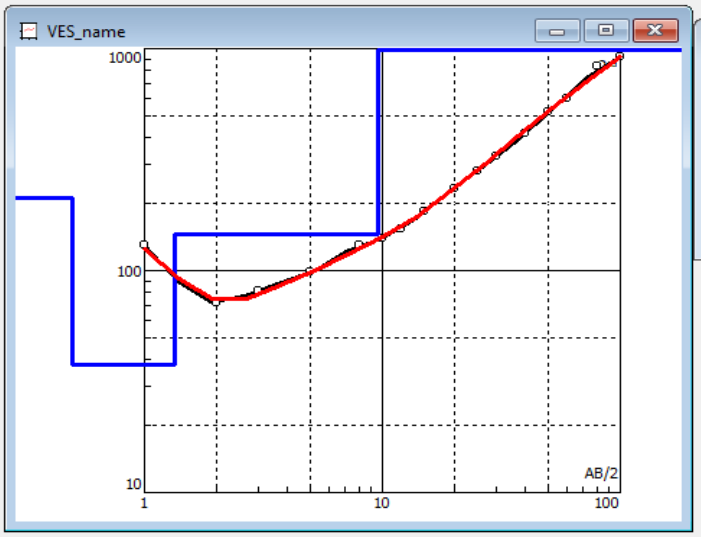
RMS=1.26%

N	ρ	h	d	Alt
1	77.7	4.89	4.89	-4.889
2	7.08	16	20.9	-20.86
3	6973			



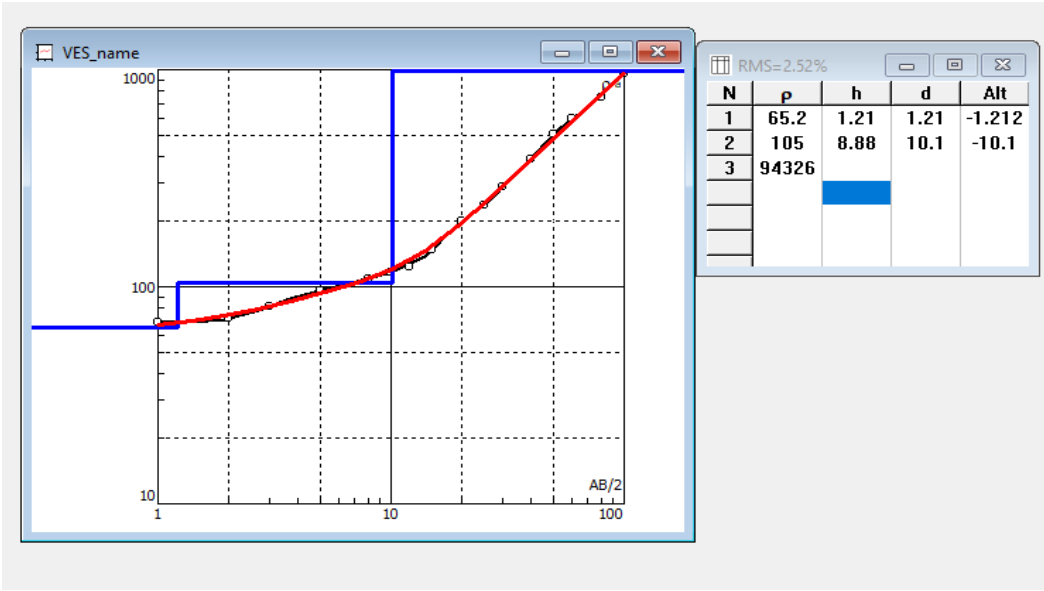
RMS=3.3%

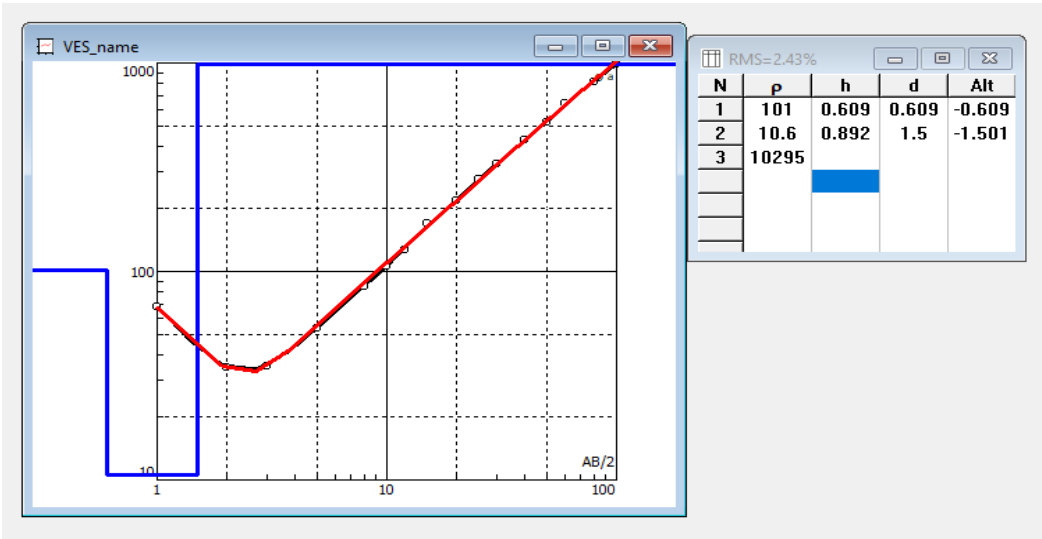
N	ρ	h	d	Alt
1	19.4	0.5	0.5	-0.5
2	359	0.836	1.34	-1.336
3	8.27	24.4	25.7	-25.74
4	2311			

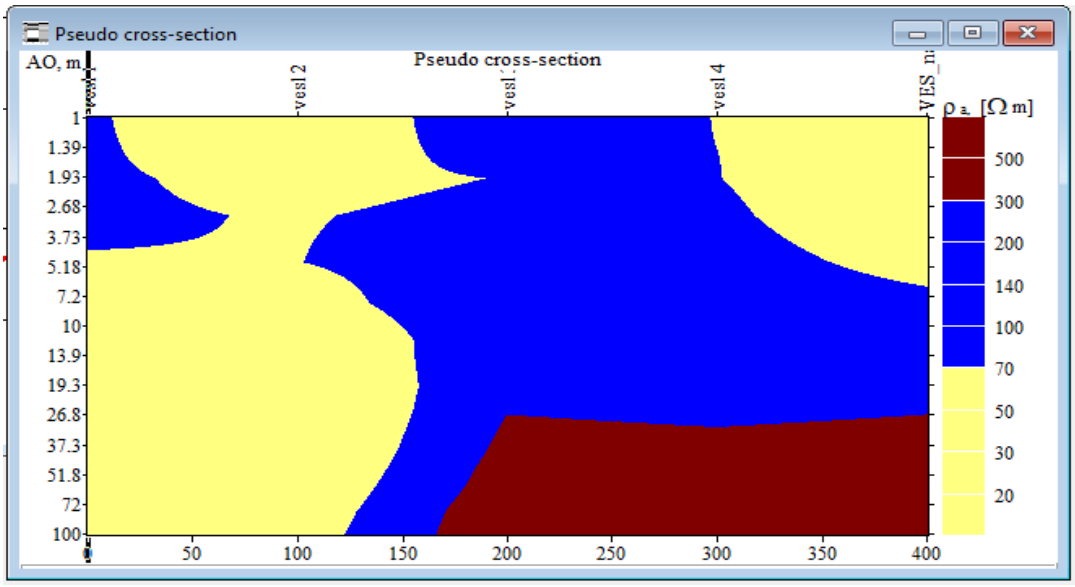


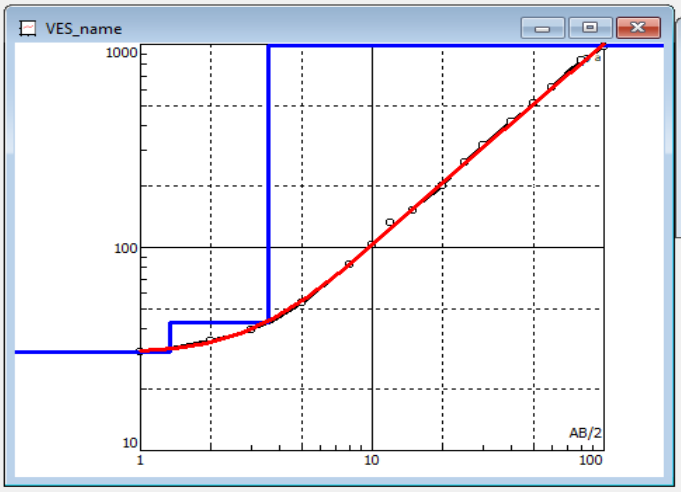
RMS=2.87%

N	ρ	h	d	Alt
1	211	0.5	0.5	-0.5
2	37.6	0.836	1.34	-1.336
3	145	8.31	9.65	-9.646
4	3210			


VES_name
1000
100
10
1
10
100
AB/2
RMS=2.52%
N ρ h d Alt
1 65.2 1.21 1.21 -1.212
2 105 8.88 10.1 -10.1
3 94326

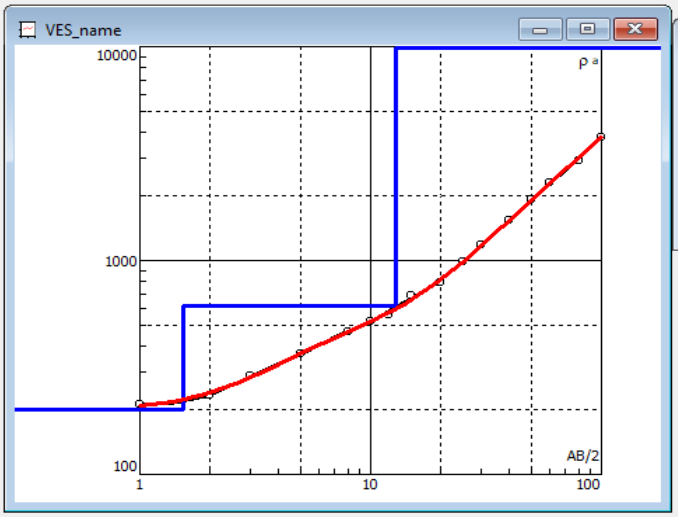

VES_name
1000
100
10
1
10
100
AB/2
RMS=2.43%
N ρ h d Alt
1 101 0.609 0.609 -0.609
2 10.6 0.892 1.5 -1.501
3 10295


Pseudo cross-section
AO, m
Pseudo cross-section
vesl 2
vesl
vesl 4
VES_n
ρ a, [Ω m]
500
300
200
140
100
70
50
30
20
1
1.39
1.93
2.68
3.73
5.18
7.2
10
13.9
19.3
26.8
37.3
51.8
72
100
50
100
150
200
250
300
350
400



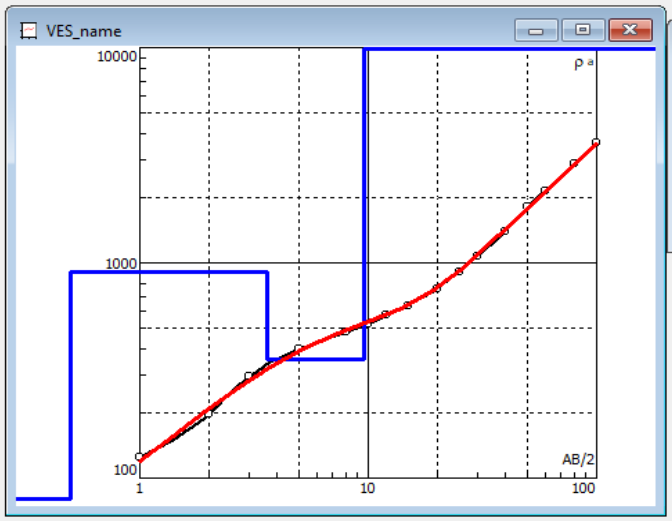
RMS=2.12%

N	ρ	h	d	Alt
1	30.4	1.34	1.34	-1.34
2	42.5	2.23	3.57	-3.57
3	32866			



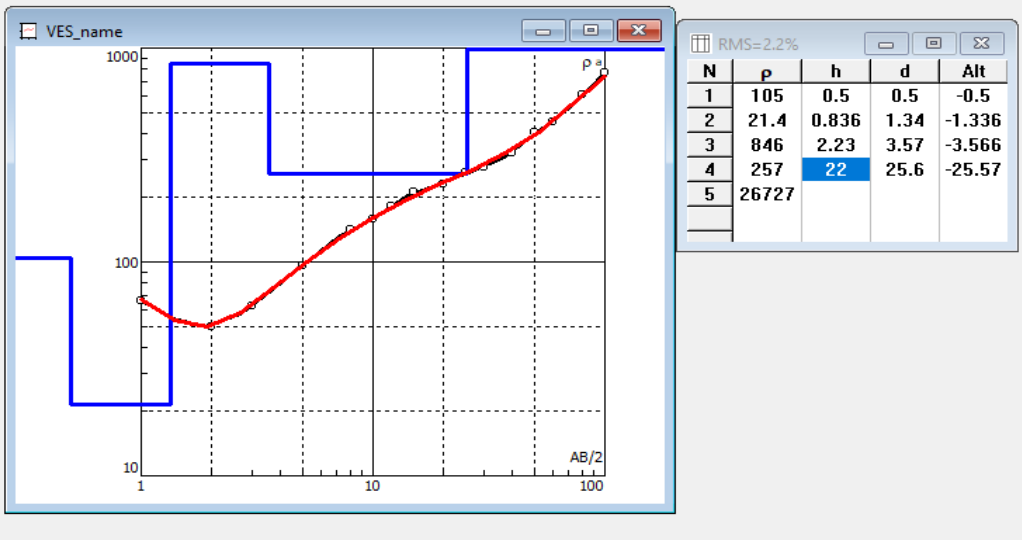
RMS=1.35%

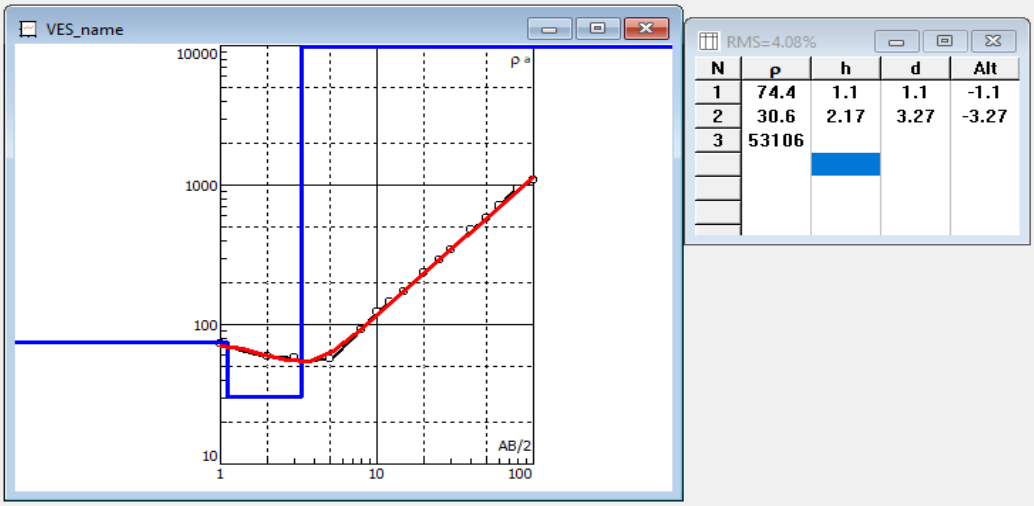
N	ρ	h	d	Alt
1	202	1.54	1.54	-1.542
2	616	11.2	12.8	-12.78
3	163195			

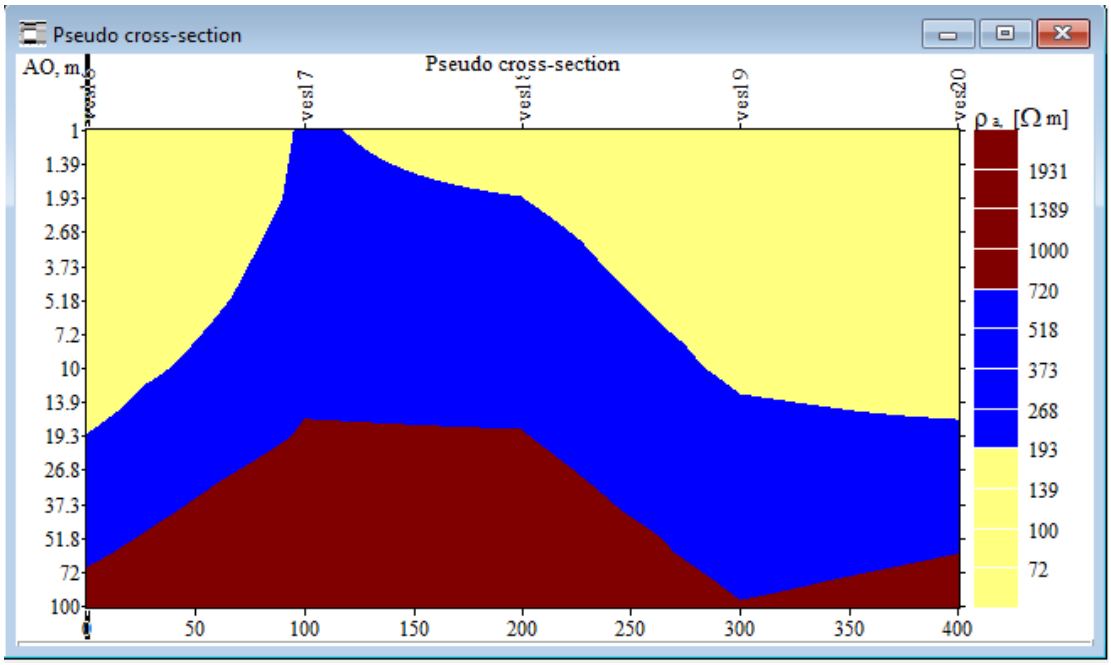


RMS=3.15%

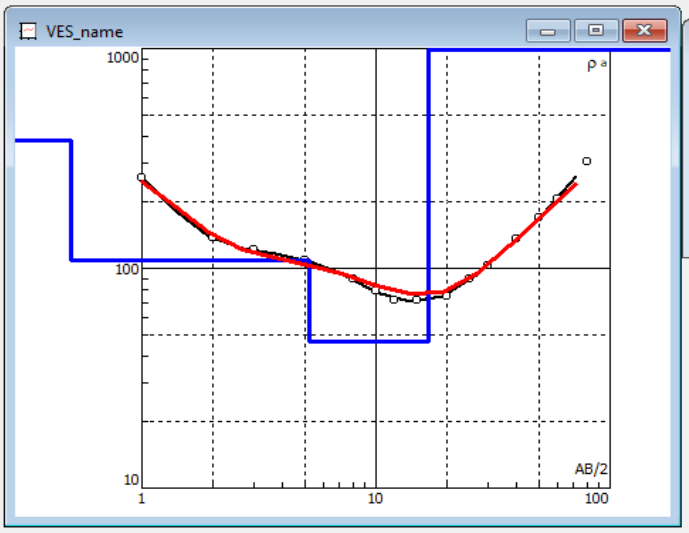
N	ρ	h	d	Alt
1	65.9	0.5	0.5	-0.5
2	912	3.09	3.59	-3.59
3	354	5.96	9.55	-9.55
4	224740			


VES_name
ρ a
1000
100
10
1
10
100
AB/2
RMS=2.2%
N ρ h d Alt
1 105 0.5 0.5 -0.5
2 21.4 0.836 1.34 -1.336
3 846 2.23 3.57 -3.566
4 257 22 25.6 -25.57
5 26727


VES_name
ρ a
10000
1000
100
10
1
10
100
AB/2
RMS=4.08%
N ρ h d Alt
1 74.4 1.1 1.1 -1.1
2 30.6 2.17 3.27 -3.27
3 53106

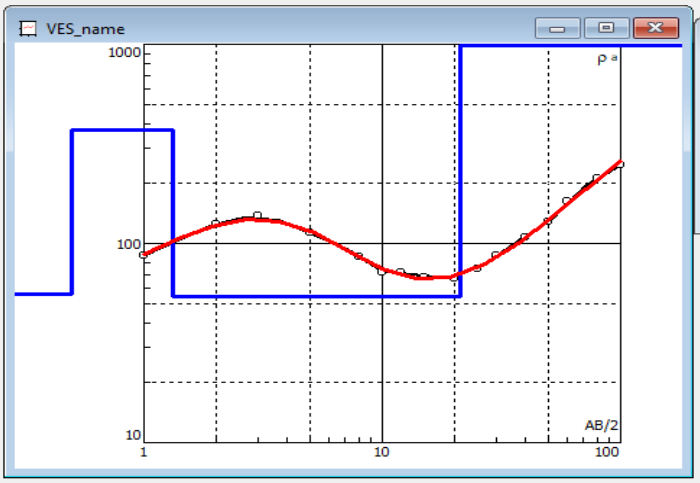

Pseudo cross-section
Pseudo cross-section
AO, m
vesl 7
vesl 9
ves20
ρ a [Ω m]
1931
1389
1000
720
518
373
268
193
139
100
72
1
1.39
1.93
2.68
3.73
5.18
7.2
10
13.9
19.3
26.8
37.3
51.8
72
100
50
100
150
200
250
300
350
400

ALOBA



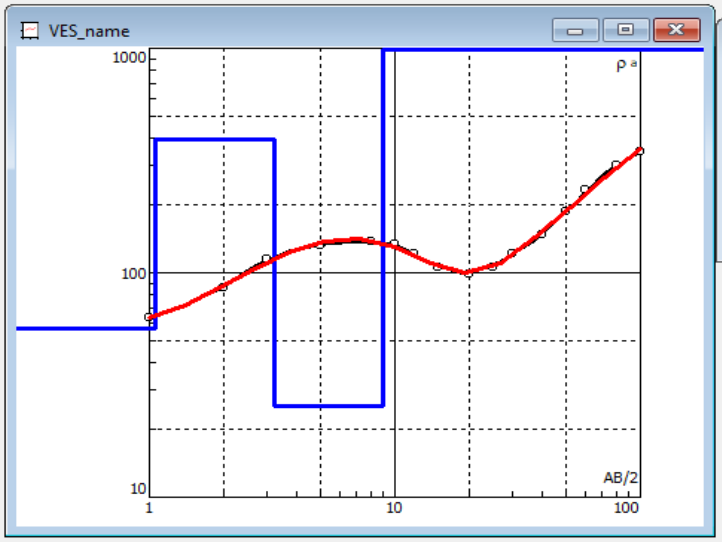
RMS=4.61%

N	ρ	h	d	Alt
1	382	0.5	0.5	-0.5
2	108	4.72	5.22	-5.22
3	46.3	11.6	16.8	-16.82
4	23134			



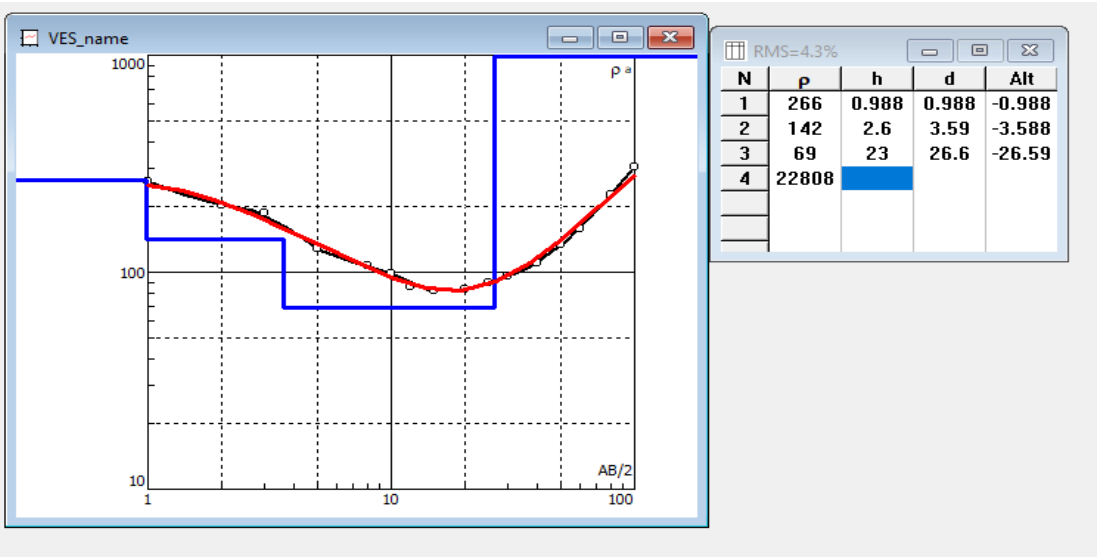
RMS=2.5%

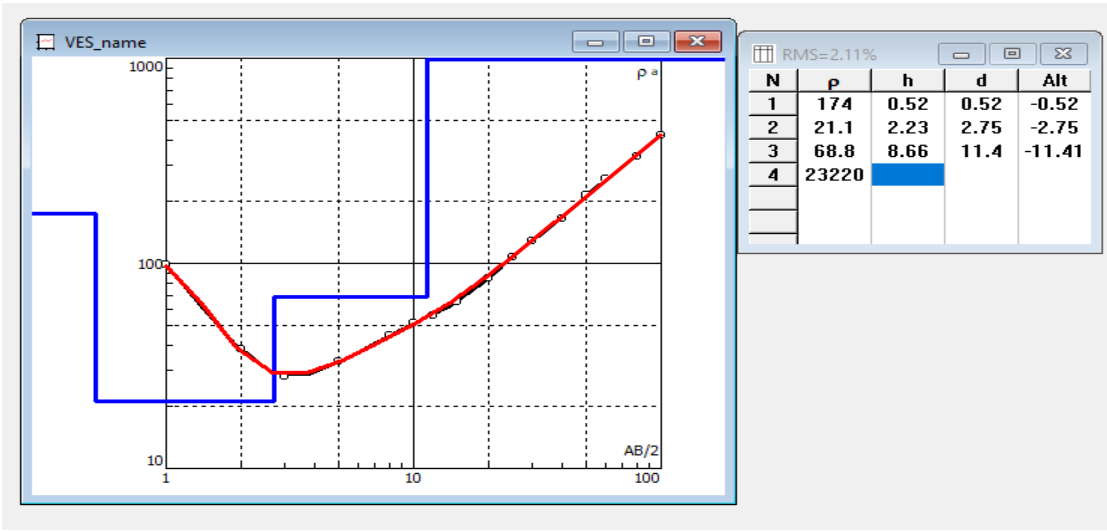
N	ρ	h	d	Alt
1	55.5	0.5	0.5	-0.5
2	371	0.817	1.32	-1.317
3	54.3	19.9	21.2	-21.22
4	10367			

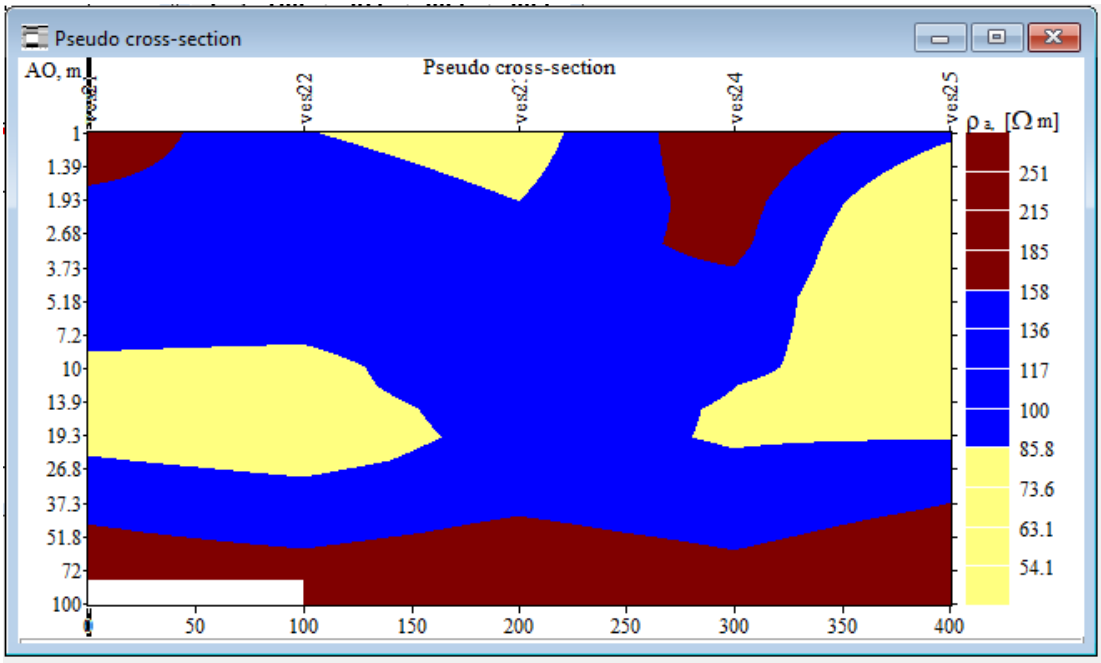


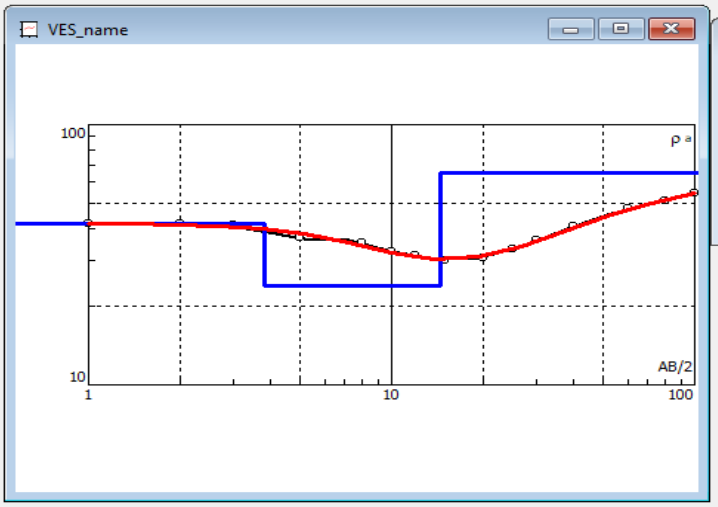
RMS=2.19%

N	ρ	h	d	Alt
1	56.1	1.06	1.06	-1.06
2	391	2.17	3.23	-3.23
3	25.5	5.77	9	-9
4	3075			


VES_name
1000
100
10
1
10
100
ρ a
AB/2
RMS=4.3%
N ρ h d Alt
1 266 0.988 0.988 -0.988
2 142 2.6 3.59 -3.588
3 69 23 26.6 -26.59
4 22808

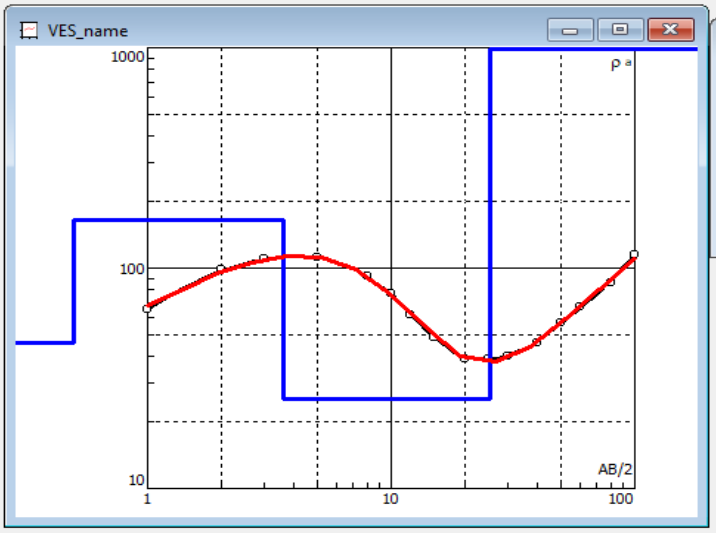

VES_name
1000
100
10
1
10
100
ρ a
AB/2
RMS=2.11%
N ρ h d Alt
1 174 0.52 0.52 -0.52
2 21.1 2.23 2.75 -2.75
3 68.8 8.66 11.4 -11.41
4 23220


Pseudo cross-section
Pseudo cross-section
AO, m
ves22
ves24
ves25
ρ a [Ω m]
1
1.39
1.93
2.68
3.73
5.18
7.2
10
13.9
19.3
26.8
37.3
51.8
72
100
50
100
150
200
250
300
350
400
251
215
185
158
136
117
100
85.8
73.6
63.1
54.1



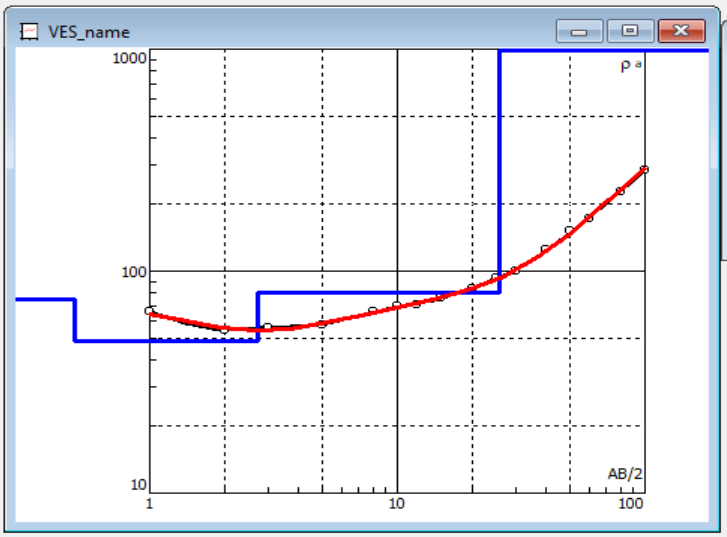
RMS=1.46%

N	ρ	h	d	Alt
1	41.6	3.81	3.81	-3.805
2	23.9	10.7	14.5	-14.53
3	65.2			



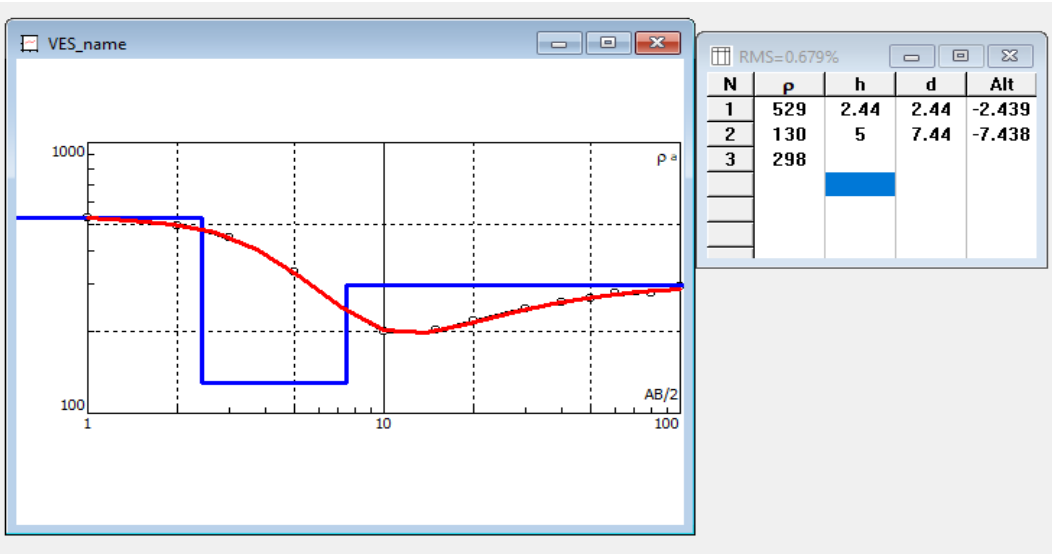
RMS=2.21%

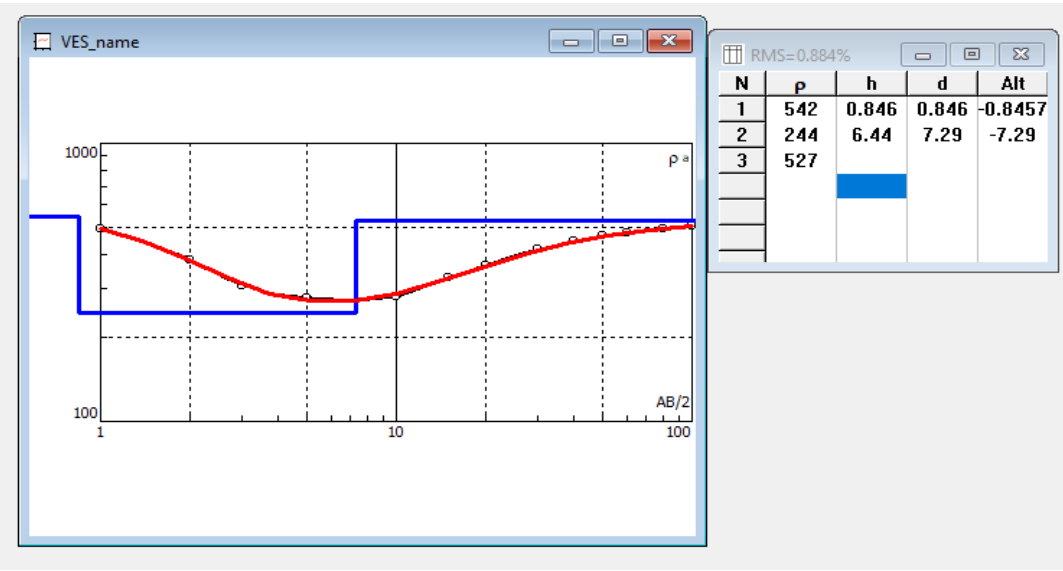
N	ρ	h	d	Alt
1	46	0.5	0.5	-0.5
2	166	3.11	3.61	-3.61
3	25.6	21.9	25.5	-25.51
4	5839			

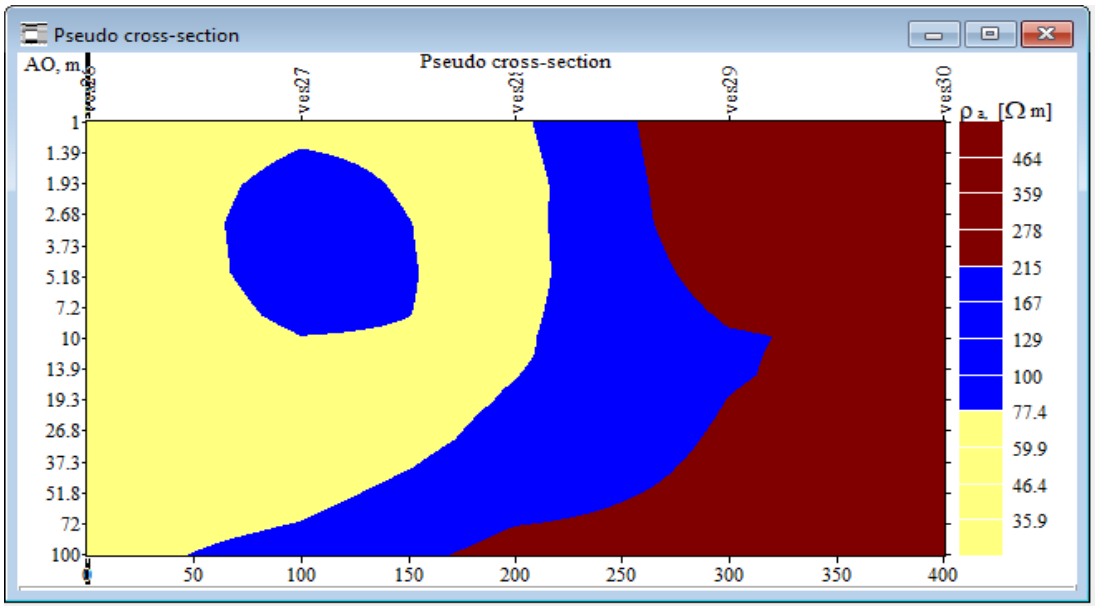


RMS=1.51%

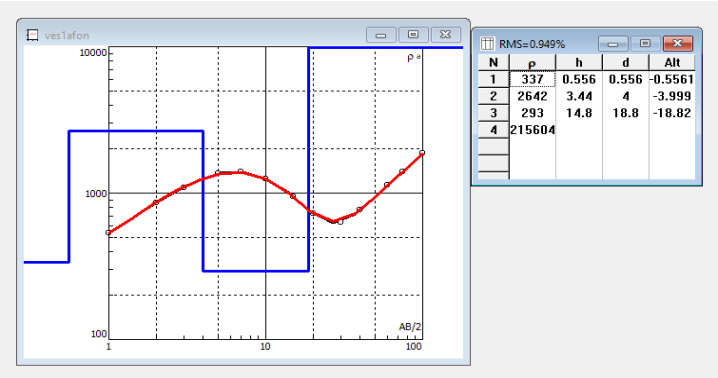
N	ρ	h	d	Alt
1	75	0.5	0.5	-0.5
2	48.5	2.24	2.74	-2.739
3	80.2	23	25.8	-25.77
4	11662			


VES_name
1000
100
ρ a
AB/2
1
10
100
RMS=0.679%
N ρ h d Alt
1 529 2.44 2.44 -2.439
2 130 5 7.44 -7.438
3 298

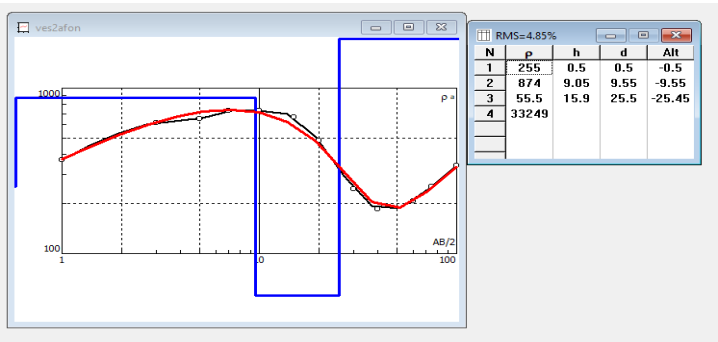

VES_name
1000
100
ρ a
AB/2
1
10
100
RMS=0.884%
N ρ h d Alt
1 542 0.846 0.846 -0.8457
2 244 6.44 7.29 -7.29
3 527


Pseudo cross-section
Pseudo cross-section
AO, m
ves27
ves28
ves29
ves30
1
1.39
1.93
2.68
3.73
5.18
7.2
10
13.9
19.3
26.8
37.3
51.8
72
100
50
100
150
200
250
300
350
400
ρ a [Ω m]
464
359
278
215
167
129
100
77.4
59.9
46.4
35.9

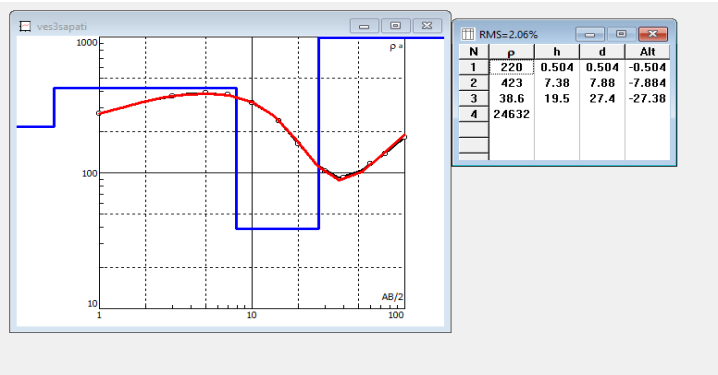
AFON



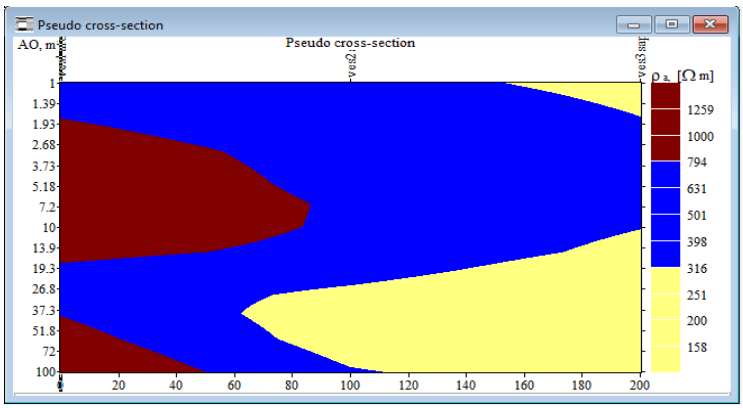
N	ρ	h	d	Alt
1	337	0.556	0.556	-0.5561
2	2642	3.44	4	-3.999
3	293	14.8	18.8	-18.82
4	215604			



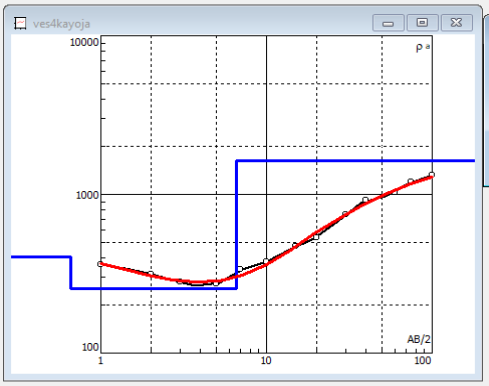
N	ρ	h	d	Alt
1	255	0.5	0.5	-0.5
2	874	9.05	9.55	-9.55
3	55.5	15.9	25.5	-25.45
4	33249			



N	ρ	h	d	Alt
1	220	0.504	0.504	-0.504
2	423	7.38	7.88	-7.884
3	38.6	19.5	27.4	-27.38
4	24632			

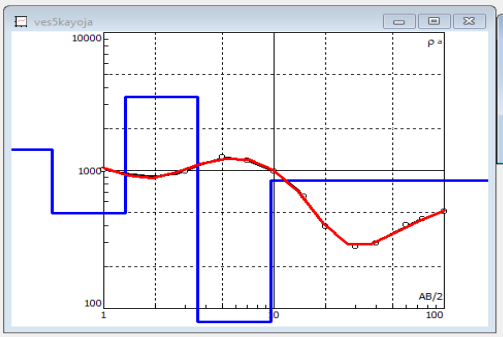


KAYOJA



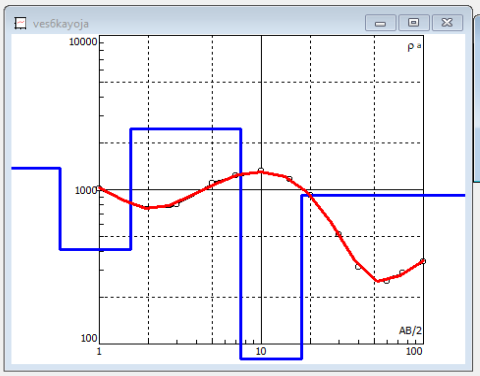
RMS=3.72%

N	ρ	h	d	Alt
1	402	0.662	0.662	-0.662
2	255	5.95	6.61	-6.612
3	1633			



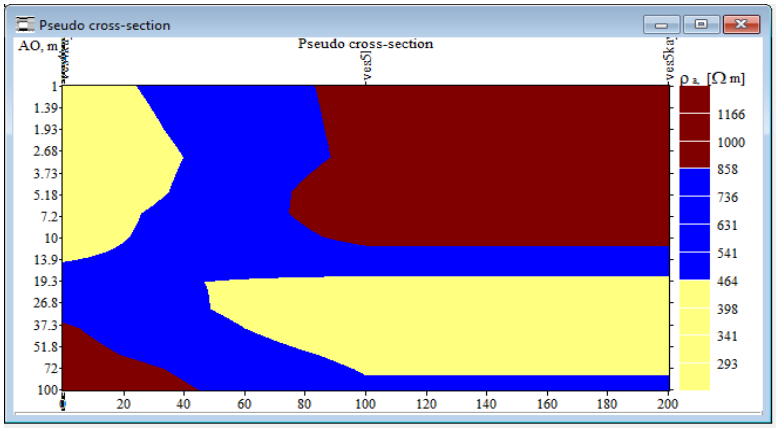
RMS=2.14%

N	ρ	h	d	Alt
1	1427	0.5	0.5	-0.5
2	493	0.836	1.34	-1.336
3	3434	2.23	3.57	-3.566
4	64.9	5.96	9.53	-9.526
5	844			

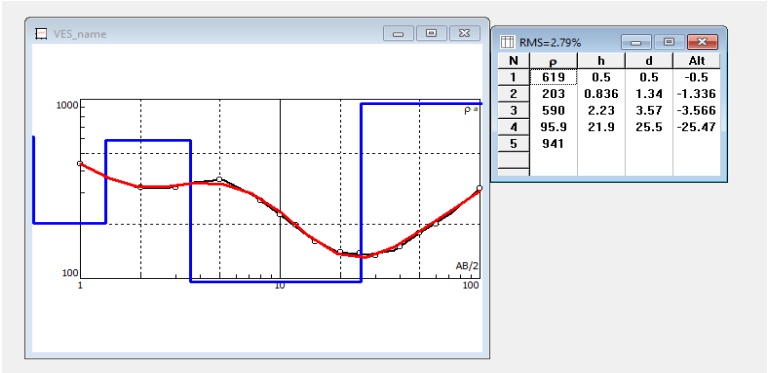


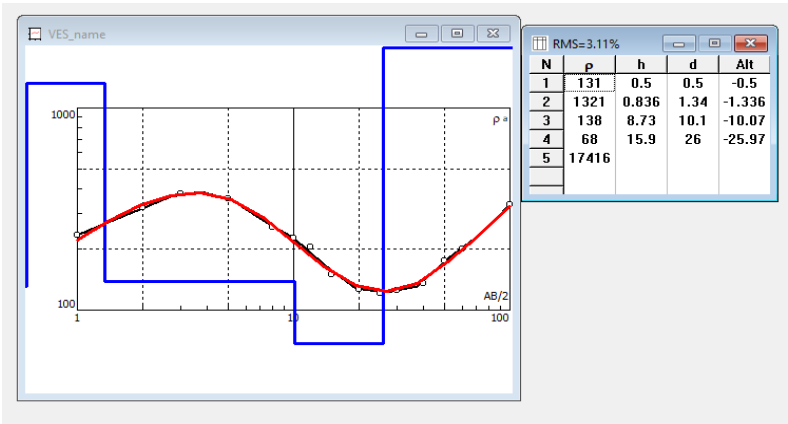
RMS=1.02%

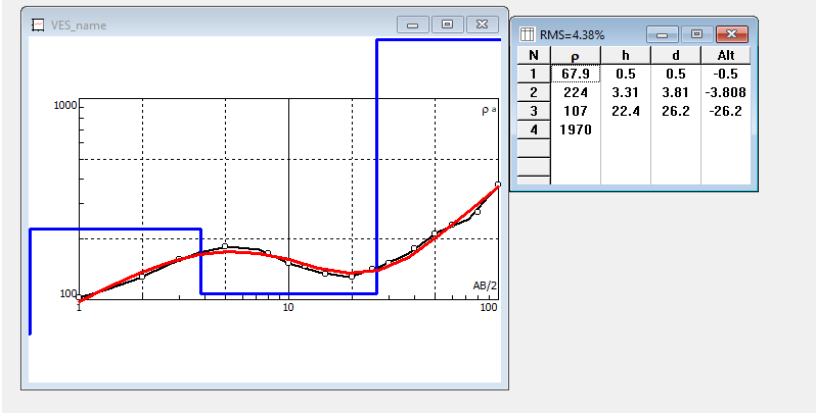
N	ρ	h	d	Alt
1	1377	0.568	0.568	-0.5683
2	409	0.984	1.55	-1.553
3	2488	5.95	7.5	-7.505
4	52.4	10.1	17.6	-17.6
5	922			

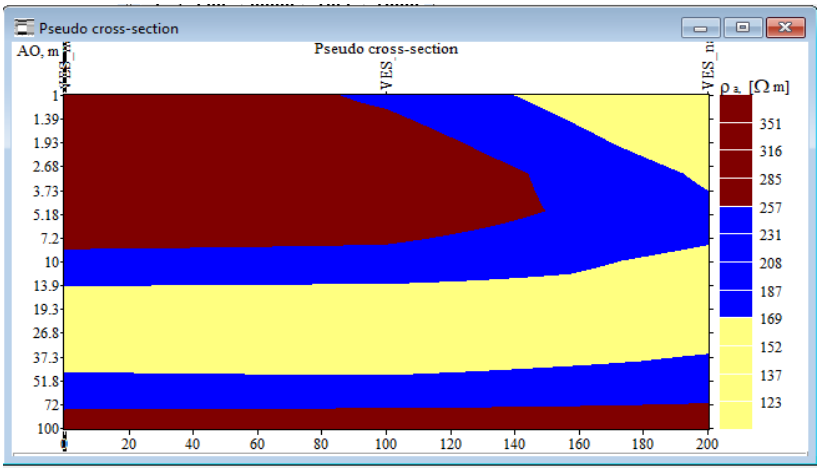


ONIYANGI

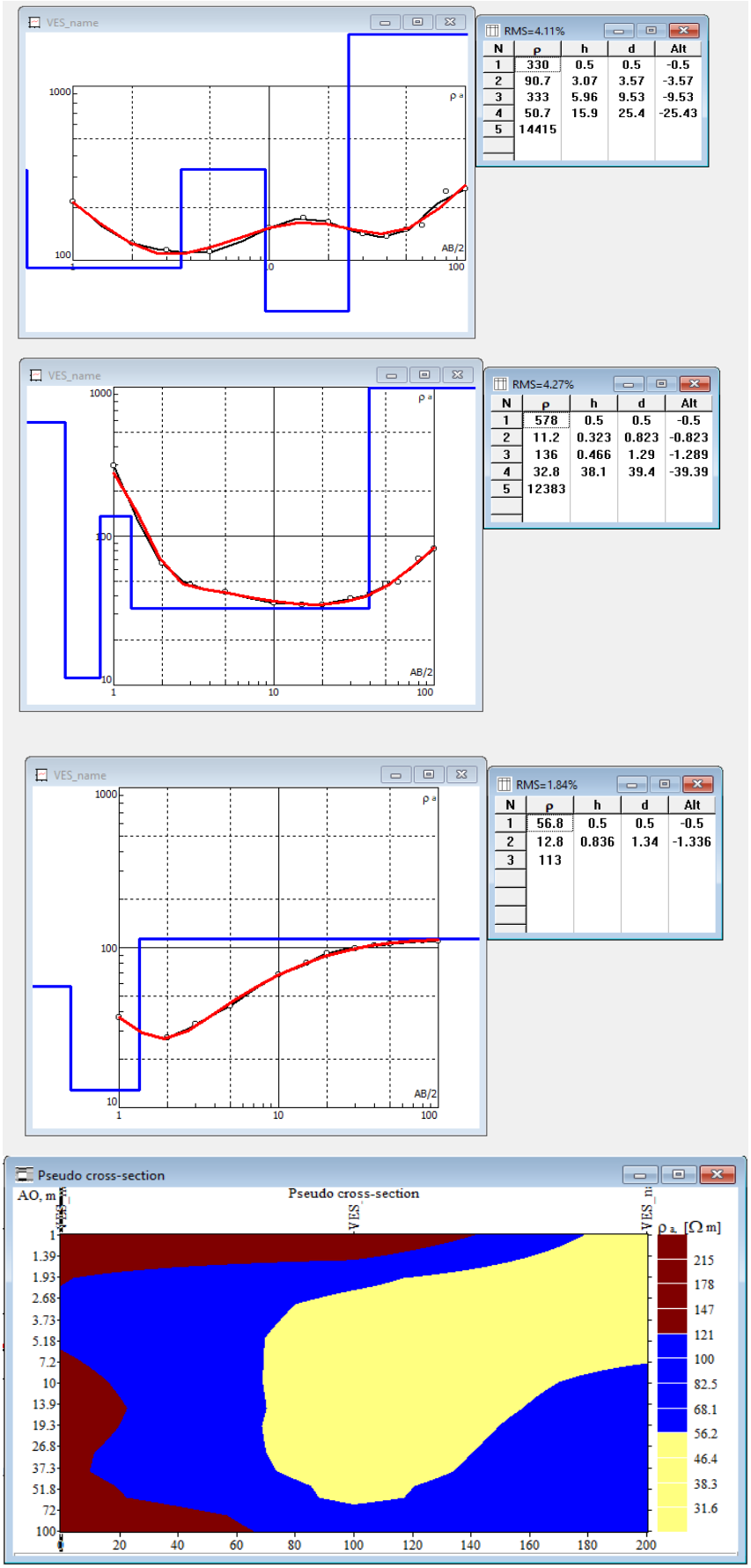

VES_name
RMS=2.79%
N ρ h d Alt
1 619 0.5 0.5 -0.5
2 203 0.836 1.34 -1.336
3 590 2.23 3.57 -3.566
4 95.9 21.9 25.5 -25.47
5 941
1000
100
1
10
100
AB/2


VES_name
RMS=3.11%
N ρ h d Alt
1 131 0.5 0.5 -0.5
2 1321 0.836 1.34 -1.336
3 138 8.73 10.1 -10.07
4 68 15.9 26 -25.97
5 17416
1000
100
1
10
100
AB/2

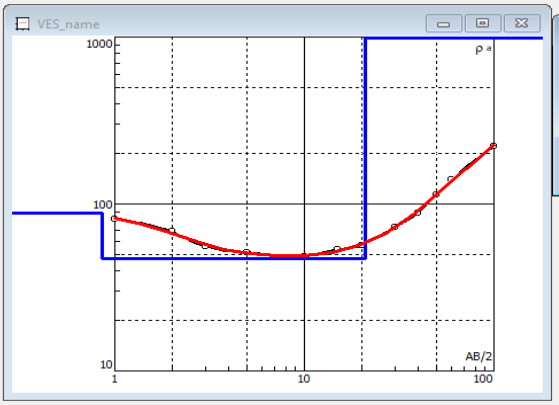

VES_name
RMS=4.38%
N ρ h d Alt
1 67.9 0.5 0.5 -0.5
2 224 3.31 3.81 -3.808
3 107 22.4 26.2 -26.2
4 1970
1000
100
1
10
100
AB/2


Pseudo cross-section
Pseudo cross-section
AO, m
VES
ρ a, [Ω m]
1
1.39
1.93
2.68
3.73
5.18
7.2
10
13.9
19.3
26.8
37.3
51.8
72
100
351
316
285
257
231
208
187
169
152
137
123
0
20
40
60
80
100
120
140
160
180
200

TERU

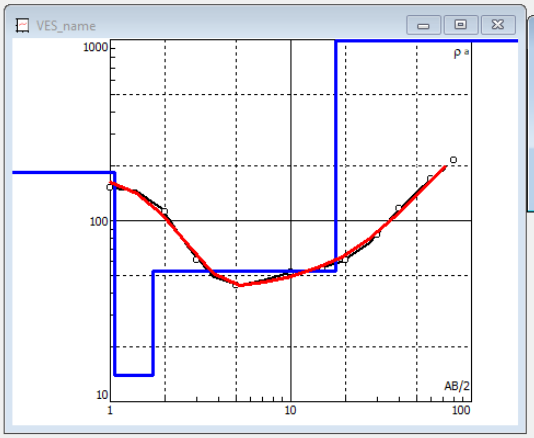

VES_name
ρ a
AB/2
RMS=4.11%
N ρ h d Alt
1 330 0.5 0.5 -0.5
2 90.7 3.07 3.57 -3.57
3 333 5.96 9.53 -9.53
4 50.7 15.9 25.4 -25.43
5 14415
VES_name
ρ a
AB/2
RMS=4.27%
N ρ h d Alt
1 578 0.5 0.5 -0.5
2 11.2 0.323 0.823 -0.823
3 136 0.466 1.29 -1.289
4 32.8 38.1 39.4 -39.39
5 12383
VES_name
ρ a
AB/2
RMS=1.84%
N ρ h d Alt
1 56.8 0.5 0.5 -0.5
2 12.8 0.836 1.34 -1.336
3 113
Pseudo cross-section
Pseudo cross-section
AO, m
VES
ρ a, [Ω m]
215
178
147
121
100
82.5
68.1
56.2
46.4
38.3
31.6

AGBOKU



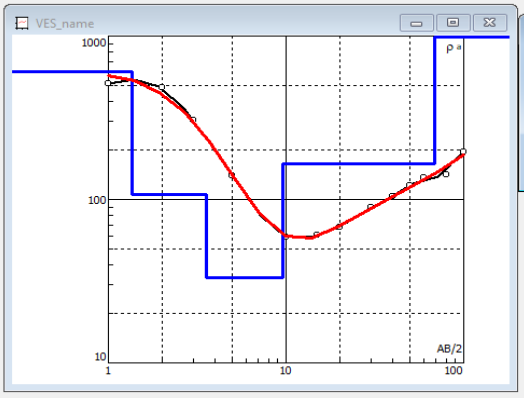
RMS=1.91%

N	ρ	h	d	Alt
1	88.7	0.853	0.853	-0.8525
2	47	20.1	21	-21
3	13096			



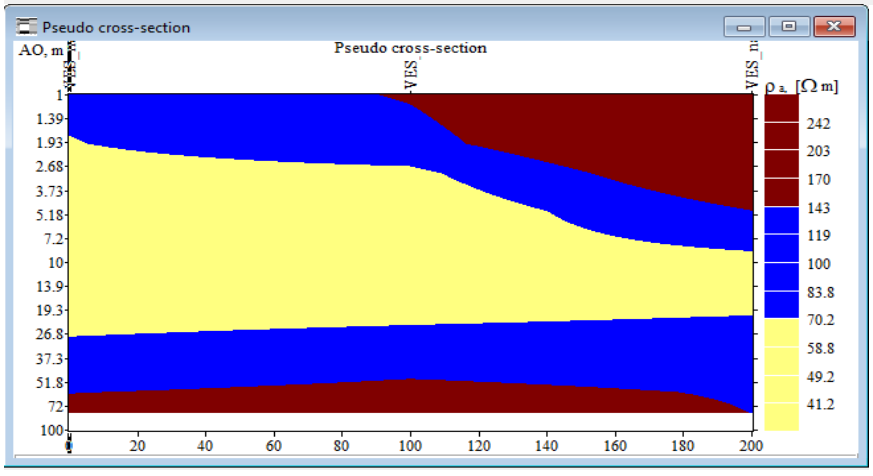
RMS=4.47%

N	ρ	h	d	Alt
1	184	1.06	1.06	-1.06
2	14	0.66	1.72	-1.72
3	52.7	16.1	17.8	-17.82
4	15671			

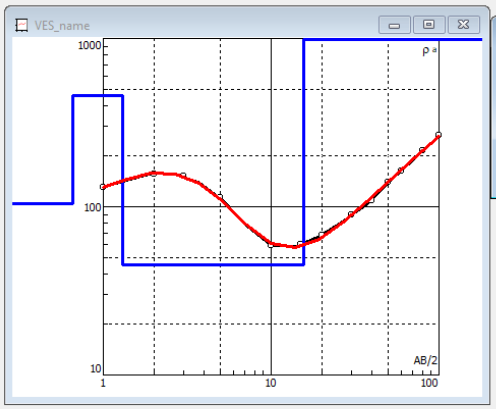


RMS=4.52%

N	ρ	h	d	Alt
1	605	1.35	1.35	-1.35
2	107	2.23	3.58	-3.58
3	33	5.96	9.54	-9.54
4	165	58.6	68.1	-68.14
5	15372			

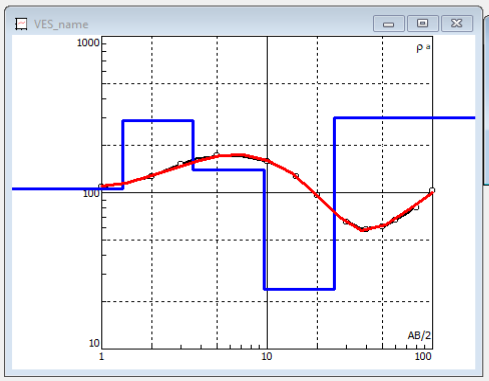


AROGUN



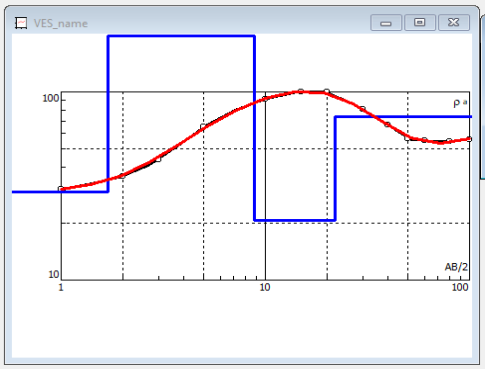
RMS=2.18%

N	ρ	h	d	Alt
1	105	0.659	0.659	-0.659
2	460	0.638	1.3	-1.297
3	44.9	14.4	15.7	-15.7
4	1644			



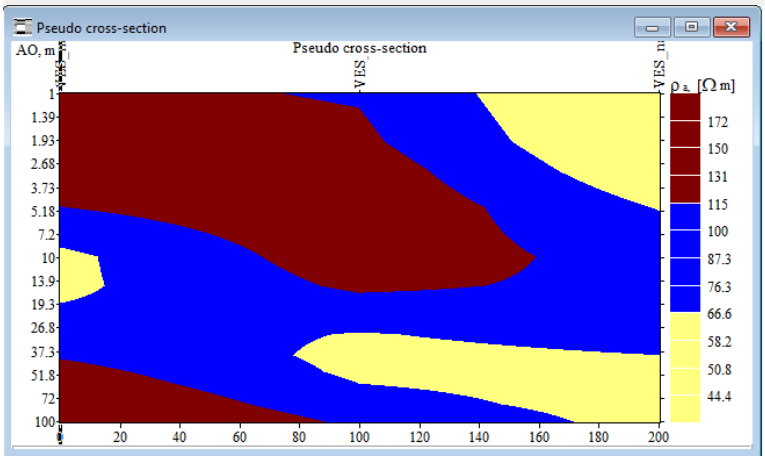
RMS=2.25%

N	ρ	h	d	Alt
1	106	1.34	1.34	-1.34
2	290	2.23	3.57	-3.57
3	140	5.96	9.53	-9.53
4	24	15.9	25.4	-25.43
5	301			

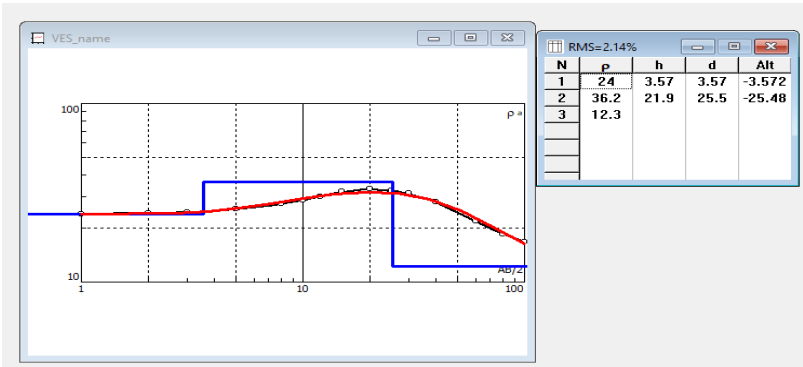


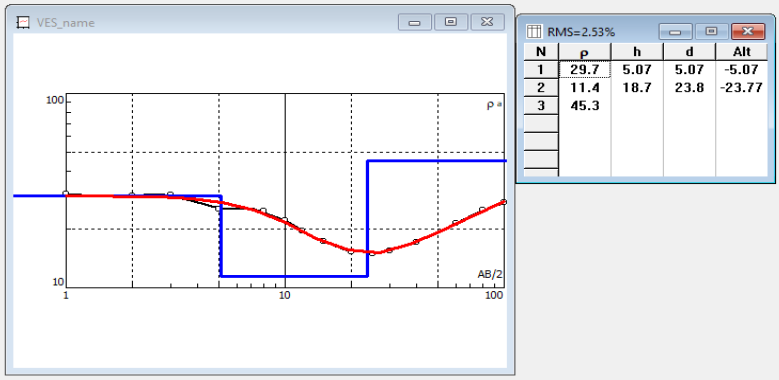
RMS=1.48%

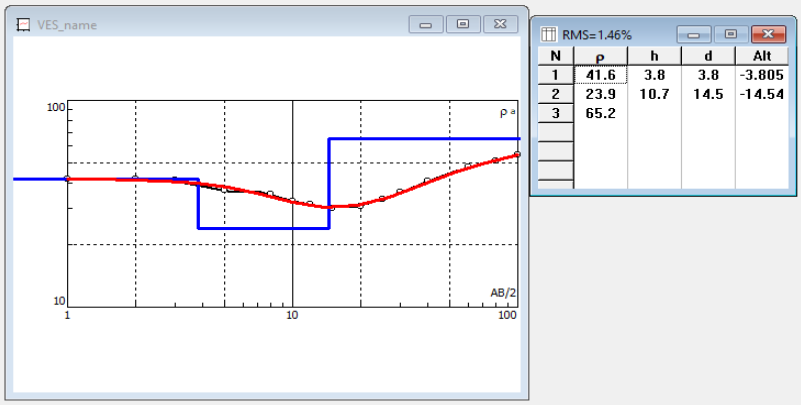
N	ρ	h	d	Alt
1	29.3	1.7	1.7	-1.695
2	213	7.18	8.87	-8.874
3	20.7	13.1	21.9	-21.94
4	74.1			

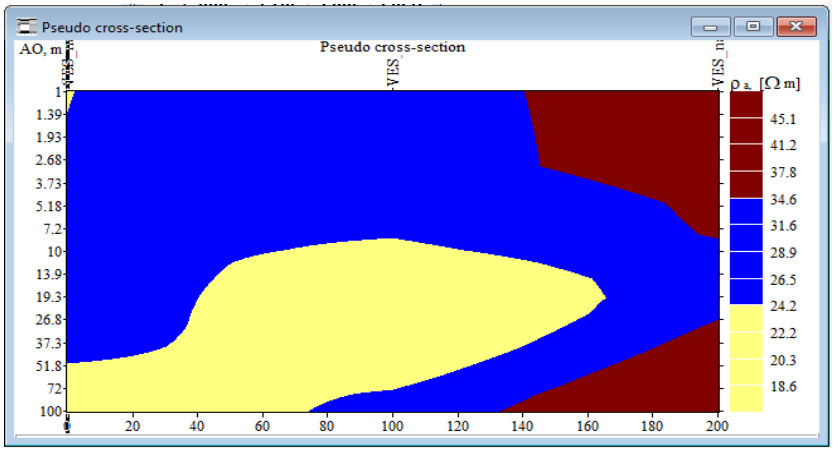


IDI AYAN

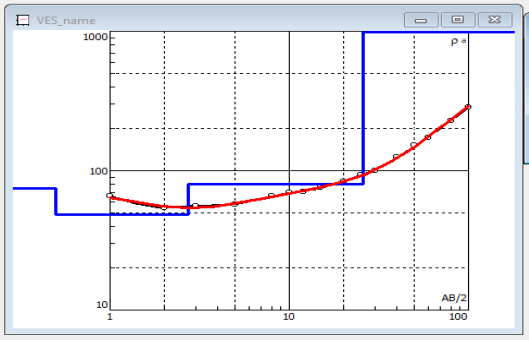

VES_name
RMS=2.14%
N ρ h d Alt
1 24 3.57 3.57 -3.572
2 36.2 21.9 25.5 -25.48
3 12.3
100
10
1
10
100
ρ a
AB/2


VES_name
RMS=2.53%
N ρ h d Alt
1 29.7 5.07 5.07 -5.07
2 11.4 18.7 23.8 -23.77
3 45.3
100
10
1
10
100
ρ a
AB/2


VES_name
RMS=1.46%
N ρ h d Alt
1 41.6 3.8 3.8 -3.805
2 23.9 10.7 14.5 -14.54
3 65.2
100
10
1
10
100
ρ a
AB/2

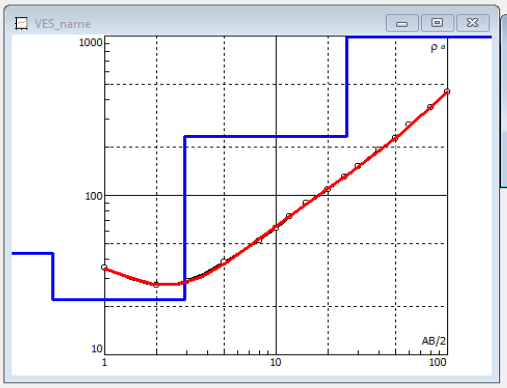

Pseudo cross-section
AO, m
Pseudo cross-section
VES_name
VES_m
ρ a [Ω m]
45.1
41.2
37.8
34.6
31.6
28.9
26.5
24.2
22.2
20.3
18.6
1
1.39
1.93
2.68
3.73
5.18
7.2
10
13.9
19.3
26.8
37.3
51.8
72
100
0
20
40
60
80
100
120
140
160
180
200

GBAJA



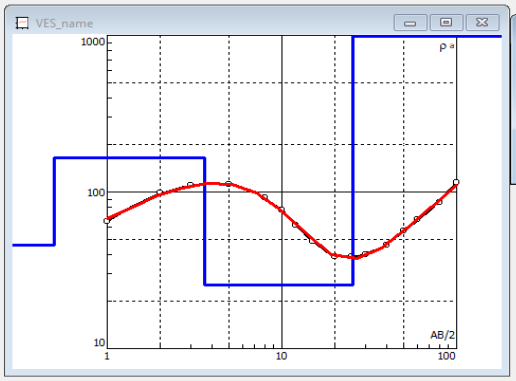
RMS=1.51%

N	ρ	h	d	Alt
1	75	0.5	0.5	-0.5
2	48.5	2.24	2.74	-2.739
3	80.2	23	25.8	-25.78
4	11662			



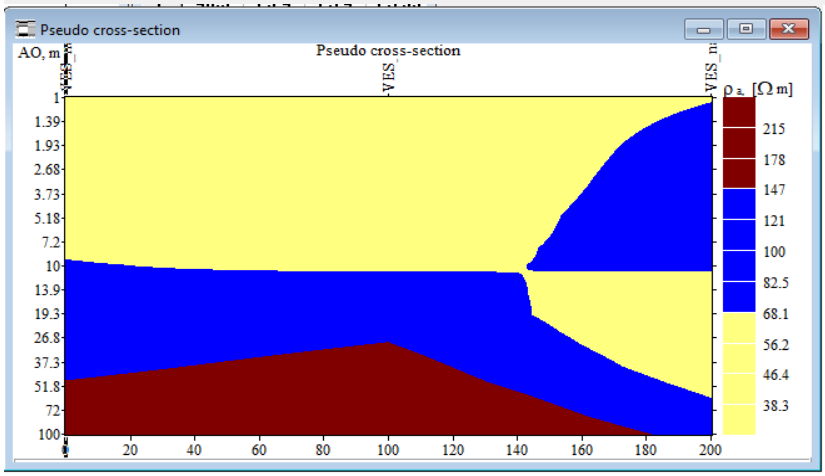
RMS=1.59%

N	ρ	h	d	Alt
1	43.5	0.5	0.5	-0.5
2	22.1	2.44	2.94	-2.936
3	234	22.7	25.7	-25.67
4	20782			

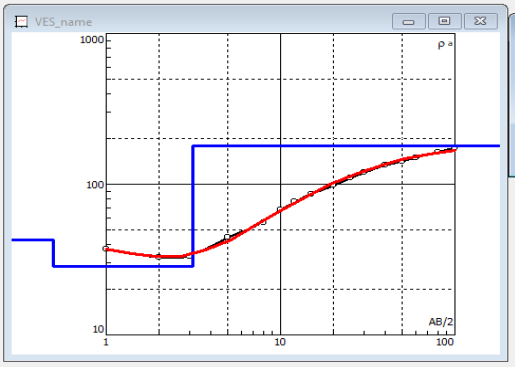


RMS=2.21%

N	ρ	h	d	Alt
1	46	0.5	0.5	-0.5
2	166	3.11	3.61	-3.61
3	25.6	21.9	25.5	-25.51
4	5839			

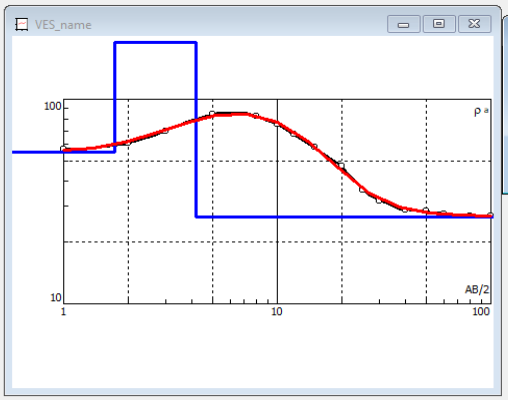


OKESO



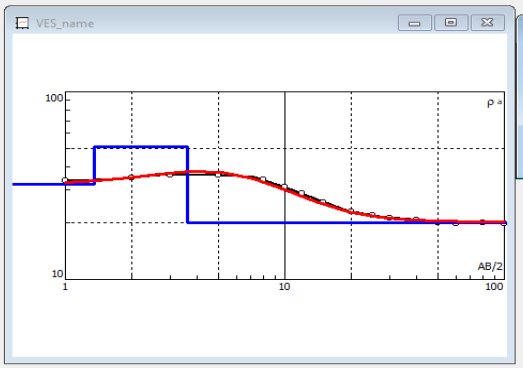
RMS=2.27%

N	ρ	h	d	Alt
1	42.9	0.5	0.5	-0.5
2	28.3	2.64	3.14	-3.14
3	180			



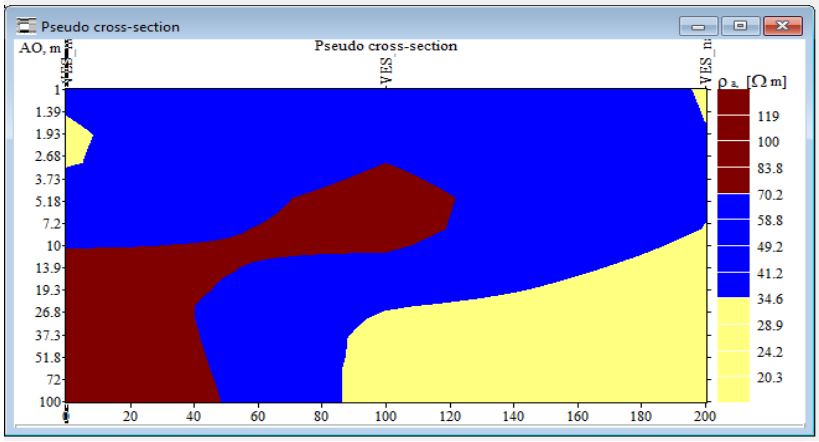
RMS=1.87%

N	ρ	h	d	Alt
1	55	1.74	1.74	-1.738
2	191	2.41	4.15	-4.147
3	26.4			

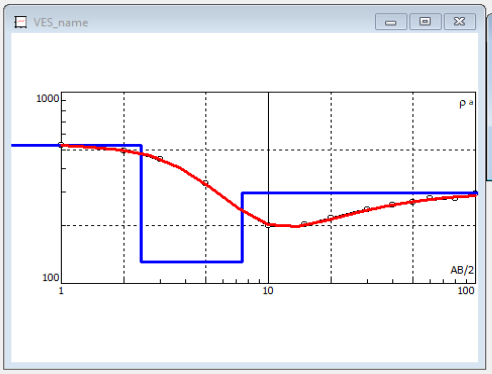


RMS=2.18%

N	ρ	h	d	Alt
1	32.3	1.35	1.35	-1.35
2	50.9	2.23	3.58	-3.58
3	20.1			

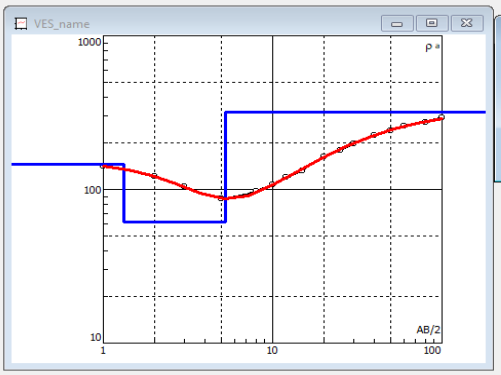


ILA



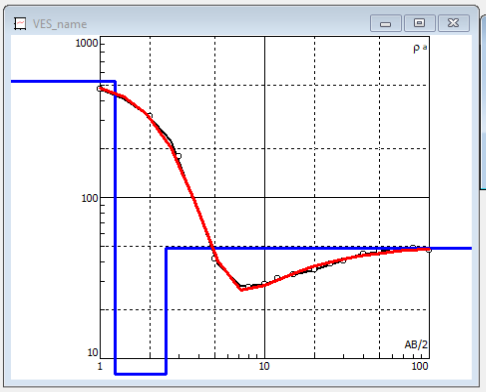
RMS=0.679%

N	ρ	h	d	Alt
1	529	2.44	2.44	-2.439
2	130	5	7.44	-7.439
3	298			



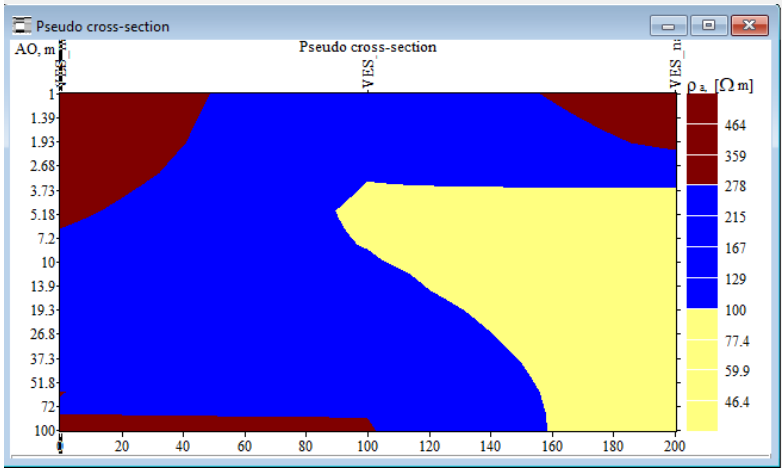
RMS=0.932%

N	ρ	h	d	Alt
1	146	1.32	1.32	-1.324
2	61.6	3.93	5.25	-5.253
3	320			

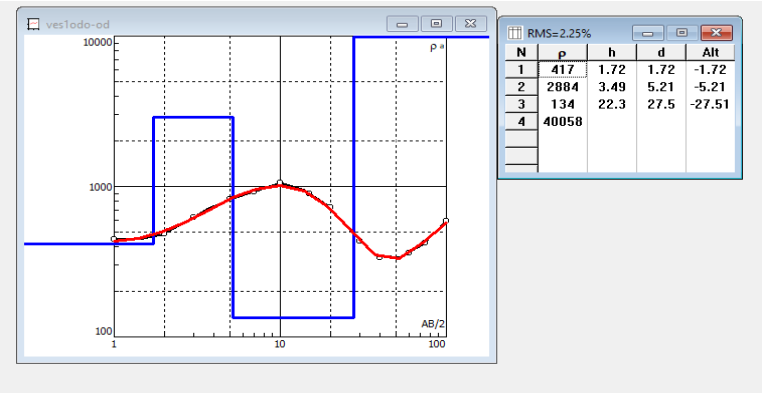


RMS=3.6%

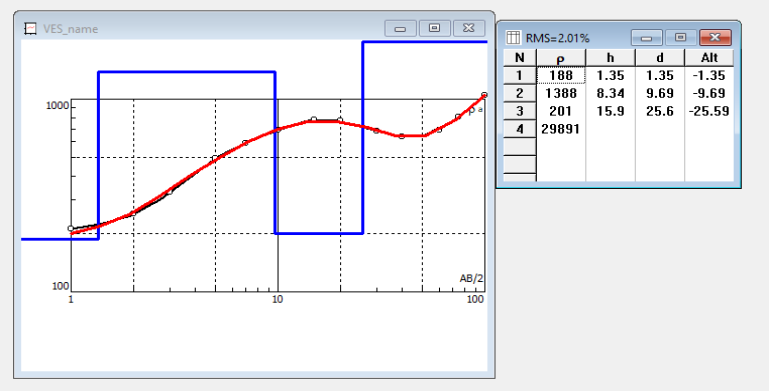
N	ρ	h	d	Alt
1	526	1.24	1.24	-1.24
2	6.97	1.28	2.52	-2.52
3	48.6			



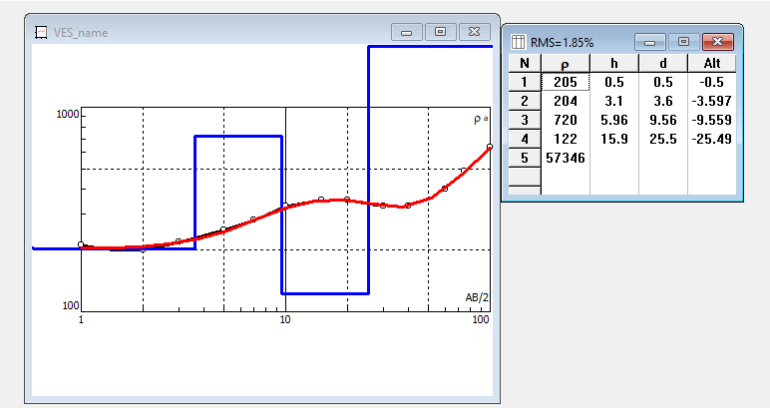
ODO ODE



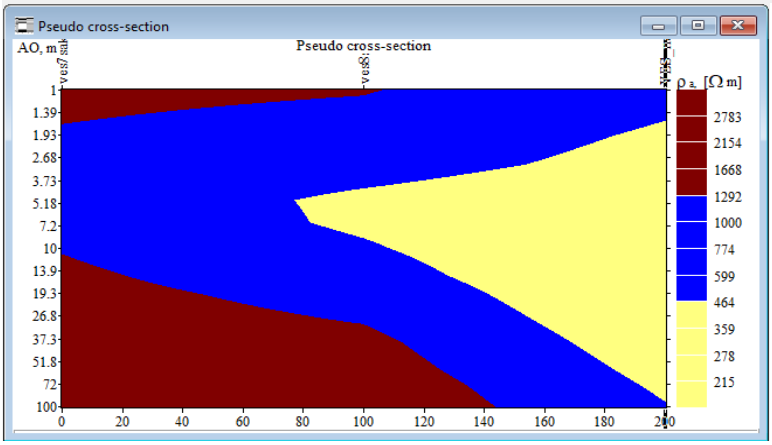
N	ρ	h	d	Alt
1	417	1.72	1.72	-1.72
2	2884	3.49	5.21	-5.21
3	134	22.3	27.5	-27.51
4	40058			



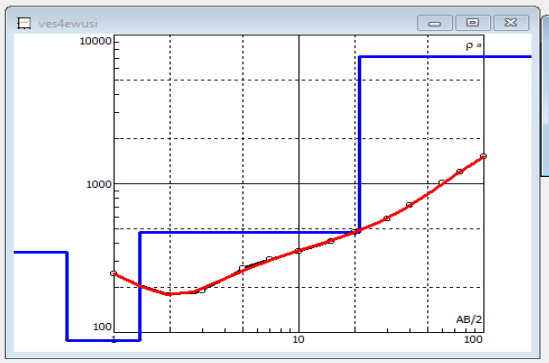
N	ρ	h	d	Alt
1	188	1.35	1.35	-1.35
2	1388	8.34	9.69	-9.69
3	201	15.9	25.6	-25.59
4	29891			



N	ρ	h	d	Alt
1	205	0.5	0.5	-0.5
2	204	3.1	3.6	-3.597
3	720	5.96	9.56	-9.559
4	122	15.9	25.5	-25.49
5	57346			

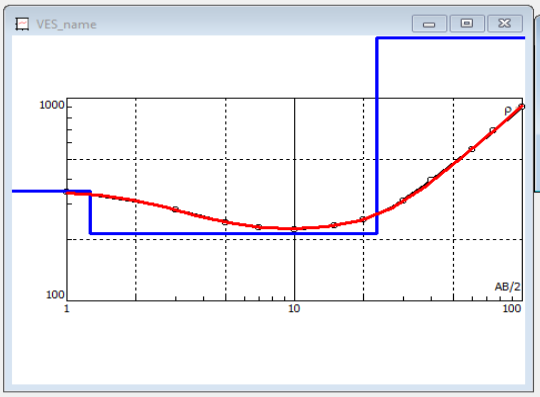


EWUSI



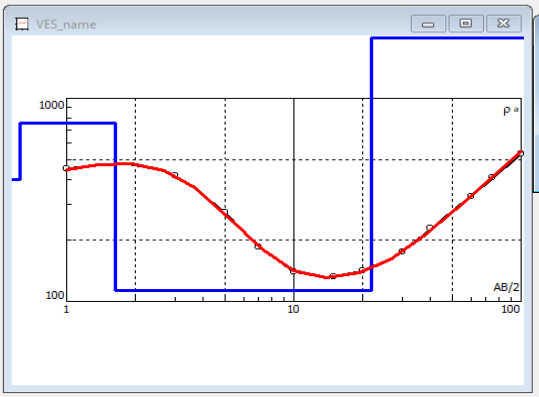
RMS=1.66%

N	ρ	h	d	Alt
1	348	0.558	0.558	-0.5582
2	88.7	0.818	1.38	-1.376
3	470	20	21.4	-21.38
4	7159			



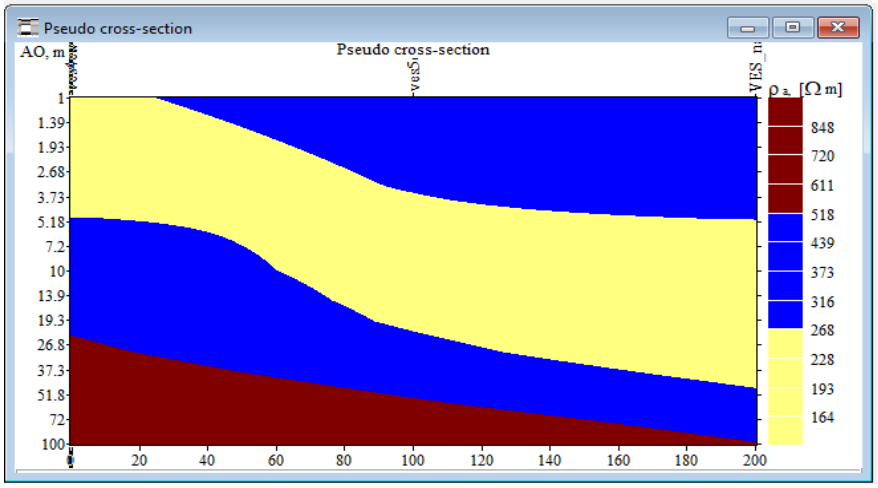
RMS=0.927%

N	ρ	h	d	Alt
1	349	1.27	1.27	-1.273
2	214	21.7	22.9	-22.94
3	22896			

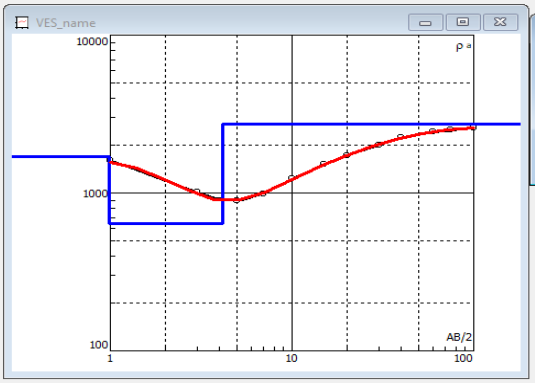


RMS=0.935%

N	ρ	h	d	Alt
1	400	0.627	0.627	-0.6265
2	758	1.01	1.63	-1.633
3	114	20.2	21.9	-21.86
4	28944			

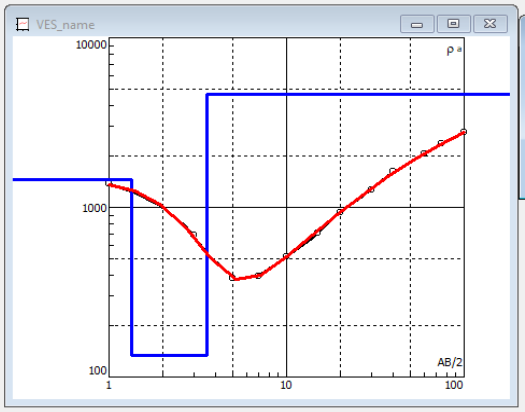


SAKAMO



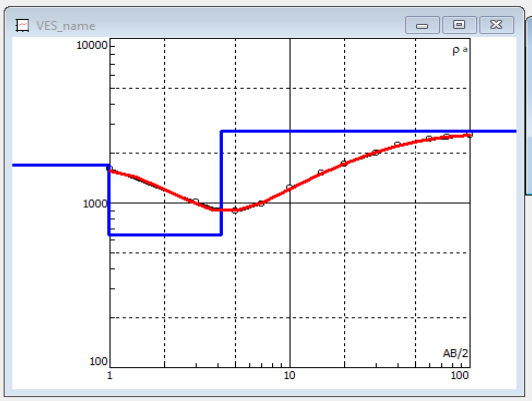
RMS=1.52%

N	ρ	h	d	Alt
1	1691	0.991	0.991	-0.9914
2	644	3.18	4.17	-4.169
3	2728			



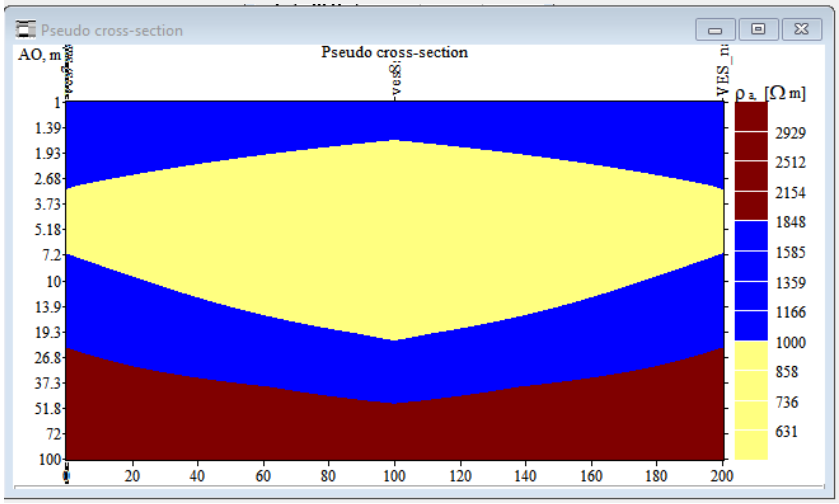
RMS=1.56%

N	ρ	h	d	Alt
1	1456	1.34	1.34	-1.336
2	134	2.23	3.57	-3.568
3	4620			

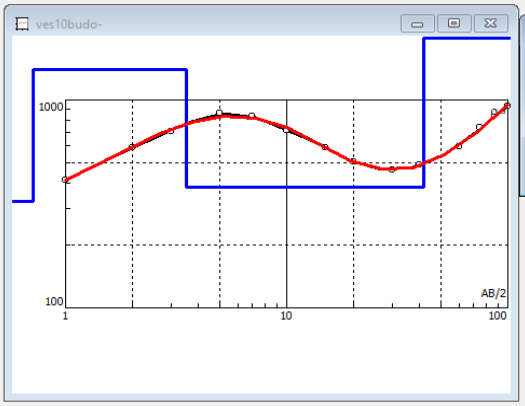


RMS=1.52%

N	ρ	h	d	Alt
1	1691	0.991	0.991	-0.9914
2	644	3.18	4.17	-4.169
3	2728			

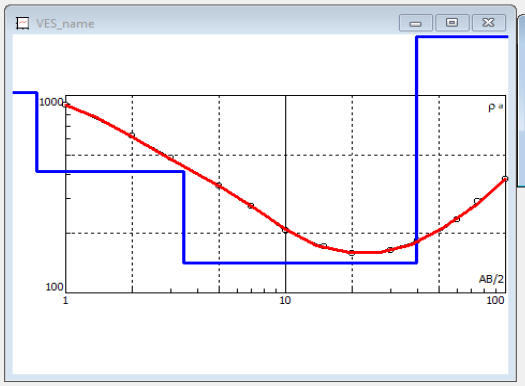


BUDO OMO



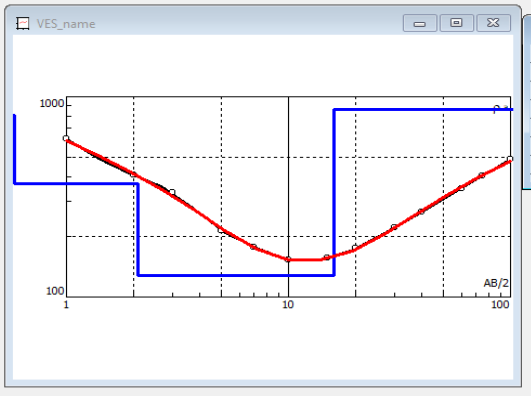
RMS=1.51%

N	ρ	h	d	Alt
1	325	0.718	0.718	-0.7176
2	1397	2.81	3.52	-3.524
3	381	38.3	41.8	-41.82
4	65628			



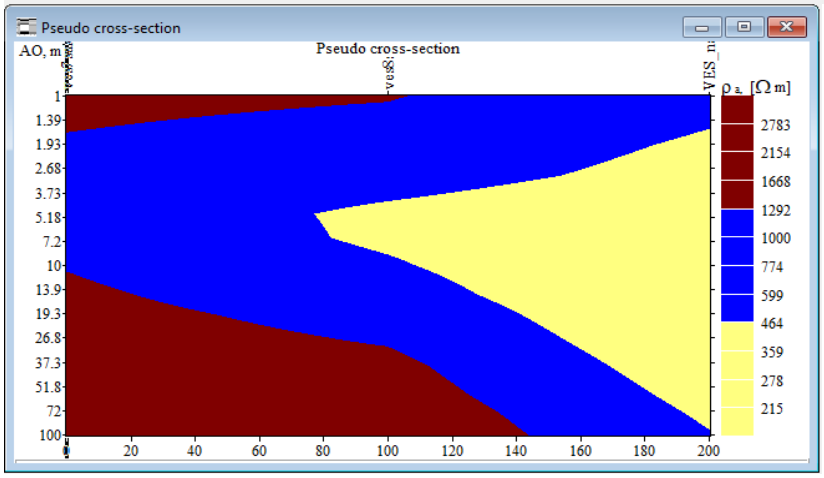
RMS=0.758%

N	ρ	h	d	Alt
1	1038	0.738	0.738	-0.7376
2	412	2.71	3.45	-3.449
3	142	36	39.5	-39.5
4	15556			

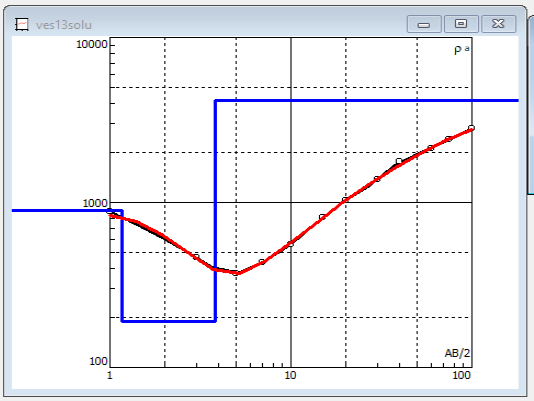


RMS=1.76%

N	ρ	h	d	Alt
1	804	0.5	0.5	-0.5
2	370	1.61	2.11	-2.105
3	129	13.9	16	-15.95
4	868			

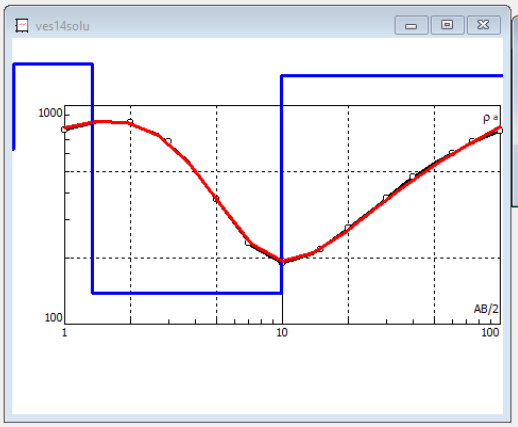


SOLU



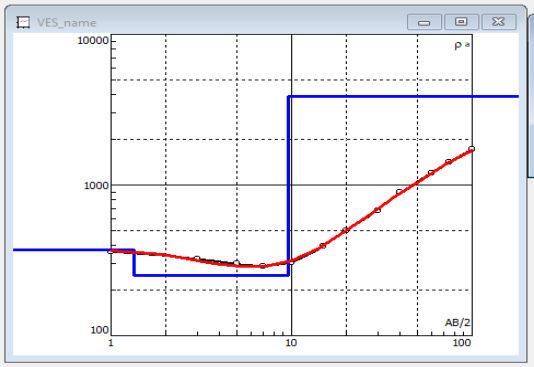
RMS=2.72%

N	ρ	h	d	Alt
1	900	1.17	1.17	-1.17
2	190	2.67	3.84	-3.84
3	4156			



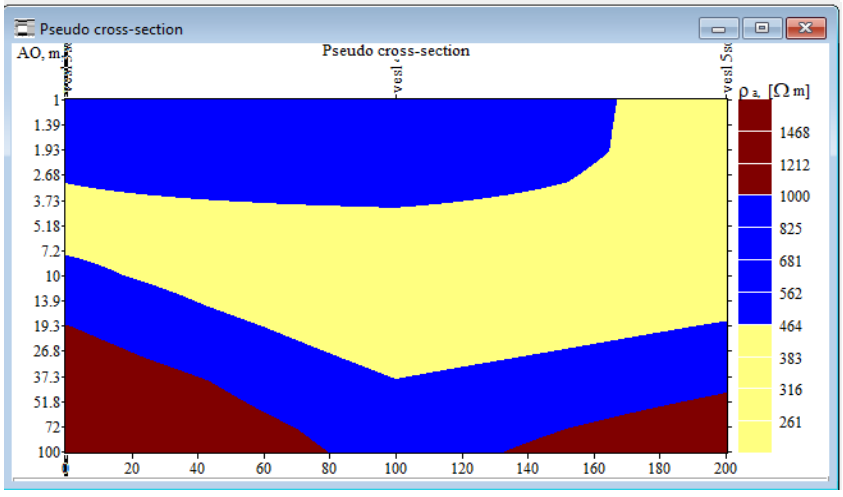
RMS=2.01%

N	ρ	h	d	Alt
1	631	0.5	0.5	-0.5
2	1556	0.836	1.34	-1.336
3	139	8.57	9.91	-9.906
4	1364			

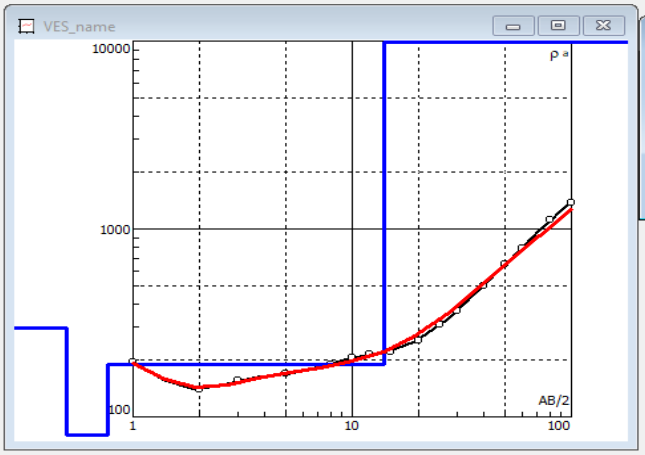


RMS=1.81%

N	ρ	h	d	Alt
1	372	1.34	1.34	-1.336
2	250	8.22	9.55	-9.551
3	3882			

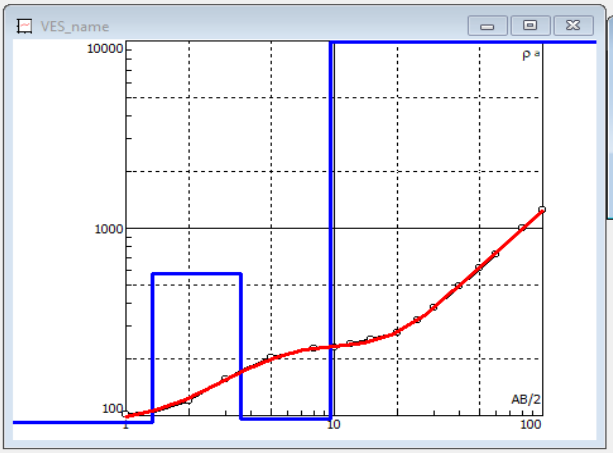


FEPOYONU



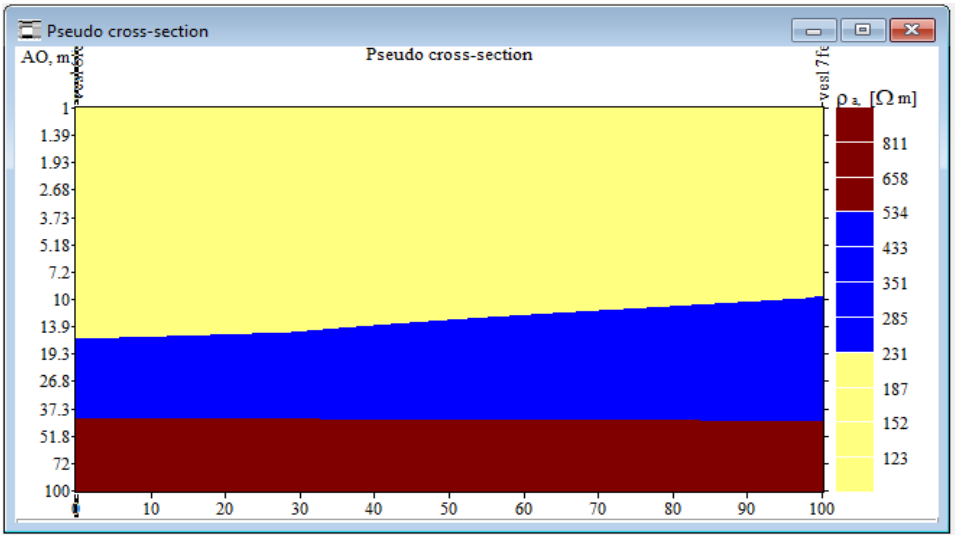
RMS=4.34%

N	ρ	h	d	Alt
1	299	0.5	0.5	-0.5
2	47.3	0.272	0.772	-0.772
3	189	13.2	14	-13.97
4	78790			

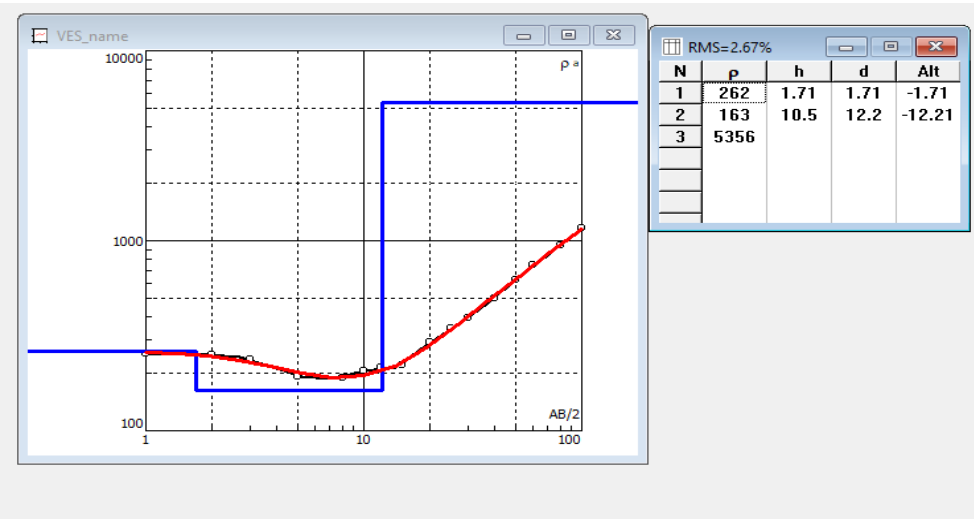


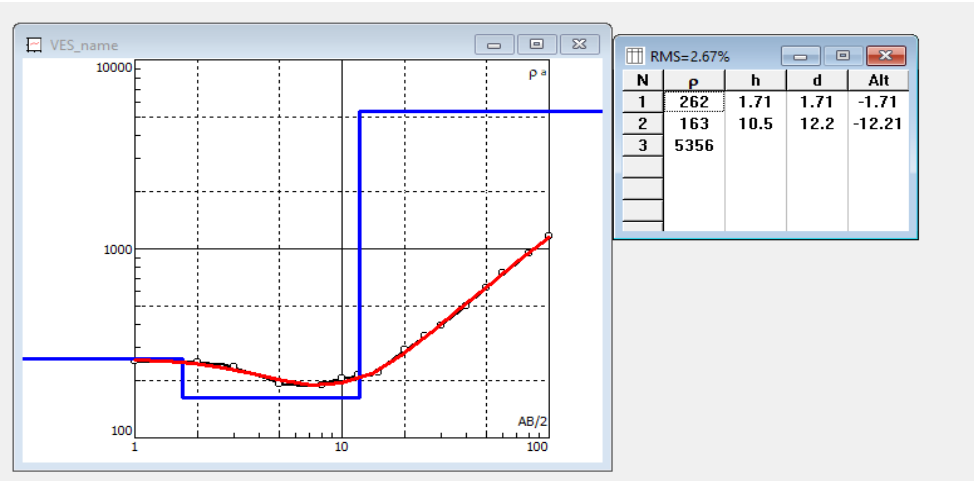
RMS=1.33%

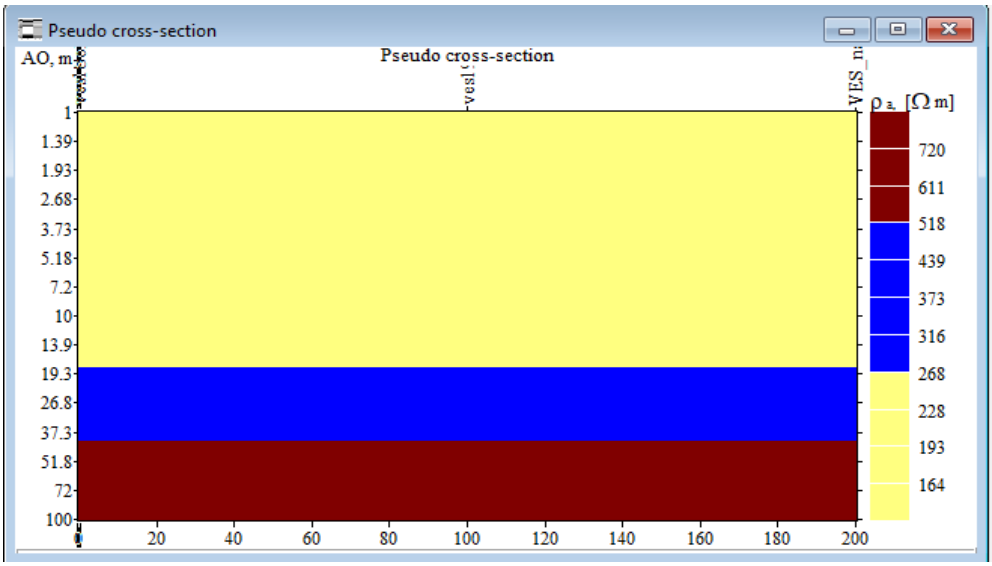
N	ρ	h	d	Alt
1	92.4	1.34	1.34	-1.337
2	569	2.23	3.57	-3.569
3	95.6	5.96	9.53	-9.531
4	182612			



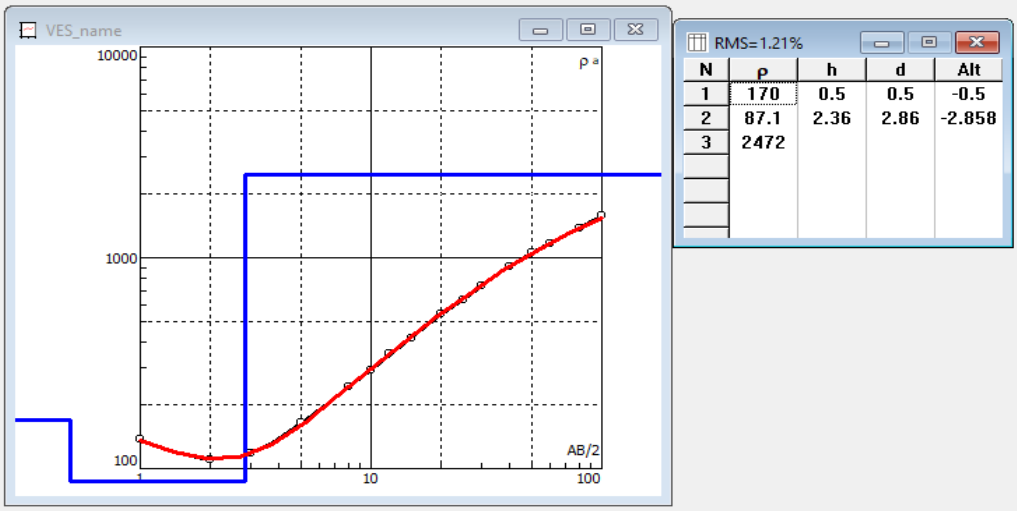
OLUPE


VES_name
10000
1000
100
1
10
100
ρ a
AB/2
RMS=2.67%
N ρ h d Alt
1 262 1.71 1.71 -1.71
2 163 10.5 12.2 -12.21
3 5356

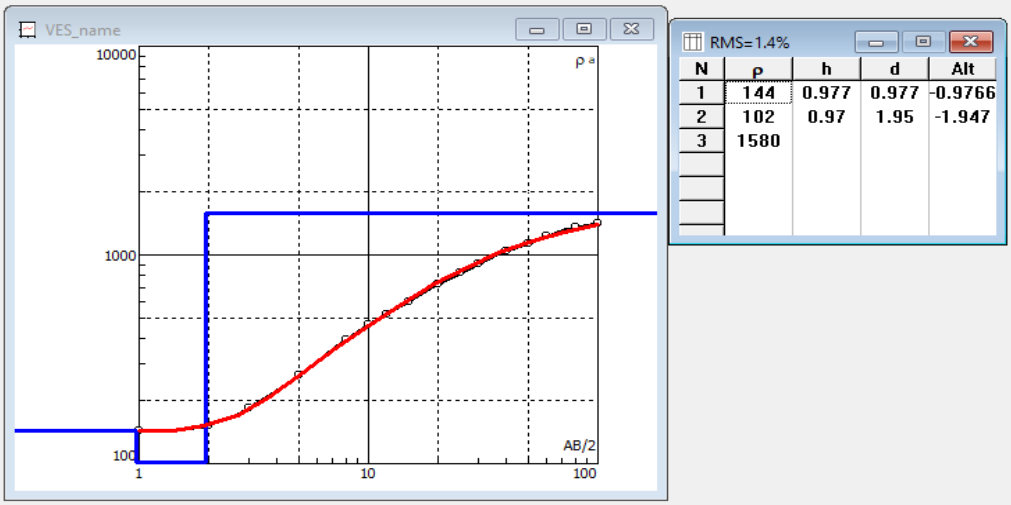

VES_name
10000
1000
100
1
10
100
ρ a
AB/2
RMS=2.67%
N ρ h d Alt
1 262 1.71 1.71 -1.71
2 163 10.5 12.2 -12.21
3 5356


Pseudo cross-section
Pseudo cross-section
AO, m
1
1.39
1.93
2.68
3.73
5.18
7.2
10
13.9
19.3
26.8
37.3
51.8
72
100
0
20
40
60
80
100
120
140
160
180
200
ρ a, [Ω m]
720
611
518
439
373
316
268
228
193
164

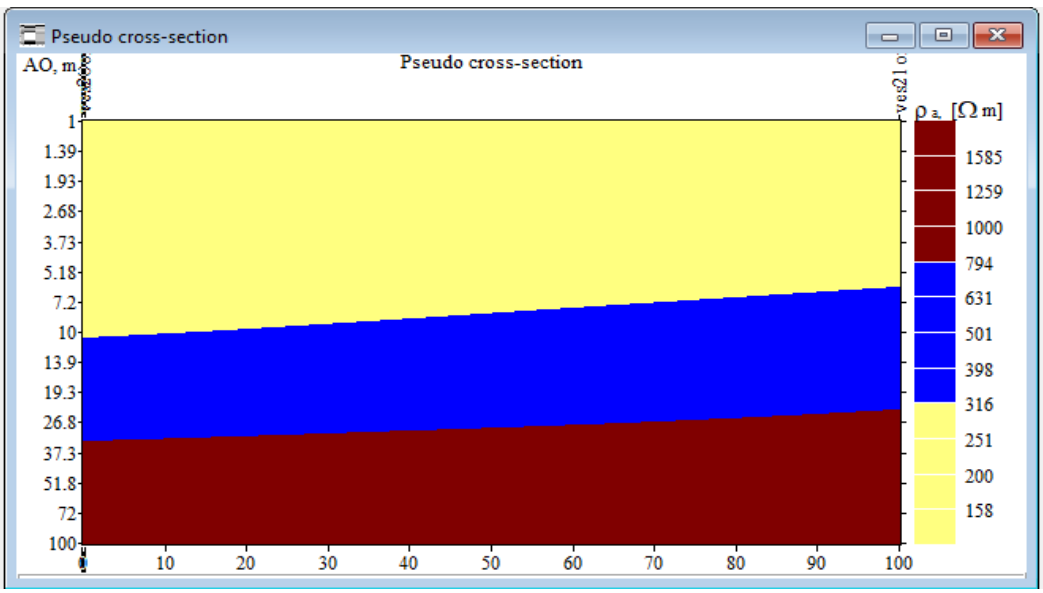
ORI OKE



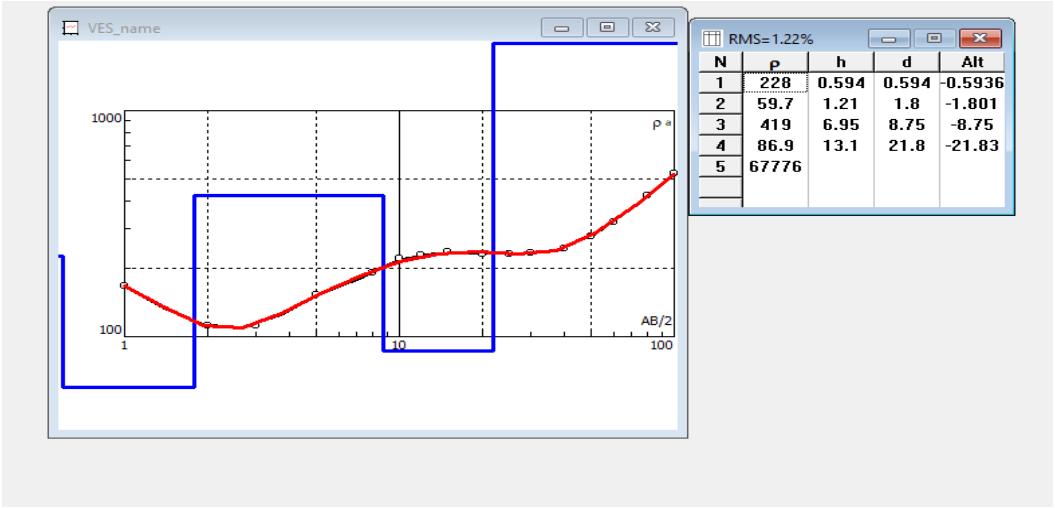
N	ρ	h	d	Alt
1	170	0.5	0.5	-0.5
2	87.1	2.36	2.86	-2.858
3	2472			



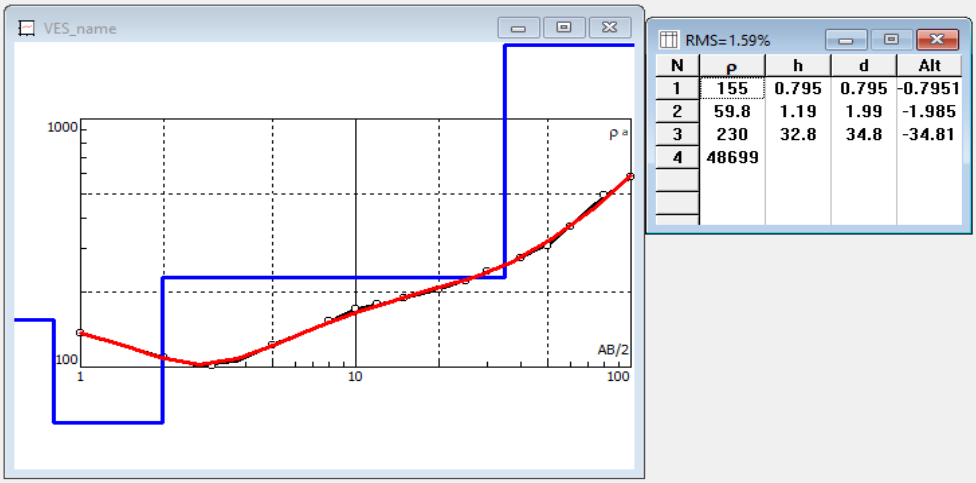
N	ρ	h	d	Alt
1	144	0.977	0.977	-0.9766
2	102	0.97	1.95	-1.947
3	1580			



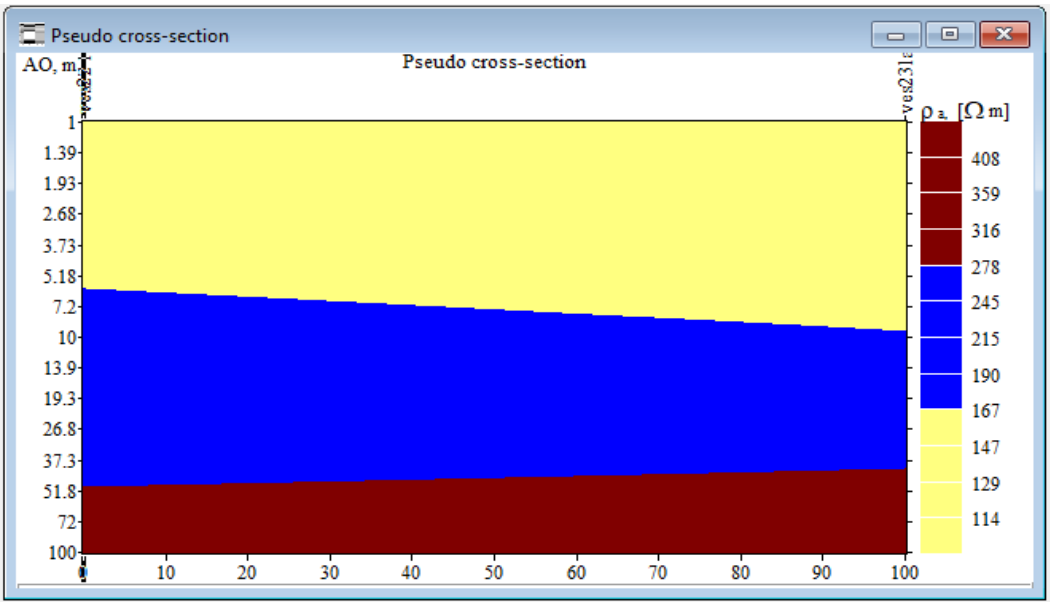
LAJ IBAMU



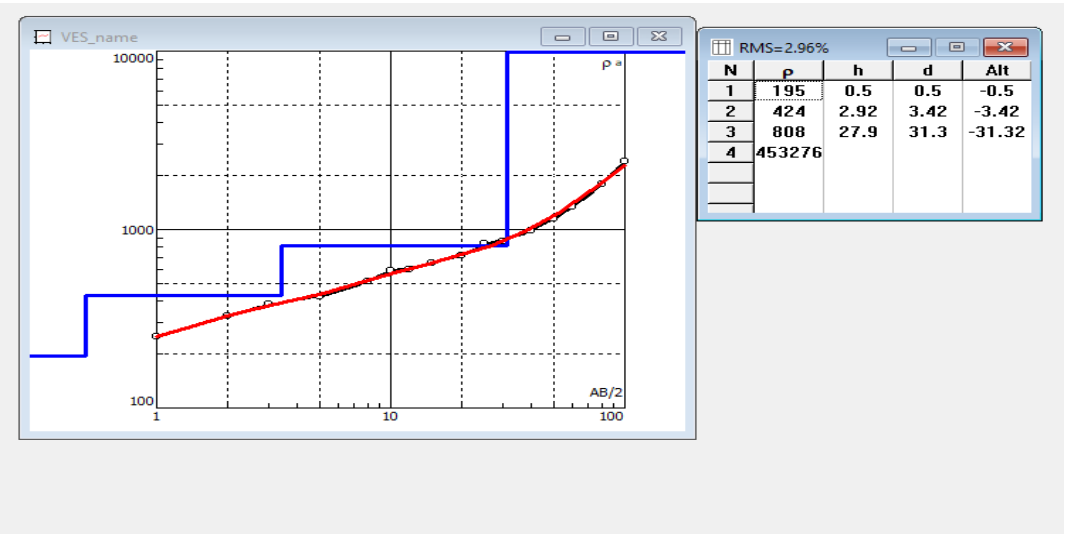
N	ρ	h	d	Alt
1	228	0.594	0.594	-0.5936
2	59.7	1.21	1.8	-1.801
3	419	6.95	8.75	-8.75
4	86.9	13.1	21.8	-21.83
5	67776			



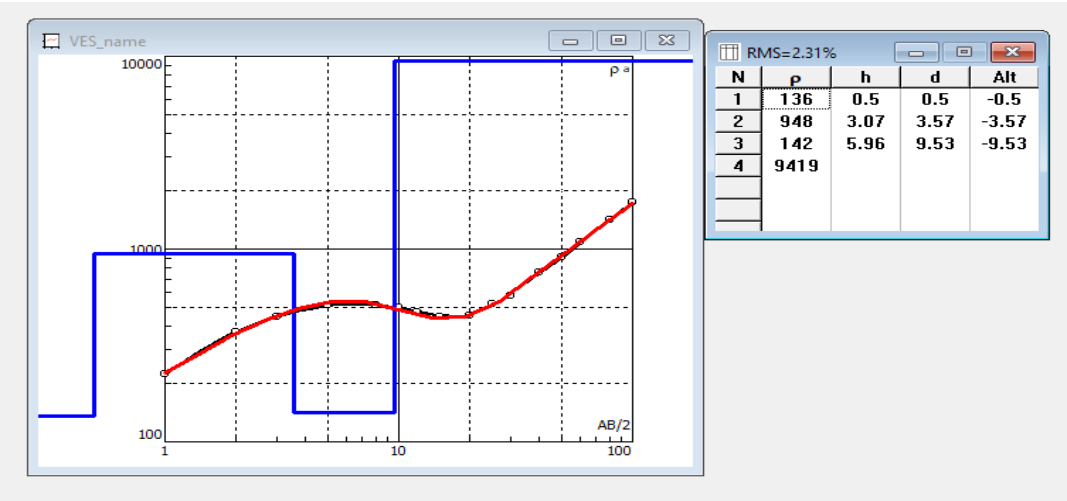
N	ρ	h	d	Alt
1	155	0.795	0.795	-0.7951
2	59.8	1.19	1.99	-1.985
3	230	32.8	34.8	-34.81
4	48699			



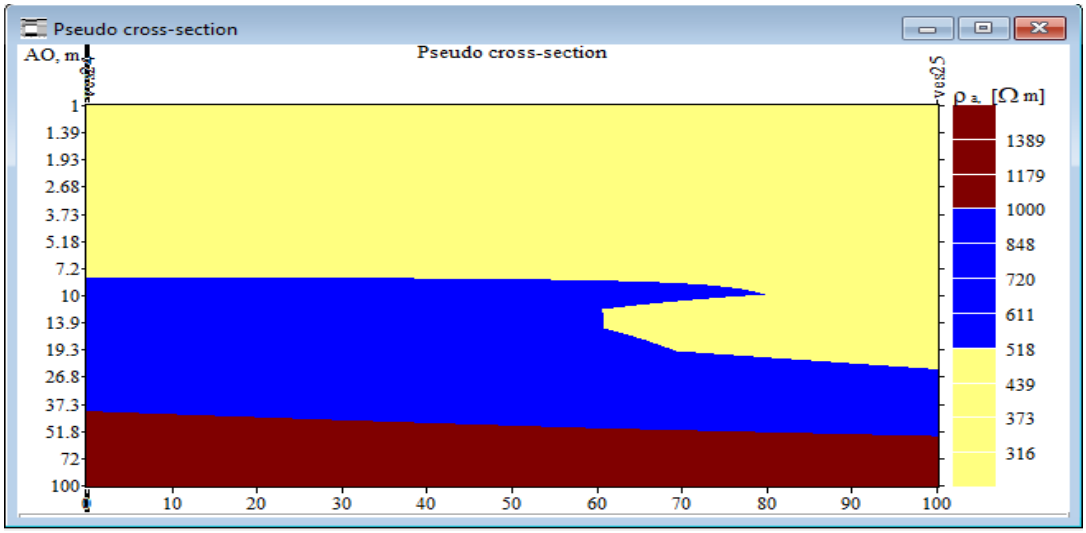
LAJI SAPATI



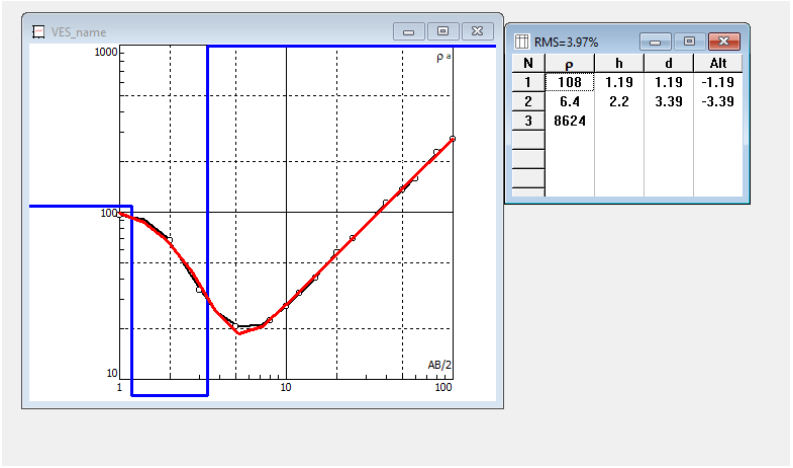
N	ρ	h	d	Alt
1	195	0.5	0.5	-0.5
2	424	2.92	3.42	-3.42
3	808	27.9	31.3	-31.32
4	453276			



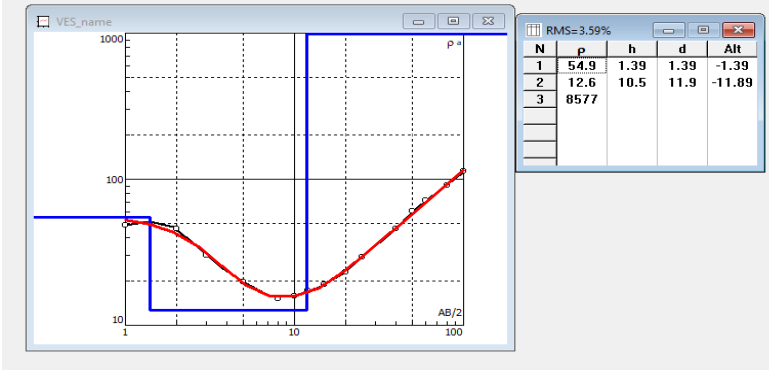
N	ρ	h	d	Alt
1	136	0.5	0.5	-0.5
2	948	3.07	3.57	-3.57
3	142	5.96	9.53	-9.53
4	9419			



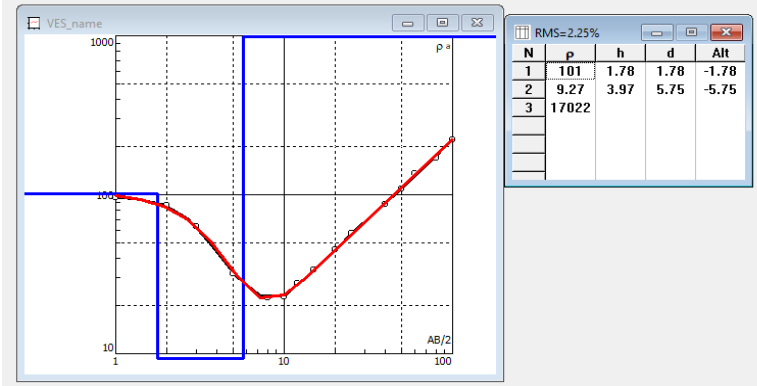
ALAJA



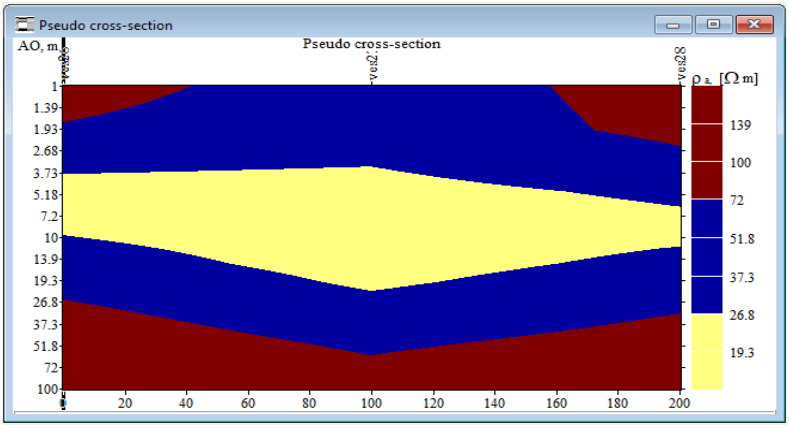
N	ρ	h	d	Alt
1	108	1.19	1.19	-1.19
2	6.4	2.2	3.39	-3.39
3	8624			



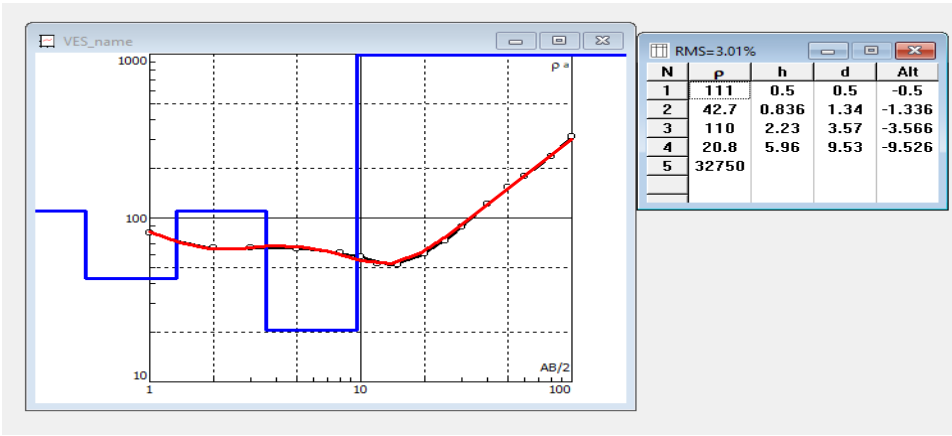
N	ρ	h	d	Alt
1	54.9	1.39	1.39	-1.39
2	12.6	10.5	11.9	-11.89
3	8577			



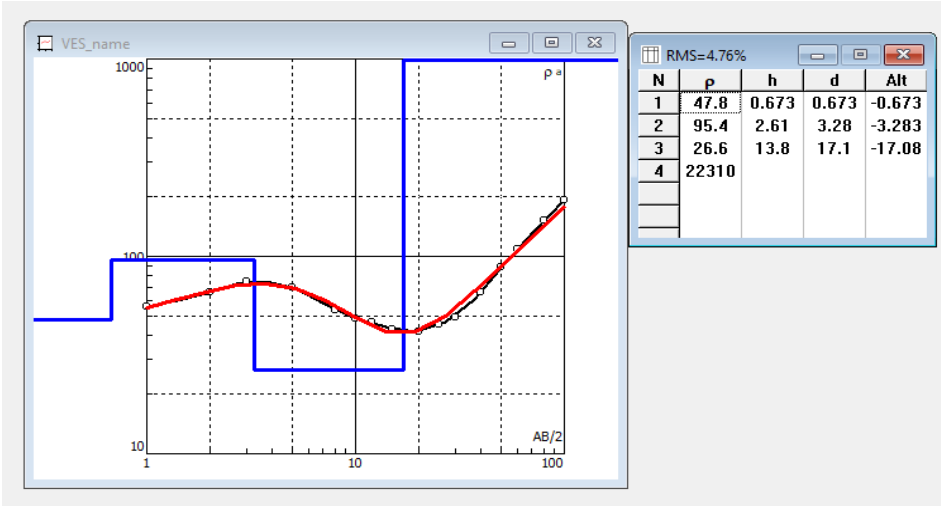
N	ρ	h	d	Alt
1	101	1.78	1.78	-1.78
2	9.27	3.97	5.75	-5.75
3	17022			



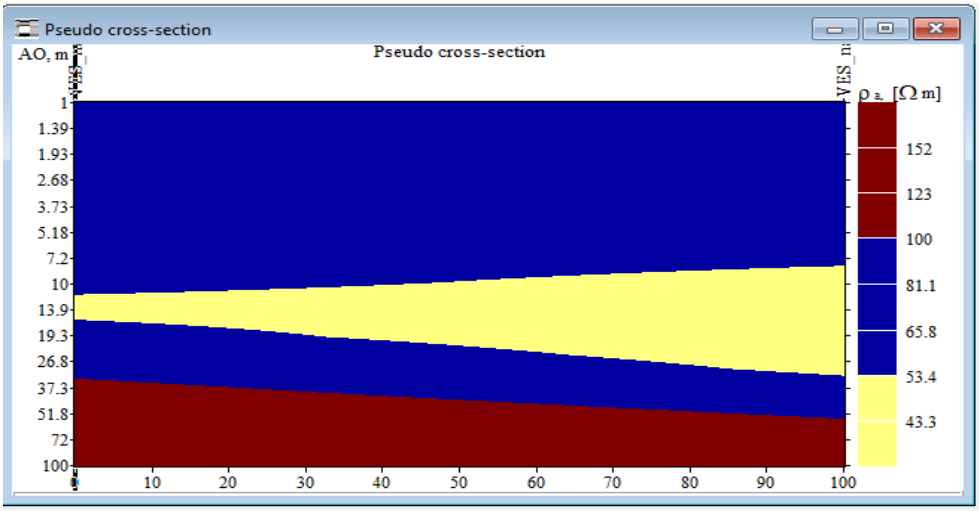
KANKAN



N	ρ	h	d	Alt
1	111	0.5	0.5	-0.5
2	42.7	0.836	1.34	-1.336
3	110	2.23	3.57	-3.566
4	20.8	5.96	9.53	-9.526
5	32750			



N	ρ	h	d	Alt
1	47.8	0.673	0.673	-0.673
2	95.4	2.61	3.28	-3.283
3	26.6	13.8	17.1	-17.08
4	22310			



APPENDIX 2: SUMMARY OF THE REMAINING RESULTS OF VERTICAL ELECTRICAL SOUNDING

GBAGEDE	VES13	3	68	3.57		A	Topsoil
			160	22.1			Weathered Basement
			1059	--	25.7		Fresh Basement.
	VES14	3	45.8	2.27		A	Topsoil
			67	13.1			Weathered Basement
			57187	--	15.4		Fresh Basement.
	VES15	3	68	3.57		A	Topsoil
			160	22.1			Weathered Basement
			1059	--	25.7		Fresh Basement.
OSIN	VES16	3	99.1	3.41		H	Topsoil
			82.3	14.1			Weathered Basement
			39086	--	17.5		Fresh Basement.
	VES17	3	83.3	0.6		H	Topsoil
			494	14.7			Weathered Basement
			3666	3666	15.3		Fresh Basement.
	VES18	3	189	1.34		A	Topsoil
			277	2.23			Weathered Basement
			784	--	3.57		Fractured Basement.
APATA	VES19	4	147	1.07		KH	Topsoil
			1810	2.03			Laterites,
			123	5.67			Weathered Basement
			2696	--	20		Fresh Basement.
	VES20	4	248	0.5		KH	Topsoil
			352	3.08			Laterites,
			182	5.96			Weathered Basement
			1860	--	9.54		Fresh Basement.
	VES21	4	259	2.18		KH	Topsoil
			625	4.38			Laterites,
			94.1	11.9			Weathered Basement
			107151	--	18.5		Fresh Basement.
ERU-OBA	VES22	4	232	1.34		KH	Topsoil
			500	2.23			Laterites,
			318	21.9			Weathered Basement
			96683		25.5		Fresh Basement.
	VES23	5	531	0.8		HKH	Topsoil
			210	3.68			Sandy Clay
			463	4.91			Laterite
			141	18.9			Weathered Basement
			1592	--	28.9		Fresh Basement.
	VES24	3	93.4	0.6		H	Topsoil
			19.8	2.07			Weathered Basement
			1383	--	2.69		Fresh Basement.

EGBEJILA	VES25	4	359	1.34	25.6	KH	Topsoil
			576	2.23			Laterites,
			125	22			Weathered Basement
			1620	--			Fresh Basement.
	VES26	3	370	2.67		H	Topsoil
			103	17.9			Weathered Basement
			294	--	20.6		Fractured Basement.
	VES27	3	795	2.43		H	Topsoil
			126	22.9			Weathered Basement
			447	--	25.3		Fractured Basement.
ONIRIN	VES28	4	41.1	0.648	5.99	H	Topsoil
			22.9	2.88			Weathered Rock
			15327	3.11			Fresh Rock
			33.3	--			Fractured Rock
	VES29	4	40.5	0.8	2.1	HA	Topsoil
			14.5	1.02			Weathered Rock
			223	10.5			Fractured Rock
			850	--			Fresh Rock
	VES30	4	53.4	0.5	2.33	HA	Topsoil
			17	0.8			Weathered Rock
			66.9	8.39			Fractured Rock
			881	--			Fresh Rock

TOWN	VES STATION	No. of Layers	Layer Resistivity ()	Thickess (m)	Depth to Bedrock (m)	Curve Type	Remark
AGO-OJA	VES 31	4	565	0.5	20	KH	Topsoil
			5108	0.8			Laterite
			45	8.2			Weathered Basement
			18559	--			Fresh Basement.
	VES 32	4	565	0.5	9.56	KH	Topsoil
			5109	0.8			Laterite
			45	8.22			Weathered Basement
			18559	--			Fresh Basement.
	VES33	3	1195	0.7	4.04	H	Topsoil
			271	3.2			Weathered Basement
			7646	--			Fresh Basement.
LADUBA	VES 34	4	918	0.5	9.56	KH	Topsoil
			1655	0.8			Laterite
			103	8.2			Weathered Basement
			86296	--			Fresh Basement.
	VES 35	3	458	3.6	9.55	H	Topsoil
			47.8	5.5			Weathered Basement
			6359	--			Fresh Basement.
	VES 36	3	286	0.5	2.5	H	Topsoil
			2 0	1.9			Weathered Basement
			655	--			Fresh Basement.
ALASAPE	VES 37	4	148	1.3	13.3	HA	Topsoil
			90.4	1.6			Weathered Rock
			20755	10.3			Fresh Rock
			108	--			Fractured Basement
	VES 38	3	82.4	0.6	1.49	A	Topsoil
			39.7	0.8			Weathered Basement
			11634	--			Fresh Basement.
	VES 39	3	106	0.5	3.92	H	Topsoil
			20	3.4			Weathered Basement
			572	--			Fractured Basement
LIFE GATE	VES40	3	1024	0.9	25.3	H	Topsoil
			372	24.4			Weathered Basement
			85678	--			Fresh Basement.
	VES41	3	2203	1.2	9.63	H	Topsoil
			56.1	8.4			Weathered Basement
			1375	--			Fresh Basement.

	VES42	3	1038	1.7			Topsoil
			218	16.6			Weathered Basement
			129921	--	18.3	H	Fresh Basement.
AKANBI ADE	VES43	3	1281	1			Topsoil
			30.3	3.8			Weathered Basement
			20754	--	4.82	H	Fresh Basement.
	VES 44	3	52.9	1.2			Topsoil
			9.92	2.3			Weathered Basement
			20369	--	4.1	H	Fresh Basement.
	VES45	3	508	0.9			Topsoil
			74.8	6.9			Weathered Basement
			593	--	7.85	H	Fractured Basement.
ALONG AFON	VES46	3	119	3.5			Topsoil
			24.1	5.9			Weathered Basement
			2031	--	9.53	H	Fresh Basement.
	VES47	5	124	1.3			Topsoil
			58.5	2.2			Clayey Sand
			16.1	5.9			Weathered Basement
			96.9	58.6			Fractured Basement.
			914	--	9.53	QHA	Fractured Basement.
	VES48	4	253	0.5			Topsoil
			116	1.5			Sandy Clay
			25.8	13.9			Weathered Basement
			223	--	15.9	QH	Fractured Basement.
ELERU	VES49	3	1418	1.75			Topsoil
			30.3	12.7			Weathered Basement
			24324	--	14.4	H	Fresh Basement.
	VES50	4	177	1.7			Topsoil
			357	1.5			Laterite
			35.8	17.3			Weathered Basement
			1016	--	20.5	KH	Fresh Basement.
LARO	VES51	3	196	1.5			Topsoil
			31.7	7.9			Weathered Basement
			342	--	9.4	H	Fractured Basement.
	VES52	4	53.9	0.5			Topsoil
			229	0.8			Laterite
			8.16	2.2			Weathered Basement
			1353		10	KH	Fresh Basement.
APATA	VES53	4	279	0.7			Topsoil
			1279	0.7			Laterite
			6.84	2.5			Weathered Basement
			194	--	22	KH	Fresh Basement.

	VES 65	3	92.9	1.6	5.22	H	Topsoil
			54.3	7			Weathered Basement
			211	--			Fractured Basement
	VES 66	3	13.2	1	12.6	A	Topsoil
			39.1	12.6			Weathered Basement
			79	--			Fractured Basement
OKE AWO	VES 67	3	263	1.7	12.2	H	Topsoil
			163	12.2			Weathered Basement
			5356	--			Fresh Basement
	VES 68	4	299	0.5	14	HA	Topsoil
			47.3	0.7			Weathered Rock
			189	14			Fractured Rock
			78790	--			Fresh Rock
	VES 69	4	92.4	1.3	9.53	KH	Topsoil
			569	3.5			Laterite
			95.6	9.53			Weathered Basement
			182612	--			Fresh Basement
	VES70	3	144	1.34	9.58	H	Topsoil
			115	9.5			Weathered Basement
			5717	--			Fresh Basement
IDIAMI	VES71	5	158	0.7	16	HKH	Topsoil

IDIAMI	VES71	5	158	0.7	16	HKH	Topsoil
			63.7	2			Clayey Sand
			475	4.8			Laterite
			118	16			Weathered Basement
			55229	--			Fresh Basement
	VES72	5	228	0.5	21.8	HKH	Topsoil
			59.7	1.8			Clayey Sand
			419	8.75			Laterite
			86.9	21.8			Weathered Basement
			67776	--			Fresh Basement
	VES 73	4	155	0.7	34.8	HA	Topsoil
			59.8	1.9			Clayey Sand
			230	34.8			Weathered Basement
			48699	--			Fresh Basement
	VES 74	3	211	0.5	9.33	H	Topsoil
			155	8.33			Weathered Basement
			78790	--			Fresh Basement
ILUIRU	VES75	4	12.9	0.5	39.2	KH	Topsoil
			159	12.5			Laterite
			55.4	39.2			Weathered Basement
			4078	--			Fresh Basement
	VES76	5	79.8	0.5	16.8	HKH	Topsoil
			32.8	1.6			Clayey Sand
			199	5.22			Laterite
			28.8	16.8			Weathered Basement

			1727	--			Fresh Basement
	VES77	4	13.9	0.5	34.1	KH	Topsoil
			121	14.8			Laterite
			45.6	34.1			Weathered Basement
			15429	--			Fresh Basement
	VES78	3	223	0.5	7.72	H	Topsoil
			132	7.7			Weathered Basement
			4050	--			Fresh Basement

AFAKU	VES79	5	14.3	0.5	25.5	AKH	Topsoil
			71.1	3.6			Clayey Sand
			244	9.6			Laterite
			44.6	25.5			Weathered Basement
			41712	--			Fresh Basement
	VES80	4	48.3	0.5	20.1	KH	Topsoil
			533	2.9			Laterite
			24.5	7.9			Weathered Basement
			1132	--			Fresh Basement
	VES81	4	384	1.3	25.5	QH	Topsoil
			223	3.5			Sandy Clay
			122	25.5			Weathered Basement
			23622	--			Fresh Basement
	VES82	3	117	0.5	7.54	H	Topsoil
			47.7	7.54			Weathered Basement
			105093	--			Fresh Basement

PAJUBA	VES83	5	479	0.5	25.6	HKH	Topsoil
			127	1.3			Clayey Sand
			474	3.5			Laterite
			93.7	25.6			Weathered Basement
			3882	--			Fresh Basement
	VES84	5	205	0.5	20.4	HKH	Topsoil
			80.3	1.3			Clayey Sand
			1050	3.5			Laterite
			129	9.5			Weathered Basement
			2857	--			Fresh Basement
	VES85	4	137	2	26.1	KH	Topsoil
			729	9.7			Laterite
			232	26.1			Weathered Basement
			11236	--			Fresh Basement
	VES 86		205	0.5	25.3	HKH	Topsoil
			80.3	1.3			Clayey Sand
			1050	3.5			Laterite
			129	9.5			Weathered Basement
			2857	9.5			Fresh Basement
GORI	VES 87	4	137	2	26.1	KH	Topsoil
			729	9.7			Laterite
			232	26.1			Weathered Basement
			11236	--			Fresh Basement

	VES 88	4	97.3	0.5	9.54	HA	Topsoil
			35.4	1.3			Weathered Rock
			68.2	9.5			Fractured Rock
			19952	--			Fresh Basement
	VES 89		126	0.5	28.9	HA	Topsoil
			65.1	2.4			Weathered Rock
			222	28.9			Fractured Rock
			1110	--			Fresh Basement
	VES 90	3	43	0.5	1.62	A	Topsoil
			102	1.6			Weathered Basement
			2460				Fresh Basement

TOWN	VES STATION	No. of Layers	Layer Resistivity ()	Thickess (m)	Depth to Bedrock (m)	Curve Type	Lithology
AROWOSAYE	VES91	3	842	1.2	15.1	H	Topsoil
			36.2	13.9			Weathered Basement
			13.9	--			Fresh Basement
	VES 92	3	187	1.2	20.5	H	Topsoil
			35.7	19.2			Weathered Basement

			231	--			Fresh Basement
	VES 93	3	276	2.1	21.1	H	Topsoil
			34.9	18.9			Weathered Basement
			241	--			Fresh Basement
	VES 94	3	63.6	2.1	22.8	H	Topsoil
			12.6	20.7			Weathered Basement
			41.2	--			Fresh Basement
	VES 95	5	32.2	2.3	8.74	H	Topsoil
			17.6	6.4			Weathered Basement
			47.8	--			Fresh Basement
	VES 96	3	24	c	25.5	K	Topsoil
			36.2	21.9			Weathered Basement
			12.3	--			Fractured Basement
IGBORESE	VES 97	3	616	1.3	23.6	H	Topsoil
			64.5	21.3			Weathered Basement

			17307	--			Fresh Basement
	VES 98		812	0.5	1.05	Q	Topsoil
			663	1.05			Weathered Basement
			231	--			Fractured Basement
	VES 99	3	232	1.3	11.3	H	Topsoil
			65	9.9			Weathered Basement
			357	--			Fractured Basement
	VES100	3	95.2	1.48	11.5	H	Topsoil
			28	10.1			Weathered Basement
			101	--			Fractured Basement
	VES101	3	40.3	2.4	8.18	H	Topsoil
			11.6	5.7			Weathered Basement
			47.9	--			Fractured Basement
	VES102	3	29.7	5	23.8	H	Topsoil
			11.4	18.7			Weathered Basement

			45.3	--			Fractured Basement
OLOKO	VES103	4	299	0.5	14	HA	Topsoil
			47.3	0.2			Weathered Rock
			189	13.2			Fractured Rock
			78790	--			Fresh Basement
	VES104	4	1207	0.5	28.8	HA	Topsoil
			89.2	0.5			Weathered Rock
			452	27.8			Fractured Rock
			57017	--			Fresh Basement
	VES105	5	92.4	1.3	19.3	KH	Topsoil
			569	2.2			Laterite
			95.53	5.9			Fractured Rock
			182612	--			Fresh Basement
	VES106	3	262	1.7	12.2	H	Topsoil
			163	10.5			Weathered Basement

			5356	--			Fresh Basement
	VES107	5	158	0.7	21.5	HKH	Topsoil
			63.7	1.3			Clayey Sand
			475	2.8			Laterite
			18	11.1			Weathered Basement
			55229	--			Fresh Basement
	VES108	3	41.6	3.8	14.5	H	Topsoil
			23.9	10.5			Weathered Basement
			65.2	--			Fractured Basement
ONIPANPO	VES109	3	54.9	1.3	11.9	H	Topsoil
			2.6	10.5			Weathered Basement
			8577	--			Fresh Basement
	VES110	4	195	0.5	31.3	AA	Topsoil
			424	2.9			Weathered Rock
			808	27.9			Fractured Rock

			453276				Fresh Basement
	VES111	4	208	0.5	25.5	AA	Topsoil
			399	3.1			Weathered Rock
			886	21.9			Fractured Rock
			3288	--			Fresh Basement
	VES 112	4	136	0.5	15.3	KH	Topsoil
			949	3.1			Laterite
			142	5.96			Weathered Basement
			9419	--			Fresh Basement
	VES113	3	114	1	5.87	H	Topsoil
			13.6	4.8			Weathered Basement
			38648	--			Fresh Basement
	VES114	4	75	0.5	25.8	HA	Topsoil
			48.5	2.3			Weathered Rock
			60.2	23.8			Fractured Rock

			11662	--			Fresh Rock
AIYEKALE	VE115	3	77.7	4.1	20.9	H	Topsoil
			7.08	16			Weathered Basement
			6973	--			Fresh Basement

	VES116	4	19.4	0.5	25.7	KH	Topsoil
			359	0.8			Laterite
			8.27	24.4			Weathered Basement
			2311	--			Fresh Basement
	VES117	4	211	0.5	9.65	HA	Topsoil
			37.6	0.8			Weathered Rock
			145	8.31			Fractured Rock
			3210	--			Fresh Rock
	VE118	3	65.2	1.2	10.1	A	Topsoil
			105	8.9			Weathered Basement

			94326	--			Fresh Basement
	VES119	3	101	0.6	1.5	H	Topsoil
			10.6	0.8			Weathered Basement
			10295	--			Fresh Basement
	VES120	4	43.5	0.5	2.94	HA	Topsoil
			22.1	2.4			Weathered Rock
			234	22.7			Fractured Rock
			20782	--			Fresh Basement
	VES134	4	1207	0.5	28.8	HA	Topsoil
			89.2	0.5			Weathered Rock
			452	27.8			Fractured Rock
			57017	--			Fresh Basement
	VES135	5	92.4	1.3	19.3	KH	Topsoil
			569	2.2			Laterite
			95.53	5.9			Fractured Rock

			182612	--			Fresh Basement
	VES136	3	262	1.7	12.2	H	Topsoil
			163	10.5			Weathered Basement
			5356	--			Fresh Basement
	VES137	5	158	0.7	21.5	HKH	Topsoil
			63.7	1.3			Clayey Sand
			475	2.8			Laterite
			18	11.1			Weathered Basement
			55229	--			Fresh Basement
	VES138	3	41.6	3.8	14.5	H	Topsoil
			23.9	10.5			Weathered Basement
			65.2	--			Fractured Basement
ONIPANPO	VES139	3	54.9	1.3	11.9	H	Topsoil
			2.6	10.5			Weathered Basement
			8577	--			Fresh Basement

	VES 140	4	195	0.5	31.3	AA	Topsoil
			424	2.9			Weathered Rock
			808	27.9			Fractured Rock
			453276				Fresh Basement
	VES141	4	208	0.5	25.5	AA	Topsoil
			399	3.1			Weathered Rock
			886	21.9			Fractured Rock
			3288	--			Fresh Basement
	VES142	4	136	0.5	15.3	KH	Topsoil
			949	3.1			Laterite
			142	5.96			Weathered Basement
			9419	--			Fresh Basement
	VES143	3	114	1	5.87	H	Topsoil
			13.6	4.8			Weathered Basement
			38648	--			Fresh Basement

	VES 144	4	75	0.5	25.8	HA	Topsoil
			48.5	2.3			Weathered Rock
			60.2	23.8			Fractured Rock
			11662	--			Fresh Rock
AIYEKALE	VES145	3	77.7	4.1	20.9	H	Topsoil
			7.08	16			Weathered Basement
			6973	--			Fresh Basement
	VES146	4	19.4	0.5	25.7	KH	Topsoil
			359	0.8			Laterite
			8.27	24.4			Weathered Basement
			2311	--			Fresh Basement
	VES147	4	211	0.5	9.65	HA	Topsoil
			37.6	0.8			Weathered Rock
			145	8.31			Fractured Rock
			3210	--			Fresh Rock

	VES148	3	65.2	1.2	10.1	A	Topsoil
			105	8.9			Weathered Basement
			94326	--			Fresh Basement
	VES149	3	101	0.6	1.5	H	Topsoil
			10.6	0.8			Weathered Basement
			10295	--			Fresh Basement
	VES150	4	43.5	0.5	2.94	HA	Topsoil
			22.1	2.4			Weathered Rock
			234	22.7			Fractured Rock
			20782	--			Fresh Basement
TOWN	VES STATION	No. of Layers	Layer Resistivity ()	Thickess (m)	Depth to Bedrock (m)	Curve Type	
AFON	VES151	4	337	0.6	18.8	KH	Topsoil
			2642	3.44			Laterite
			293	14.8			Weathered Basement
			215604	--			Fresh Basement
	VES152	4	255	0.5	25.5	KH	Topsoil
			874	9.05			Laterite
			55.5	15.9			Weathered Basement
			33249	--			Fresh Basement

	VES 153		220	0.5	27.4	KH	Topsoil
			423	7.38			Laterite
			38.6	19.5			Weathered Basement
			24632	--			Fresh Basement
KAYOJA	VES 154	3	402	0.6	6.62	H	Topsoil
			255	6.1			Weathered Basement
			1633	--			Fresh Basement
	VES 155	5	1427	0.5	9.53	HKH	Topsoil
			493	0.836			Sandy Clay
			3434	2.23			Laterite
			64.9	5.96			Weathered basement
			844	--			Fractured Basement
	VES 156	5	1377	0.6	17.6	HKH	Topsoil
			409	0.9			Sandy Clay
			2488	5.95			Laterite
			52.4	10.1			Weathered basement
			922	--			Fractured Basement
ONIYANGI	VES157	5	619	0.5	25.5	HKH	Topsoil
			203	0.8			Sandy Clay
			590	2.23			Laterite
			95.9	21.9			Weathered basement
			941	--			Fractured Basement
	VES 158	5	131	0.5	26	KH	Topsoil
			1321	0.8			Sand
			138	8.73			Sandy Clay
			68	15.9			Weathered basement
			17416	--			Fresh Basement
	VES 159	4	67.9	0.5	26.2	KH	Topsoil
			224	3.31			Laterite
			107	22.4			Weathered basement
			1970	--			Fresh Basement

TERU	VES160	5	330	0.5	25.4	HKH	Topsoil
			90.7	3.07			Clay
			333	5.96			Laterite
			50.7	15.9			Weathered Basement
			14415	--			Fresh Basement
	VES161	5	578	0.5	39.4	HKH	Topsoil
			11.2	0.3			Clay
			136	0.46			Laterite
			32.8	30.1			Weathered Rock
			12383	--			Fresh Rock
	VES162	4	56.8	0.5	1.34	H	Topsoil
			12.8	0.836			Weathered Basement
			113	--			Fractured Basement
AGBOKU	VES 163	3	88.7	0.9	21	H	Topsoil
			47	20.1			Weathered Basement
			13096	--			Fresh Basement
	VES164	4	184	1.06	17.8	HA	Topsoil
			14	0.66			Weathered Rock
			52.7	16.1			Fractured Rock
			15671	--			Fresh Rock
	VES165		605	1.35	9.54	HA	Topsoil
			107	2.23			Sandy Clay
			33	5.96			Weathered Rock
			165	58.6			Fractured Rock
			15372	--			Fresh Rock
AROGUN	VES166	4	105	0.66	15.7	KH	Topsoil
			460	0.64			Laterite
			44.9	14.4			Weathered Basement
			1644	--			Fresh Basement
	VES167	5	106	1.34	25.4	KQA	Topsoil
			290	2.23			Sandy Clay
			140	5.96			Laterite
			24	15.9			Weathered Basement
			301	--			Fractured

							Basement
	VES168	4	29.3	1.7	21.9	KH	Topsoil
			213	7.18			Laterite
			20.7	13.1			Weathered Basement
			74.1	--			Fractured Basement
IDI AYAN	VES169	3	24	3.57	3.57	K	Topsoil
			36.2	21.9			Weathered Basement
			12.3	--			Fractured Basement
	VES 170	3	29.7	5.07	23.8	H	Topsoil
			11.4	18.7			Weathered Basement
			45.3	--			Fractured Basement
	VES171	3	41.6	3.8	14.5	H	Topsoil
			23.9	10.7			Weathered Basement
			65.2	--			Fractured Basement
GBAJA	VES172	4	75	0.5	2.74	HA	Topsoil
			40.5	2.24			Weathered Rock
			80.2	23			Fractured Rock
			11662	--			Fresh Rock
	VES173	4	43.5	0.5	2.94	HA	Topsoil
			22.1	2.44			Weathered Rock
			234	22.7			Fractured Rock
			20782	--			Fresh Rock
	VES174	4	46	0.5	25.5	KH	Topsoil
			166	3.11			Laterite
			25.6	21.9			Weathered Basement
			5839	--			Fresh Basement
OKESO	VES175	3	42.9	0.5	3.14	H	Topsoil
			28.3	2.64			Weathered Basement
			180	--			Fractured Basement

TOWN	VES STATION	No. of Layers	Layer Resistivity ()	Thickess (m)	Depth to Bedrock (m)	Curve Type	Lithology
ODO ODE	VES181	4	417	1.7	27.5	KH	Topsoil

			2884	3.49			Laterite
			134	22.3			Weathered Basement
			40058	--			Fresh Basement
	VES182	4	188	1.34	25.6	KH	Topsoil
			1388	8.34			Laterite
			201	15.9			Weathered Basement
			29891	--			Fresh Basement
	VES183	5	205	0.5	25.5	HKH	Topsoil
			204	3.1			Sandy Clay
			720	5.96			Laterite
			122	15.9			Weathered Basement
			57346	--			Fresh Basement
EWUSI	VES184	4	348	0.6	1.3	HA	Topsoil
			88.7	0.8			Weathered Basement
			470	20			Fractured Rock
			7159	--			Fresh Basement
	VES185	3	349	1.27	22.9	H	Topsoil
			214	21.7			Weathered Basement
			22896	--			Fresh Rock
	VES186	4	400	0.62	21.9	KH	Topsoil
			758	1.01			Laterite
			114	20.2			Weathered Basement
			28944	--			Fresh Basement
SAKAMO	VES187	3	1691	0.99	4.17	H	Topsoil
			644	3.18			Weathered Basement
			2728	--			Fresh Rock
	VES 188	3	1456	1.34	3.57	H	Topsoil
			134	2.23			Weathered Basement
			4620	--			Fresh Rock
	VES189	3	1691	0.99	4.17	H	Topsoil
			644	3.18			Weathered

							Basement
			2728	--			Fresh Rock
BUDO OMO	VES190	4	325	0.7	41.8	KH	Topsoil
			1397	2.81			Laterite
			381	38.3			Weathered Basement
			65628	--			Fresh Basement
	VES191	4	1038	0.74	30	QH	Topsoil
			412	2.71			Sandy Clay
			142	36			Weathered Basement
			15556	--			Fresh Basement
	VES192	4	804	0.5	16	QA	Topsoil
			370	1.61			Sandy Clay
			129	13.9			Weathered Basement
			868	--			Fractured Basement
SOLU	VES193	3	900	1.17	4.3	H	Topsoil
			190	2.67			Weathered Basement
			4156	--			Fresh Rock
	VES194	5	631	0.5	9.91	KH	Topsoil
			1556	0.84			Laterite
			139	8.6			Weathered Basement
			1364	--			Fresh Basement
	VES195	3	372	1.34	9.55	H	Topsoil
			250	8.22			Weathered Basement
			3882	--			Fresh Rock
FEPOFOYO	VES196	4	299	0.5	14	HA	Topsoil
			47.3	0.3			Weathered Rock
			189	13.2			Fractured Rock
			78790	--			Fresh Rock
	VES197	4	92.4	1.3	9.5	KH	Topsoil
			569	2.23			Laterite
			95.6	5.96			Weathered

							Basement
			182612	--			Fresh Basement
OLUPE	VES198		1458	1.71	10.3	H	Topsoil
		3	125	8.57			Weathered Basement
			5356	--			Fresh Basement
	VES199	3	262	1.71	12.2	H	Topsoil
			163	10.5			Weathered Basement
			5356	--			Fresh Basement
ORI OKE	VES200		170	0.5	2.86	H	Topsoil
		3	87.1	2.36			Weathered Basement
			2472	--			Fresh Basement
	VES201	3	144	0.9	1.95	H	Topsoil
			102	0.9			Weathered Basement
			1500	--			Fresh Basement
LAJIBAMU	VES202	5	228	0.59	2.5	HKH	Topsoil
			59.7	1.21			Clay
			419	6.95			Laterite
			86.9	13.1			Weathered Basement
			6.7776	--			Fresh Basement
	VES203	4	155	0.8	3.1	HA	Topsoil
			59.8	1.19			Weathered Rock
			230	32.8			Fractured Rock
			48699	--			Fresh Rock
LAJI-SAPATI	VES204	4	195	0.5	30	AA	Topsoil
			424	2.92			Laterite
			808	27.9			Weathered Rock
			453276	--			Fresh Rock
	VES205	4	136	0.5	9.53	KH	Topsoil
			948	3.07			Laterite
			142	5.96			Weathered Basement
			9419	--			Fresh Basement

ALAJA	VES206	3	108	1.19	3.39	H	Topsoil
			6.4	2.2			Weathered Basement
			8624	--			Fresh Basement
	VES207		54.9	1.39	11.9	H	Topsoil
			12.6	10.5			Weathered Basement
			8577	--			Fresh Basement
	VES208	3	101	1.78	5.75	H	Topsoil
			9.27	3.97			Weathered Basement
			17022	--			Fresh Basement
KANKAN	VES209	5	111	0.5	9.53	HKH	Topsoil
			42.7	0.8			Clay
			110	2.23			Laterite
			20.8	5.96			Weathered Basement
			32750	--			Fresh Basement
	VES210	4	47.8	0.7	17.1	KH	Top soil
			95.4	2.61			Laterite
			26.6	13.8			Weathered Basement
			22310	--			Fresh Basement

APPENDIX 3: TABLE 4(a-f) SHOWING CALCULATED VALUES OF DAR-ZAROUK PARAMETERS

Table 4a: Calculated values of Dar-Zarouk Parameters

SN	Longitudinal conductance (S)	Transverse resistance (T)	Longitudinal resistivity (ρ_L)	SN	Longitudinal conductance (S)	Transverse resistance (T)	Longitudinal resistivity (ρ_L)
1	0.068864	5132.4	1.294652015	44	12.22	22.816	28.106
2	0.075972	6084.5	1.633392226	45	124.8	3740	6240
3	0.027439	2228.7	0.214569825	46	30	142.19	177
4	0.402286	123.2	2.832091429	47	576.87	32733.87	36804.306
5	0.132936	7322.64	4.147592671	48	184.4	7464	11064
6	0.372203	2682.84	11.76160188	49	43	384.81	546.1
7	0.176768	6930	6.186868687	50	53.1	619.34	918.63
8	0.356771	526.08	4.887760417	51	243.8	10647.6	13896.6
9	0.13022	388.206	0.925862637	52	10.36	17.952	22.792
10	0.28777	500.4	3.45323741	53	9.34	17.1	23.35
11	0.07581	3343.2	1.206887619	54	382.1	8960.7	9590.71
12	0.333618	4559.1	13.01112062	55	87.7	651.9	719.14
13	0.138125	3536	3.0525625	56	87.7	651.9	719.14
14	0.195522	877.7	2.561343284	57	109.6	679.8	723.36
15	0.138125	3536	3.0525625	58	208.2	1792.8	1873.8
16	0.171324	1160.43	2.415674362	59	208.5	1795.5	1876.5
17	0.029757	7261.8	0.43742915	60	446	21505	24530
18	0.083129	23395.05	3.665994345	61	218.7055	5862.344	5751.955702
19	0.046098	697.41	0.261373171	62	214.5476	3748.08	5535.329112
20	0.032747	1084.72	0.195173626	63	18.29476	1884.974	40.248472
21	0.126461	1119.79	1.504888417	64	92.46522	5425.7	1026.363942
22	0.068868	6964.2	1.508207547	65	233.5147	3137.288	6538.410256
23	0.134043	2664.9	2.533404255	66	225.4343	2275.54	6086.725722
24	0.104545	40.986	0.216409091	67	87.444	2484.858	918.162
25	0.176	2750	3.872	68	108.8058	1862.04	1419.915657
26	0.223174	8793.55	9.886599496	69	49.24859	2081.39	290.5666586
27	0.167539	13752	8.041884817	70	68.52598	8842	561.9130475

28	1.042705	823.33	30.55124555	71	91.7312	2502.39	1009.0432
29	0.294737	4156.25	10.31578947	72	109.3694	9023.18	1432.739112
30	0.868421	1517.34	31.52368421	73	274.1561	1703.84	8992.320421
31	53.2	369	436.24	74	73.63864	2359.26	648.0200109
32	53.22	369.9	437.4684	75	222.3362	1292.88	5936.377608
33	274.2	867.2	877.44	76	98.37435	1571.38	1160.817285
34	18.2	82	149.24	77	161.0859	1073.09	3108.957241
35	53.3	262.9	293.15	78	60.33051	3363.1	435.5863179
36	21.9	38	41.61	79	129.2979	458.72	2004.11745
37	143.2	4364.8	6300.8	80	40.9219	4733.2	200.5173301
38	40.5	31.76	32.4	81	183.1063	1099.77	4010.027843
39	345	14504	16905	82	59.43145	5866.2	421.9633071
40	396.4	9076.8	9672.16	83	183.0356	1522.2	4026.7832
41	64.5	471.24	541.8	84	49.14351	7609.6	289.9467273
42	234.6	3618.8	3894.36	85	136.7599	1227.3	2242.862281
43	34.1	115.14	129.58	86	49.2569	7881.62	290.6157059

Table 4b: Calculated values of Dar-Zarouk Parameters

SN	Longitudinal conductance (S)	Transverse resistance (T)	Longitudinal resistivity (ρ_L)	SN	Longitudinal conductance (S)	Transverse resistance (T)	Longitudinal resistivity (ρ_L)
87	136.6727	588.6	2241.431952	130	1587.5	88.5	39687.5
88	75.08978	4076.82	675.808029	131	113.28	23.08	1812.48
89	237.2229	122.4	6737.129542	132	201.788	32.67	4923.6272
90	10.03503	0	12.04203888	133	830.83	100.4	7560.553
91	503.18	50.1	6994.202	134	924	113.8	8131.2
92	685.44	54.9	13160.448	135	8.48	11.4	6.784
93	659.61	53.8	12466.629	136	93.5	44.7	205.7
94	260.82	33.3	5398.974	137	6899.2	627.2	77271.04
95	112.64	24	720.896	138	2088.6	359.9	12322.74
96	531.075	46.15	11630.5425	139	5654	279	124388
97	14121.9	684.3	30079.647	140	67.32	32.8	148.104
98	469.35	448.05	492.8175	141	537.08	57.9	6230.128
99	2088.9	220.9	20680.11	142	1080.57	74.2	21503.343
100	651.45	74.6	6579.645	143	147.9	31.3	857.82
101	169.575	35.45	966.5775	144	1587	92	36501
102	530.145	47.05	9913.7115	145	489.955	55.85	5340.5095
103	1709.28	133.1	24613.632	146	1058.4	68.1	25401.6
104	7657.98	298.9	21672.0834	147	558.45	47.4	12230.055
105	563.627	101.43	3325.3993	148	1212.5	73.5	30312.5
106	1711.5	173.5	17970.75	149	4494	235	94374
107	199.8	29.1	2217.78	150	8481	407.5	1865.82
108	453.9	54.7	4629.78	151	4336.4	307.8	64178.72
109	27.3	13.1	286.65	152	882.45	71.4	14030.955
110	18972.8	646.8	584362.24	153	752.7	58.1	14677.65
111	16062.5	667.5	401562.5	154	1555.5	261.1	9488.55

112	846.32	147.96	5044.0672	155	23631.4	506.45	12288.328
113	65.28	18.4	313.344	156	23902.2	536.8	1171207.8
114	1418.535	80.45	37023.7635	157	26440.95	569.45	13484.8845
115	113.28	23.08	1812.48	158	1081.2	83.9	17191.08
116	224.48	33.6	2065.216	159	2396.8	129.4	5368.832
117	831.743	100.41	7577.17873	160	806.13	66.6	12817.467
118	934.5	113.9	8317.05	161	987.28	62.9	29717.128
119	8.48	11.4	6.784	162	3145	112.9	157250
120	3225.35	153.6	8095.6285	163	944.7	67.1	18988.47
121	2763.52	133.55	7074.6112	164	558.946	50.11	9367.93496
122	495.67	60.8	4807.999	165	5375.7	153.3	291900.51
123	6154.65	240.6	17910.0315	166	646.56	59.3	9310.464
124	800.73	77.4	9848.979	167	8368.75	214	430990.625
125	4864.5	234.5	11188.35	168	2417.4	98.4	123287.4
126	9015.6	431.8	198343.2	169	1261	76.25	65572
127	334.8	126.7	903.96	170	837.775	64.825	39375.425
128	348	147.4	835.2	171	1737.45	83.55	39687.5
129	403	133.1	1249.3	172	1523.234	85.59	1812.48

Table 4c: Calculated values of Dar-Zarouk Parameters

SN	Longitudinal conductance (S)	Transverse resistance (T)	Longitudinal resistivity (ρ_L)	SN	Longitudinal conductance (S)	Transverse resistance (T)	Longitudinal resistivity (ρ_L)
173	3220.458	153.2	67760.55	192	4135.25	153.15	184032
174	560.64	47.5	38446.42616	193	507.3	192.67	144733.75
175	74.712	30.94	80994.50613	194	1195.4	147.6	1354.491
176	2230.6	96.7	12278.016	195	2055	258.22	10280.44
177	1365	74	197.23968	196	4371.55	155.15	16892.1
178	10700	264	84762.8	197	569.776	101.56	161747.35
179	23868	519	53235	198	1071.25	133.57	3395.86496
180	1070.1	68.78	535000	199	1711.5	173.5	9180.6125
181	2988.2	156.3	1217268	200	205.556	89.46	17970.75
182	3195.9	216.9	48154.5	201	91.8	102.9	485.11216
183	1939.8	137.9	66636.86	202	1138.39	100	82.62
184	5810.48	300.15	50814.81	203	4910.661	178.79	14912.909
185	4643.8	235.7	30842.82	204	22543.2	835.9	166422.3013
186	2302.8	134.2	120857.984	205	846.32	147.96	628955.28
187	2047.92	647.18	100770.46	206	14.08	8.6	5044.0672
188	298.82	136.23	46516.56	207	132.3	23.1	30.976
189	2047.92	647.18	6512.3856	208	36.8019	13.24	1389.15
190	14592.3	419.3	666.3686	209	123.968	26.76	146.103543
191	5112	178	6512.3856	210	2196	97	738.84928

Table 4d: Calculated values of Dar-Zarouk Parameters

SN	Coefficient of anisotropy(λ)	Transverse resistivity(ρ_t)	SN	Coefficient of anisotropy(λ)	Transverse resistivity(ρ_t)
1	0.030809158	0.039887138	44	44.34536521	1246.370835
2	0.029754449	0.048600685	45	20.85687053	130146.8721
3	0.029579361	0.006346838	46	42.37728814	7500.78
4	0.480754286	1.361540092	47	75.44346548	277664.389
5	0.035887554	0.148846957	48	25.67283799	28404.2795
6	0.099321767	1.168183079	49	28.31533071	15463.0021
7	0.042428788	0.262501339	50	25.69827907	23607.2101
8	0.219023672	1.070535234	51	35.77786386	497190.6629
9	0.154214615	0.142781551	52	39.43585329	898.8219682
10	0.201278177	0.695061332	53	31.1814032	728.0857647
11	0.040013852	0.048292223	54	127.2013792	1219951.54
12	0.07196337	0.936324092	55	89.2957122	64216.11847
13	0.052580625	0.160505644	56	89.39848162	64290.02407
14	0.12570909	0.321984132	57	139.293297	100759.1993
15	0.052700738	0.160872295	58	194.2670015	364017.5075
16	0.102439854	0.247461329	59	193.6038333	363297.5933
17	0.017085848	0.007473848	60	67.84559298	1664252.396
18	0.015928403	0.058393437	61	69.15252964	397762.2872
19	0.068557724	0.01791915	62	69.15252964	382782.0105
20	0.046385764	0.009053278	63	69.15252964	2783.283653
21	0.089817407	0.135165175	64	69.39223204	71221.68482
22	0.026511006	0.0399841	65	69.55241416	454762.2181
23	0.059858929	0.151646866	66	69.71278094	424322.5769
24	0.426753434	0.092353323	67	69.355584	63679.66172
25	0.0673848	0.260913946	68	69.51572384	98706.46466

26	0.042482161	0.420004114	69	69.67604834	20245.53655
27	0.029467079	0.236970851	70	69.83655751	39242.07285
28	0.299647687	9.154610059	71	69.54225664	70171.14118
29	0.070987023	0.732287186	72	69.70261172	99865.65805
30	0.20189756	6.364554918	73	69.86315146	628231.8436
31	54.42879024	23744.01546	74	70.02387587	45376.8728
32	54.37898528	23789.08768	75	69.34225984	411641.8386
33	720.5134549	632207.3258	76	69.5023843	80679.56906
34	18.60594878	2776.751796	77	69.66269343	216578.3352
35	81.33104176	23842.19489	78	69.82318722	30414.02502
36	96.84546537	4029.739814	79	69.58562724	139457.7698
37	27.18554364	171290.6733	80	69.74603229	13985.28818
38	423.3621431	13716.93344	81	69.906622	280327.5006
39	58.94795327	996515.15	82	70.06739637	29565.87029
40	135.5168131	1310740.299	83	69.21907204	278730.1964
41	64.12535482	34743.11724	84	69.37905429	20116.22973
42	118.1595122	460155.678	85	69.5392212	155966.8963
43	74.81270789	9694.230689	86	69.69957279	1246.370835

Table 4e: Calculated values of Dar-Zarouk Parameters (Continues)

SN	Coefficient of anisotropy(λ)	Transverse resistivity(ρ_t)	SN	Coefficient of anisotropy(λ)	Transverse resistivity(ρ_t)
87	69.45055569	20255.79054	130	1090.41036	1362249.663
88	69.61080507	155668.6946	131	533.2336935	21162712.21
89	69.77123911	47043.54097	132	58.770372	106520.1238
90	69.93185783	470057.8762	133	68.72790943	338390.6043
91	302.56322	842.1221509	134	759.6267734	5743198.481
92	298.7272113	2116188.278	135	874.621335	7111720.999
93	292.3683982	3931383.93	136	88.3969616	599.6849875
94	105.6752802	3644848.352	137	354.8301625	72988.56443
95	147.7790336	570538.0902	138	5148.869264	397858482.9
96	202.543275	106533.3142	139	2962.329702	365040.71
97	5543.945667	2355688.168	140	2153.087404	267818236
98	3742.068546	1667599287	141	256.6538586	38011.46307
99	1768.417797	1844156.866	142	390.33215	2431819.257
100	541.202472	36571074.57	143	458.2979187	9854937.342
101	249.9102638	3560920.139	144	215.467809	184832.5959
102	236.81889	241557.638	145	583.693563	21305398.74
103	992.6891683	2347754.153	146	380.6786732	2033018.071
104	2265.630431	24433685.88	147	373.9038345	9497755.642
105	800.7541453	491009316.5	148	216.447927	2647170.052
106	1367.869268	2662827.274	149	412.1415055	12493039.39
107	151.22601	24581636.65	150	1820.577608	171815191.2
108	374.291903	335386.0205	151	3283.296176	612603967
109	21.7412	1732889.167	152	2436.7638	156388381.6
110	5156.911144	6232.11498	153	462.1045995	6483768.841

111	5384.932565	3013504148	154	321.7625748	4722718.456
112	1191.497434	2162386983	155	2116.2705	20080338.45
113	114.2459296	6009993.126	156	3775.892805	4639940928
114	457.0859458	35798.27656	157	4057.67552	4752381219
115	59.204376	16923041.95	158	4287.06305	5781055007
116	204.2721396	107306.7474	159	562.945412	9677639.613
117	765.2234634	421866.0911	160	886.839326	47612913.52
118	881.057835	5798234.951	161	419.18253	5372858.245
119	89.0467416	7327802.067	162	271.5022952	8068268.459
120	1080.716483	604.093095	163	521.2597222	81968091.32
121	897.161655	87490791.56	164	388.1965	7371257.594
122	425.1780099	63470698.93	165	275.7747852	2583440.251
123	1761.819957	2044255.446	166	819.593082	239239638.6
124	542.9162277	315542509.3	167	370.60011	3450458.983
125	1765.884564	5347170.525	168	1342.820213	578742922.6
126	3425.495661	197573345.6	169	392.1457932	48346635.26
127	1037.700696	679423771	170	200.72695	13162067.57
128	1214.833635	938039.9212	171	147.7159354	5816377.737
129	3742.068546	1014629.052	172	1090.41036	25045270.42

Table 4f: Calculated values of Dar-Zarouk Parameters (Continues)

SN	Coefficient of anisotropy(λ)	Transverse resistivity(ρ_t)
173	369.6143319	19197216.76
174	499.32383	85910105.02
175	1060.690522	2606638.277
176	212.3012608	46224.13085
177	234.35513	41251055.71
178	486.6646183	15465360.01
179	290.51113	949820489
180	1775.3654	4731608130
181	3887.071812	9521987.139
182	197.738262	73966181.59
183	1109.989	84703964.39
195	1666.914909	11844837.7
196	1012.931596	35045271.28
197	2306.03425	158534555.1
198	1768.626326	2696274.467
199	943.260852	948586.866
200	5337.4076	24241180.77
201	1111.866206	353697.8906
202	5349.783992	70624.56067
203	3144.1263	10706988.47
204	1173.191078	199466471.7
205	977.2798517	4198206051
206	1573.086	5923886.076
207	1152.172251	1637.079122
208	2074.6545	144706.8573
209	980.136955	11210.22634
210	793.9875404	127384.3542

APPENDIX 4: TABLE 6(a-e) SHOWING CALCULATED VALUES OF AQUIFER PARAMETERS

Table 6(a): Calculated values of Aquifer Parameters

SN	Resistivity (Ωm)	Depth (m)	Thickness (m)	Hydro. Conduc.(m/day)	Transmissivity(m^2/day)
1	273	1.3	18.8	1.955413	38.67584
2	283	1.3	21.5	1.886318	38.80094
3	285	0.7	7.82	1.87308	38.92622
4	17.5	1.3	7.04	30.50445	38.69315
5	234.7	3.6	31.2	2.274512	38.81828
6	84.9	0.5	31.6	6.287725	38.94359
7	198	1.3	35	2.6961	38.72227
8	38.4	0.6	13.7	13.90177	38.84738
9	54.6	0.5	7.11	9.777067	38.97267
10	41.7	0.9	12	12.80163	38.6394
11	210	1.2	15.92	2.542037	38.76438
12	116.9	1.7	39	4.566534	38.88954
13	160	1	22.1	3.336424	38.8289
14	67	1.2	13.1	7.96758	38.95418
15	160	0.9	22.1	3.336424	39.07965
16	82.3	3.5	14.1	6.486365	38.55068
17	494	3.5	14.7	1.080623	38.67572
18	530.5	2	44.1	1.006273	38.80094
19	123	1.75	5.67	4.340064	38.40965
20	182	3.2	5.96	2.93312	38.53454
21	94.1	1.5	11.9	5.672985	38.65961
22	318	1.3	21.9	1.678704	38.13368
23	141	1.4	18.9	3.786013	38.25825
24	19.8	1.3	2.07	26.961	38.383
25	125	1.3	22	4.270623	38.05641

26	198.5	1.5	44.3	2.689309	38.18085
27	286.5	1.5	48	1.863274	38.30548
28	28.1	0.5	29.3	18.99743	38.12537
29	118.75	1.9	35	4.495393	38.24988
30	41.8	2.5	36.3	12.771	38.37457
31	45	0.5	8.2	11.08845	90.9253
32	45	0.6	8.22	11.08845	91.14707
33	271	1.76	3.2	2.077258	6.647225
34	10	1.72	8.2	45.10318	369.846
35	47.8	2.01	5.5	10.48133	57.64731
36	20	0.701	1.9	23.62639	44.89013
37	99.2	1.28	44	5.304337	233.3908
38	39.7	2.26	0.8	12.46342	9.970739
39	296	1.02	49	1.913119	93.74285
40	372	1.09	24.4	1.545815	37.71789
41	56.1	2.01	8.4	9.02718	75.82831
42	218	3.57	16.6	2.544806	42.24379
43	30.3	2.27	3.8	16.03626	60.93777
44	9.92	3.57	2.3	45.44239	104.5175
45	74.8	3.41	50	6.902485	345.1243
46	24.1	0.6	5.9	19.8541	117.1392
47	513.07	1.34	63.8	1.145257	73.06741
48	124.4	1.3	60	4.294631	257.6778

Table 6(b): Aquifer Parameters

SN	Resistivity (Ωm)	Depth (m)	Thickness (m)	Hydro. Conduc.(m/day)	Transmissivity(m^2/day)
49	30.3	4.0	12.7	16.03626	203.6605
50	35.8	4.2	17.3	13.72551	237.4513
51	186.8	6.42	57	2.939197	167.5342
52	8.16	3.57	2.2	54.52368	119.9521
53	6.84	8,23	2.5	64.27939	160.6985
54	357	0.6	25.1	1.606318	40.31859
55	79.5	3.57	8.2	6.521052	53.47262
56	79.5	2.67	8.2	6.521052	53.47262
57	103	2.43	6.6	5.121559	33.80229
58	199.2	0.648	9	2.768159	24.91343
59	199.5	0.8	9	2.764276	24.87848
60	391	0.5	55	1.475628	81.15954
61	201	3.02	26.3	2.745028	80.06117
62	216	1.8	25.8	2.56678	44.53933
63	15.4	1.3	2.2	30.14964	3690.343
64	26.085	0.5	11.1	18.44103	3835.749
65	132.65	1.6	28	4.04494	95.66634
66	59.09	1	27	8.600342	331.1969
67	163	1.7	10.5	3.33766	50.88105
68	118.15	0.5	13.05	4.506182	71.01728
69	95.6	3.5	5.9	5.490433	119.5369
70	115	1.3	8.2	4.621217	355.3113
71	118	4.8	11	4.511526	95.67455
72	86.9	7.6	13.1	6.001521	623.1623
73	230	1.9	32.8	2.420731	17.93278
74	155	0.5	8.8	3.498082	53.24442
75	55.4	12.5	26.7	9.133535	213.151

76	28.8	5.2	11.8	16.81404	917.4043
77	45.6	14.8	19.3	10.95229	257.7367
78	132	0.5	7.22	4.063518	103.5304
79	44.6	10.5	15.5	11.18119	115.0008
80	24.5	2.9	4.9	19.55156	3777.201
81	122	3.5	21.9	4.373389	39.42395
82	47.7	0.5	7.1	10.50183	1291.526
83	93.7	3.5	22	5.594217	90.88065
84	129	3.5	5.9	4.151602	244.8995
85	232	9.7	16.4	2.401259	12.70287
86	129	3.5	5.9	4.151602	253.6539
87	232	9.7	16.4	2.401259	6.092159
88	51.8	0.5	9	9.724312	765.3334
89	143.55	0.5	28.4	3.75768	3.204041
90	102	0.5	1.2	5.168382	0
91	36.2	1.2	13.9	13.58398	18.79993
92	35.7	1.2	19.2	13.76137	21.16244
93	34.9	2.1	18.9	14.0554	21.66707
94	12.6	2.1	20.7	36.3562	96.08424
95	17.6	2.3	6.4	26.61862	36.29812

Table 6 (c) Aquifer Parameters

SN	Resistivity (Ωm)	Depth (m)	Thickness (m)	Hydro. Conduc.(m/day)	Transmissivity(m^2/day)
96	24.25	35.7	21.9	19.73951	37.56613
97	663	1.3	21.3	0.901664	0.930631
98	447	0.5	1.05	1.302419	1.305478
99	211	1.3	9.9	2.623474	2.746566
100	64.5	1.48	10.1	7.925479	9.166523
101	29.75	2.4	5.7	16.31264	19.43809
102	28.35	5	18.7	17.06287	28.31774
103	118.7	0.5	14.4	4.486702	5.031003
104	270.6	0.5	28.3	2.080122	2.297666
105	95.53	3.5	5.9	5.494186	5.83351
106	163	1.7	10.5	3.33766	3.552663
107	18	4.8	11.1	26.06641	42.1407
108	44.5	3.8	10.2	11.20463	13.77288
109	2.6	1.3	10.5	158.4665	798.4275
110	616	0.5	30.8	0.965678	1.013962
111	642.5	0.5	25	0.928472	0.964599
112	142	3.6	5.96	3.795928	3.95525
113	13.6	1	4.8	33.85618	45.80543
114	54.35	0.5	26.1	9.29803	13.76314
115	7.08	4.1	16	62.24444	202.9099
116	24.4	1.3	9.2	19.62629	27.02637
117	91.3	0.5	9.11	5.731274	6.303146
118	105	1.2	8.9	5.030499	5.456894
119	10.6	0.6	0.8	42.71703	45.94096
120	128.5	0.5	25.1	4.166669	4.980548
121	107.95	1.3	25.6	4.902144	6.064672
122	51.1	0.5	9.7	9.848517	11.718

123	211.5	0.5	29.1	2.617688	2.977852
124	65.1	1.3	12.3	7.857319	9.341881
125	211.5	0.5	23	2.617688	2.902354
126	409.8	0.7	22	1.41238	1.488203
127	124	0.5	2.7	4.307552	4.401346
128	145	1	2.4	3.722616	3.784231
129	130	1.7	3.1	4.121804	4.220093
130	63.5	1.3	25	8.041845	11.20793
131	7.08	4.8	16	62.24444	202.9099
132	8.27	1.3	24.4	53.84687	212.7179
133	91.3	0.5	9.1	5.731274	6.302518
134	105	1.2	8.8	5.030499	5.452103
135	10.6	0.6	0.8	42.71703	45.94096
136	42.5	1.3	2.2	11.69572	12.30115
137	616	1.5	11.2	0.965678	0.983236
138	354	3.6	5.9	1.619013	1.645997
139	257	3.5	22	2.182625	2.369465
140	30.6	1.1	2.2	15.88955	17.03194
141	46.3	5.2	11.6	10.79775	13.50302
142	54.3	1.3	19.9	9.306016	12.71651
143	25.5	3.2	5.8	18.83537	23.1195
144	69	3.5	23	7.442237	9.922983
145	44.95	0.5	10.9	11.09996	13.7916

Table 6 (d): Aquifer Parameters

SN	Resistivity (Ωm)	Depth (m)	Thickness (m)	Hydro. Conduc.(m/day)	Transmissivity(m^2/day)
146	44.1	3.8	24	11.2994	17.44874
147	25.5	3.6	21.9	18.83537	35.01164
148	48.5 80.2	0.5	25	10.34015	15.67012
149	214	2.4	21	2.58915	2.843226
150	385.5	0.8	22	1.495258	1.58059
151	293	4.04	14.8	1.931386	2.028944
152	55.5	10	15.9	9.118183	11.73042
153	38.6	7.88	19.5	12.79443	19.25793
154	255	0.6	6.1	2.19859	2.251184
155	454.45	3.5	52	1.282491	1.429239
156	487.8	7.5	49	1.200507	1.321099
157	518.45	3.5	51	1.134167	1.245735
158	68	10	15.9	7.544281	9.308311
159	107	3.8	22.4	4.942732	5.977472
160	50.7	8.4	15.9	9.920979	13.03229
161	32.8	1.2	30.1	14.89308	28.56021
162	62.9	0.5	50	8.11338	14.56281
163	47	0.9	20.1	10.64766	15.20123
164	33.35	1.06	16.76	14.66384	22.03313
165	99	3.58	54.3	5.314333	8.229164
166	44.9	1.24	14.4	11.11149	14.67508
167	162.5	8.4	51.5	3.347239	4.408057
168	47.4	8.88	51	10.56382	21.92995
169	24.25	3.57	52	19.73951	62.06754
170	17.825	5.07	47	26.30506	95.66481
171	44.55	3.8	39	11.1929	20.99139
172	60.35	0.5	25.24	8.432725	11.95952

173	128.05	0.5	25.15	4.180327	5.001375
174	25.6	3.61	21.9	18.76673	34.82108
175	28.3	0.5	2.64	17.09099	18.68534
176	58.7	1.74	38	8.653632	14.25564
177	35	1.35	39	14.01794	29.63793
178	214	2.44	50	2.58915	3.194092
179	468	1.32	51	1.247819	1.3838
180	23.78	1.24	45	20.10321	58.14545
181	134	5.19	22.3	4.006913	4.673735
182	201	9.68	15.9	2.745028	2.962172
183	122	8.56	15.9	4.373389	4.943363
184	279.35	0.6	20.8	2.019279	2.169631
185	214	1.27	21.7	2.58915	2.851695
186	114	1.63	20.2	4.65902	5.484566
187	644	0.99	3.18	0.926455	0.931029
188	134	1.34	2.23	4.006913	4.073596
189	644	0.99	3.18	0.926455	0.931029
190	381	3.51	38.3	1.511725	1.663691
191	142	3.9	36	3.795928	4.758276
192	118.15	2.11	35	4.506182	5.841065

Table 6 (e): Aquifer Parameters

SN	Resistivity (Ωm)	Depth (m)	Thickness (m)	Hydro. Conduc.(m/day)	Transmisivity (m^2/day)
193	190	1.17	2.67	2.892993	2.933647
194	139	1.34	8.6	3.872297	4.111878
195	250	1.34	8.22	2.239581	2.313218
196	118.15	0.5	37	4.506182	5.917344
197	95.6	3.53	5.96	5.490433	5.832723
198	125	1.71	8.57	4.275398	4.568519
199	163	1.71	10.5	3.33766	3.552663
200	87.1	0.5	2.36	5.988664	6.150929
201	102	0.9	0.9	5.168382	5.213986
202	86.9	8.56	13.1	6.001521	6.906238
203	144.9	0.8	33.89	3.725012	4.596238
204	808	3.42	27.9	0.74975	0.775639
205	142	3.57	5.96	3.795928	3.95525
206	6.4	1.19	2.2	68.39246	91.90237
207	12.6	1.39	10.5	36.3562	66.65303
208	9.27	1.78	3.97	48.40789	69.1392
209	20.8	3.35	5.96	22.77761	29.30427
210	61	0.7	36	8.348874	13.27608

APPENDIX 5: PRINCIPLES AND PROCEDURES OF THE METHODS USED IN THE WATER SAMPLES' ANALYSIS

PRINCIPLES AND PROCEDURES OF THE METHODS USED IN AAS ANALYSIS

Principle of the method

The principle is based on the absorption of radiant energy of various wavelengths by atoms present in the sample in their ground states. The atoms of elements strongly absorb radiation at certain characteristic wavelengths that coincide with the emission lines of spectral wavelengths of the particular element.

Procedure for analysis

Sample solution is aspirated through a nebulizer and sprayed as a fine aerosol in to the mixing chamber where it is mixed with fuel and oxidant gases. The mixture is then carried to the head of a flame or burner for sample vaporization and atomization. The sample is then passed through the light beam which is a hollow – Cathode lamp. These cathode lamps are designed to emit the atomic spectrum of a particular element and the specific lamps are selected for use depending on the element to be determined. For example, if calcium is to be measured, a calcium lamp is selected to be used. The atomic vapour of the sample absorbs some of the energy from a cathode lamp used as a radiant source. The energy absorbed and the remaining energy are passed into the monochromator which selects and isolate the wavelengths of energy of elements of interest. The wavelength of light isolated by the monochromator is then directed to the detector, which serves as the eye of the instrument. This detector is a photo-multiplier tube; produce an electrical current dependent on the light intensity.

The electrical current is then amplified and processed by the instrument electronics to produce a signal, which is a measure of the light attenuation occurring in the sample cell. This signal is further processed to produce instrument readout directly in concentration units.

Digestion procedure for "AAS"analysis

1. Put 1 or 2 mls of the sample is in to an empty beaker
2. Measure 9 mls of Conc. HNO_3, 3 mls of HCL and 1ml of pacloric acid into the same beaker
3. Add 10 mls of de-ionized or distilled water into the same beaker
4. Leave the sample for about 2 to 3 hours
5. Filter the sample using a filter paper
6. Pour the filtrate into 100ml volumetric flask
7. The filtrate would be toped-up to 100 ml meniscus level using de-ionized or distilled water

   That's the digested samples. The digested samples would then be run through AAS machine

Determination of Chloride (Cl^-) by Argentimetric method

Principle of the method

The simplest and most widely used method for the estimation of chlorides in water is Argentimetric method. This method is based on the titration of a halide such as Chloride (Cl^-) with standard Silver nitrate $(AgNO_3)$ in the presence of Potassium chlorate (K_2CrO_4) as indicator. The end point of the titration is indicated when the solution changes from pure yellow to reddish brown. This is caused by the start of the precipitation of insoluble reddish brown silver chromate when all the chloride has reacted with Silver nitrate solution.

The reactions involved in the process are:

$$NaCl \quad \times \quad AgNO_3 \rightarrow AgCl_4 \times NaNO_3$$

(In water) (Std-solution) (In-soluble white ppt.)

$AgNO_3 \times K_2CrO_4 \rightarrow Ag_2CrO_4 \times 2KNO_3$ (In-soluble reddish brown ppt)

Procedure for analysis

A 100 ml of water sample is exactly measured in to a conical flask of 250 ml and 1.0..ml of potassium chromate indicator solution is added to it. The sample in the flask is then titrated with standard silver nitrate solution of 0.0141N until there is a perceptible colouration end point. The concentration of chloride is calculated from this below expression.

The expression goes thus:

$$Cl\ (Mg/l) = \frac{A \times N \times 35450}{Ml\ of\ sample\ taken\ for\ analysis}$$

Where:

$A = Ml\ of\ titration\ for\ sample$

$N = Normality\ of\ Silver\ nitrate\ solution\ (N = 0141)$

Determination of Carbonate and Bi-Carbonate byTitrinetric Method

Principle of the method:

This technique is based on titration of water sample with standard solution of Sulphuric acid (H_2SO_4) in the presence of phenolphthalein and methyl orange as indicators. The end point of the titration will be indicated when the colour of the solution changes from orange – yellow to red.

Procedure for analysis: Carbonate $(\boldsymbol{CO_3^-})$0.0ml of water sample is measured in a conical flask and 2-5 drops of phenolphthalein indicator is added to it. The solution is then titrated

with 0.02N H_2SO_4 till the pink colour disappears. The volume of acid used is recorded and the concentration of CO_3^- is calculated as:

$$\frac{2 \times Normality\ of\ Acid\ \times Volume\ of\ water\ used\ \times 100}{Aliquot\ taken\ (mls\ of\ acid\ used)}$$

Bicarbonate(HCO_3^-): To the same solution as above 2-5 drops of methyl –orange is added and then titrated until the colour changes which indicates the end point of the titration. The volume of acid used is recorded.

$$\frac{2 \times Normality\ of\ Acid\ \times Volume\ H_2O\ \times 100}{Aliquot\ taken\ (mls\ of\ acid\ used)}$$

N.B: 2 = constant values given

Digestion processes for nitrogen to calculate nitrate

There are three stages to get N_2

1. **Digestion**: To expose nitrogen out of the sample

   Use 0.5 g of $CuSo_4$

   Use 5 g of $NaSo_4$

   Use selenium powder or crystal as a catalyst (very small quantity) just a (speck)

   Use 25 ml of conc. H_2So_4

   All these would be added to 2 ml of the sample (liquid) or 2 g if it is solid.

   Pour the solution into kjeldahal digestion flask. Heat the solution in a digestion stove (fume cupboard) from black to brown and it will later turn greenish. Pour the greenish

solution after cooling into a standard volumetric flask (250 ml) and top it with distilled water after filtration. Pour the sample to digest bottle.

2. **Distillation**

Get: 5 ml of the digested sample

5 ml of 40% NaOH solution

5ml of boric acid

Pour the sample into the distillation flask with NaOH. The boric acid would be put into a small flask of 100ml. Distillation starts; one side would be distillating the sample while the other side would be condensing it. The boric acid would be trapping Nitrogen in the sample until it becomes greenish up to 50 ml.

3. **Titrration**

0.01 molar HCl acid would be titrated with 50 ml of distillate until it turns blue like boric acid. The tire value would be used to calculate Nitrogen

$$\% N = \frac{0.014\ g \times 0.01\ m\ HCl \times 250/5 \times titre\ value \times 100\%}{2\ ml\ of\ the\ sample}$$

Nitrate Concentration = % N × 4.43 ml

ProQuest Number: 29326803

INFORMATION TO ALL USERS
The quality and completeness of this reproduction is dependent on the quality
and completeness of the copy made available to ProQuest.



Distributed by ProQuest LLC (2022).
Copyright of the Dissertation is held by the Author unless otherwise noted.

This work may be used in accordance with the terms of the Creative Commons license
or other rights statement, as indicated in the copyright statement or in the metadata
associated with this work. Unless otherwise specified in the copyright statement
or the metadata, all rights are reserved by the copyright holder.

This work is protected against unauthorized copying under Title 17,
United States Code and other applicable copyright laws.

Microform Edition where available © ProQuest LLC. No reproduction or digitization
of the Microform Edition is authorized without permission of ProQuest LLC.

ProQuest LLC
789 East Eisenhower Parkway
P.O. Box 1346
Ann Arbor, MI 48106 - 1346 USA